Visualization of Some Energy Levels of Even-Even Nuclei

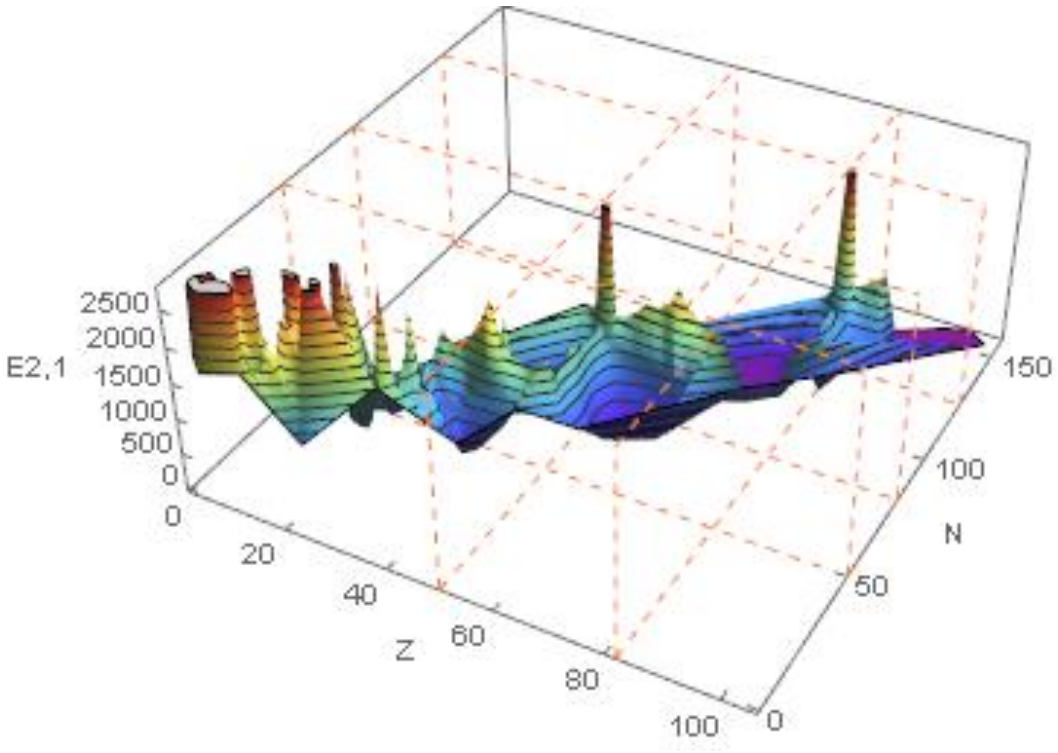

M. M. Hammad, M. M. Yahia, and S. B. Doma

Visualization of Some Energy Levels of Even-Even Nuclei

Visualization of Some Energy Levels of Even-Even Nuclei

An Atlas for the energy levels of the even-even nuclei

by

M. M. Hammad

Department of Mathematics

Faculty of Science

Damanhour University, Egypt

https://orcid.org/0000-0003-0306-9719

m_hammad@sci.dmu.edu.eg

M. M. Yahia

Department of Mathematics

Faculty of Science

Damanhour University, Egypt

S. B. Doma

Department of Mathematics and Computer Science

Faculty of Science

Alexandria University, Egypt

https://orcid.org/0000-0003-4563-1079

sbdoma@yahoo.com

Abstract

The properties of the lowest excited states of atomic nuclei offer a very sensitive test for nuclear structure theories. To identify and distinguish the shape phase transitions, one needs the variation behaviors of the energy ratios with respect to the neutron or proton number of the nuclei. The possibility of generating images of the variation behaviors of energy levels and energy ratios by exploiting the large body of data on stable and near-stable nuclei, whose accumulation over the past decades now permits, prompted us to produce this atlas which illustrates in a simple and effective way these behaviors. The atlas represents the experimental data of the energy levels and energy ratios of the 2_1^+, 4_1^+, 2_2^+ and 4_2^+ states of 645 even-even nuclei. The interpolation surfaces of the values of energy levels and energy ratios, $E_{2_1^+}$, $E_{2_2^+}$, $E_{4_1^+}$, $E_{4_2^+}$, $E_{4_1^+}/E_{2_1^+}$, $E_{4_2^+}/E_{2_2^+}$, $E_{2_2^+}/E_{2_1^+}$, $E_{4_2^+}/E_{4_1^+}$, $E_{4_2^+}/E_{2_1^+}$ and $E_{4_1^+}/E_{2_2^+}$, through all points of the even-even nuclear landscape are presented. The variation of these values with respect to each chain of isotopes and isotones are displayed using two-dimensional figures. Visualization of the data through visual imagery has been considered an effective way for connecting abstract and concrete ideas as well as allowing the emergence of the significant patterns. Moreover, we will see that it is possible, in many if not most cases, to understand the detailed results of complex calculations of the nuclear structure theories with an absolute minimum of formalism and often by inspection. The introduction of this atlas contains a brief account of some topics of present-day interest in theoretical nuclear structure. These topics can be used to explain the existence of a few typical patterns of nuclear spectra as well as some of the systematic changes in these patterns over sequences of nuclei. Researchers working on nuclear theory will find this atlas handy to understand the nuclear structure theories.

Contents

List of Figures

Introduction

Chapter I: Three dimensional figures of the values of energy levels and energy ratios over all even–even nuclei

Chapter II: Two dimensional figures of the values of energy levels and energy ratios over all even–even nuclei for different isotopes.

Chapter III: Two dimensional figures of the values of energy levels and energy ratios over all even–even nuclei for each chain of isotopes.

Chapter IV: Two dimensional figures of the values of energy levels and energy ratios over all even–even nuclei for different isotones.

Chapter V: Two dimensional figures of the values of energy levels and energy ratios over all even–even nuclei for each chain of isotones.

Chapter VI: Scatter plots showing relationship between the values of energy levels (2_1^+, 2_2^+, 4_1^+ and 4_2^+) for all even–even nuclei.

Glossary of Acronyms

NSM	Nuclear shell model
GCM	Geometrical collective model
IBM	Interacting boson model
QSPTs	Quantum shape phase transitions
CPSs	Critical point symmetries
DS	Dynamical symmetry
SGA	Spectrum generating algebra
COs	Casimir operators
IBM-2	Proton-Neutron version of interacting boson model
IBFM	Interacting boson-fermion model
QAs	Quantum algebras
PES	Potential energy surface
GSB	The ground state band

Introduction

The purpose of this introduction is to give short overview of some topics in theoretical nuclear structure. The topics selected are nuclear chart, nuclear shell model (NSM), geometrical collective model (GCM), interacting boson model (IBM), quantum shape phase transitions (QSPTs), shape coexistence, critical point symmetries (CPSs), energy ratios and energy correlations. These topics can be used to explain the existence of a few typical patterns of nuclear spectra as well as some of the systematic changes in these patterns over sequences of nuclei. So, the reader will be able to understand each specific type of nuclei occurring in the chart as well as the evolution of structure from one type to another.

Since Rutherford's discovery of the nucleus in 1910 using collisions of alpha particles against thin gold sheets [1], the knowledge about the nucleus has been substantially improved. The atomic nucleus is a small dense region located at the center of an atom. It consists of a number of neutrons and protons bound together by the short-ranged attractive nuclear force [2]. The chart of nuclides, or the Segré chart, figure 1, is a two-dimensional graph in which one axis represents the number of neutrons and the other represents the number of protons in an atomic nucleus. Each point plotted on the graph, thus, represents the nuclide of a real or hypothetical chemical element. This system of ordering nuclides can offer a greater insight into the characteristics of isotopes than the well-known periodic table, which shows only elements instead of each of their isotopes.

There are several thousand nuclides, or isotopes, that inhabit the nuclear landscape. The interplay between the nuclear force and the Coulomb repulsive force leads to nuclei, with certain combinations of neutrons and protons, which are stable. These are situated along the line of stability in the nuclear chart. Exactly 288 nuclei form the so-called valley of stability [3,4]. For the lightest of the stable nuclei, equal numbers of neutrons and protons are energetically favored. Heavier stable nuclei, on the other hand, require a neutron excess to balance the Coulomb repulsion provided by the increasing number of protons. Nuclei which are removed from the line of stability are unstable and undergo radioactive decay. On the neutron-rich side, nuclei convert neutrons into protons via β^- decay in order to approach stability. Similarly, proton-rich nuclei decay through β^+ emission or electron capture, converting protons into neutrons. The heaviest of nuclei can decay by emitting tightly-bound α particles. The vast majority of our current knowledge, concerning the foundations of many nuclear models, is derived from nuclei near the line of stability. The neutron and proton drip lines represent the limits of the nuclear landscape. While the proton drip line is measured experimentally up to rather high Z-values, the location of the neutron drip line for absolute majority of elements is based on theoretical predictions [5,6].

Fundamentally, the behavior of the nuclear system is entirely determined by the interaction of its constituents, but it is largely impossible to deduce even the most basic structural behavior of the system directly from the intrinsic properties of these constituents. This limitation arises in part since the underlying interactions of protons and neutrons in the nuclear medium are not entirely understood, but, more importantly, the computational problem of describing a system of tens or hundreds of interacting protons and neutrons is intractable without the benefit of some additional simplifications. Consequently, there is a need for "phenomenological" models of nuclear structure. The theoretical nuclear structure landscape comprises a rich collection of nuclear models. The different models provide a basic understanding of the variety of phenomena observed in atomic nuclei which have not been explained under the framework of a single unifying model. However, it is not so that a model developed for one group of nuclei will necessarily be successful in describing the properties of a different group of nuclei.

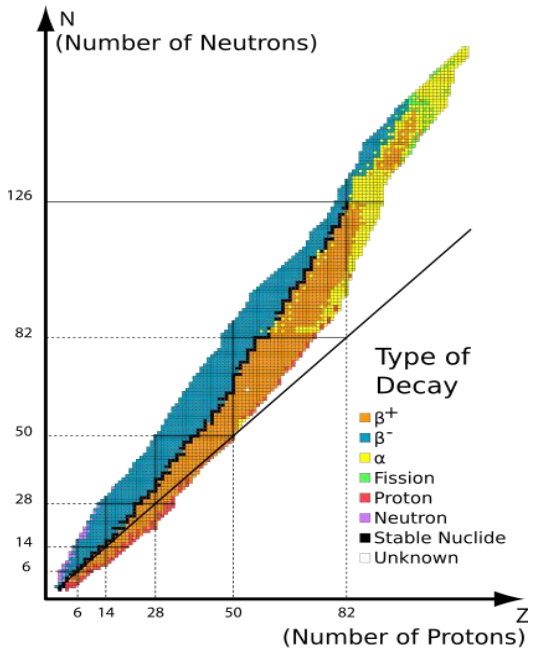

Figure 1. Graph of isotopes by type of nuclear decay. Orange and blue nuclides are unstable, with the black squares between these regions representing stable nuclides. The unbroken line passing below many of the nuclides represents the theoretical position on the graph of nuclides for which proton number is the same as neutron number. The chart shows the location of all nuclei as a function of their neutron number (N) and proton number (Z). Dashed lines represent magic numbers, which correspond to full shells of protons or neutrons. Doubly magic nuclei lie at the intersections of magic-number lines.

The available models can be grouped into roughly three categories: single particle, collective, and models combining both collective and single-particle degrees of freedom. Most nuclei exhibit the properties of both single-particle and collective excitations. In this regard, experimental studies, exploring the interplay of collective and single-particle degrees of freedom, help bridge the gap between the different types of models.

Early in the development of the theory of the nucleus there arose two very different models. The liquid drop model of Neils Bohr took a very classical view of the nucleus as a drop of some nuclear liquid, and using hydrodynamics with some quantum corrections, the binding energies of all known nuclei were reproduced quite well [7], along with a useful model for nuclear fission [8,9]. This model failed in many other respects. The second model is the NSM, developed by Mayer and Jensen, which has its foundation in the single-particle motion of the constituent nucleons in a mean-field potential, much like electrons in the atom [10-13]. The wave function of any quantum-mechanical state of a nucleus with A nucleons satisfies the Schrodinger equation [14,15]

$$H\Psi(\xi_1,\xi_2,\dots,\xi_A) = E\Psi(\xi_1,\xi_2,\dots,\xi_A), \tag{1}$$

with the Hamiltonian

$$H = \sum_{i=1}^{A} \frac{p_i^2}{2m_i} + \sum_{i<j}^{A} V_2(\xi_i,\xi_j) + \sum_{i<j<k}^{A} V_3(\xi_i,\xi_j,\xi_k) + \cdots. \tag{2}$$

The notation ξ_i is used to denote all coordinates of nucleon i, not only its position vector $\boldsymbol{r}_i$. The term $p_i^2/2m_i$ is the kinetic energy of nucleon i and acts on a single nucleon only. The operator

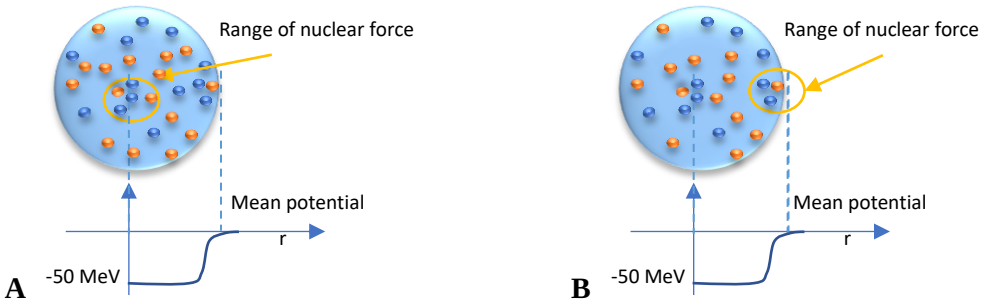

Figure 2. Panels A and B are schematic illustration of the mean potential for a nucleon inside the nuclear surface and at the nuclear surface, respectively.

$V_2(\xi_i, \xi_j)$ is the two-body interaction between the nucleons i and j. The operator $V_3(\xi_i, \xi_j, \xi_k)$ is the three-body interaction. Considering at most two-body interactions, the Hamiltonian becomes

$$H = \sum_{i=1}^{A} \frac{p_i^2}{2m_i} + \sum_{i=1}^{A} V_1(\xi_i) + \sum_{i<j}^{A} V_2(\xi_i, \xi_j) - \sum_{i=1}^{A} V_1(\xi_i) = H_{\text{ip}} + V_{\text{ri}}, \qquad (3)$$

where the independent-particle potential is $H_{\text{ip}} = \sum_{i=1}^{A} p_i^2/2m_i + V_1(\xi_i)$, and the residual interaction V_{ri} is given by $V_{\text{ri}} = \sum_{i<j}^{A} V_2(\xi_i, \xi_j) - \sum_{i=1}^{A} V_1(\xi_i)$. Moreover, if we choose H_{ip} such that a large part of the effect of the two-body interaction in (3) is included, the residual interaction V_{ri} will be sufficiently weak that, in some cases, it may even be adequate to ignore it. This gives us various independent particle models. Alternatively, we can make use of the energies of independent-particle potential to reduce the Hilbert space to a manageable size and solve the eigenvalue problem with the residual interaction in the truncated space. Hence, the first step in developing the NSM is the choice of the potential. Figure 2, panel A, depicts this situation, a nucleon well inside the nucleus feels the nucleon-nucleon interaction from the surrounding nucleons within range of the interaction, which is about 1 fm. As the density of the nucleons is constant inside the nucleus, the mean effect from surrounding nucleons should be almost constant, and the mean potential should be almost flat. Figure 2, panel B, also indicates the effect from surrounding nucleons for a nucleon at the surface. The number of the surrounding nucleons becomes smaller, as this nucleon moves out, resulting in less binding. Therefore, the single- particle shell model treats each nucleon as an independent particle that acts within a mean field of all the rest. Popular choices of the independent-particle potential are harmonic-oscillator potential, square-well potential and Woods-Saxon potential.

The NSM centers on the fact that the individual nucleon-nucleon collisions which occur within the nucleus in its ground-state, do not supply enough energy to move nucleons from one major shell to another. The energy required to remove a nucleon from a closed shell is on the order of a few MeV or more. Thus, the closed shell nucleons can be approximated as a closed system which is not open to interactions with external nucleons. The closed shell is often called the (inert) core. In general, there can be some protons (or neutrons) occupying the next shell just above the closed shell. This shell is called the valence shell, and its nucleons are referred to as valence nucleons. The valence shell is, by definition, only partially occupied. Generally, core nucleons are strongly bound and difficult to excite whereas valence nucleons are more loosely bound and easier to excite. An approximation usually (though not always) made in the NSM is to assume that the independent-particle Hamiltonian H_{ip} suffices to describe the core nucleons and to include the residual interaction V_{ri} between valence nucleons only. Given that in this approach the core must be in a unique state coupled to angular momentum $J = 0$, this in effect corresponds to an inert-core assumption, that is, the contribution of the core to the total energy is constant for all quantum states of the nucleus and can be neglected unless one is interested in binding energies.

The NSM is founded on the experimental observation that nuclei with proton or neutron numbers $N = Z = 2,8,20,28,50,82$ and 126, known as the magic numbers, have unique properties compared to other nearby nuclei in the nuclear chart. The nuclear magic numbers are shown in the chart of nuclides in figure 1. Points at which the magic lines intersect are thought to correspond to doubly magic isotopes. Among the thousands of atomic nuclei studied to date, doubly magic nuclei form a very small and exclusive club. The doubly magic nuclei are the best examples of rigidly spherical nuclear systems. To date, six nuclei have had their membership in the doubly magic club confirmed through observation of their rigid sphericity. Five of them are among the stable isotopes found in nature. The sixth is radioactive and is proton rich, it would need two more neutrons to be stable [16,17].

The NSM holds up well near magic nuclei. However, the model cannot describe features such as rotations and vibrations in nuclei, observed in regions of the nuclear chart distanced from the magic nuclei. In other words, a major problem for both the liquid drop and NSM was the deviation of the nuclear distribution from spherical symmetry, in particular the large quadrupole moments observed in some elements. These types of nuclei are characterized by a series of low-lying excitations with large transition probabilities. This suggested that certain nuclei are themselves deformed, a situation that could not be satisfactorily explained by either model. The third model is GCM developed by Bohr and Mottelson [18]. The GCM, contrary to single particle ones, describes the motions exhibited by the nucleus as a whole, not considering the behavior of individual nucleons [19,20]. Nuclei can be viewed as incompressible, charged liquid drops, which vibrate and, if deformed, also rotate. In other words, the GCM describes certain properties of the nucleus in terms of its surface that, under the influence of a restoring force, can perform quadrupole (or, more generally, multipole) oscillations around an equilibrium ellipsoidal shape that can be spherical or deformed. To calculate the restoring force, we must know the potential energy landscape as a function of shape variables. This is a very complicated problem of quantum dynamics. However, in the liquid drop model, it can be relatively easily solved if we assume that the mass formula is valid not only for ground state binding energies but also in the process of deformation. If the deformation is small, the change of the surface energy should be described by the same surface tension as in the global surface energy. Any deviation from the spherical shape at fixed volume increases the surface area and surface energy. Thus, the surface tension always provides us with the restoring force. In contrast to the surface energy, the electrostatic repulsion prefers the deformation that would increase distances between the charge elements. In heavy nuclei, the gain of Coulomb energy becomes comparable with the loss of surface energy. Their balance defines the stability of the drop. Too heavy nuclei cannot be stable because of too strong Coulomb repulsion.

With these assumptions, the moving nuclear surface may be described by an expansion in spherical harmonics $Y_{\lambda,\mu}(\theta,\phi)$ with time-dependent shape parameters as coefficients [19,20]:

$$R(\theta,\phi,t) = R_0\left(1 + \sum_{\lambda=0}^{\infty}\sum_{\mu=-\lambda}^{\lambda} \alpha^*_{\lambda,\mu}(t) Y_{\lambda,\mu}(\theta,\phi)\right), \tag{4}$$

where $R(\theta,\phi,t)$ denotes the nuclear radius in the direction (θ,ϕ) at time t. If all coefficients $\alpha_{\lambda,\mu} = 0$ the nuclear surface becomes spherical with radius R_0. The coefficients, $\alpha_{\lambda,\mu}$, act as the collective coordinates of the nucleus, being the $Y_{\lambda,\mu}(\theta,\phi)$ the directional vectors. Plain sections through nuclear shapes with deformation of order $\lambda = 1,2,3,4$ are presented in figure 3.

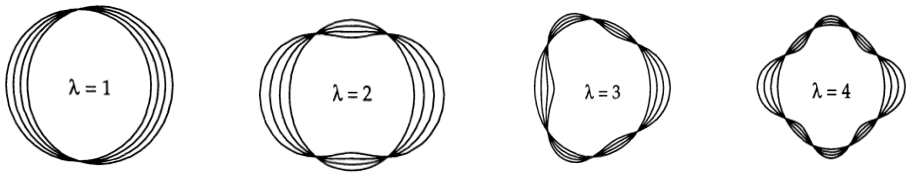

Figure 3. Illustration of the multipole deformations for $\lambda = 1,2,3,4$.

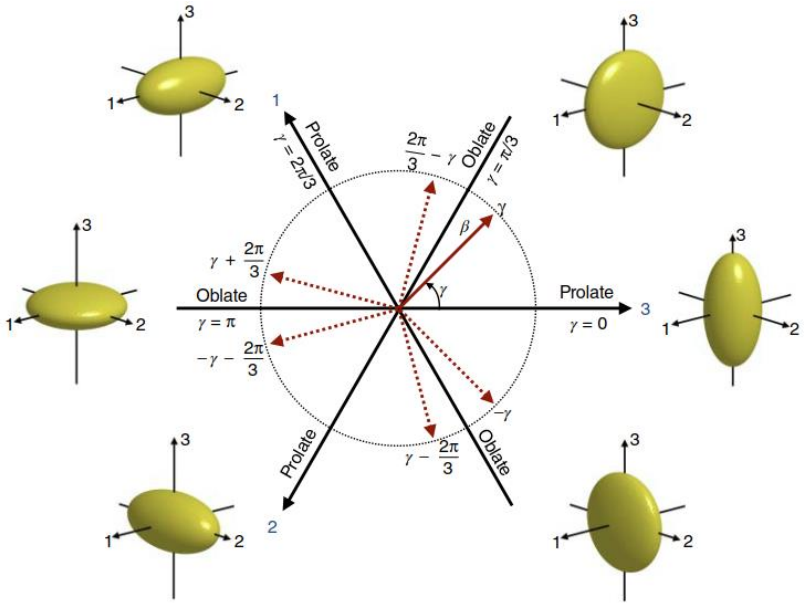

Figure 4. A polar diagram in the deformation plane (β, γ). Any quadrupole shape can be identified within a region $\beta \geq 0$ and $0 \leq \gamma \leq \pi / 3$; on a full polar plane, symmetry, transformations allow for six equivalent representations as illustrated. Values of γ multiples of 60 correspond to restoration of axial symmetry along axis whose number is indicated and direction points toward prolate shape; the shapes are illustrated.

Quadrupolar deformations, $\lambda = 2$, are the most important multipole deformations because the associated excitation modes are the most common collective excitations of the nucleus. Following A. Bohr, each shape is uniquely defined by five quadrupole shape variables: two, β and γ, that encode the extent of quadrupole deformation and the asymmetry in the intrinsic frame of reference and three Euler angles, that govern the orientation in space of the intrinsic ellipsoid with respect to a laboratory frame. This transcription is suitable for a clear visual interpretation: the parameter β controls the amplitude of the deformations and the "angle" γ is related to the direction where the deformation occurs. The angular dependence of the deformation parameters along all axes shows the same cosine behavior, except of the phase shift $2\pi k/3$, $k = 0,1,2$, figure 4.

In general, spherical nuclei are found around closed shells. This is easy to understand. The single-particle spectrum for nucleons is not uniform. Instead, the states are separated into groups, with energy differences between states within a group smaller than those between groups. This makes it more favorable for nucleons to fill up each group, or shells, before occupying those in the next one. A closed shell nucleus is formed when all the single-particle states in a group are fully occupied. When this condition is met, the total M-value, the projection of spin along the quantization axis, of the nuclear state is zero. Such an object is then invariant under a rotation of the coordinate system and must, therefore, be spherical in shape.

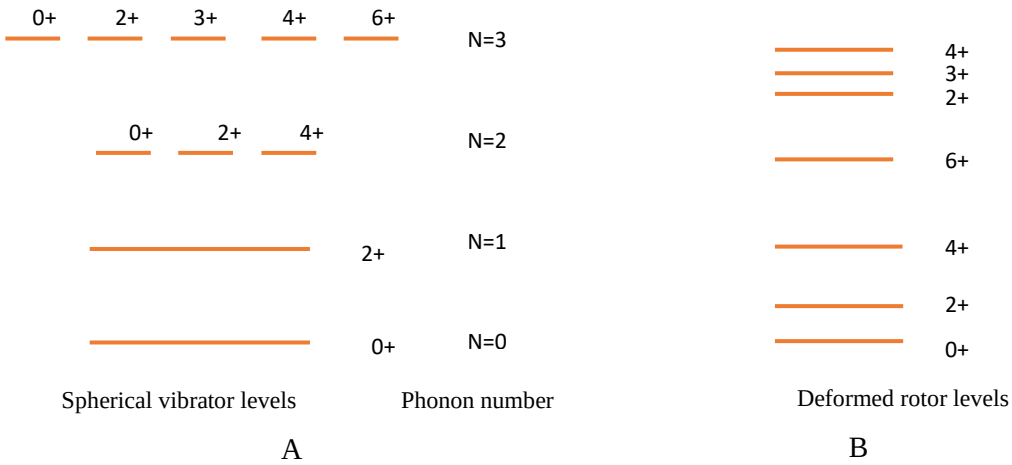

Figure 5. Panels A and B are the energy spectra of the spherical vibrator and the deformed rotor, respectively.

At the same time, the interplay between short-range nuclear force and long-range repulsive Coulomb force may well favor a non-spherical or deformed equilibrium shape. The deformed nuclei are classified into prolate, oblate and triaxial. Prolate and oblate nuclei are axially symmetric. If the third axis of the nucleus is longer than the others, the nucleus is prolate and if it is shorter, the nucleus is oblate. For triaxial nuclei, the three axes are different. In nature, prolate nuclei dominate over oblate ones. It is found that 86 % of the even-even nuclei are prolate in the ground state and triaxial shapes are very rare for them. The effect of Coulomb repulsion between protons is to deform the nucleus more into an elongated shape than to a flattened shape. The spin-orbit potential (coupling) between nucleons plays a role favoring stable prolate shape for nuclei. The shell structure of nuclei is also responsible for the variety of shapes, depending on the number of valance nucleons between the two closed shells. Prolate shape occurs just after closed shells and towards the end of closed shells, oblate shape is observed.

Quantum mechanically, there cannot be a rotational degree of freedom associated with a spherical object. For a sphere, the square of its wave function is, by definition, independent of angles; it appears to be the same from all directions. As a result, there is no way to distinguish the wave functions before and after a rotation. Rotation is therefore not a quantity that can be observed in this case and, consequently, cannot correspond to a degree of freedom in the system with energy associated with it. In contrast, rotational motion of a deformed object, such as an ellipsoid, may be detected, for example, by observing the changes in the orientation of the axis of symmetry with time. In the historical development of the GCM, it was supposed that the nucleus should vibrate and rotate as an irrotational liquid drop. In this model, the internal degrees of freedom of the nucleus are suppressed and the nucleus is regarded as a homogeneous fluid characterized only by a set of shape coordinates. However, in the two-fluid model the nucleus is represented as a rotationally invariant super fluid core that does not participate in the rotational motion, plus a deformed normal fluid that rotates bodily about it [19].

In the framework of GCM, a variety of models such as the anharmonic spherical vibrator, the deformed rotor-vibrator, or the γ-unstable rotor were derived. Figure 5, panel A, shows typical vibrational nuclei where the first excited state is a quadrupole phonon excitation of a basically spherical shape. At about twice and three times of this energy, there are groups of states that can be described as two- and three-phonon excitations of the basic spherical structure. Figure 5, panel B, shows typical even-even deformed nuclei. The lowest levels of spin $J = 0, 2, 4, 6, \ldots$ form a rotational structure whose energies closely follow the $J(J+1)$ law for a rotating symmetric top. Above these are groups of levels.

On the other hand, since the birth of quantum mechanics, symmetry has acquired a central role in all branches of physics, and group theory provides the mathematical tool to formulate symmetry principles. Historically, symmetries have played an important role in nuclear physics. Examples are Wigner's spin–isospin $\mathfrak{su}(4)$ symmetry [21], Elliott's rotational $\mathfrak{su}(3)$ [22,23], Racah's pairing $\mathfrak{su}(2)$ [24,25] and its extension to proton–neutron pairing with $j-j$ coupling giving $\mathfrak{so}(5)$ [26,27], Hecht and Arima's pseudospin [28,29], and Rowe's $Sp(3,R)$ [30]. Modern developments in symmetry are putting more emphasis on the concept of dynamical symmetry (DS). The DS is a type of symmetry in which the Hamiltonian is expanded in elements of a Lie algebra, (G_0), called the spectrum generating algebra (SGA) [31,32]. The DS occurs if the Hamiltonian can be written in terms of the Casimir operators (COs) of a chain of nested algebras, $G_0 \supset G_1 \supset \cdots \supset G_n$. The main advantage of DS is that, whenever one such symmetry occurs, the following properties are then observed. (i) Analytic expressions are available for physical observables. (ii) All states are classified by quantum numbers $\lambda_0, \lambda_1, \ldots, \lambda_n$ which are the labels of the irreducible representations of the subalgebras in SGA.

The notable application of DS and SGA in nuclear physics is the study of collective states for even-even nuclei using the IBM. In its simplest form, Arima and Iachello assumed that an even-even nucleus consists of an inert core plus some valence particles. Furthermore, they assume that the valence particles, which are those outside the major closed shells at 50, 82, 126, tend to pair together in states with angular momentum $l = 0$ and 2, and treat these pairs as bosons [33-38]. The identical bosons with angular momentum l are referred to as the l- bosons. Hence, the nucleus is described in terms of interacting s- ($l = 0$) and d- ($l = 2$) bosons. The SGA of the IBM is the unitary algebra $\mathfrak{u}(6)$. The IBM is a model for collective behavior. It has become customary to refer to collective models of the Bohr-Mottelson type as "geometric" models and those of the IBM or other group theory-based approaches as "algebraic" models. The IBM quickly became a popular model for the interpretation of nuclear data and acquired the center stage of discussions within the nuclear-structure community. One of its strengths is that it offers a unified view of several descriptions which existed separately. The IBM includes the three descriptions (anharmonic spherical vibrator, the deformed rotor-vibrator, or the γ-unstable rotor) as special cases of its Hamiltonian. Not only do such cases turn out to be analytically solvable using DSs but, in addition, one may easily interpolate in the IBM between the different geometric solutions.

An appropriate formalism to describe the IBM is provided by second quantization. The most general Hamiltonian of the sd-boson model with one- and two-body rotationally invariant interactions is written as [38]

$$\begin{aligned} H = E_0 + \varepsilon_s\left(s^\dagger \cdot \tilde{s}\right) + \varepsilon_d\left(d^\dagger \cdot \tilde{d}\right) + \sum_{L=0,2,4} \frac{1}{2}(2L+1)\, c_L \left[\left[d^\dagger \otimes d^\dagger\right]_L \otimes \left[\tilde{d} \otimes \tilde{d}\right]_L\right]_0 \\ + \frac{1}{\sqrt{2}} v_2 \left[\left[d^\dagger \otimes d^\dagger\right]_2 \otimes \left[\tilde{d} \otimes \tilde{s}\right]_2 + \left[d^\dagger \otimes s^\dagger\right]_2 \otimes \left[\tilde{d} \otimes \tilde{d}\right]_2\right]_0 \\ + \frac{1}{2} v_0 \left[\left[d^\dagger \otimes d^\dagger\right]_0 \otimes [\tilde{s} \otimes \tilde{s}]_0 + \left[s^\dagger \otimes s^\dagger\right]_0 \otimes \left[\tilde{d} \otimes \tilde{d}\right]_0\right]_0 \\ + u_2 \left[\left[d^\dagger \otimes s^\dagger\right]_2 \otimes \left[\tilde{d} \otimes \tilde{s}\right]_2\right]_0 + \frac{1}{2} u_0 \left[\left[s^\dagger \otimes s^\dagger\right]_0 \otimes [\tilde{s} \otimes \tilde{s}]_0\right]_0, \end{aligned} \tag{5}$$

where, as usual, ($s^\dagger$, $d^\dagger$) and ($\tilde{s} = s$, $\tilde{d}_m = (-1)^m d_{-m}$) are denoted to the s and d creation and modified annihilation operators, respectively. The tensor product $[A_a \otimes B_b]_e$ of two spherical tensors A_a and B_b is defined as the tensor of rank e whose components $[A_a \otimes B_b]_{e\epsilon}$ can be expressed in terms of $A_{a\alpha}$ and $B_{b\beta}$ according to $[A_a \otimes B_b]_{e\epsilon} = \sum_{\alpha\beta} C^{e\epsilon}_{a\alpha b\beta} A_{a\alpha} B_{b\beta}$, where $C^{e\epsilon}_{a\alpha b\beta}$ are the Clebsch-Gordan coefficients [39]. The matrix elements of the boson interaction are treated in IBM as parameters.

There are thus two one-body terms, specified by the parameters ε_s, ε_d, and seven two body terms, specified by the parameters c_L $(L = 0,2,4)$, v_L $(L = 0,2)$ and u_L $(L = 0,2)$. Moreover, the multipole form of the Hamiltonian in the sd-boson space is

$$H = \epsilon n_d + \kappa Q \cdot Q + \acute{\kappa} L \cdot L + q_3 T_3 \cdot T_3 + q_4 T_4 \cdot T_4, \tag{6}$$

where n_d, Q, L, T_3 and T_4 terms are the d-boson number operator, the quadrupole operator, the angular momentum operator and the octupole and hexadecapole operators, respectively, and they are defined in terms of s and d bosons as; $n_d = \sqrt{5}\left[d^{\dagger}\otimes\tilde{d}\right]_0^{(0)}$, $Q = \left[d^{\dagger}\otimes\tilde{s} + s^{\dagger}\otimes\tilde{d}\right]^{(2)} + \chi\left[d^{\dagger}\otimes\tilde{d}\right]^{(2)}$, $L = \sqrt{10}\left[d^{\dagger}\otimes\tilde{d}\right]^{(1)}$, $T_3 = \left[d^{\dagger}\otimes\tilde{d}\right]^{(3)}$, $T_4 = \left[d^{\dagger}\otimes\tilde{d}\right]^{(4)}$.

One of the most interesting aspects of the IBM is that of having suggested the occurrence of three types of DSs

I	$\mathfrak{u}(6) \supset \mathfrak{u}(5) \supset \mathfrak{o}(5) \supset \mathfrak{o}(3)$,	anharmonic spherical vibrator,	(7.a)
II	$\mathfrak{u}(6) \supset \mathfrak{su}(3) \supset \mathfrak{o}(3)$,	Axially deformed rotovibrator,	(7.b)
III	$\mathfrak{u}(6) \supset \mathfrak{o}(6) \supset \mathfrak{o}(5) \supset \mathfrak{o}(3)$,	γ–unstable deformed rotovibrator.	(7.c)

The Hamiltonians corresponding to these group chains are

$$H^{I} = e_0 + e_1 C_1[\mathfrak{u}(6)] + e_2 C_2[\mathfrak{u}(6)] + \varepsilon C_1[\mathfrak{u}(5)] + \alpha C_2[\mathfrak{u}(5)] + \rho C_2[\mathfrak{o}(5)] + \omega C_2[\mathfrak{o}(3)], \tag{8.a}$$
$$H^{II} = e_0 + e_1 C_1[\mathfrak{u}(6)] + e_2 C_2[\mathfrak{u}(6)] + \delta C_2[\mathfrak{su}(3)] + \omega C_2[\mathfrak{o}(3)], \tag{8.b}$$
$$H^{III} = e_0 + e_1 C_1[\mathfrak{u}(6)] + e_2 C_2[\mathfrak{u}(6)] + \eta C_2[\mathfrak{o}(6)] + \rho C_2[\mathfrak{o}(5)] + \omega C_2[\mathfrak{o}(3)]. \tag{8.c}$$

where $C_1[G]$ and $C_2[G]$ are the linear and quadratic COs of the algebra G. The irreducible representations corresponding to these group chains which label the states of a nucleus are

$$\left|\begin{array}{cccccccc} \mathfrak{u}(6) & \supset & \mathfrak{u}(5) & \supset & \mathfrak{o}(5) & \supset & \mathfrak{o}(3) & \supset \mathfrak{o}(2) \\ \downarrow & & \downarrow & & \downarrow & & \downarrow & \downarrow \\ [N] & & n_d & & \nu & n_{\triangle} & L & M \end{array}\right\rangle, \tag{9.a}$$

$$\left|\begin{array}{cccccc} \mathfrak{u}(6) & \supset & \mathfrak{su}(3) & \supset & \mathfrak{o}(3) & \supset \mathfrak{o}(2) \\ \downarrow & & \downarrow & & \downarrow & \downarrow \\ [N] & & (\lambda,\mu) & K & L & M \end{array}\right\rangle, \tag{9.b}$$

$$\left|\begin{array}{cccccccc} \mathfrak{u}(6) & \supset & \mathfrak{o}(6) & \supset & \mathfrak{o}(5) & \supset & \mathfrak{o}(3) & \supset \mathfrak{o}(2) \\ \downarrow & & \downarrow & & \downarrow & & \downarrow & \downarrow \\ [N] & & \sigma & & \tau & \nu_{\triangle} & L & M \end{array}\right\rangle. \tag{9.c}$$

According to the spectrum generation principle and the branch rules of the irreducible representations of the groups which label the states of a nucleus, we have the energy spectrum of the states in each of the symmetries as:

$$E^{I}(N, n_d, \nu, n_{\triangle}, L, M) = E_0 + \varepsilon n_d + \alpha n_d(n_d + 4) + 2\rho\nu(\nu + 3) + 2\omega L(L + 1), \tag{10.a}$$
$$E^{II}(N, (\lambda,\mu), K, L, M) = E_0 + \frac{2}{3}\delta(\lambda^2 + \mu^2 + \lambda\mu + 3\lambda + 3\mu) + 2\omega L(L + 1), \tag{10.b}$$
$$E^{III}(N, \sigma, \tau, \nu_{\triangle}, L, M) = E_0 + 2\eta\sigma(\sigma + 4) + 2\rho\tau(\tau + 3) + 2\omega L(L + 1), \tag{10.c}$$

where $E_0 = e_0 + e_1 N + e_2 N(N+5)$. This term contributes only to binding energies and not to excitation energies.

The $\mathfrak{u}(6) \supset \mathfrak{u}(5)$ reduction rule takes the form $n_d = N, N-1, \ldots, 0$. The reduction $\mathfrak{u}(5) \supset \mathfrak{o}(5)$ is given by $v = n_d, n_d - 2, \ldots, 1 \text{ or } 0$ (n_d odd or even). There is the following algorithm for the reduction $\mathfrak{o}(5) \supset \mathfrak{o}(3)$. First, partition n_d as $n_d = 2n_\beta + 3n_\triangle + \lambda$ where $n_\beta = (n_d - v)/2$: $n_\beta = 0,1, \ldots, n_d/2$ or $(n_d-1)/2$ and $n_\triangle = 0,1,2, \ldots$. The allowed angular momenta are $L = \lambda, \lambda+1, \ldots, 2\lambda-2, 2\lambda$. Note that $2\lambda - 1$ is missing and $L = 1$ will never occur. A typical $\mathfrak{u}(5)$ DS spectrum exhibits n_d-multiplets of a spherical vibrator, with a two-phonon (n_d = 2) triplet of states (L = 4, 2, 0) at an energy $E(n_d = 2) \approx 2E(n_d = 1)$ above the ground state (n_d = L = 0), and a three-phonon (n_d =3) quintuplet of states (L= 6, 4, 3, 2, 0) at $E(n_d = 3) \approx 3E(n_d = 1)$. The spectrum of states corresponding to (10.a) is shown in figure 6.

The $\mathfrak{u}(6) \supset \mathfrak{su}(3)$ reduction rule takes the form $(\lambda, \mu) = (2N, 0) \oplus (2N-4, 2) \oplus (2N-8, 4) \oplus \ldots \oplus \{(0, N), (2, N-1)\}\{N = \text{even or } N = \text{odd}\} \oplus \ldots$. There is the following algorithm for the reduction $\mathfrak{su}(3) \supset \mathfrak{o}(3)$. If $K \neq 0$, where $K = \text{integer} = \min\{\lambda, \mu\}, \min\{\lambda, \mu\} - 2, \ldots, 1 \text{ or } 0$, ($\min\{\lambda, \mu\} = $ odd or even). The allowed angular momenta are $L = K, K+1, K+2 \ldots, K + \max\{\lambda, \mu\}$. However, in the case of $K = 0$, the allowed angular momenta are $L = \max\{\lambda, \mu\}, \max\{\lambda, \mu\} - 2, \ldots, 1 \text{ or } 0$, ($\max\{\lambda, \mu\} = $ odd or even). In the $\mathfrak{su}(3)$ symmetry scheme the "ground" band appears as the representation $(\lambda, \mu) = (2N, 0)$, while the "β" and "γ" bands appear as the representation $(\lambda, \mu) = (2N-4, 2)$ with $K = 0$ and $K = 2$. Because the $\mathfrak{su}(3)$ eigenvalues, (10. b), do not depend on K, states of the "β " and "γ " bands of identical angular momentum (L = 0,2,4,…) are degenerate in $\mathfrak{su}(3)$. The spectrum of states corresponding to (10.b) is shown in figure 6.

The $\mathfrak{u}(6) \supset \mathfrak{o}(6)$ reduction rule takes the form $\sigma = N, N-2, \ldots, 1 \text{ or } 0$, ($N$ = odd or even). The reduction $\mathfrak{o}(6) \supset \mathfrak{o}(5)$ is given by $\tau = \sigma, \sigma - 1, \ldots, 1, 0$. There is the following algorithm for the reduction $\mathfrak{o}(5) \supset \mathfrak{o}(3)$. First, partition τ as $\tau = 3v_\triangle + \lambda$ and $v_\triangle$ =0, 1, 2 …. The allowed angular momenta are $L = \lambda, \lambda+1, \ldots, 2\lambda-2, 2\lambda$. It is easy to see that the ground state and the lowest-energy states have an $\mathfrak{o}(6)$ quantum number $\sigma = N$ and $\mathfrak{o}(5)$ symmetry. The $\mathfrak{o}(6)$ symmetry then predicts a repetition of structural patterns with $\mathfrak{o}(5)$ symmetry at higher excitation energies and $\mathfrak{o}(6)$ quantum number $\sigma = N-2, N-4$, etc. The spectrum of states corresponding to (10.c) is shown in figure 6.

The eigenvalue problem for Hamiltonian H can be solved in closed form when H can be written in terms only of COs of chain of groups $G \supset \acute{G} \supset \cdots$. Most nuclei are not in this ideal situation and thus one needs to treat the full Hamiltonian H. After that of the DSs in which all properties can be calculated analytically, the next situation, in order of complexity, arises when the Hamiltonian can be written in terms of operators of two chains. One can schematically depict the situation as in figure 7, called Casten triangle. The three limits, DSs, are placed at the vertices of the triangle. Situations in which H contains only COs of the two chains are placed along the sides of the triangle, and situations in which COs of all chains appear are placed inside the triangle. One can thus divide nuclei into four transitional classes. Class A, nuclei with properties intermediate between I and II; Class B, nuclei with properties intermediate between II and III; Class C, nuclei with properties intermediate between III and I; and Class D, nuclei with properties intermediate between all three limits.

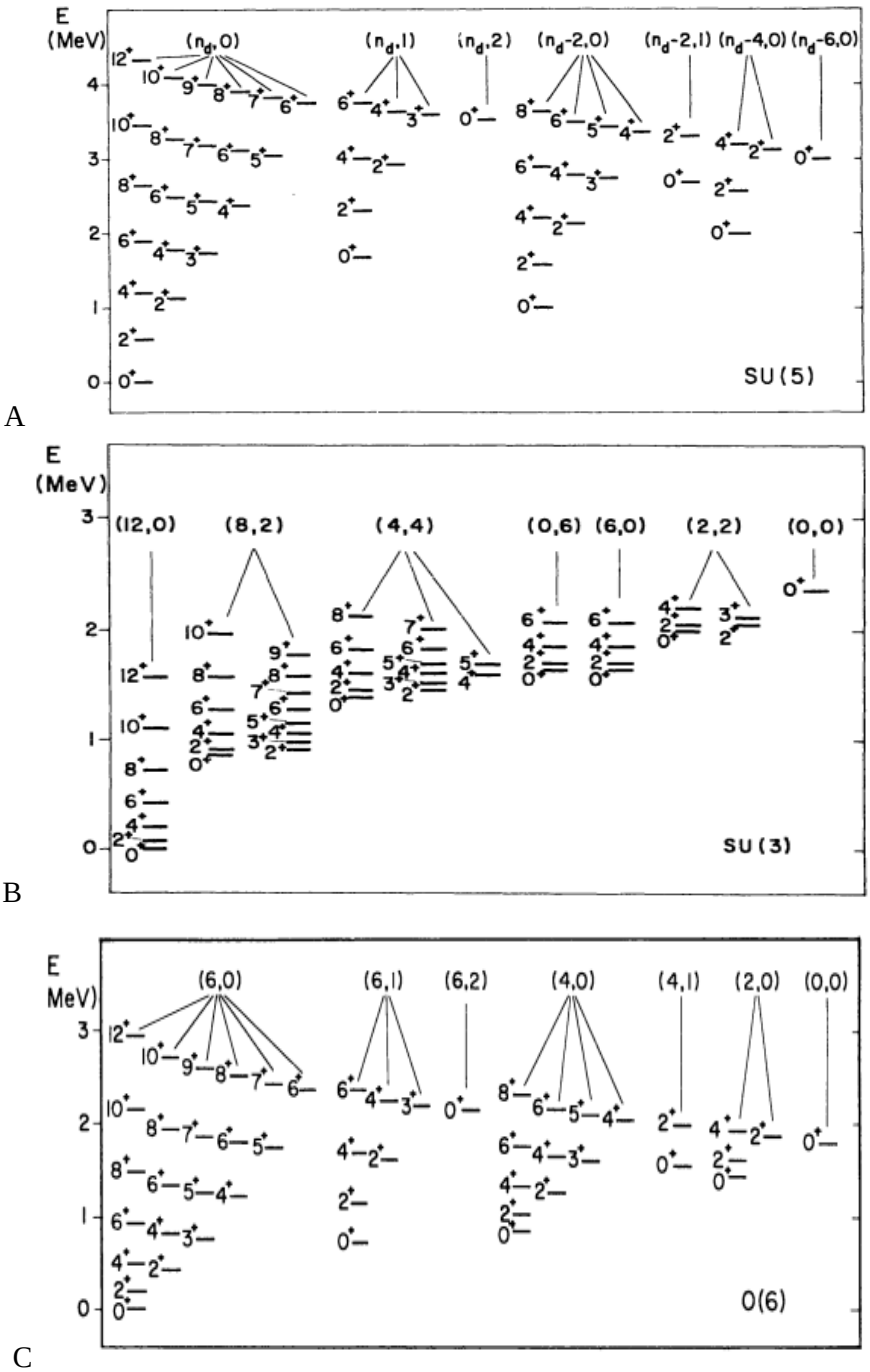

Figure 6. Panels A, B, and C represent spectra with $\mathfrak{u}(5)$, $\mathfrak{su}(3)$, and $\mathfrak{o}(6)$ DSs, respectively, and $N = 6$. The angular momentum L of each state is shown to the left.

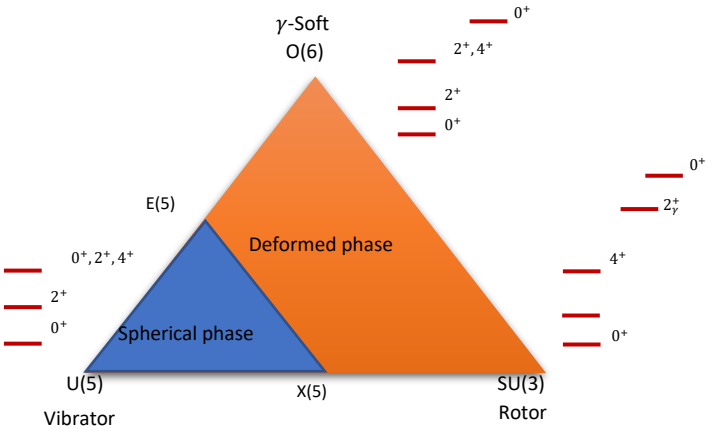

Figure 7. Representation of the IBM phase diagram as a Casten triangle. The three DSs are located in the vertices. Critical points E(5) (second order) and X(5) (first order).

Many extensions of IBM are developed to cover many situations. One remarkable extension is g-IBM in which the next even angular momentum is considered hence to include a g- ($l = 4$) boson [40-45]. The $\mathfrak{u}(15)$ is the SGA of the g-IBM. In addition to those mentioned above, more important versions of the IBM consist of additional angular momenta (p, f with $l = 1, 3$, respectively) together with the s and d boson. In the extensions of IBM, the bosons with p, f and g angular momentum are useful mostly as supplements of dipole and octupole degrees of freedom, which are generated by the system of the s and d bosons [46-48]. Over the last few years, more attention has been paid to the development of the IBM in a more general form. The two-level boson model, or s-a boson model, is described in terms of interacting s- and a- boson where a is the positive integer angular momentum [49,50]. The SGA of the s-a IBM is $\mathfrak{u}(n_a + 1)$, where $n_a = 2a + 1$ [51,52]. The generic three-level boson model or s-ab boson model can be defined in terms of the s, a and b- bosons [53]. The SGA of the s-ab IBM is $\mathfrak{u}(n_a + n_b + 1)$, where $n_a = 2a + 1$ and $n_b = 2b + 1$. Two versions of IBM in this class include the $\mathfrak{u}(15)$ sdg-IBM and the $\mathfrak{u}(9)$ spd-IBM. Clearly, such an algebraic approach is preferable not only because it gives the opportunity to expand the model to other cases without having to develop a completely new model, but also because it provides the analytical expressions of physical observations.

Since the beginning of the discussion of magnetic properties of collective even-even nuclei in the IBM the proton-neutron version (IBM-2) [54-61] has become increasingly important. Even-even nuclei are modeled in the IBM-2 as a system of proton (π) and neutron (ν) bosons that interact via two-body forces. The charge character of the bosons can be introduced in two different ways: 1- One considers two distinct systems for proton and neutron bosons and treats them exactly as in the IBM-1. 2- One considers the boson charge states as the components of a two-valued state vector and labels them with the quantum number called F -spin, $|F = 1/2, M_F = 1/2\rangle = |N_\pi\rangle$ and $|F = 1/2, M_F = -1/2\rangle = |N_\nu\rangle$, where N_π and N_ν are the numbers of proton and neutron bosons, respectively. Wave functions with good F-spin can be eigenstates of Hamiltonians that commute with the quadratic F-spin operator, $[H, F^2] = 0$. The SGA of IBM-2 is $\mathfrak{u}(12)$ as a single boson carries 12 degrees of freedom (6 from s and d and two from π and ν). Then there are the well-known $\mathfrak{u}(6)\otimes\mathfrak{su}^F(2)$ with the $\mathfrak{su}^F(2)$ algebra generating F spin and the $\mathfrak{u}^\pi(6)\otimes\mathfrak{u}^\nu(6)$ symmetry limits in this model.

In the interacting boson-fermion model (IBFM) odd-even nuclei are treated by coupling the single particle (fermion) degrees of freedom of the odd nucleon to the collective (boson) degrees of freedom of the even-even core nucleus. The structure of many odd-even nuclei has been successfully

described in the framework of the IBFM, both in the IBFM-1 version where the IBM-1 core is built from one type of bosons, and in the IBFM-2 version where the IBM-2 core is based on the concept of two types of bosons: proton bosons and neutron bosons. For odd-odd nuclei only interacting boson-fermion-fermion model IBFFM-1, the version with one type of bosons, was extensively used. On the other hand, there have not been so many calculations in the proton-neutron interacting boson-fermion-fermion model (IBFFM-2). The IBFFM-2, where proton, neutron, proton boson, and neutron boson degrees of freedom are present, gives the rare opportunity to analyses the full scale of boson-fermion interactions. Consequently, the concept of symmetry has been extended with the introduction of supersymmetries. The generators of supersymmetry transformations form a graded Lie algebra whose even subalgebra is an ordinary Lie algebra while the odd generators, which mix bosons and fermions, close under anti-commutation. The best studied examples of these supersymmetries are $\mathfrak{u}(6/4)$, $\mathfrak{u}(6/12)$ and $\mathfrak{u}(6/20)$ graded Lie algebras in which the rotation group, $so(3)$, is embedded [62-72].

On the other hand, quantum algebras (QAs) are deformed versions of the Lie algebras, to which they are reduced when the deformation parameter q is set equal to unity. The growing interest in the QAs is related to the correspondence of the properties of QAs and those of Lie algebras regarding the representation theory and their numerous physical applications. QAs have now become a significant and widely used concept in nuclear and molecular physics [73-77]. The QA $\mathfrak{su}_q(2)$, in particular, has been used for the description of rotational bands in the deformed and super-deformed nuclei. Deformed versions of the $\mathfrak{v}(6)$ and $\mathfrak{u}(5)$ DSs of the IBM have been discussed in Ref [78]. Recently [79], the q-deformed Hamiltonian for the $\mathfrak{sv}(6)$-$\mathfrak{u}(5)$ transitional case in IBM is constructed by using affine $\mathfrak{su}_q(1,1)$ Lie algebra in the both IBM-1 and 2 versions and IBFM. In addition, a deformed version of sdl- and $sdll'$ -boson models are produced (where l and l' are any two angular momenta) [80]. It is important to note that, the quantum algebraic treatment extends the applicability of the analytical solutions and it works in the near neighborhood of the exact DS. Thus, an equivalent of a large numerical problem is obtained in terms of a simple analytical expression [81-84].

A geometric shape visualization of the even-even nuclei is made by plotting the potential energy surface (PES), denoted by $E(N,\beta,\gamma)$, in the (β,γ) plane. Based on the coherent state formalism and making use of results and an algorithm developed by Gilmore and Feng, [85-87] a technique for going from an IBM Hamiltonian to a PES in the variables β and γ, has been outlined in Ref. [88]. The $E(N,\beta,\gamma)$ can be obtained by calculating the expectation value of the Hamiltonian (5) in the coherent state and is given in the following form

$$E(N,\beta,\gamma)=\frac{N}{\beta^2+1}(\varepsilon_s+\varepsilon_d\beta^2)+\frac{N(N-1)}{(\beta^2+1)^2}\left\{x_1\beta^4+x_2\beta^3\cos 3\gamma+x_3\beta^2+\frac{1}{2}u_0\right\}, \tag{11}$$

with

$$x_1=\frac{1}{10}c_0+\frac{1}{7}c_2+\frac{9}{35}c_4\,, \tag{12.a}$$

$$x_2=-2\sqrt{\frac{1}{35}}v_2, \tag{12.b}$$

$$x_3=\sqrt{\frac{1}{5}}(v_0+u_2), \tag{12.c}$$

where N is number of bosons, β, γ are deformation parameters (usually, $\beta\geq 0$, $0\leq\gamma\leq 60$) and other terms are the same as in the Hamiltonian (5). Equation (11) can be used to analyze the shape structure of the three DSs.

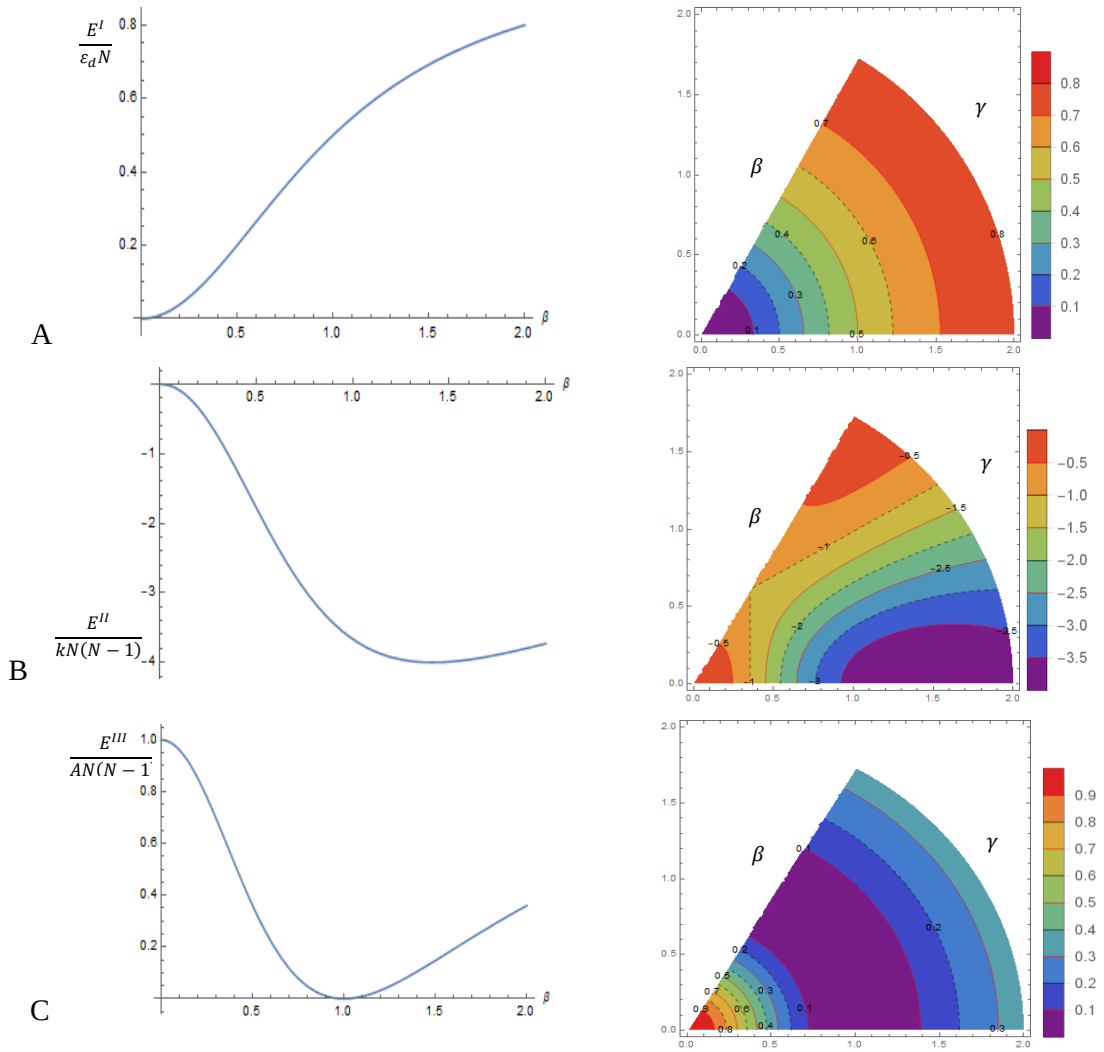

Figure 8. Panel A represents the PES E^I as a function of β ($E_0 = 0, x_1 = 0$) and β-γ plot. Panel B illustrates the PES E^{II} as a function of β ($\gamma = 0, \acute{k} = \frac{3}{4}k, E_0 = 10kN$) and the corresponding β-γ plot. Panel C r explains the PES E^{III} in the case $B = C = 0, E_0 = 0$ and the corresponding β-γ plot.

We have

$$E^I(N,\beta,\gamma) = E_0 + \varepsilon_d N\frac{\beta^2}{\beta^2+1} + x_1 N(N-1)\frac{\beta^4}{(\beta^2+1)^2}, \tag{13.a}$$

$$E^{II}(N,\beta,\gamma) = E_0 - 2k\left[\frac{N}{\beta^2+1}\left(5+\frac{11}{4}\beta^2\right) + \frac{N(N-1)}{(\beta^2+1)^2}\left(\frac{\beta^4}{2} + 2\sqrt{2}\beta^3\cos 3\gamma + 4\beta^2\right)\right] - \acute{k}\frac{6N\beta^2}{(\beta^2+1)}, \tag{13.b}$$

$$E^{III}(N,\beta,\gamma) = E_0 + (2B+6C)\frac{N\beta^2}{\beta^2+1} + \frac{A}{4}N(N-1)\left(\frac{1-\beta^2}{1+\beta^2}\right)^2. \tag{13.c}$$

where $k = -\frac{2}{3}\delta$, $\acute{k} = -\frac{1}{2}\delta - 2\omega$, $A = -8\eta$, $B = 12\rho$ and $C = 2\omega$. From (13), we know that E^I and E^{III} are γ independent. Figure 8 represents PES, E^I, E^{II}, and E^{III} as a function of β.

The concept of QSPT refers to the sudden change of the atomic nucleus ground state structure as a function of a control parameter. Such control parameter can be, e.g., the neutron number and, therefore, a QSPT can appear in an isotopic chain where the ground state deformation varies in an abrupt way when passing from an isotope to its neighbor. The QSPT have been the subject of numerous theoretical and experimental studies and present a rapidly growing field of research. Theoretical analyses have typically been based on algebraic models of nuclear structure or phenomenological geometric models of nuclear shapes and potentials, but more recently several attempts have been made towards a fully microscopic description of QSPT starting from nucleonic degrees of freedom [88-92]. Generally, the form of the Hamiltonian used to describe the QSPT from phase A to phase B is often built as

$$H_\lambda = (1-\lambda)H_A + \lambda H_B, \quad \lambda \in [0,1]. \tag{14}$$

The terms H_A and H_B with $[H_A, H_B] \neq 0$ represent two modes of motion- suppose that they are classified by two different DSs and H_λ is intermediate between them for $\lambda \in [0,1]$. The parameter λ controls the transition between both DSs. The onset of a QSPT is denoted by the existence of a critical value of the control parameter, λ, for which the structure of the system passes from one phase with symmetry A to another phase with symmetry B.

The simple consistent-Q formalism can be used for characterizing all situations of transitional patterns in the IBM-1 if only one- and two-body interactions are taken into consideration. The consistent-Q Hamiltonian [93-98] can be written as:

$$H = \alpha\left(\eta N_d + \frac{\eta-1}{N} Q^\chi(\zeta)\cdot Q^\chi(\zeta)\right), \tag{15}$$

with $Q^\chi = \left[d^\dagger \otimes \tilde{s} + s^\dagger \otimes \tilde{d}\right]^{(2)} + \chi\left[d^\dagger \otimes \tilde{d}\right]^{(2)}$. Here η and χ play the role of the control parameters and α is an overall energy scaling factor. N is the number of bosons and equals half the number of valence nucleons. The parameter η governs the transition between spherical and deformed, and χ the transition between prolate and oblate deformation. The Hamiltonian, (15), contains the three DSs of the IBM: $\mathfrak{u}(5)$ when $\eta = 1$, $\mathfrak{o}(6)$ when $\eta = 0$ and $\chi = 0$ and $\mathfrak{su}(3)$ when $\eta = 0$ and $\chi = -\sqrt{7}/2$ as well as the $\overline{\mathfrak{su}(3)}$ limit when $\eta = 0$ and $\chi = +\sqrt{7}/2$.

Various nuclear QSPT can be explored within the transitional patterns among different symmetries in the IBM. For example, the QSPT from spherical to axially deformed shape is characterized as the $\mathfrak{u}(5)$- $\mathfrak{su}(3)$ transition; the QSPT from spherical to the γ-soft motion is described by the $\mathfrak{u}(5)$- $\mathfrak{o}(6)$ transition; and the QSPT from prolate to oblate shape is often described by the $\mathfrak{su}(3)$-$\mathfrak{o}(6)$-$\overline{\mathfrak{su}(3)}$ transition, in which the prolate and oblate phase are described by the $\mathfrak{su}(3)$ and $\overline{\mathfrak{su}(3)}$ symmetry limit respectively, and the $\mathfrak{o}(6)$ symmetry limit emerges exactly at the critical point since the traditional Hamiltonian is designed to pass the $\mathfrak{o}(6)$ limit via a nonlinear dependence on the control parameter. The extended Casten triangle maps also the QSPTs which occurs inside the triangle. They are the first order transition between oblate and prolate shapes occurring on the $\mathfrak{o}(6)$-$\mathfrak{u}(5)$ axis to the point where the nucleus changes from spherical to deformed. From there on the first order transition between spherical and deformed goes outwards to the legs. The central point itself represents the second order transition and can be seen as the triple point of nuclear deformation where spherical, prolate and oblate deformation coexist. Figure 9 illustrates the obtained phase diagram and indicates the position of the first and second order QSPTs. The two key differences between first- and second-order QSPTs are that, in a first-order QSPT, the

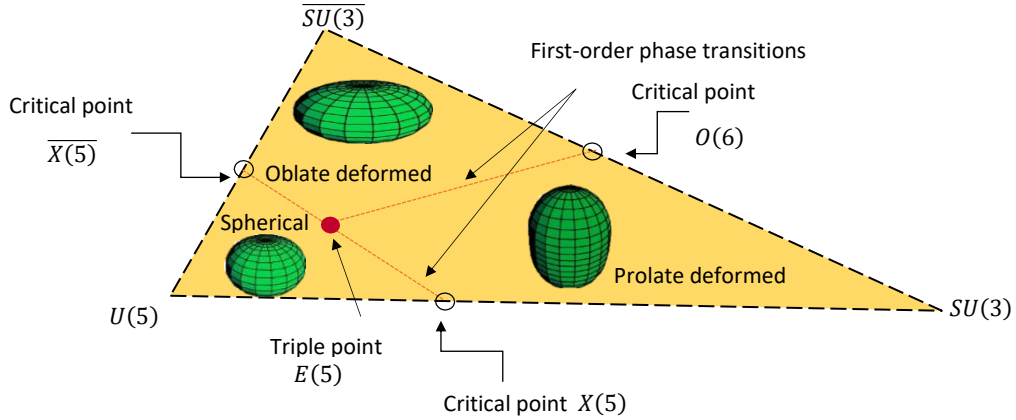

Figure 9. The extended Casten triangle. Dashed lines indicate the first order QSPTs and the filled dot the isolated second order transition. The open circles indicate the location of the different DSs. The three different phases are spherical (I), prolate deformed (II) and oblate deformed (III).

order parameter (the quadrupole deformation) changes discontinuously at the phase transition and there is a coexistence of spherical and deformed phases. In a second-order QSPT, the deformation grows continuously and there is only a single phase.

Furthermore, there are several extensions of QSPT to sdg-IBM [99], proton–neutron IBM [100-103], and excited state QSPT [104]. More interestingly, QSPT are also studied in odd-A nuclei within the IBFM model [105-108].

Besides QSPTs atomic nuclei might also exhibit shape coexistence. Shape coexistence in nuclear physics was first proposed by Morinaga in the 1950's and since then it has given rise to a property of atomic nuclei that appears throughout the entire nuclear landscape, especially to those nuclei at or near shell or sub-shell closures [109]. Shape coexistence presents certain distinct experimental features: a U shape in the energy systematics of certain excited bands, lowering of certain excited 0+ states, a rapid change in the value of spectroscopic quadrupole moments, and the existence of strong E0 transitions. All of them are enhanced and present an almost symmetric behavior with respect to the corresponding mid-shell. Shape coexistence can be understood in terms of two major theoretical approaches, namely the spherical NSM and the mean field. The appearance of intruder configurations reflects the competition between the energy gap, that tends to maintain spherical shapes, and the residual interaction, that favors the deformation of the nucleus and lower, in some cases considerably, the excitation energy of the intruder states [109].

With QSPT, from the point of view of experiments, an important question arises: is it possible to obtain analytical predictions for observables at the phase transition point, i.e., are there solvable models or symmetries that describe the structure at the phase transition point? The introduction of CPSs concept, describing nuclei at points of QSPT between different limiting symmetries, was originally suggested by Iachello [110,111]. It is still one of the hot topics in nuclear structure physics [112-149]. A much development, in this direction, has been mainly accomplished by both phenomenological models: the GCM as well as the IBM. The CPS of the QSPT between the $\mathfrak{u}(5)$ and $\mathfrak{v}(6)$ DSs defines the $E(5)$ symmetry and it was experimentally identified for the first time in ^{134}Ba. It has been found that there are many nuclei in the transitional region with the $E(5)$ CPS, such as ^{102}Pd, ^{104}Ru, ^{106}Mo, ^{106}Cd, ^{108}Cd, ^{124}Te and ^{128}Xe [114-126]. The critical-point description of the transition from a deformed rotor to a spherically vibrator, denoted as $X(5)$, is located on the $\mathfrak{u}(5)$-$\mathfrak{su}(3)$ leg of the Casten's triangle and it was experimentally identified for the first time in the ^{152}Sm nucleus. There are many nuclei in the transitional region with the $X(5)$ CPS, such as ^{150}Nd, ^{154}Gd, ^{156}Dy [127-136].

All these CPSs have been constructed by considering the original Bohr equation, separating the collective β and γ variables, and making different assumptions about the $u(\beta)$ and $u(\gamma)$ potentials involved ($V(\beta,\gamma) = u(\beta) + u(\gamma)$). The original Bohr Hamiltonian is written as

$$H = -\frac{\hbar^2}{2B}\left\{\frac{1}{\beta^4}\frac{\partial}{\partial\beta}\beta^4\frac{\partial}{\partial\beta} + \frac{1}{\beta^2}\left(\frac{1}{\sin 3\gamma}\frac{\partial}{\partial\gamma}\sin 3\gamma\frac{\partial}{\partial\gamma} - \frac{1}{4}\sum_k \frac{\acute{L}_k^2}{\sin^2\left(\gamma - \frac{2}{3}k\pi\right)}\right)\right\} + V(\beta,\gamma) \qquad (16)$$

where β and γ are the deformation variables, B is the collective mass parameter, and $\acute{L}_k$ $(k = 1,2,3)$ are the projections of the angular momentum on the body-fixed k-axis. In the $E(5)$ case the potential is supposed to depend only on the collective variable β and not on γ. Then exact separation of variables is achieved and the equation containing β can be solved exactly for an infinite square well potential in β, the eigenfunctions being Bessel functions of the first kind. In the $X(5)$ case the potential is supposed to be of the form $u(\beta) + u(\gamma)$. Then approximate separation of variables is achieved in the special case of $\gamma \simeq 0$, the β-equation with an infinite square well potential leading to Bessel eigenfunctions, while the γ-equation with a harmonic oscillator potential having a minimum at $\gamma = 0$ leads to a two-dimensional harmonic oscillator with Laguerre eigenfunctions. Even more, $Y(5)$ [137] and $Z(5)$ [138] CPSs describe the transitions from axial rotor to triaxial rotor and from prolate rotor to oblate rotor, respectively. A γ-rigid version (with $\gamma = 0$) of the $X(5)$ CPS was constructed [139]. The model was called $X(3)$ since it was proved to contain three degrees of freedom. Experimental realizations of $X(3)$ appear to occur in ^{172}Os and ^{186}Pt. Recently, the CPS called $T(5)$ [140] has been introduced by approximately separating variables in the Bohr Hamiltonian for any given γ value. It was shown that the $T(5)$ model provides a dynamical connection between the original $X(5)$ and $Z(5)$ CPSs, of which the two CPSs just correspond to the limiting cases of the $T(5)$ model. It was also shown that the model provides a better description of the spectral patterns of ^{148}Ce, ^{160}Yb, ^{192}Pt, and ^{194}Pt, which in turn indicates that possible triaxial deformation may be involved to some extent in these transitional nuclei.

In Ref. [145] the $E(5/4)$ model of critical-point symmetry for odd- mass systems was developed, based on the concept of dynamical supersymmetry. The $E(5/4)$ model describes the coupling of an unpaired $j = 3/2$ nucleon to the even-even boson core with $E(5)$ symmetry. In fact, the first test of the $E(5/4)$ Bose-Fermi symmetry considered the low-energy spectrum of ^{135}Ba [146] in terms of the neutron $2d_{3/2}$ orbital coupled to the $E(5)$ boson core ^{134}Ba. If the odd nucleon lives in a system of levels with $j = 1/2,3/2,5/2$, the $E(5/12)$ model [147] is obtained. Similarly, the $X(n/2j + 1)$ scheme [148,149] with $n = 3$ or 5 was proposed by coupling the $X(n)$ core with a particle in a single-j shell.

The easiest experimental signature for each type of behavior is the energy ratios. By analyzing the energy ratios, we can identify the shape phases. The energy ratio $R_{4_1^+/2_1^+}$ is one of the most remarkable structural signatures and, furthermore, is one of the few whose absolute value is directly meaningful. This ratio has the limiting value 2 for a quadrupole vibrator, 2.5 for a non-axial γ-soft rotor and 3.33 for an ideally symmetric rotor, figure 10. However, our understanding of the low-lying excitations is frequently complicated by coexisting shapes or intruder configurations. It would be useful to identify a clear signature for these coexisting structures which alter the low-lying level spectra. Such a signature could possibly point to a unified origin

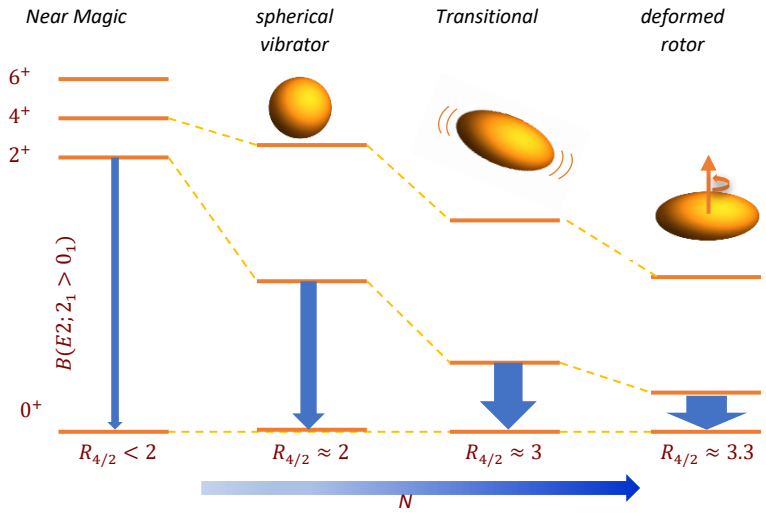

Figure 10. Pictorial description of the quadrupole collective states of atomic nucleus. When departing from the closed shell (Near Magic) with the increase of the valence nucleon number N, the shape changes from spherical vibrator to deformed rotor, passing through the transitional nuclei in between.

	$R(6/2)$	$R(4/0)$	$R(6/0)$
Vibrational nuclei	3.00	1.00	1.50
γ-unstable nuclei	4.50	5/9	1.00
Rotational nuclei	7.00	0.00	0.00

Table 1. Energy ratios take different values in different shape phases.

of the source for these intruders. It has been suggested [150] that plots of $R(6/4) = E(6_1^+)/E(4_1^+)$ versus $R(4/2) = E(4_1^+)/E(2_1^+)$ show a smooth systematic behavior, deviations from which indicate coexistence of collective and noncollective configurations. Consequently, the care should be taken in using only $R(4/2)$ values as an indication of the collective shape, since frequently this value is affected by coexisting structures. For the safe determination of the character of a collective band, especially in nuclei where mixing of different bands occurs, in which case the $R(4/2)$ ratio might be seriously affected, the series of ratios $R(J+2/J)$, $J = 2, 4, 6, \ldots$ used to construct a quantity showing distinctly different behavior in the vibrational, rotational, and γ-unstable limits [151]. In the rotational limit the members of ground-state bands have excitation energies $E(J) = AJ(J+I)$, where A is the rotational constant. Then, in this limit, the relevant ratio is $R(J+2/J)_{rot} = (J+2)(J+3)/J(J+1)$. In the vibrational limit, the members of the band are $E(J) = BJ$, so that the relevant ratio is $R(J+2/J)_{vib} = (J+2)/J$. For the ground band, the following ratio is constructed for each J, $r(J+2/J) = [R(J+2/J)_{exp} - R(J+2/J)_{vib}]/[(J+2/J)_{rot} - R(J+2/J)_{vib}]$, where $R(J+2/J)_{exp}$ is the experimental value of the ratio. These ratios show distinctive different behaviors in the vibrational, rotational, and γ-unstable limits. This ratio should be close to one for a rotational nucleus and close to zero for a vibrational nucleus, while it should have intermediate values for γ-unstable nuclei ($0.1 \le r \le 0.35$, $0.4 \le r \le 0.6$ and $0.6 \le r \le 1.0$ for vibrational, transitional and rotational nuclei, respectively). Moreover, table 1 shows clearly that other energy ratios between the states in the ground state band (e.g., $R(6/2)$) and those in different bands (e.g., $R(4/0)$ and $R(6/0)$) take different values in different shape phases [152].

As we see from the previous discussion, the properties of the lowest excited states of atomic nuclei offer a very sensitive test for nuclear structure theories. During the last two decades a remarkable set of correlations has been discovered [153-161] among the excitation energies of quasi-band structures in collective nuclei. These discoveries have been possible by exploiting the large body of data on stable and near-stable nuclei whose accumulation over the past decades now permits a global perspective and a synthesis of heretofore seemingly disparate behavior. The correlations found to apply to nuclei near stability offer benchmarks and challenges for confronting data soon to be obtained on exotic nuclei far from stability. They also draw attention to the value of a ‘‘horizontal’’ approach to structural evolution, as a complement to the usual ‘‘vertical’’ approach that focuses on individual level schemes. In this horizontal approach, instead of studying the yrast energies of even-even nuclei, $E(2_1^+)$, $E(4_1^+)$, $E(6_1^+)$, . . . or their ratios, such as $R(4/2)$, as functions of Z, A or other similar quantities, as usually done, the relationships between the energies themselves are studied.

Almost 60 years ago, Mallmann showed [162] that the data for the $R(6/2) = E(6^+)/E(2^+)$ and $R(8/2) = E(8^+)/E(2^+)$ energy ratios for the ground state band (GSB) of even–even nuclei represented as functions of $R(4/2) = E(4^+)/E(2^+)$ lie on two universal curves, respectively. After that, it was found that Mallmann-type ratios for higher spin states in the GSB define also compact, unique patterns. The correlations between energy ratios within bands have a universal character: various bands in all collective nuclei (even–even, odd–even, and odd–odd), and even the super-deformed bands, display a similar behavior.

Such simple and almost universal correlations were not predicted in advance by any nuclear model and there is still no microscopic understanding of the observed behavior and its universality. Nevertheless, macroscopic approaches such as the IBM, as well as the IBFM, automatically reproduce, in a natural way, the observed behavior. The fact that the GSB structure in the even-even nuclei follows a simple systematic incited to the development of many theoretical and phenomenological approaches aiming at understanding this behavior. Among the early various approaches to the description of the yrast excitation energies, important steps are the variable moment of inertia model [163], the anharmonic vibrator [164] and the empirical relation of Ejiri [165]. It was shown that the anharmonic vibrator relations: $E(J) = nE(2_1^+) + n(n-1)\varepsilon_4/2$, where n is the number of phonons, fit very well all the energies in the ground-state band of all even–even nuclei, where $J = 2n$. This expression is equivalent with the two-parameter formula proposed on purely empirical grounds by Ejiri, $E(J) = aJ + bJ(J+1)$ (a, b are parameters) and, in fact, is a second-degree polynomial in J: $E(J) = \alpha J + \beta J^2$. In this case the Mallmann-type relations are: $R(J/2) = [R(4/2)n(n-1)]/2 - n(n-2)$. In particular $R(6/2) = 3R(4/2) - 3$ and $R(8/2) = 6R(4/2) - 8$. It is found experimentally that with increasing n (spin) the plots increase in scattering but with highly correlated deviations, a fact which indicates the need of additional anharmonicities. The second order anharmonic vibrator expression, $E(J) = nE(2_1^+) + n(n-1)^2\varepsilon_4 + [n(n-1)(n-2)\varepsilon_6]/6$, describes quite well the experimental GSB's of all collective even–even nuclei. This formula, in fact, is equivalent to the third order polynomial in J: $E(J) = \alpha J + \beta J^2 + \gamma J^3$.Moreover, based on the spin dependence of the energy of the states, recurrence relations between energy ratios was obtained. These relations can be used to predict with high accuracy (if there is no perturbation of the band) the energy of higher members of the band.

Finally, we hope that, with the background provided in this introduction, reader can now begin to develop an understanding of each specific type of nuclei occurring in the chart as well as the evolution of structure from one type to another.

Now, in this work, we present an atlas of 645 even-even nuclei containing the experimental data of four energy levels. Besides the usual 2_1^+ and 4_1^+ states, we consider the following excited states: 2_2^+ and 4_2^+, which are experimentally known in many nuclei. The “non-collective” nuclei (that

is, those with $R(4/2) < 2.0$) were also included, thus, covering the whole range of nuclear structures. We visualized the values of energy levels and energy ratios, $E_{2_1^+}$, $E_{2_2^+}$, $E_{4_1^+}$, $E_{4_2^+}$, $E_{4_1^+}/E_{2_1^+}$, $E_{4_2^+}/E_{2_2^+}$, $E_{2_2^+}/E_{2_1^+}$, $E_{4_2^+}/E_{4_1^+}$, $E_{4_2^+}/E_{2_1^+}$ and $E_{4_1^+}/E_{2_2^+}$, in all even-even nuclei. The ENSDF database [166] has been extensively used in extracting the relevant data. The atlas is organized as follows.

In chapter I, we provide three dimensional figures of the values of energy levels and energy ratios over all even–even nuclei. The experimental values of the energy levels and energy ratios plotted as a function of neutron number N along the x axis and proton number Z along the y axis. The dashed horizontal and vertical lines indicate the positions of magic numbers. The values of energy levels (keV) and energy ratios are indicated by the scale shown on the right of the graphs.

In chapter II, two dimensional figures of the values of energy level and energy ratios over all even–even nuclei for different isotopes are presented. The experimental values of the energy levels and energy ratios plotted as a function of neutron number N along the x axis for different isotopes. The proton numbers Z for different isotopes are indicated by legend below graph.

In chapter III, two dimensional figures of the values of energy levels and energy ratios for each chain of isotopes are presented. Each figure consists of four panels. Panel A represents the comparison of the experimental values of energy levels of the 2_1^+, 2_2^+, 4_1^+ and 4_2^+ states for each chain of isotopes. Panels B, C, D represent the comparison of the experimental energy ratios ($E_{4_1^+}/E_{2_1^+}$ and $E_{4_2^+}/E_{2_2^+}$), ($E_{2_2^+}/E_{2_1^+}$and $E_{4_2^+}/E_{4_1^+}$) and ($E_{4_2^+}/E_{2_1^+}$ and $E_{4_1^+}/E_{2_2^+}$), respectively, for each chain of isotopes.

In chapter IV, we provide two dimensional figures of the values of energy levels and energy ratios for different isotones. The experimental values of the energy levels and energy ratios plotted as a function of proton number Z along the x axis for different isotones. The neutron numbers N for different isotones are indicated by legend below graphs.

In chapter V, two dimensional figures of the values of energy levels and energy ratios for each chain of isotones are presented. Each figure consists of four panels. Panel A represents the comparison of the experimental values of energy levels of the lowest 2_1^+, 2_2^+, 4_1^+ and 4_2^+ states for each chain of isotones. Panels B, C, D represent the comparison of the experimental energy ratios ($E_{4_1^+}/E_{2_1^+}$ and $E_{4_2^+}/E_{2_2^+}$), ($E_{2_2^+}/E_{2_1^+}$and $E_{4_2^+}/E_{4_1^+}$) and (($E_{4_2^+}/E_{2_1^+}$ and $E_{4_1^+}/E_{2_2^+}$), respectively, for each chain of isotones.

In chapter VI, we provide scatter plots showing relationship between the values of energy levels $E_{2_1^+}$, $E_{2_2^+}$, $E_{4_1^+}$ and $E_{4_2^+}$ for all even–even nuclei.

In chapter VII, we provide a table of experimental data. In order are given: the nuclide, Z, N, A, $E_{2,1}$, $E_{2,2}$, $E_{4,1}$, $E_{4,2}$, $\frac{E_{4,2}}{E_{2,1}}$, $\frac{E_{4,2}}{E_{2,2}}$, $\frac{E_{4,2}}{E_{4,1}}$, $\frac{E_{4,1}}{E_{2,1}}$, $\frac{E_{4,1}}{E_{2,2}}$, $\frac{E_{2,2}}{E_{2,1}}$, and reference.

Chapter I

Three dimensional figures of the values of energy levels and energy ratios over all even–even nuclei

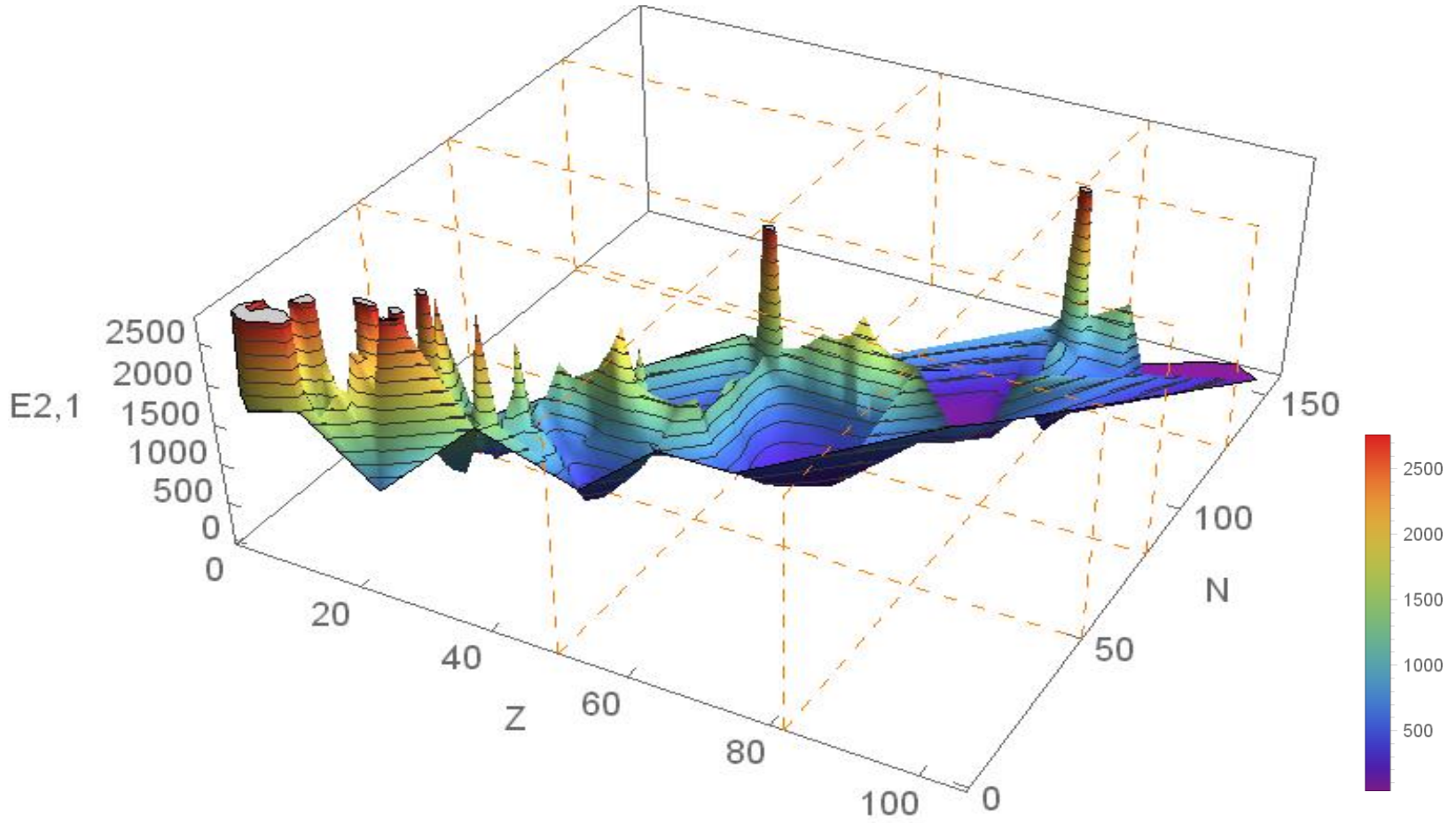

Figure I. 1 (color online) The experimental values of the energy of the first-excited 2^+ state (the interpolation surface of $E_{2_1^+}$) for all even–even nuclei plotted as a function of neutron number N along the x axis and proton number Z along the y axis. The dashed horizontal and vertical lines indicate the positions of magic numbers. The value of $E_{2_1^+}$ (Kev) is indicated by the scale shown on the right.

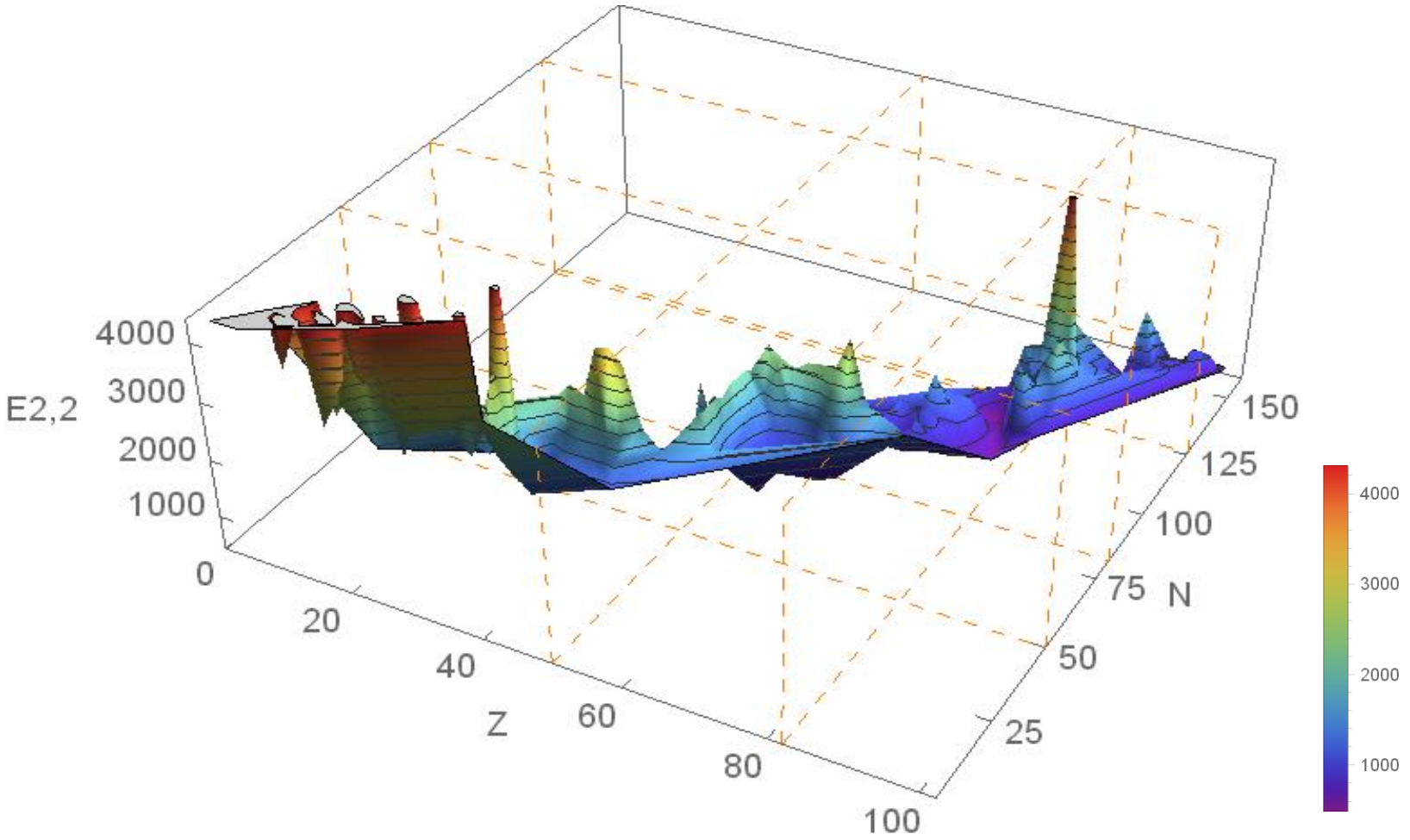

Figure I. 2 (color online) The experimental values of the energy of the second-excited 2^+ state (the interpolation surface of $E_{2_2^+}$) for all even–even nuclei plotted as a function of neutron number N along the x axis and proton number Z along the y axis. The dashed horizontal and vertical lines indicate the positions of magic numbers. The value of $E_{2_2^+}$ (Kev) is indicated by the scale shown on the right.

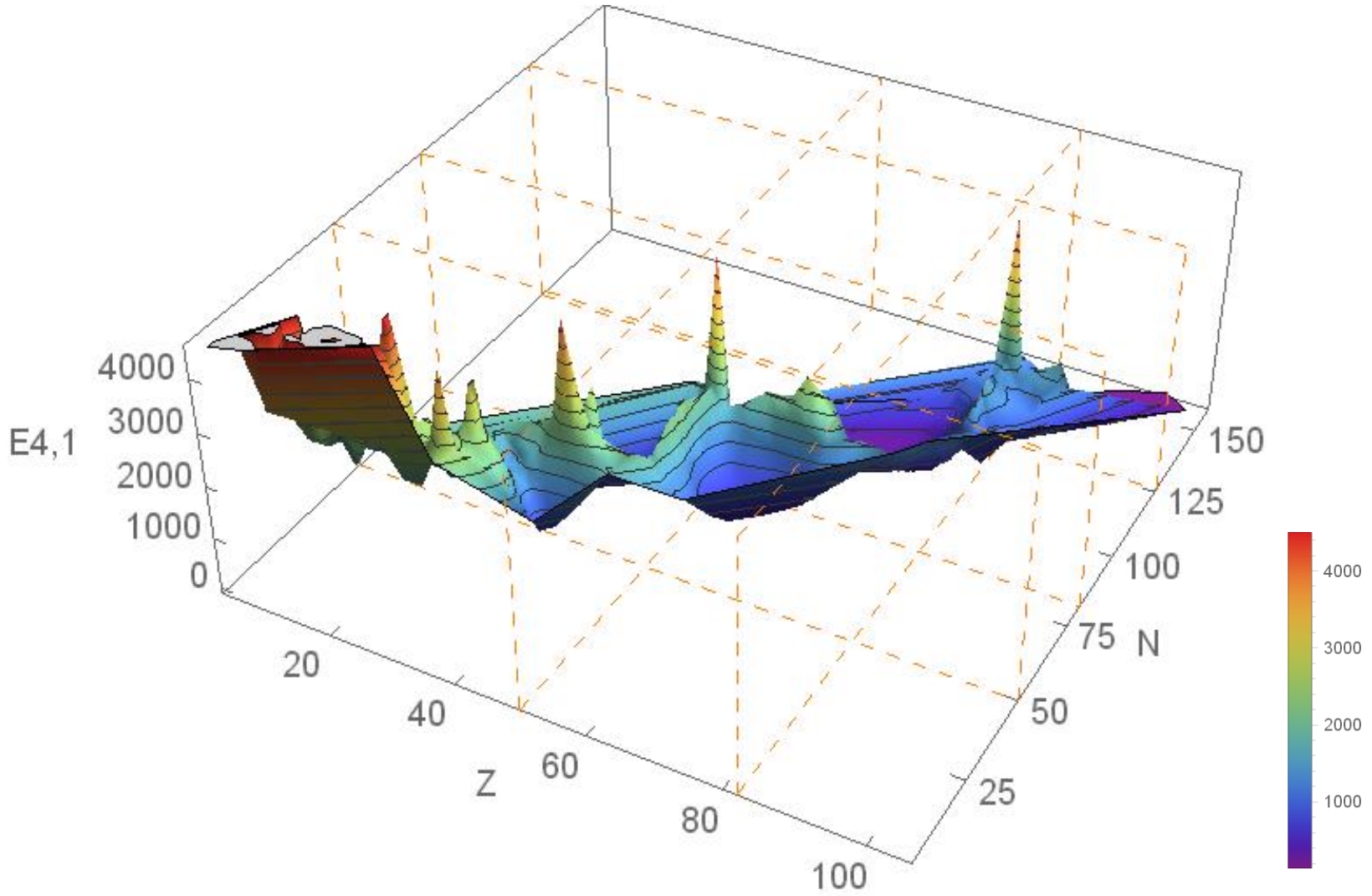

Figure I. 3 (color online) The experimental values of the energy of the first-excited 4^+ state (the interpolation surface of $E_{4_1^+}$) for all even–even nuclei plotted as a function of neutron number N along the x axis and proton number Z along the y axis. The dashed horizontal and vertical lines indicate the positions of magic numbers. The value of $E_{4_1^+}$ (Kev) is indicated by the scale shown on the right.

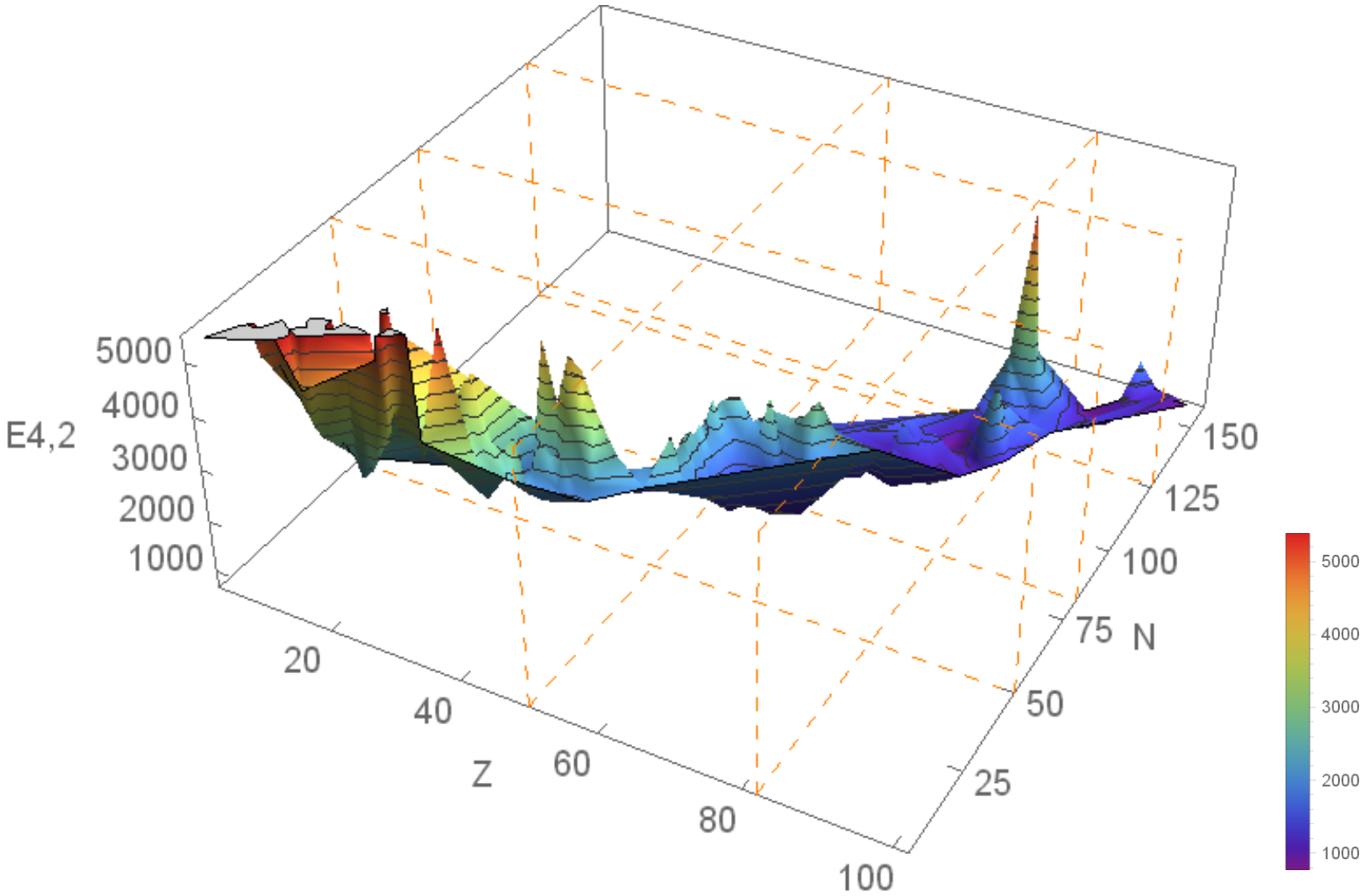

Figure I. 4 (color online) The experimental values of the energy of the second-excited 4^+ state (the interpolation surface of $E_{4_2^+}$) for all even–even nuclei plotted as a function of neutron number N along the x axis and proton number Z along the y axis. The dashed horizontal and vertical lines indicate the positions of magic numbers. The value of $E_{4_2^+}$ (Kev) is indicated by the scale shown on the right.

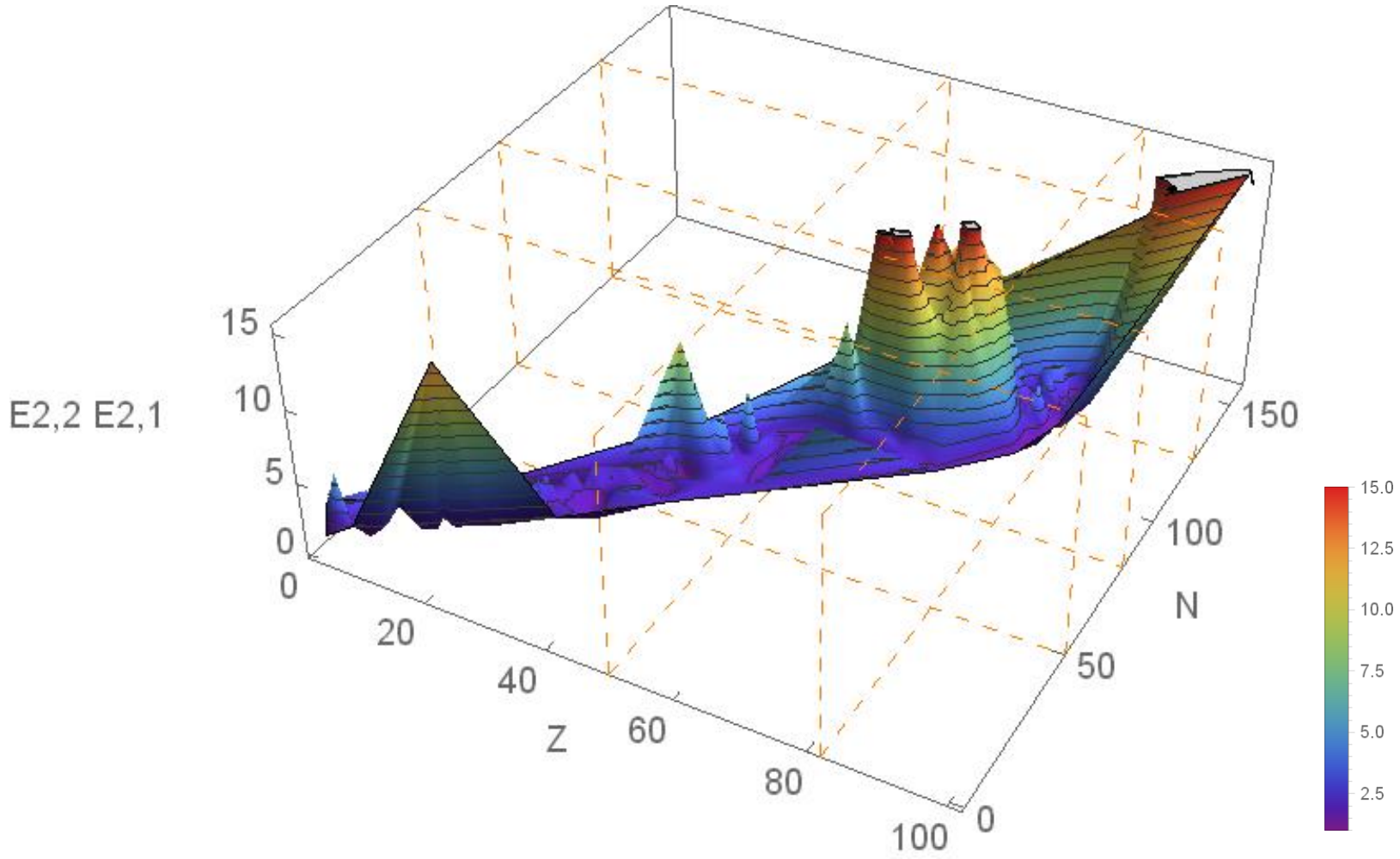

Figure I. 5 (color online) The experimental values of the energy ratio $E_{2_2^+}/E_{2_1^+}$ (the interpolation surface of $E_{2_2^+}/E_{2_1^+}$) for all even–even nuclei plotted as a function of neutron number N along the x axis and proton number Z along the y axis. The dashed horizontal and vertical lines indicate the positions of magic numbers. The value of $E_{2_2^+}/E_{2_1^+}$ is indicated by the scale shown on the right.

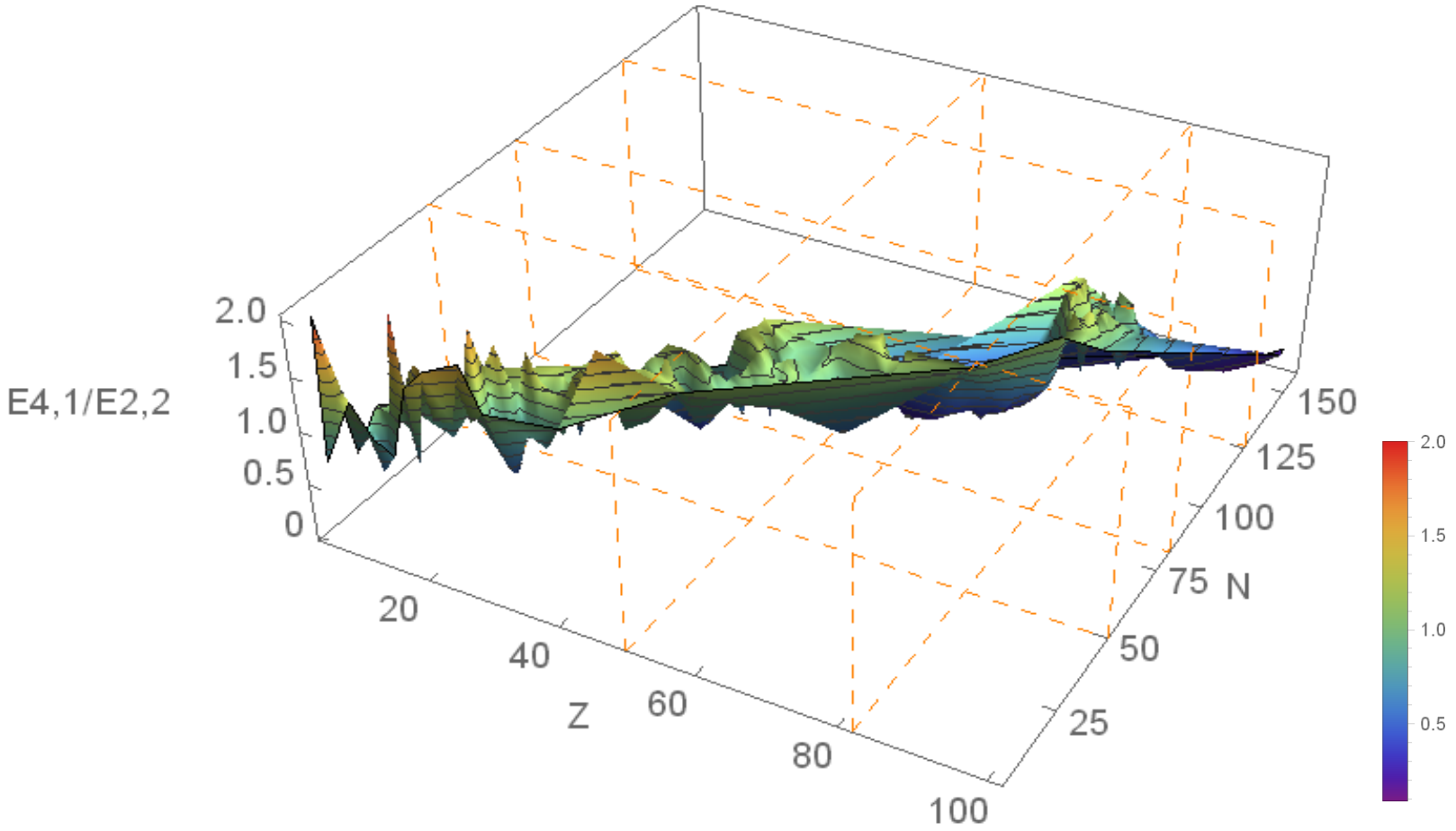

Figure I. 6 (color online) The experimental values of the energy ratio $E_{4_1^+}/E_{2_2^+}$ (the interpolation surface of $E_{4_1^+}/E_{2_2^+}$) for all even–even nuclei plotted as a function of neutron number N along the x axis and proton number Z along the y axis. The dashed horizontal and vertical lines indicate the positions of magic numbers. The value of $E_{4_1^+}/E_{2_2^+}$ is indicated by the scale shown on the right.

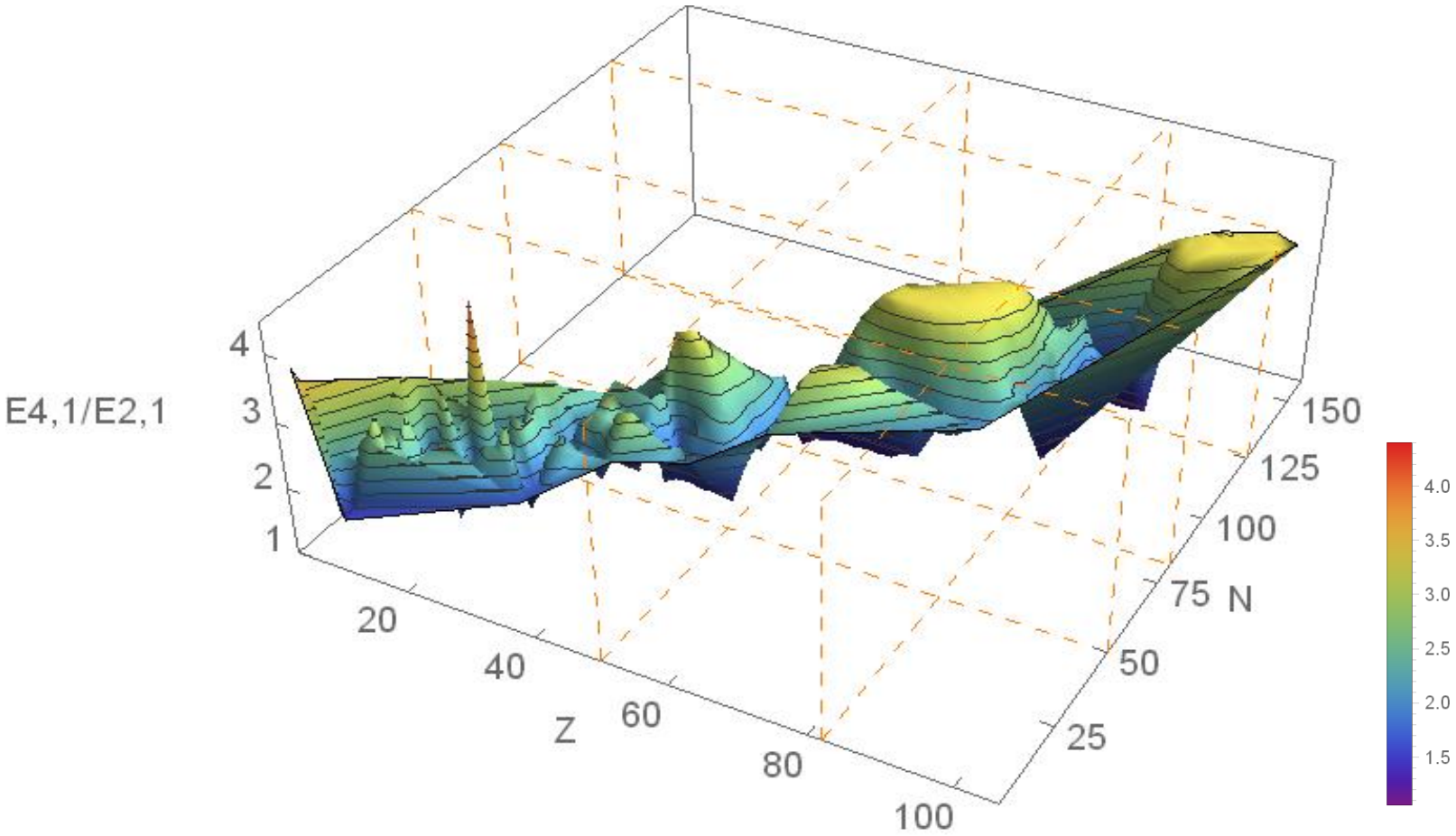

Figure I. 7 (color online) The experimental values of the energy ratio $E_{4_1^+}/E_{2_1^+}$ (the interpolation surface of $E_{4_1^+}/E_{2_1^+}$) for all even–even nuclei plotted as a function of neutron number N along the x axis and proton number Z along the y axis. The dashed horizontal and vertical lines indicate the positions of magic numbers. The value of $E_{4_1^+}/E_{2_1^+}$ is indicated by the scale shown on the right.

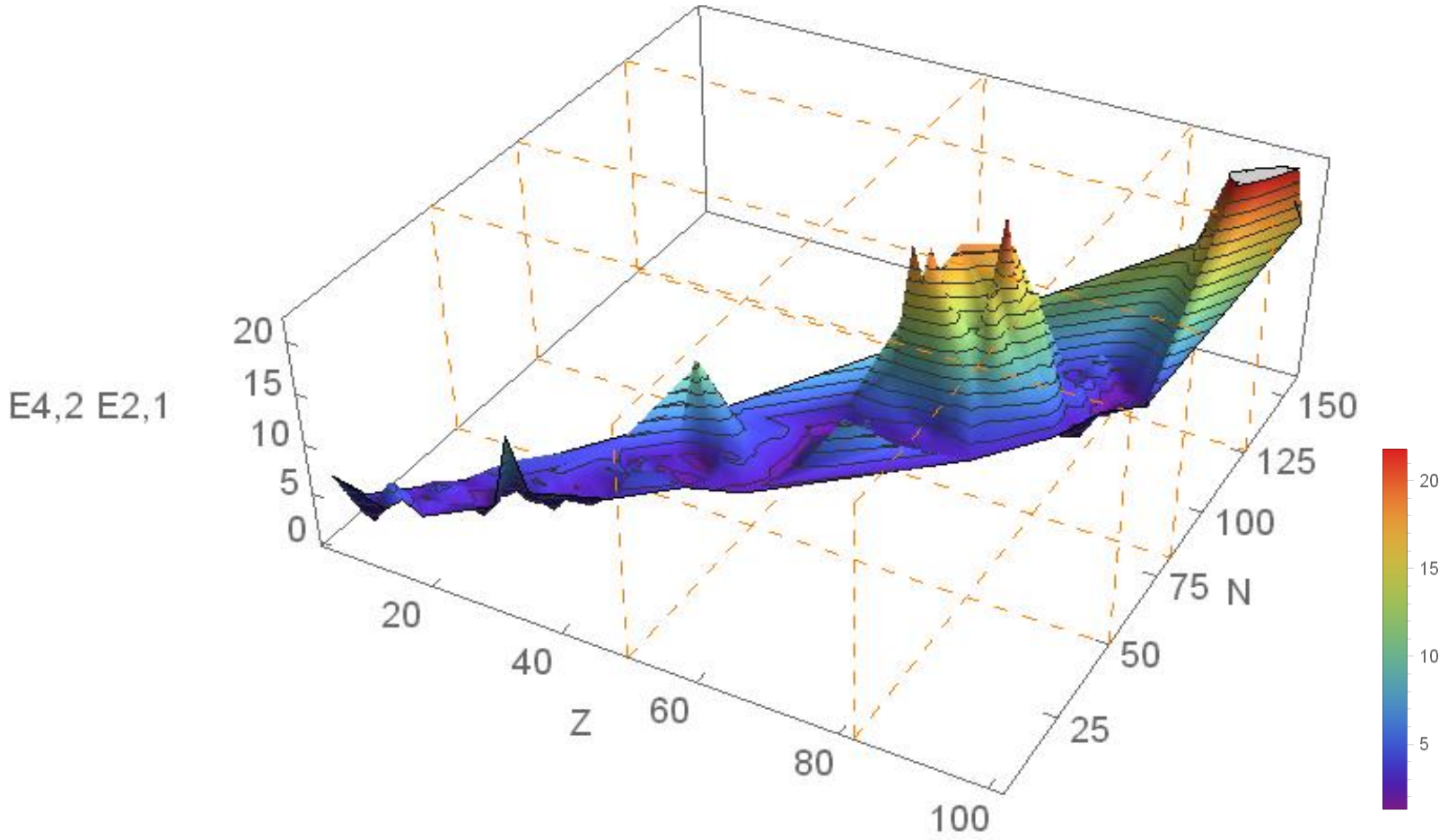

Figure I. 8 (color online) The experimental values of the energy ratio $E_{4_2^+}/E_{2_1^+}$ (the interpolation surface of $E_{4_2^+}/E_{2_1^+}$) for all even–even nuclei plotted as a function of neutron number N along the x axis and proton number Z along the y axis. The dashed horizontal and vertical lines indicate the positions of magic numbers. The value of $E_{4_2^+}/E_{2_1^+}$ is indicated by the scale shown on the right.

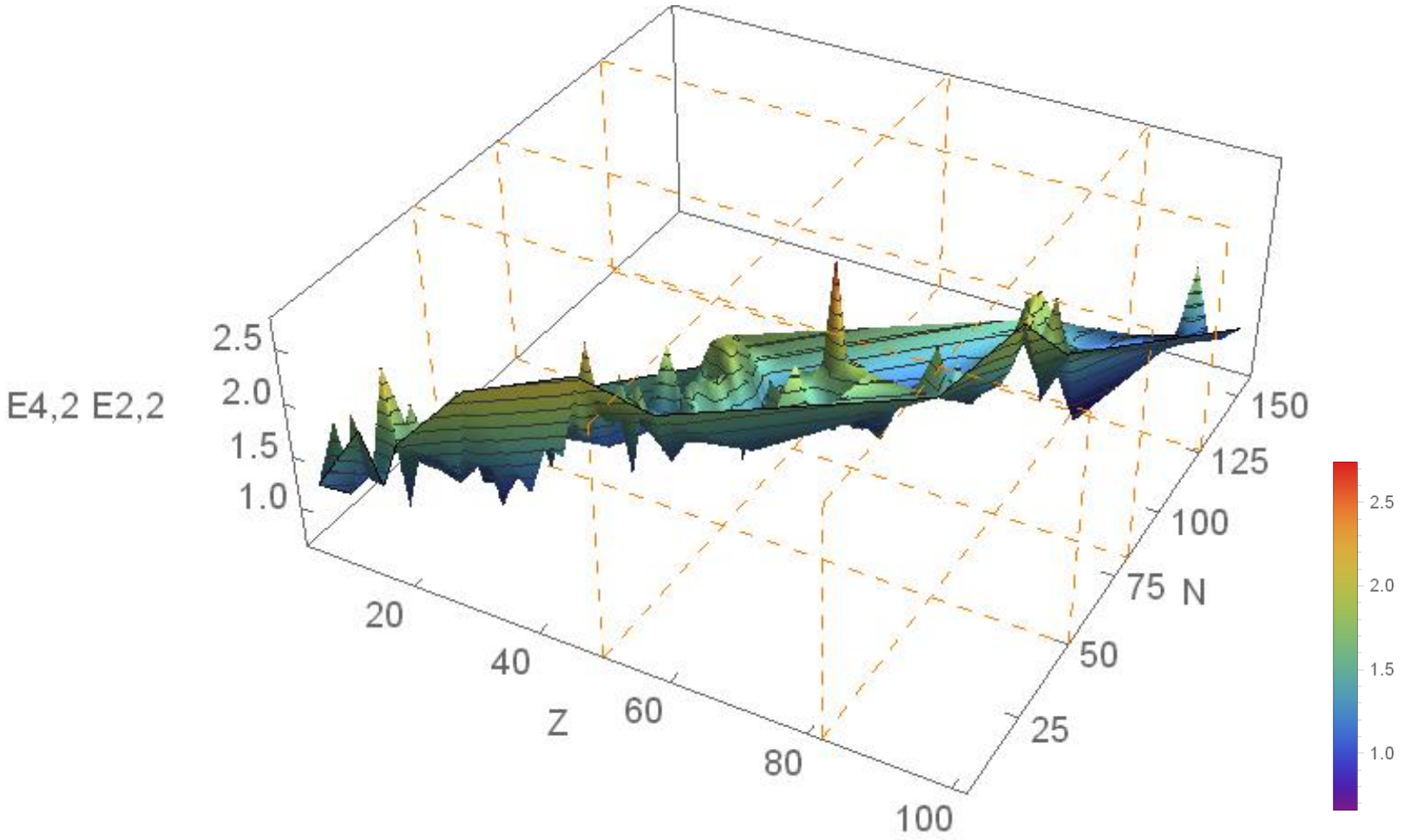

Figure I. 9 (color online) The experimental values of the energy ratio $E_{4_2^+}/E_{2_2^+}$ (the interpolation surface of $E_{4_2^+}/E_{2_2^+}$) for all even–even nuclei plotted as a function of neutron number N along the x axis and proton number Z along the y axis. The dashed horizontal and vertical lines indicate the positions of magic numbers. The value of $E_{4_2^+}/E_{2_2^+}$ is indicated by the scale shown on the right.

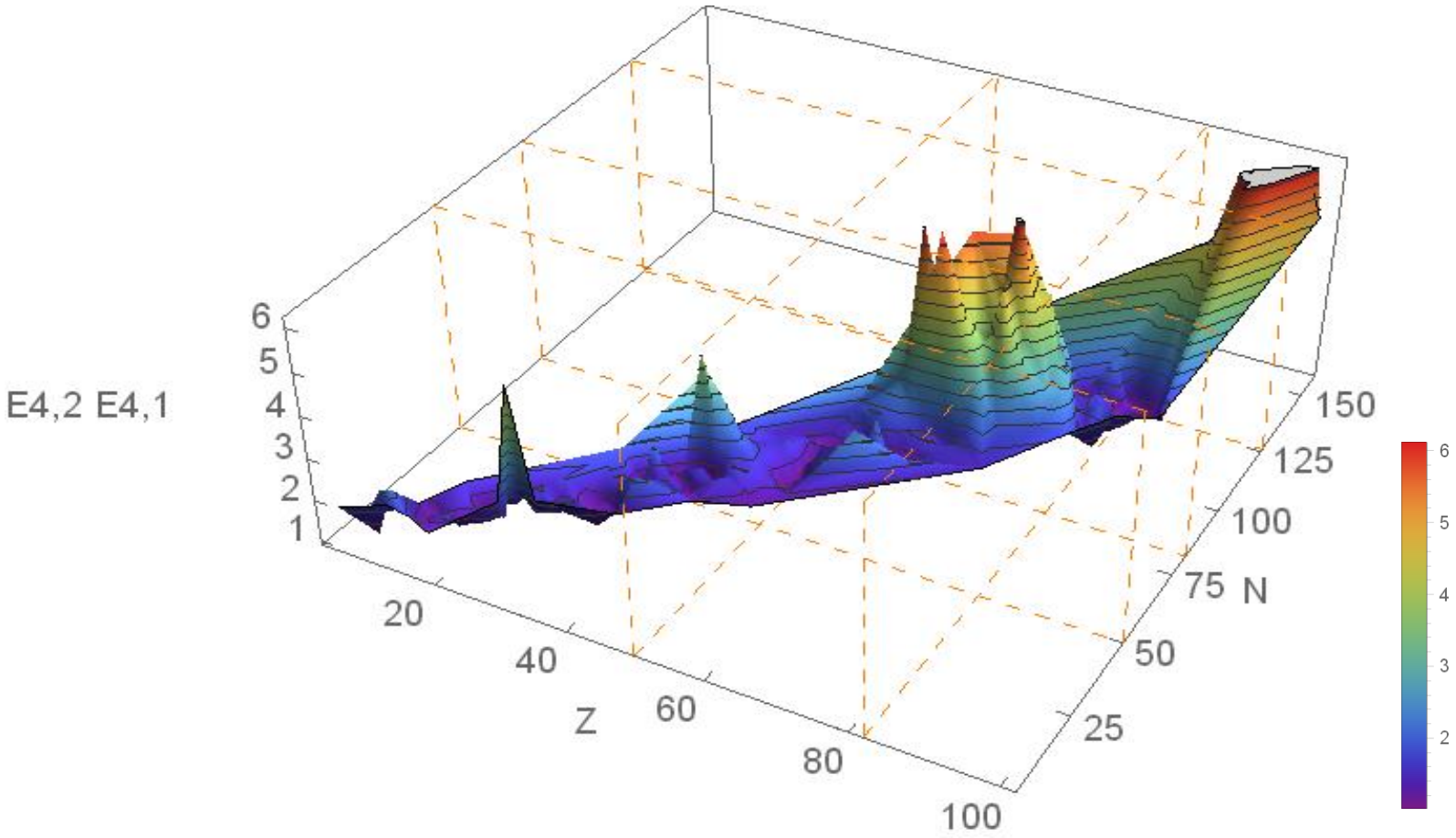

Figure I. 10 (color online) The experimental values of the energy ratio $E_{4_2^+}/E_{4_1^+}$ (the interpolation surface of $E_{4_2^+}/E_{4_1^+}$) for all even–even nuclei plotted as a function of neutron number N along the x axis and proton number Z along the y axis. The dashed horizontal and vertical lines indicate the positions of magic numbers. The value of $E_{4_2^+}/E_{4_1^+}$ is indicated by the scale shown on the right.

Chapter II

Two dimensional figures of the values of energy levels and energy ratios over all even–even nuclei for different isotopes

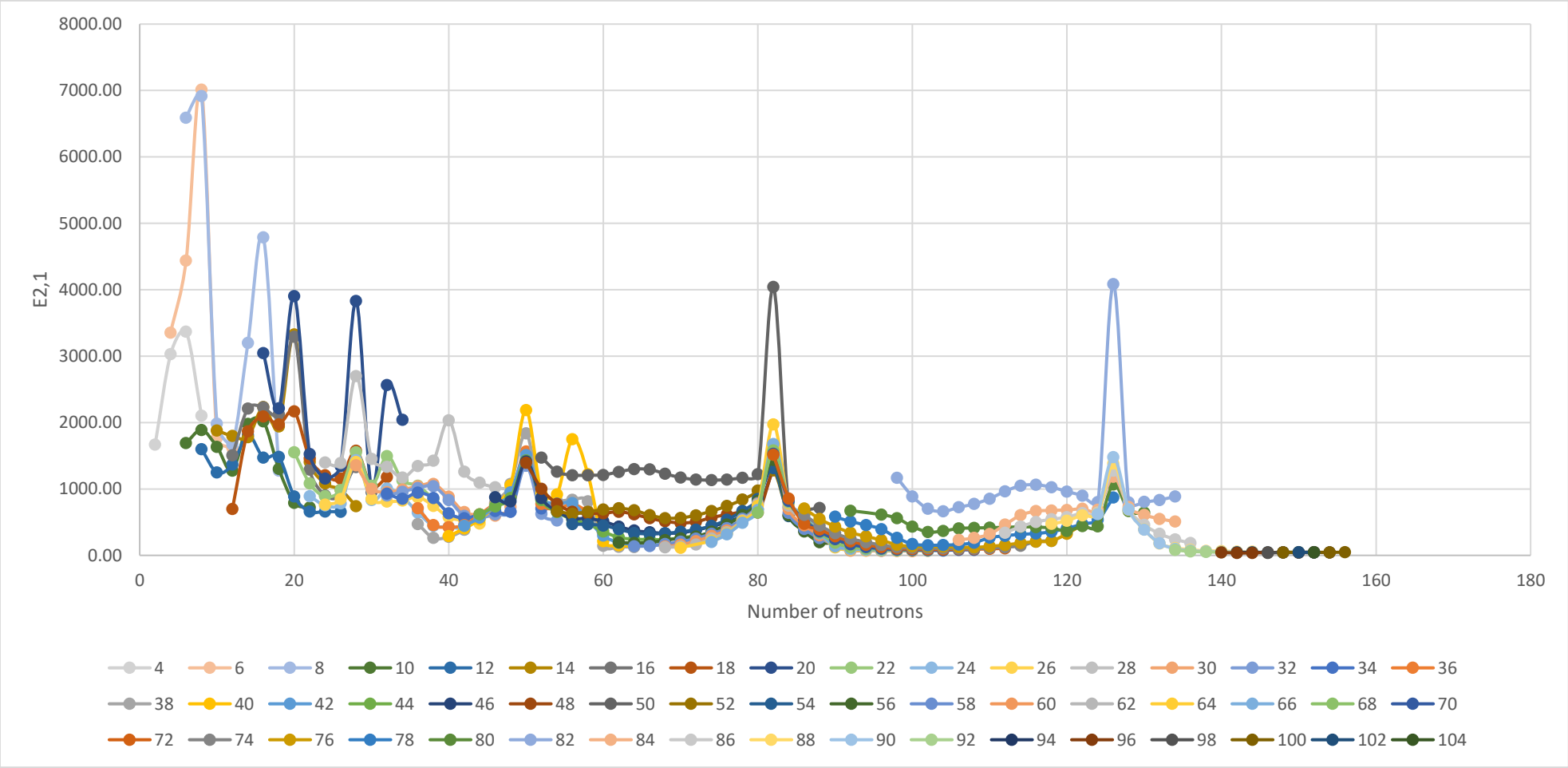

Figure II. 1 (color online) The experimental values of the energy of the first -excited 2^+ state ($E_{2_1^+}$) for all even–even nuclei plotted as a function of neutron number N along the x axis for different isotopes. The proton numbers Z for different isotopes are indicated by legend below graph.

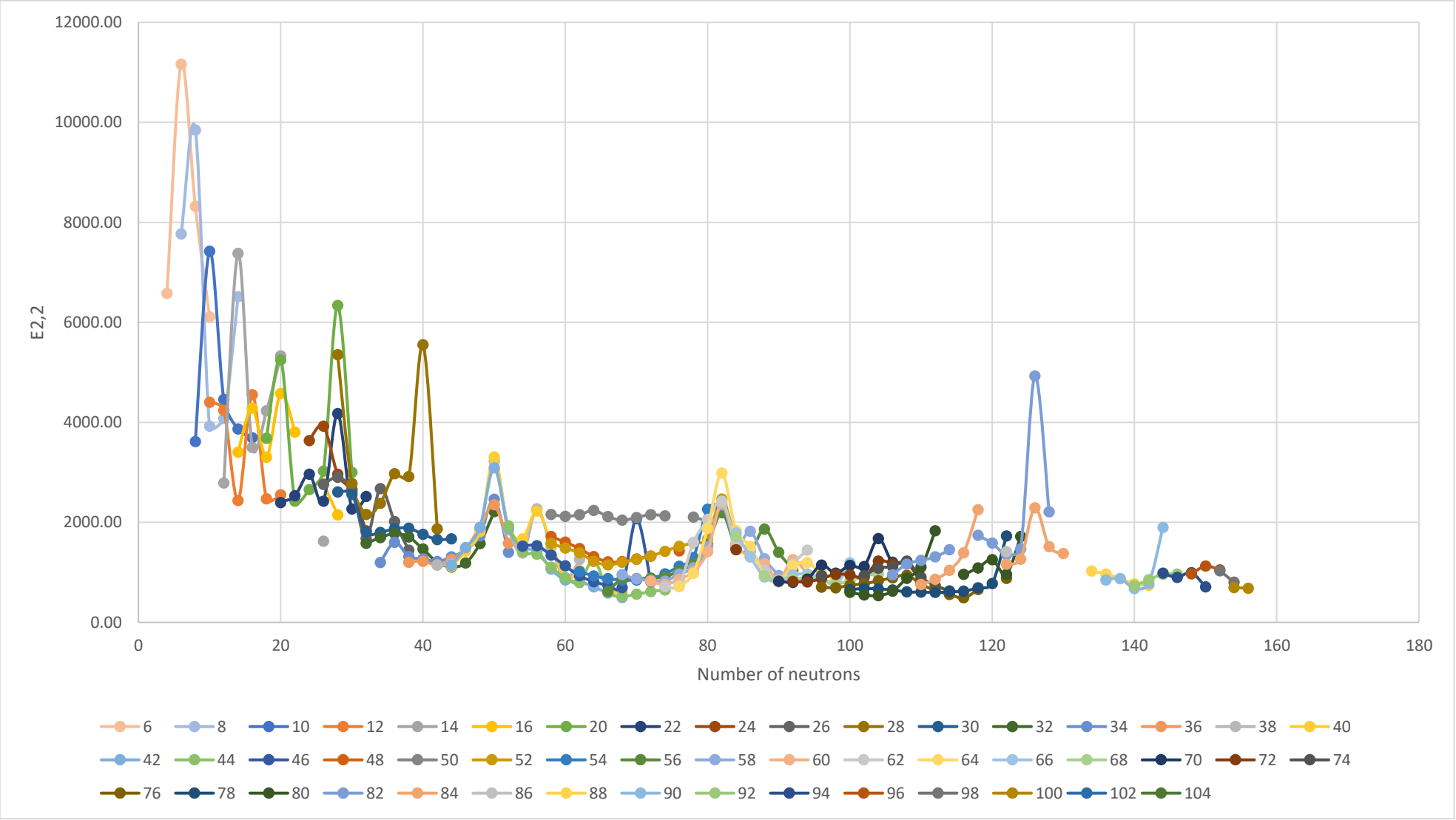

Figure II. 2 (color online) The experimental values of the energy of the second-excited 2^+ state ($E_{2_2^+}$) for all even–even nuclei plotted as a function of neutron number N along the x axis for different isotopes. The proton numbers Z for different isotopes are indicated by legend below graph.

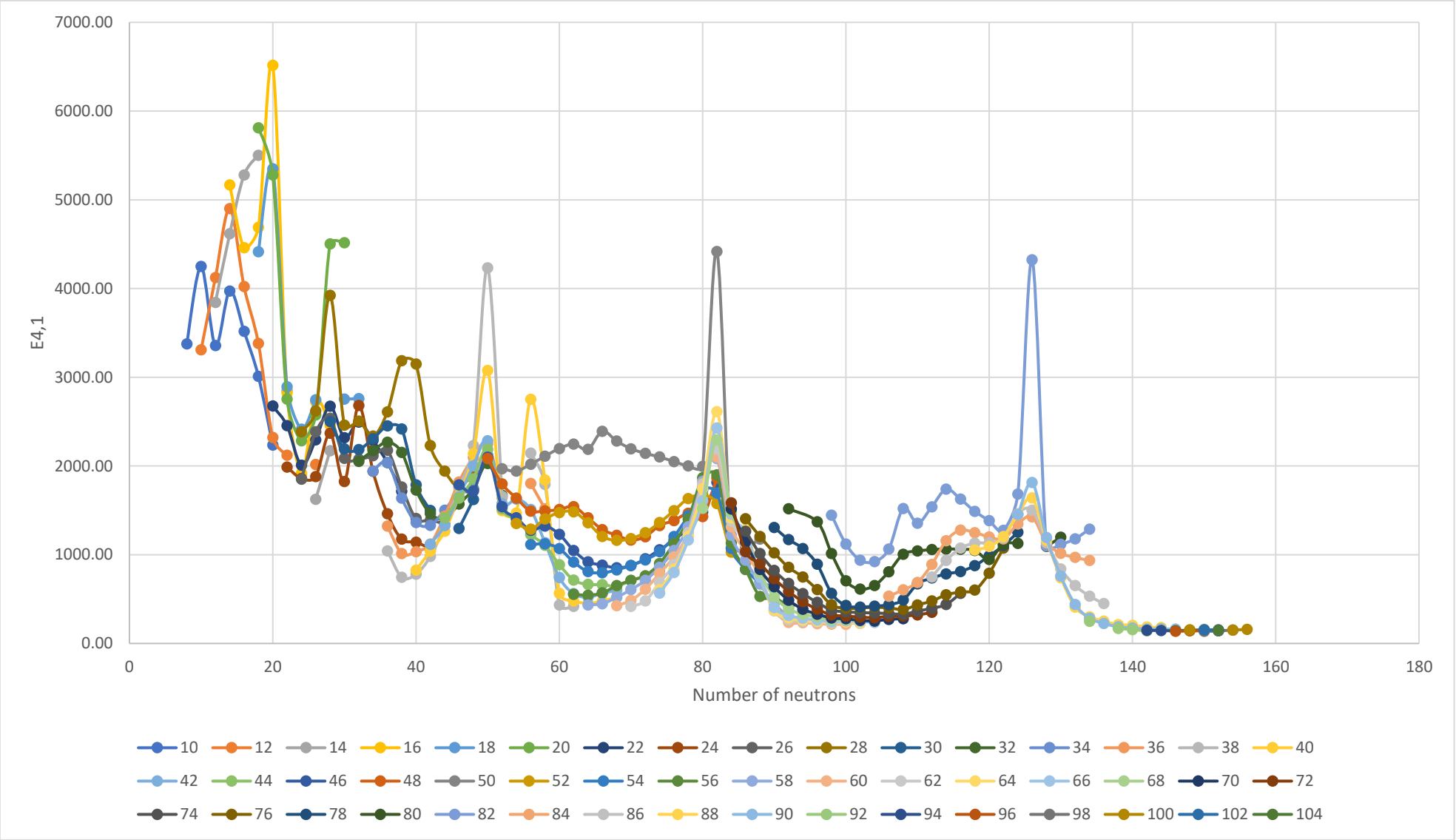

Figure II. 3 (color online) The experimental values of the energy of the first- excited 4^+ state ($E_{4_1^+}$) for all even–even nuclei plotted as a function of neutron number N along the x axis for different isotopes. The proton numbers Z for different isotopes are indicated by legend below graph.

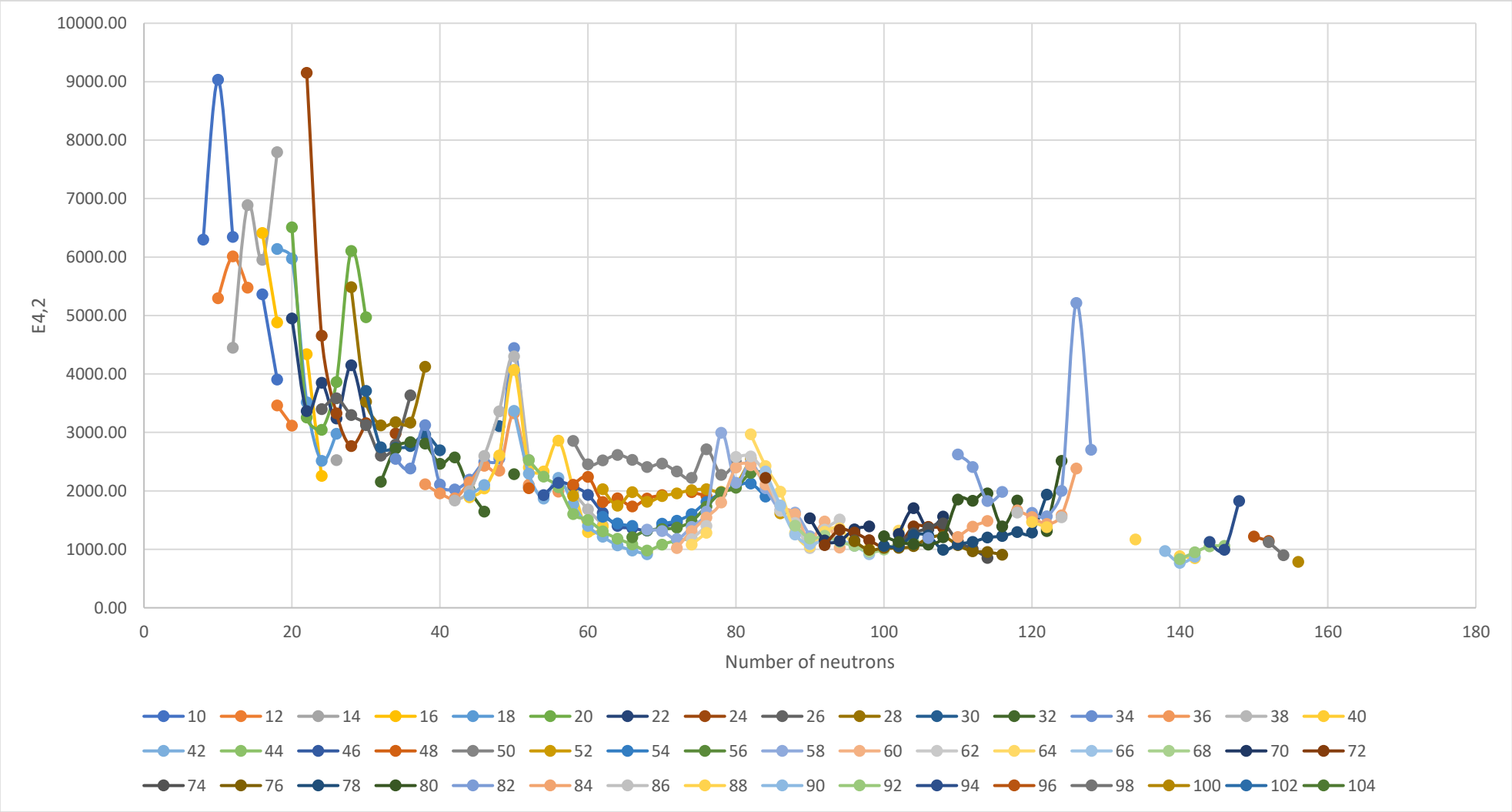

Figure II. 4 (color online) The experimental values of the energy of the second-excited 4^+ state ($E_{4_2^+}$) for all even–even nuclei plotted as a function of neutron number N along the x axis for different isotopes. The proton numbers Z for different isotopes are indicated by legend below graph.

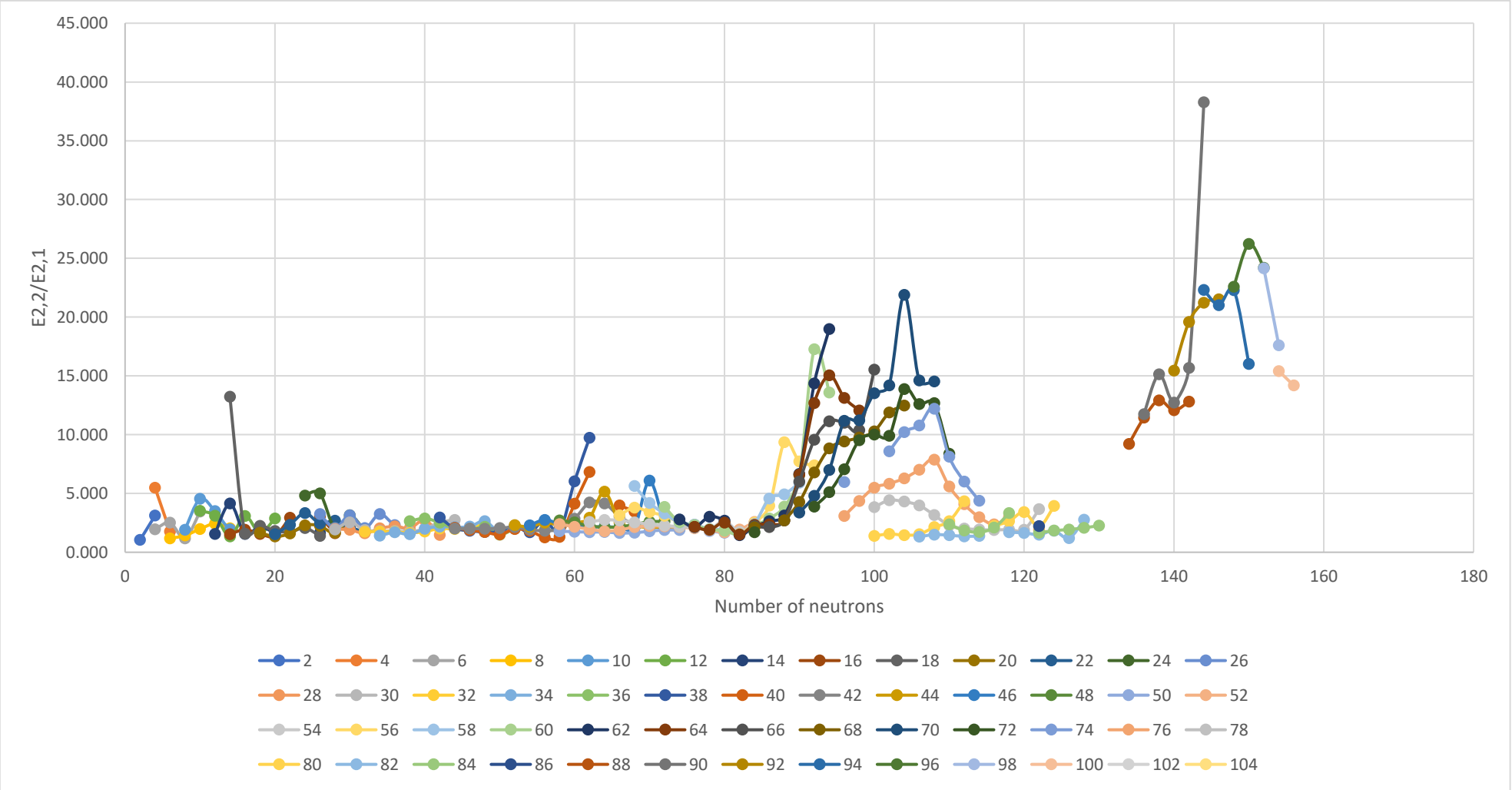

Figure II. 5 (color online) The experimental values of the energy ratio $E_{2_2^+}/E_{2_1^+}$ for all even–even nuclei plotted as a function of neutron number N along the x axis for different isotopes. The proton numbers Z for different isotopes are indicated by legend below graph.

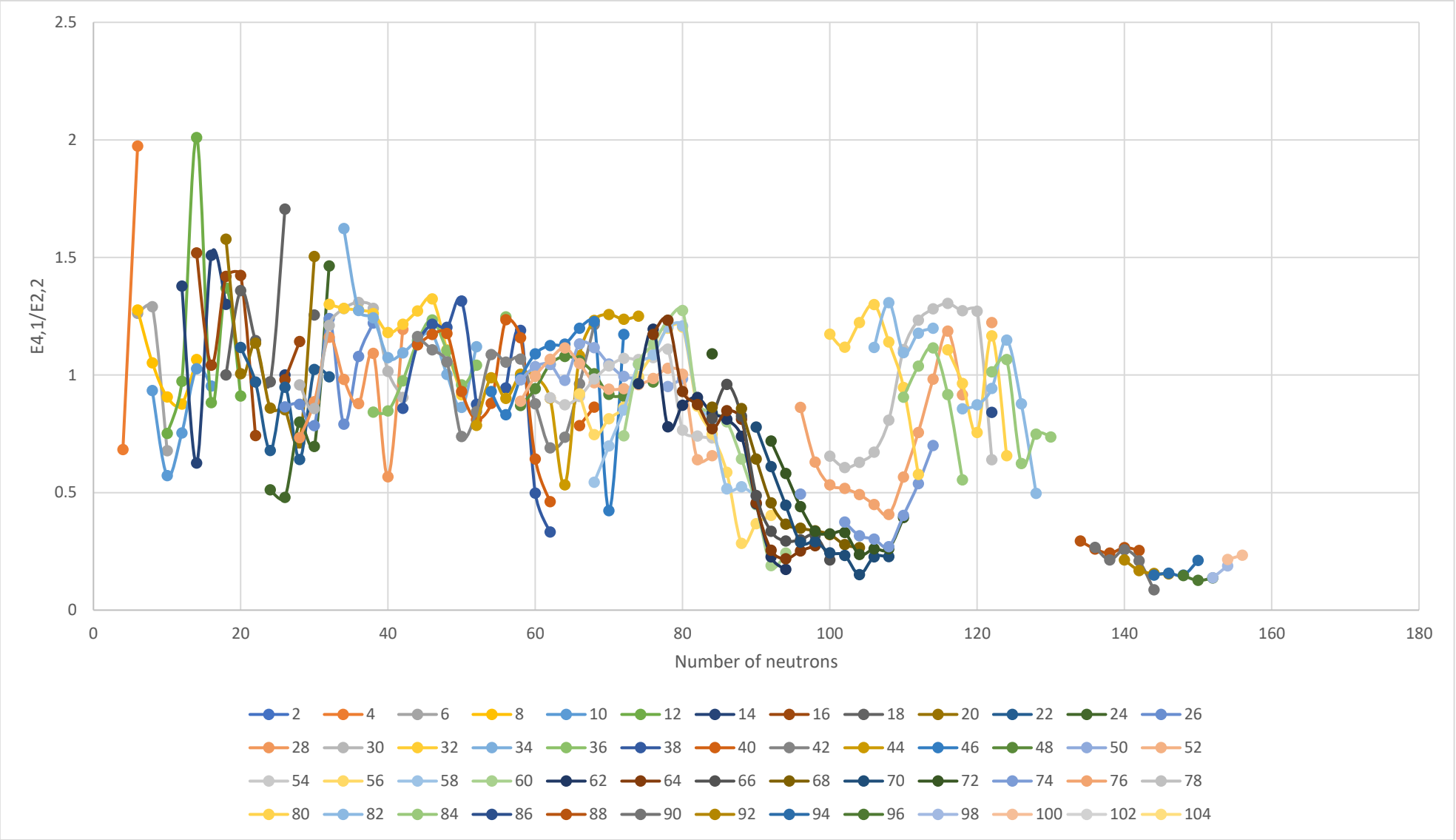

Figure II. 6 (color online) The experimental values of the energy ratio $E_{4_1^+}/E_{2_2^+}$ for all even–even nuclei plotted as a function of neutron number N along the x axis for different isotopes. The proton numbers Z for different isotopes are indicated by legend below graph.

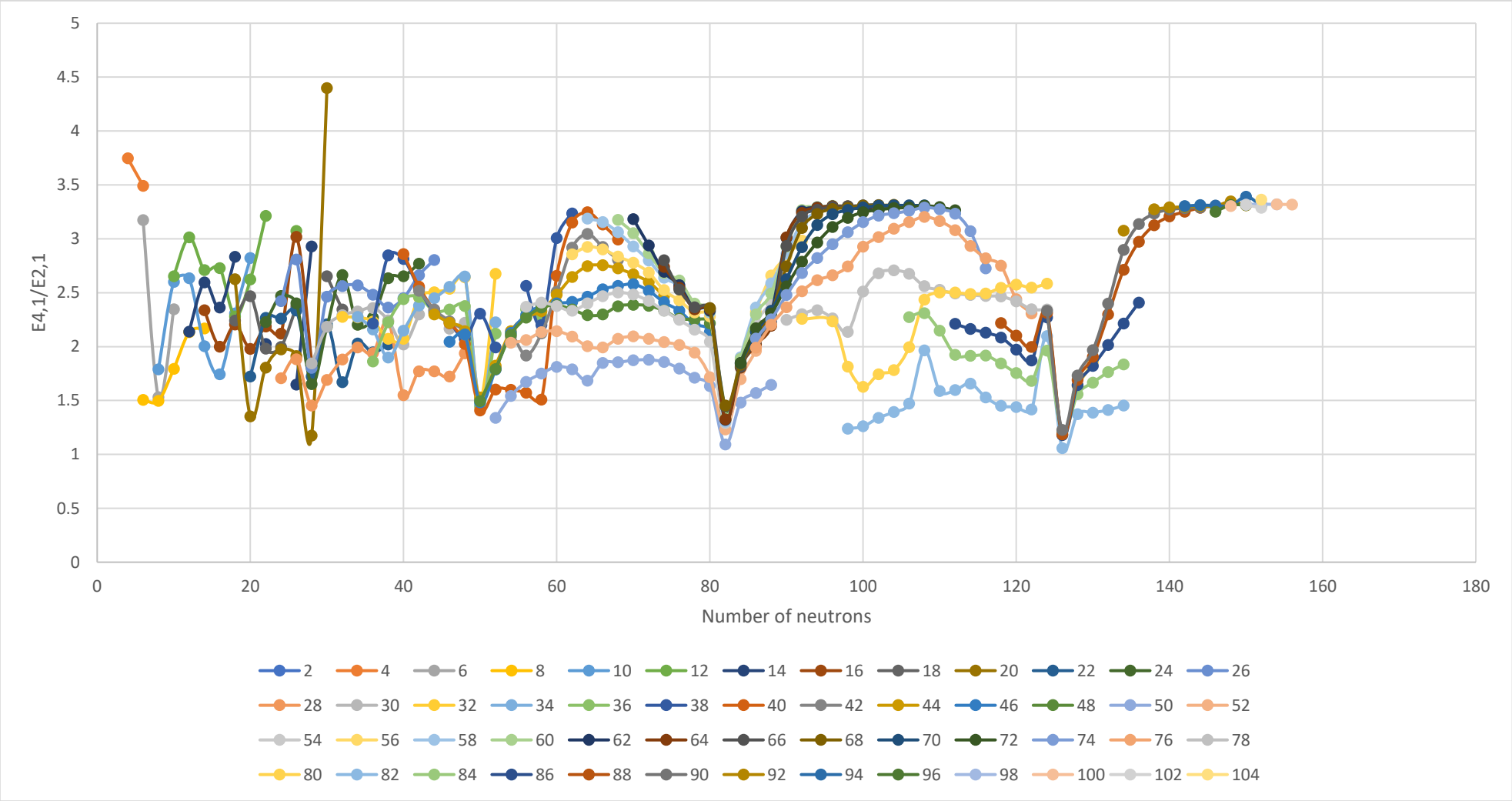

Figure II. 7 (color online) The experimental values of the energy ratio $E_{4_1^+}/E_{2_1^+}$ for all even–even nuclei plotted as a function of neutron number N along the x axis for different isotopes. The proton numbers Z for different isotopes are indicated by legend below graph.

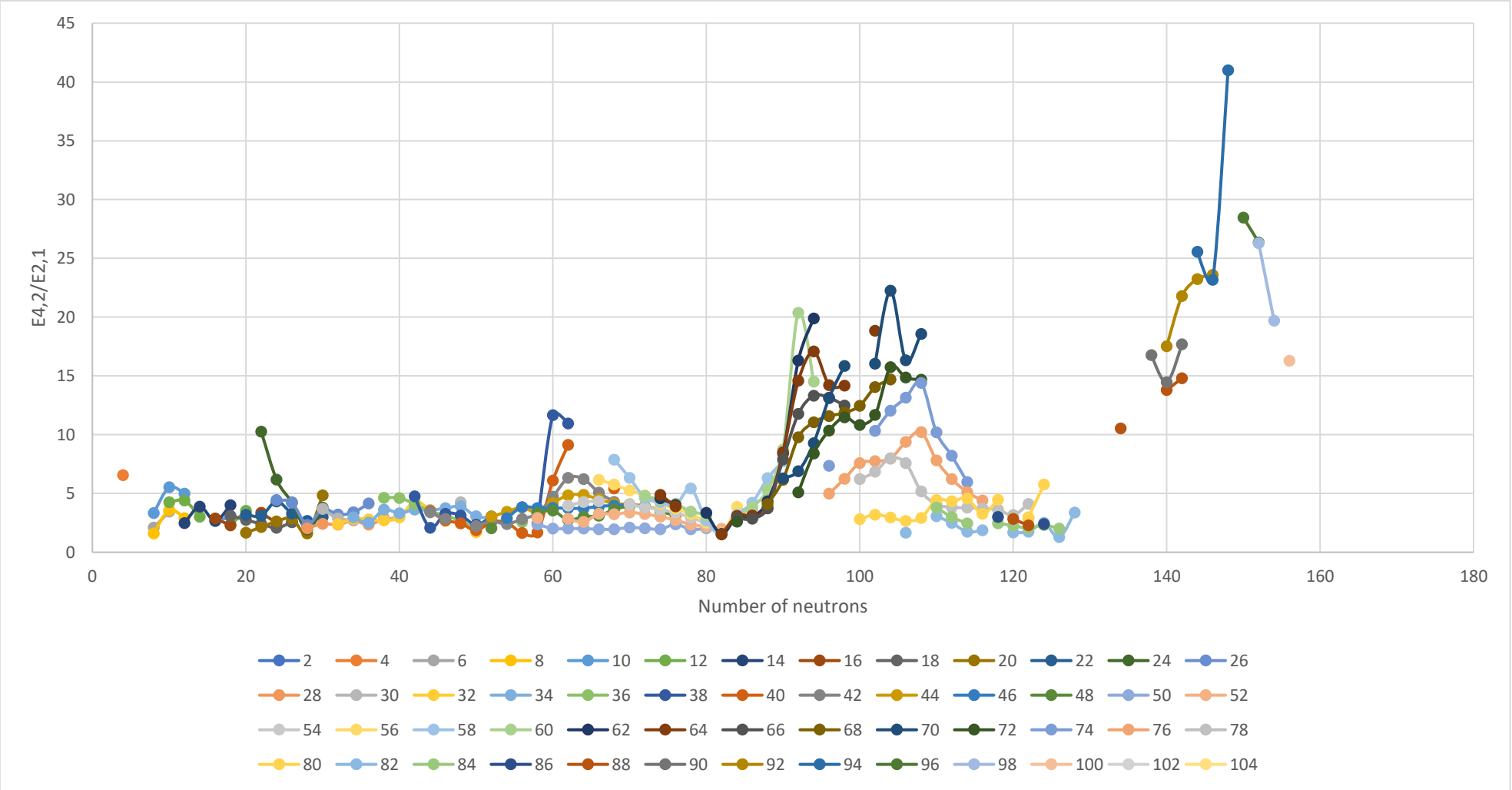

Figure II. 8 (color online) The experimental values of the energy ratio $E_{4_2^+}/E_{2_1^+}$ for all even–even nuclei plotted as a function of neutron number N along the x axis for different isotopes. The proton numbers Z for different isotopes are indicated by legend below graph.

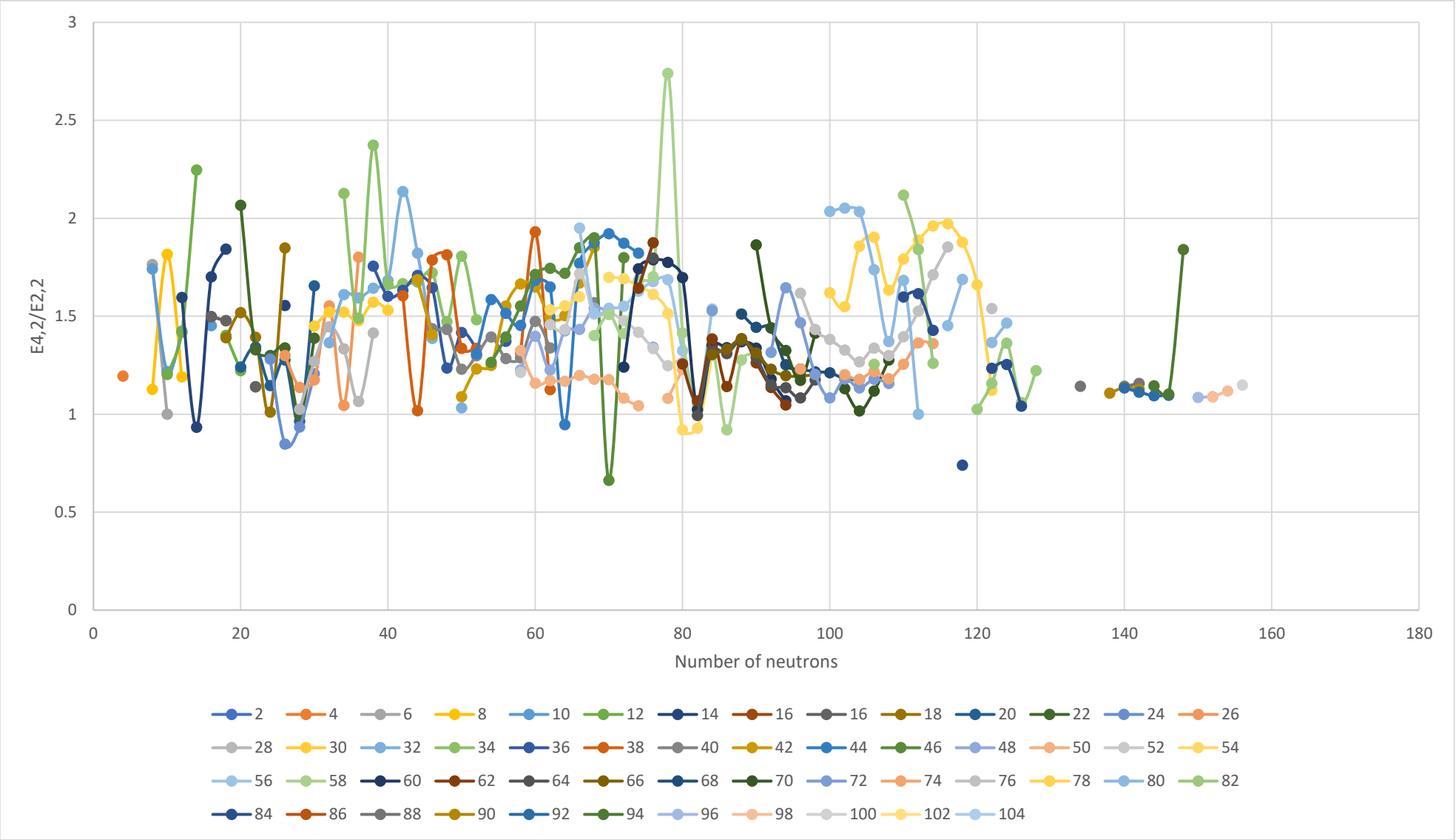

Figure II. 9 (color online) The experimental values of the energy ratio $E_{4_2^+}/E_{2_2^+}$ for all even–even nuclei plotted as a function of neutron number N along the x axis for different isotopes. The proton numbers Z for different isotopes are indicated by legend below graph.

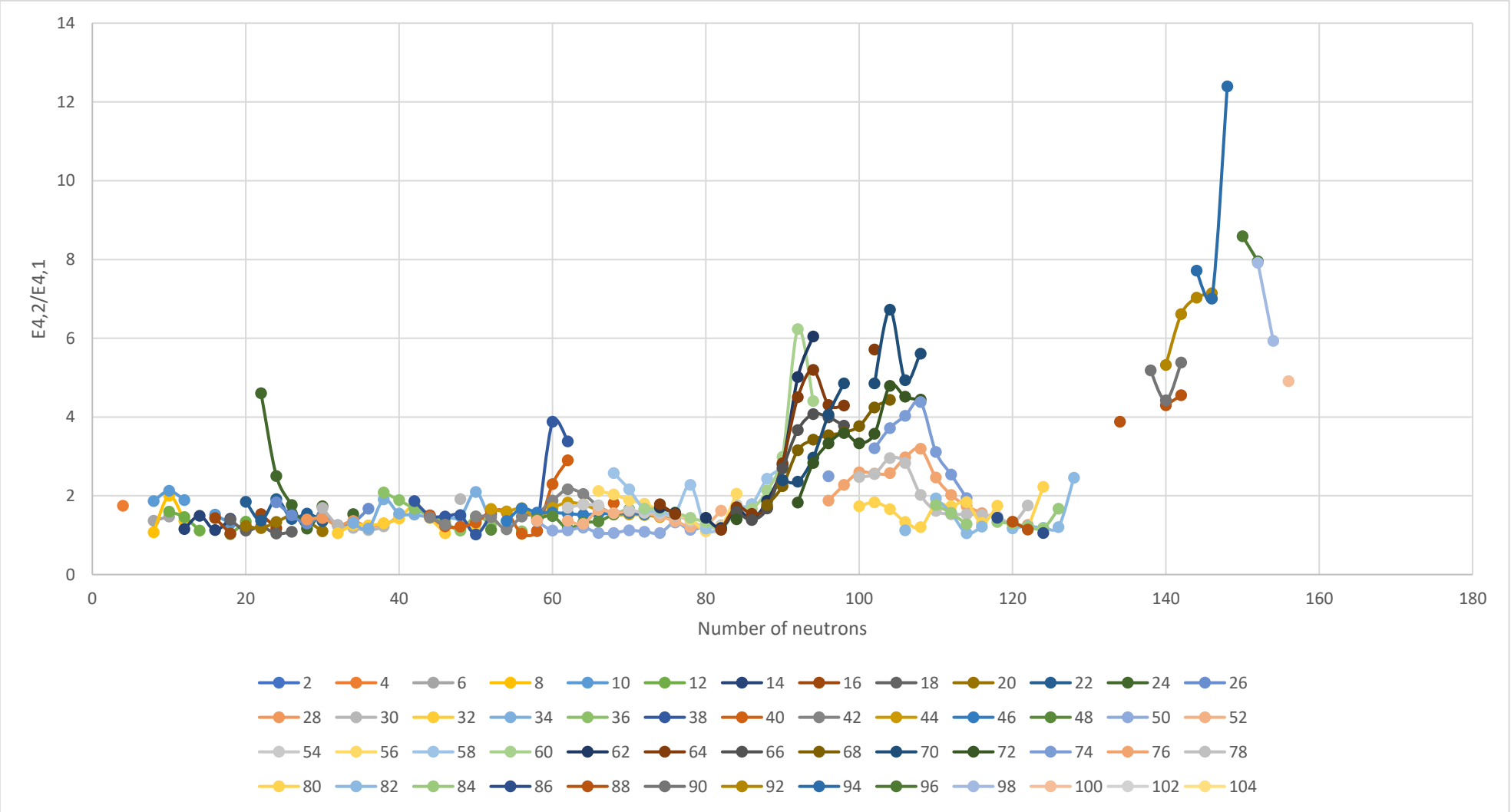

Figure II. 10 (color online) The experimental values of the energy ratio $E_{4_2^+}/E_{4_1^+}$ for all even–even nuclei plotted as a function of neutron number N along the x axis for different isotopes. The proton numbers Z for different isotopes are indicated by legend below graph.

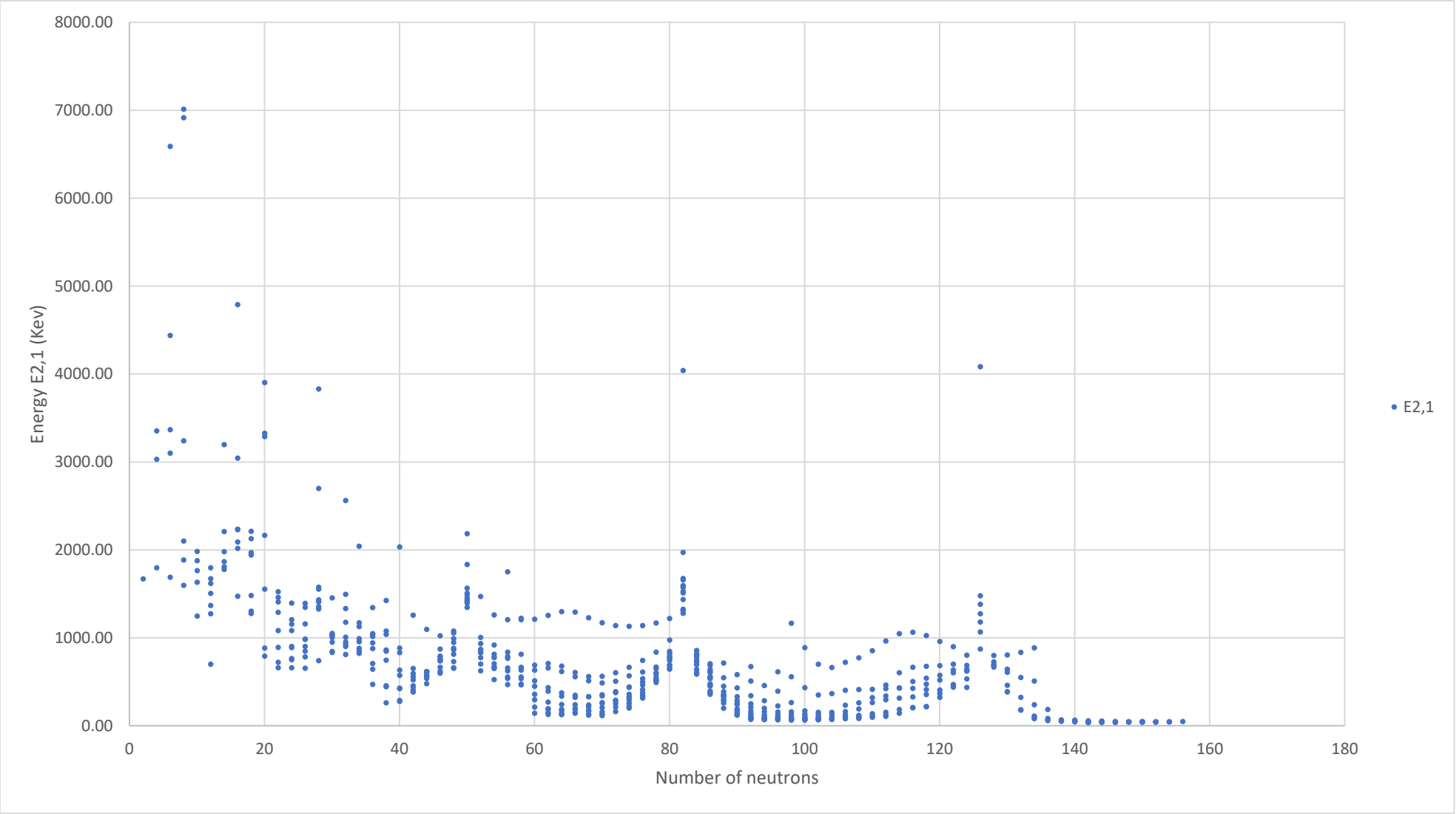

Figure II. 11 (color online) The experimental values of the energy of the first -excited 2^+ state ($E_{2_1^+}$) for all even–even nuclei plotted as a function of neutron number N along the x axis (in general).

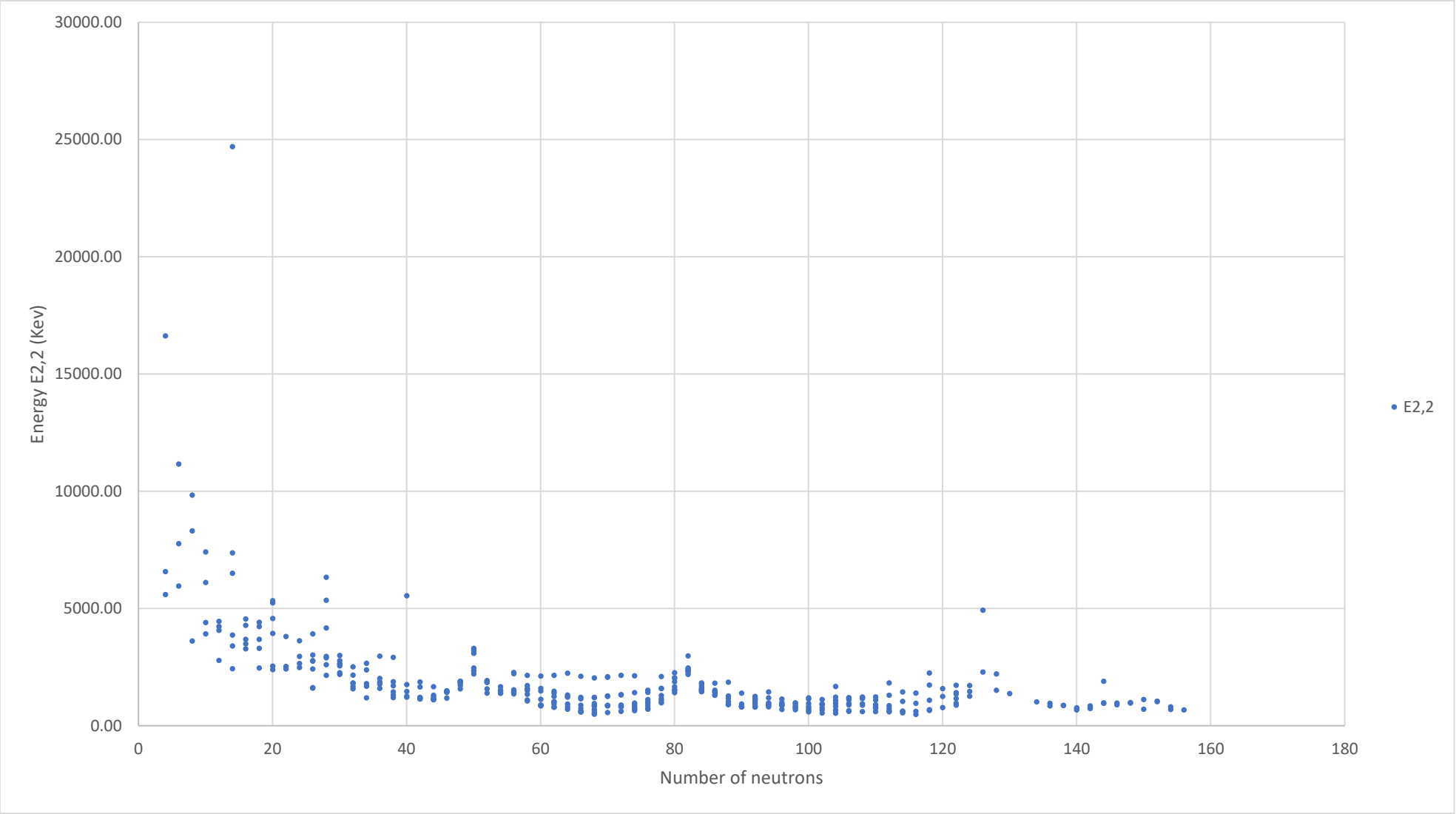

Figure II. 12 (color online) The experimental values of the energy of the second -excited 2^+ state ($E_{2_2^+}$) for all even–even nuclei plotted as a function of neutron number N along the x axis (in general).

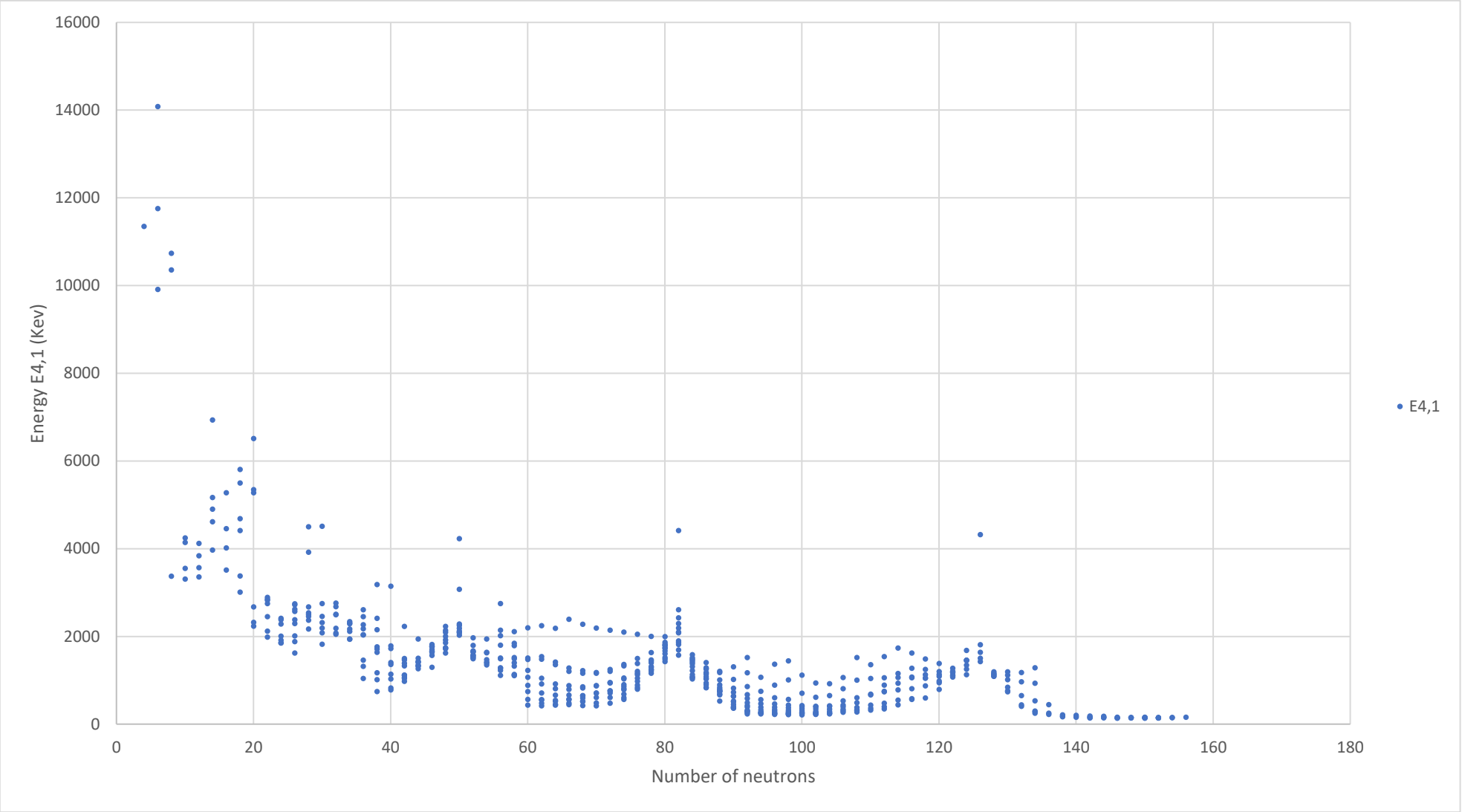

Figure II. 13 (color online) The experimental values of the energy of the first -excited 4^+ state ($E_{4_1^+}$) for all even–even nuclei plotted as a function of neutron number N along the x axis (in general).

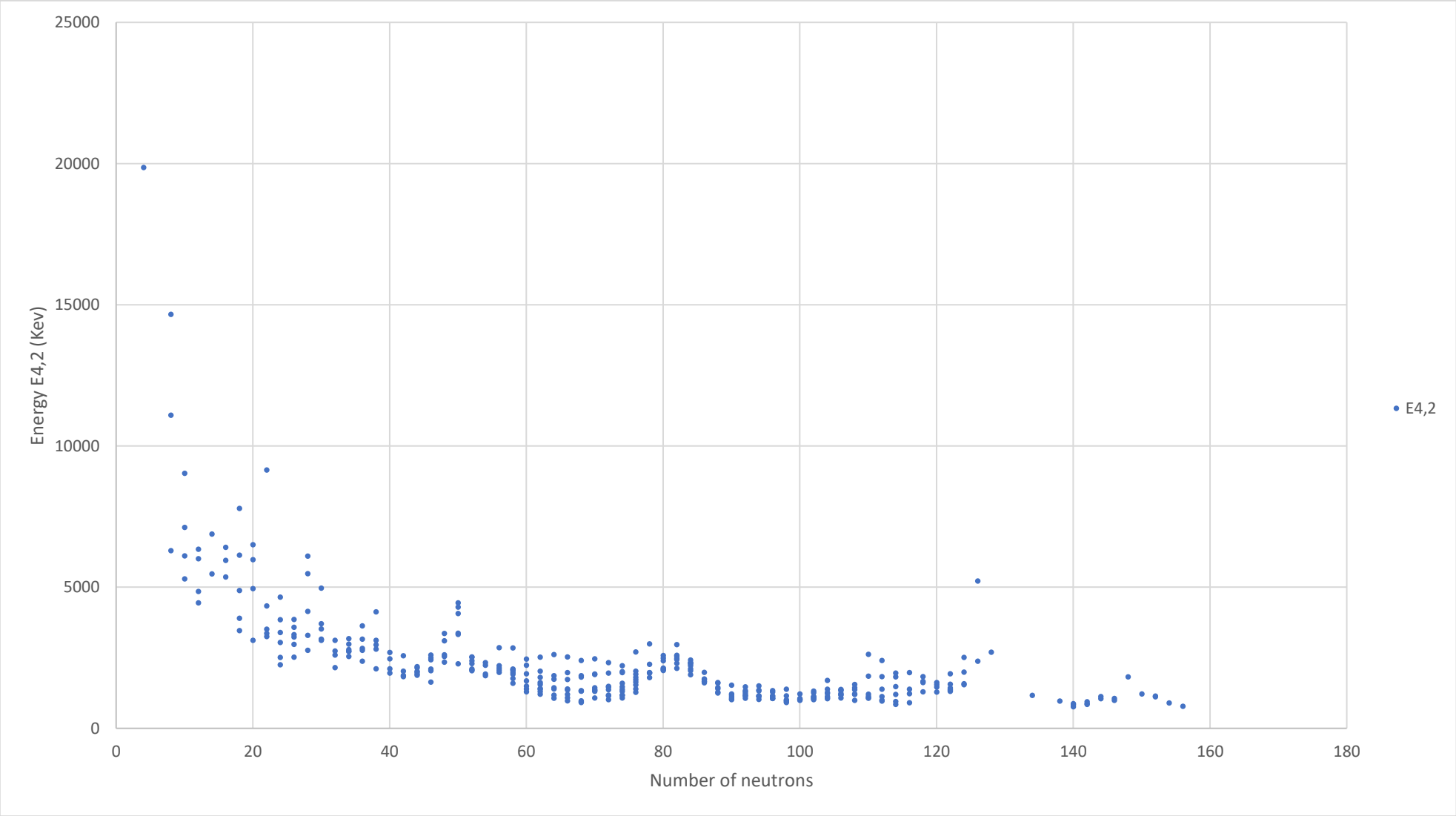

Figure II. 14 (color online) The experimental values of the energy of the second -excited 4^+ state ($E_{4_2^+}$) for all even–even nuclei plotted as a function of neutron number N along the x axis (in general).

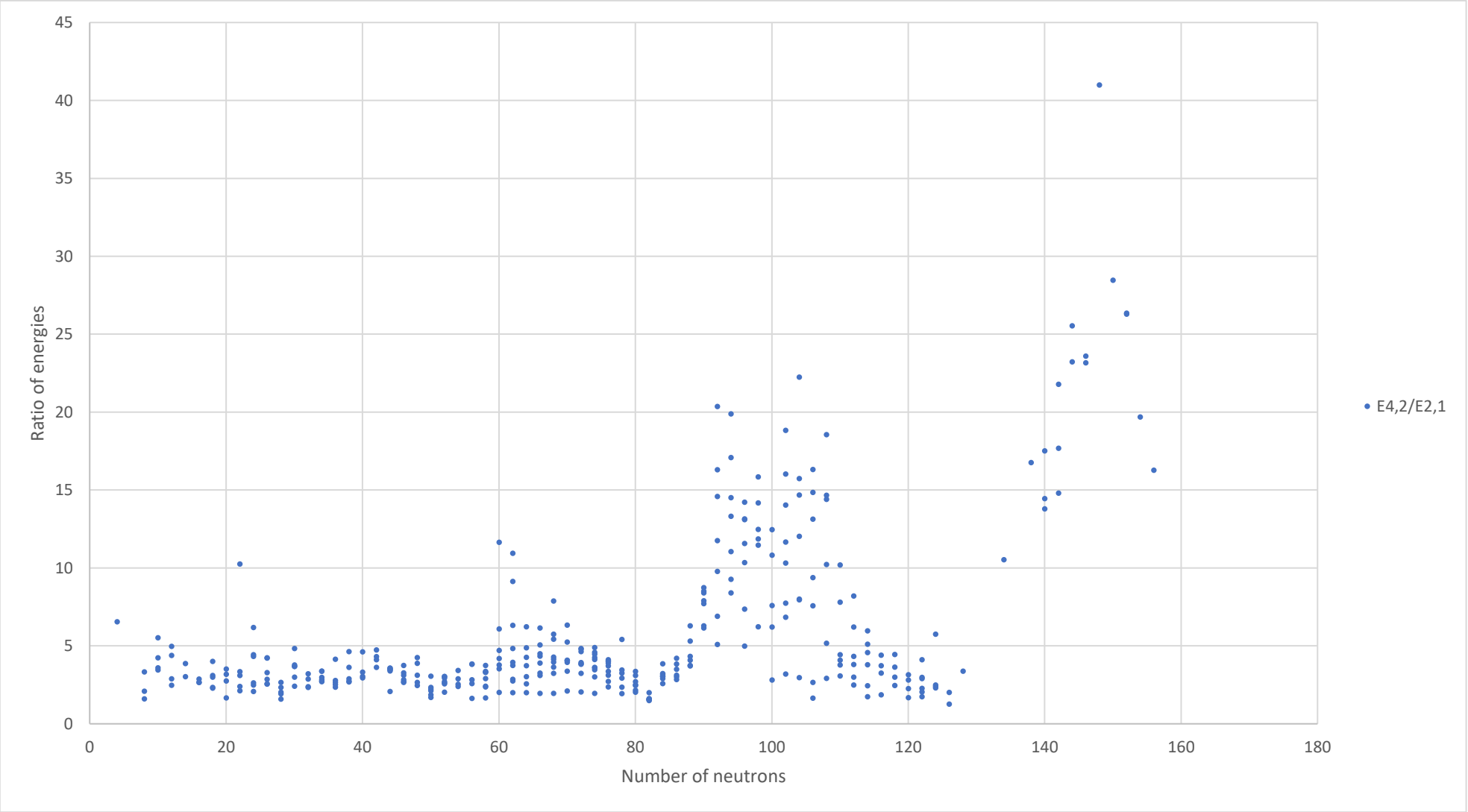

Figure II. 15 (color online) The experimental values of the energy ratio $E_{4_2^+}/E_{2_1^+}$ for all even–even nuclei plotted as a function of neutron number N along the x axis (in general).

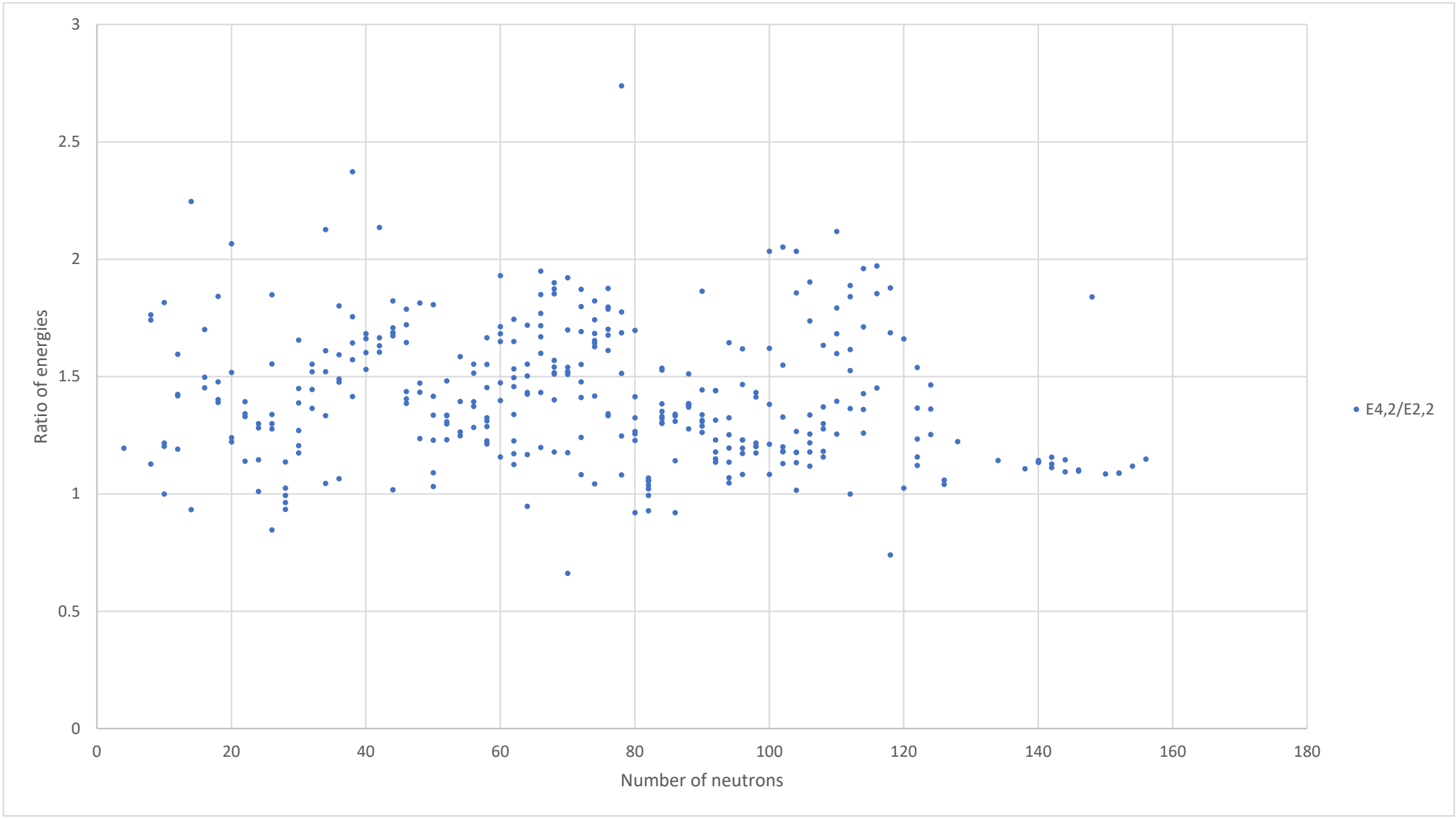

Figure II. 16 (color online) The experimental values of the energy ratio $E_{4_2^+}/E_{2_2^+}$ for all even–even nuclei plotted as a function of neutron number N along the x axis (in general).

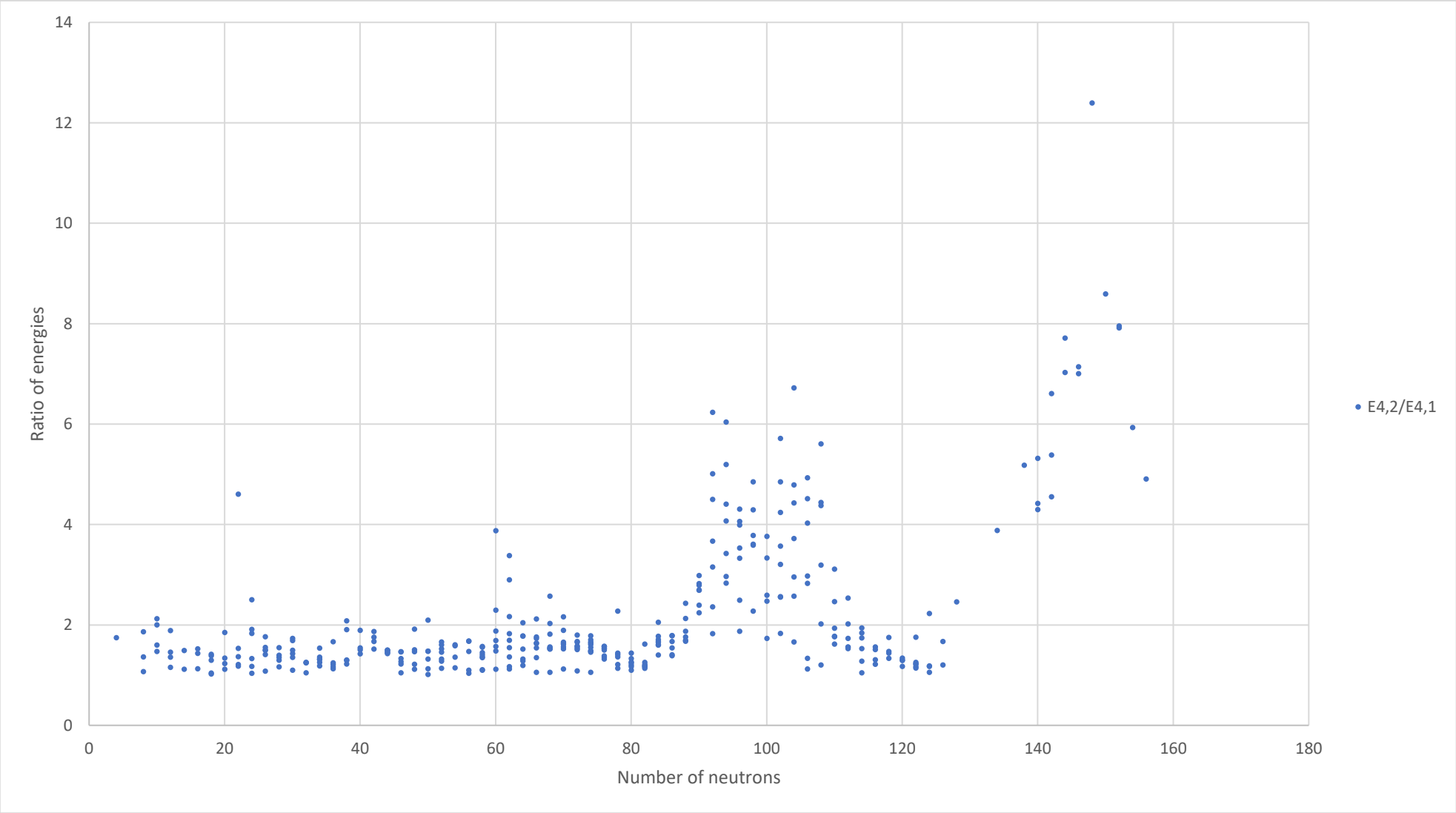

Figure II. 17 (color online) The experimental values of the energy ratio $E_{4_2^+}/E_{4_1^+}$ for all even–even nuclei plotted as a function of neutron number N along the x axis (in general).

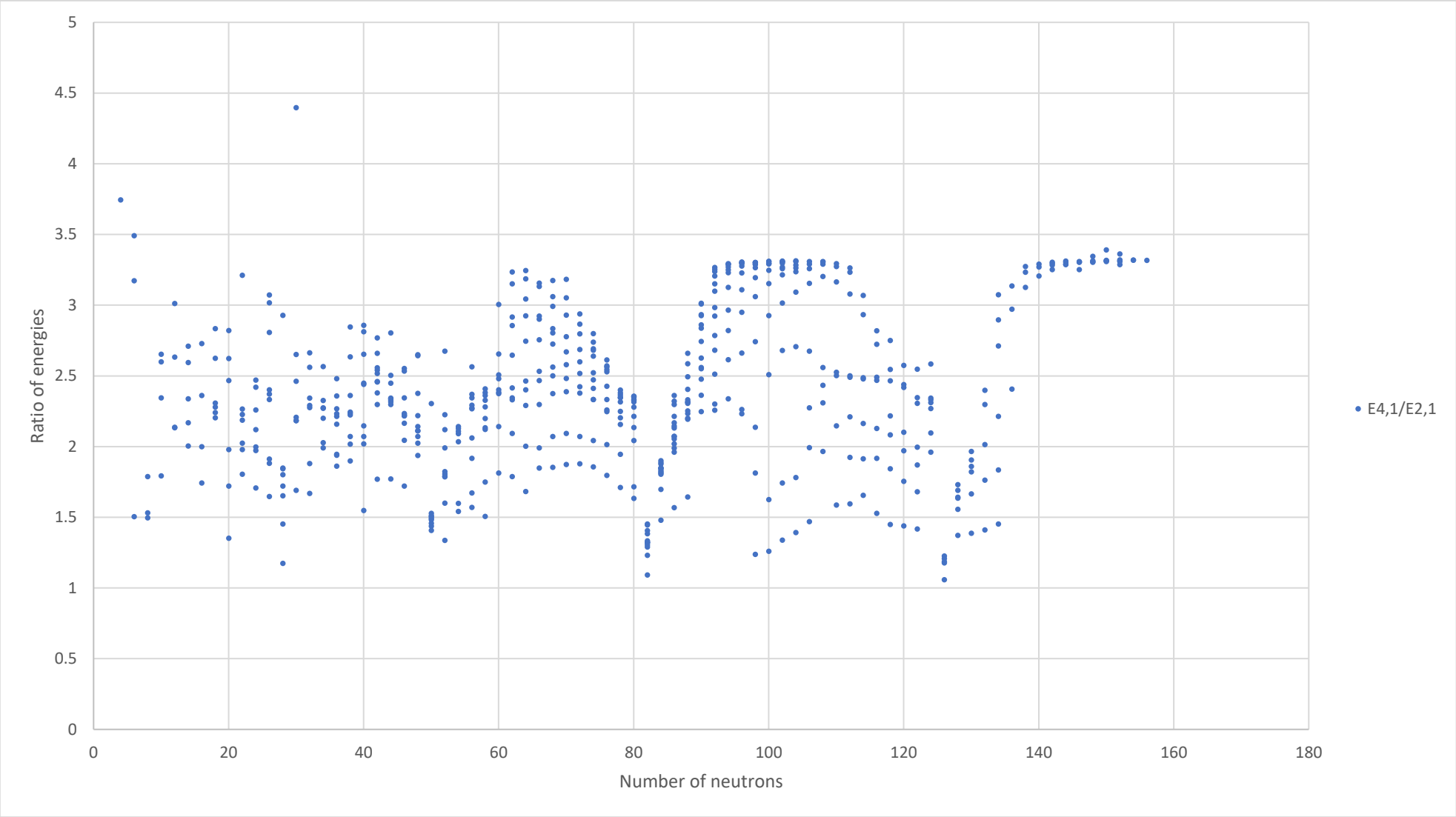

Figure II. 18 (color online) The experimental values of the energy ratio $E_{4_1^+}/E_{2_1^+}$ for all even–even nuclei plotted as a function of neutron number N along the x axis (in general).

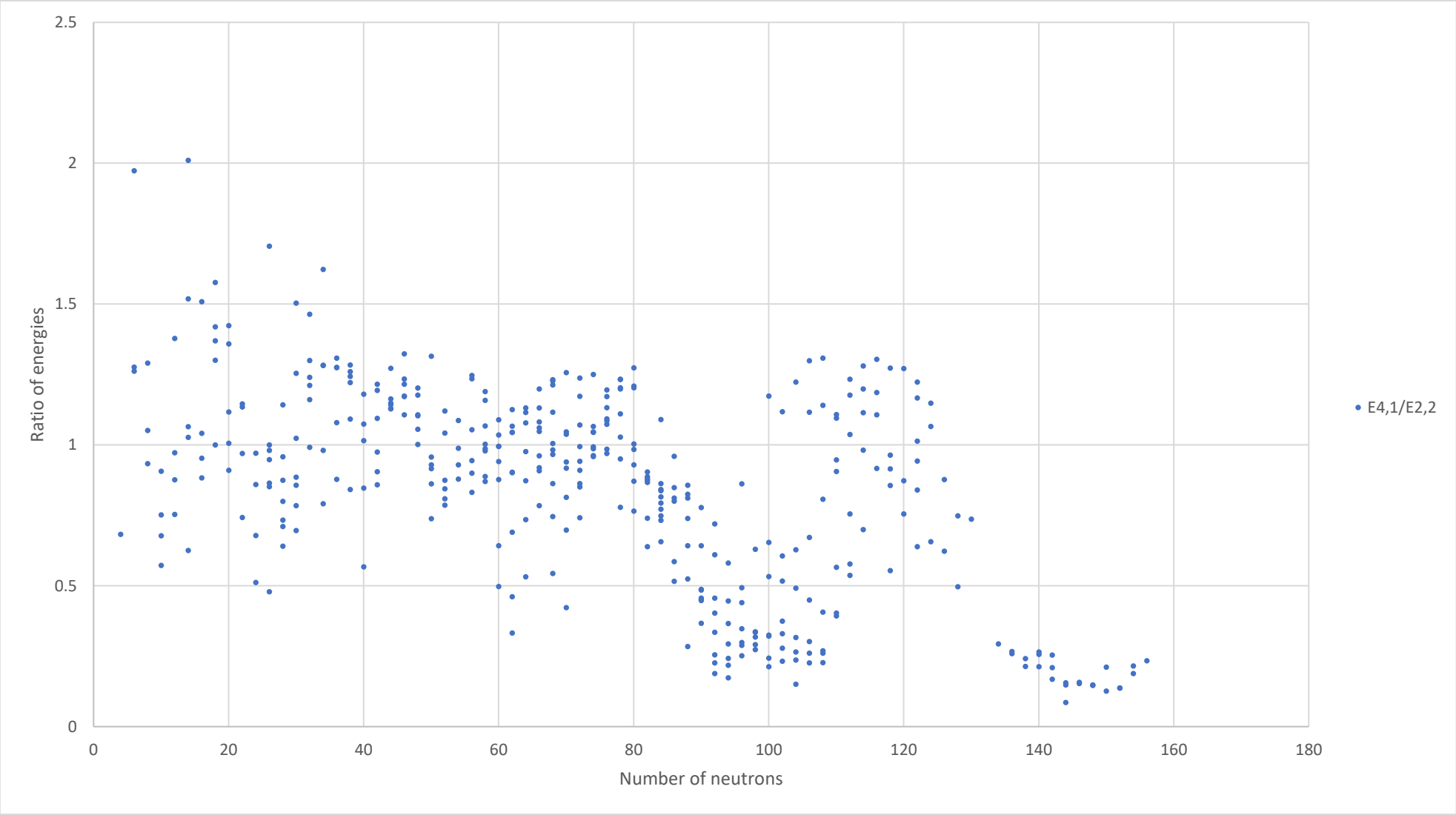

Figure II. 19 (color online) The experimental values of the energy ratio $E_{4_1^+}/E_{2_2^+}$ for all even–even nuclei plotted as a function of neutron number N along the x axis (in general).

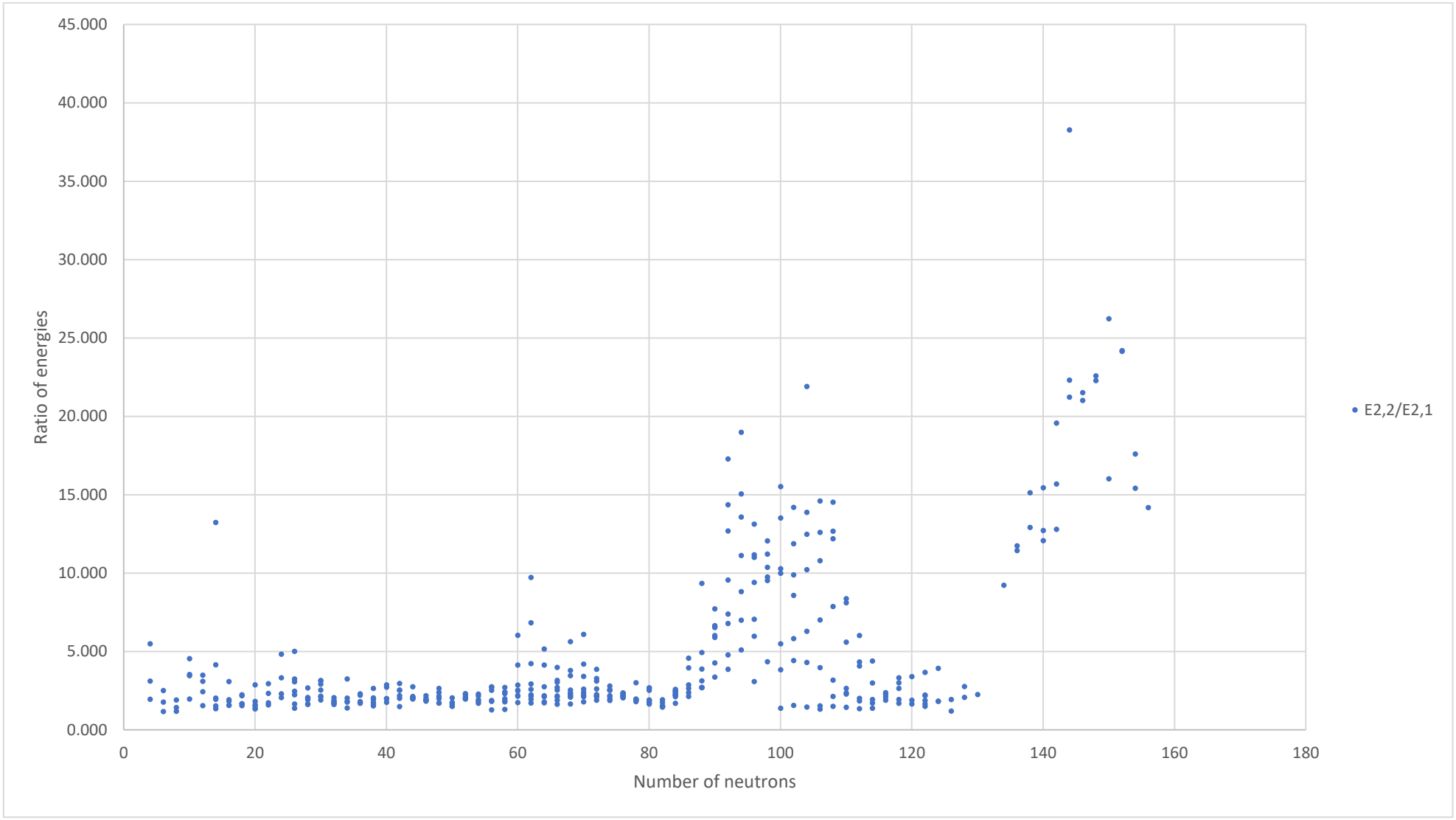

Figure II. 20 (color online) The experimental values of the energy ratio $E_{2_2^+}/E_{2_1^+}$ for all even–even nuclei plotted as a function of neutron number N along the x axis (in general).

Chapter III

Two dimensional figures of the values of energy levels and energy ratios over all even–even nuclei for each chain of isotopes

He isotopes (Z=2)

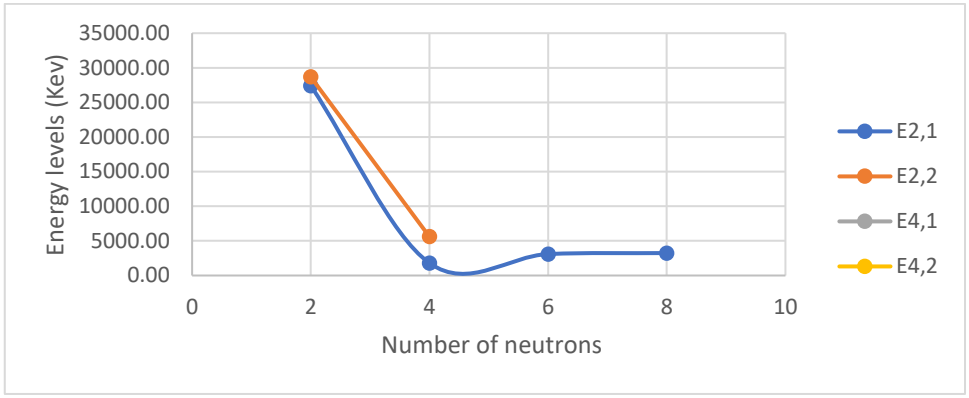

A

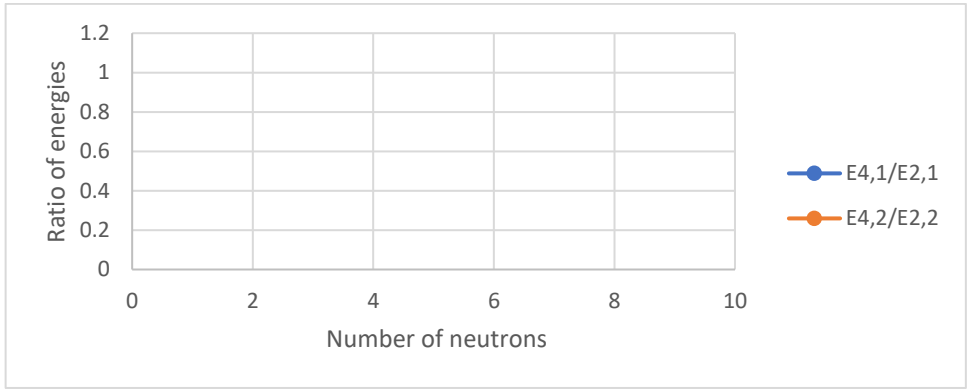

B

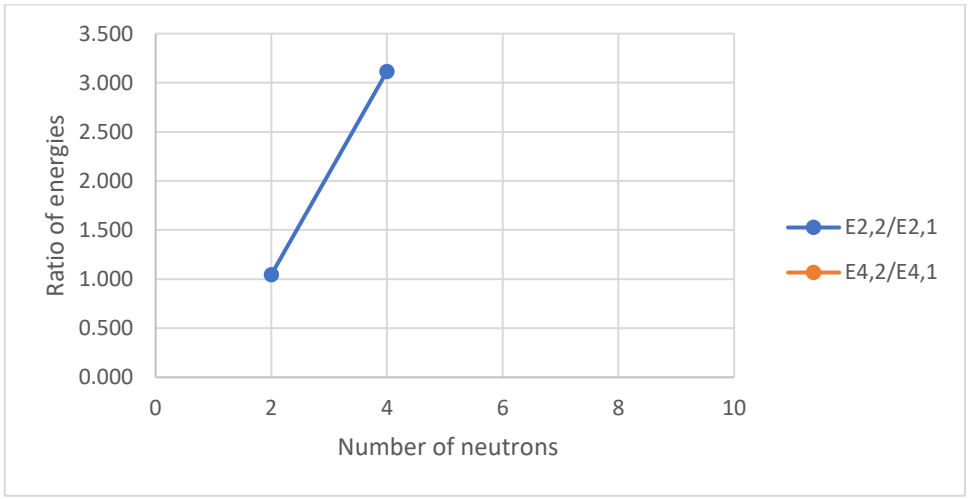

C

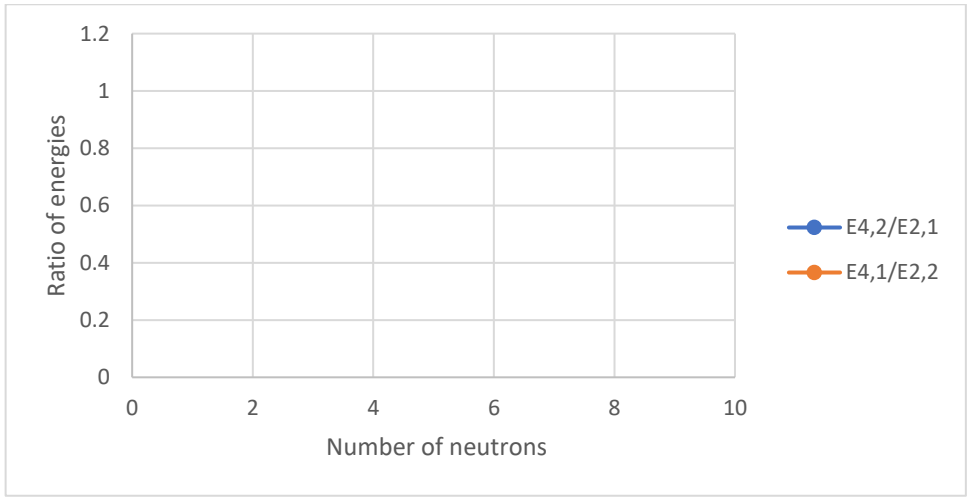

D

Figure III. 1 (color online) Panel **A** represents the comparison of the experimental energy levels of the lowest 2_1^+, 2_2^+, 4_1^+ and 4_2^+ states for the chain of He isotopes. Panels **B, C, D** represent the comparison of the experimental energy ratios ($E_{4_1^+}/E_{2_1^+}$ and $E_{4_2^+}/E_{2_2^+}$), ($E_{2_2^+}/E_{2_1^+}$ and $E_{4_2^+}/E_{4_1^+}$) and ($E_{4_2^+}/E_{2_1^+}$ and $E_{4_1^+}/E_{2_2^+}$), respectively, for the chain of He isotopes.

Be isotopes (Z=4)

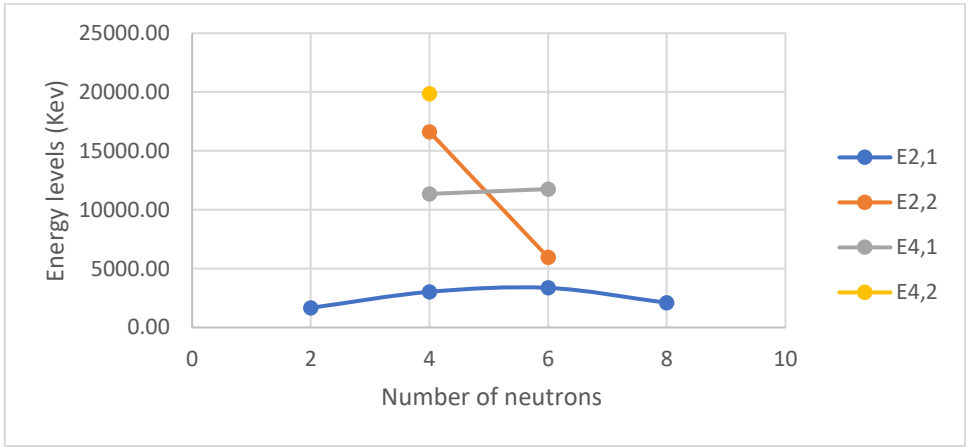

A

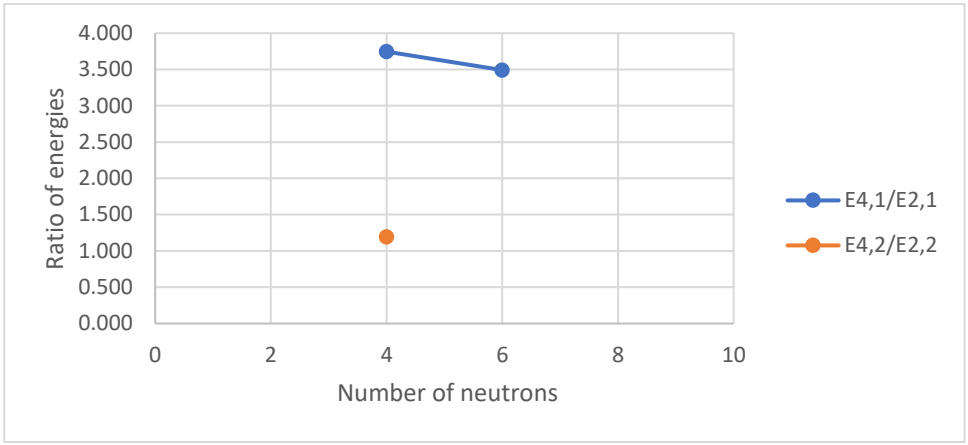

B

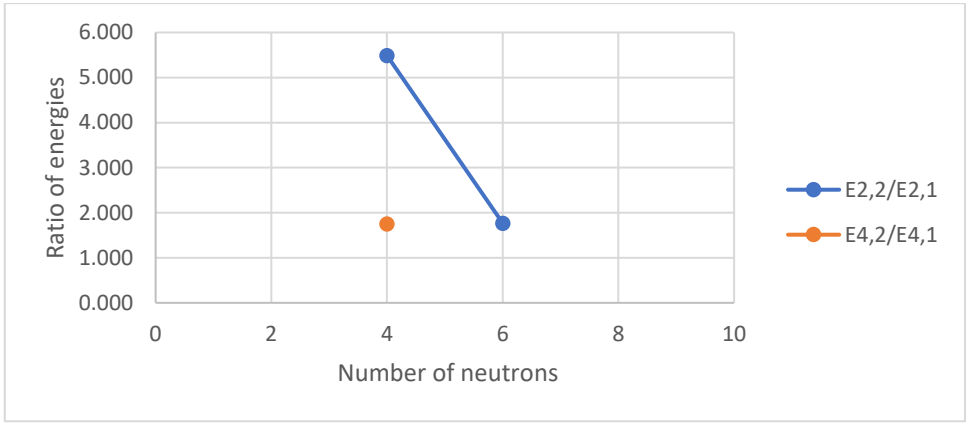

C

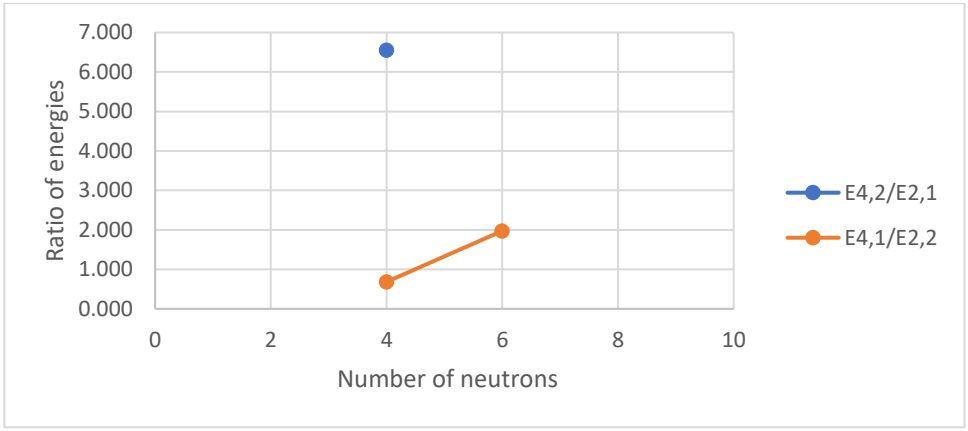

D

Figure III. 2 (color online) Panel **A** represents the comparison of the experimental energy levels of the lowest 2_1^+, 2_2^+, 4_1^+ and 4_2^+ states for the chain of Be isotopes. Panels **B, C, D** represent the comparison of the experimental energy ratios ($E_{4_1^+}/E_{2_1^+}$ and $E_{4_2^+}/E_{2_2^+}$), ($E_{2_2^+}/E_{2_1^+}$ and $E_{4_2^+}/E_{4_1^+}$) and ($E_{4_2^+}/E_{2_1^+}$ and $E_{4_1^+}/E_{2_2^+}$), respectively, for the chain of Be isotopes.

C isotopes (Z=6)

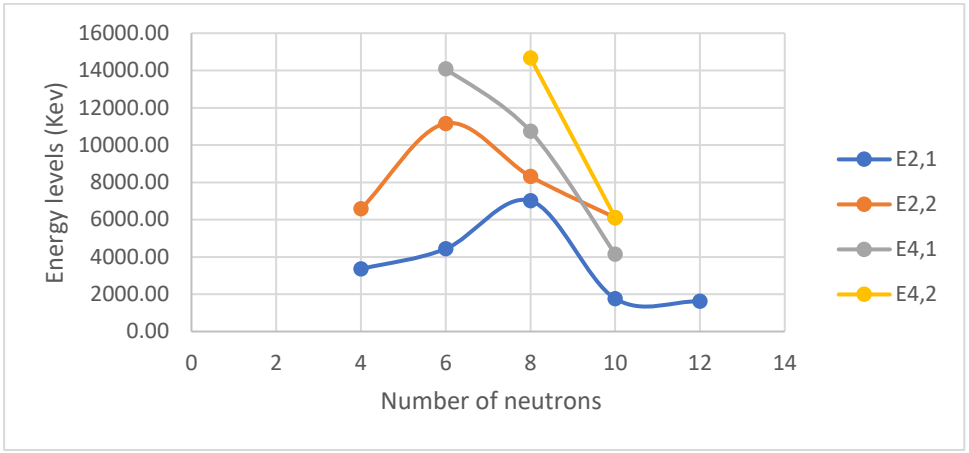

A

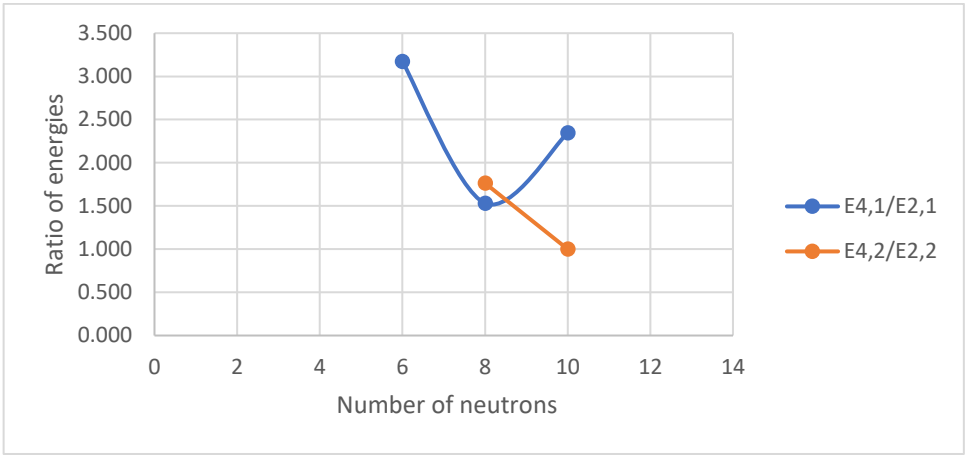

B

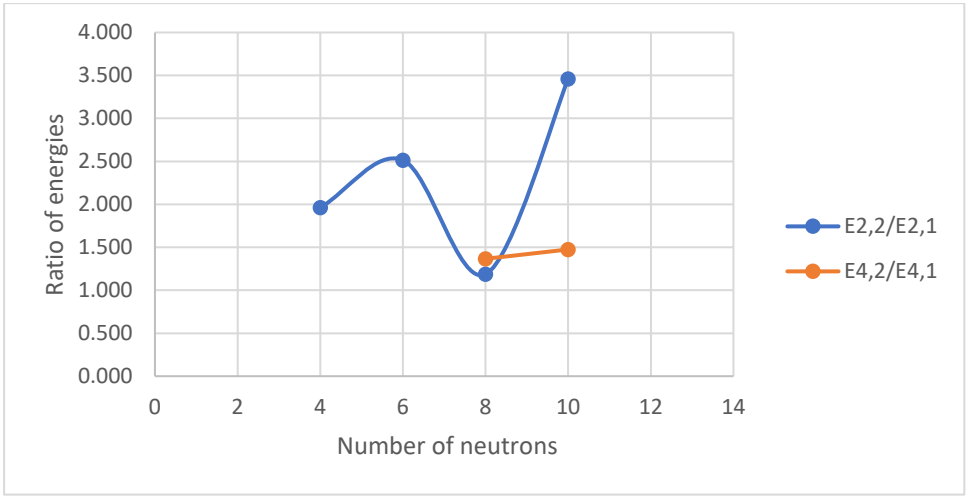

C

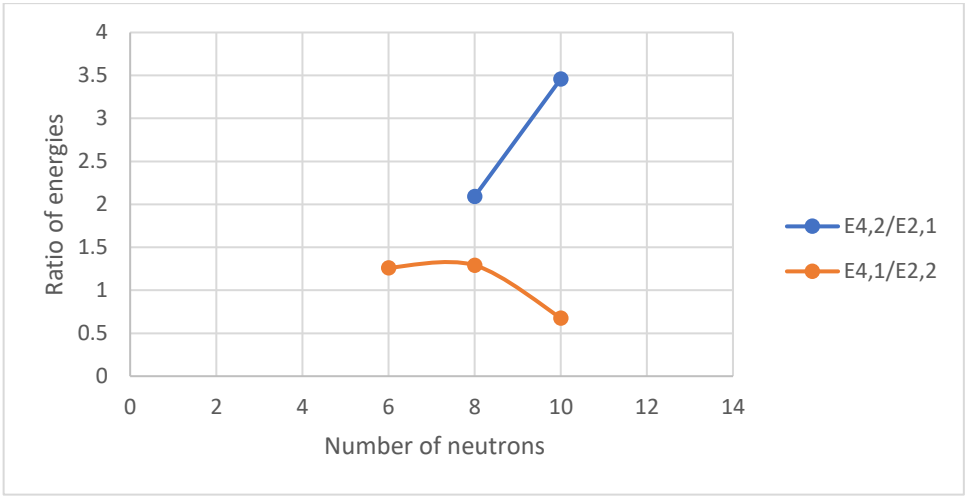

D

Figure III. 3 (color online) Panel **A** represents the comparison of the experimental energy levels of the lowest 2_1^+, 2_2^+, 4_1^+ and 4_2^+ states for the chain of C isotopes. Panels **B, C, D** represent the comparison of the experimental energy ratios ($E_{4_1^+}/E_{2_1^+}$ and $E_{4_2^+}/E_{2_2^+}$), ($E_{2_2^+}/E_{2_1^+}$ and $E_{4_2^+}/E_{4_1^+}$) and ($E_{4_2^+}/E_{2_1^+}$ and $E_{4_1^+}/E_{2_2^+}$), respectively, for the chain of C isotopes.

O isotopes (Z =8)

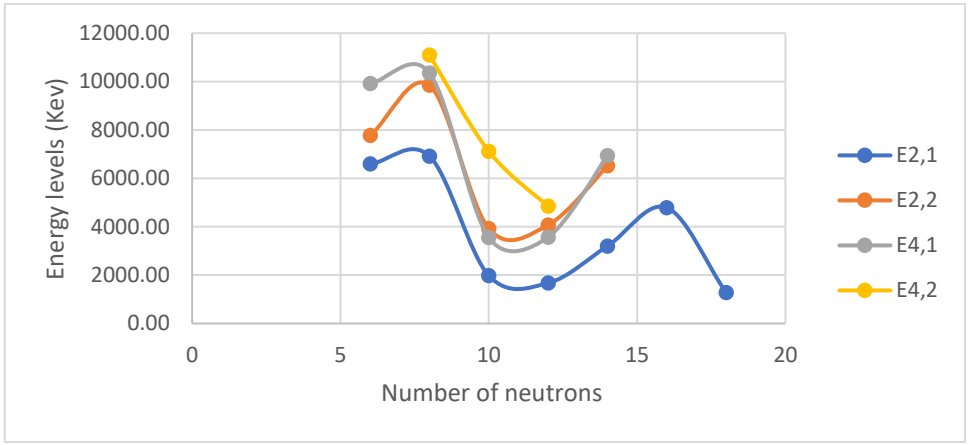

A

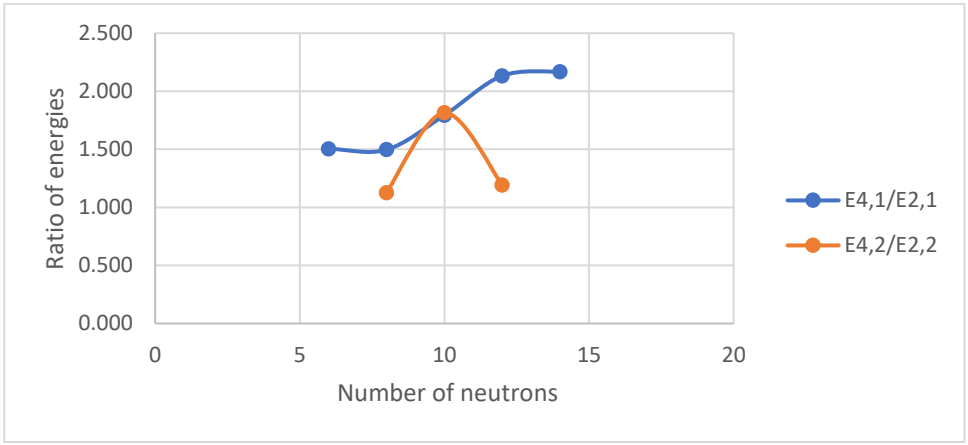

B

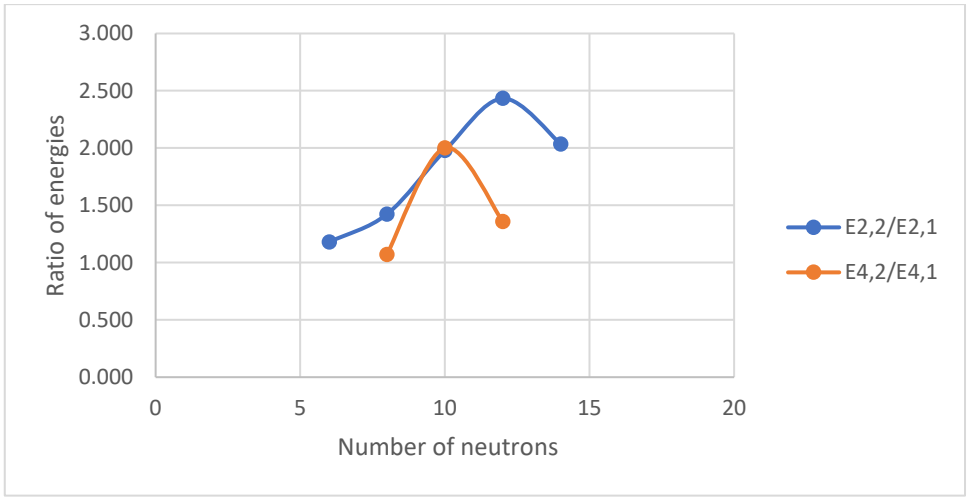

C

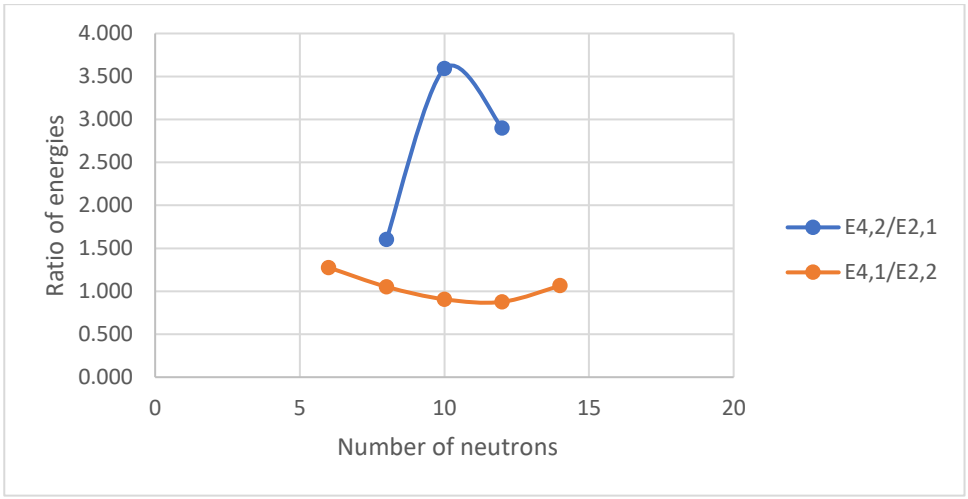

D

Figure III. 4 (color online) Panel **A** represents the comparison of the experimental energy levels of the lowest 2_1^+, 2_2^+, 4_1^+ and 4_2^+ states for the chain of O isotopes. Panels **B, C, D** represent the comparison of the experimental energy ratios ($E_{4_1^+}/E_{2_1^+}$ and $E_{4_2^+}/E_{2_2^+}$), ($E_{2_2^+}/E_{2_1^+}$ and $E_{4_2^+}/E_{4_1^+}$) and ($E_{4_2^+}/E_{2_1^+}$ and $E_{4_1^+}/E_{2_2^+}$), respectively, for the chain of O isotopes.

Ne isotopes (Z =10)

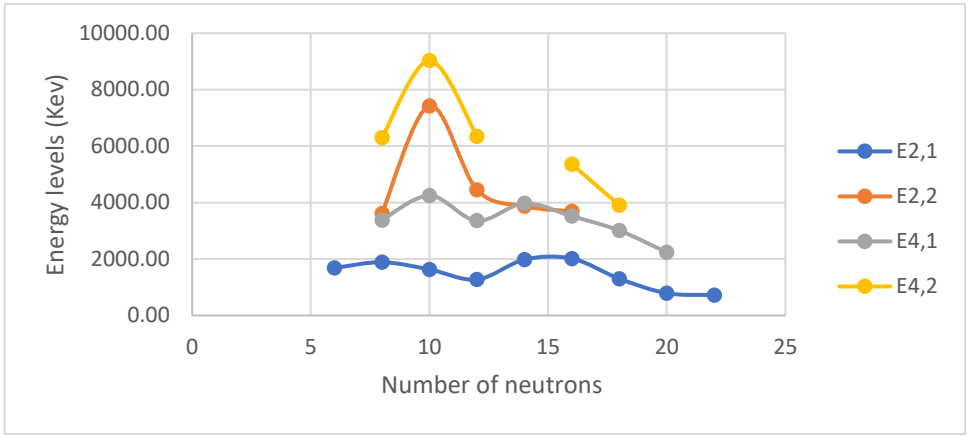

A

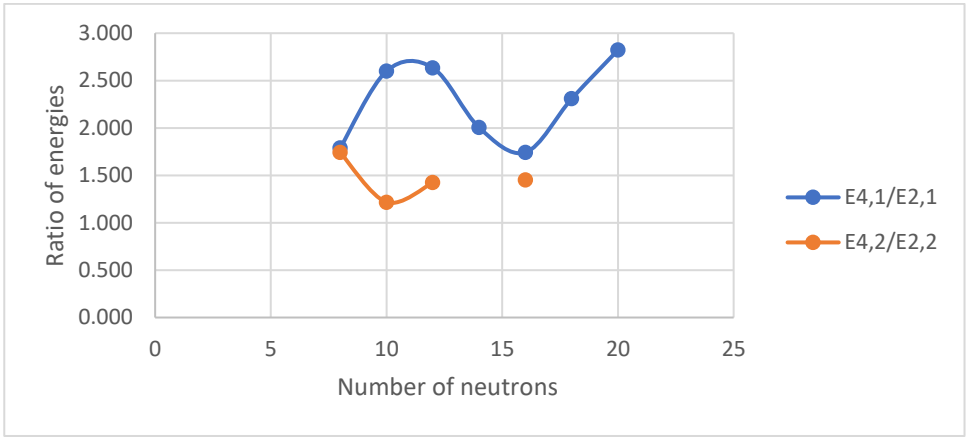

B

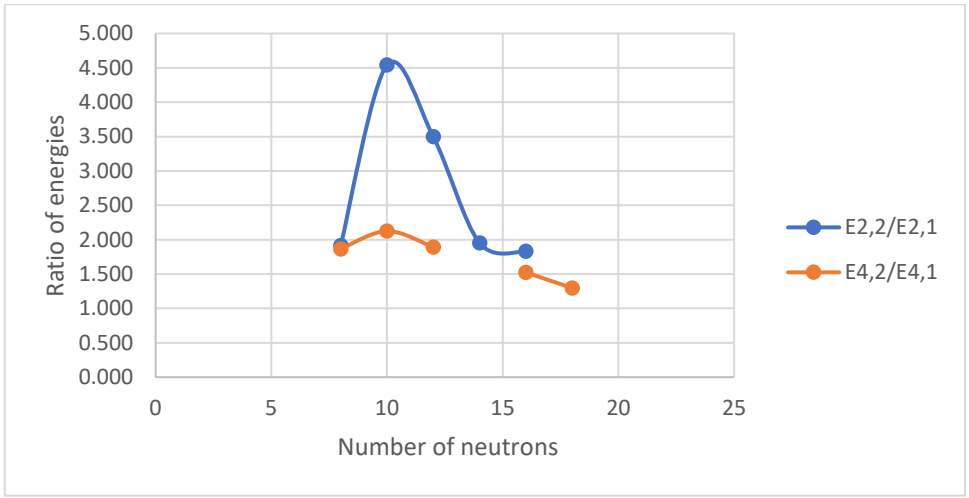

C

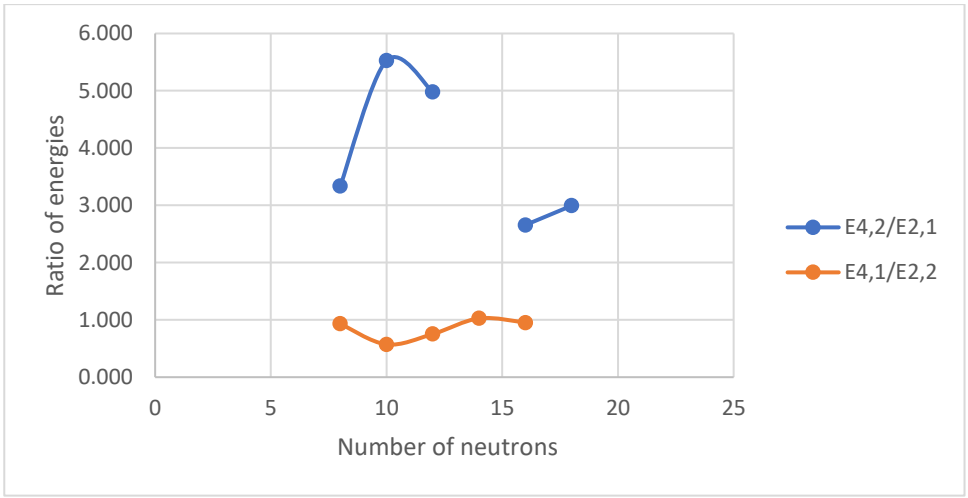

D

Figure III. 5 (color online) Panel **A** represents the comparison of the experimental energy levels of the lowest 2_1^+, 2_2^+, 4_1^+ and 4_2^+ states for the chain of Ne isotopes. Panels **B, C, D** represent the comparison of the experimental energy ratios ($E_{4_1^+}/E_{2_1^+}$ and $E_{4_2^+}/E_{2_2^+}$), ($E_{2_2^+}/E_{2_1^+}$ and $E_{4_2^+}/E_{4_1^+}$) and ($E_{4_2^+}/E_{2_1^+}$ and $E_{4_1^+}/E_{2_2^+}$), respectively, for the chain of Ne isotopes.

Mg isotopes (Z =12)

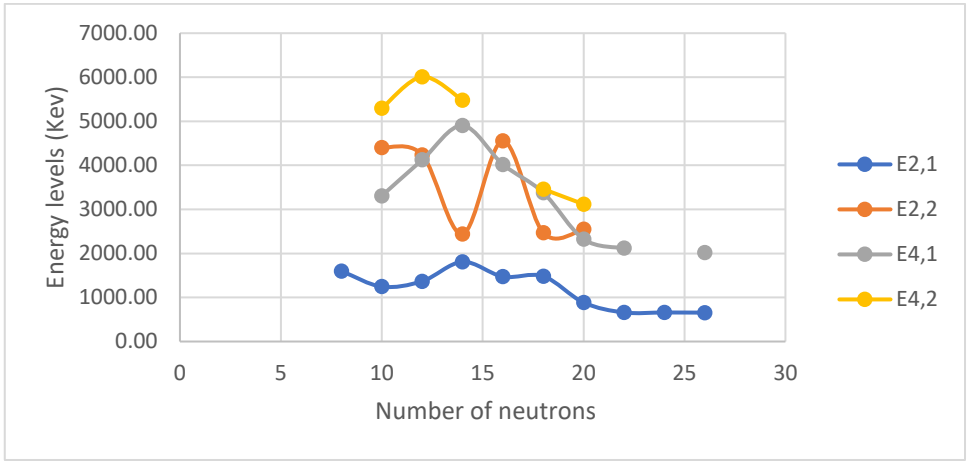

A

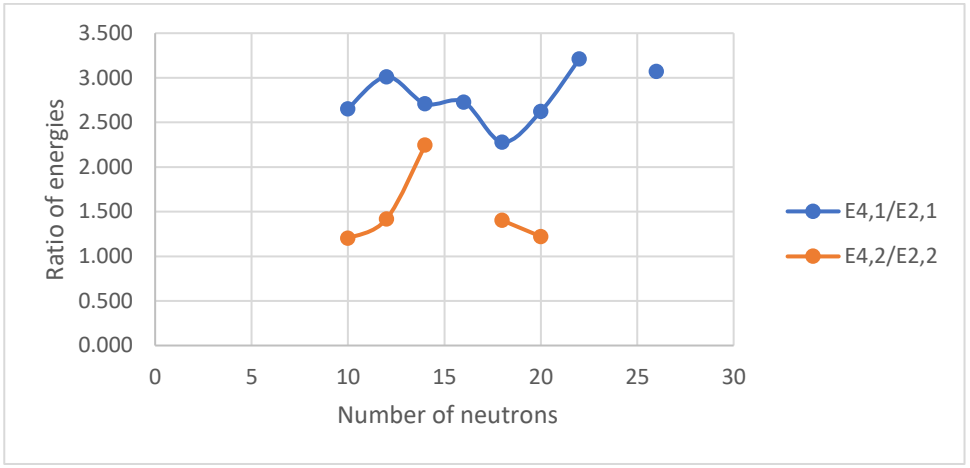

B

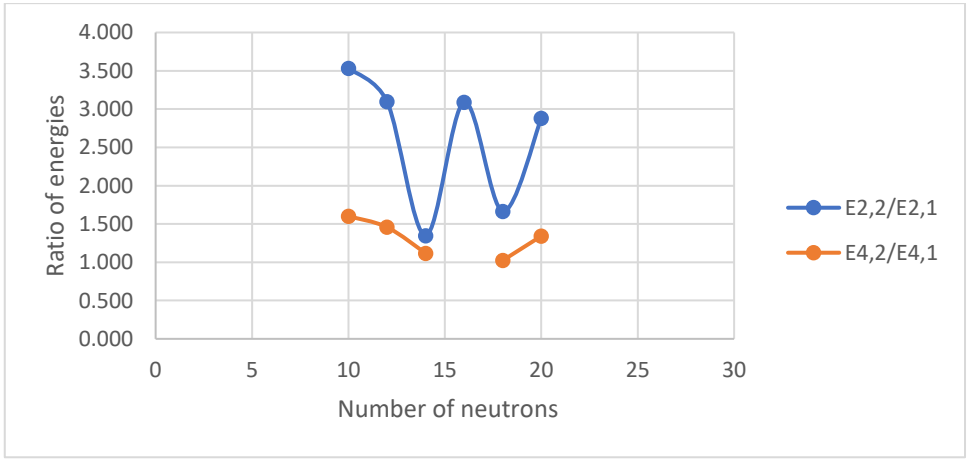

C

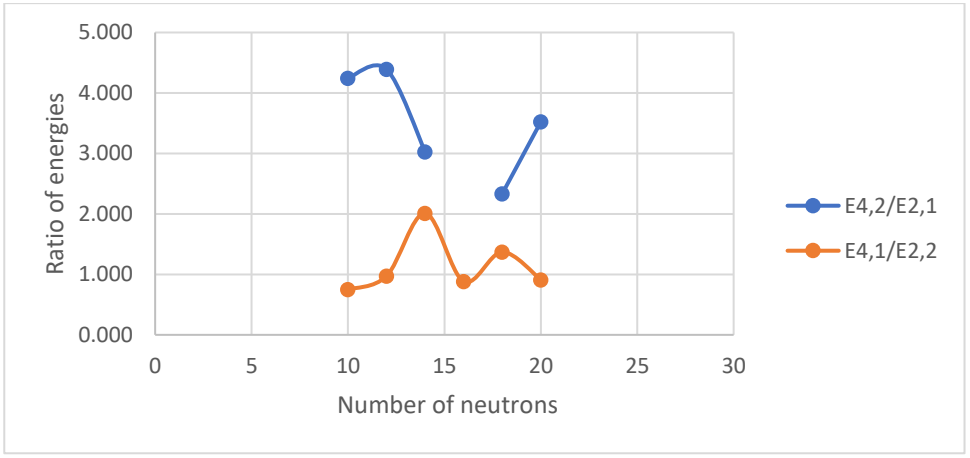

D

Figure III. 6 (color online) Panel **A** represents the comparison of the experimental energy levels of the lowest 2_1^+, 2_2^+, 4_1^+ and 4_2^+ states for the chain of Mg isotopes. Panels **B, C, D** represent the comparison of the experimental energy ratios ($E_{4_1^+}/E_{2_1^+}$ and $E_{4_2^+}/E_{2_2^+}$), ($E_{2_2^+}/E_{2_1^+}$ and $E_{4_2^+}/E_{4_1^+}$) and ($E_{4_2^+}/E_{2_1^+}$ and $E_{4_1^+}/E_{2_2^+}$), respectively, for the chain of Mg isotopes.

Si isotopes (Z =14)

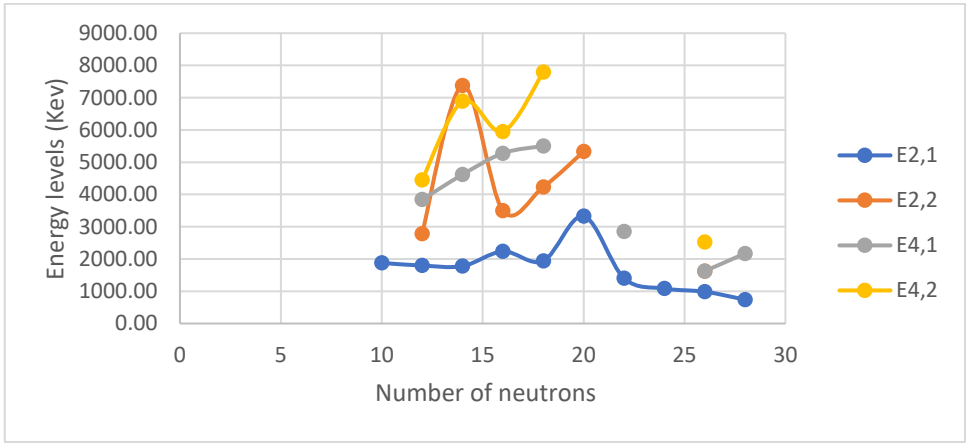

A

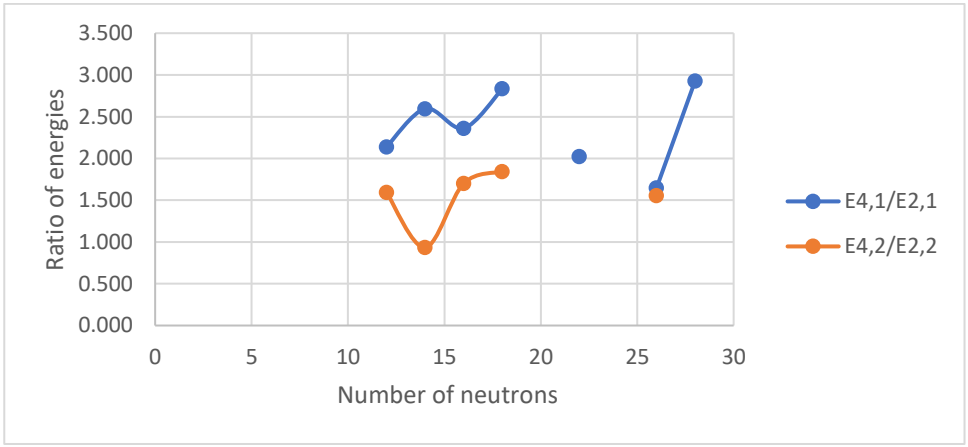

B

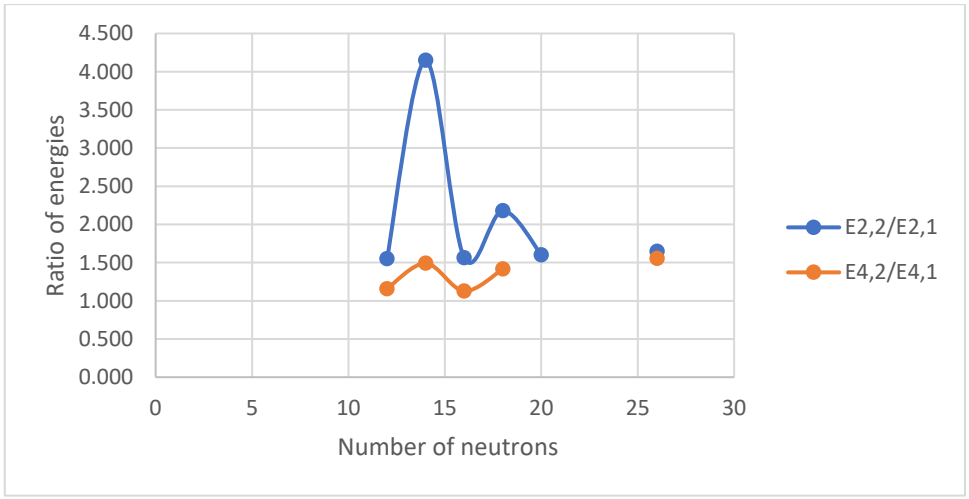

C

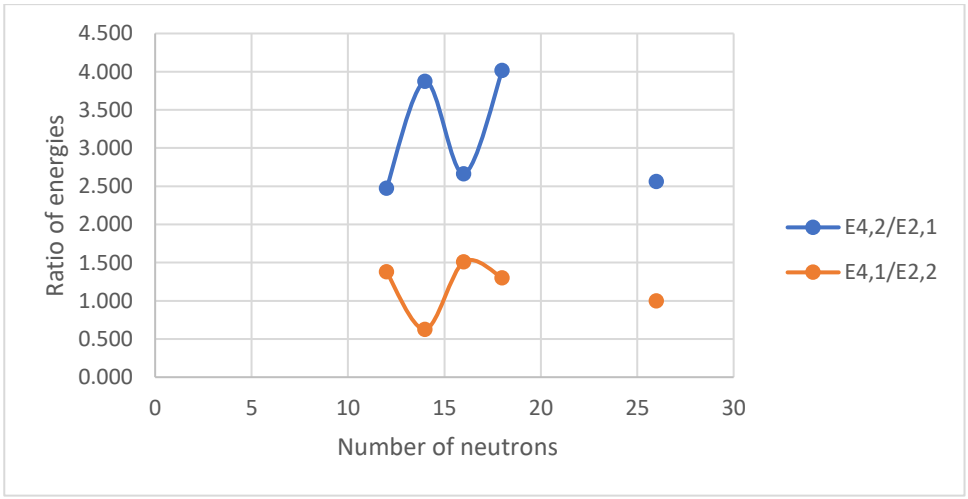

D

Figure III. 7 (color online) Panel **A** represents the comparison of the experimental energy levels of the lowest 2_1^+, 2_2^+, 4_1^+ and 4_2^+ states for the chain of Si isotopes. Panels **B, C, D** represent the comparison of the experimental energy ratios ($E_{4_1^+}/E_{2_1^+}$ and $E_{4_2^+}/E_{2_2^+}$), ($E_{2_2^+}/E_{2_1^+}$ and $E_{4_2^+}/E_{4_1^+}$) and ($E_{4_2^+}/E_{2_1^+}$ and $E_{4_1^+}/E_{2_2^+}$), respectively, for the chain of Si isotopes.

S isotopes (Z =16)

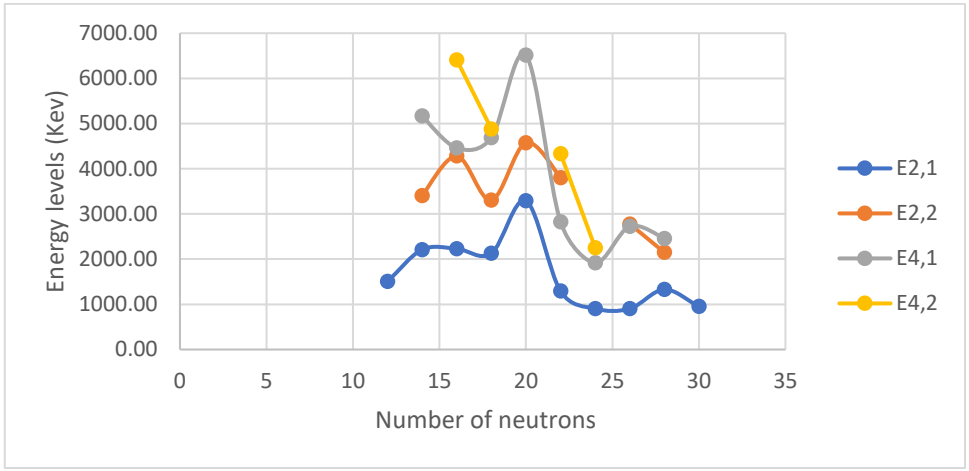

A

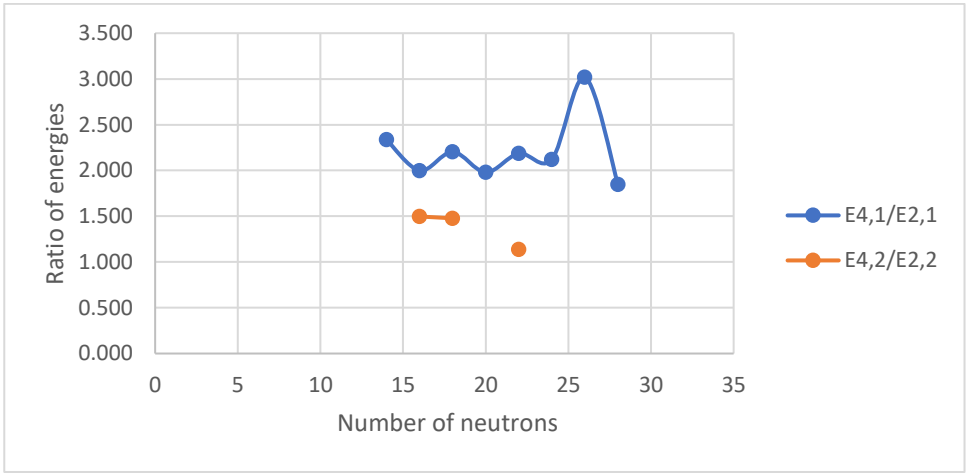

B

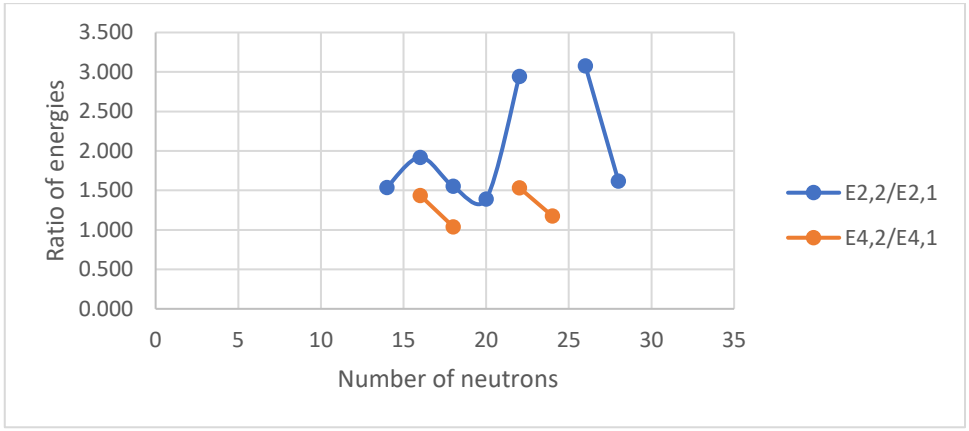

C

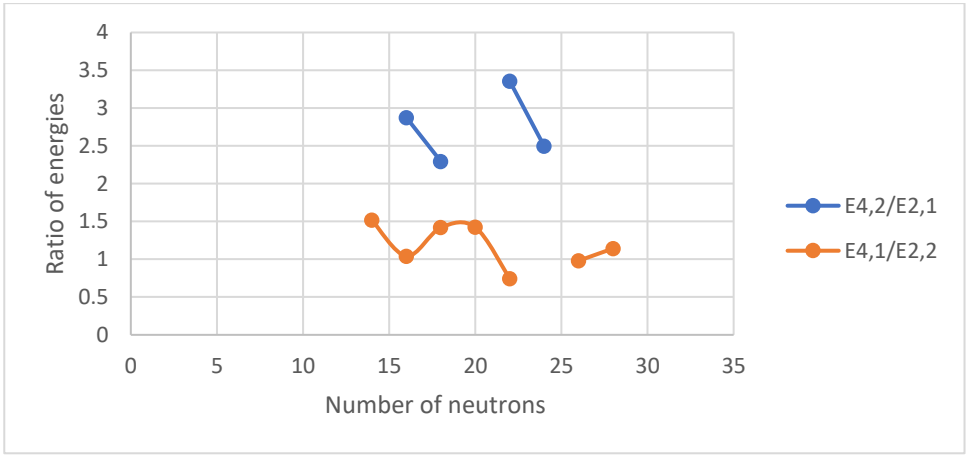

D

Figure III. 8 (color online) Panel **A** represents the comparison of the experimental energy levels of the lowest 2_1^+, 2_2^+, 4_1^+ and 4_2^+ states for the chain of S isotopes. Panels **B, C, D** represent the comparison of the experimental energy ratios ($E_{4_1^+}/E_{2_1^+}$ and $E_{4_2^+}/E_{2_2^+}$), ($E_{2_2^+}/E_{2_1^+}$ and $E_{4_2^+}/E_{4_1^+}$) and ($E_{4_2^+}/E_{2_1^+}$ and $E_{4_1^+}/E_{2_2^+}$), respectively, for the chain of S isotopes.

Ar isotopes (Z =18)

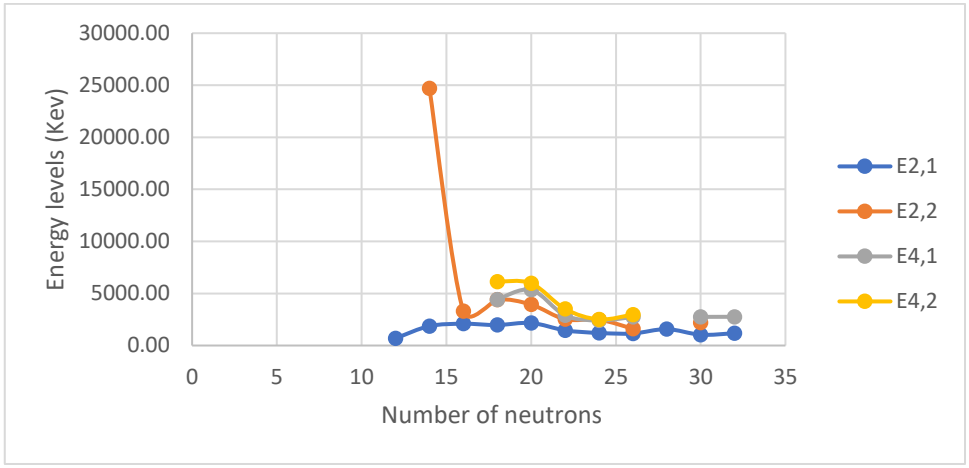

A

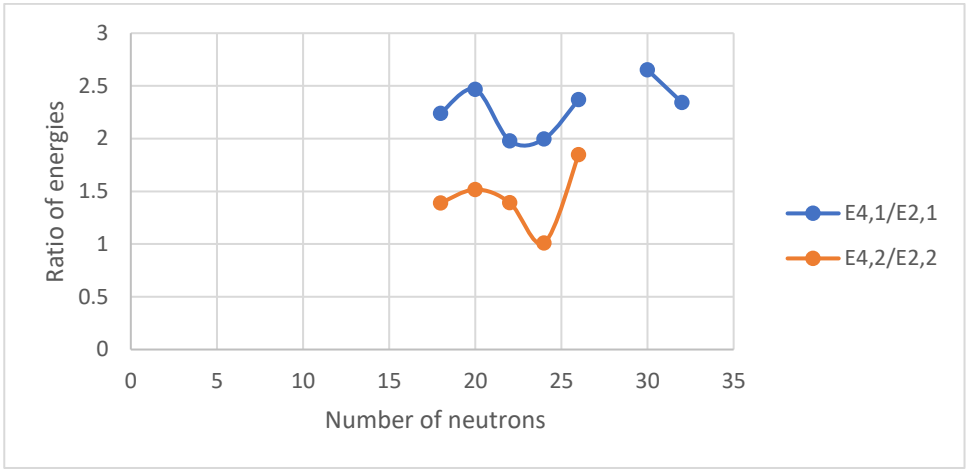

B

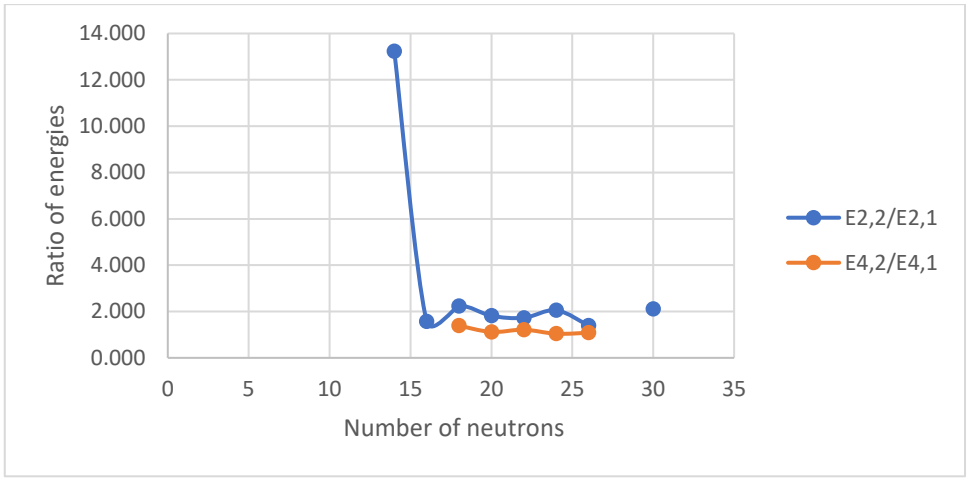

C

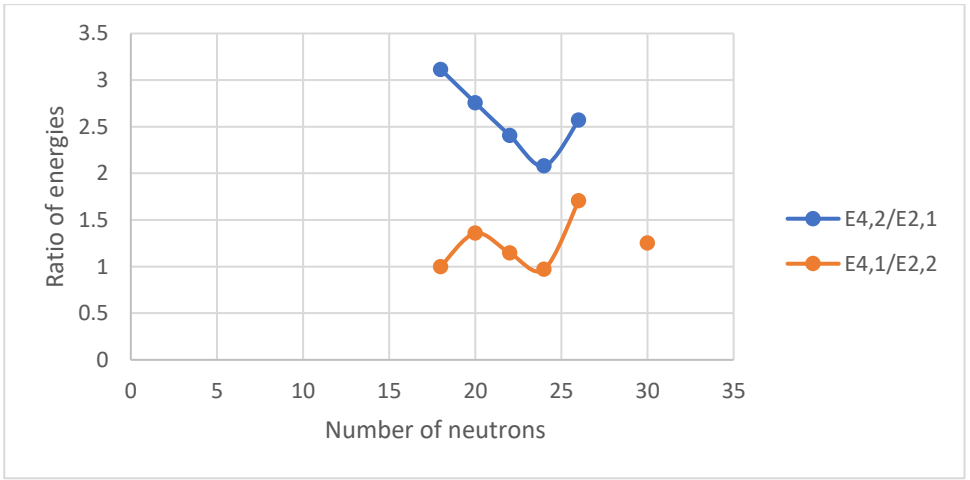

D

Figure III. 9 (color online) Panel **A** represents the comparison of the experimental energy levels of the lowest 2_1^+, 2_2^+, 4_1^+ and 4_2^+ states for the chain of Ar isotopes. Panels **B, C, D** represent the comparison of the experimental energy ratios ($E_{4_1^+}/E_{2_1^+}$ and $E_{4_2^+}/E_{2_2^+}$), ($E_{2_2^+}/E_{2_1^+}$ and $E_{4_2^+}/E_{4_1^+}$) and ($E_{4_2^+}/E_{2_1^+}$ and $E_{4_1^+}/E_{2_2^+}$), respectively, for the chain of Ar isotopes.

Ca isotopes (Z =20)

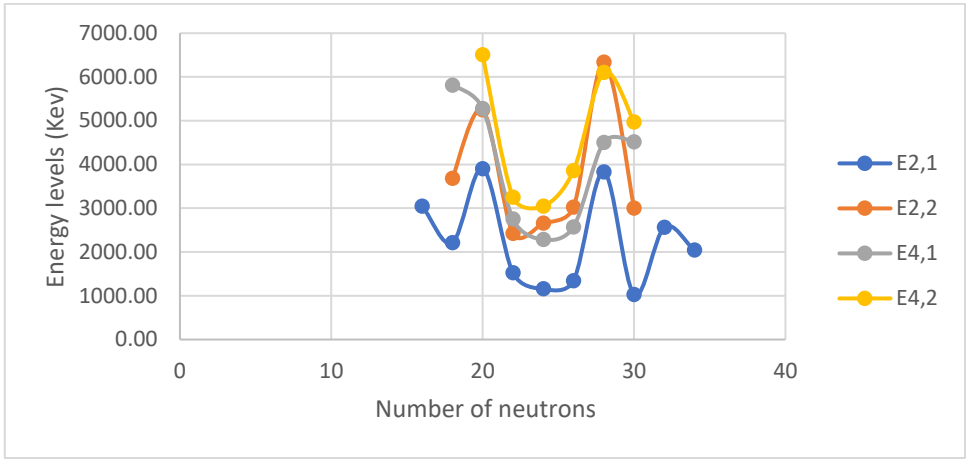

A

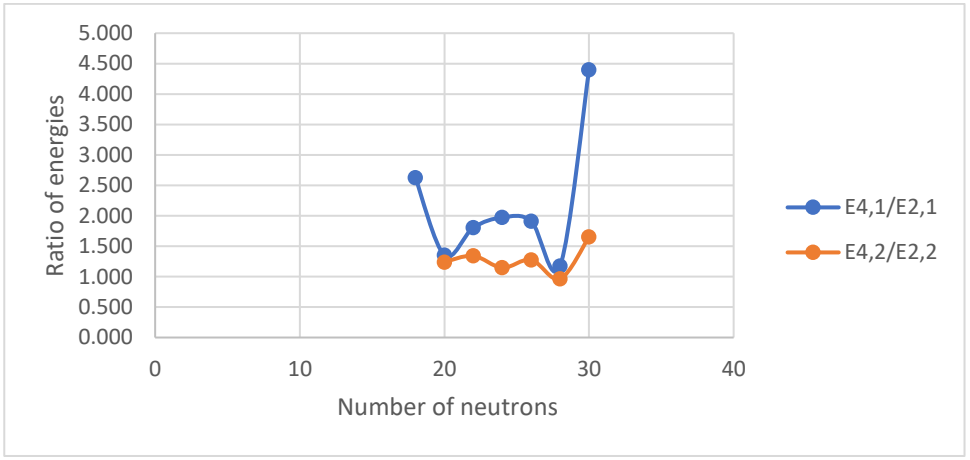

B

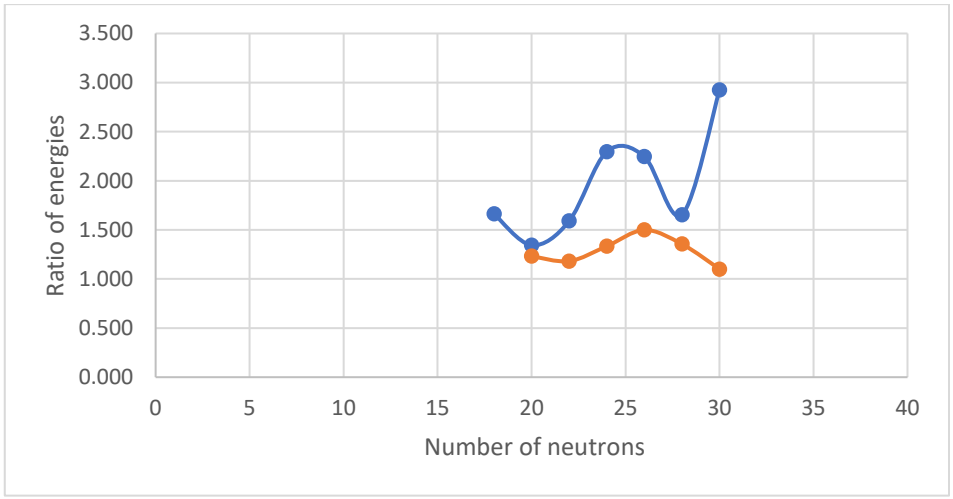

C

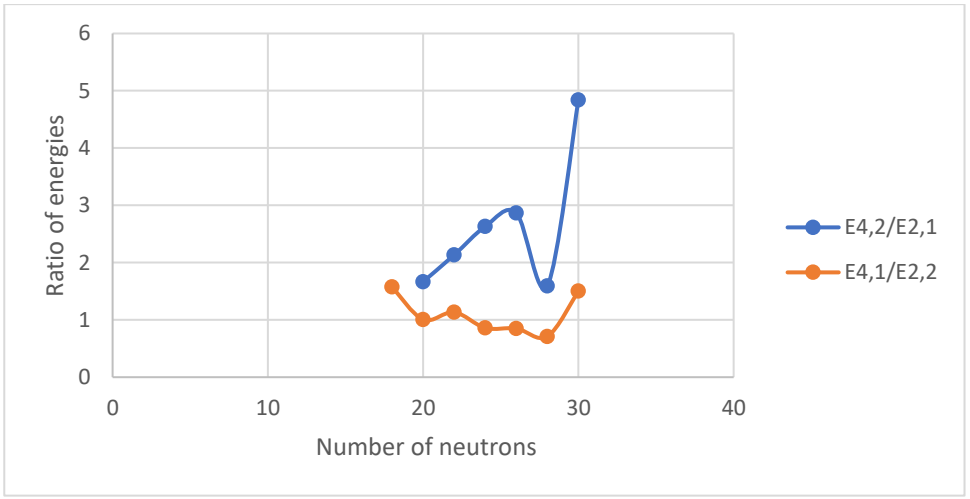

D

Figure III. 10 (color online) Panel **A** represents the comparison of the experimental energy levels of the lowest 2_1^+, 2_2^+, 4_1^+ and 4_2^+ states for the chain of Ca isotopes. Panels **B, C, D** represent the comparison of the experimental energy ratios ($E_{4_1^+}/E_{2_1^+}$ and $E_{4_2^+}/E_{2_2^+}$), ($E_{2_2^+}/E_{2_1^+}$ and $E_{4_2^+}/E_{4_1^+}$) and ($E_{4_2^+}/E_{2_1^+}$ and $E_{4_1^+}/E_{2_2^+}$), respectively, for the chain of Ca isotopes.

Ti isotopes (Z =22)

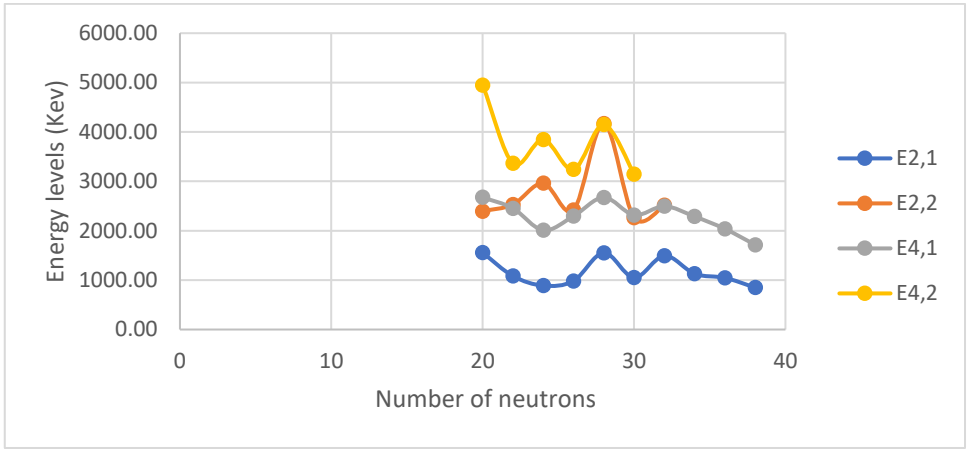

A

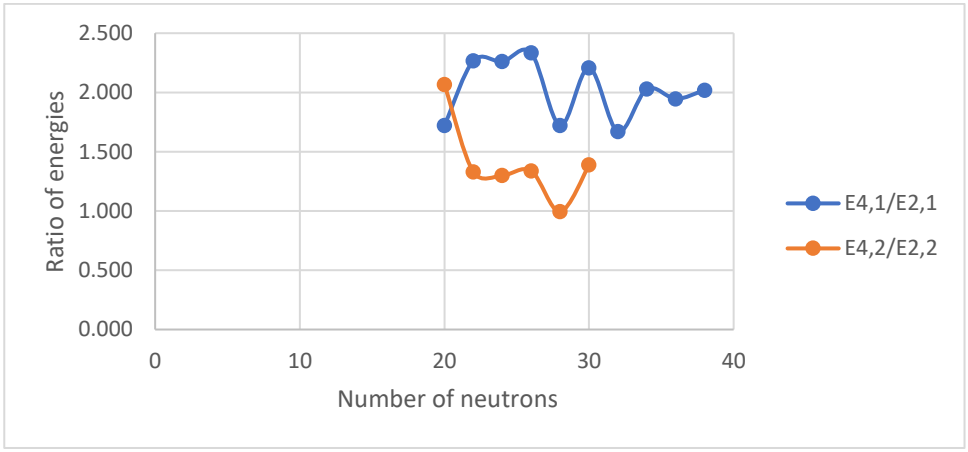

B

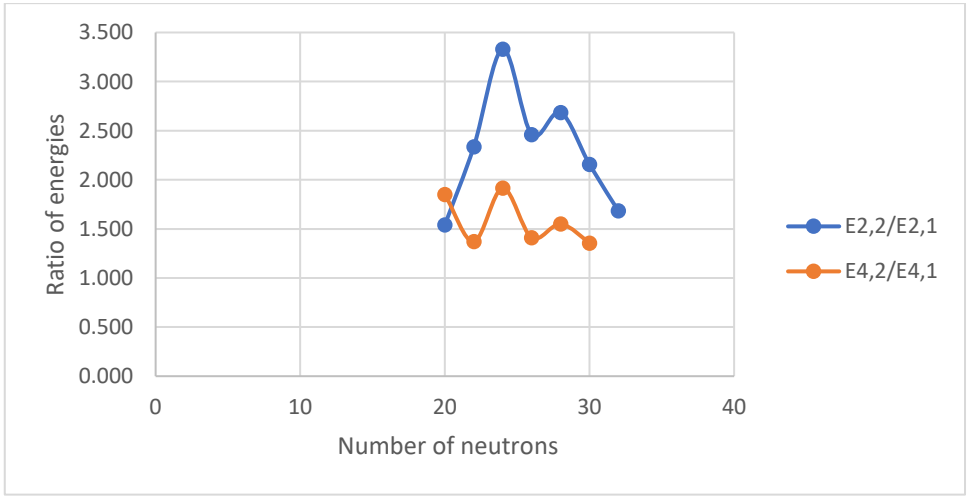

C

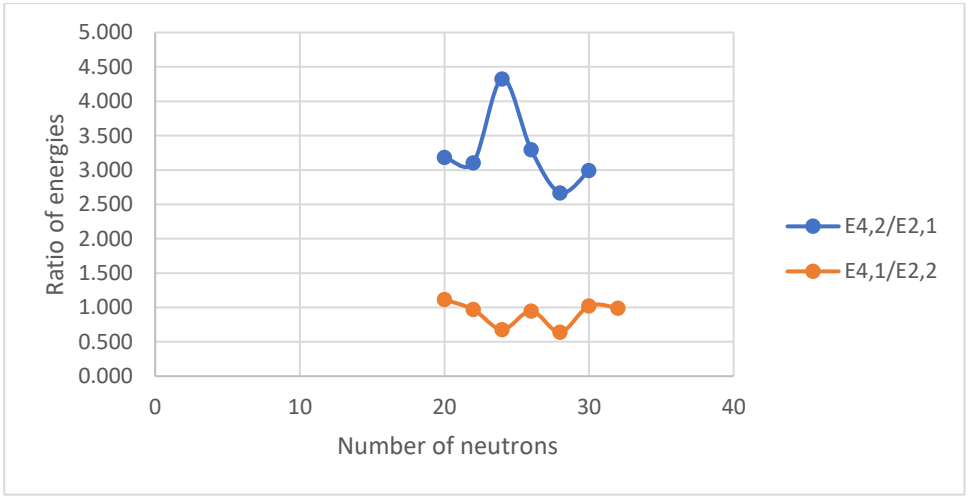

D

Figure III. 11 (color online) Panel **A** represents the comparison of the experimental energy levels of the lowest 2_1^+, 2_2^+, 4_1^+ and 4_2^+ states for the chain of Ti isotopes. Panels **B, C, D** represent the comparison of the experimental energy ratios ($E_{4_1^+}/E_{2_1^+}$ and $E_{4_2^+}/E_{2_2^+}$), ($E_{2_2^+}/E_{2_1^+}$ and $E_{4_2^+}/E_{4_1^+}$) and ($E_{4_2^+}/E_{2_1^+}$ and $E_{4_1^+}/E_{2_2^+}$), respectively, for the chain of Ti isotopes.

Cr isotopes (Z =24)

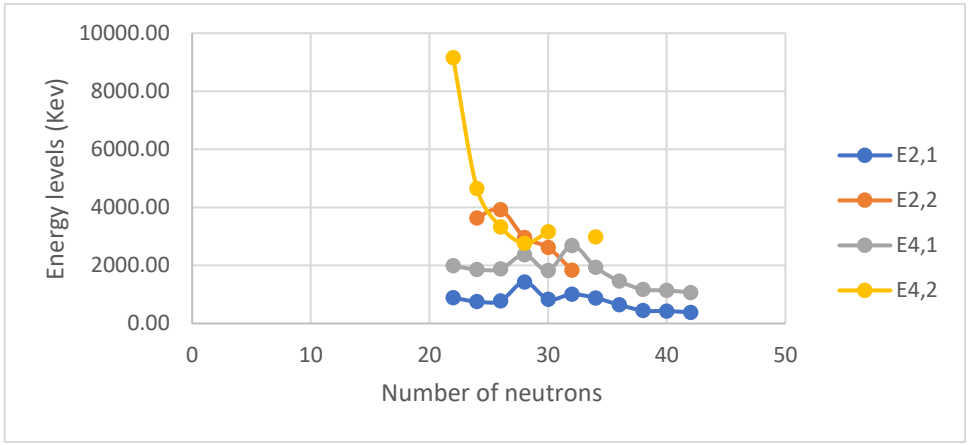

A

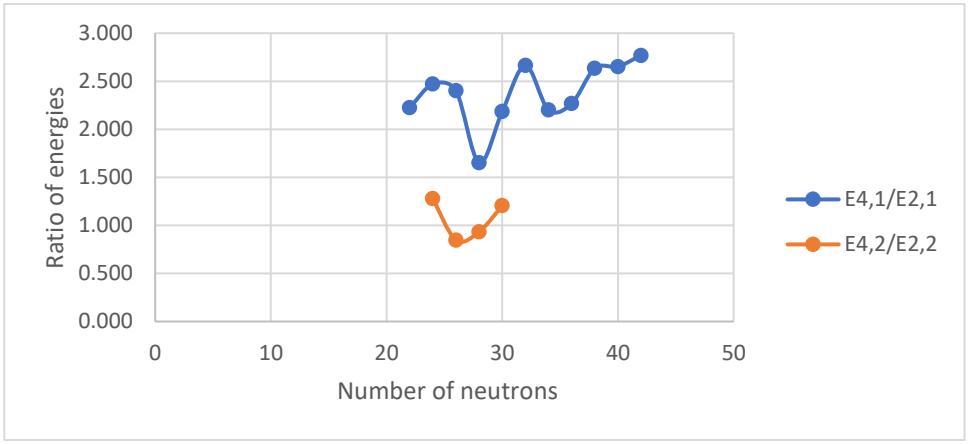

B

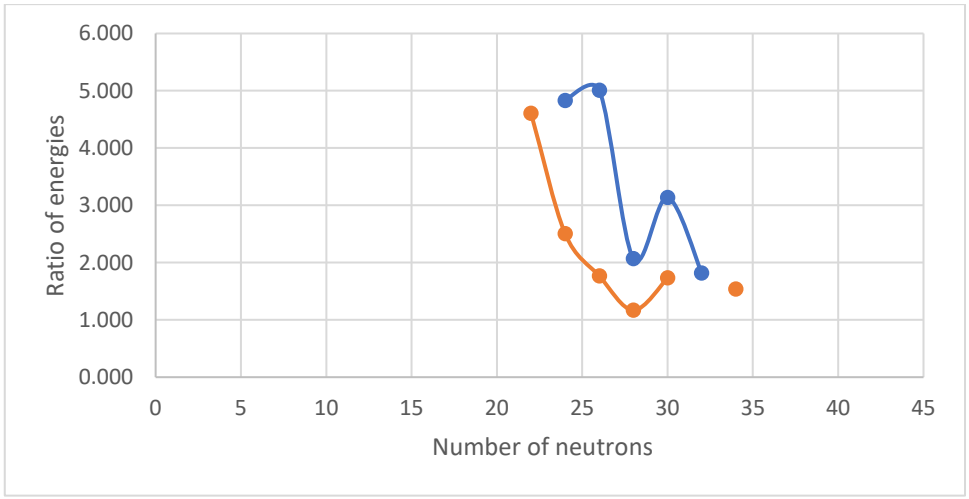

C

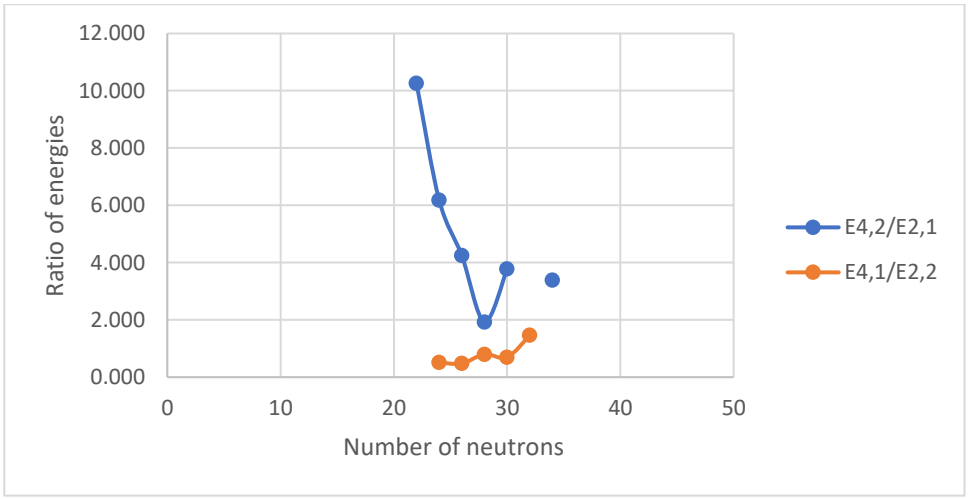

D

Figure III. 12 (color online) Panel **A** represents the comparison of the experimental energy levels of the lowest 2_1^+, 2_2^+, 4_1^+ and 4_2^+ states for the chain of Cr isotopes. Panels **B, C, D** represent the comparison of the experimental energy ratios ($E_{4_1^+}/E_{2_1^+}$ and $E_{4_2^+}/E_{2_2^+}$), ($E_{2_2^+}/E_{2_1^+}$ and $E_{4_2^+}/E_{4_1^+}$) and ($E_{4_2^+}/E_{2_1^+}$ and $E_{4_1^+}/E_{2_2^+}$), respectively, for the chain of Cr isotopes.

Fe isotopes (Z =26)

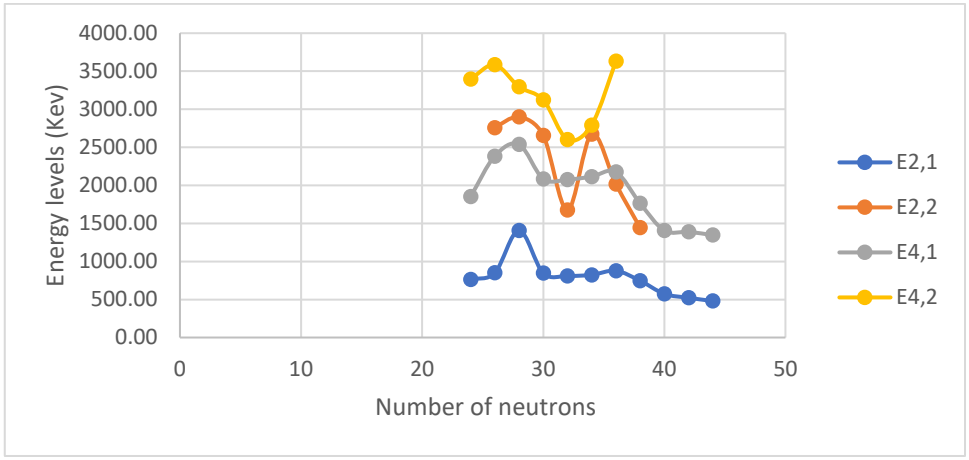

A

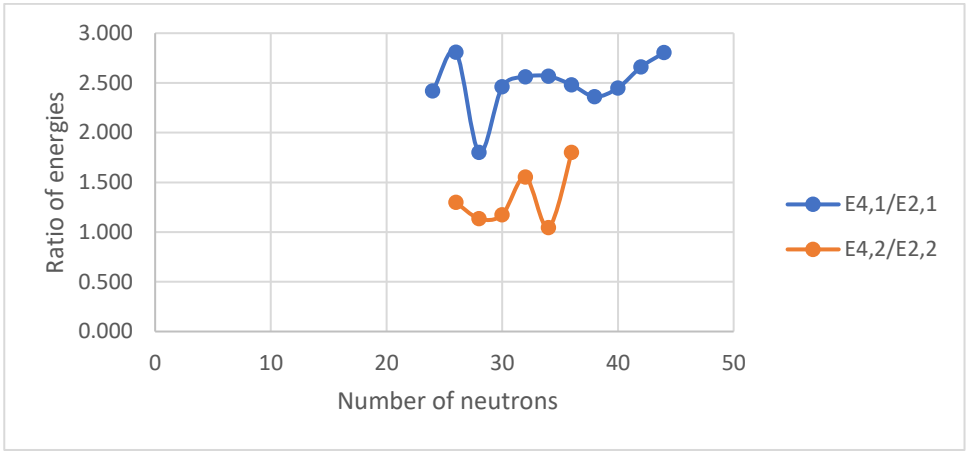

B

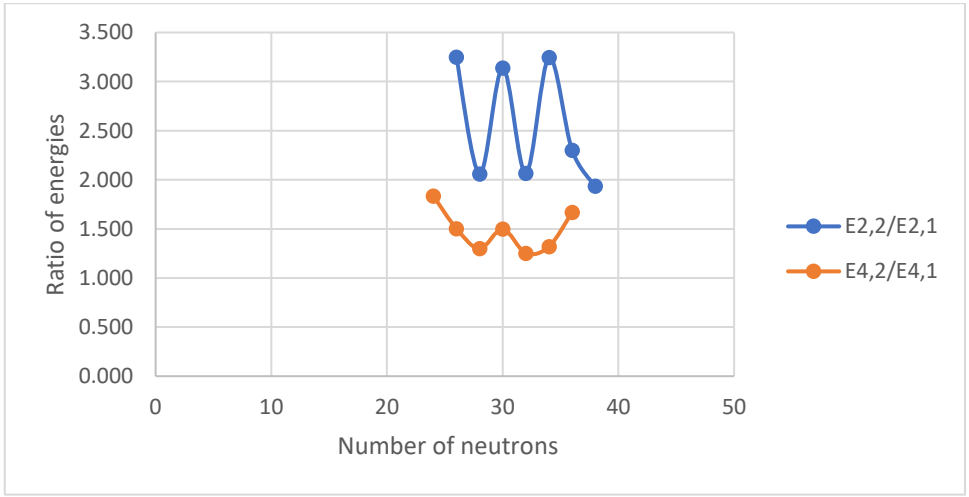

C

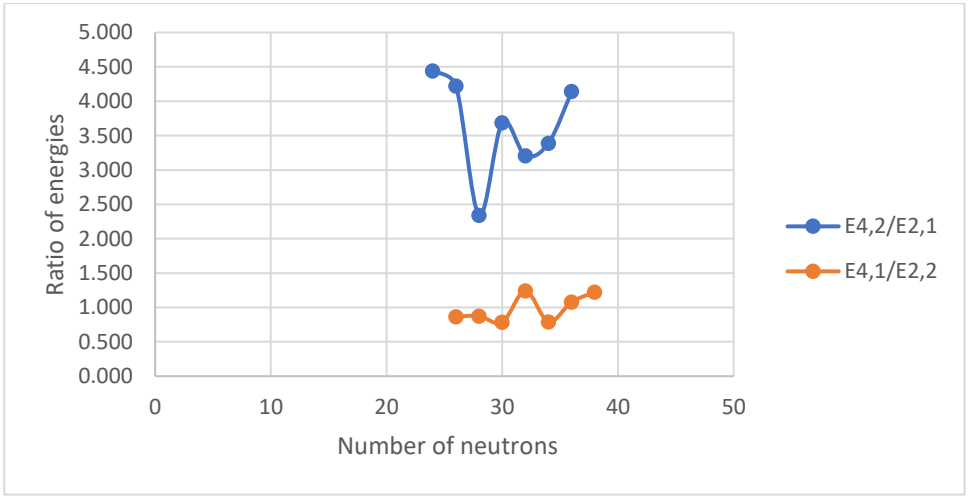

D

Figure III. 13 (color online) Panel **A** represents the comparison of the experimental energy levels of the lowest 2_1^+, 2_2^+, 4_1^+ and 4_2^+ states for the chain of Fe isotopes. Panels **B, C, D** represent the comparison of the experimental energy ratios ($E_{4_1^+}/E_{2_1^+}$ and $E_{4_2^+}/E_{2_2^+}$), ($E_{2_2^+}/E_{2_1^+}$ and $E_{4_2^+}/E_{4_1^+}$) and ($E_{4_2^+}/E_{2_1^+}$ and $E_{4_1^+}/E_{2_2^+}$), respectively, for the chain of Fe isotopes.

Ni isotopes (Z =28)

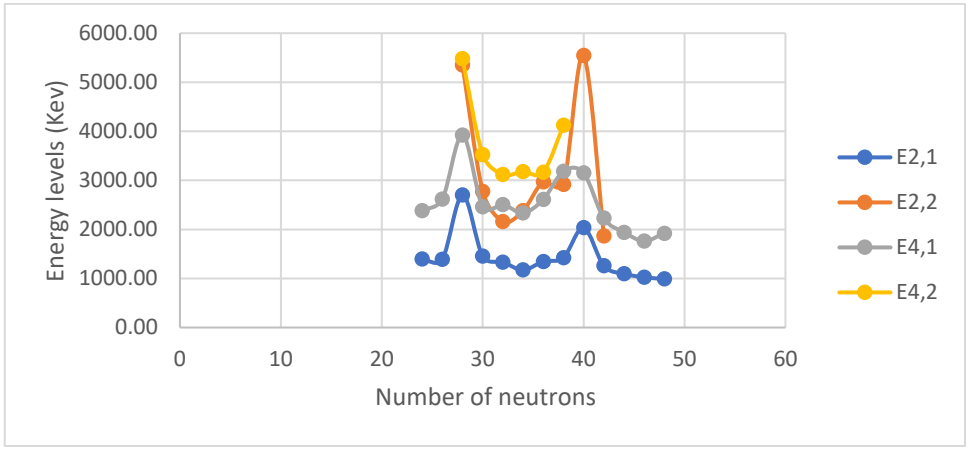

A

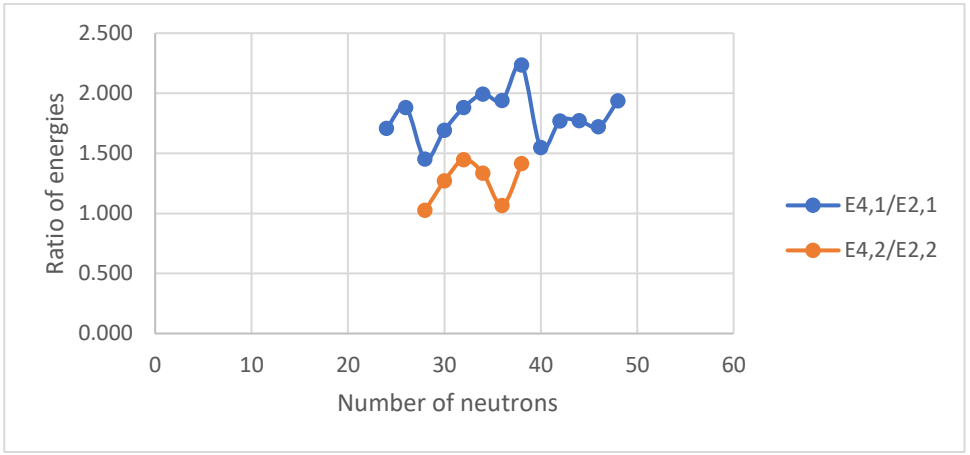

B

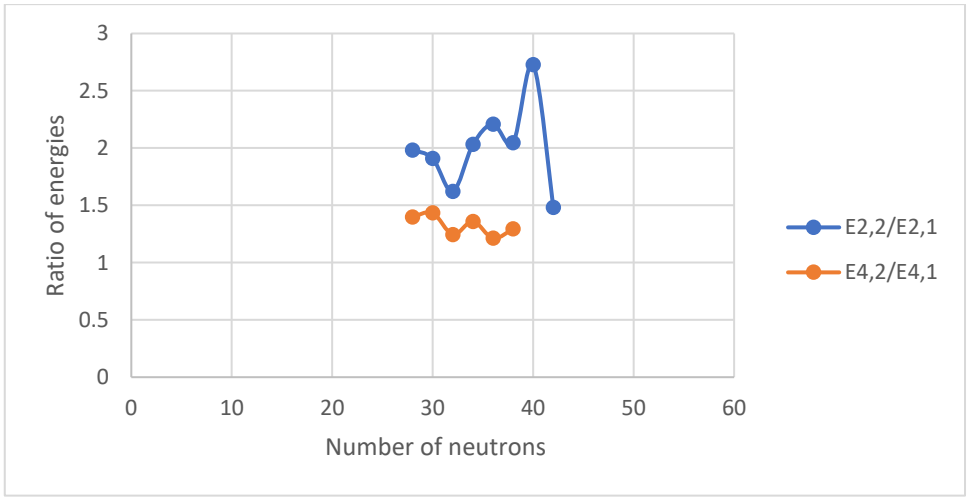

C

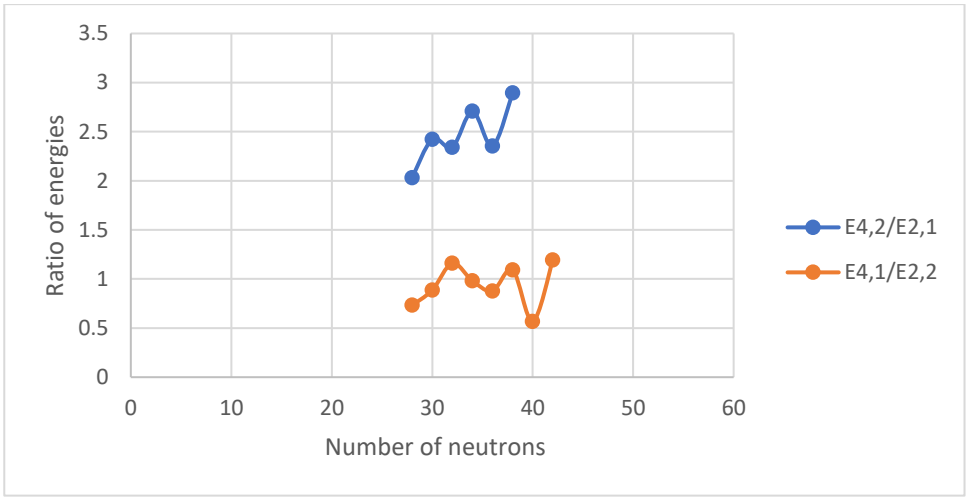

D

Figure III. 14 (color online) Panel **A** represents the comparison of the experimental energy levels of the lowest 2_1^+, 2_2^+, 4_1^+ and 4_2^+ states for the chain of Ni isotopes. Panels **B, C, D** represent the comparison of the experimental energy ratios ($E_{4_1^+}/E_{2_1^+}$ and $E_{4_2^+}/E_{2_2^+}$), ($E_{2_2^+}/E_{2_1^+}$ and $E_{4_2^+}/E_{4_1^+}$) and ($E_{4_2^+}/E_{2_1^+}$ and $E_{4_1^+}/E_{2_2^+}$), respectively, for the chain of Ni isotopes.

Zn isotopes (Z =30)

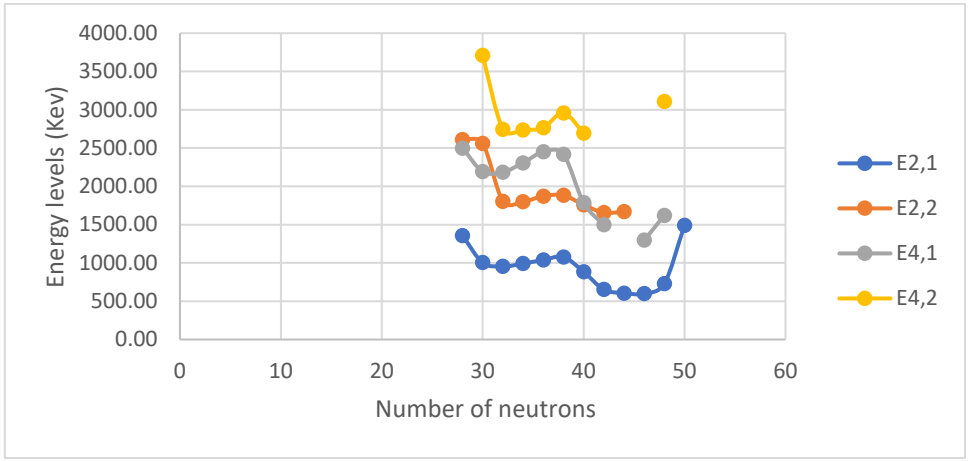

A

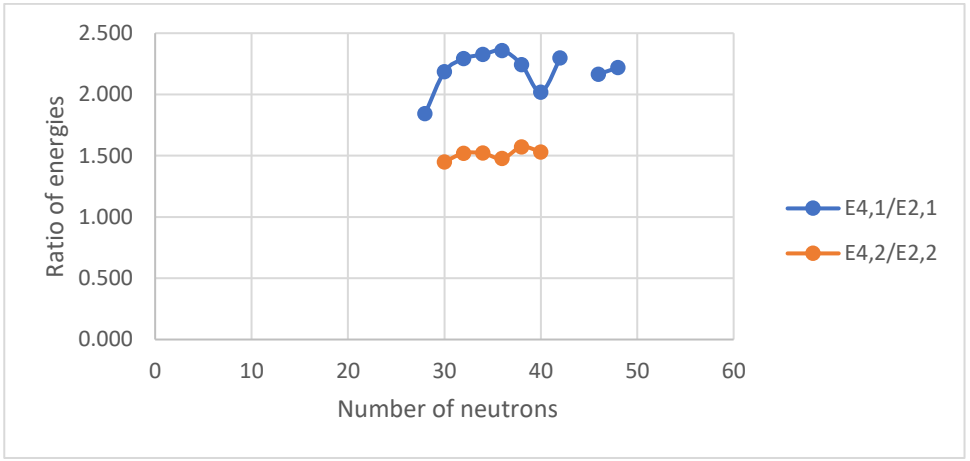

B

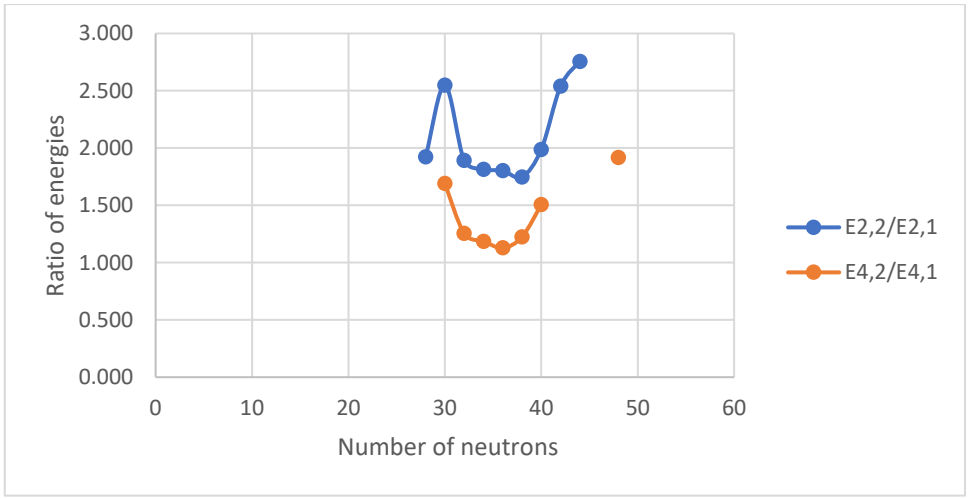

C

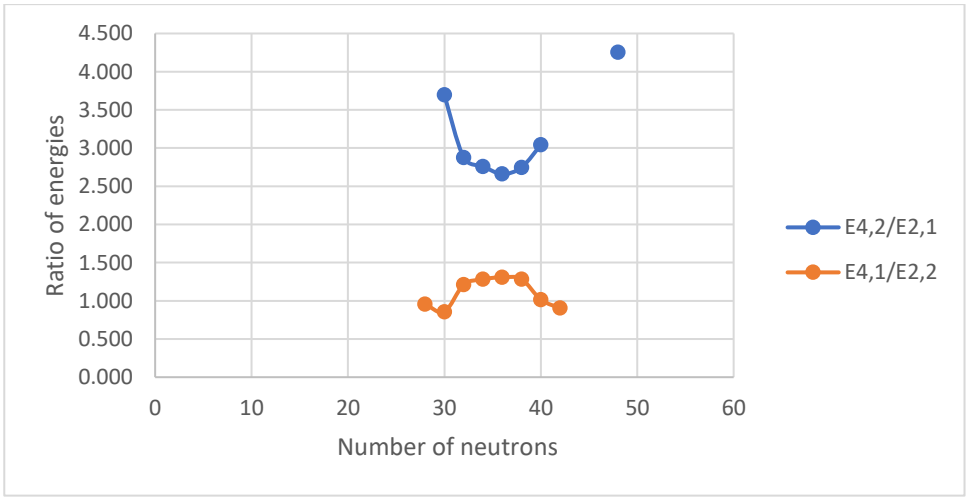

D

Figure III. 15 (color online) Panel **A** represents the comparison of the experimental energy levels of the lowest 2_1^+, 2_2^+, 4_1^+ and 4_2^+ states for the chain of Zn isotopes. Panels **B, C, D** represent the comparison of the experimental energy ratios ($E_{4_1^+}/E_{2_1^+}$ and $E_{4_2^+}/E_{2_2^+}$), ($E_{2_2^+}/E_{2_1^+}$ and $E_{4_2^+}/E_{4_1^+}$) and ($E_{4_2^+}/E_{2_1^+}$ and $E_{4_1^+}/E_{2_2^+}$), respectively, for the chain of Zn isotopes.

Ge isotopes (Z =32)

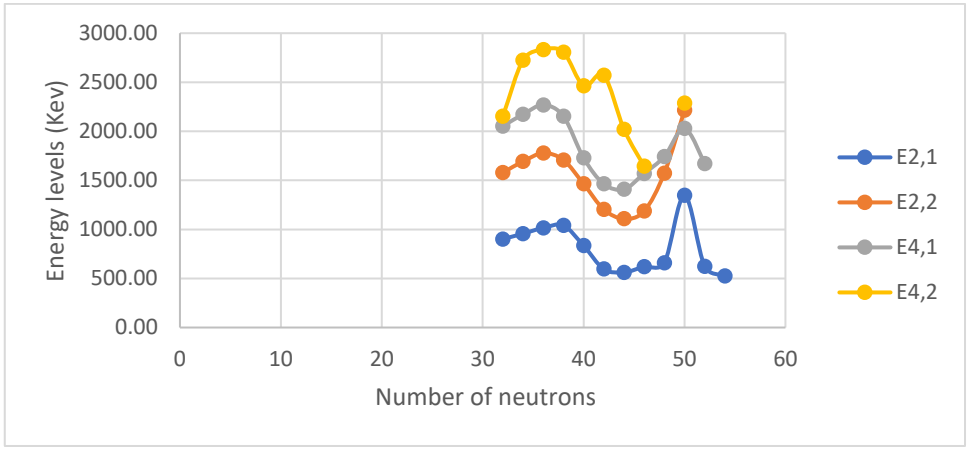

A

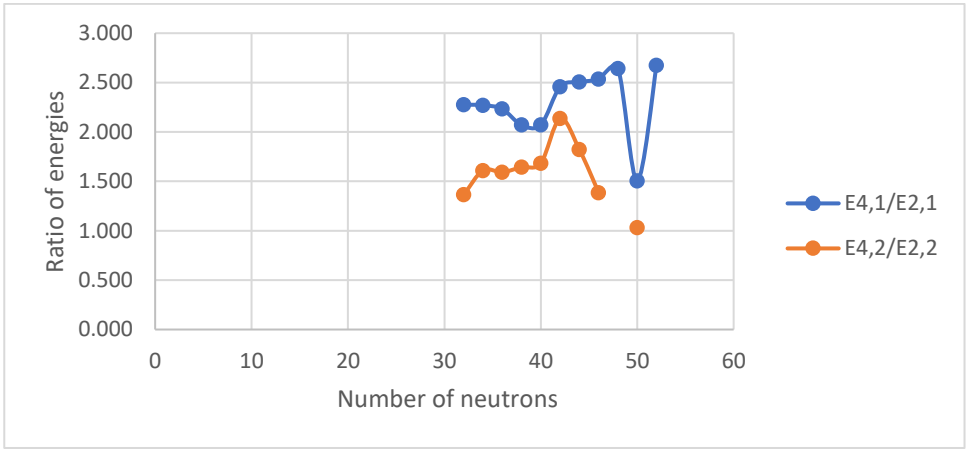

B

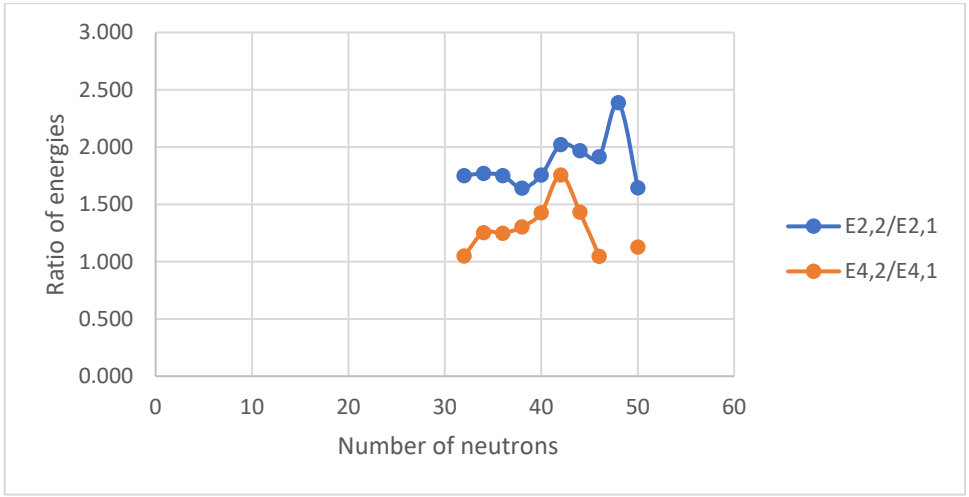

C

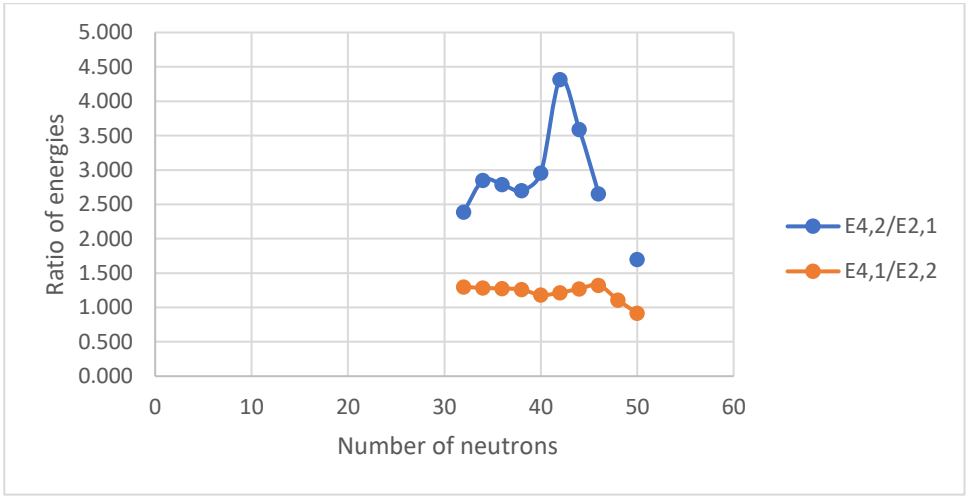

D

Figure III. 16 (color online) Panel **A** represents the comparison of the experimental energy levels of the lowest 2_1^+, 2_2^+, 4_1^+ and 4_2^+ states for the chain of Ge isotopes. Panels **B, C, D** represent the comparison of the experimental energy ratios ($E_{4_1^+}/E_{2_1^+}$ and $E_{4_2^+}/E_{2_2^+}$), ($E_{2_2^+}/E_{2_1^+}$ and $E_{4_2^+}/E_{4_1^+}$) and ($E_{4_2^+}/E_{2_1^+}$ and $E_{4_1^+}/E_{2_2^+}$), respectively, for the chain of Ge isotopes.

Se isotopes (Z =34)

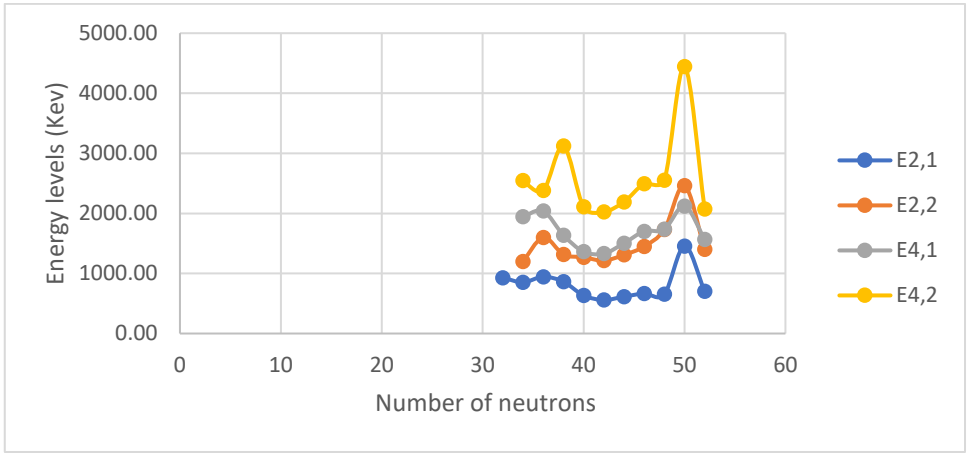

A

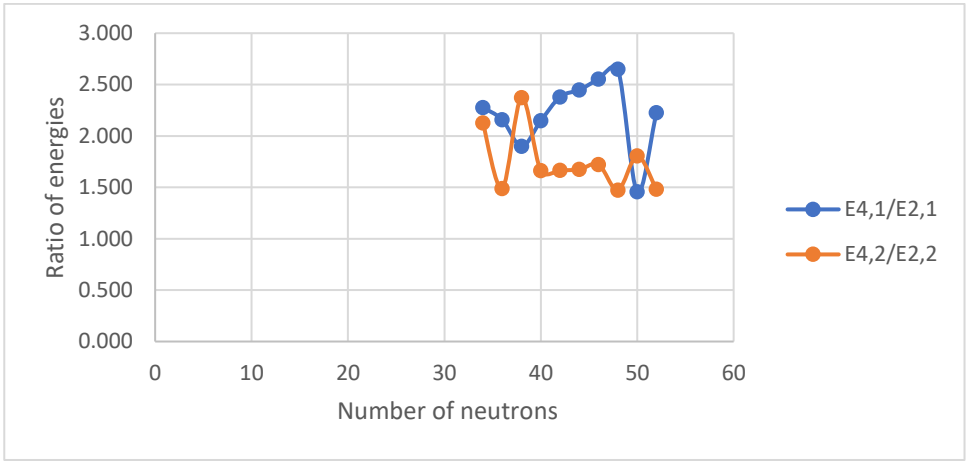

B

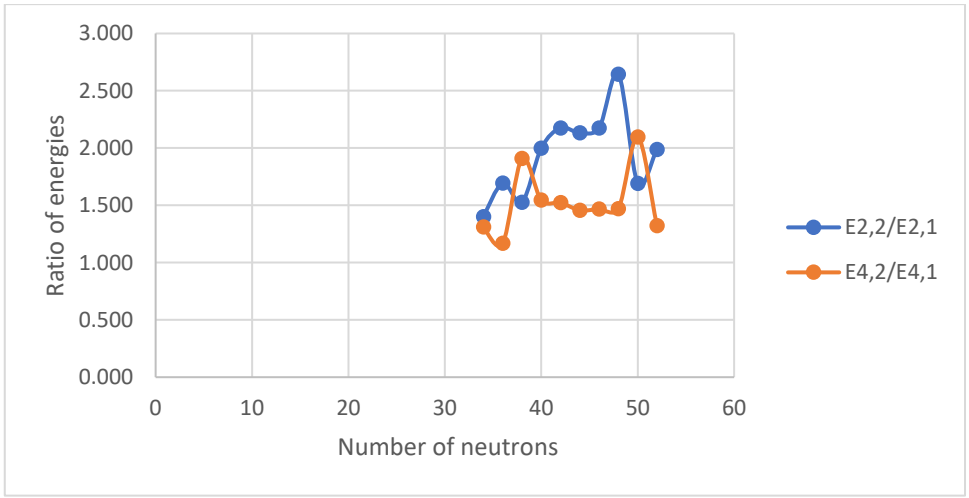

C

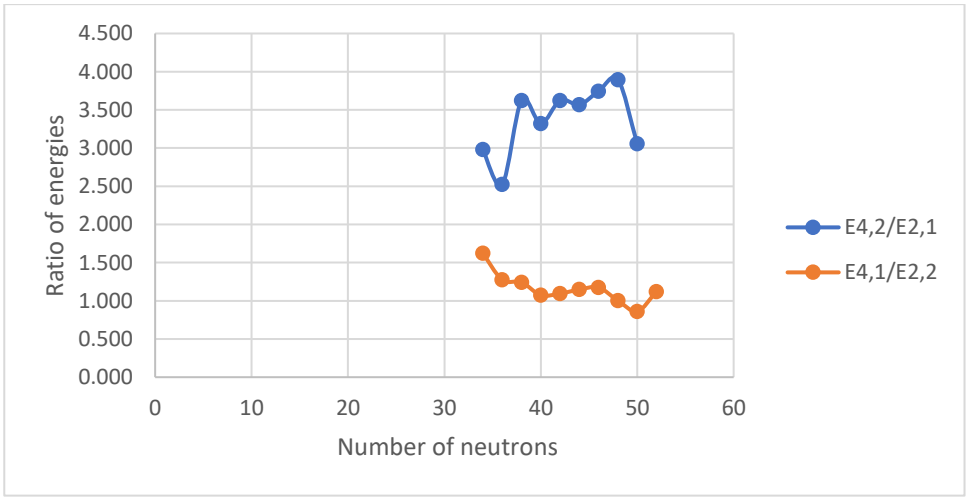

D

Figure III. 17 (color online) Panel **A** represents the comparison of the experimental energy levels of the lowest 2_1^+, 2_2^+, 4_1^+ and 4_2^+ states for the chain of Se isotopes. Panels **B, C, D** represent the comparison of the experimental energy ratios ($E_{4_1^+}/E_{2_1^+}$ and $E_{4_2^+}/E_{2_2^+}$), ($E_{2_2^+}/E_{2_1^+}$ and $E_{4_2^+}/E_{4_1^+}$) and ($E_{4_2^+}/E_{2_1^+}$ and $E_{4_1^+}/E_{2_2^+}$), respectively, for the chain of Se isotopes.

Kr isotopes (Z =36)

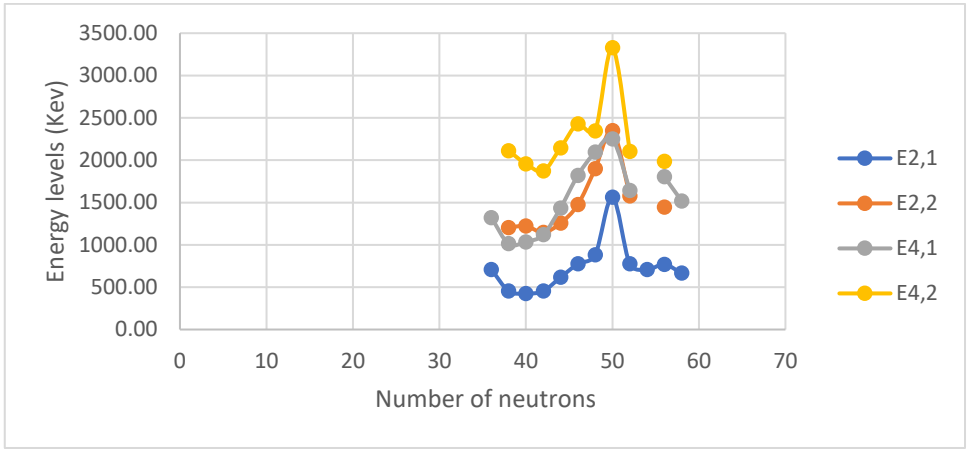

A

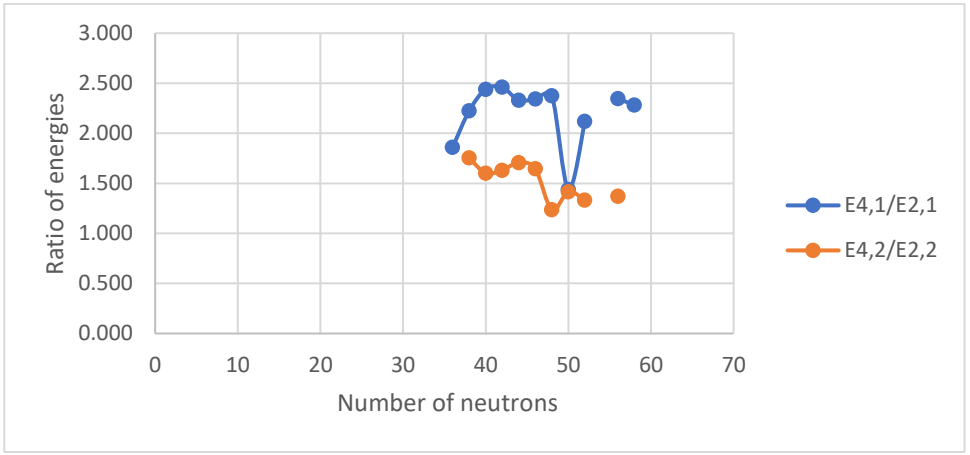

B

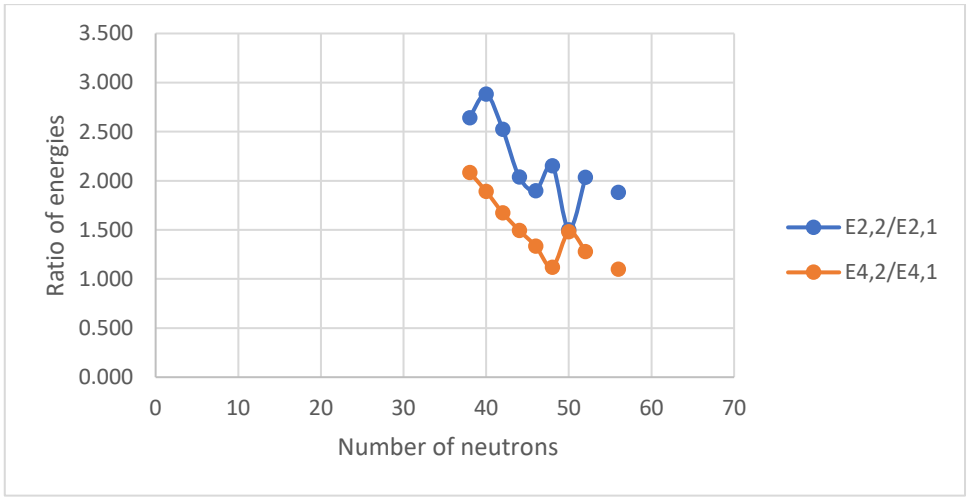

C

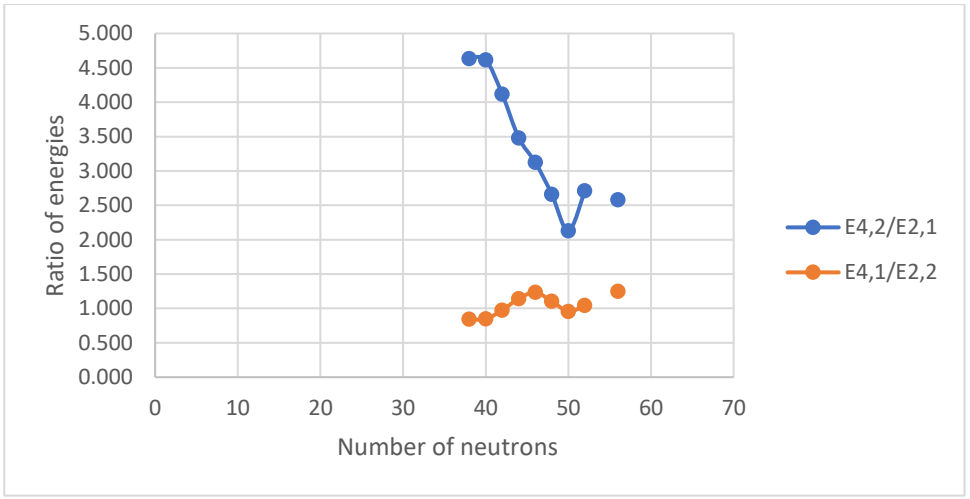

D

Figure III. 18 (color online) Panel **A** represents the comparison of the experimental energy levels of the lowest 2_1^+, 2_2^+, 4_1^+ and 4_2^+ states for the chain of Kr isotopes. Panels **B, C, D** represent the comparison of the experimental energy ratios ($E_{4_1^+}/E_{2_1^+}$ and $E_{4_2^+}/E_{2_2^+}$), ($E_{2_2^+}/E_{2_1^+}$ and $E_{4_2^+}/E_{4_1^+}$) and ($E_{4_2^+}/E_{2_1^+}$ and $E_{4_1^+}/E_{2_2^+}$), respectively, for the chain of Kr isotopes.

Sr isotopes (Z =38)

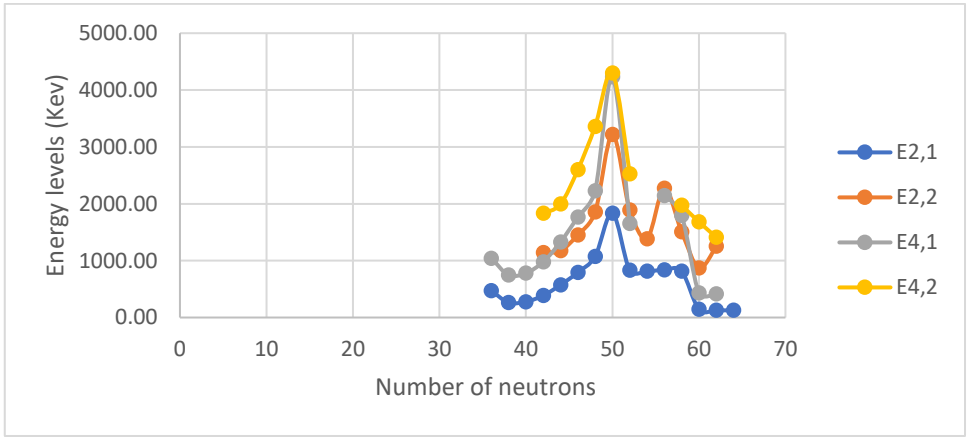

A

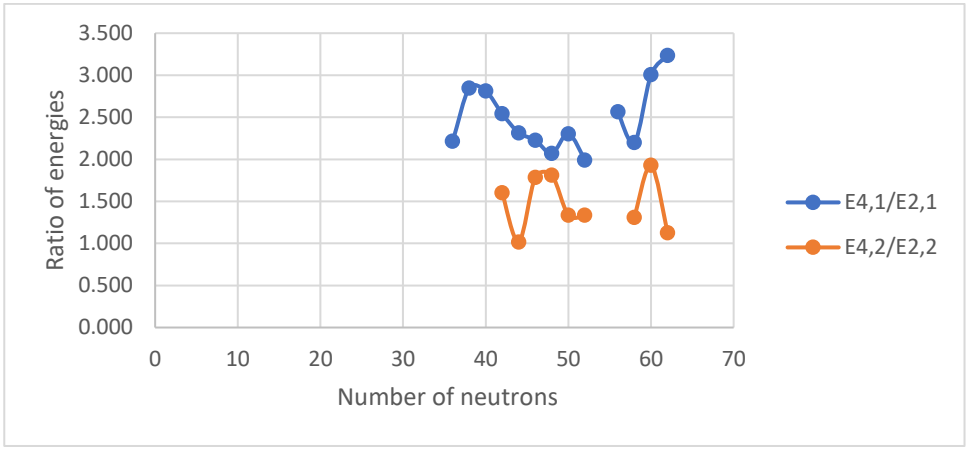

B

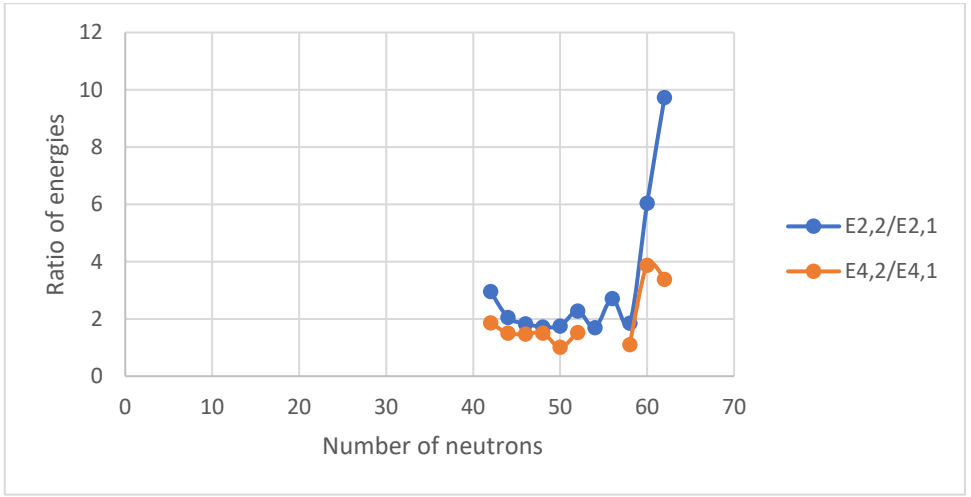

C

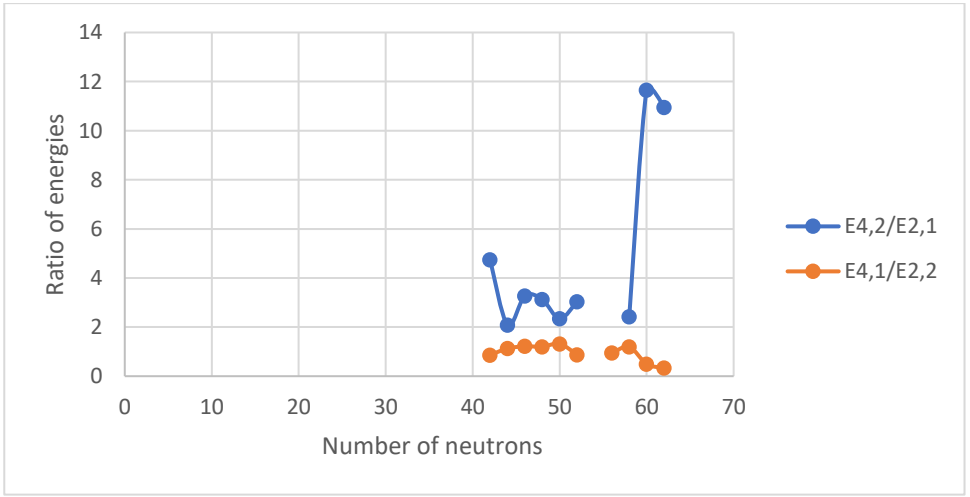

D

Figure III. 19 (color online) Panel **A** represents the comparison of the experimental energy levels of the lowest 2_1^+, 2_2^+, 4_1^+ and 4_2^+ states for the chain of Sr isotopes. Panels **B, C, D** represent the comparison of the experimental energy ratios ($E_{4_1^+}/E_{2_1^+}$ and $E_{4_2^+}/E_{2_2^+}$), ($E_{2_2^+}/E_{2_1^+}$ and $E_{4_2^+}/E_{4_1^+}$) and ($E_{4_2^+}/E_{2_1^+}$ and $E_{4_1^+}/E_{2_2^+}$), respectively, for the chain of Sr isotopes.

Zr isotopes (Z =40)

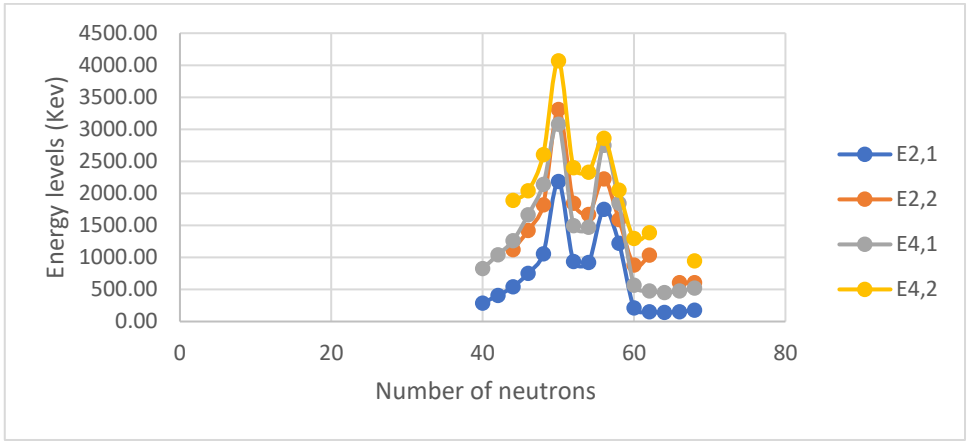

A

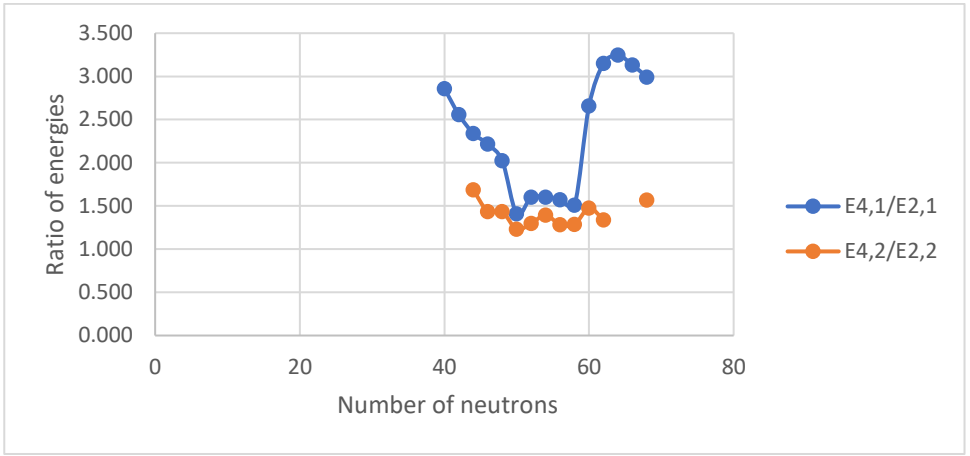

B

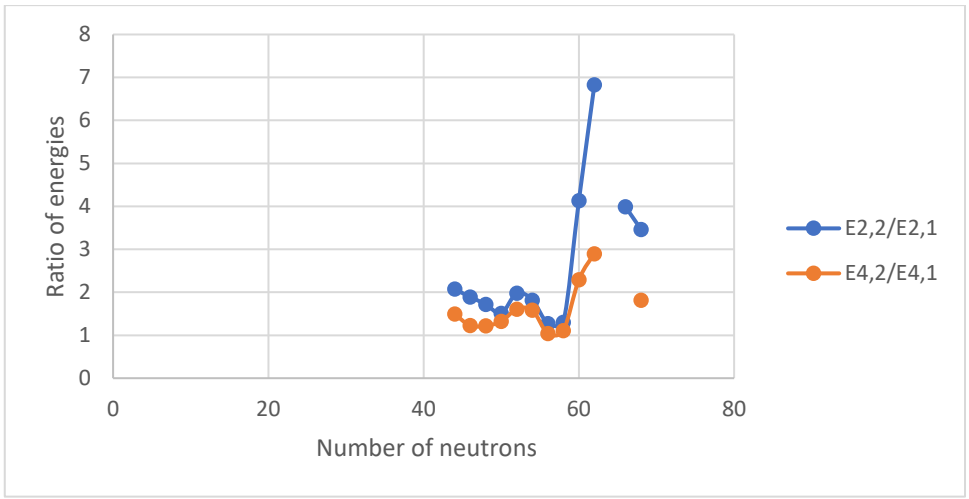

C

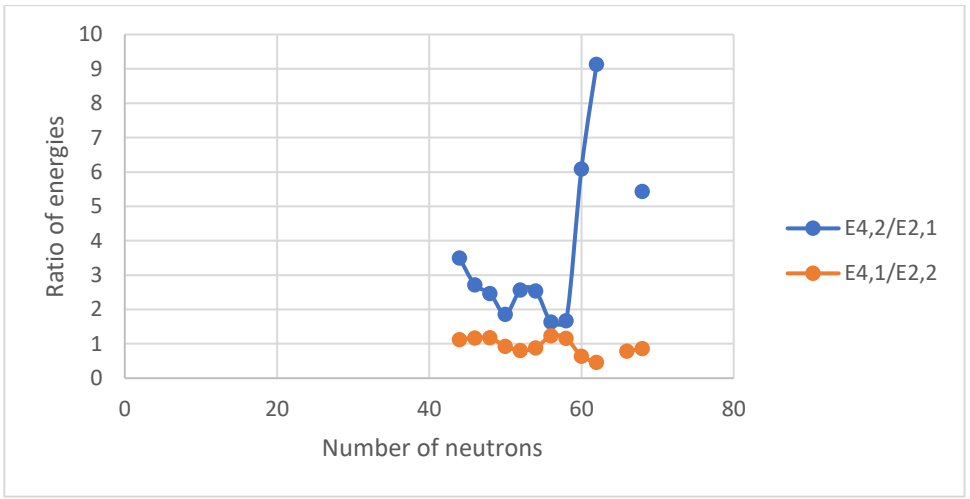

D

Figure III. 20 (color online) Panel **A** represents the comparison of the experimental energy levels of the lowest 2_1^+, 2_2^+, 4_1^+ and 4_2^+ states for the chain of Zr isotopes. Panels **B, C, D** represent the comparison of the experimental energy ratios ($E_{4_1^+}/E_{2_1^+}$ and $E_{4_2^+}/E_{2_2^+}$), ($E_{2_2^+}/E_{2_1^+}$ and $E_{4_2^+}/E_{4_1^+}$) and ($E_{4_2^+}/E_{2_1^+}$ and $E_{4_1^+}/E_{2_2^+}$), respectively, for the chain of Zr isotopes.

Mo isotopes (Z =42)

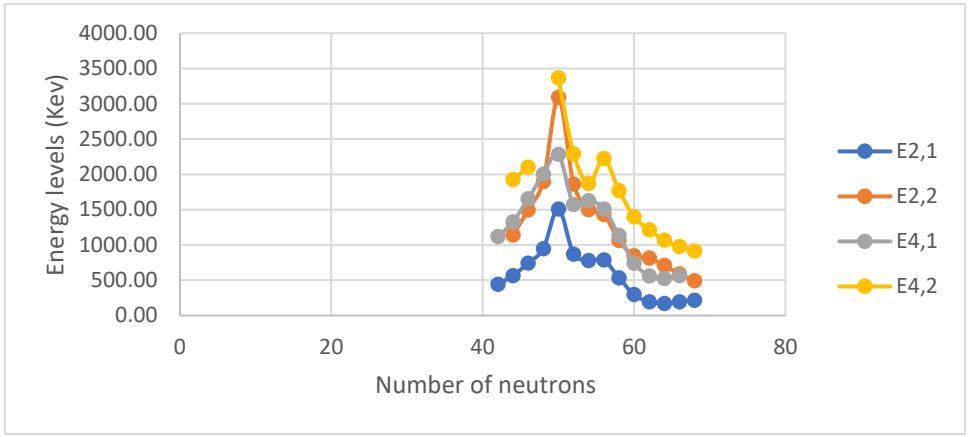

A

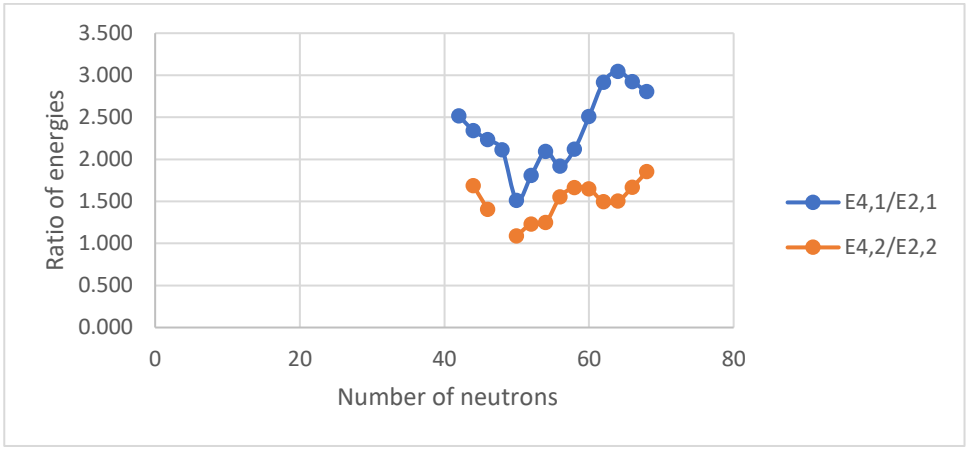

B

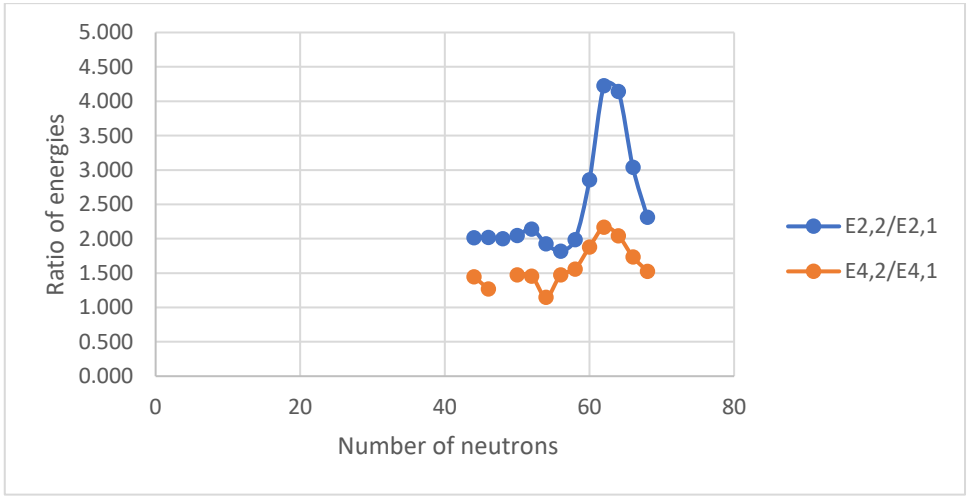

C

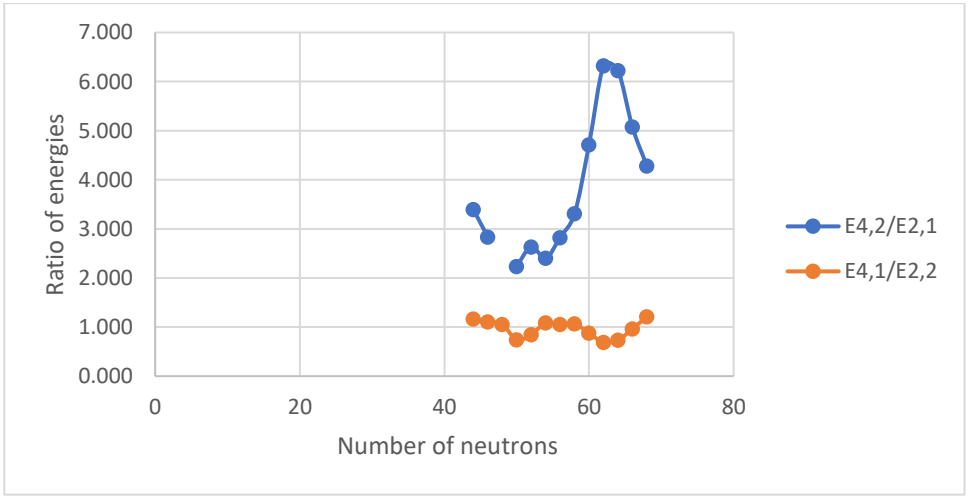

D

Figure III. 21 (color online) Panel **A** represents the comparison of the experimental energy levels of the lowest 2_1^+, 2_2^+, 4_1^+ and 4_2^+ states for the chain of Mo isotopes. Panels **B, C, D** represent the comparison of the experimental energy ratios ($E_{4_1^+}/E_{2_1^+}$ and $E_{4_2^+}/E_{2_2^+}$), ($E_{2_2^+}/E_{2_1^+}$ and $E_{4_2^+}/E_{4_1^+}$) and ($E_{4_2^+}/E_{2_1^+}$ and $E_{4_1^+}/E_{2_2^+}$), respectively, for the chain of Mo isotopes.

Ru isotopes (Z =44)

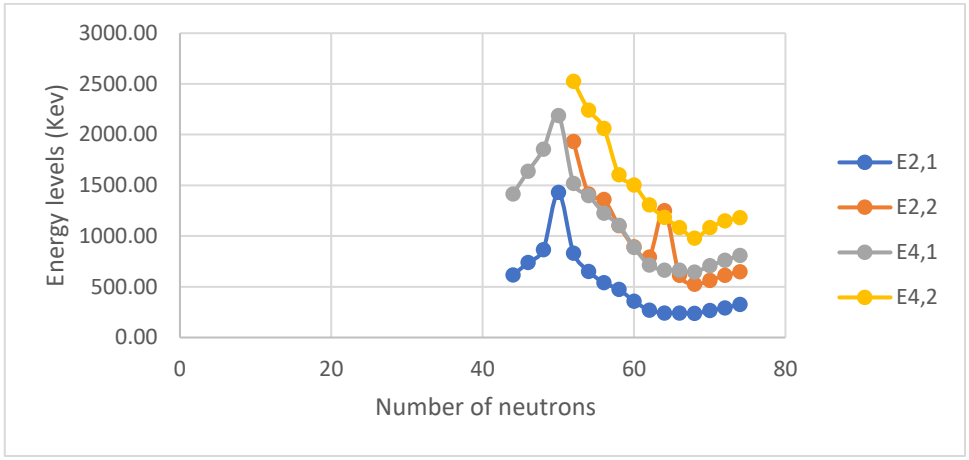

A

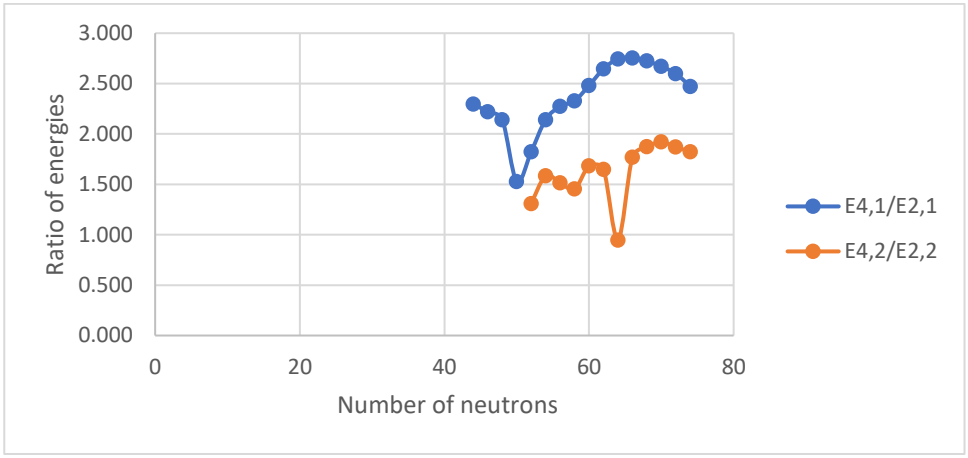

B

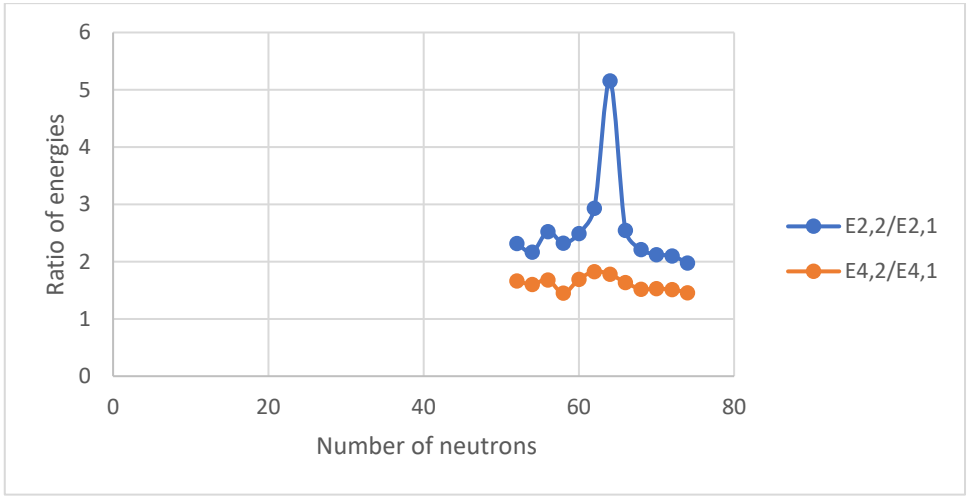

C

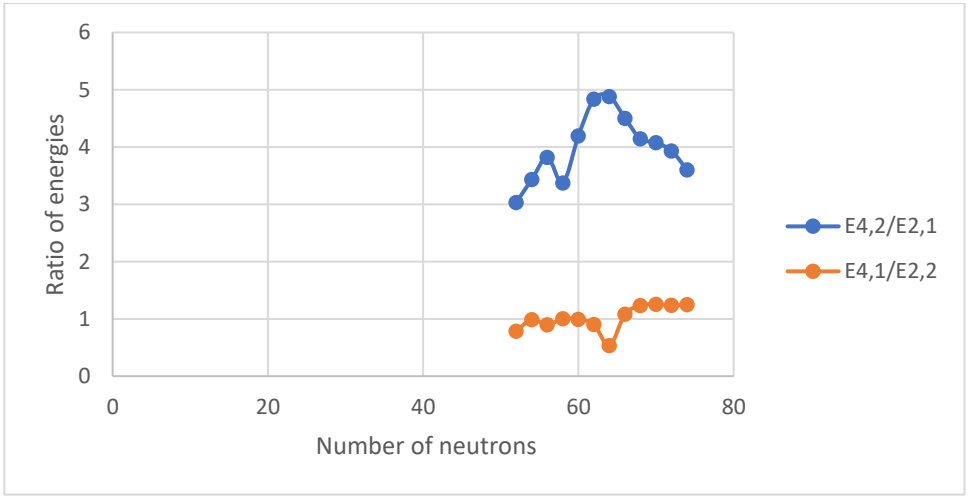

D

Figure III. 22 (color online) Panel **A** represents the comparison of the experimental energy levels of the lowest 2_1^+, 2_2^+, 4_1^+ and 4_2^+ states for the chain of Ru isotopes. Panels **B, C, D** represent the comparison of the experimental energy ratios ($E_{4_1^+}/E_{2_1^+}$ and $E_{4_2^+}/E_{2_2^+}$), ($E_{2_2^+}/E_{2_1^+}$ and $E_{4_2^+}/E_{4_1^+}$) and ($E_{4_2^+}/E_{2_1^+}$ and $E_{4_1^+}/E_{2_2^+}$), respectively, for the chain of Ru isotopes.

Pd isotopes (Z =46)

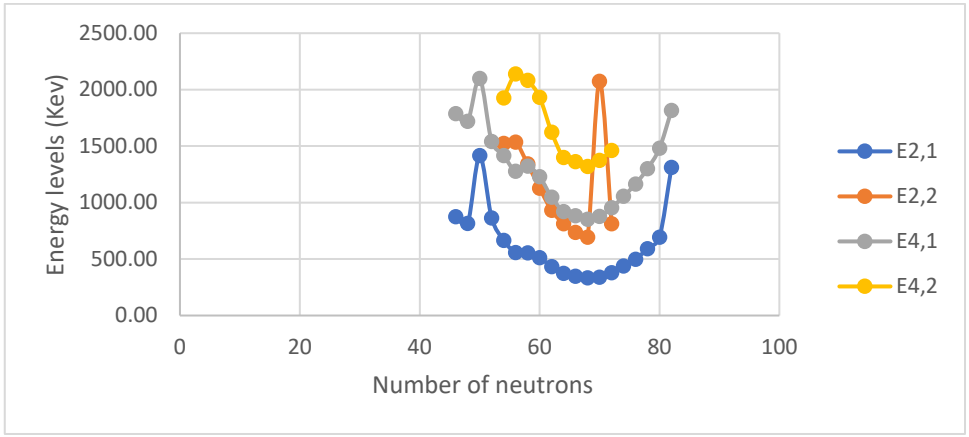

A

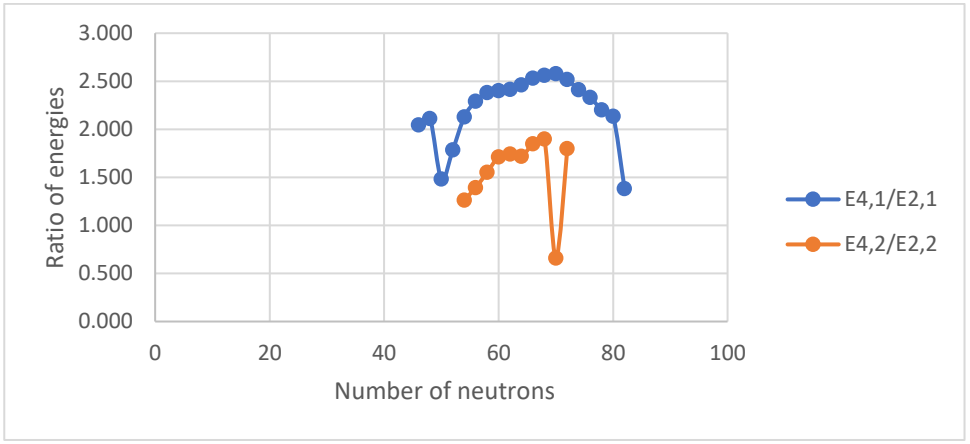

B

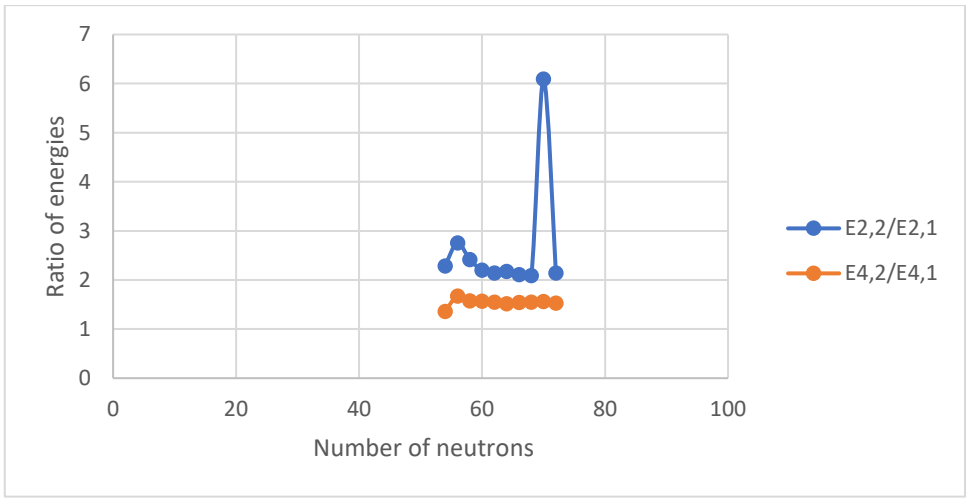

C

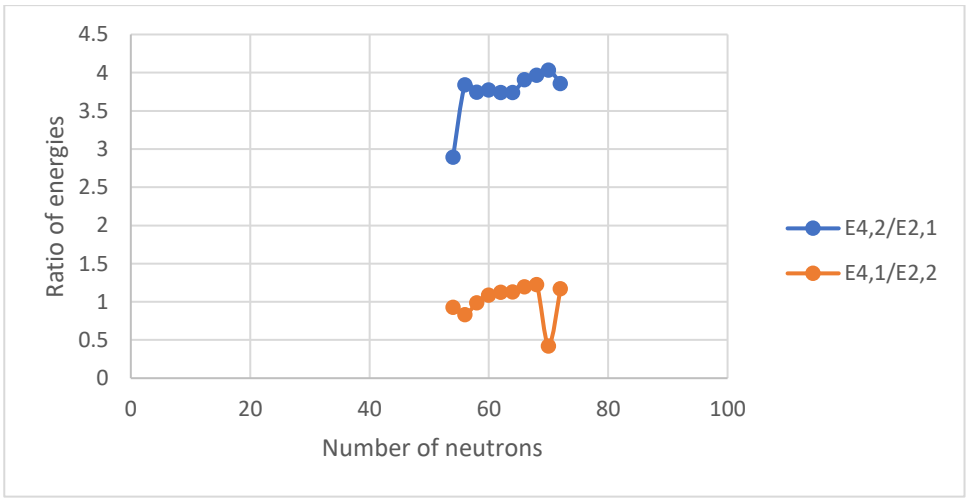

D

Figure III. 23 (color online) Panel **A** represents the comparison of the experimental energy levels of the lowest 2_1^+, 2_2^+, 4_1^+ and 4_2^+ states for the chain of Pd isotopes. Panels **B, C, D** represent the comparison of the experimental energy ratios ($E_{4_1^+}/E_{2_1^+}$ and $E_{4_2^+}/E_{2_2^+}$), ($E_{2_2^+}/E_{2_1^+}$ and $E_{4_2^+}/E_{4_1^+}$) and ($E_{4_2^+}/E_{2_1^+}$ and $E_{4_1^+}/E_{2_2^+}$), respectively, for the chain of Pd isotopes.

Cd isotopes (Z =48)

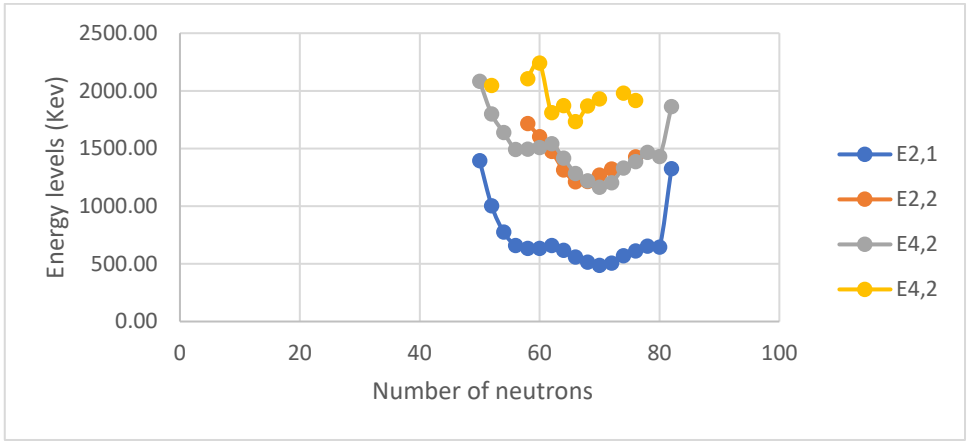

A

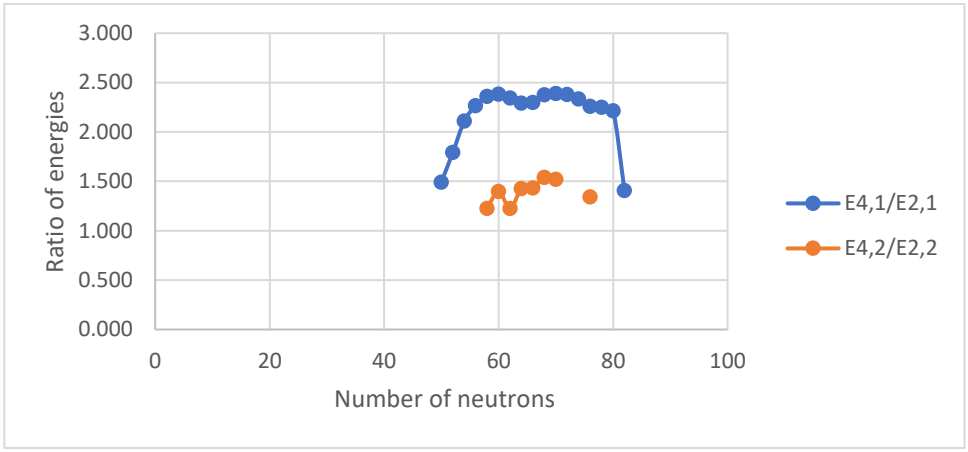

B

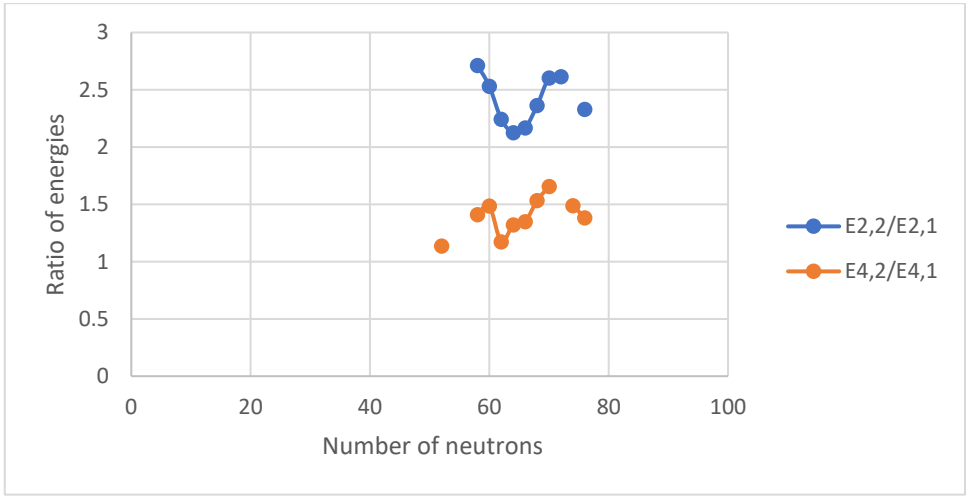

C

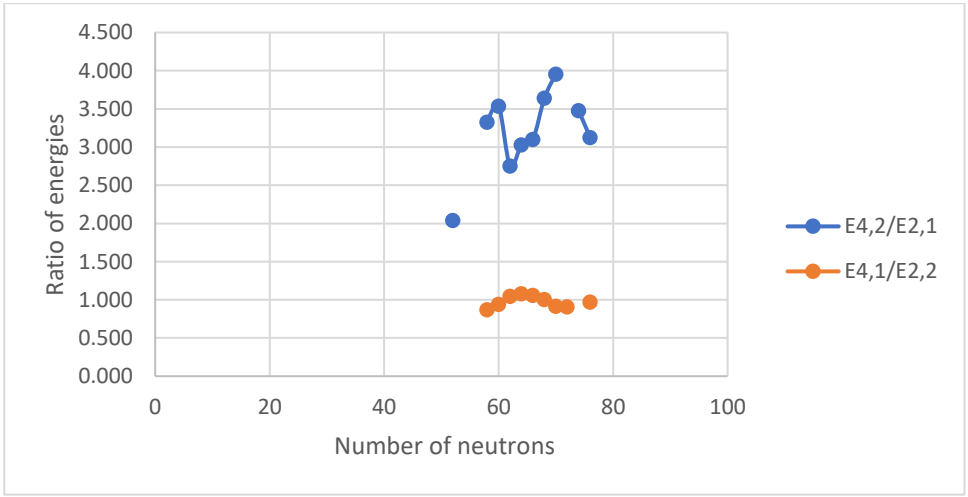

D

Figure III. 24 (color online) Panel **A** represents the comparison of the experimental energy levels of the lowest 2_1^+, 2_2^+, 4_1^+ and 4_2^+ states for the chain of Cd isotopes. Panels **B, C, D** represent the comparison of the experimental energy ratios ($E_{4_1^+}/E_{2_1^+}$ and $E_{4_2^+}/E_{2_2^+}$), ($E_{2_2^+}/E_{2_1^+}$ and $E_{4_2^+}/E_{4_1^+}$) and ($E_{4_2^+}/E_{2_1^+}$ and $E_{4_1^+}/E_{2_2^+}$), respectively, for the chain of Cd isotopes.

Sn isotopes (Z =50)

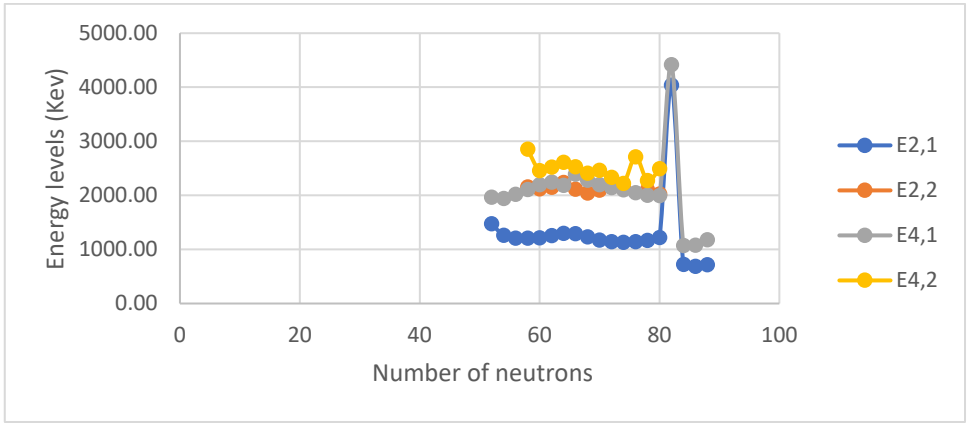

A

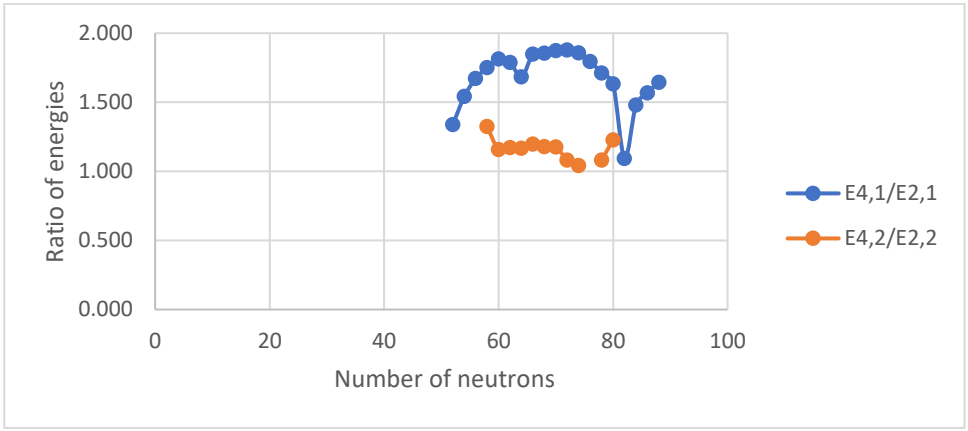

B

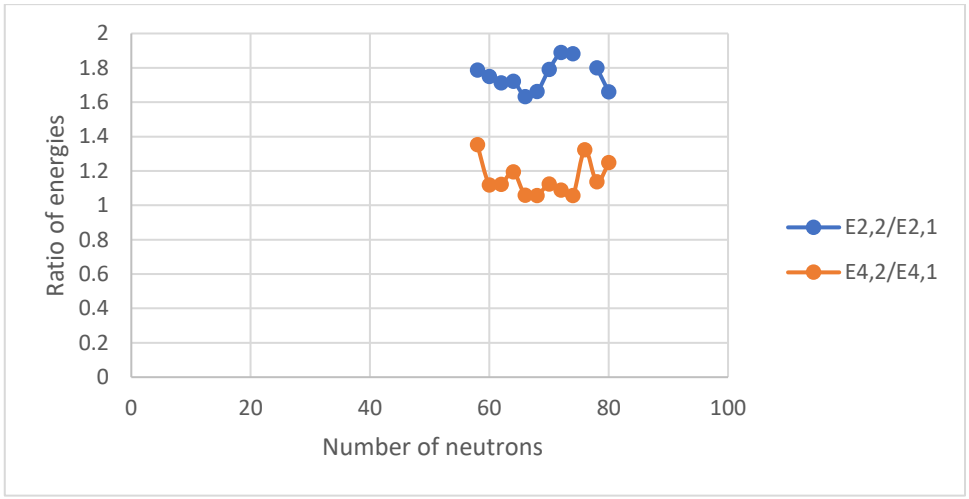

C

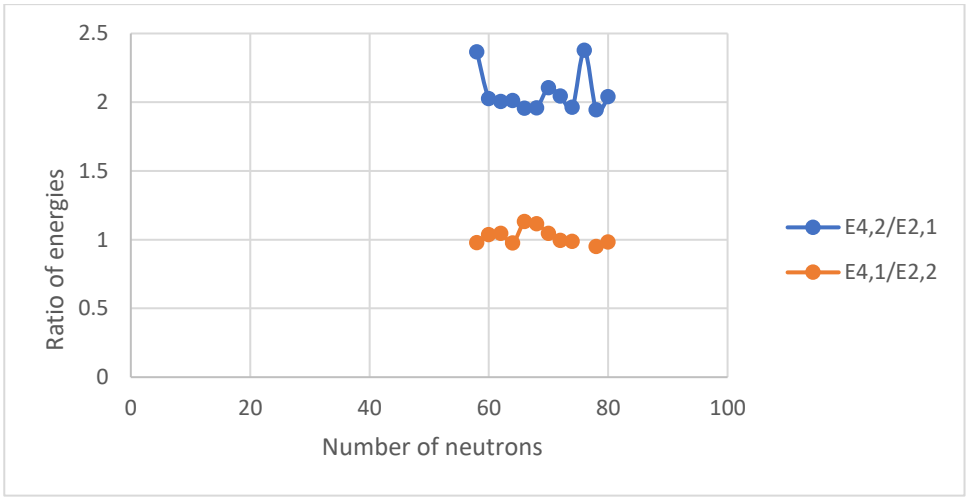

D

Figure III. 25 (color online) Panel **A** represents the comparison of the experimental energy levels of the lowest 2_1^+, 2_2^+, 4_1^+ and 4_2^+ states for the chain of Sn isotopes. Panels **B, C, D** represent the comparison of the experimental energy ratios ($E_{4_1^+}/E_{2_1^+}$ and $E_{4_2^+}/E_{2_2^+}$), ($E_{2_2^+}/E_{2_1^+}$ and $E_{4_2^+}/E_{4_1^+}$) and ($E_{4_2^+}/E_{2_1^+}$ and $E_{4_1^+}/E_{2_2^+}$), respectively, for the chain of Sn isotopes.

Te isotopes (Z =52)

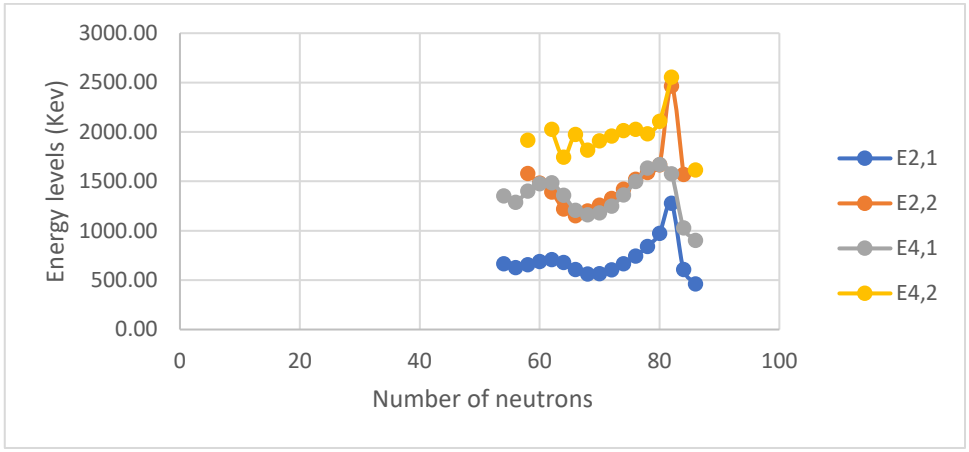

A

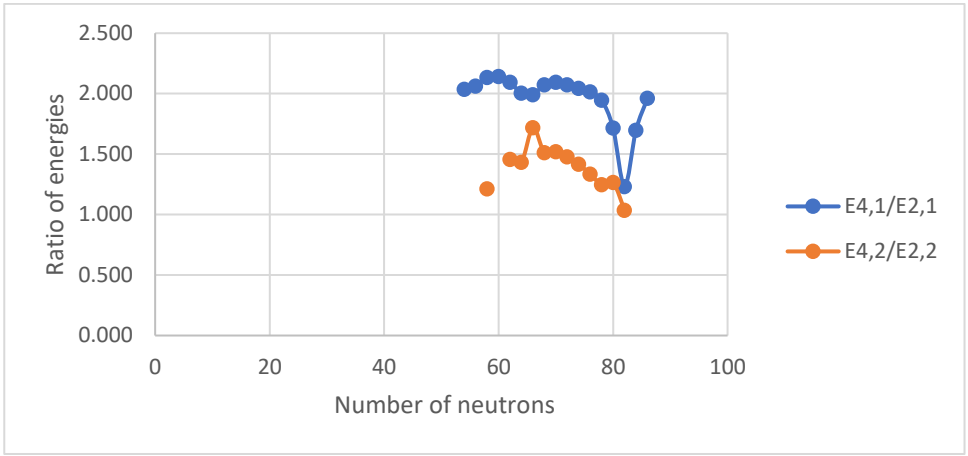

B

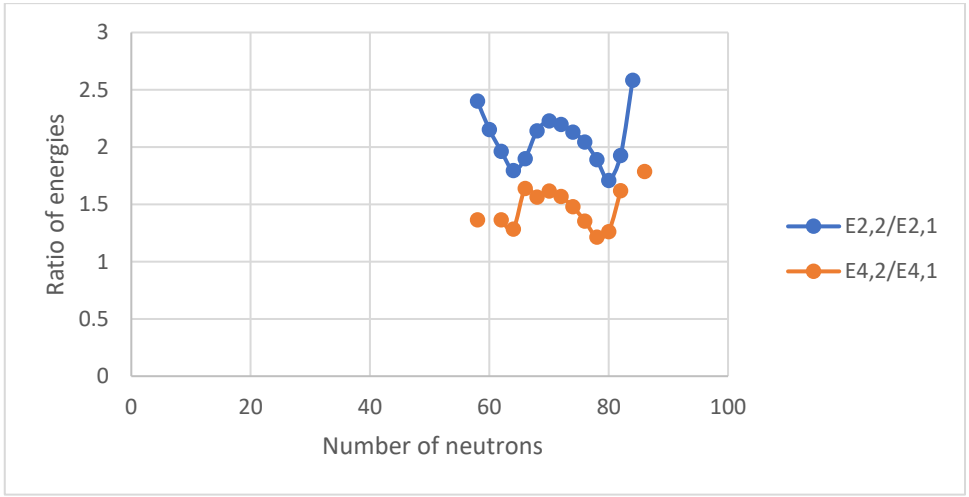

C

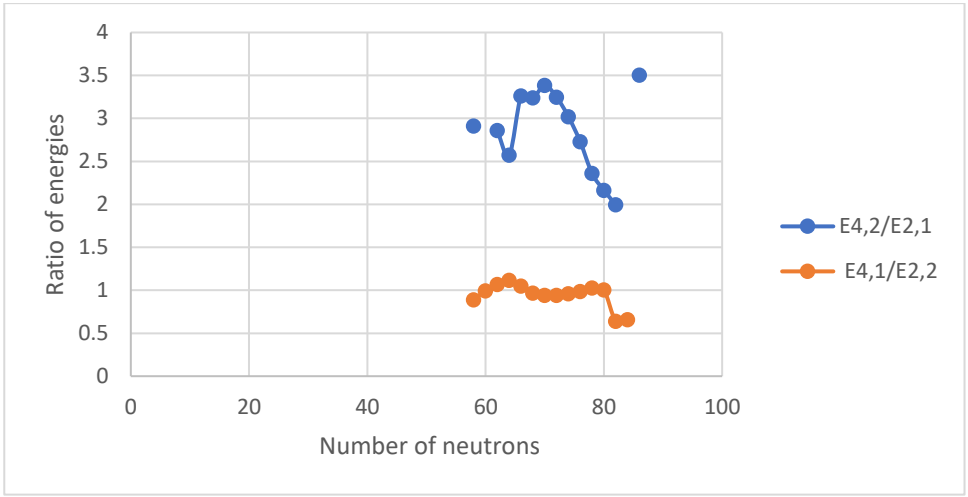

D

Figure III. 26 (color online) Panel **A** represents the comparison of the experimental energy levels of the lowest 2_1^+, 2_2^+, 4_1^+ and 4_2^+ states for the chain of Te isotopes. Panels **B, C, D** represent the comparison of the experimental energy ratios ($E_{4_1^+}/E_{2_1^+}$ and $E_{4_2^+}/E_{2_2^+}$), ($E_{2_2^+}/E_{2_1^+}$ and $E_{4_2^+}/E_{4_1^+}$) and ($E_{4_2^+}/E_{2_1^+}$ and $E_{4_1^+}/E_{2_2^+}$), respectively, for the chain of Te isotopes.

Xe isotopes (Z =54)

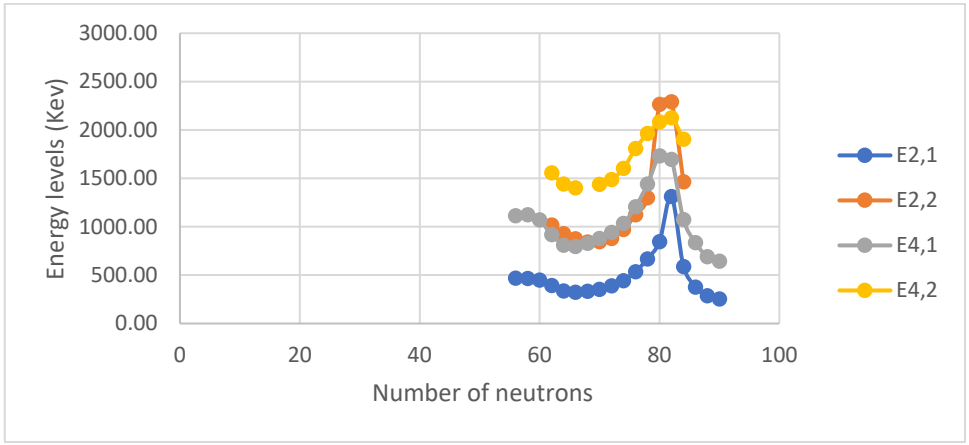

A

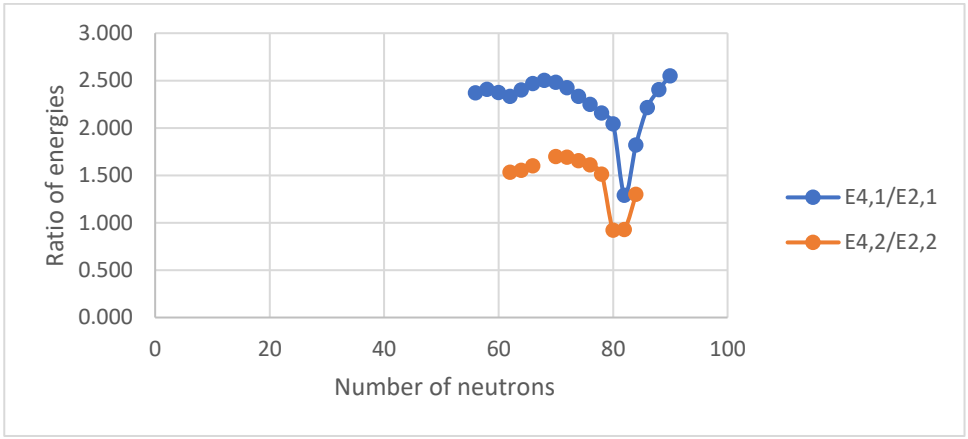

B

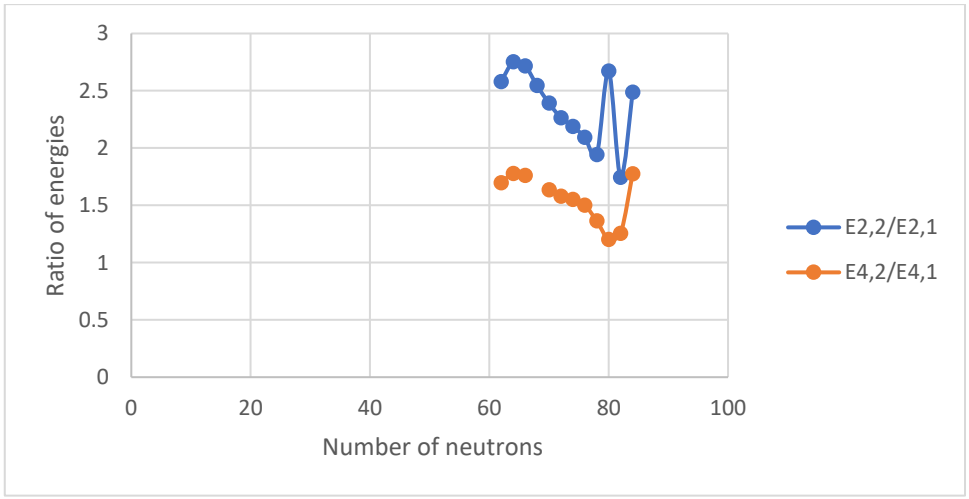

C

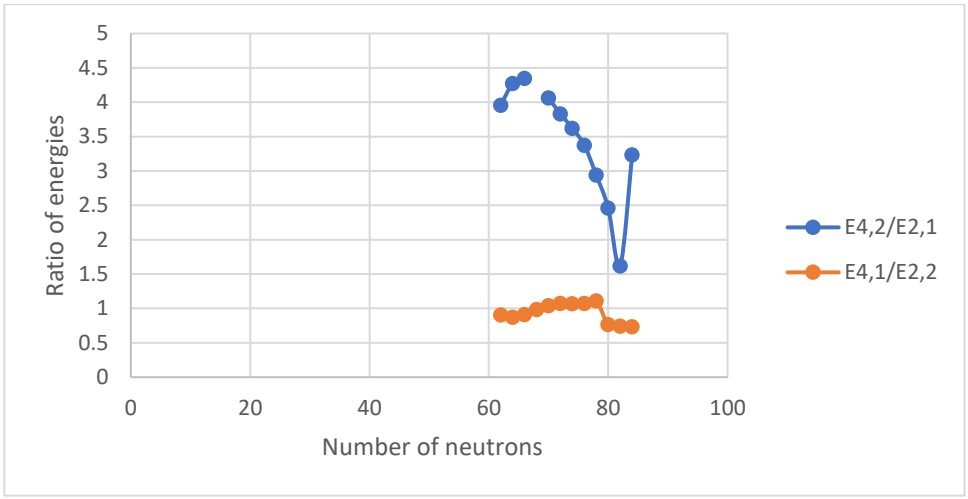

D

Figure III. 27 (color online) Panel **A** represents the comparison of the experimental energy levels of the lowest 2_1^+, 2_2^+, 4_1^+ and 4_2^+ states for the chain of Xe isotopes. Panels **B, C, D** represent the comparison of the experimental energy ratios ($E_{4_1^+}/E_{2_1^+}$ and $E_{4_2^+}/E_{2_2^+}$), ($E_{2_2^+}/E_{2_1^+}$ and $E_{4_2^+}/E_{4_1^+}$) and ($E_{4_2^+}/E_{2_1^+}$ and $E_{4_1^+}/E_{2_2^+}$), respectively, for the chain of Xe isotopes.

Ba isotopes (Z =56)

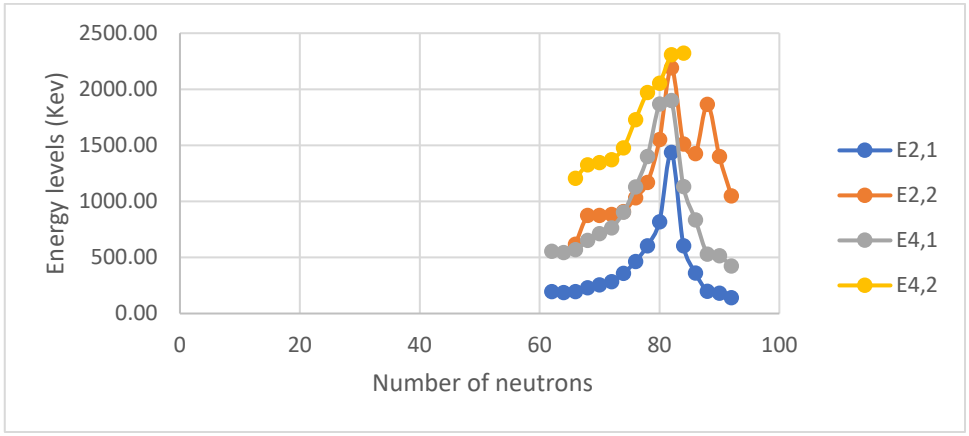

A

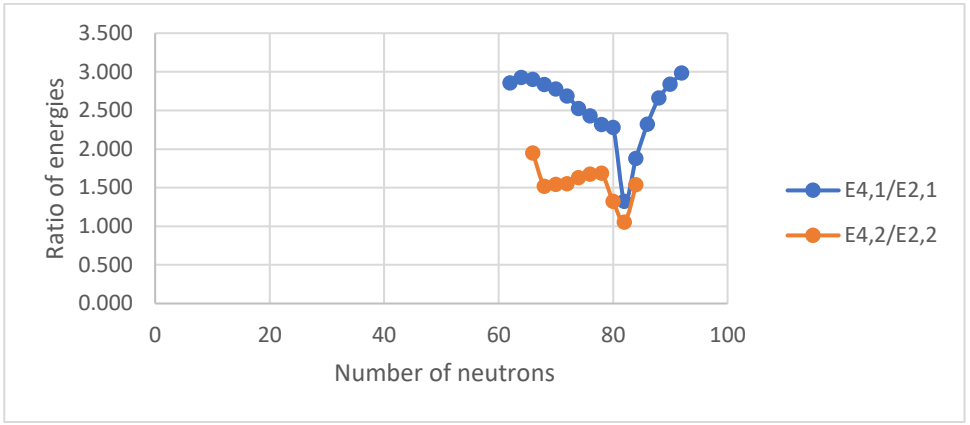

B

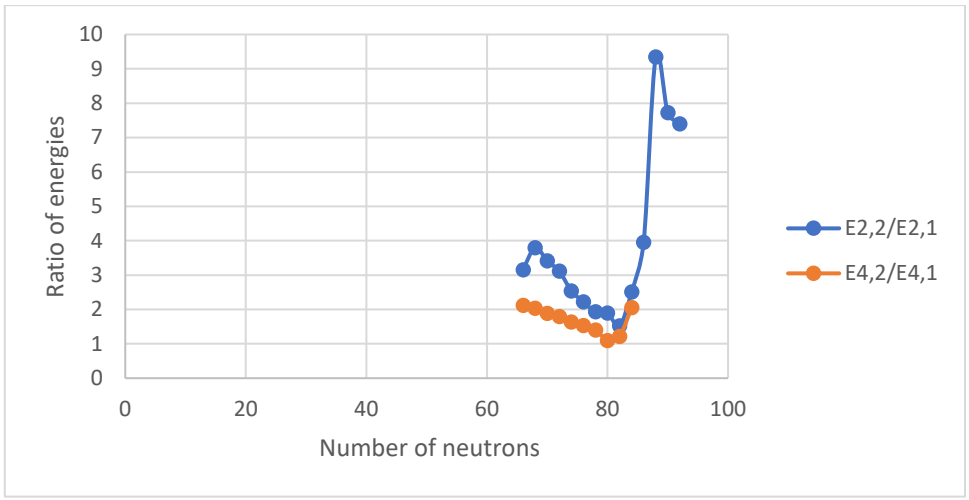

C

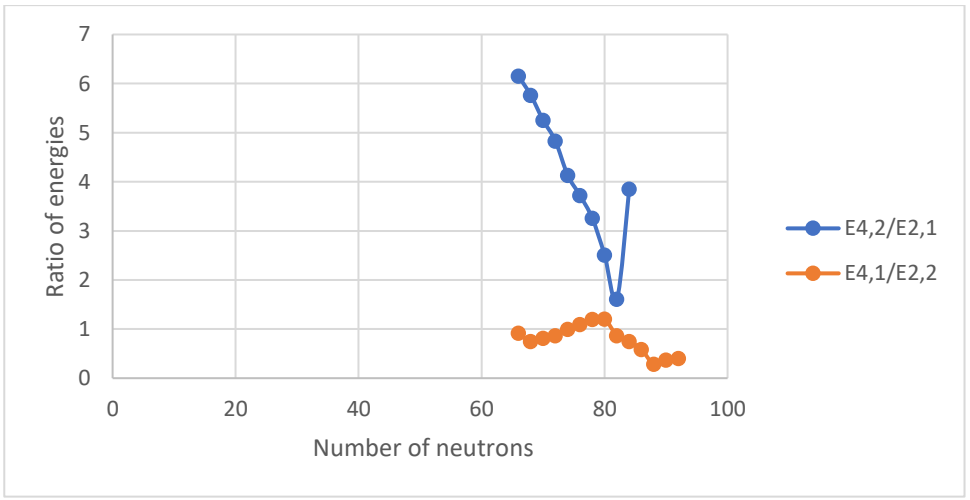

D

Figure III. 28 (color online) Panel **A** represents the comparison of the experimental energy levels of the lowest 2_1^+, 2_2^+, 4_1^+ and 4_2^+ states for the chain of Ba isotopes. Panels **B, C, D** represent the comparison of the experimental energy ratios ($E_{4_1^+}/E_{2_1^+}$ and $E_{4_2^+}/E_{2_2^+}$), ($E_{2_2^+}/E_{2_1^+}$ and $E_{4_2^+}/E_{4_1^+}$) and ($E_{4_2^+}/E_{2_1^+}$ and $E_{4_1^+}/E_{2_2^+}$), respectively, for the chain of Ba isotopes.

Ce isotopes (Z =58)

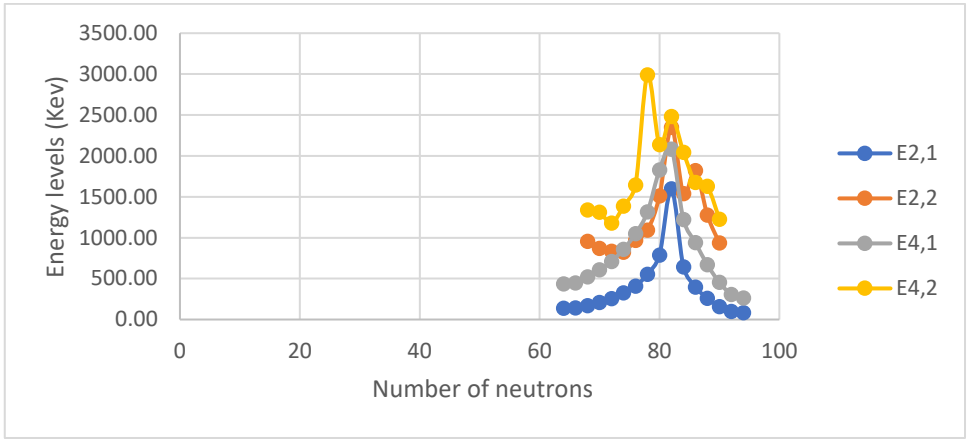

A

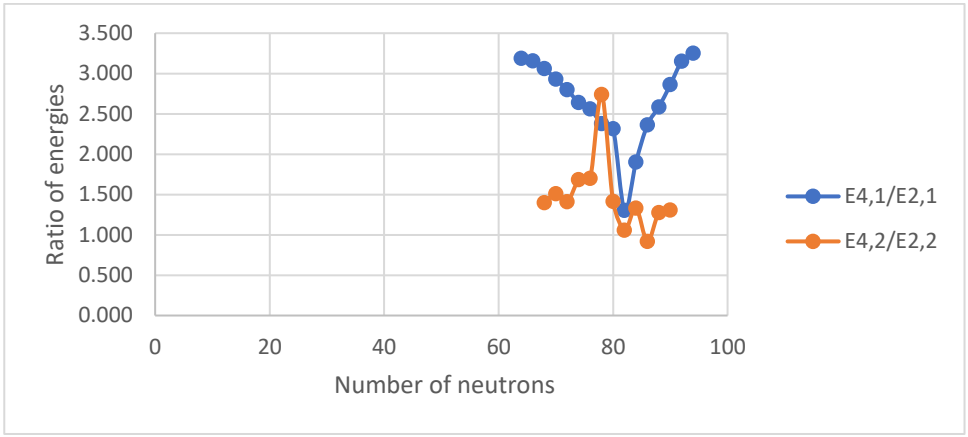

B

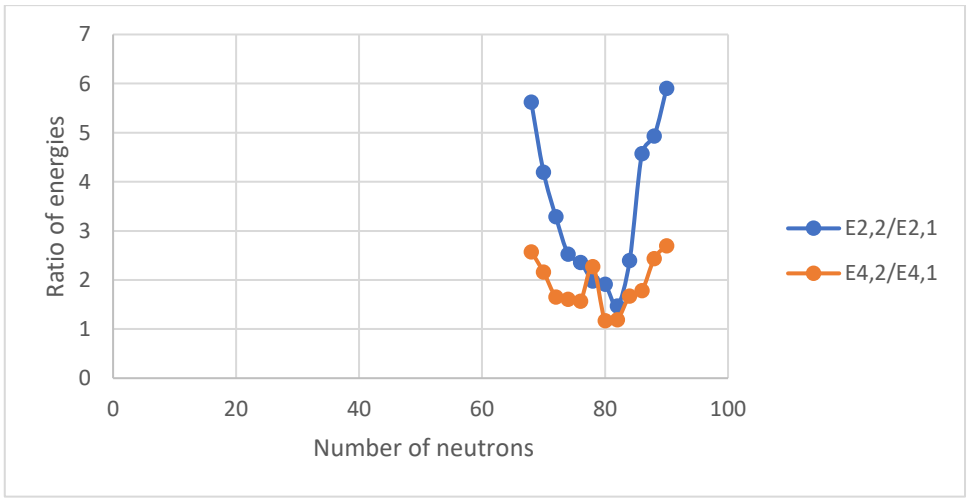

C

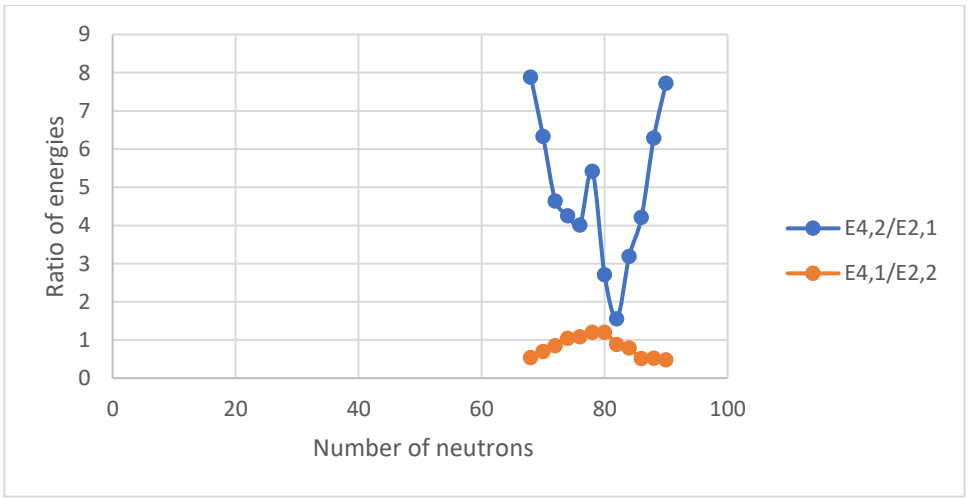

D

Figure III. 29 (color online) Panel **A** represents the comparison of the experimental energy levels of the lowest 2_1^+, 2_2^+, 4_1^+ and 4_2^+ states for the chain of Ce isotopes. Panels **B, C, D** represent the comparison of the experimental energy ratios ($E_{4_1^+}/E_{2_1^+}$ and $E_{4_2^+}/E_{2_2^+}$), ($E_{2_2^+}/E_{2_1^+}$ and $E_{4_2^+}/E_{4_1^+}$) and ($E_{4_2^+}/E_{2_1^+}$ and $E_{4_1^+}/E_{2_2^+}$), respectively, for the chain of Ce isotopes.

Nd isotopes (Z =60)

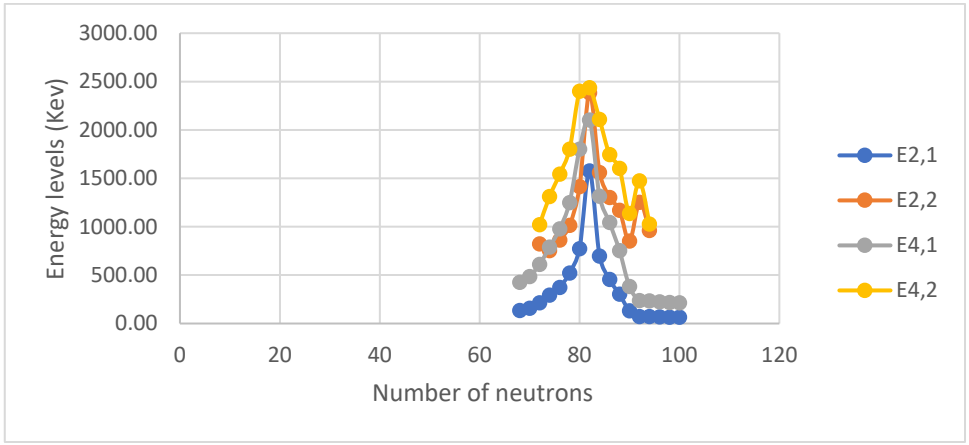

A

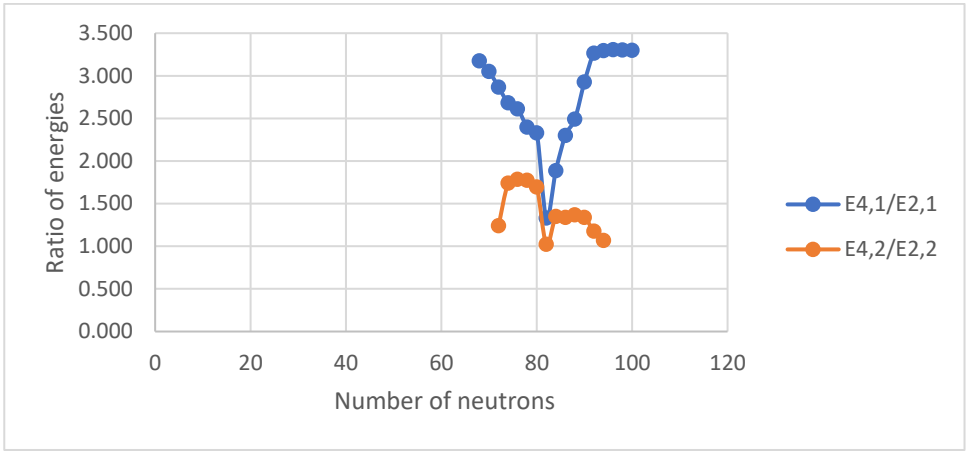

B

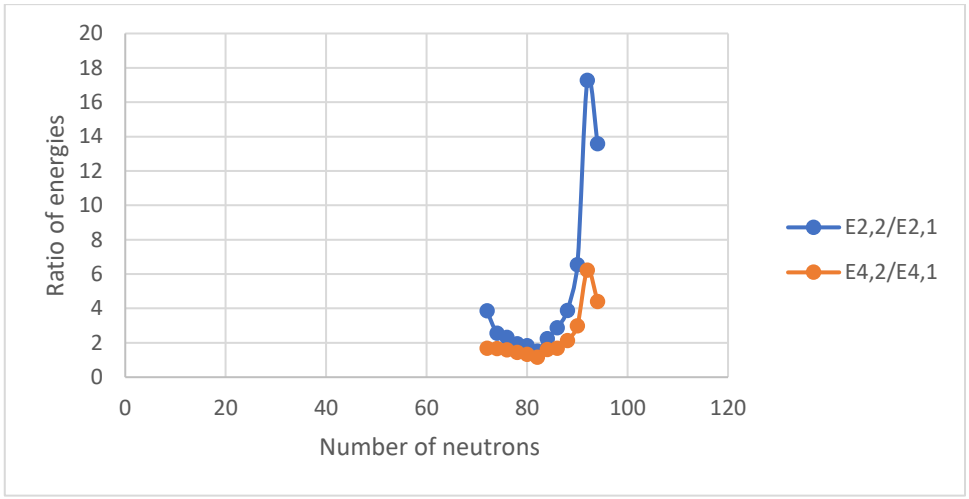

C

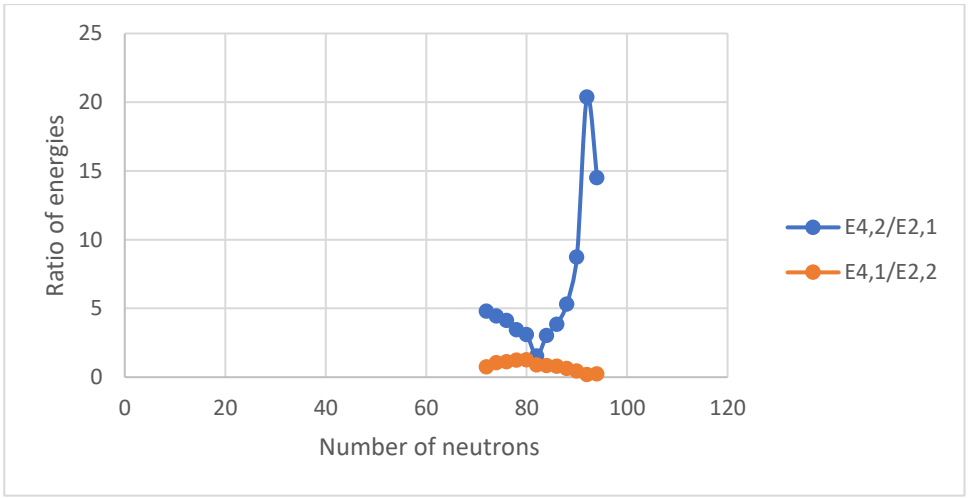

D

Figure III. 30 (color online) Panel **A** represents the comparison of the experimental energy levels of the lowest 2_1^+, 2_2^+, 4_1^+ and 4_2^+ states for the chain of Nd isotopes. Panels **B, C, D** represent the comparison of the experimental energy ratios ($E_{4_1^+}/E_{2_1^+}$ and $E_{4_2^+}/E_{2_2^+}$), ($E_{2_2^+}/E_{2_1^+}$ and $E_{4_2^+}/E_{4_1^+}$) and ($E_{4_2^+}/E_{2_1^+}$ and $E_{4_1^+}/E_{2_2^+}$), respectively, for the chain of Nd isotopes.

Sm isotopes (Z =62)

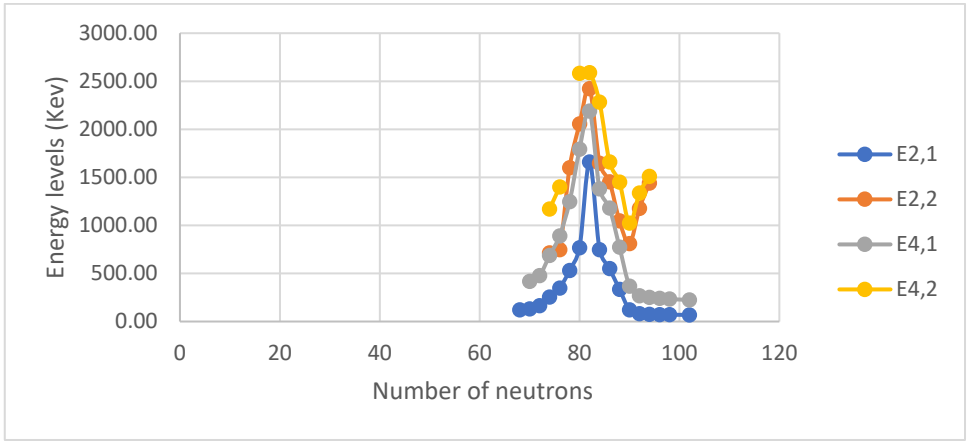

A

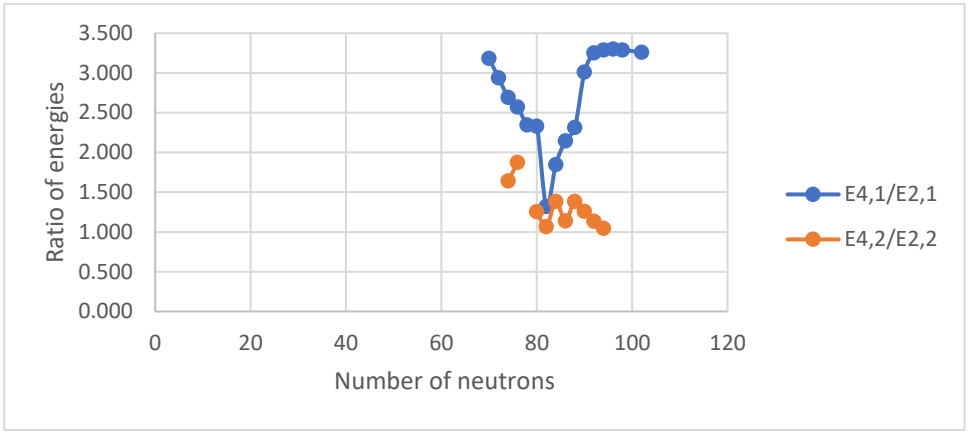

B

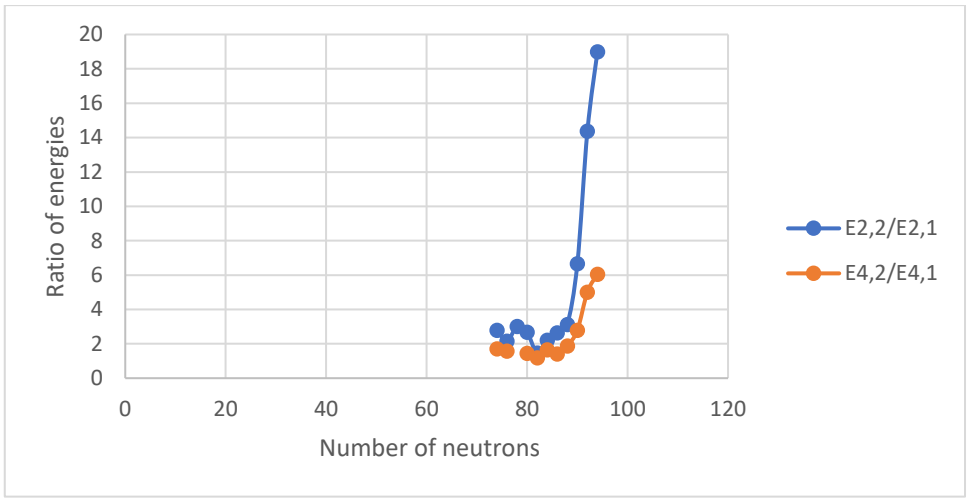

C

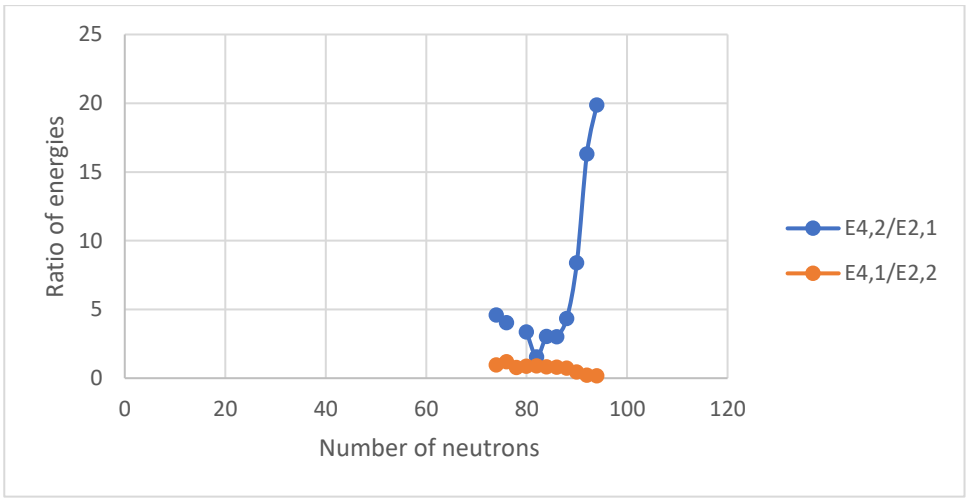

D

Figure III. 31 (color online) Panel **A** represents the comparison of the experimental energy levels of the lowest 2_1^+, 2_2^+, 4_1^+ and 4_2^+ states for the chain of Sm isotopes. Panels **B, C, D** represent the comparison of the experimental energy ratios ($E_{4_1^+}/E_{2_1^+}$ and $E_{4_2^+}/E_{2_2^+}$), ($E_{2_2^+}/E_{2_1^+}$ and $E_{4_2^+}/E_{4_1^+}$) and ($E_{4_2^+}/E_{2_1^+}$ and $E_{4_1^+}/E_{2_2^+}$), respectively, for the chain of Sm isotopes.

Gd isotopes (Z =64)

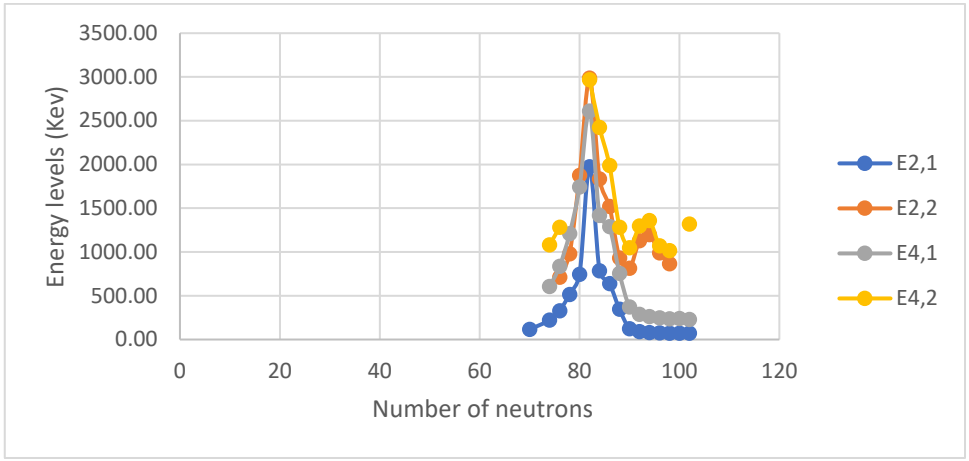

A

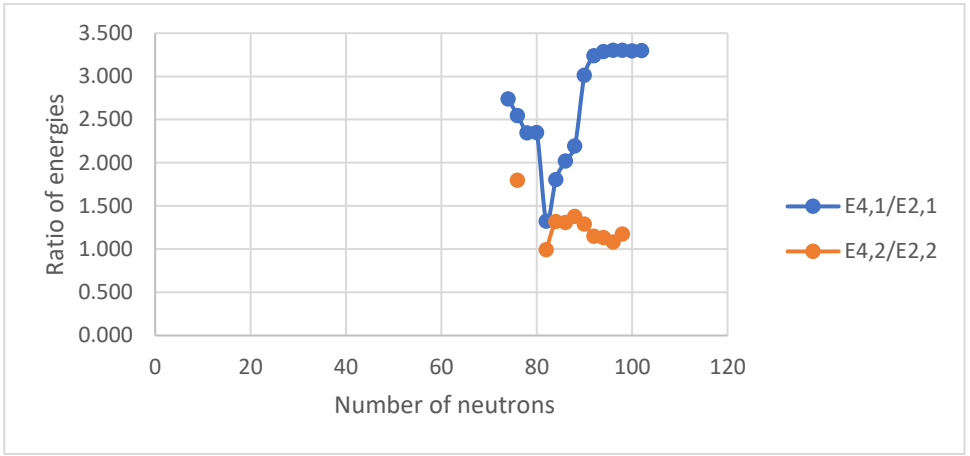

B

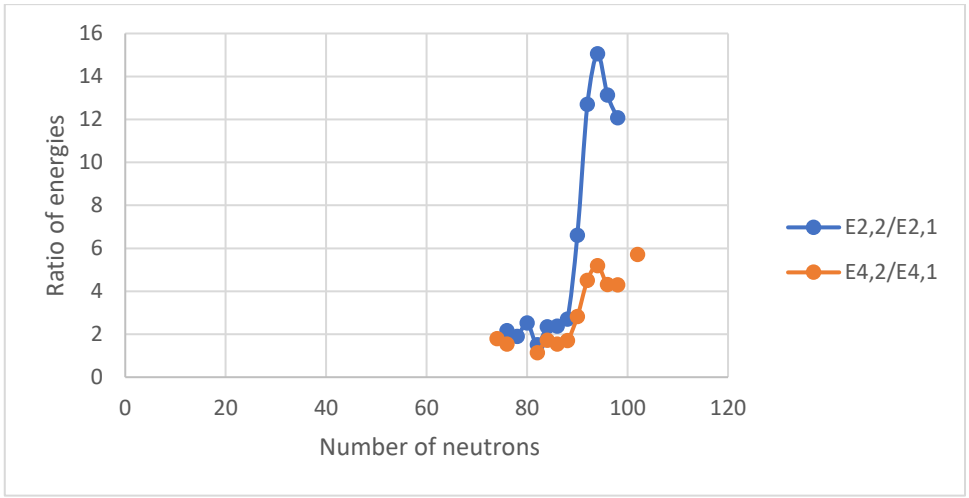

C

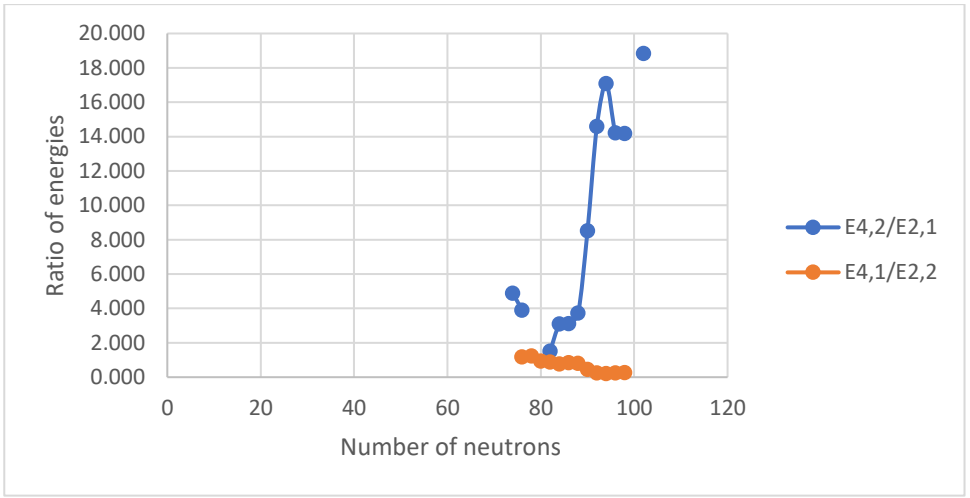

D

Figure III. 32 (color online) Panel **A** represents the comparison of the experimental energy levels of the lowest 2_1^+, 2_2^+, 4_1^+ and 4_2^+ states for the chain of Gd isotopes. Panels **B, C, D** represent the comparison of the experimental energy ratios ($E_{4_1^+}/E_{2_1^+}$ and $E_{4_2^+}/E_{2_2^+}$), ($E_{2_2^+}/E_{2_1^+}$ and $E_{4_2^+}/E_{4_1^+}$) and ($E_{4_2^+}/E_{2_1^+}$ and $E_{4_1^+}/E_{2_2^+}$), respectively, for the chain of Gd isotopes.

Dy isotopes (Z =66)

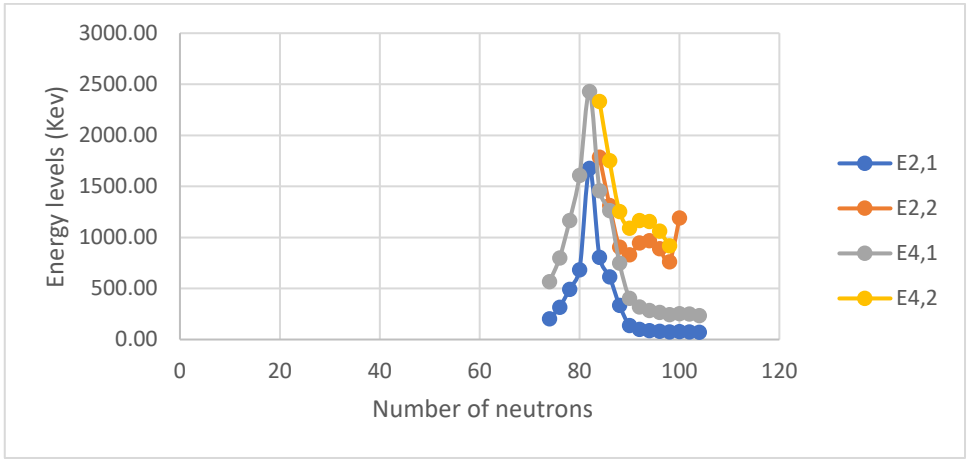

A

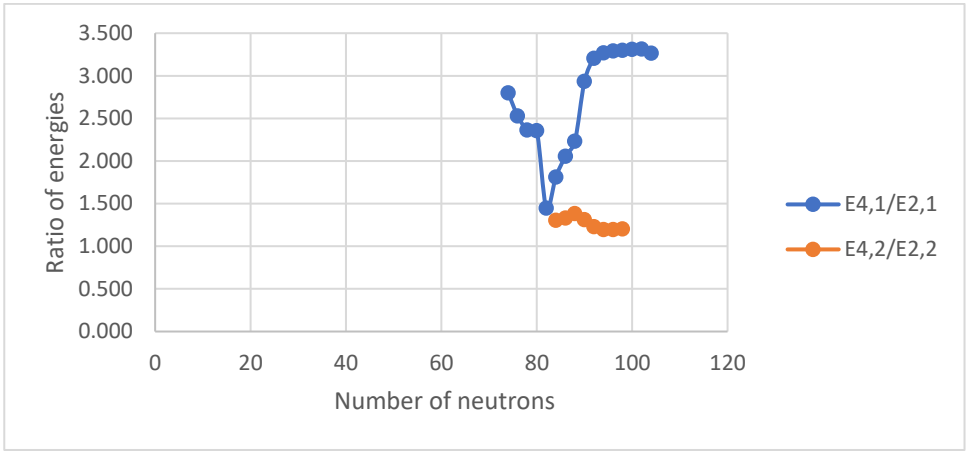

B

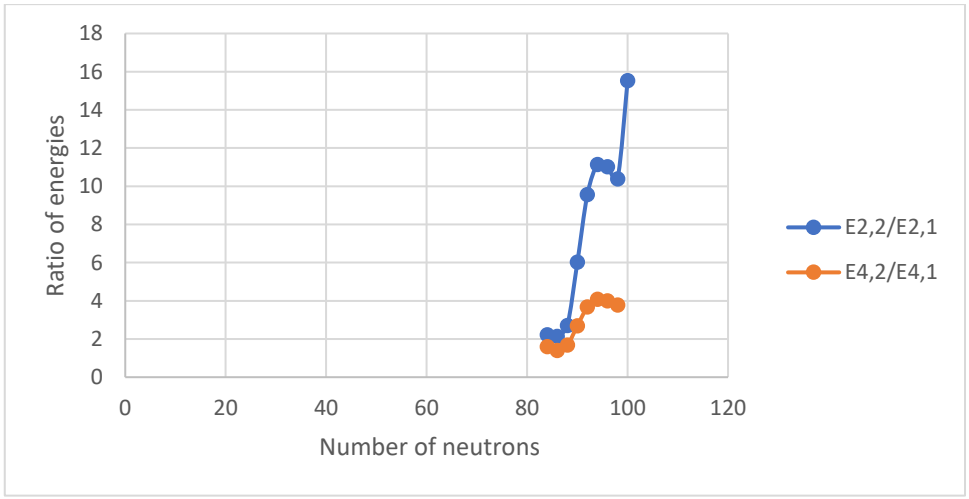

C

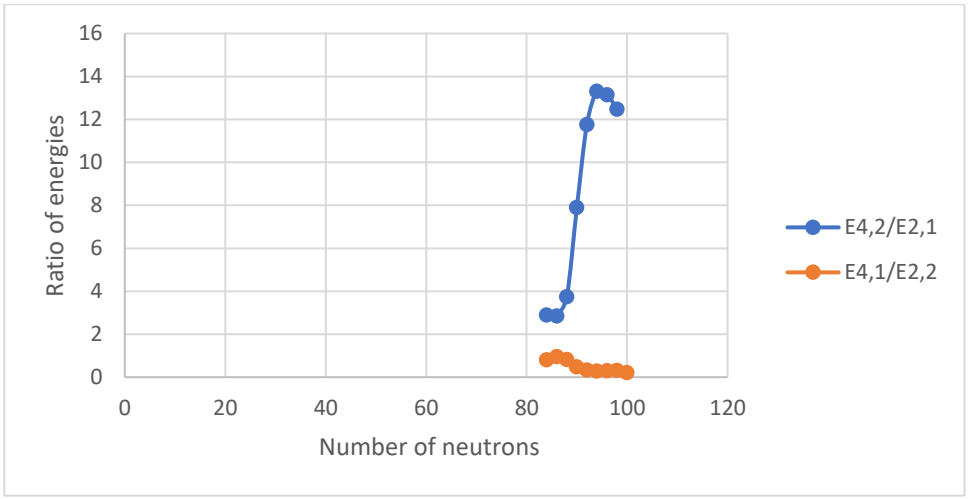

D

Figure III. 33 (color online) Panel **A** represents the comparison of the experimental energy levels of the lowest 2_1^+, 2_2^+, 4_1^+ and 4_2^+ states for the chain of Dy isotopes. Panels **B, C, D** represent the comparison of the experimental energy ratios ($E_{4_1^+}/E_{2_1^+}$ and $E_{4_2^+}/E_{2_2^+}$), ($E_{2_2^+}/E_{2_1^+}$ and $E_{4_2^+}/E_{4_1^+}$) and ($E_{4_2^+}/E_{2_1^+}$ and $E_{4_1^+}/E_{2_2^+}$), respectively, for the chain of Dy isotopes.

Er isotopes (Z =68)

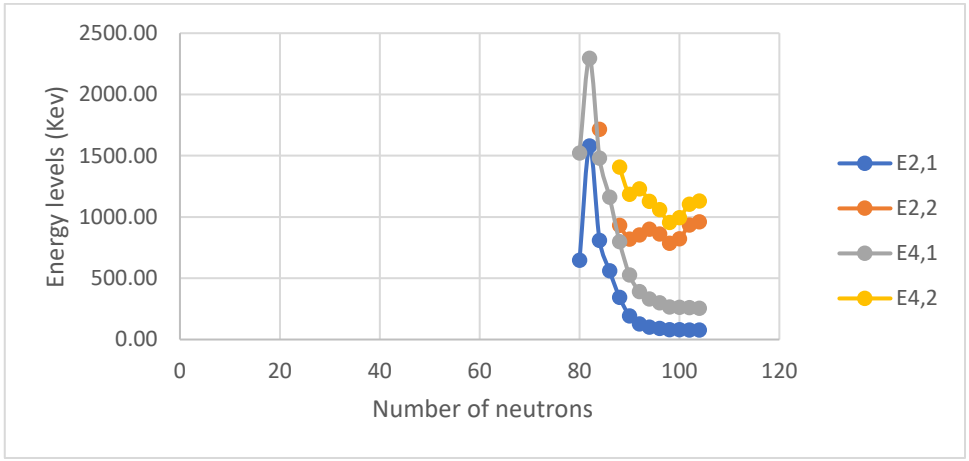

A

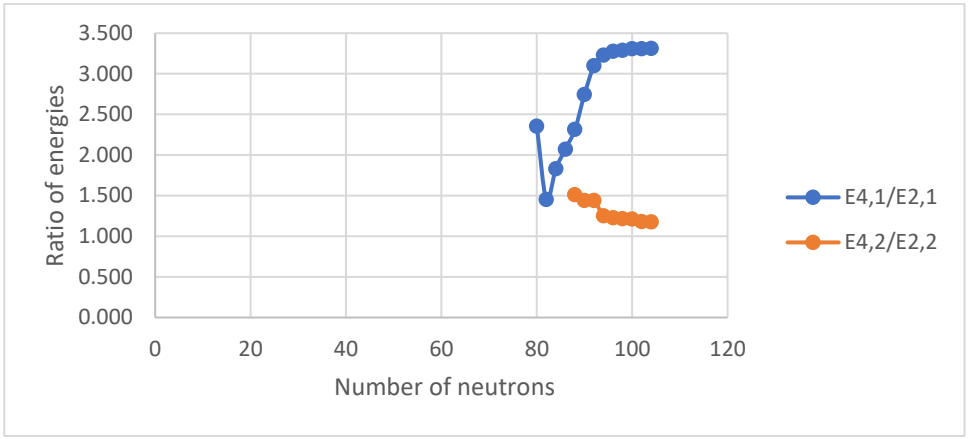

B

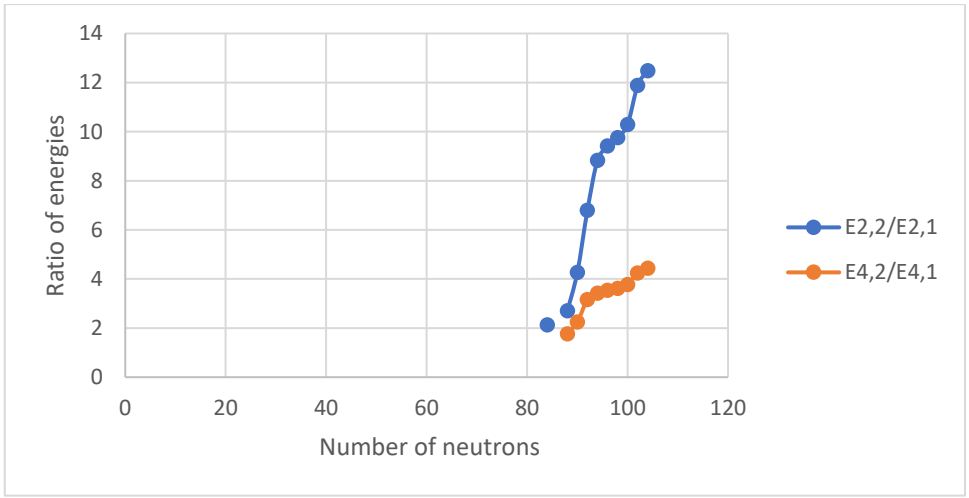

C

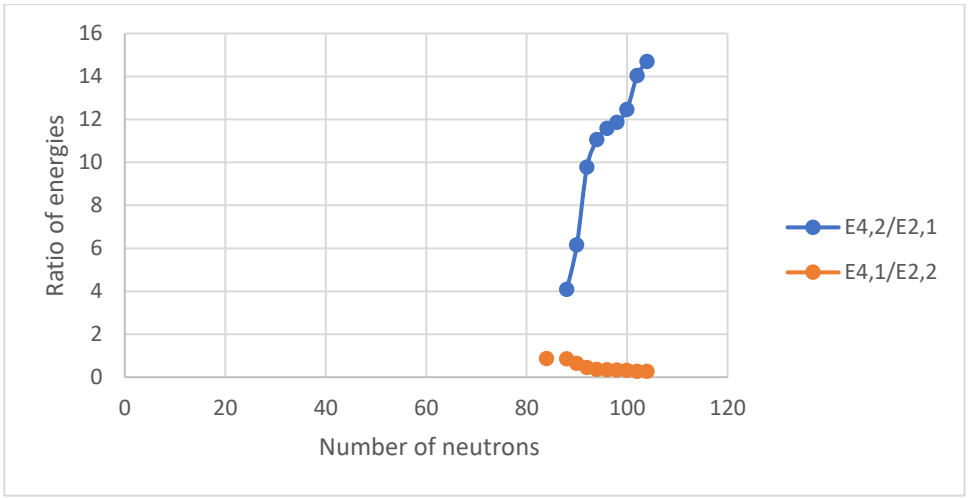

D

Figure III. 34 (color online) Panel **A** represents the comparison of the experimental energy levels of the lowest 2_1^+, 2_2^+, 4_1^+ and 4_2^+ states for the chain of Er isotopes. Panels **B, C, D** represent the comparison of the experimental energy ratios ($E_{4_1^+}/E_{2_1^+}$ and $E_{4_2^+}/E_{2_2^+}$), ($E_{2_2^+}/E_{2_1^+}$ and $E_{4_2^+}/E_{4_1^+}$) and ($E_{4_2^+}/E_{2_1^+}$ and $E_{4_1^+}/E_{2_2^+}$), respectively, for the chain of Er isotopes.

Yb isotopes (Z =70)

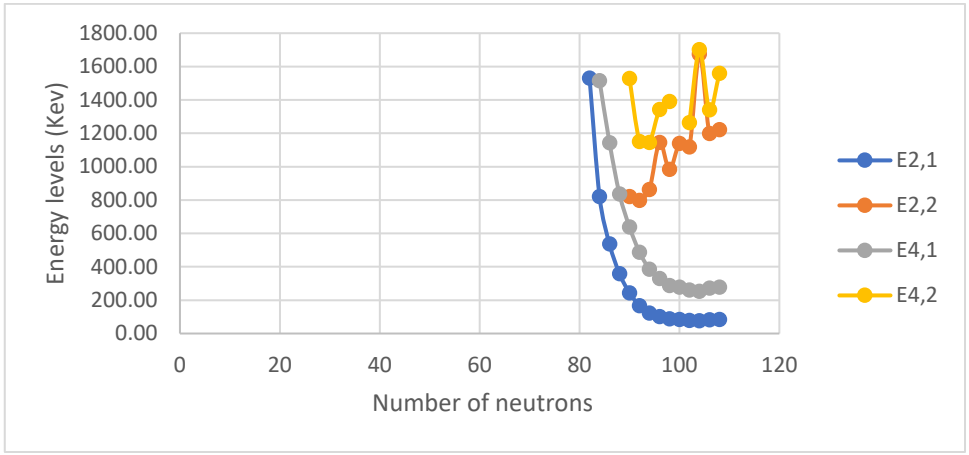

A

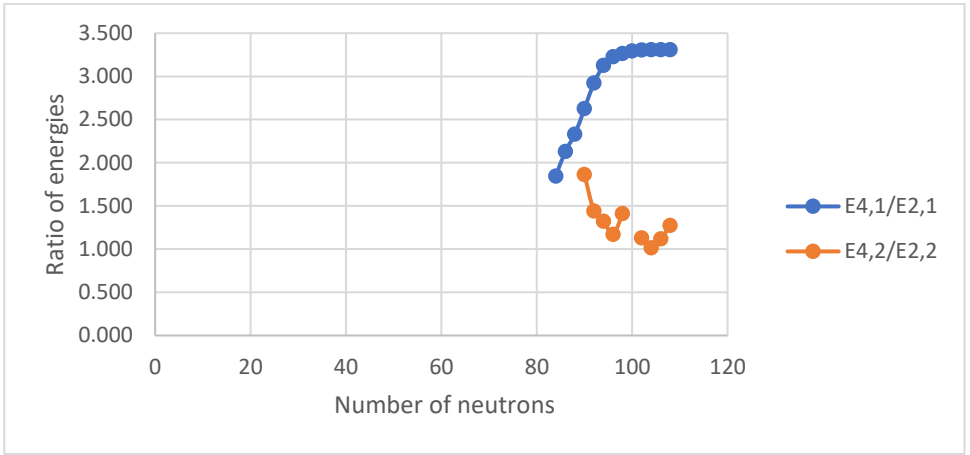

B

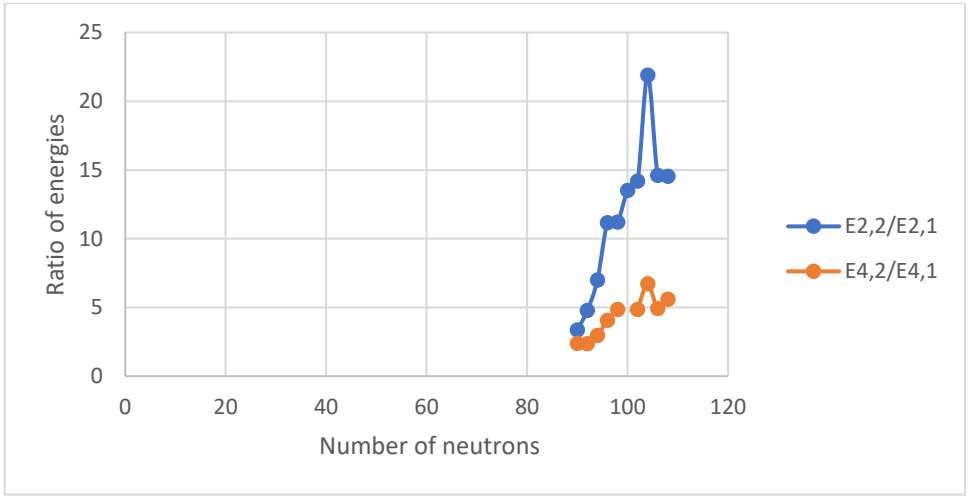

C

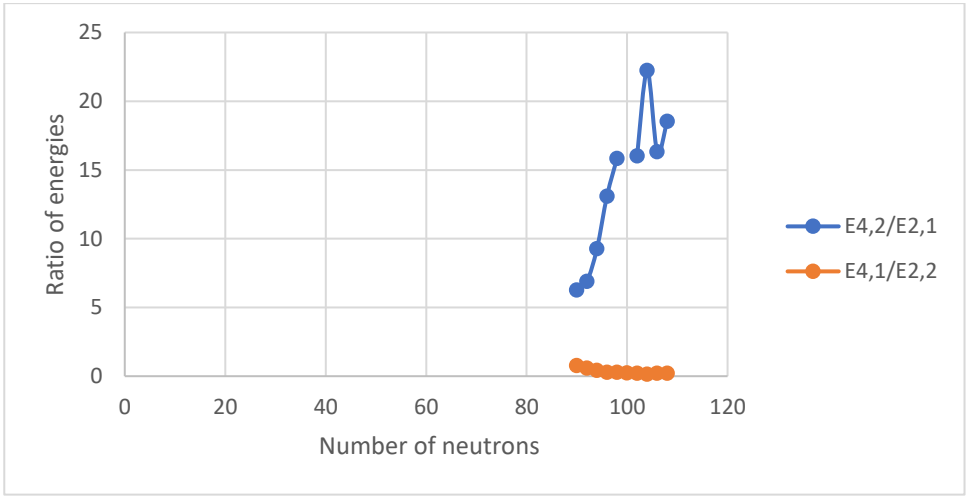

D

Figure III. 35 (color online) Panel **A** represents the comparison of the experimental energy levels of the lowest 2_1^+, 2_2^+, 4_1^+ and 4_2^+ states for the chain of Yb isotopes. Panels **B, C, D** represent the comparison of the experimental energy ratios ($E_{4_1^+}/E_{2_1^+}$ and $E_{4_2^+}/E_{2_2^+}$), ($E_{2_2^+}/E_{2_1^+}$ and $E_{4_2^+}/E_{4_1^+}$) and ($E_{4_2^+}/E_{2_1^+}$ and $E_{4_1^+}/E_{2_2^+}$), respectively, for the chain of Yb isotopes.

Hf isotopes (Z =72)

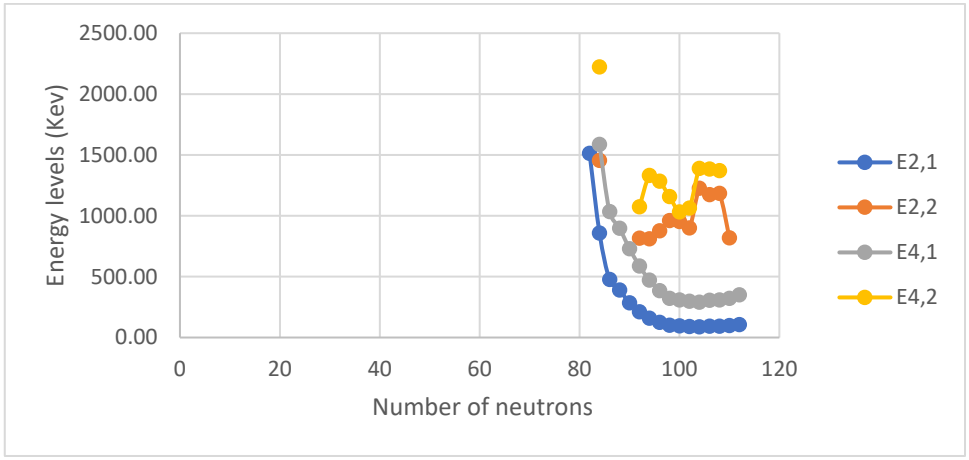

A

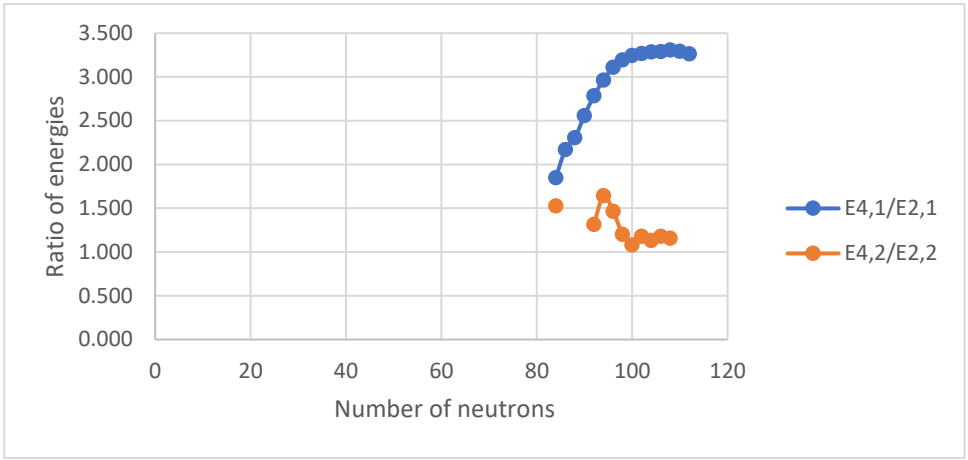

B

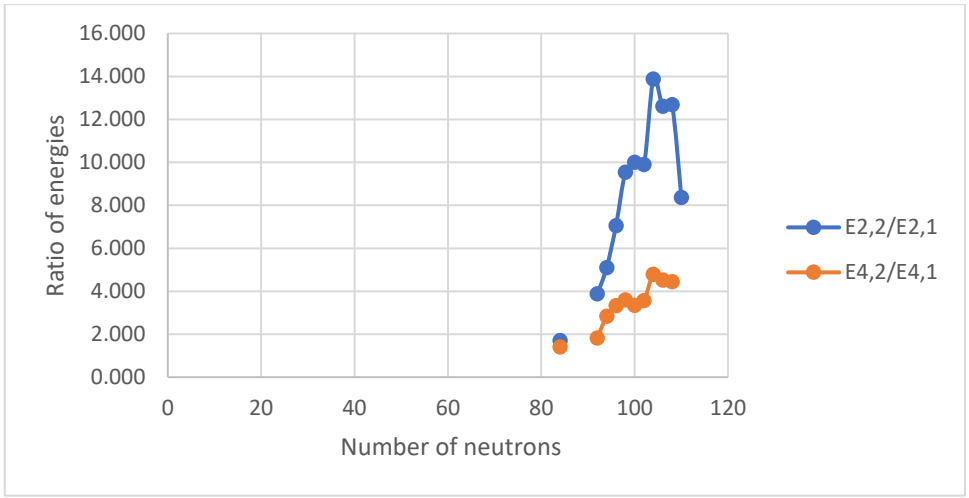

C

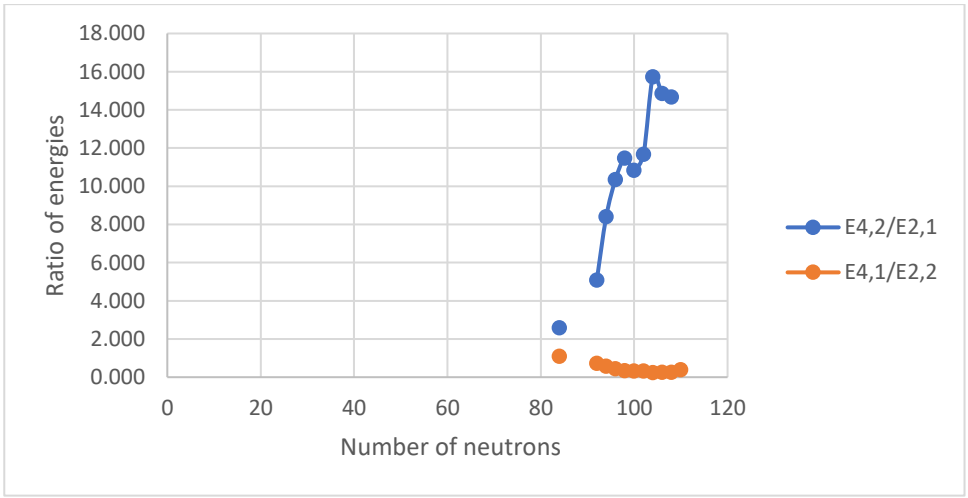

D

Figure III. 36 (color online) Panel **A** represents the comparison of the experimental energy levels of the lowest 2_1^+, 2_2^+, 4_1^+ and 4_2^+ states for the chain of Hf isotopes. Panels **B, C, D** represent the comparison of the experimental energy ratios ($E_{4_1^+}/E_{2_1^+}$ and $E_{4_2^+}/E_{2_2^+}$), ($E_{2_2^+}/E_{2_1^+}$ and $E_{4_2^+}/E_{4_1^+}$) and ($E_{4_2^+}/E_{2_1^+}$ and $E_{4_1^+}/E_{2_2^+}$), respectively, for the chain of Hf isotopes.

W isotopes (Z =74)

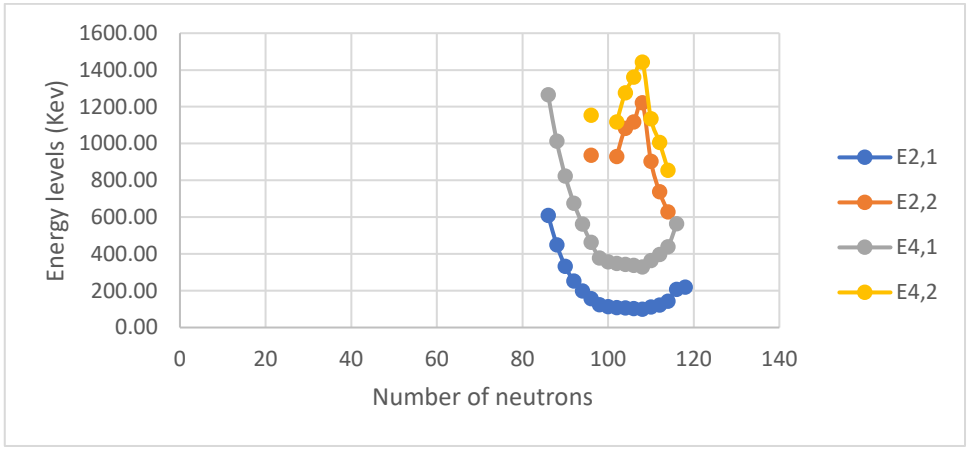

A

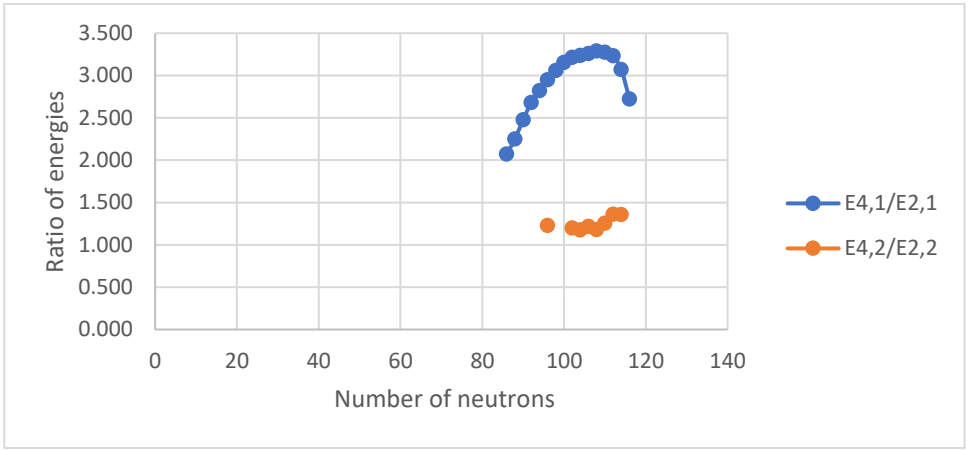

B

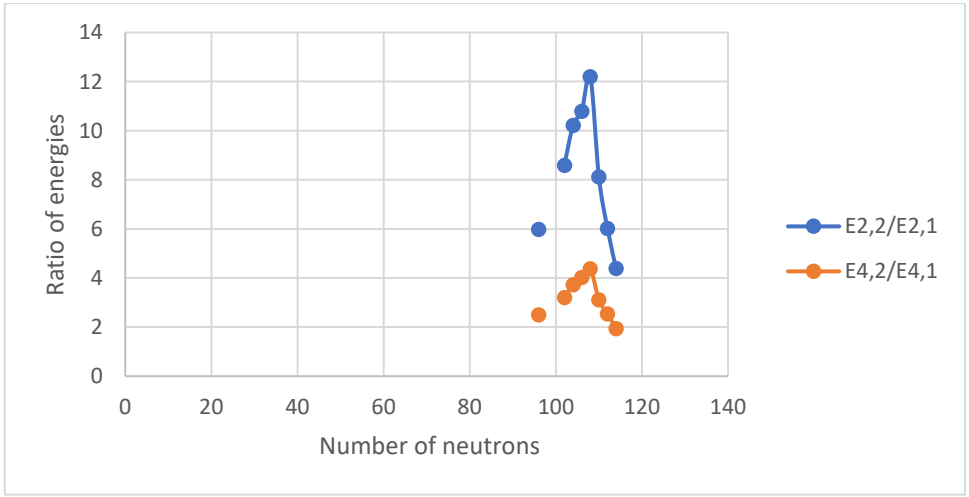

C

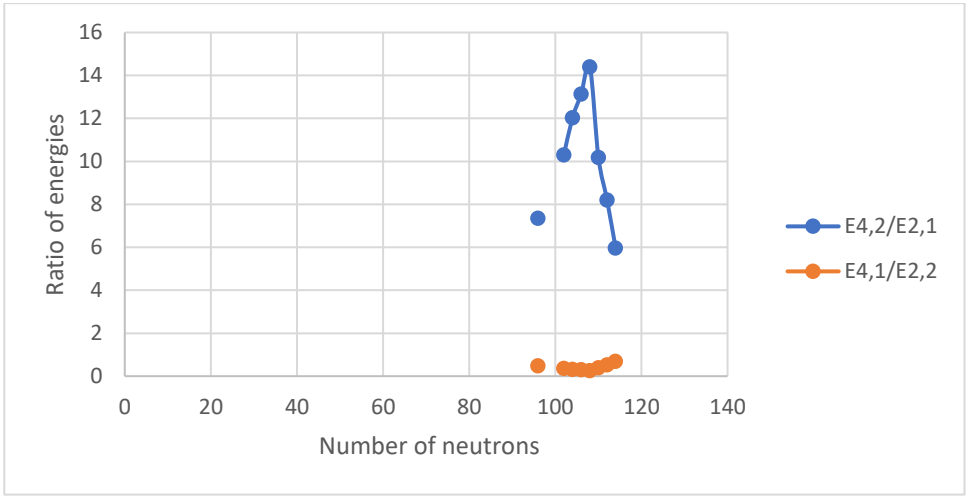

D

Figure III. 37 (color online) Panel **A** represents the comparison of the experimental energy levels of the lowest 2_1^+, 2_2^+, 4_1^+ and 4_2^+ states for the chain of W isotopes. Panels **B, C, D** represent the comparison of the experimental energy ratios ($E_{4_1^+}/E_{2_1^+}$ and $E_{4_2^+}/E_{2_2^+}$), ($E_{2_2^+}/E_{2_1^+}$ and $E_{4_2^+}/E_{4_1^+}$) and ($E_{4_2^+}/E_{2_1^+}$ and $E_{4_1^+}/E_{2_2^+}$), respectively, for the chain of W isotopes.

Os isotopes (Z =76)

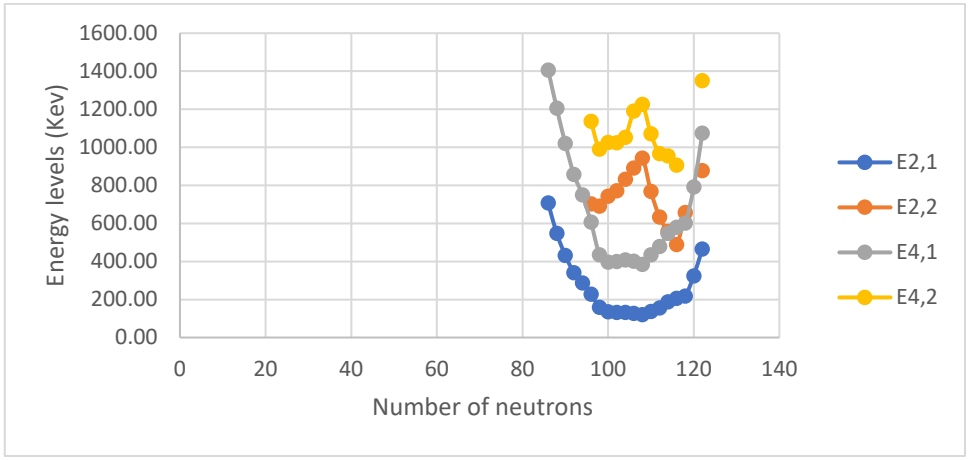

A

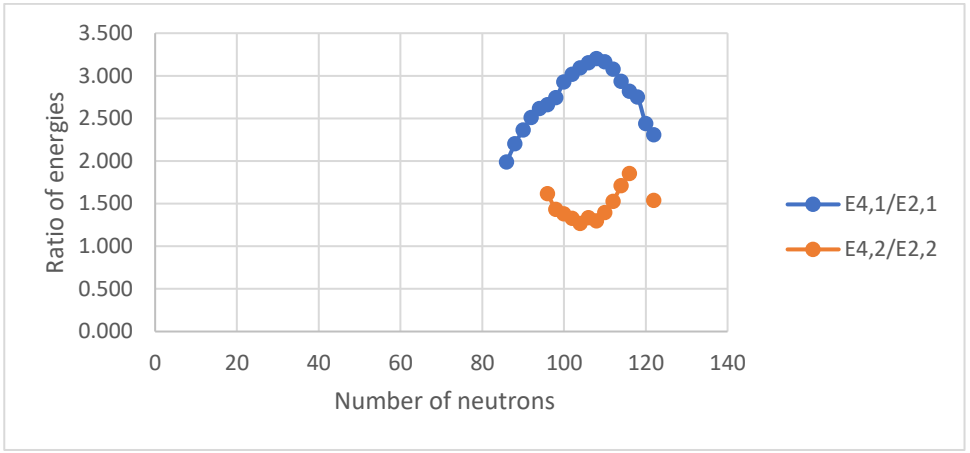

B

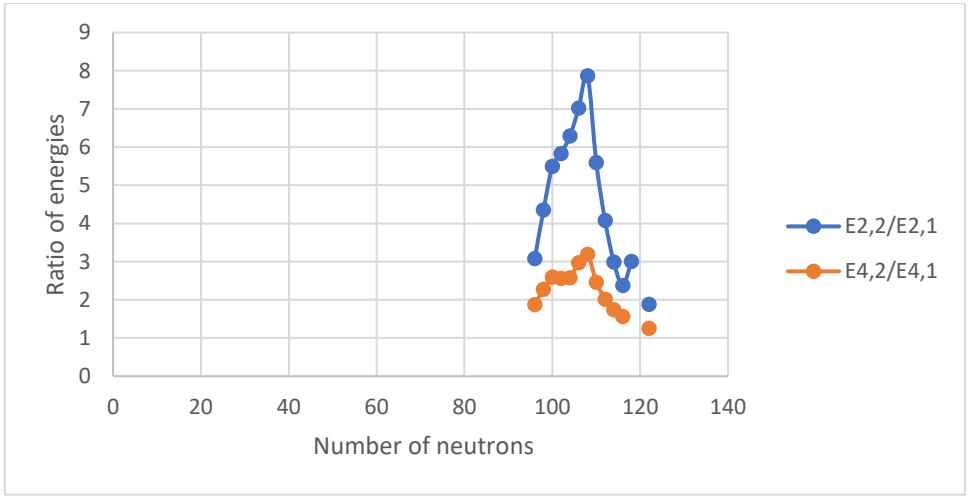

C

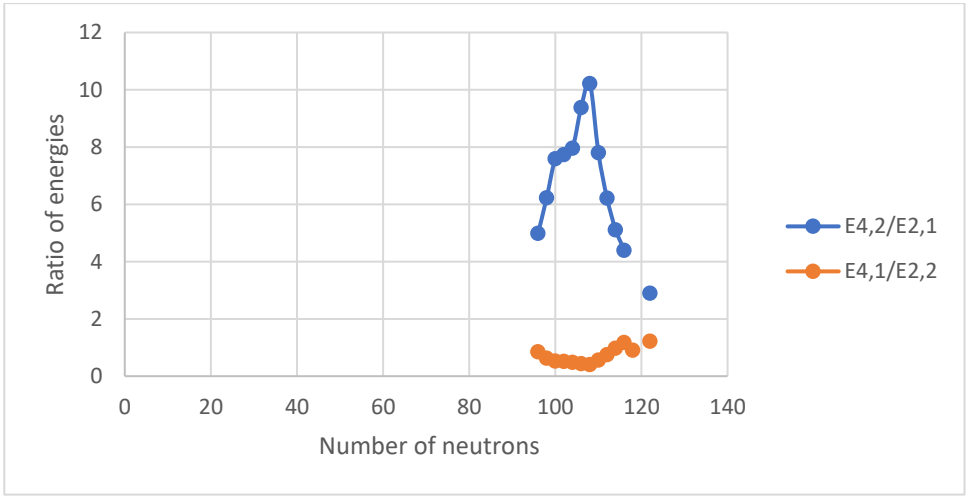

D

Figure III. 38 (color online) Panel **A** represents the comparison of the experimental energy levels of the lowest 2_1^+, 2_2^+, 4_1^+ and 4_2^+ states for the chain of Os isotopes. Panels **B, C, D** represent the comparison of the experimental energy ratios ($E_{4_1^+}/E_{2_1^+}$ and $E_{4_2^+}/E_{2_2^+}$), ($E_{2_2^+}/E_{2_1^+}$ and $E_{4_2^+}/E_{4_1^+}$) and ($E_{4_2^+}/E_{2_1^+}$ and $E_{4_1^+}/E_{2_2^+}$), respectively, for the chain of Os isotopes.

Pt isotopes (Z =78)

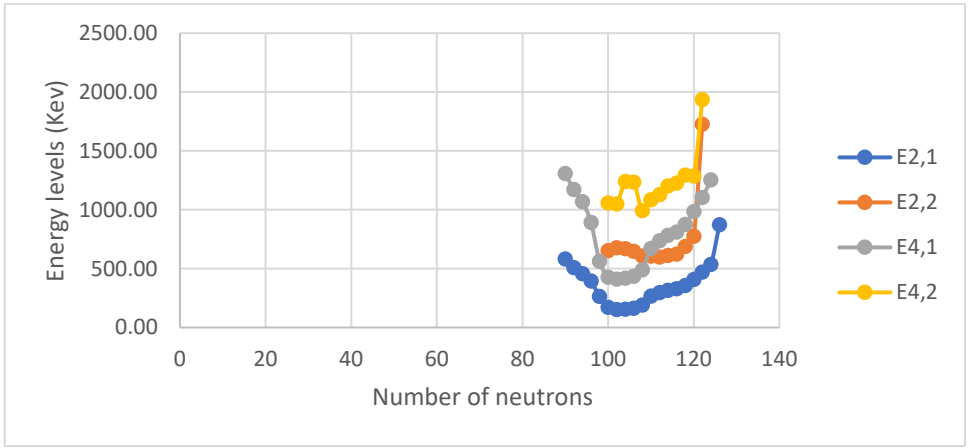

A

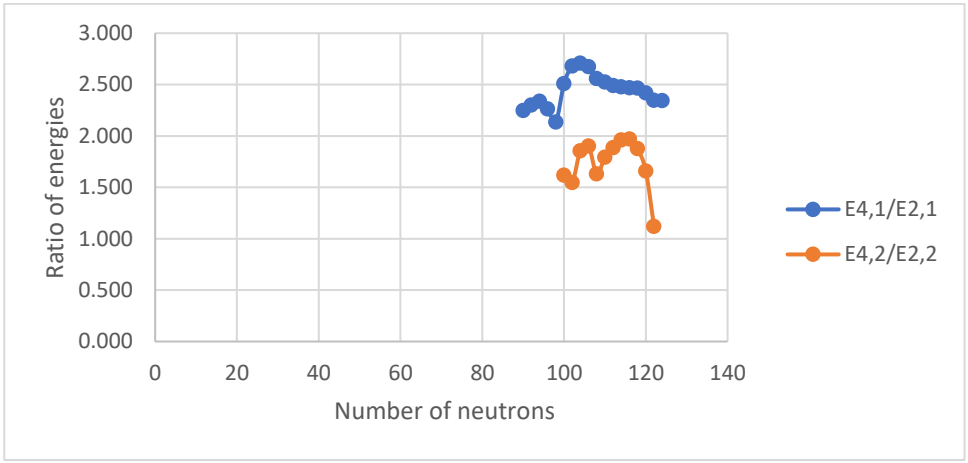

B

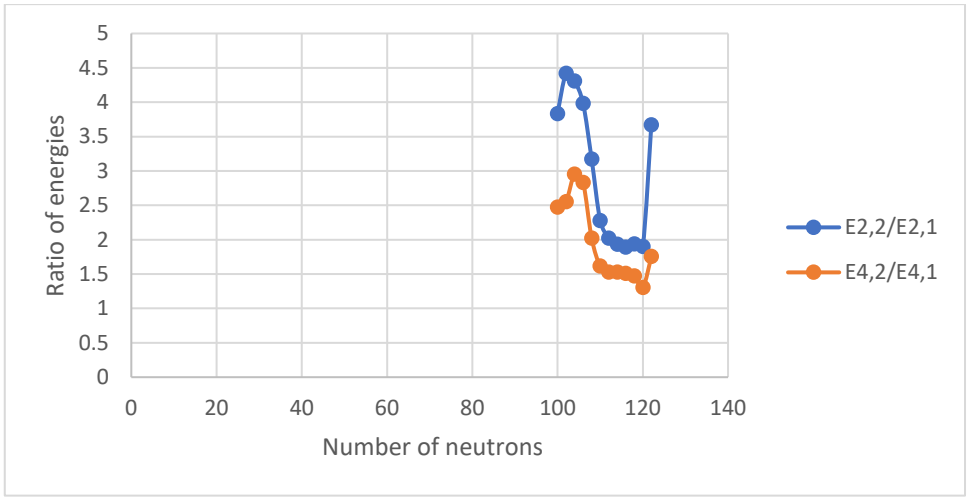

C

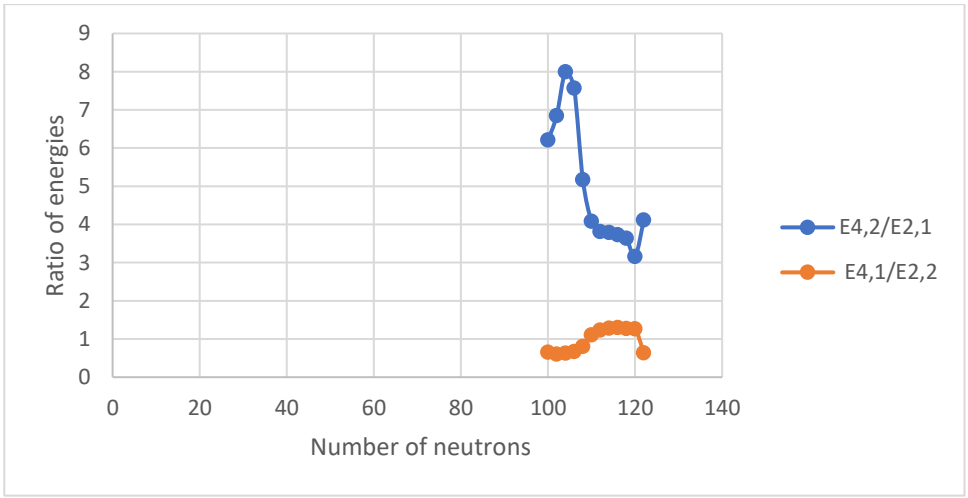

D

Figure III. 39 (color online) Panel **A** represents the comparison of the experimental energy levels of the lowest 2_1^+, 2_2^+, 4_1^+ and 4_2^+ states for the chain of Pt isotopes. Panels **B, C, D** represent the comparison of the experimental energy ratios ($E_{4_1^+}/E_{2_1^+}$ and $E_{4_2^+}/E_{2_2^+}$), ($E_{2_2^+}/E_{2_1^+}$ and $E_{4_2^+}/E_{4_1^+}$) and ($E_{4_2^+}/E_{2_1^+}$ and $E_{4_1^+}/E_{2_2^+}$), respectively, for the chain of Pt isotopes.

Hg isotopes (Z =80)

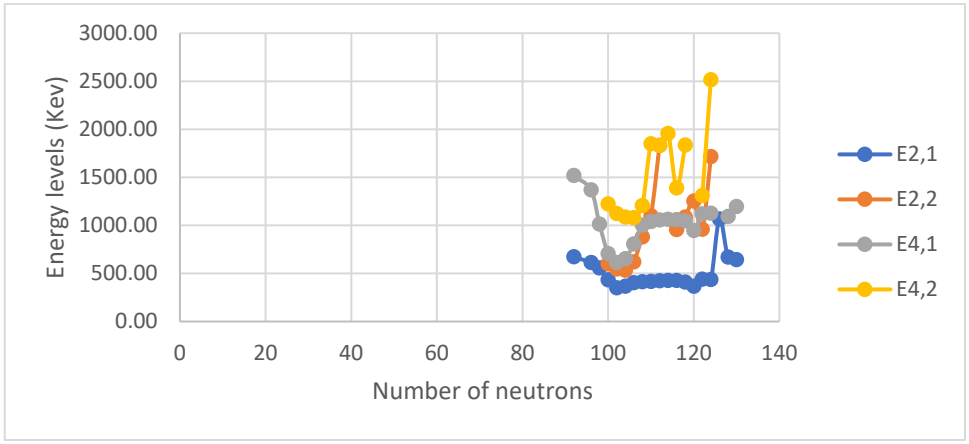

A

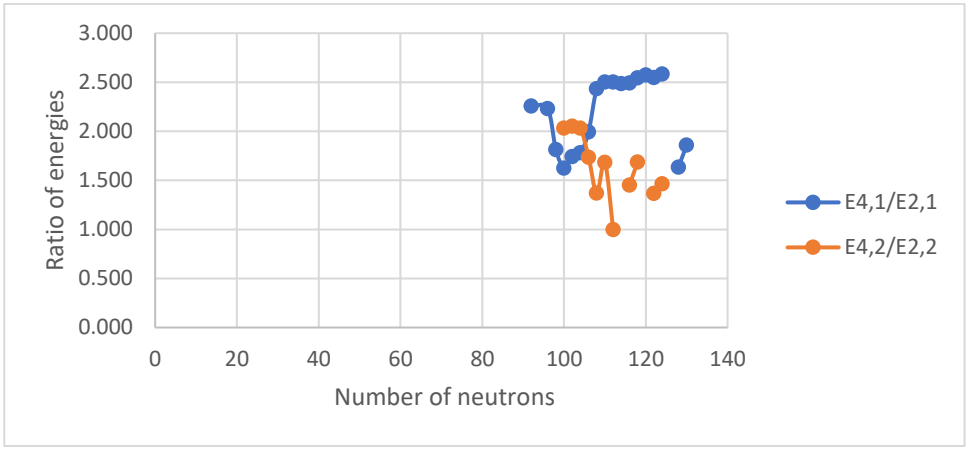

B

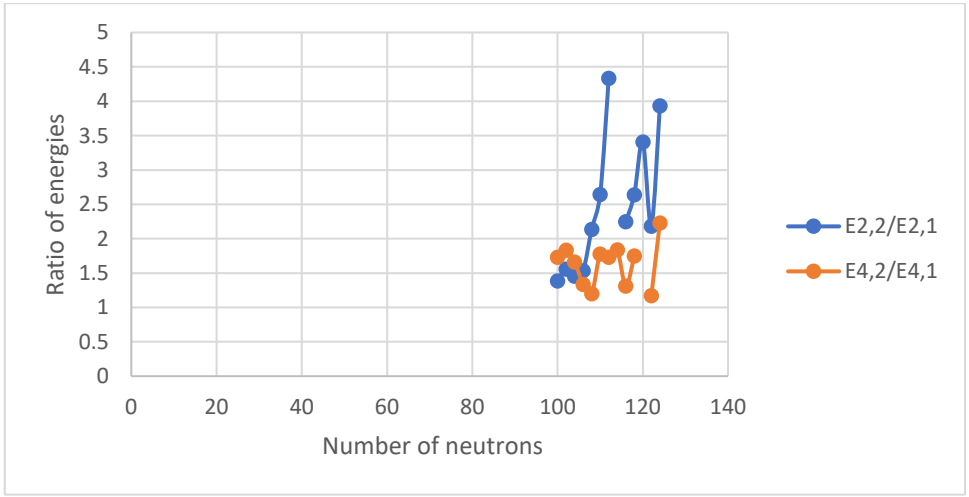

C

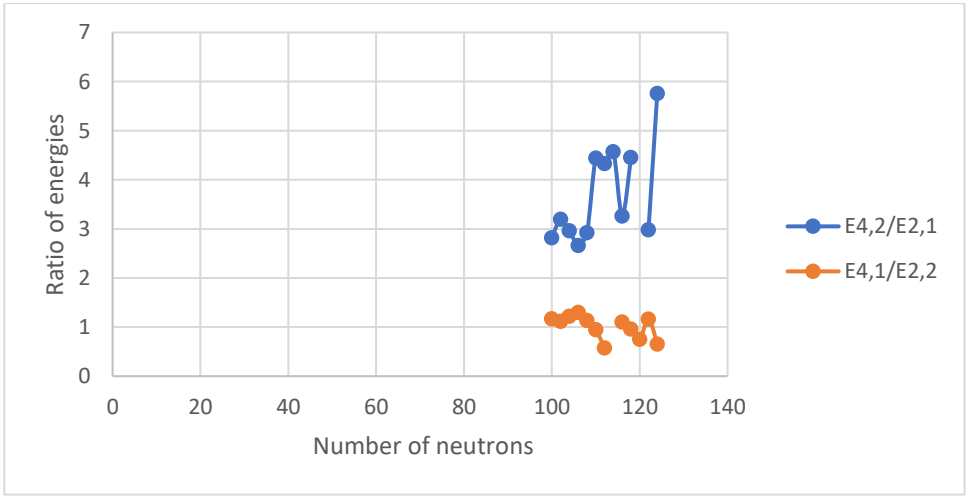

D

Figure III. 40 (color online) Panel **A** represents the comparison of the experimental energy levels of the lowest 2_1^+, 2_2^+, 4_1^+ and 4_2^+ states for the chain of Hg isotopes. Panels **B, C, D** represent the comparison of the experimental energy ratios ($E_{4_1^+}/E_{2_1^+}$ and $E_{4_2^+}/E_{2_2^+}$), ($E_{2_2^+}/E_{2_1^+}$ and $E_{4_2^+}/E_{4_1^+}$) and ($E_{4_2^+}/E_{2_1^+}$ and $E_{4_1^+}/E_{2_2^+}$), respectively, for the chain of Hg isotopes.

Pb isotopes (Z =82)

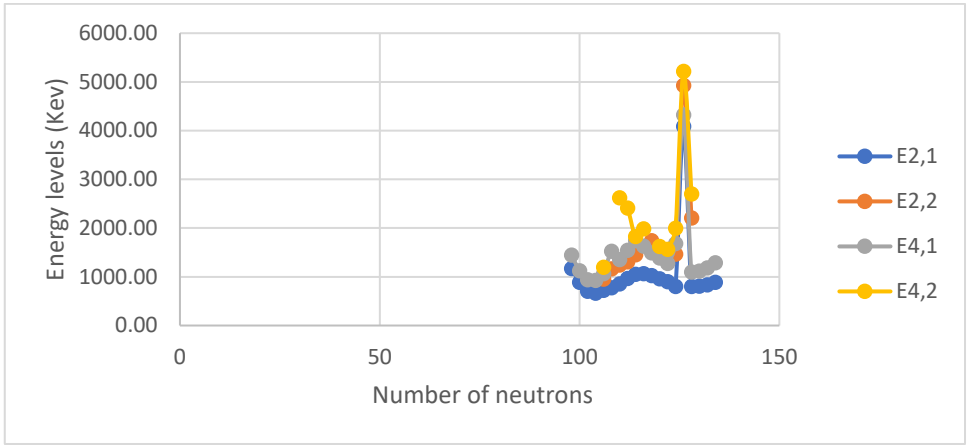

A

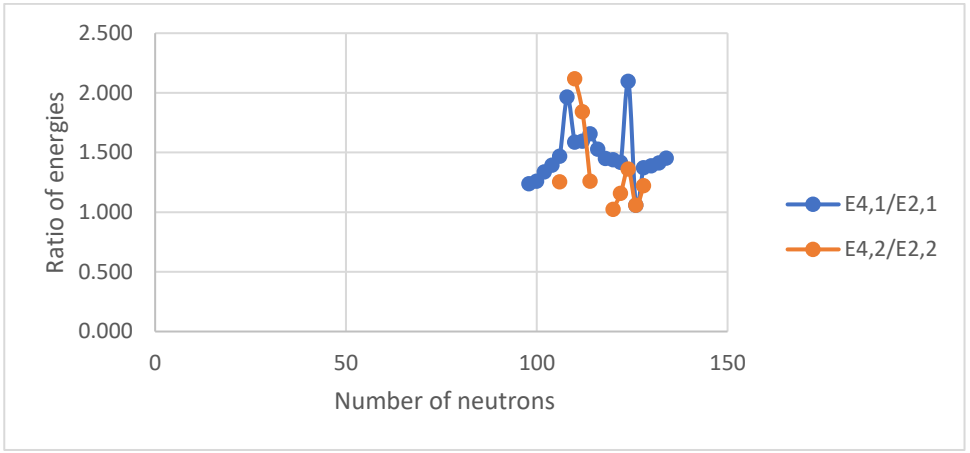

B

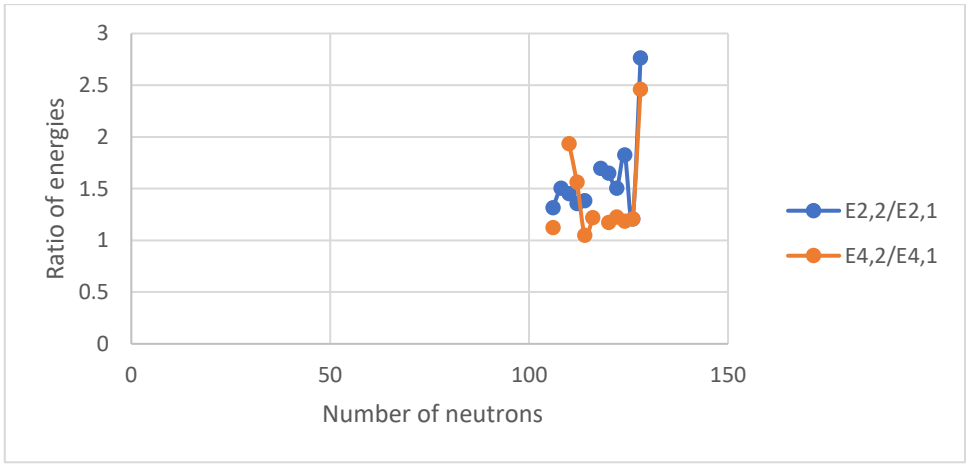

C

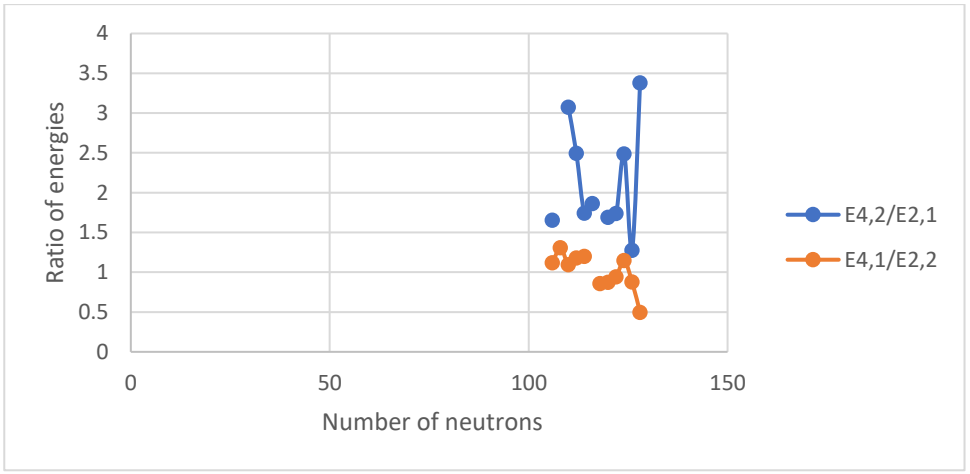

D

Figure III. 41 (color online) Panel **A** represents the comparison of the experimental energy levels of the lowest 2_1^+, 2_2^+, 4_1^+ and 4_2^+ states for the chain of Pb isotopes. Panels **B, C, D** represent the comparison of the experimental energy ratios ($E_{4_1^+}/E_{2_1^+}$ and $E_{4_2^+}/E_{2_2^+}$), ($E_{2_2^+}/E_{2_1^+}$ and $E_{4_2^+}/E_{4_1^+}$) and ($E_{4_2^+}/E_{2_1^+}$ and $E_{4_1^+}/E_{2_2^+}$), respectively, for the chain of Pb isotopes.

Po isotopes (Z =84)

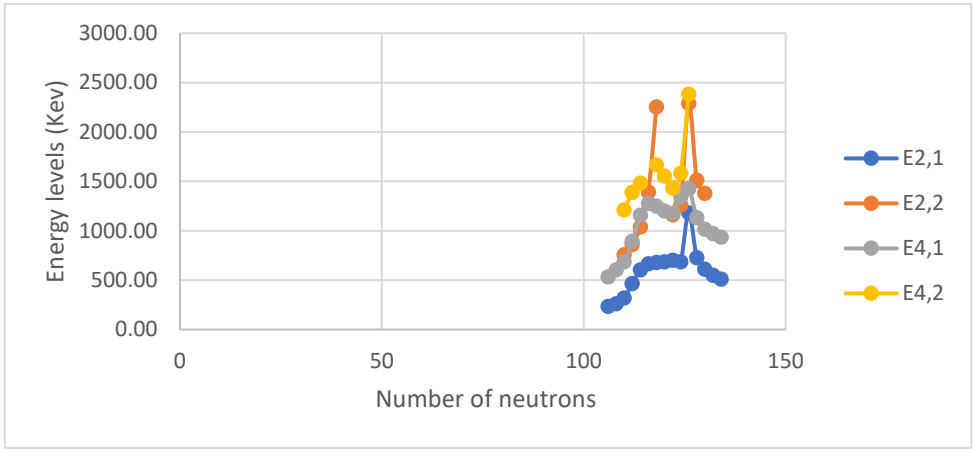

A

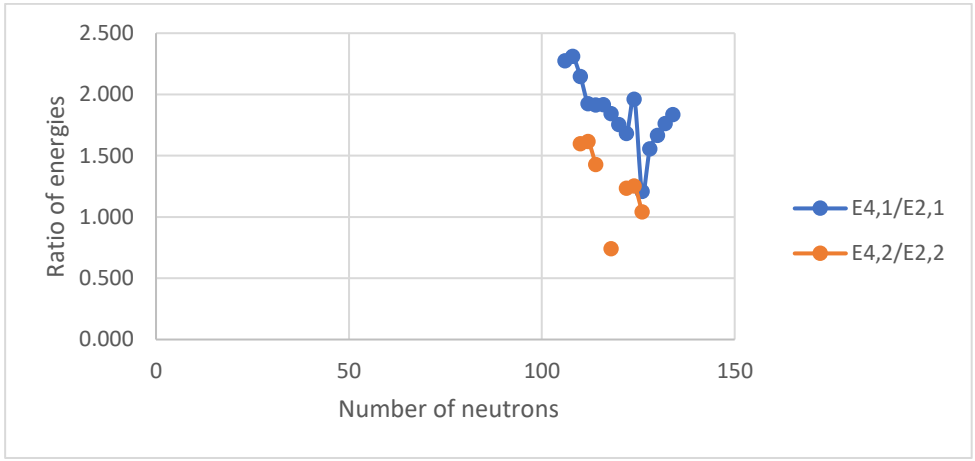

B

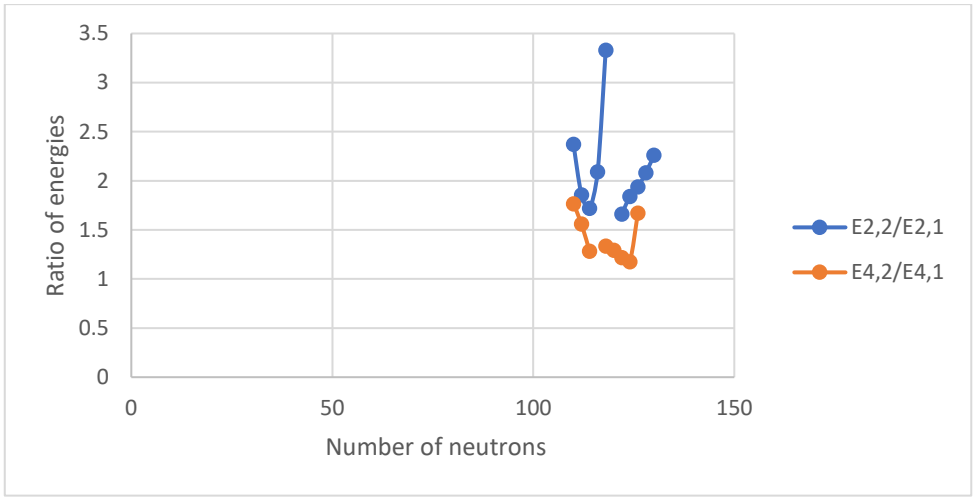

C

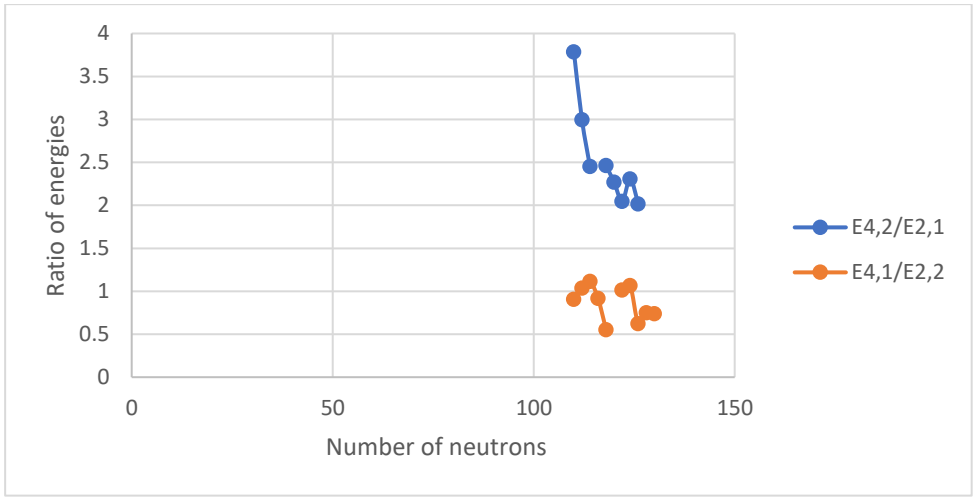

D

Figure III. 42 (color online) Panel **A** represents the comparison of the experimental energy levels of the lowest 2_1^+, 2_2^+, 4_1^+ and 4_2^+ states for the chain of Po isotopes. Panels **B, C, D** represent the comparison of the experimental energy ratios ($E_{4_1^+}/E_{2_1^+}$ and $E_{4_2^+}/E_{2_2^+}$), ($E_{2_2^+}/E_{2_1^+}$ and $E_{4_2^+}/E_{4_1^+}$) and ($E_{4_2^+}/E_{2_1^+}$ and $E_{4_1^+}/E_{2_2^+}$), respectively, for the chain of Po isotopes.

Rn isotopes (Z =86)

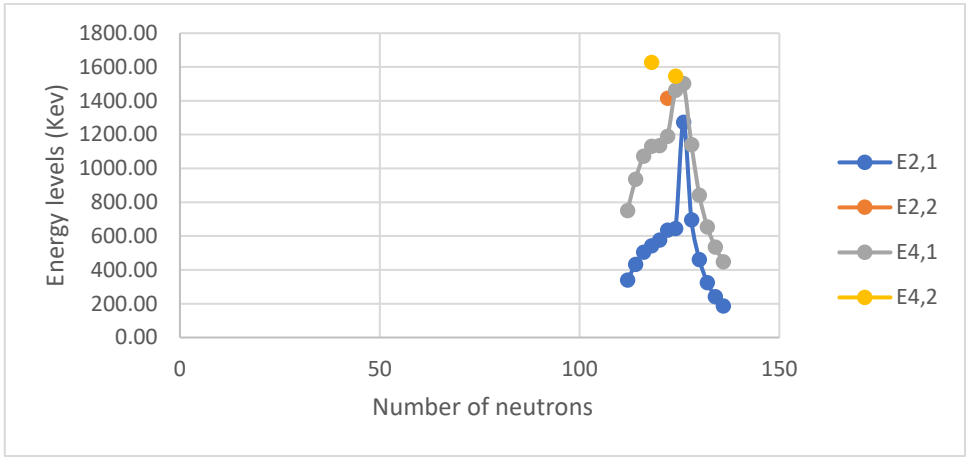

A

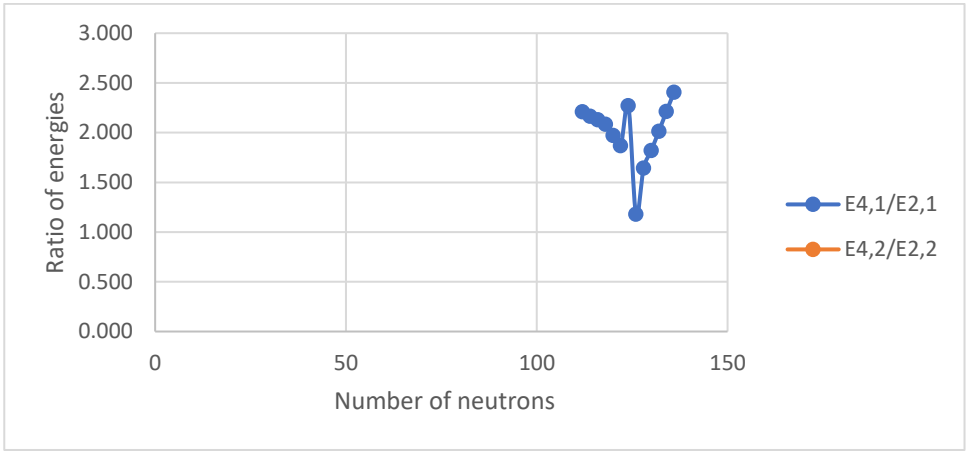

B

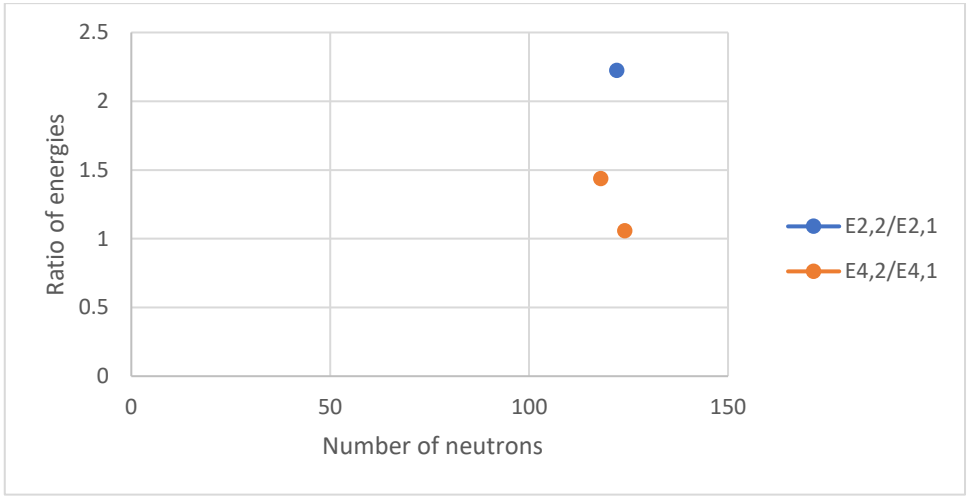

C

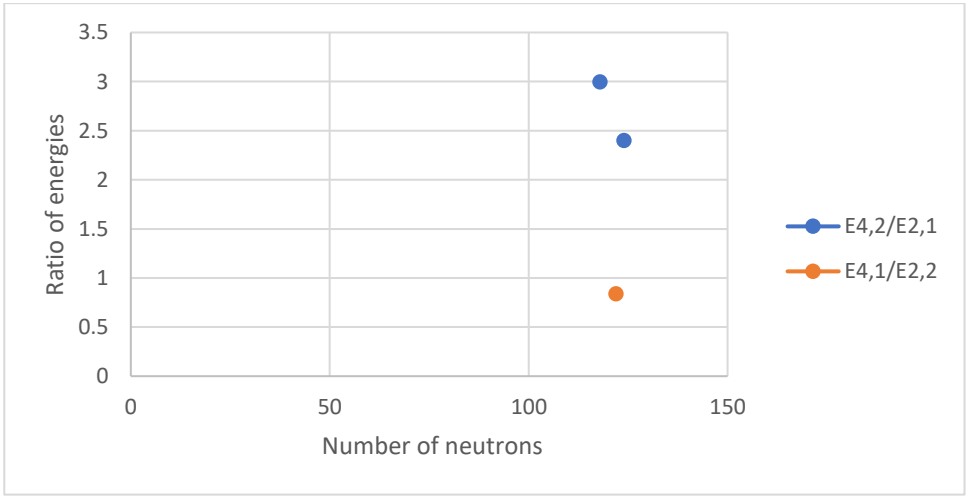

D

Figure III. 43 (color online) Panel **A** represents the comparison of the experimental energy levels of the lowest 2_1^+, 2_2^+, 4_1^+ and 4_2^+ states for the chain of Rn isotopes. Panels **B, C, D** represent the comparison of the experimental energy ratios ($E_{4_1^+}/E_{2_1^+}$ and $E_{4_2^+}/E_{2_2^+}$), ($E_{2_2^+}/E_{2_1^+}$ and $E_{4_2^+}/E_{4_1^+}$) and ($E_{4_2^+}/E_{2_1^+}$ and $E_{4_1^+}/E_{2_2^+}$), respectively, for the chain of Rn isotopes.

Ra isotopes (Z =88)

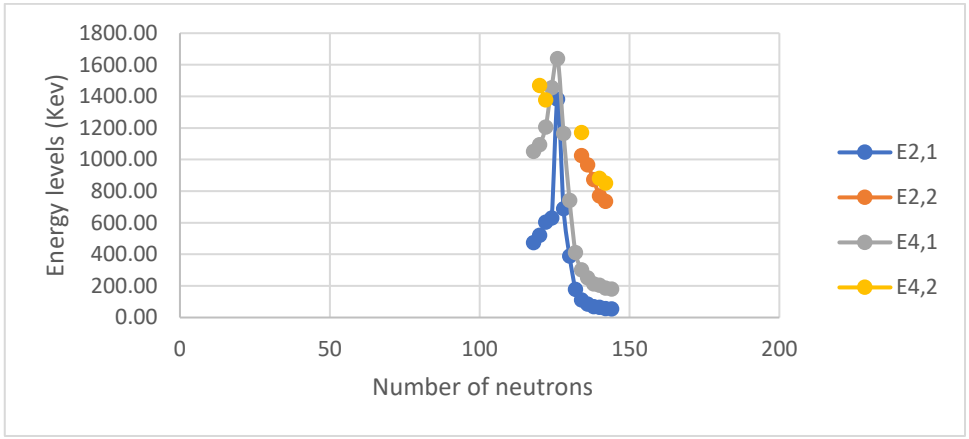

A

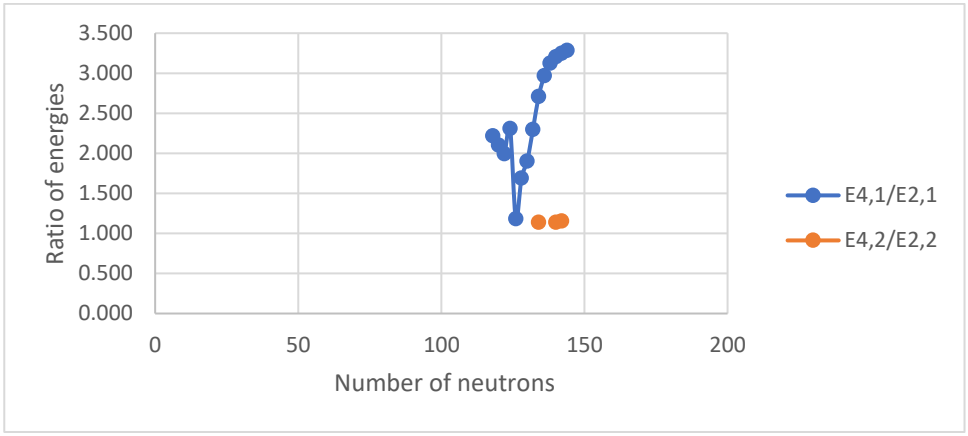

B

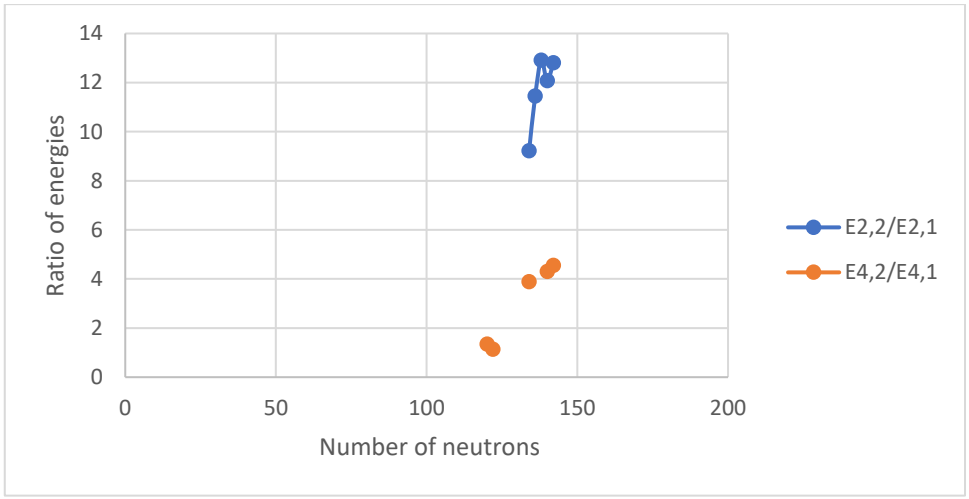

C

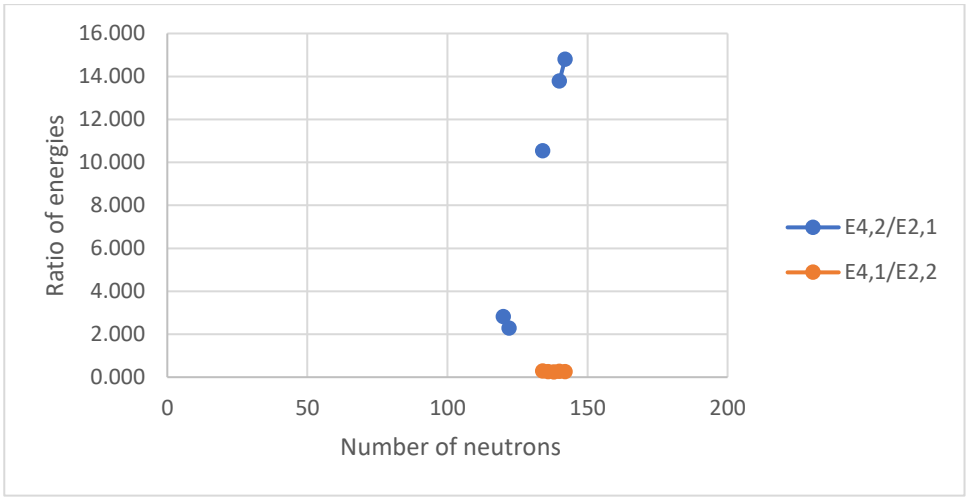

D

Figure III. 44 (color online) Panel **A** represents the comparison of the experimental energy levels of the lowest 2_1^+, 2_2^+, 4_1^+ and 4_2^+ states for the chain of Ra isotopes. Panels **B, C, D** represent the comparison of the experimental energy ratios ($E_{4_1^+}/E_{2_1^+}$ and $E_{4_2^+}/E_{2_2^+}$), ($E_{2_2^+}/E_{2_1^+}$ and $E_{4_2^+}/E_{4_1^+}$) and ($E_{4_2^+}/E_{2_1^+}$ and $E_{4_1^+}/E_{2_2^+}$), respectively, for the chain of Ra isotopes.

Th isotopes (Z =90)

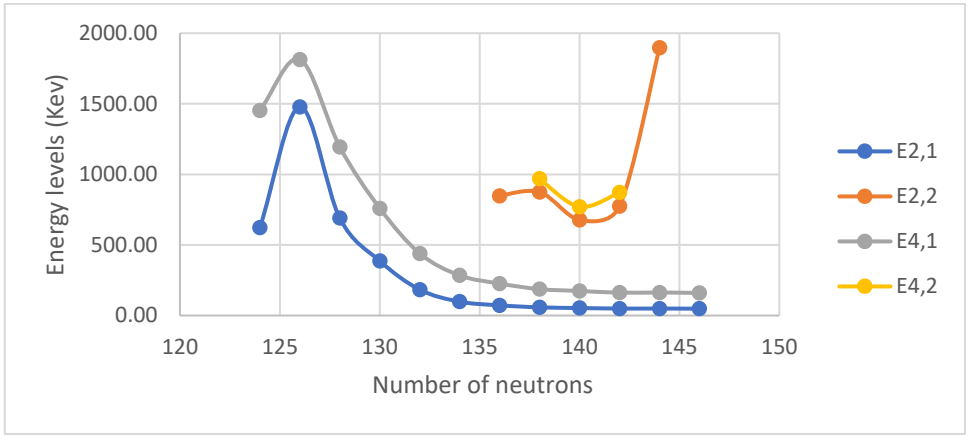

A

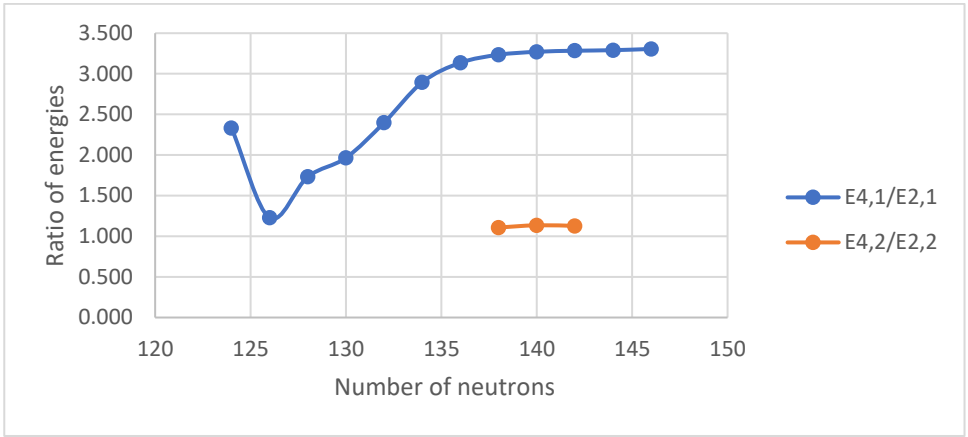

B

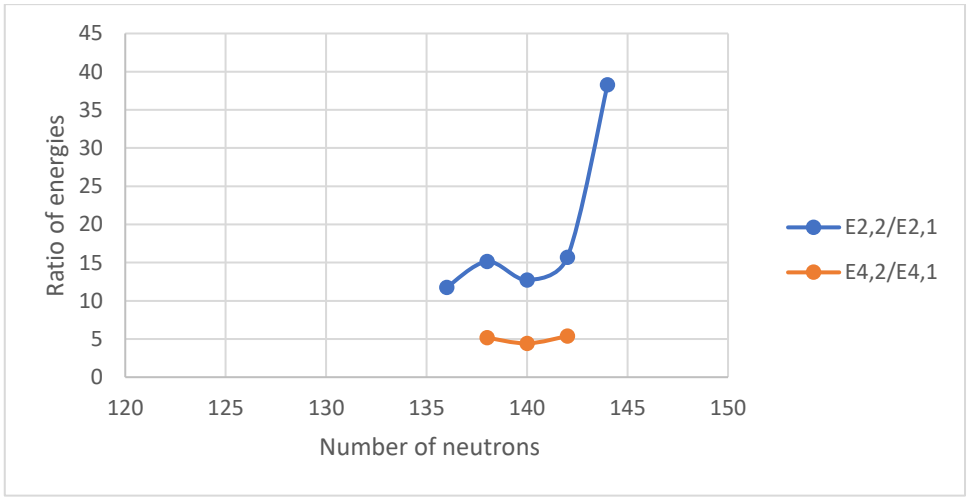

C

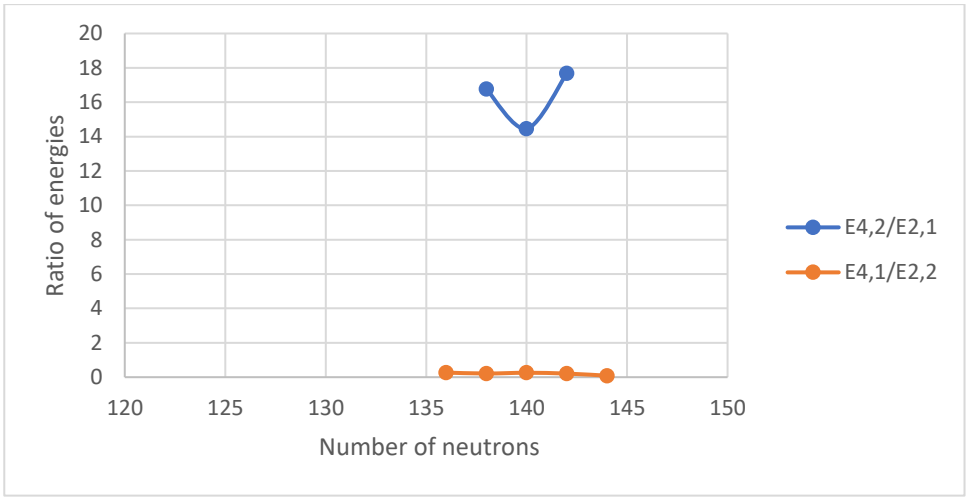

D

Figure III. 45 (color online) Panel **A** represents the comparison of the experimental energy levels of the lowest 2_1^+, 2_2^+, 4_1^+ and 4_2^+ states for the chain of Th isotopes. Panels **B, C, D** represent the comparison of the experimental energy ratios ($E_{4_1^+}/E_{2_1^+}$ and $E_{4_2^+}/E_{2_2^+}$), ($E_{2_2^+}/E_{2_1^+}$ and $E_{4_2^+}/E_{4_1^+}$) and ($E_{4_2^+}/E_{2_1^+}$ and $E_{4_1^+}/E_{2_2^+}$), respectively, for the chain of Th isotopes.

U isotopes (Z =92)

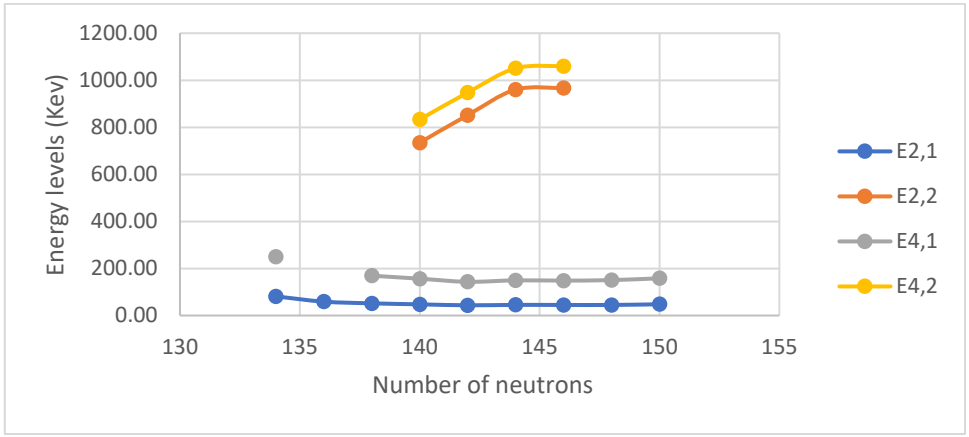

A

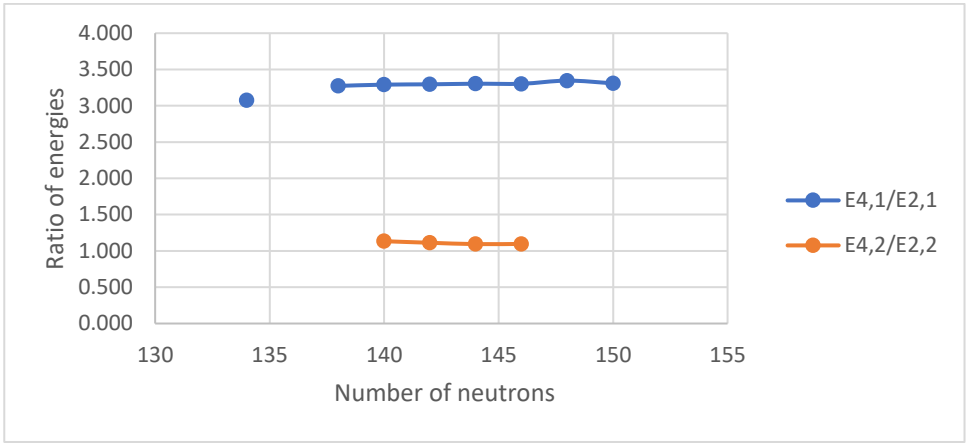

B

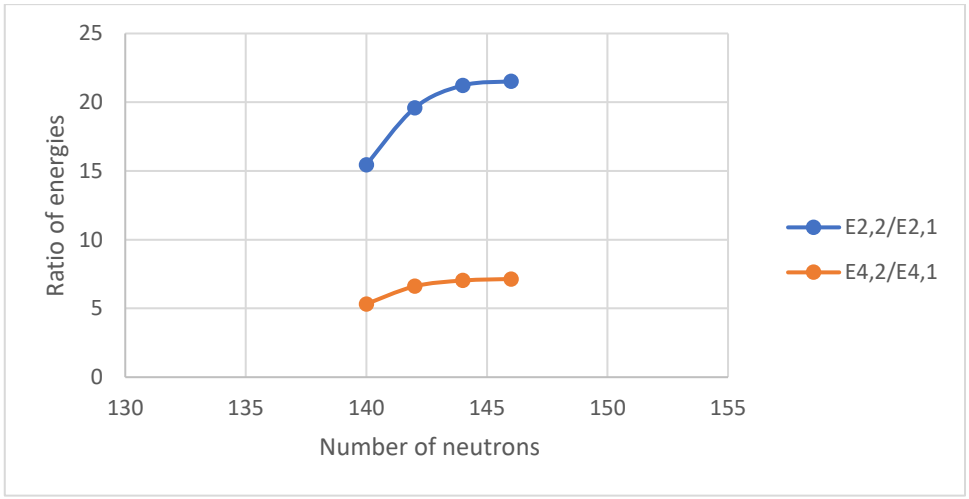

C

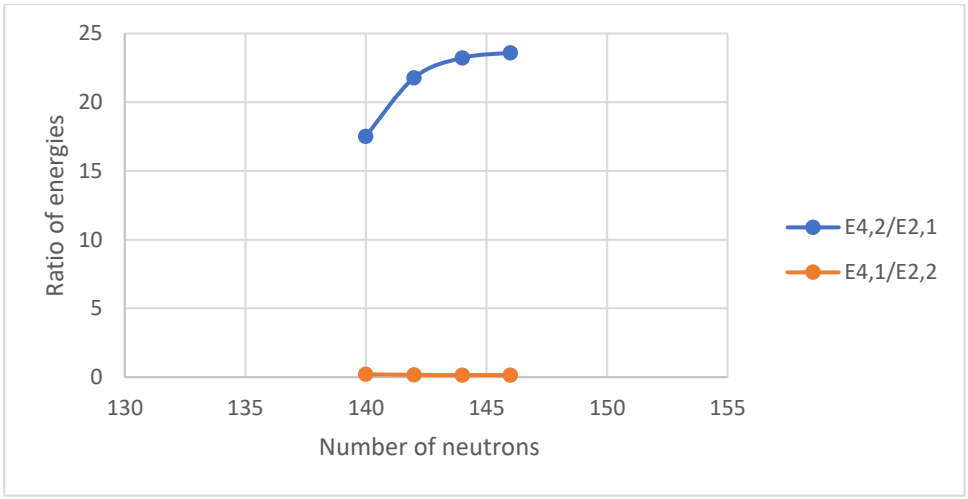

D

Figure III. 46 (color online) Panel **A** represents the comparison of the experimental energy levels of the lowest 2_1^+, 2_2^+, 4_1^+ and 4_2^+ states for the chain of U isotopes. Panels **B, C, D** represent the comparison of the experimental energy ratios ($E_{4_1^+}/E_{2_1^+}$ and $E_{4_2^+}/E_{2_2^+}$), ($E_{2_2^+}/E_{2_1^+}$ and $E_{4_2^+}/E_{4_1^+}$) and ($E_{4_2^+}/E_{2_1^+}$ and $E_{4_1^+}/E_{2_2^+}$), respectively, for the chain of U isotopes.

Pu isotopes (Z =94)

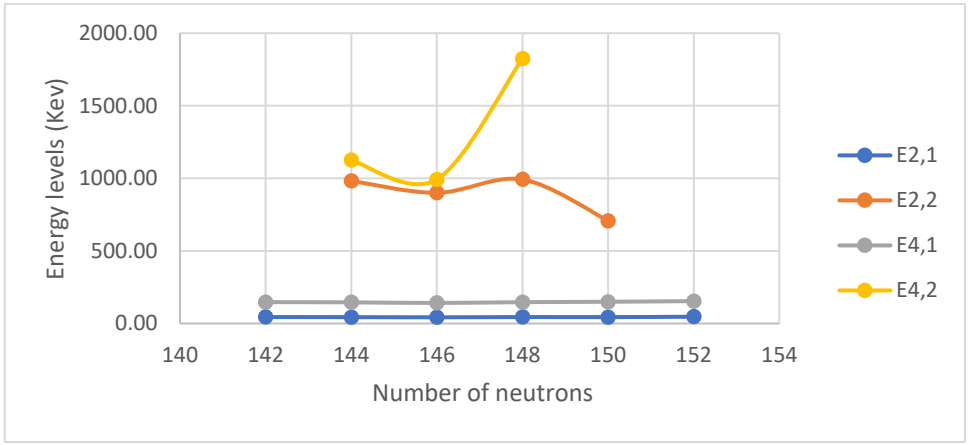

A

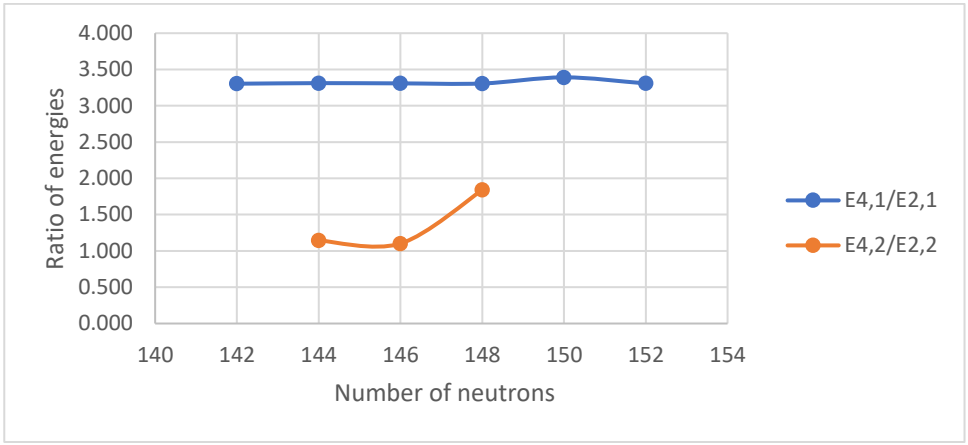

B

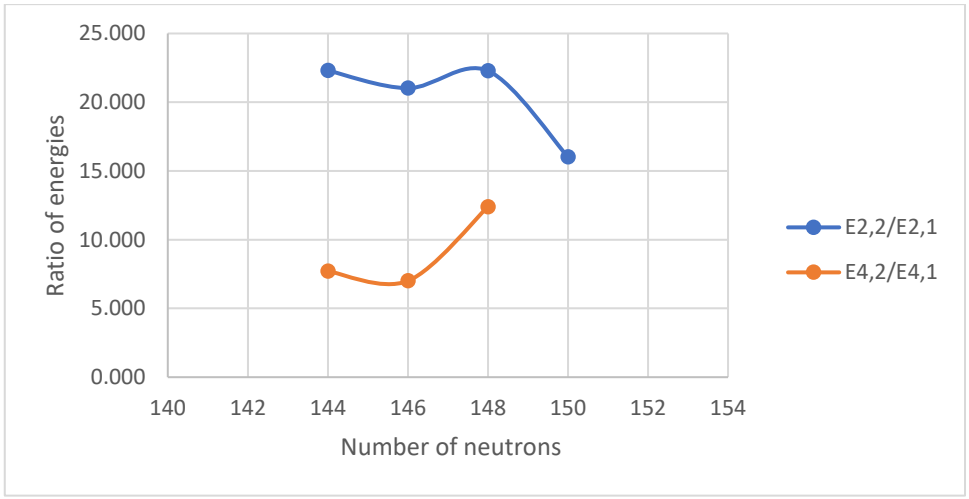

C

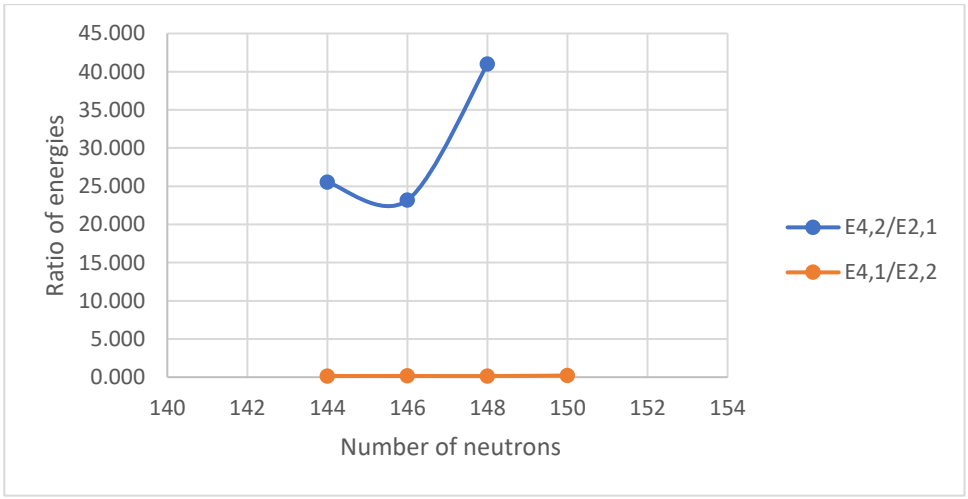

D

Figure III. 47 (color online) Panel **A** represents the comparison of the experimental energy levels of the lowest 2_1^+, 2_2^+, 4_1^+ and 4_2^+ states for the chain of Pu isotopes. Panels **B, C, D** represent the comparison of the experimental energy ratios ($E_{4_1^+}/E_{2_1^+}$ and $E_{4_2^+}/E_{2_2^+}$), ($E_{2_2^+}/E_{2_1^+}$ and $E_{4_2^+}/E_{4_1^+}$) and ($E_{4_2^+}/E_{2_1^+}$ and $E_{4_1^+}/E_{2_2^+}$), respectively, for the chain of Pu isotopes.

Cm isotopes (Z =96)

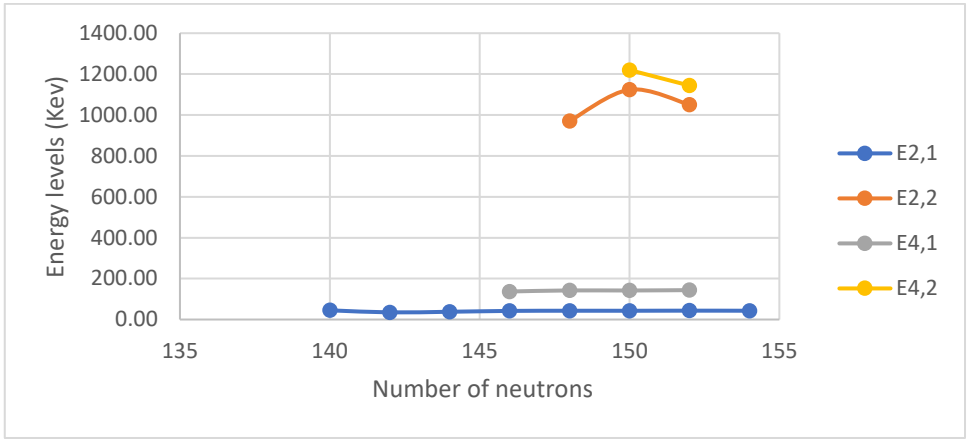

A

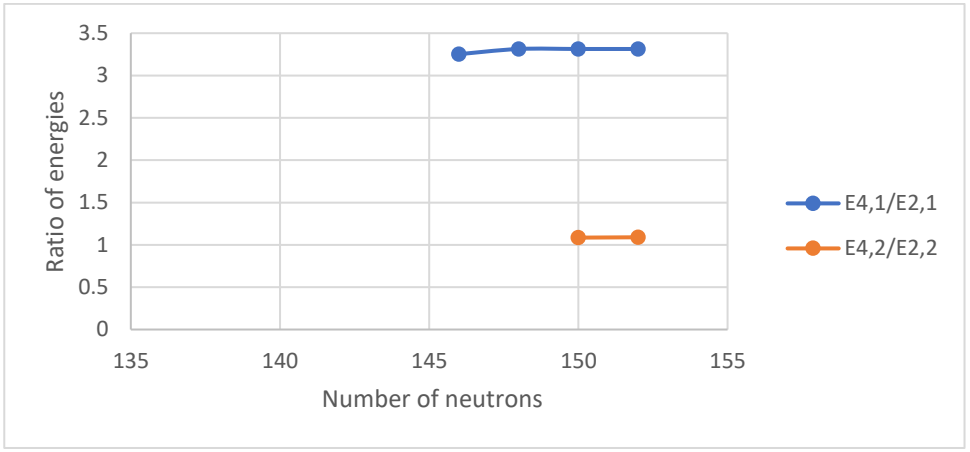

B

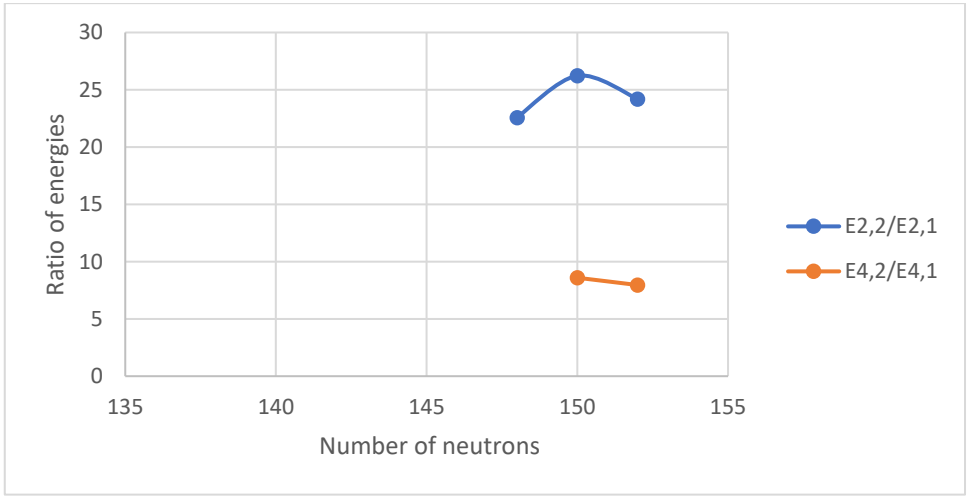

C

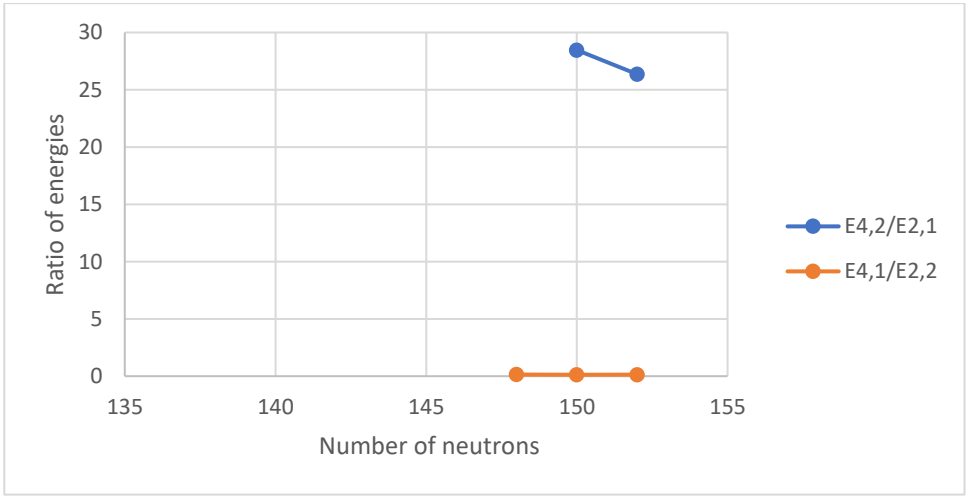

D

Figure III. 48 (color online) Panel **A** represents the comparison of the experimental energy levels of the lowest 2_1^+, 2_2^+, 4_1^+ and 4_2^+ states for the chain of Cm isotopes. Panels **B, C, D** represent the comparison of the experimental energy ratios ($E_{4_1^+}/E_{2_1^+}$ and $E_{4_2^+}/E_{2_2^+}$), ($E_{2_2^+}/E_{2_1^+}$ and $E_{4_2^+}/E_{4_1^+}$) and ($E_{4_2^+}/E_{2_1^+}$ and $E_{4_1^+}/E_{2_2^+}$), respectively, for the chain of Cm isotopes.

Cf isotopes (Z =98)

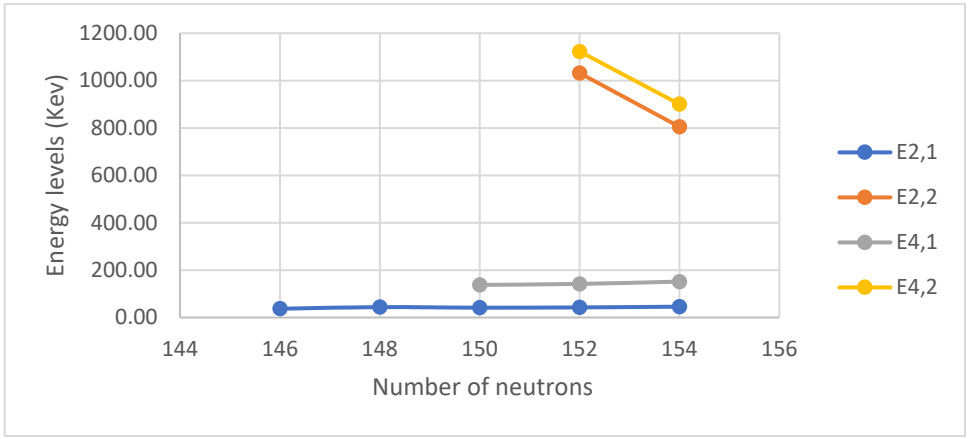

A

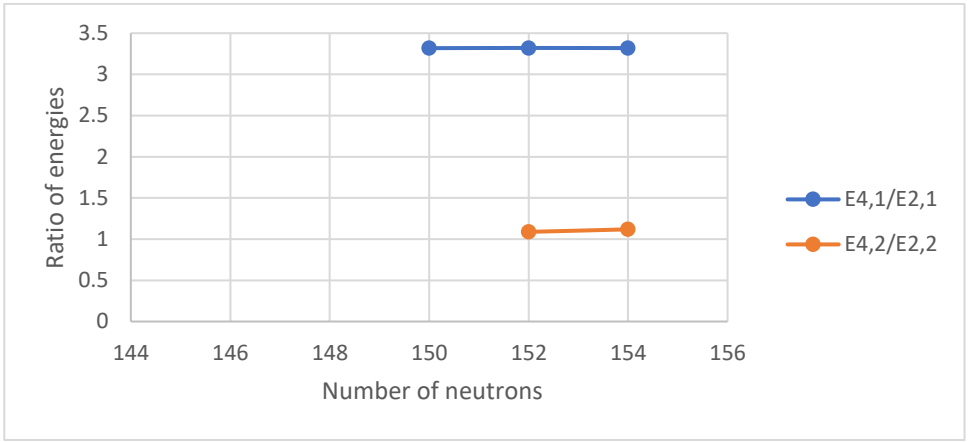

B

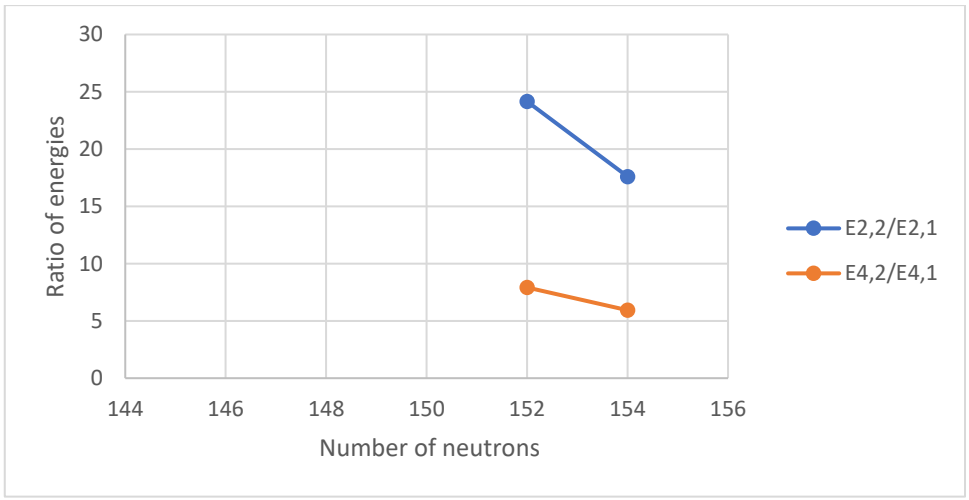

C

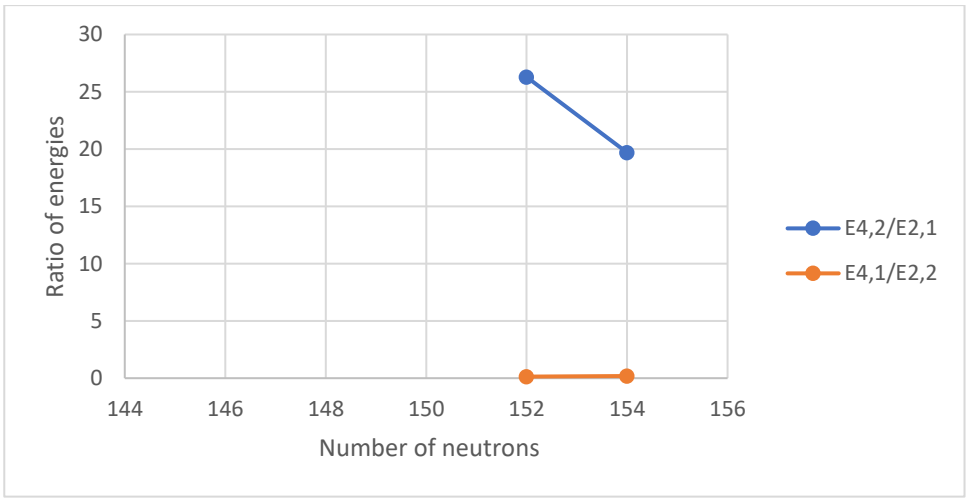

D

Figure III. 49 (color online) Panel **A** represents the comparison of the experimental energy levels of the lowest 2_1^+, 2_2^+, 4_1^+ and 4_2^+ states for the chain of Cf isotopes. Panels **B, C, D** represent the comparison of the experimental energy ratios ($E_{4_1^+}/E_{2_1^+}$ and $E_{4_2^+}/E_{2_2^+}$), ($E_{2_2^+}/E_{2_1^+}$ and $E_{4_2^+}/E_{4_1^+}$) and ($E_{4_2^+}/E_{2_1^+}$ and $E_{4_1^+}/E_{2_2^+}$), respectively, for the chain of Cf isotopes.

Fm isotopes (Z =100)

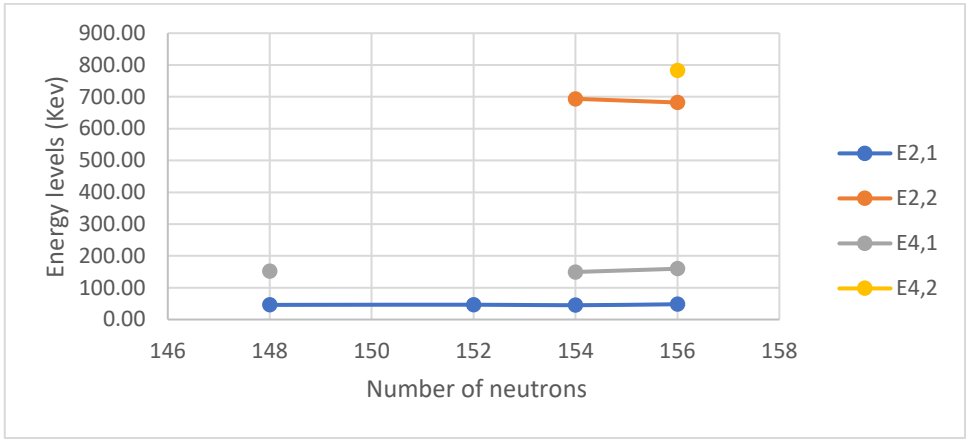

A

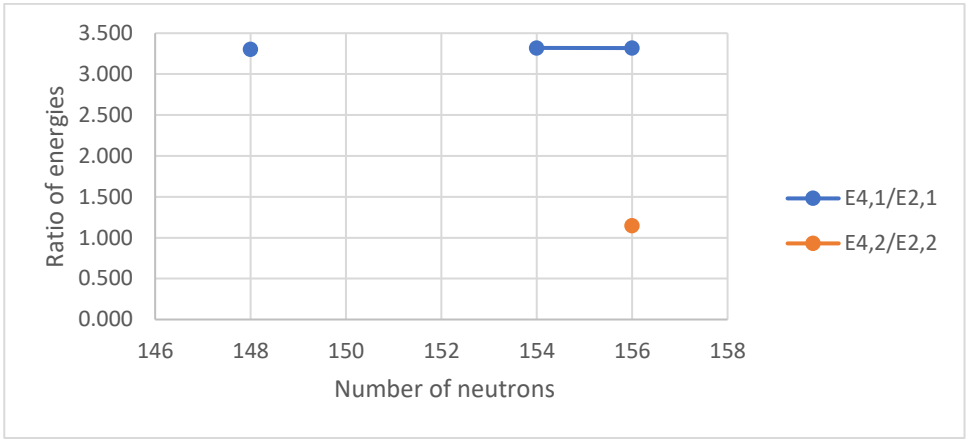

B

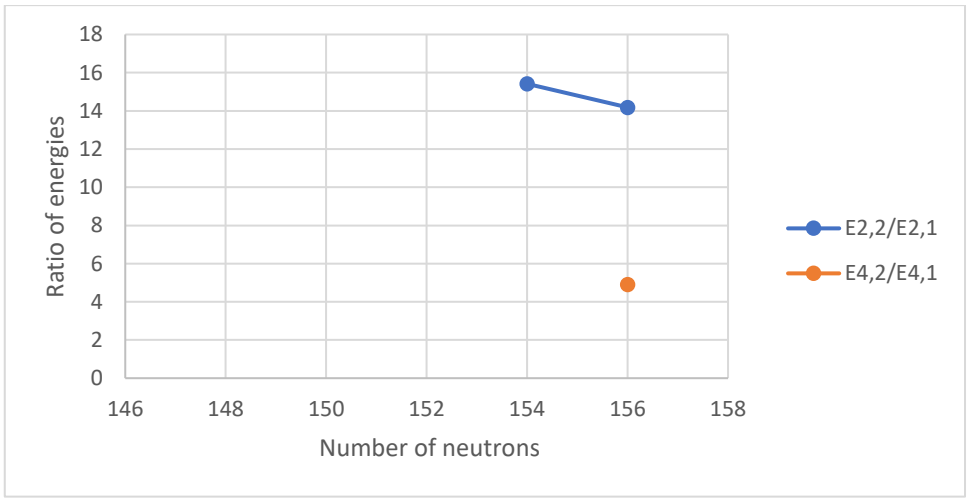

C

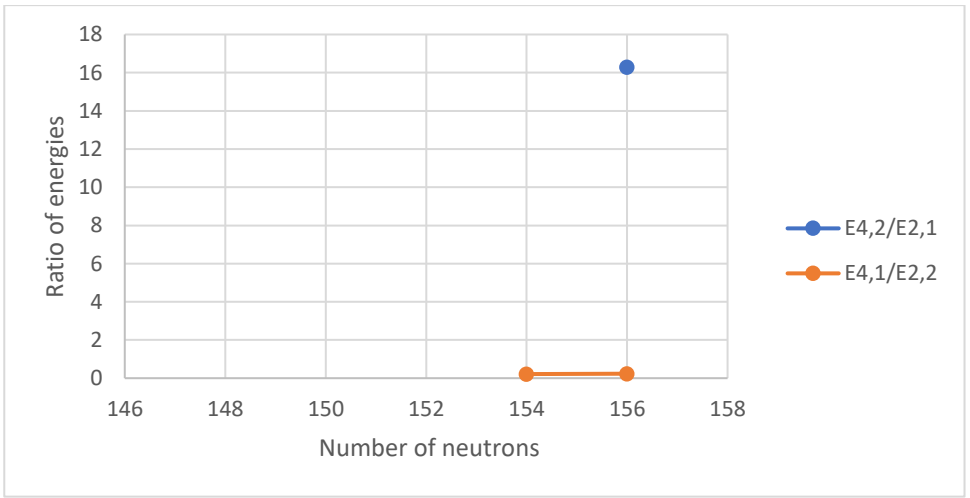

D

Figure III. 50 (color online) Panel **A** represents the comparison of the experimental energy levels of the lowest 2_1^+, 2_2^+, 4_1^+ and 4_2^+ states for the chain of Fm isotopes. Panels **B, C, D** represent the comparison of the experimental energy ratios ($E_{4_1^+}/E_{2_1^+}$ and $E_{4_2^+}/E_{2_2^+}$), ($E_{2_2^+}/E_{2_1^+}$ and $E_{4_2^+}/E_{4_1^+}$) and ($E_{4_2^+}/E_{2_1^+}$ and $E_{4_1^+}/E_{2_2^+}$), respectively, for the chain of Fm isotopes.

No isotopes (Z =102)

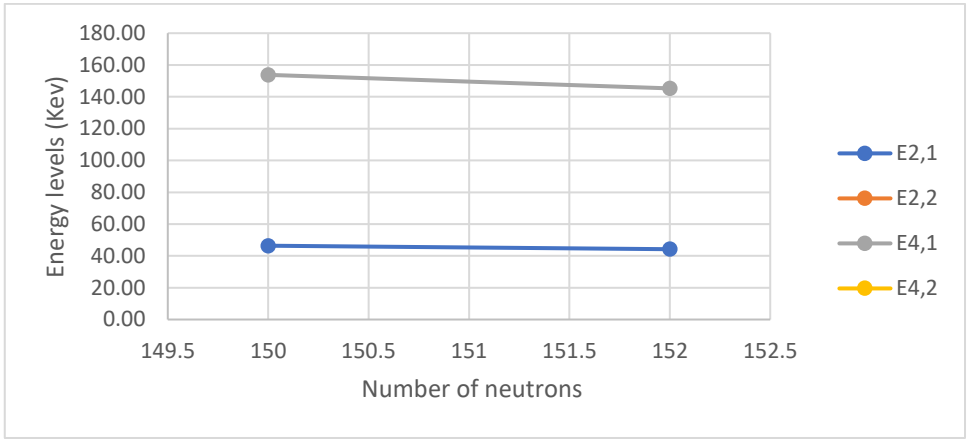

A

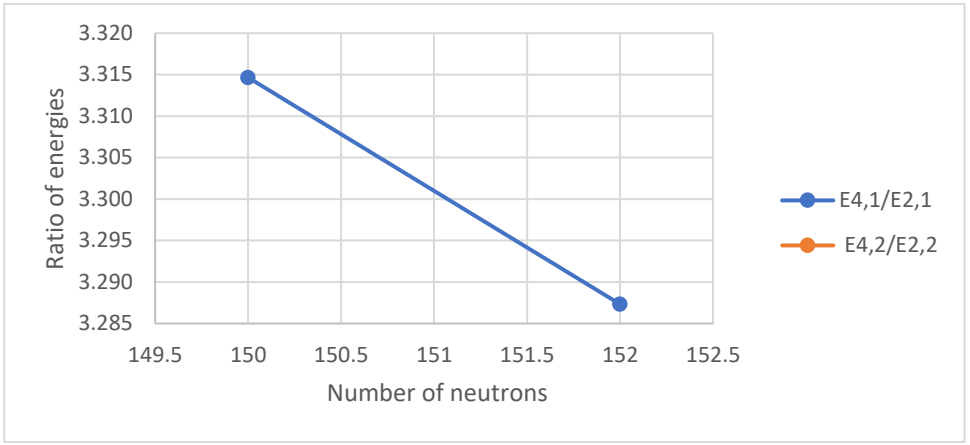

B

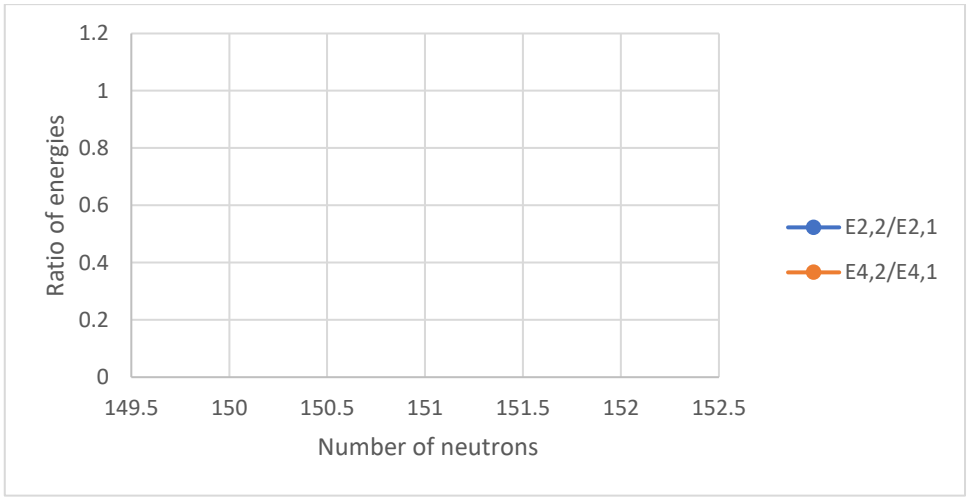

C

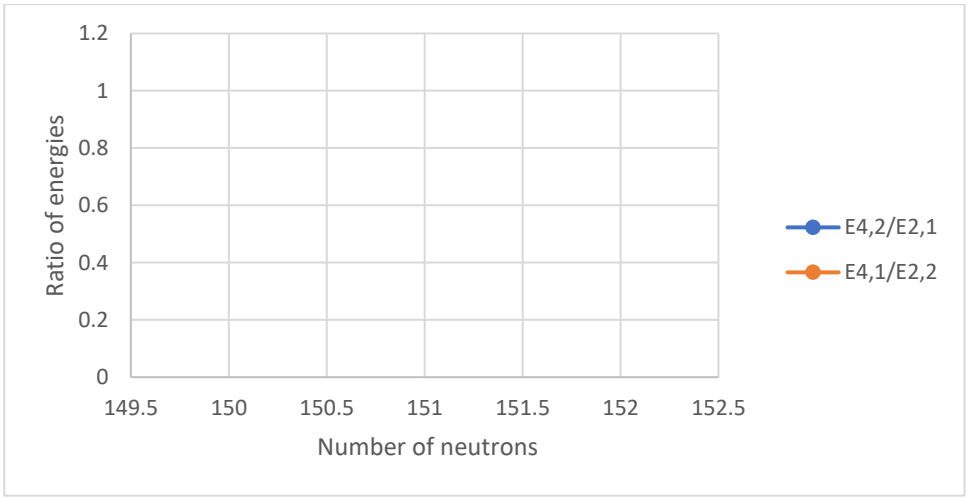

D

Figure III. 51 (color online) Panel **A** represents the comparison of the experimental energy levels of the lowest 2_1^+, 2_2^+, 4_1^+ and 4_2^+ states for the chain of No isotopes. Panels **B, C, D** represent the comparison of the experimental energy ratios ($E_{4_1^+}/E_{2_1^+}$ and $E_{4_2^+}/E_{2_2^+}$), ($E_{2_2^+}/E_{2_1^+}$ and $E_{4_2^+}/E_{4_1^+}$) and ($E_{4_2^+}/E_{2_1^+}$ and $E_{4_1^+}/E_{2_2^+}$), respectively, for the chain of No isotopes.

Rf isotopes (Z =104)

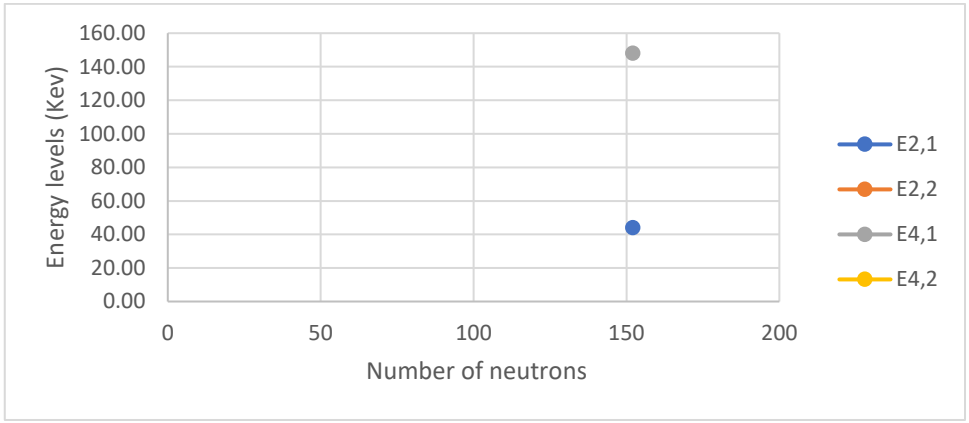

A

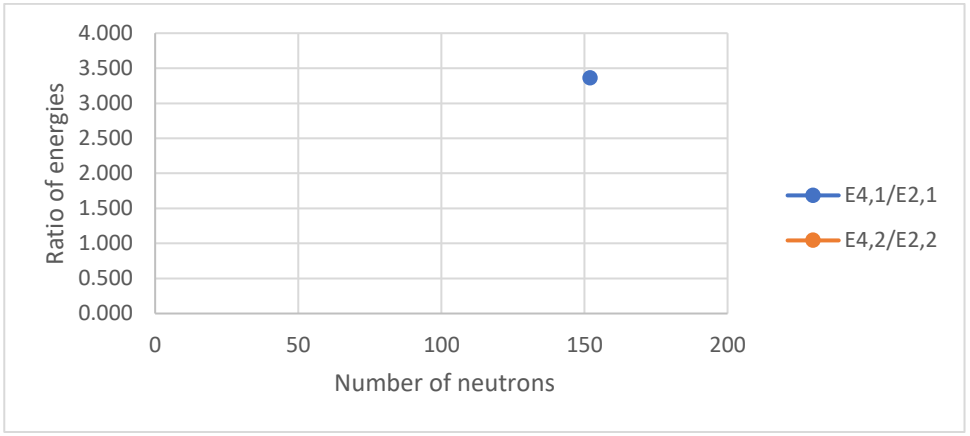

B

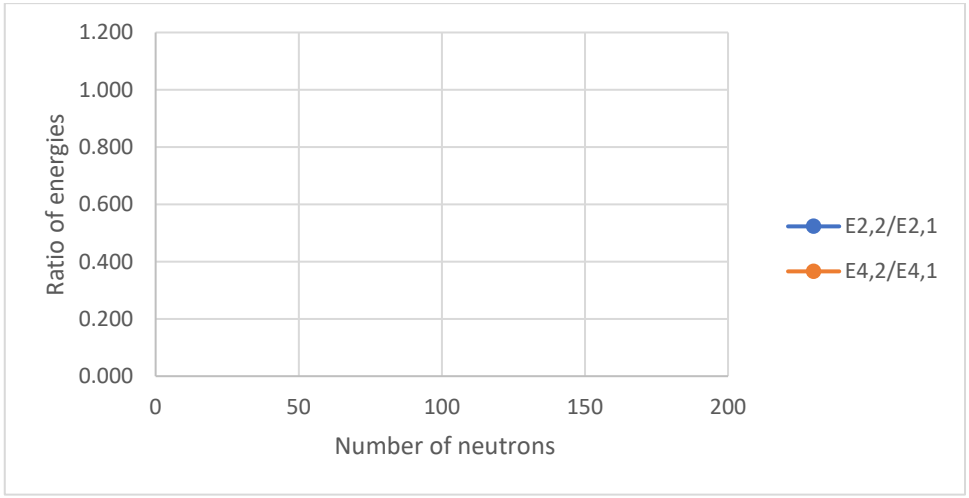

C

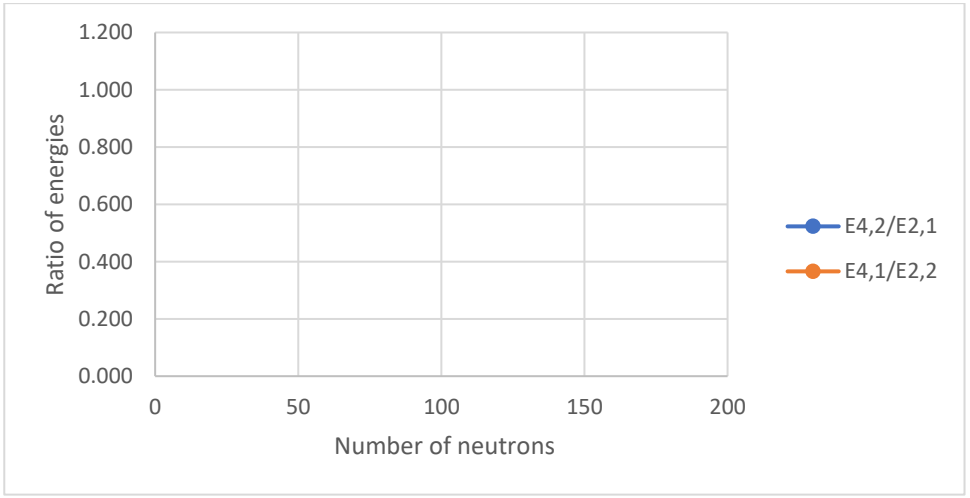

D

Figure III. 52 (color online) Panel **A** represents the comparison of the experimental energy levels of the lowest 2_1^+, 2_2^+, 4_1^+ and 4_2^+ states for the chain of Rf isotopes. Panels **B, C, D** represent the comparison of the experimental energy ratios ($E_{4_1^+}/E_{2_1^+}$ and $E_{4_2^+}/E_{2_2^+}$), ($E_{2_2^+}/E_{2_1^+}$ and $E_{4_2^+}/E_{4_1^+}$) and ($E_{4_2^+}/E_{2_1^+}$ and $E_{4_1^+}/E_{2_2^+}$), respectively, for the chain of Rf isotopes.

Chapter IV

Two dimensional figures for the values of energy levels and energy ratios over all even–even nuclei for different isotones

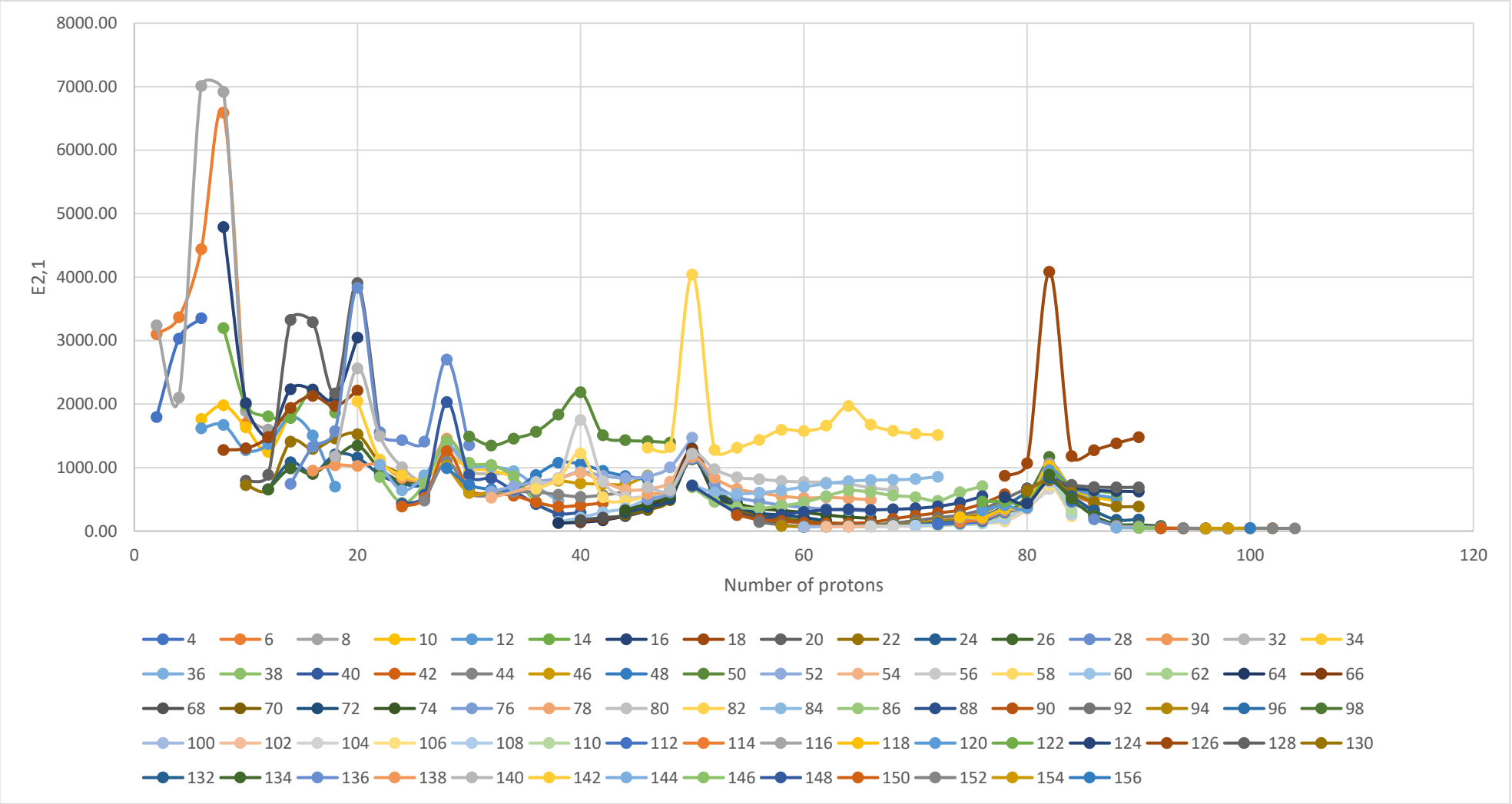

Figure IV. 1 (color online) The experimental values of the energy of the first -excited 2^+ state ($E_{2_1^+}$) for all even–even nuclei plotted as a function of proton number Z along the x axis for different isotones. The neutron numbers N for different isotones are indicated by legend below graph.

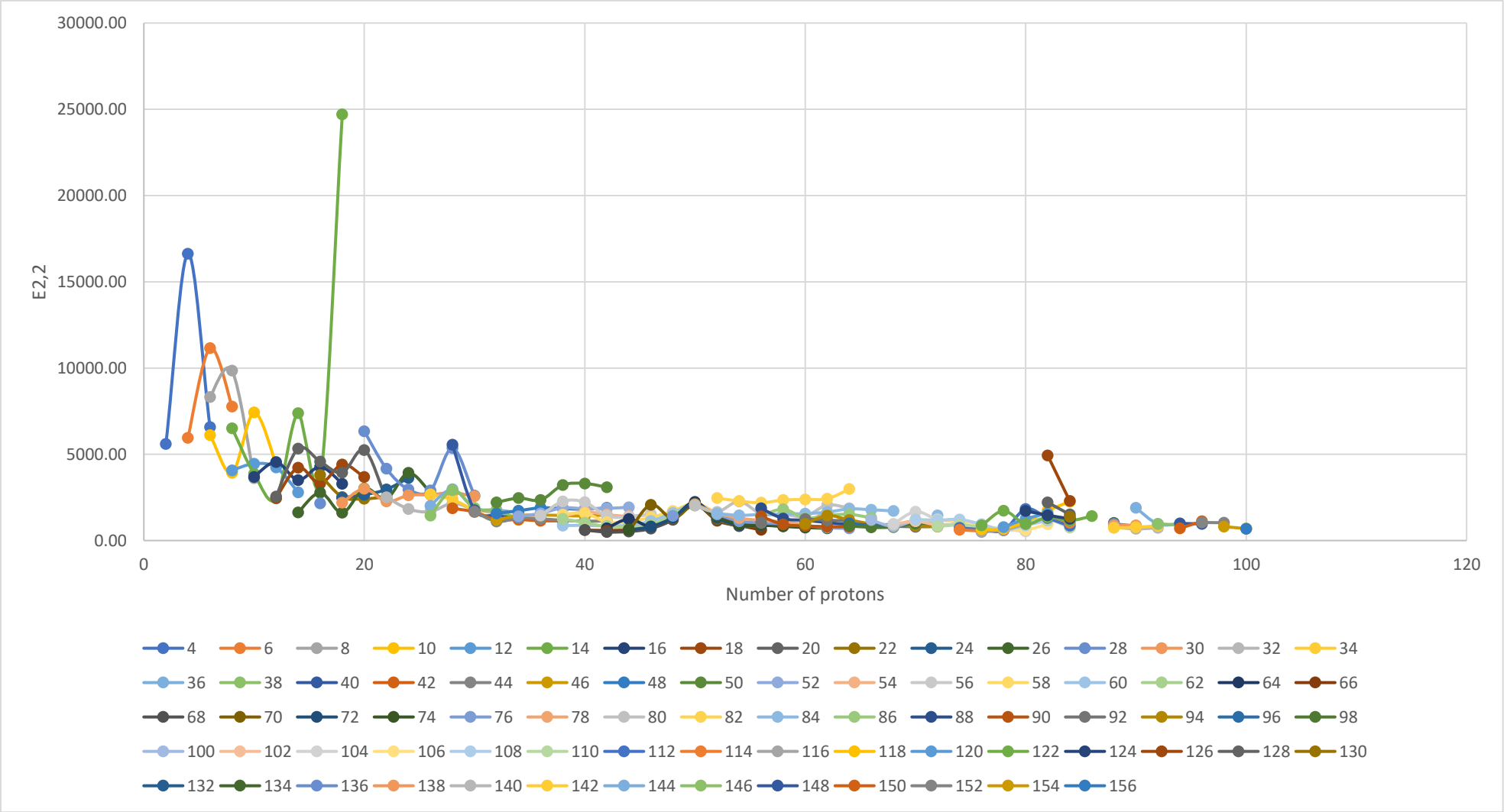

Figure IV. 2 (color online) The experimental values of the energy of the second -excited 2^+ state ($E_{2_2^+}$) for all even–even nuclei plotted as a function of proton number Z along the x axis for different isotones. The neutron numbers N for different isotones are indicated by legend below graph.

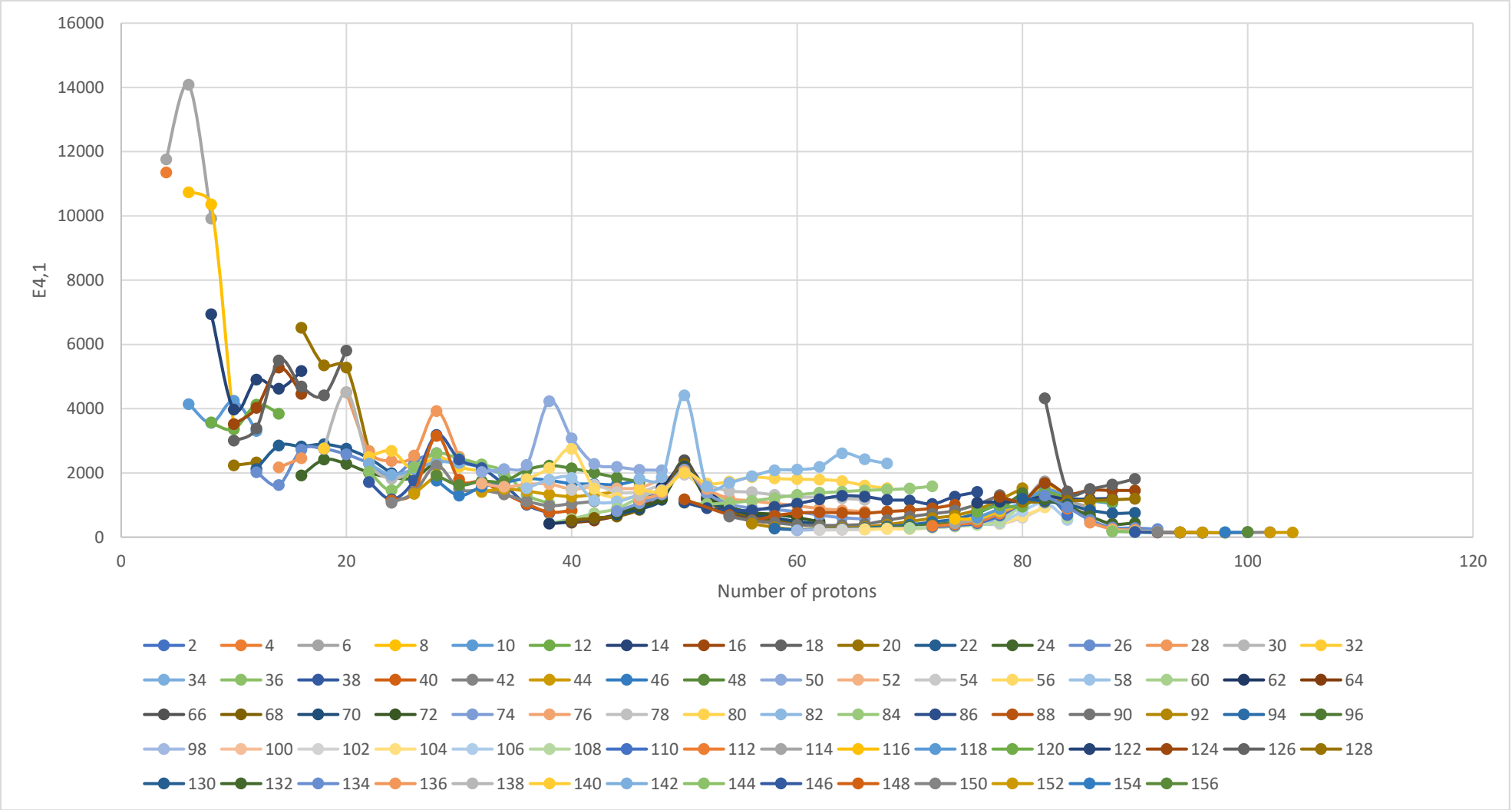

Figure IV. 3 (color online) The experimental values of the energy of the first -excited 4^+ state ($E_{4_1^+}$) for all even–even nuclei plotted as a function of proton number Z along the x axis for different isotones. The neutron numbers N for different isotones are indicated by legend below graph.

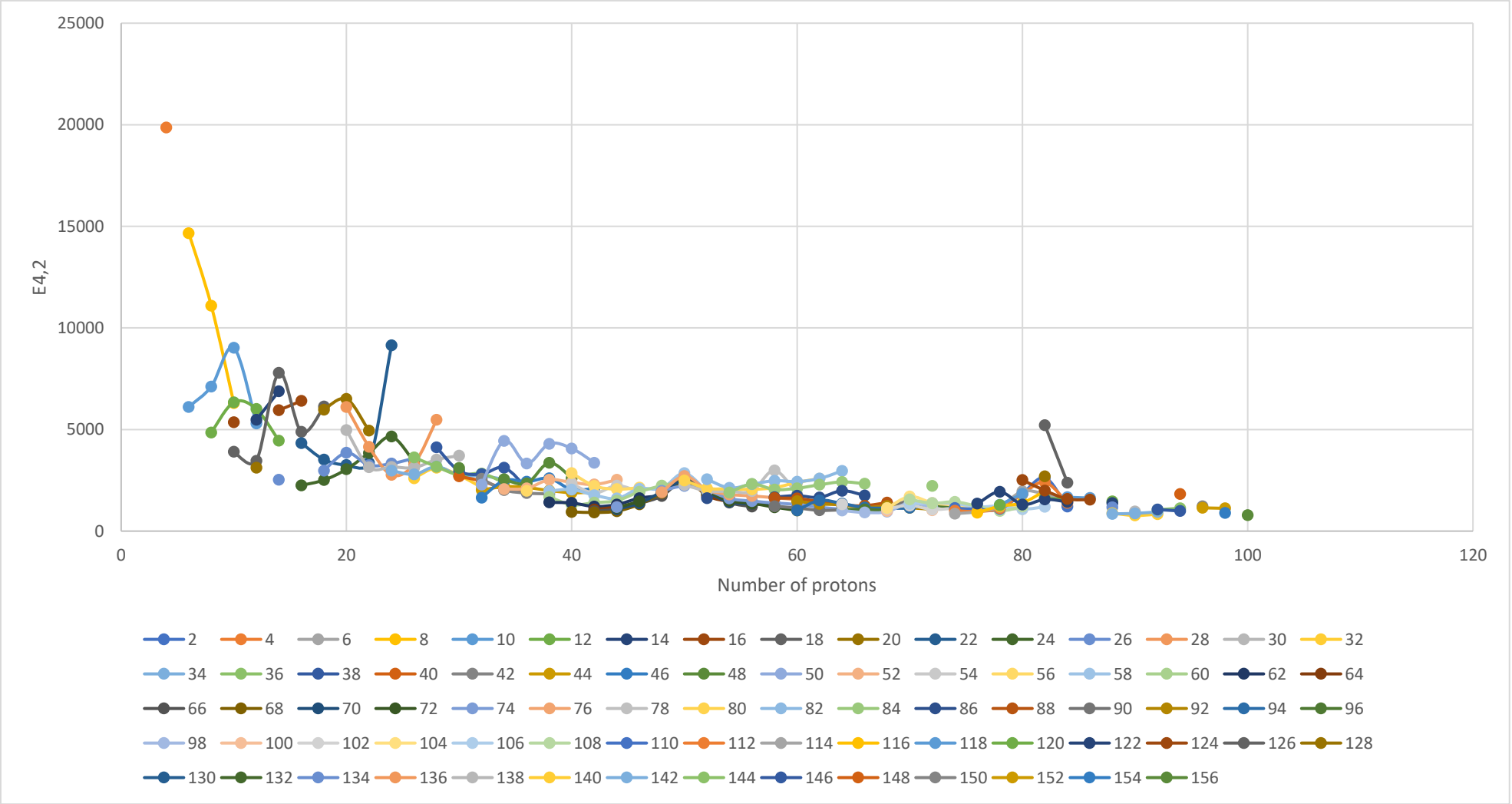

Figure IV. 4 (color online) The experimental values of the energy of the second -excited 4^+ state ($E_{4_2^+}$) for all even–even nuclei plotted as a function of proton number Z along the x axis for different isotones. The neutron numbers N for different isotones are indicated by legend below graph.

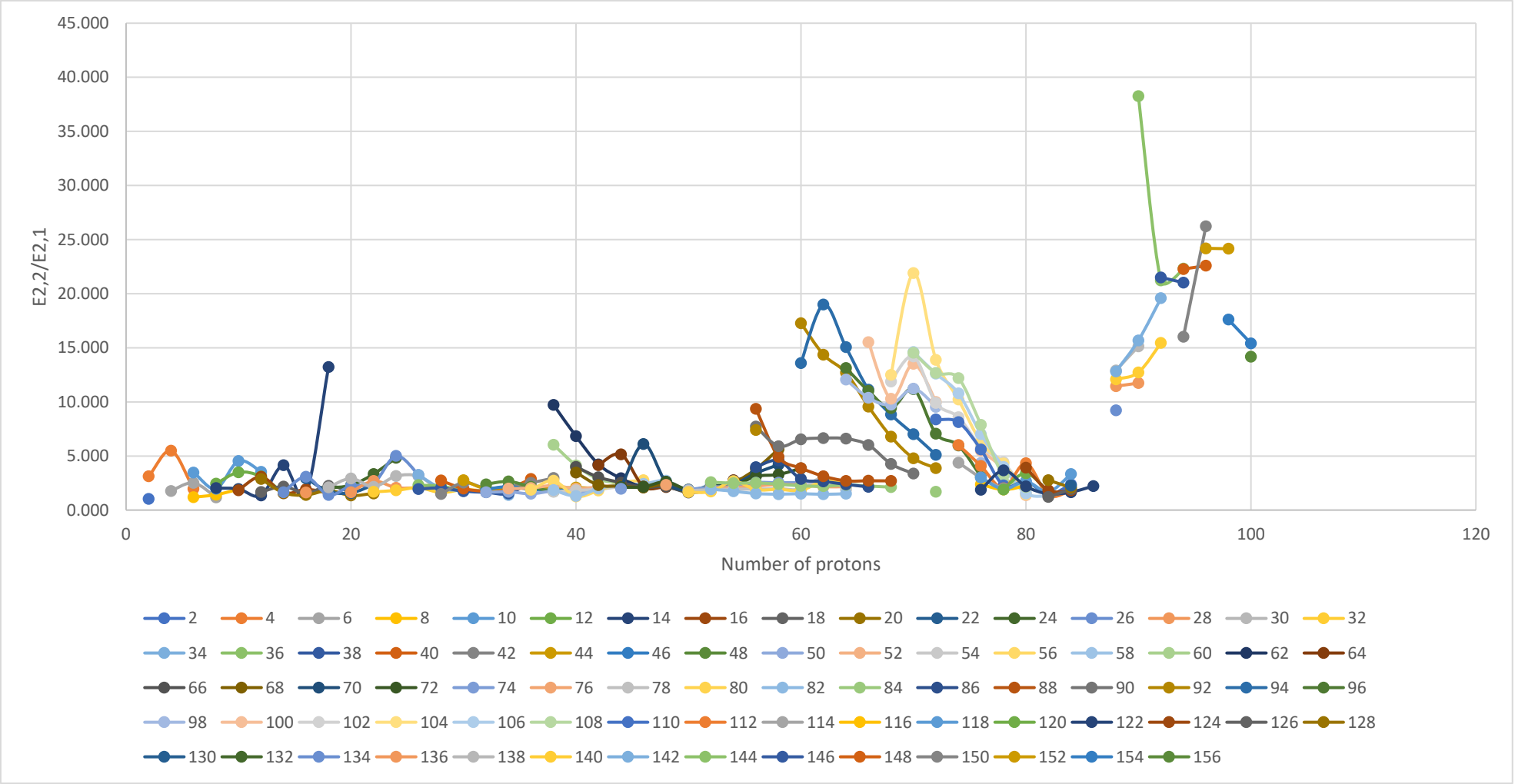

Figure IV. 5 (color online) The experimental values of the energy ratio $E_{2_2^+}/E_{2_1^+}$ for all even–even nuclei plotted as a function of proton number Z along the x axis for different isotones. The neutron numbers N for different isotones are indicated by legend below graph.

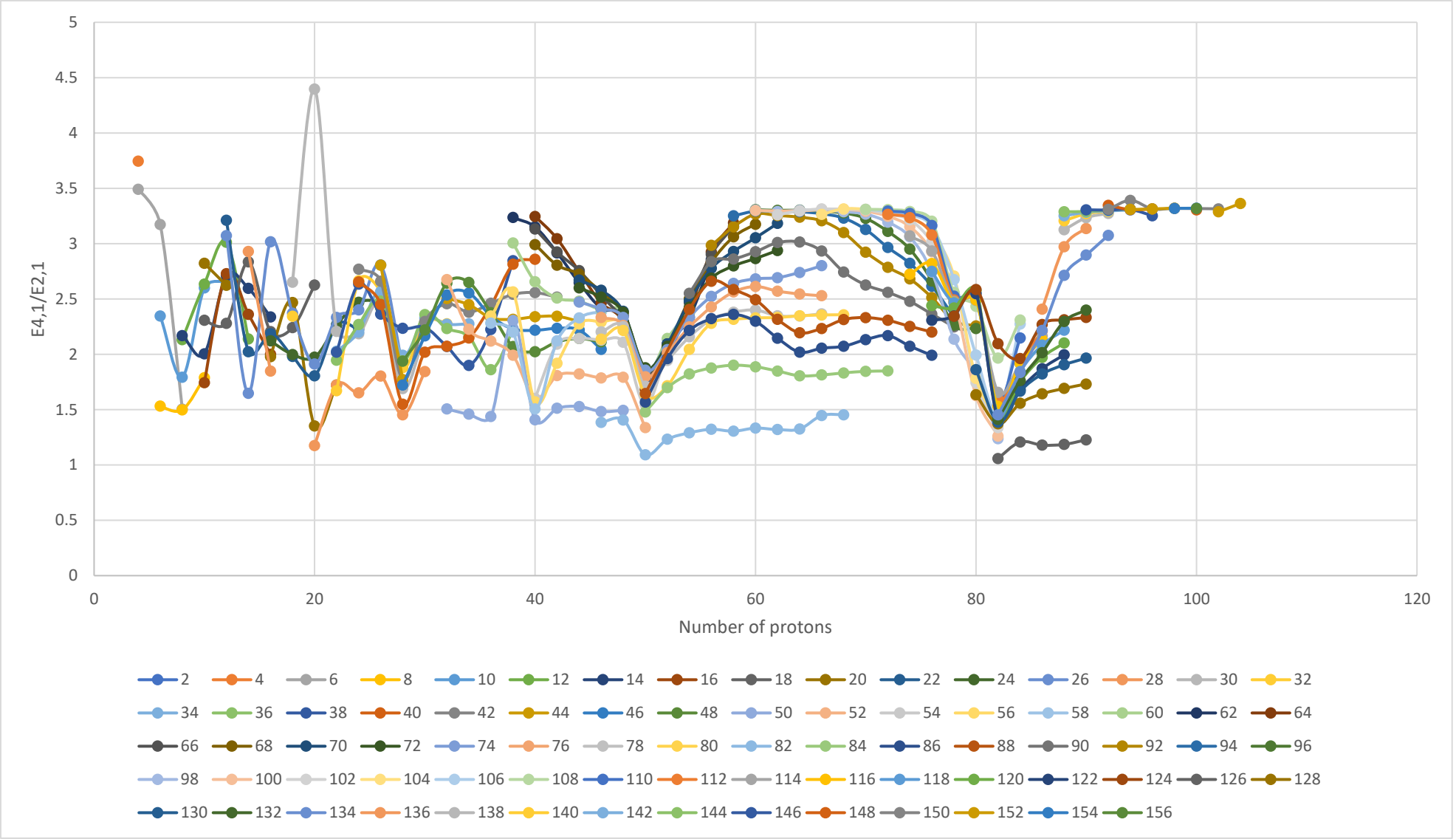

Figure IV. 6 (color online) The experimental values of the energy ratio $E_{4_1^+}/E_{2_1^+}$ for all even–even nuclei plotted as a function of proton number Z along the x axis for different isotones. The neutron numbers N for different isotones are indicated by legend below graph.

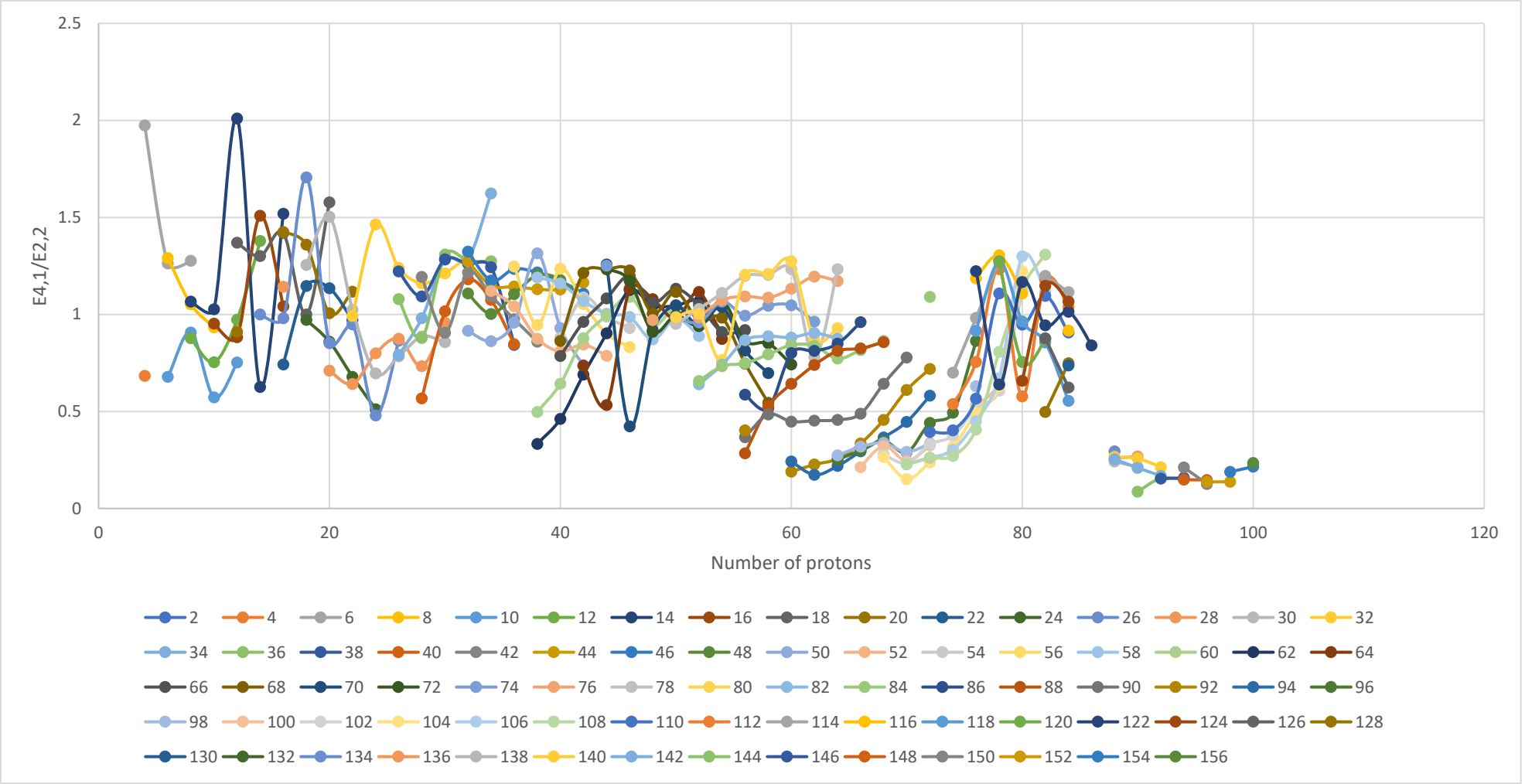

Figure IV. 7 (color online) The experimental values of the energy ratio $E_{4_1^+}/E_{2_2^+}$ for all even–even nuclei plotted as a function of proton number Z along the x axis for different isotones. The neutron numbers N for different isotones are indicated by legend below graph.

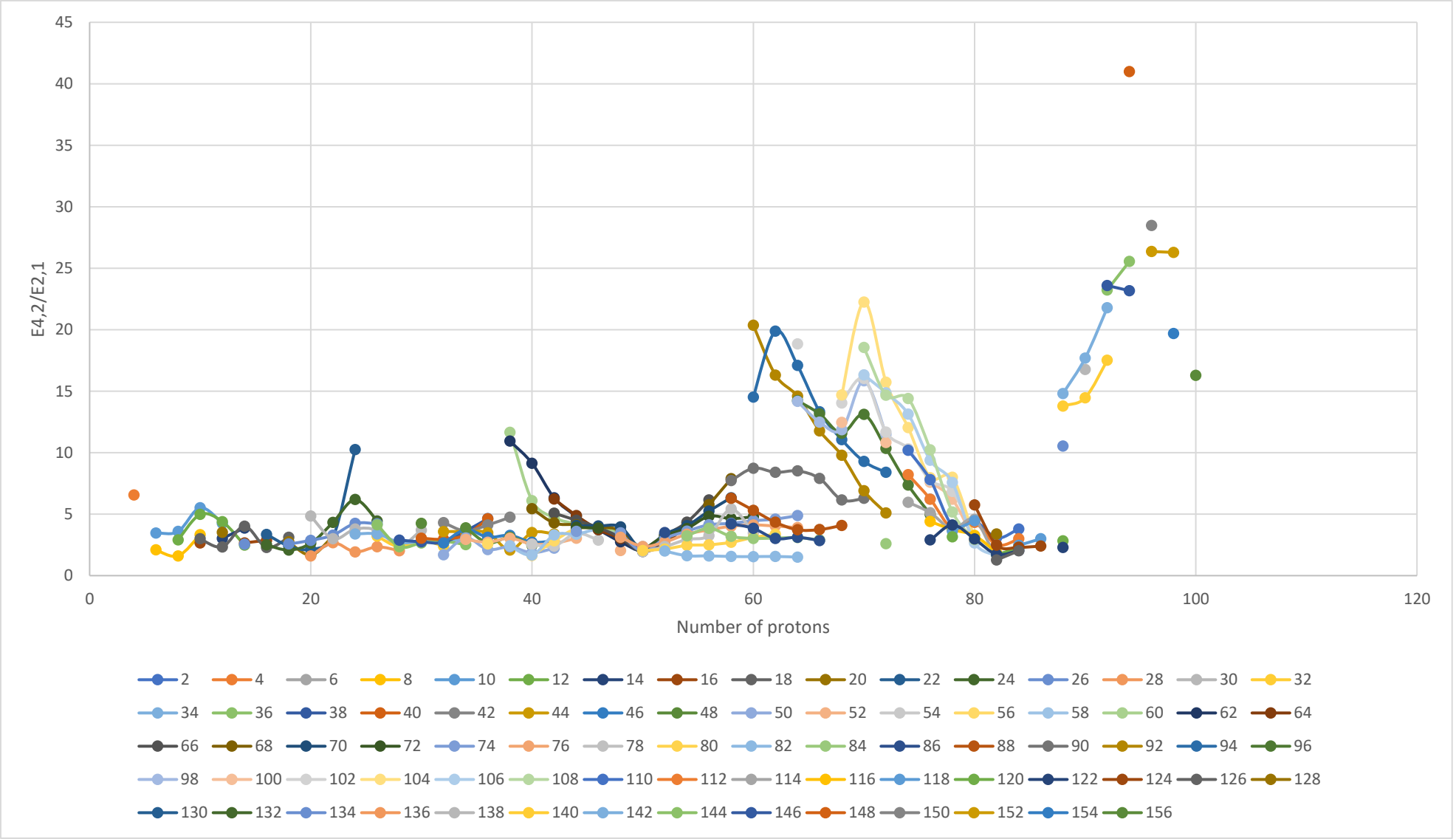

Figure IV. 8 (color online) The experimental values of the energy ratio $E_{4_2^+}/E_{2_1^+}$ for all even–even nuclei plotted as a function of proton number Z along the x axis for different isotones. The neutron numbers N for different isotones are indicated by legend below graph.

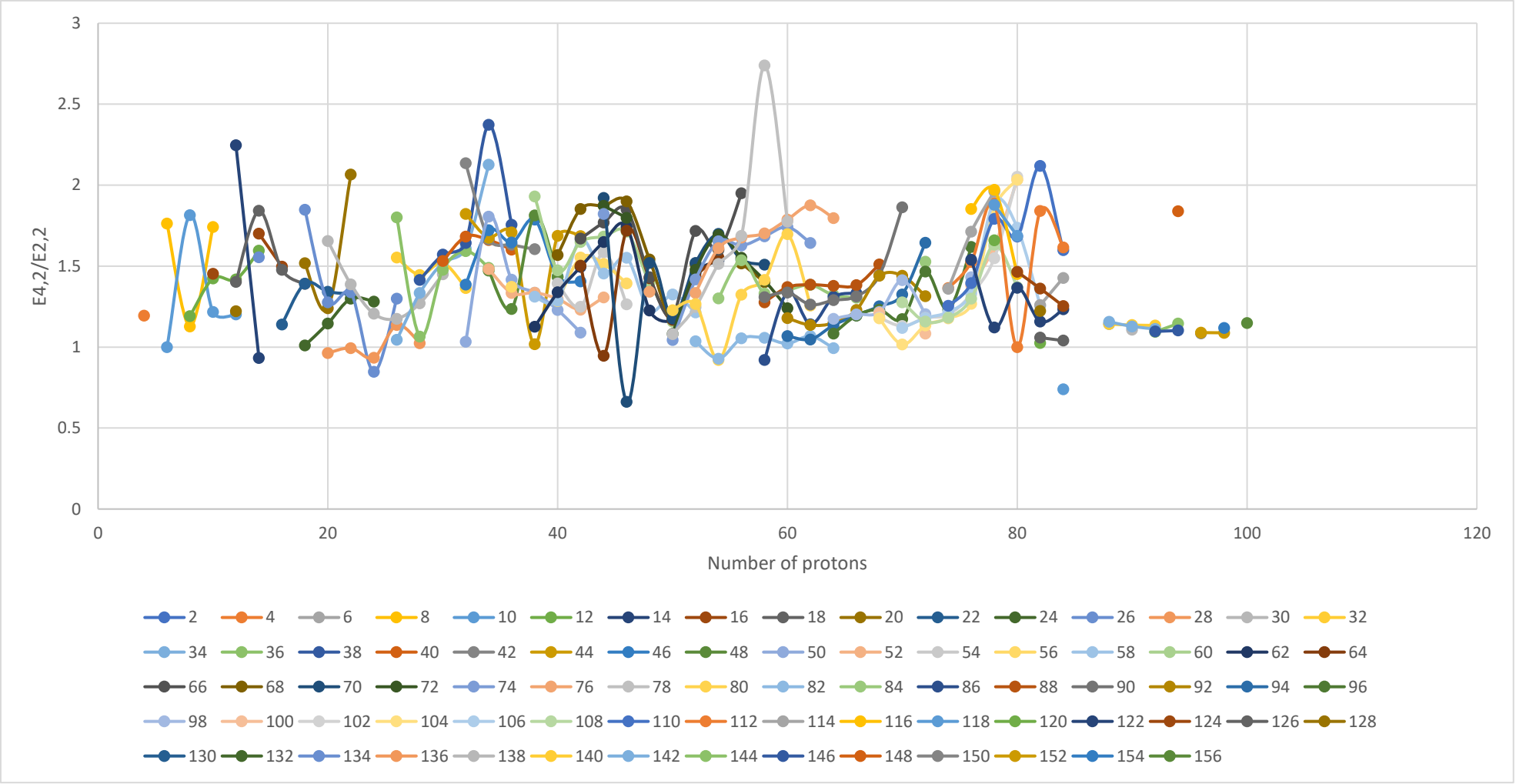

Figure IV. 9 (color online) The experimental values of the energy ratio $E_{4_2^+}/E_{2_2^+}$ for all even–even nuclei plotted as a function of proton number Z along the x axis for different isotones. The neutron numbers N for different isotones are indicated by legend below graph.

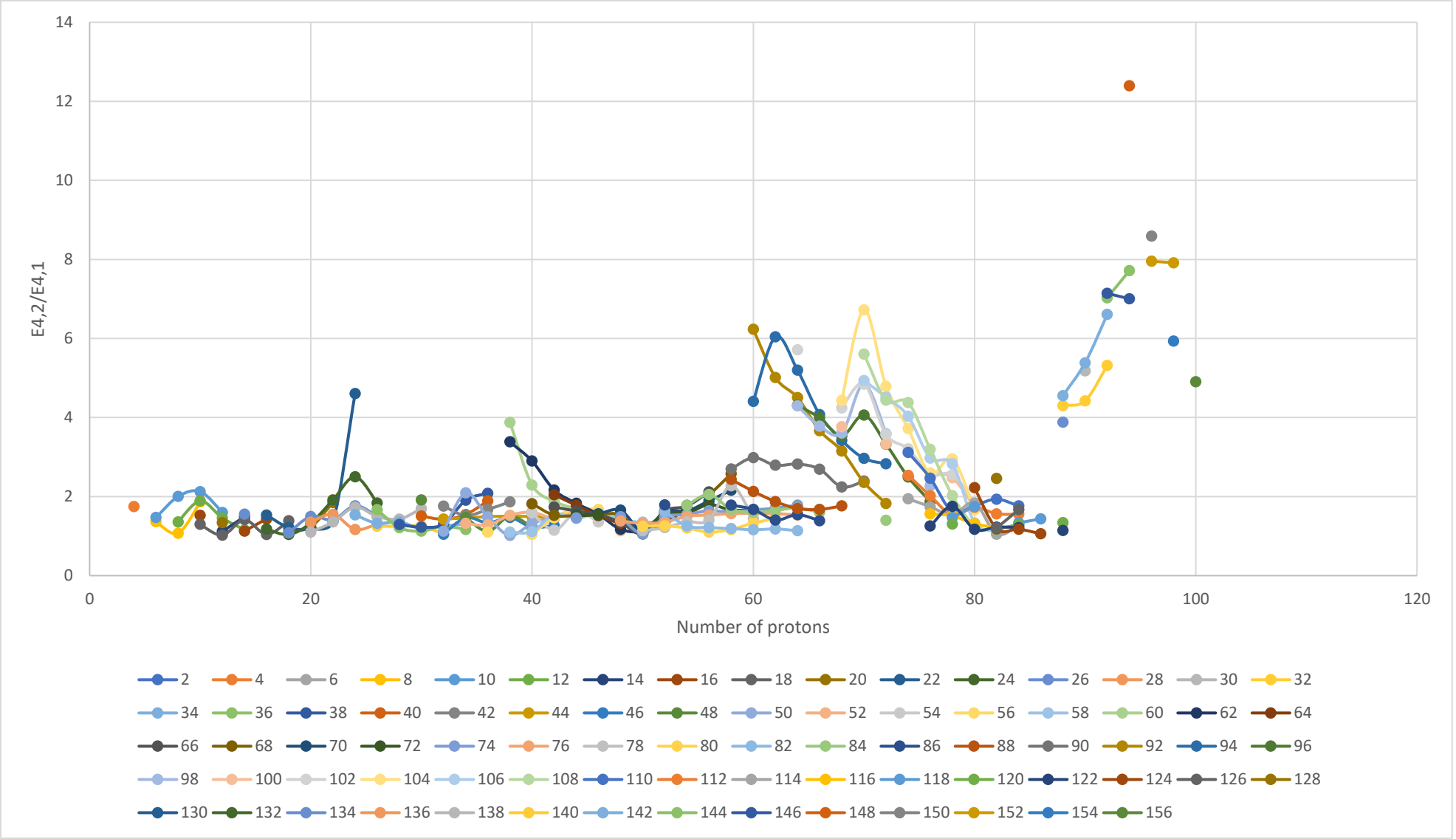

Figure IV. 10 (color online) The experimental values of the energy ratio $E_{4_2^+}/E_{4_1^+}$ for all even–even nuclei plotted as a function of proton number Z along the x axis for different isotones. The neutron numbers N for different isotones are indicated by legend below graph.

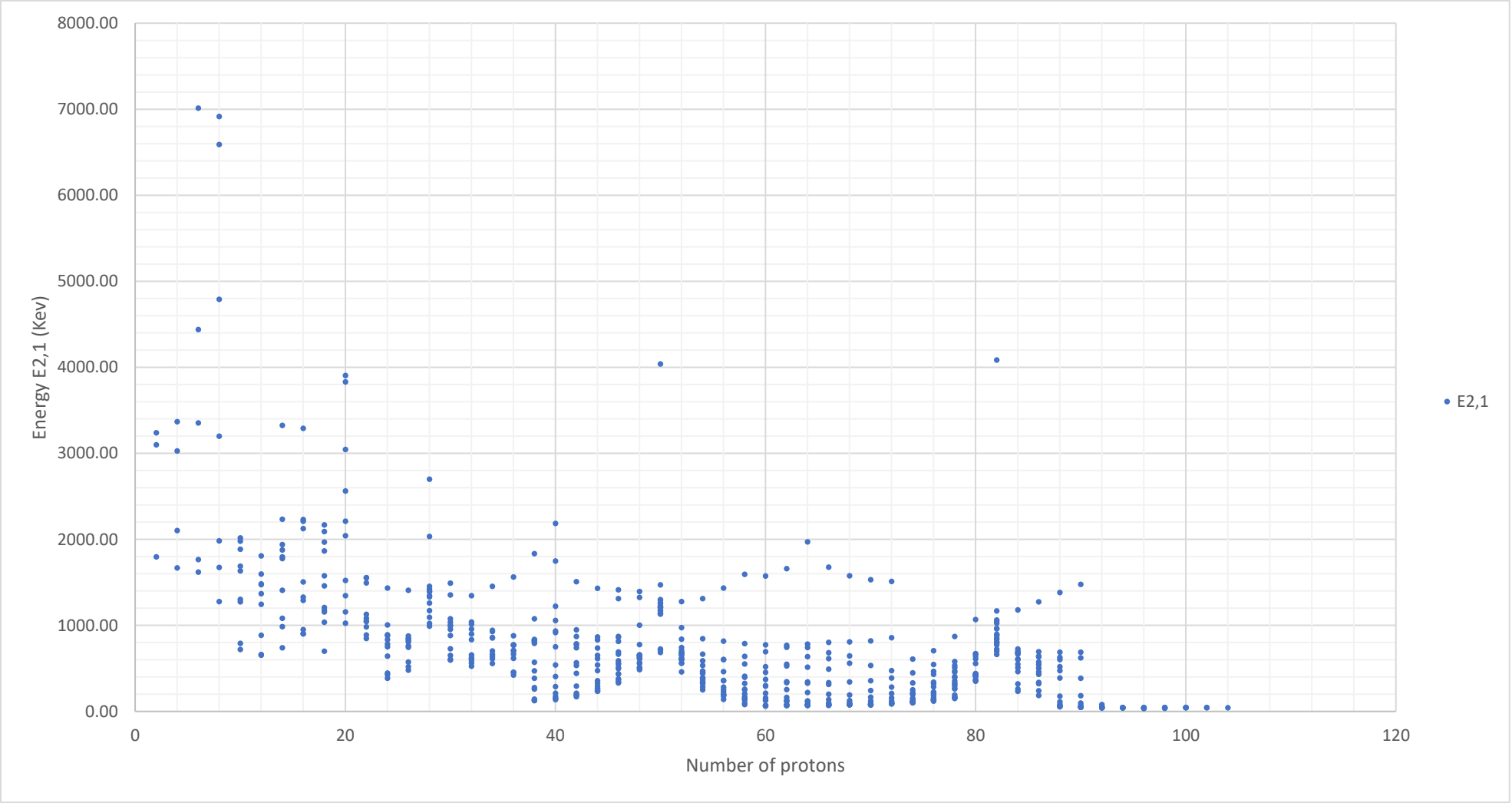

Figure IV. 11 (color online) The experimental values of the energy of the first -excited 2^+ state ($E_{2_1^+}$) for all even–even nuclei plotted as a function of proton number Z along the x axis (in general).

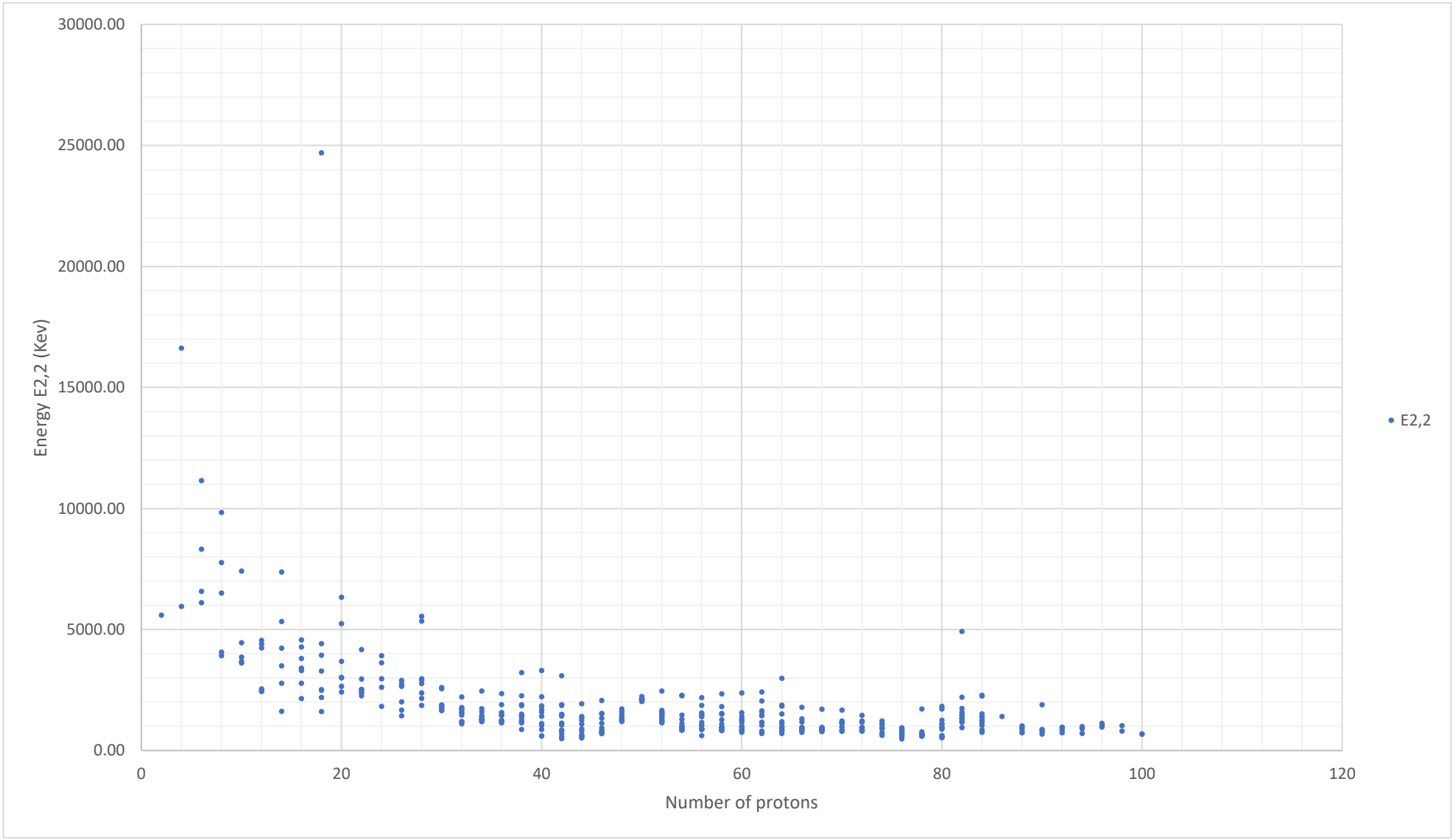

Figure IV. 12 (color online) The experimental values of the energy of the second -excited 2^+ state ($E_{2_2^+}$) for all even–even nuclei plotted as a function of proton number Z along the x axis (in general).

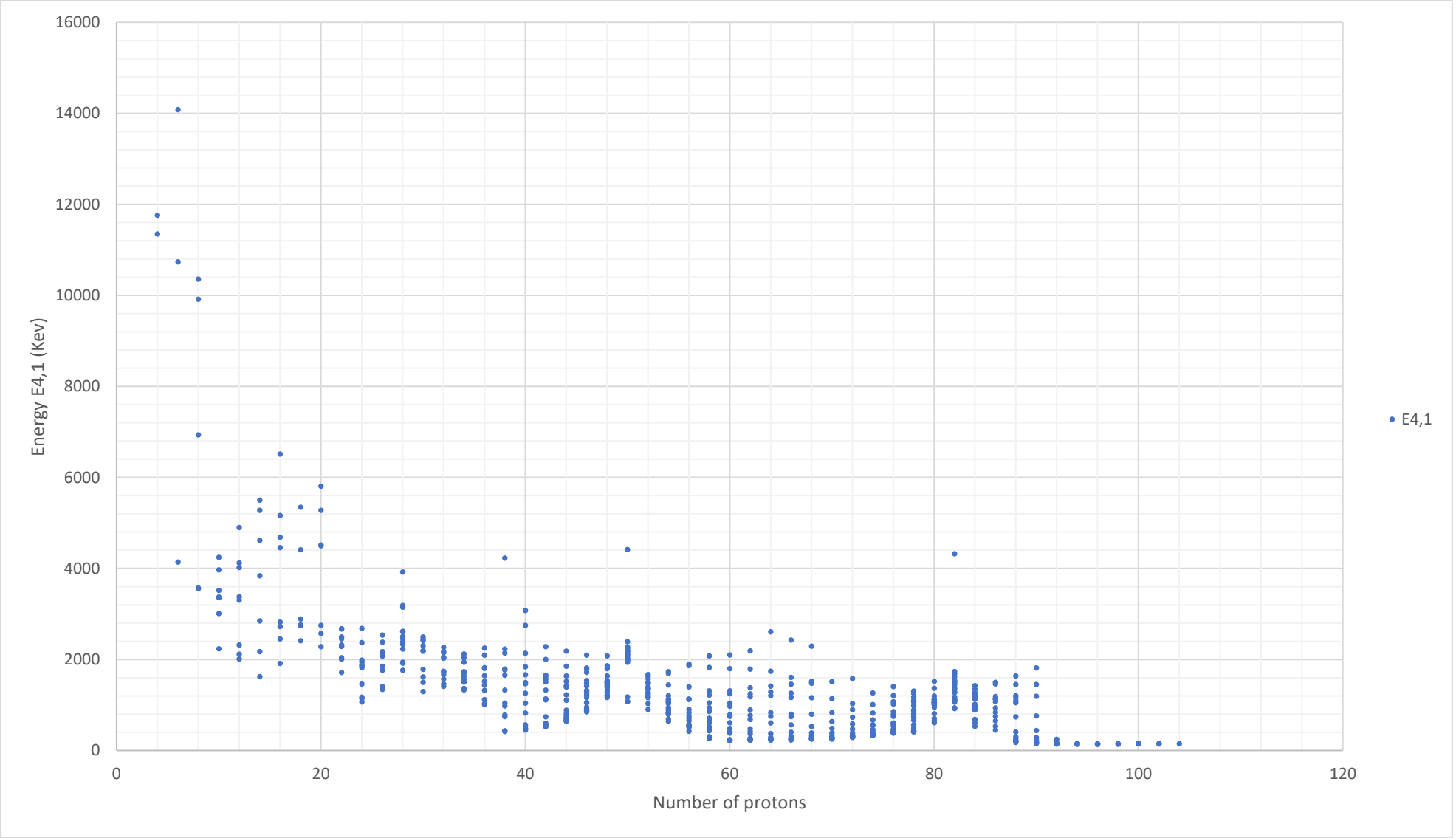

Figure IV. 13 (color online) The experimental values of the energy of the first -excited 4^+ state ($E_{4_1^+}$) for all even–even nuclei plotted as a function of proton number Z along the x axis (in general).

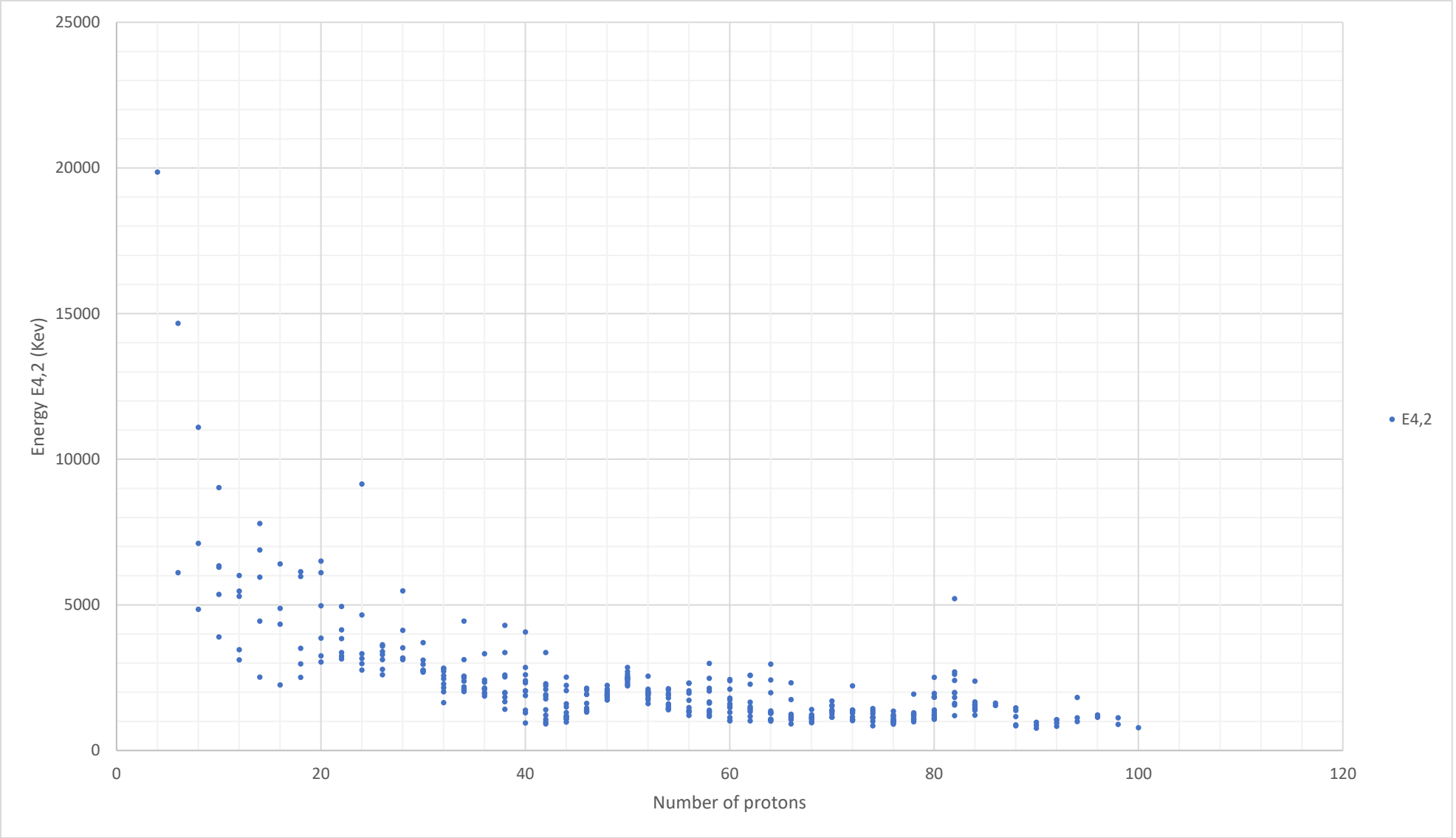

Figure IV. 14 (color online) The experimental values of the energy of the second -excited 4^+ state ($E_{4_2^+}$) for all even–even nuclei plotted as a function of proton number Z along the x axis (in general).

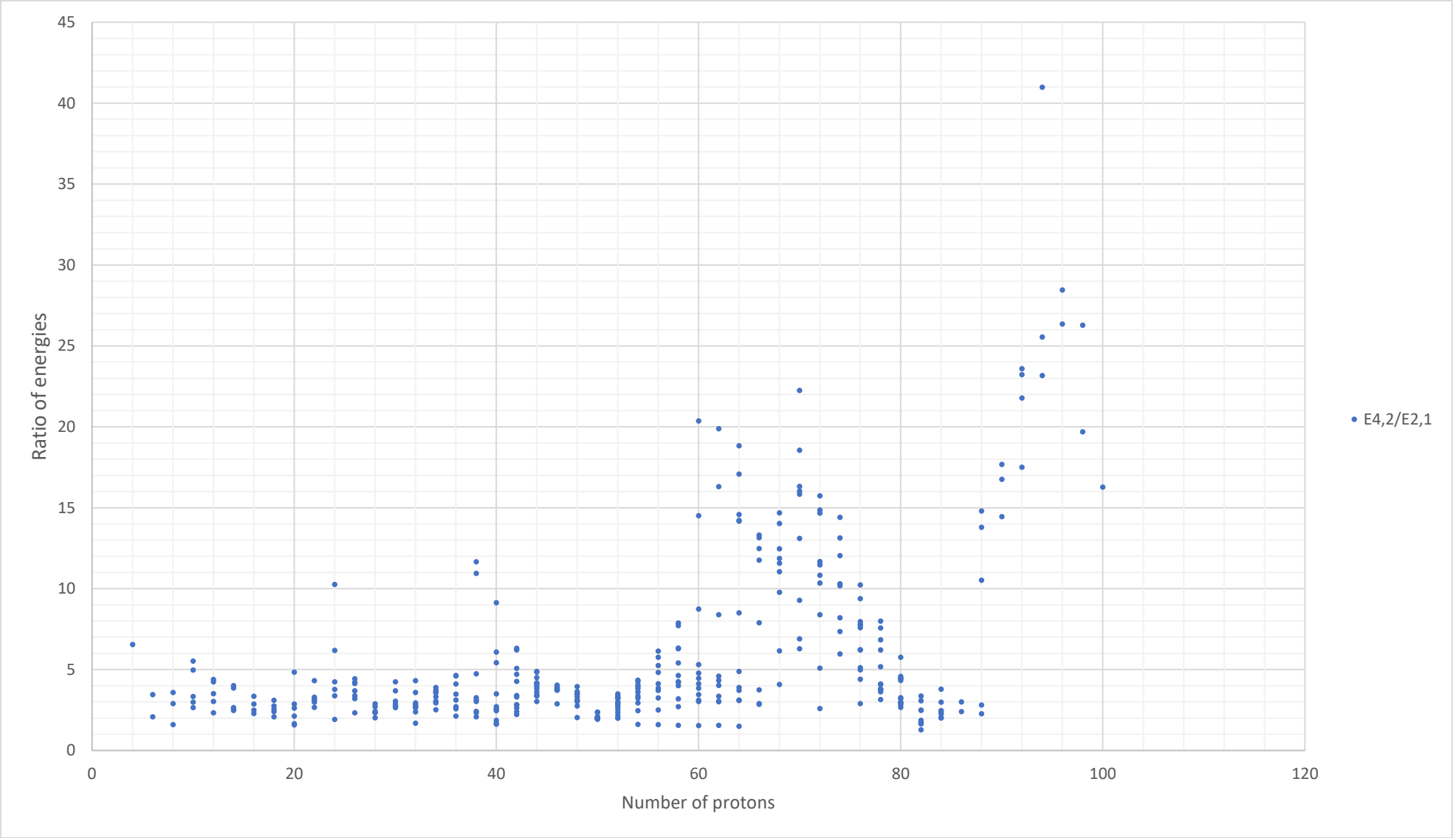

Figure IV. 15 (color online) The experimental values of the energy ratio $E_{4_2^+}/E_{2_1^+}$ for all even–even nuclei plotted as a function of proton number Z along the x axis (in general).

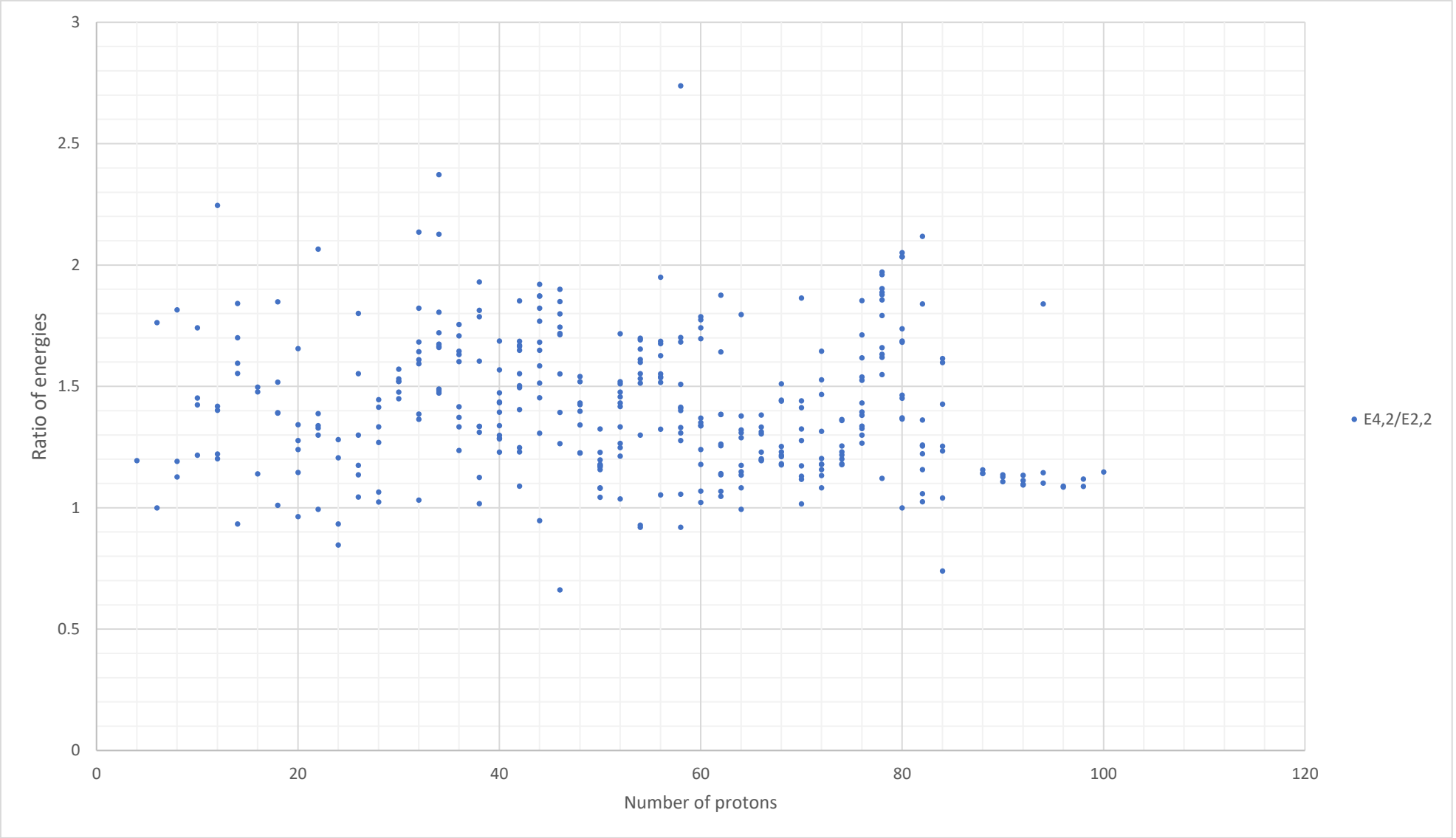

Figure IV. 16 (color online) The experimental values of the energy ratio $E_{4_2^+}/E_{2_2^+}$ for all even–even nuclei plotted as a function of proton number Z along the x axis (in general).

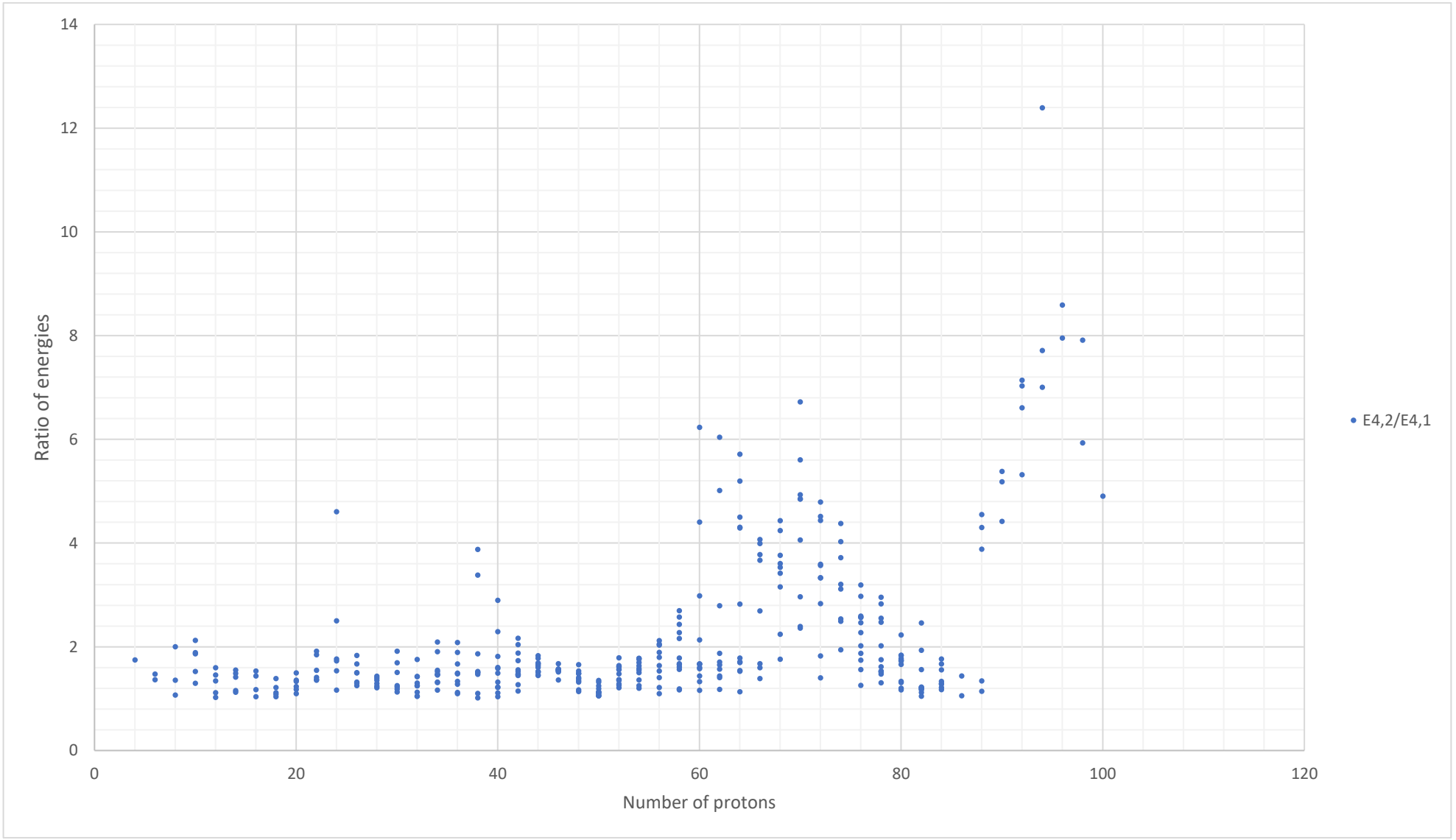

Figure IV. 17 (color online) The experimental values of the energy ratio $E_{4_2^+}/E_{4_1^+}$ for all even–even nuclei plotted as a function of proton number Z along the x axis (in general).

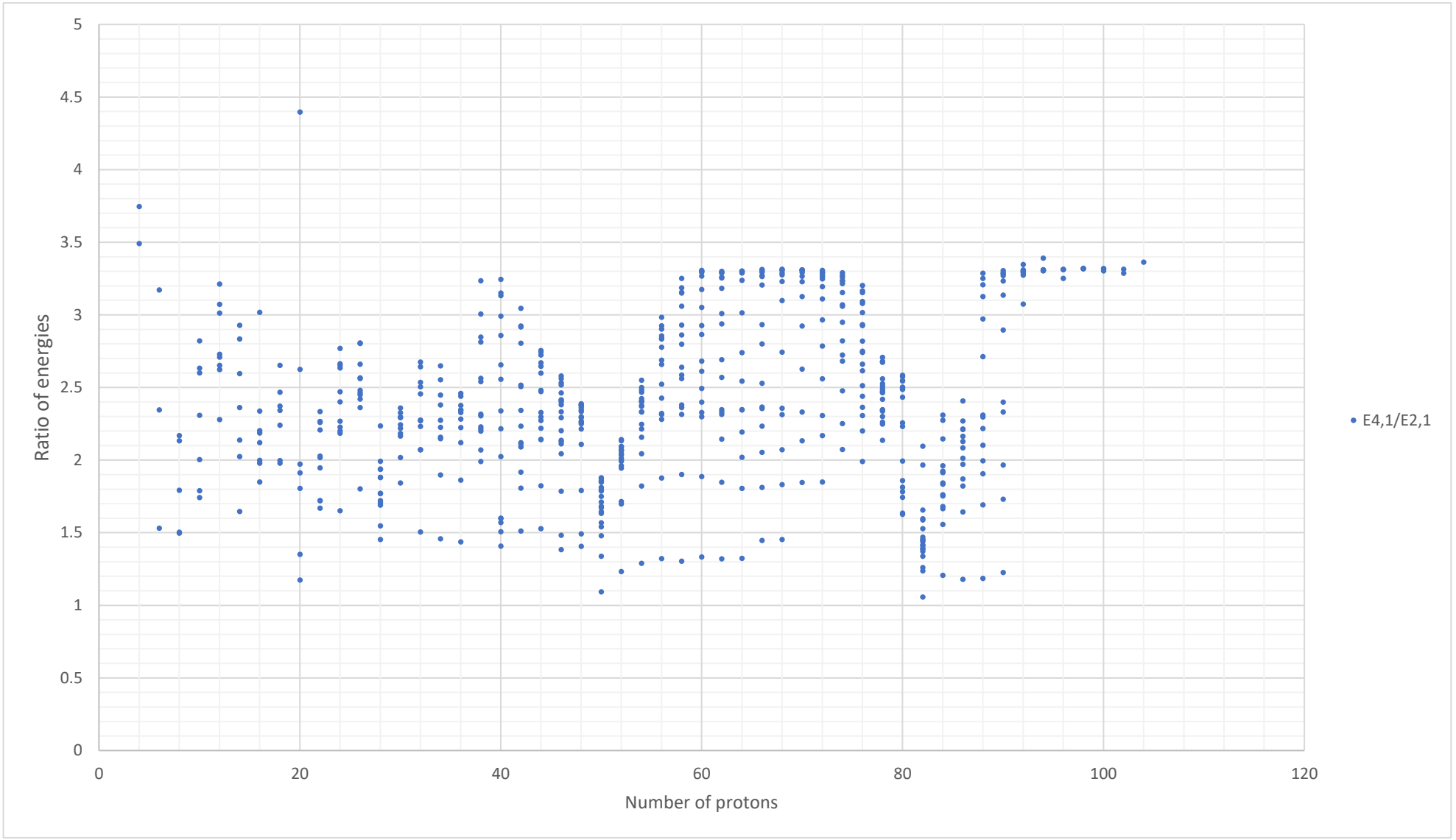

Figure IV. 18 (color online) The experimental values of the energy ratio $E_{4_1^+}/E_{2_1^+}$ for all even–even nuclei plotted as a function of proton number Z along the x axis (in general).

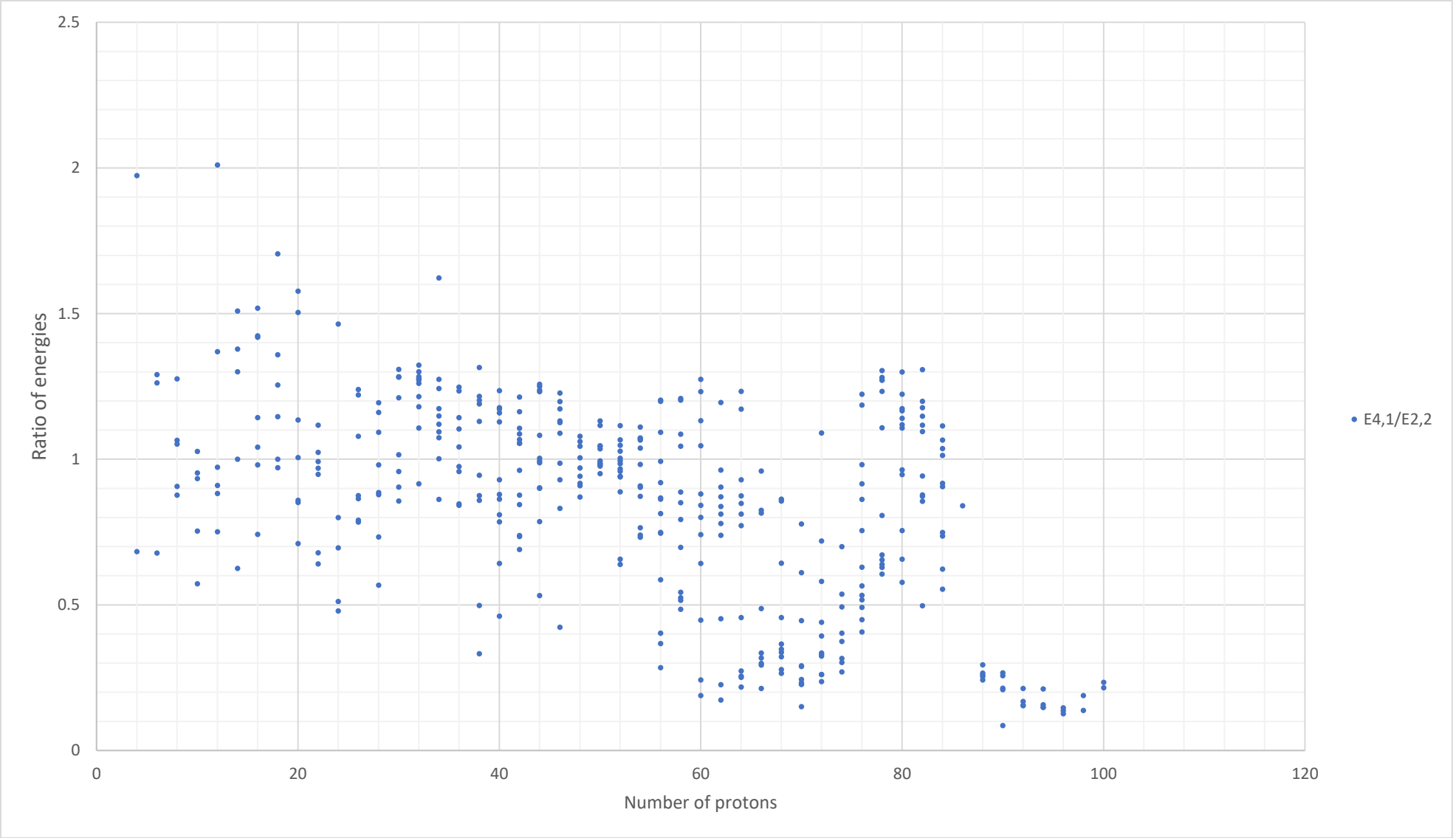

Figure IV. 19 (color online) The experimental values of the energy ratio $E_{4_1^+}/E_{2_2^+}$ for all even–even nuclei plotted as a function of proton number Z along the x axis (in general).

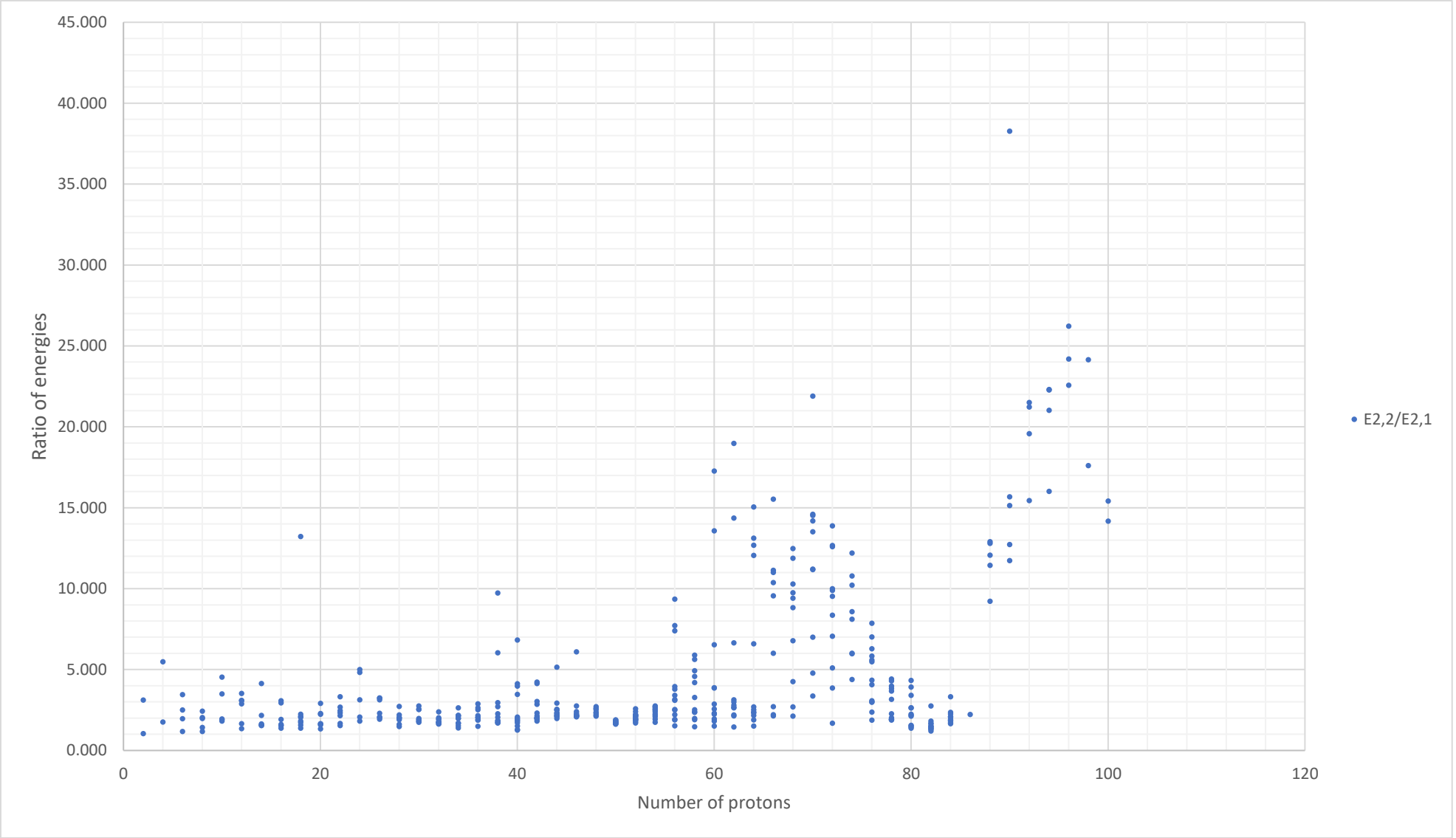

Figure IV. 20 (color online) The experimental values of the energy ratio $E_{2_2^+}/E_{2_1^+}$ for all even–even nuclei plotted as a function of proton number Z along the x axis (in general).

Chapter V

Two dimensional figures of the values of energy levels and energy ratios over all even–even nuclei for each chain of Isotones

Isotones (N=2)

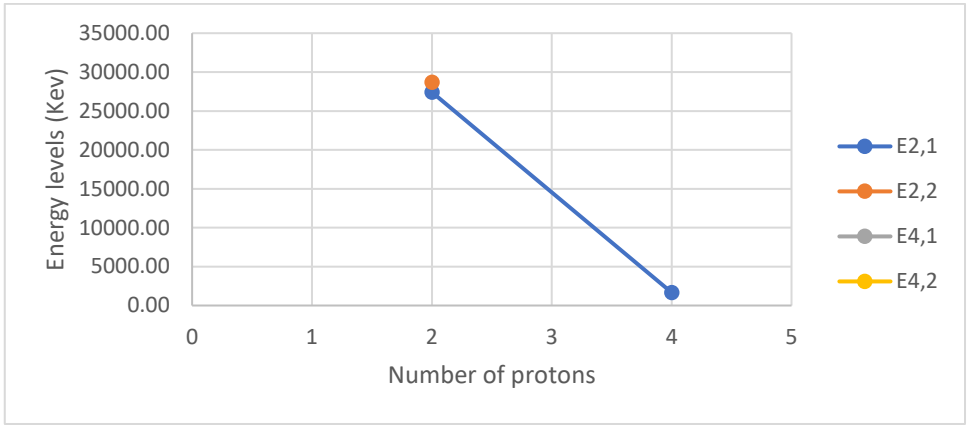

A

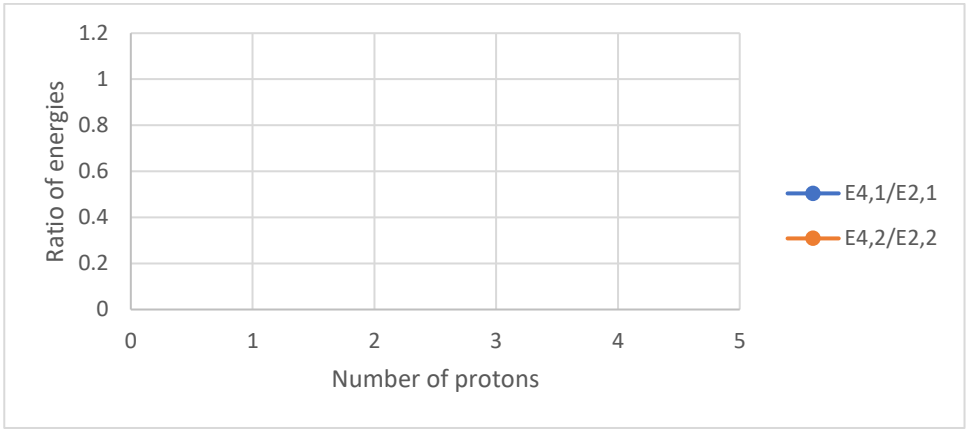

B

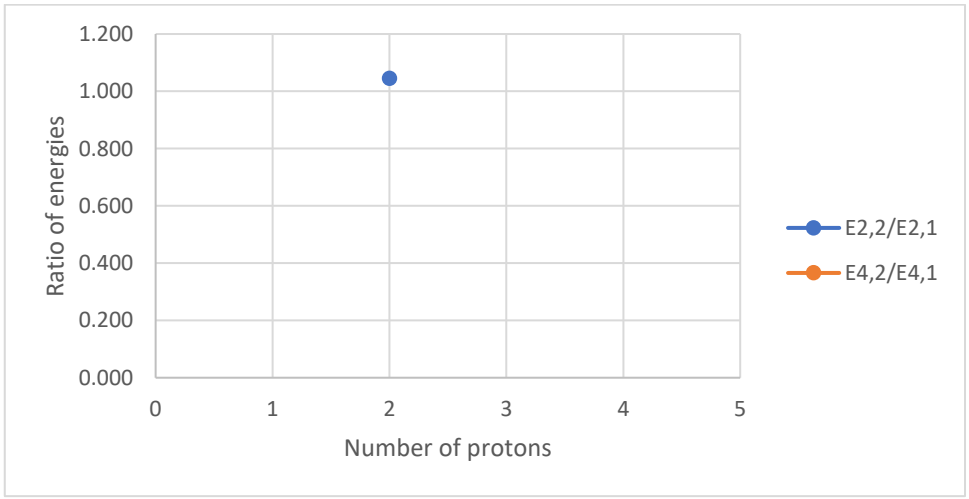

C

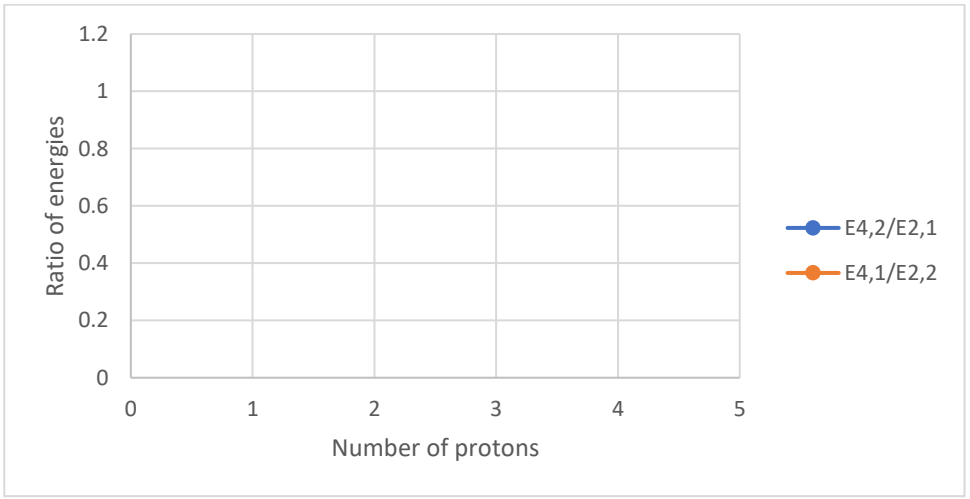

D

Figure V. 1 (color online) Panel **A** represents the comparison of the experimental energy levels of the lowest 2_1^+, 2_2^+, 4_1^+ and 4_2^+ states for the chain of N=2 isotones. Panels **B, C, D** represent the comparison of the experimental energy ratios ($E_{4_1^+}/E_{2_1^+}$ and $E_{4_2^+}/E_{2_2^+}$), ($E_{2_2^+}/E_{2_1^+}$ and $E_{4_2^+}/E_{4_1^+}$) and ($E_{4_2^+}/E_{2_1^+}$ and $E_{4_1^+}/E_{2_2^+}$), respectively, for the chain of N=2 isotones.

Isotones (N=4)

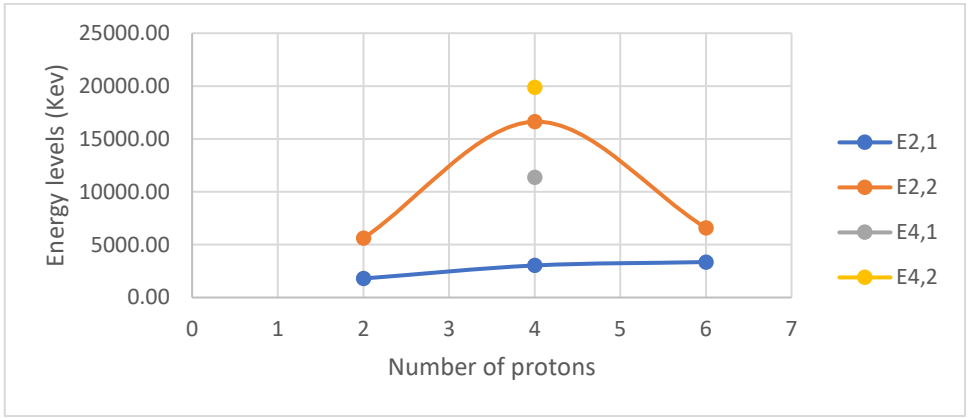

A

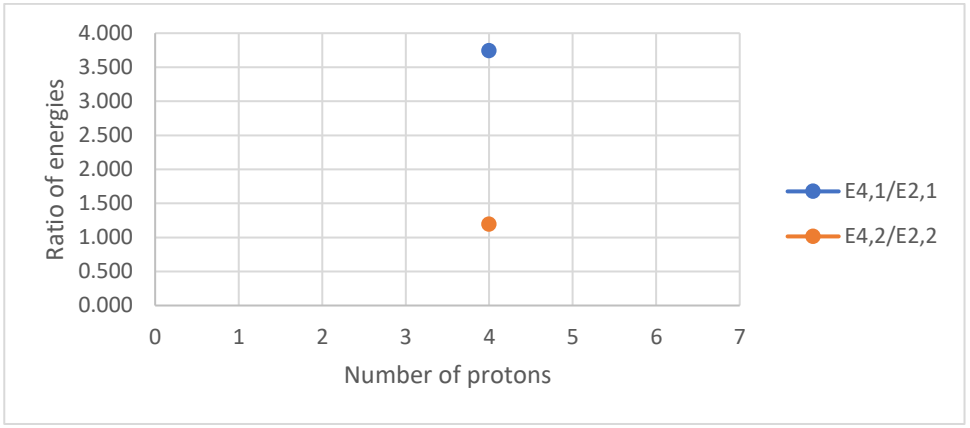

B

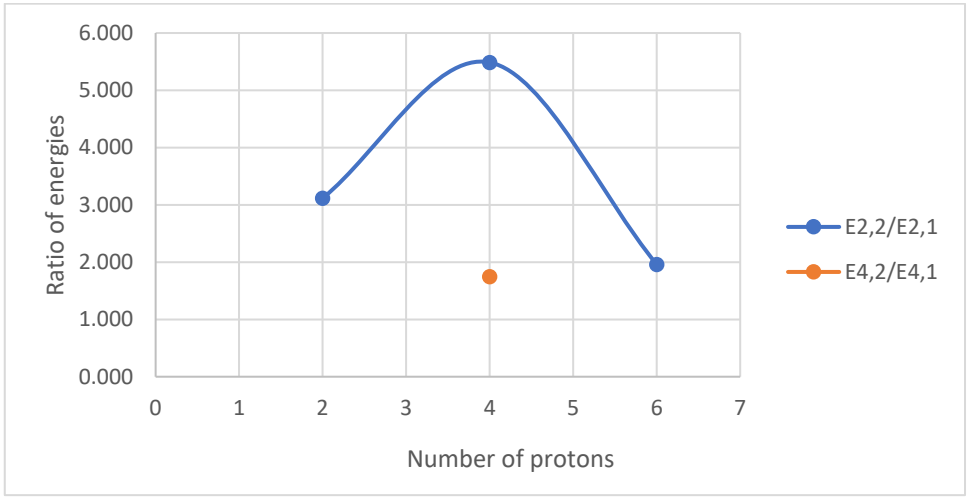

C

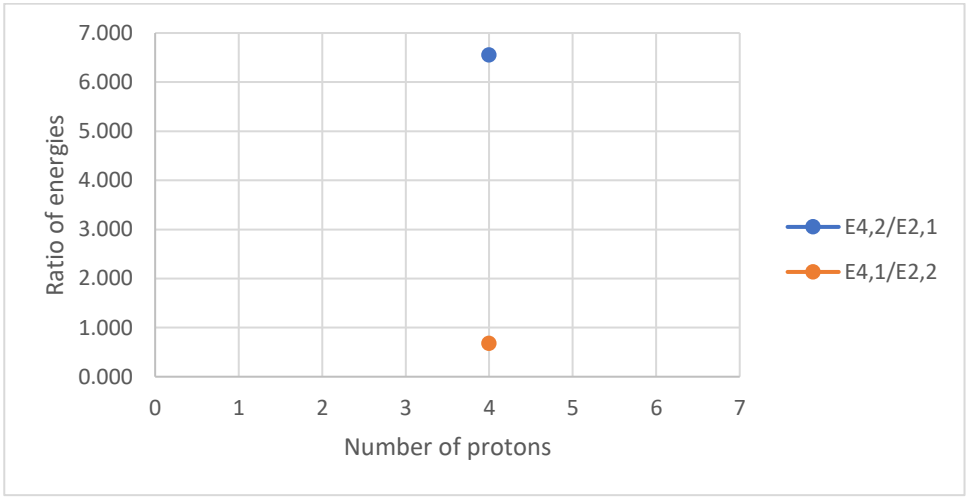

D

Figure V. 2 (color online) Panel **A** represents the comparison of the experimental energy levels of the lowest 2_1^+, 2_2^+, 4_1^+ and 4_2^+ states for the chain of N=4 isotones. Panels **B, C, D** represent the comparison of the experimental energy ratios ($E_{4_1^+}/E_{2_1^+}$ and $E_{4_2^+}/E_{2_2^+}$), ($E_{2_2^+}/E_{2_1^+}$ and $E_{4_2^+}/E_{4_1^+}$) and ($E_{4_2^+}/E_{2_1^+}$ and $E_{4_1^+}/E_{2_2^+}$), respectively, for the chain of N=4 isotones.

Isotones (N=6)

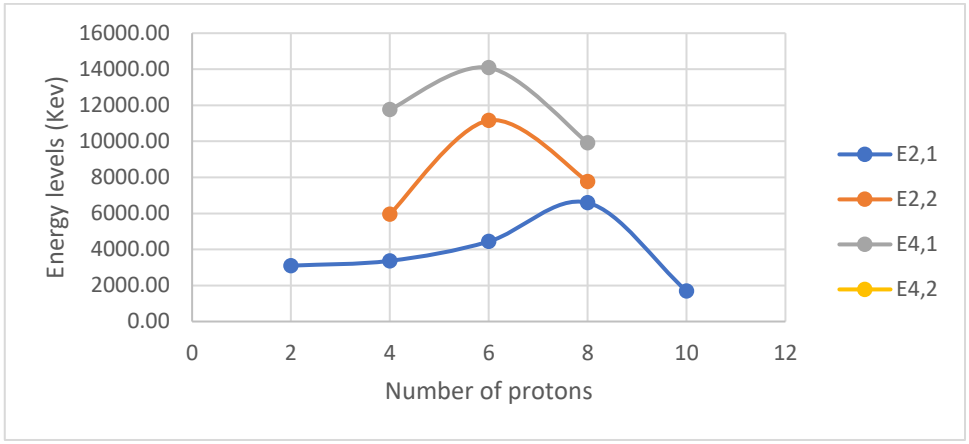

A

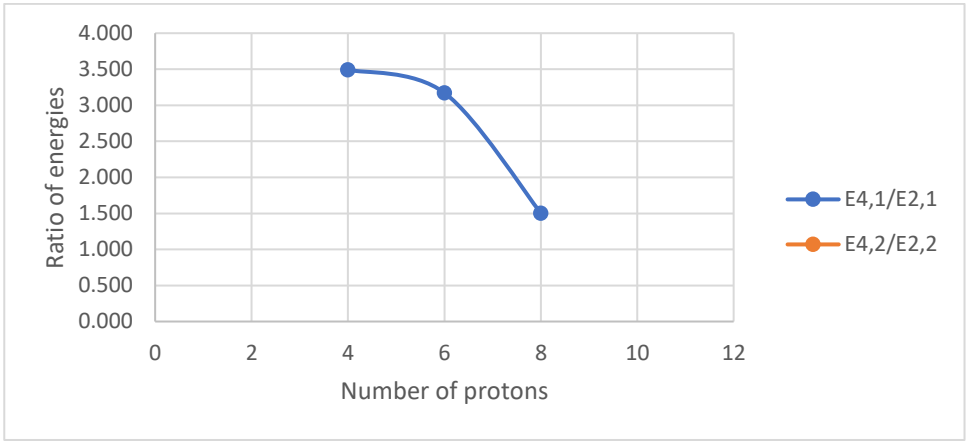

B

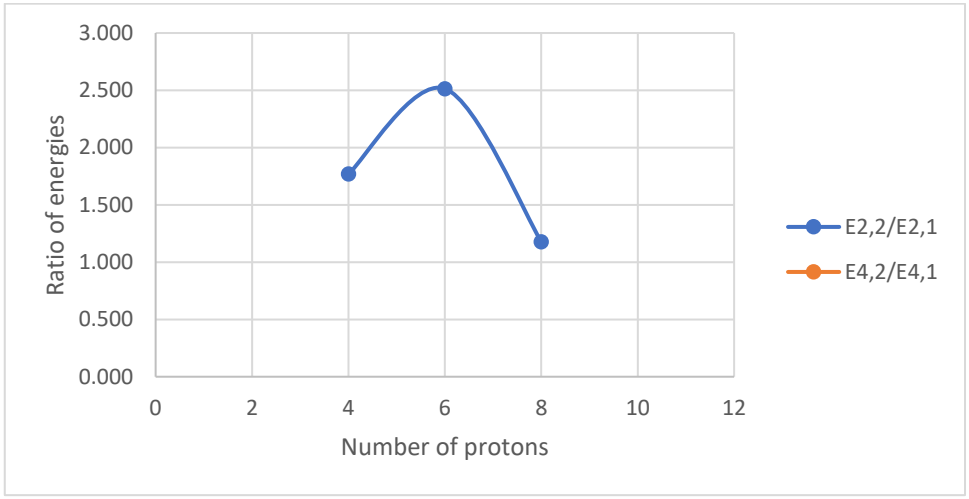

C

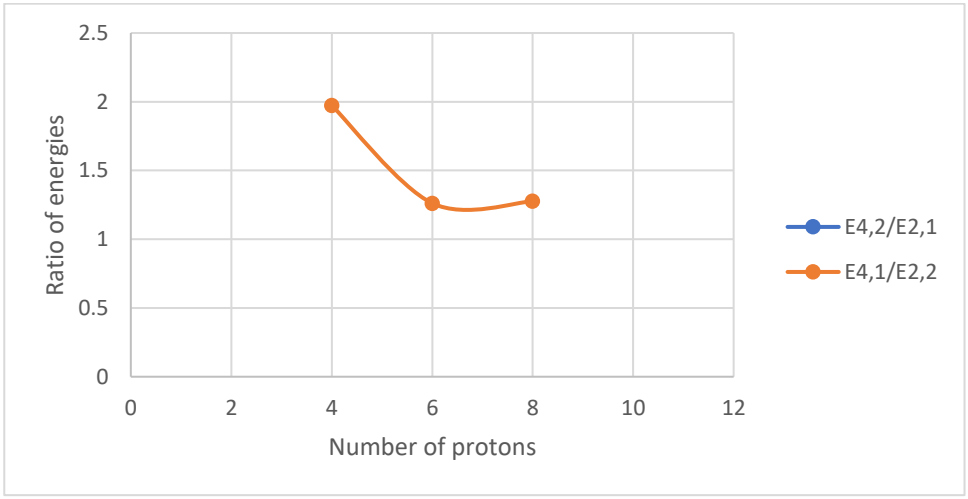

D

Figure V. 3 (color online) Panel **A** represents the comparison of the experimental energy levels of the lowest 2_1^+, 2_2^+, 4_1^+ and 4_2^+ states for the chain of N=6 isotones. Panels **B, C, D** represent the comparison of the experimental energy ratios ($E_{4_1^+}/E_{2_1^+}$ and $E_{4_2^+}/E_{2_2^+}$), ($E_{2_2^+}/E_{2_1^+}$ and $E_{4_2^+}/E_{4_1^+}$) and ($E_{4_2^+}/E_{2_1^+}$ and $E_{4_1^+}/E_{2_2^+}$), respectively, for the chain of N=6 isotones.

Isotones (N=8)

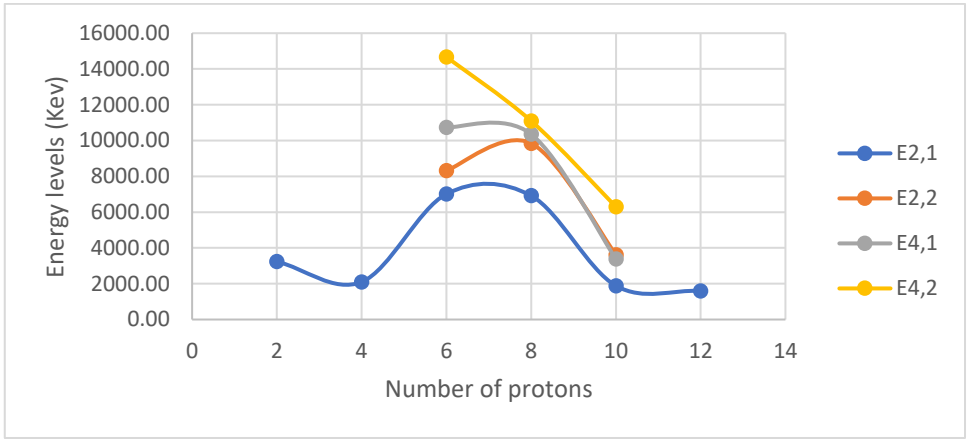

A

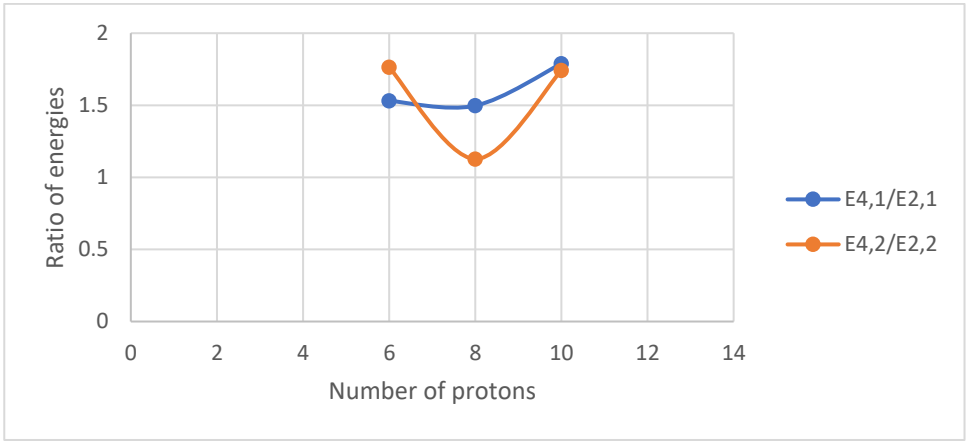

B

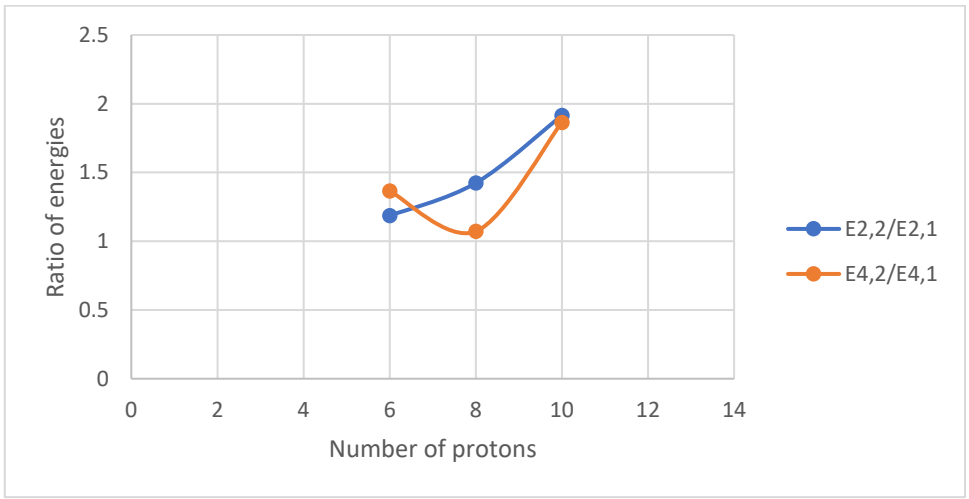

C

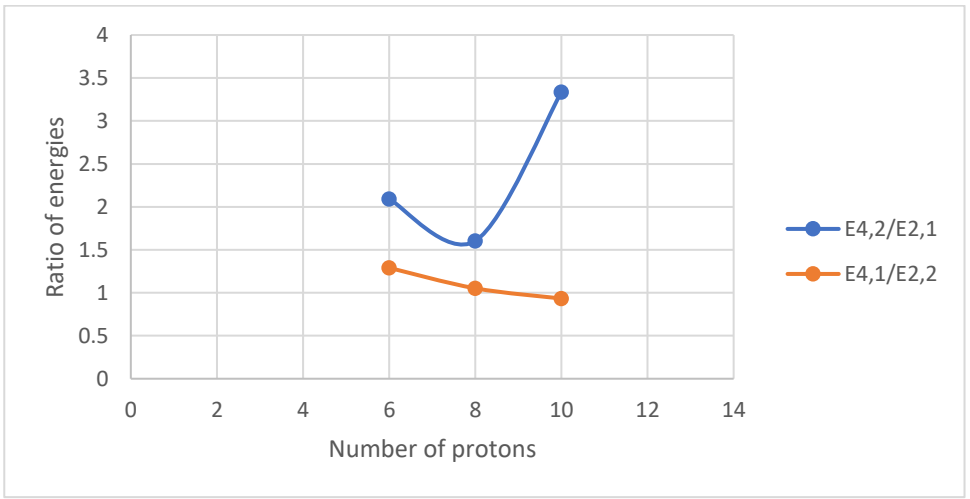

D

Figure V. 4 (color online) Panel **A** represents the comparison of the experimental energy levels of the lowest 2_1^+, 2_2^+, 4_1^+ and 4_2^+ states for the chain of N=8 isotones. Panels **B, C, D** represent the comparison of the experimental energy ratios ($E_{4_1^+}/E_{2_1^+}$ and $E_{4_2^+}/E_{2_2^+}$), ($E_{2_2^+}/E_{2_1^+}$ and $E_{4_2^+}/E_{4_1^+}$) and ($E_{4_2^+}/E_{2_1^+}$ and $E_{4_1^+}/E_{2_2^+}$), respectively, for the chain of N=8 isotones.

Isotones (N=10)

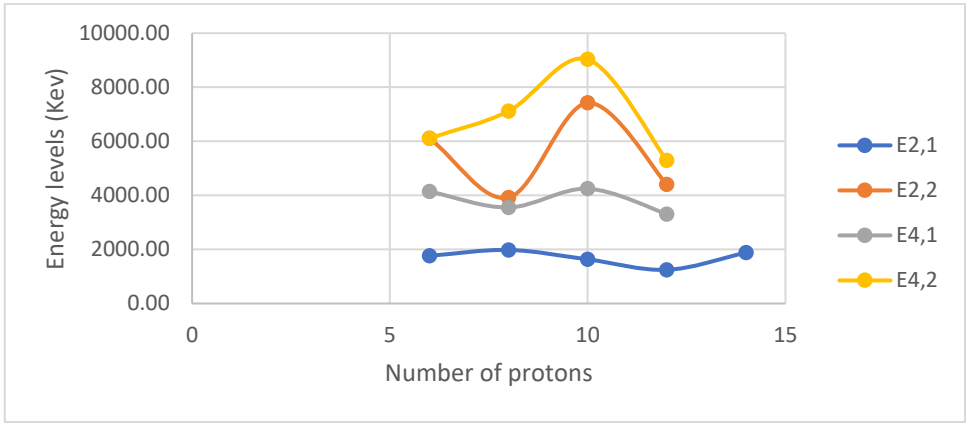

A

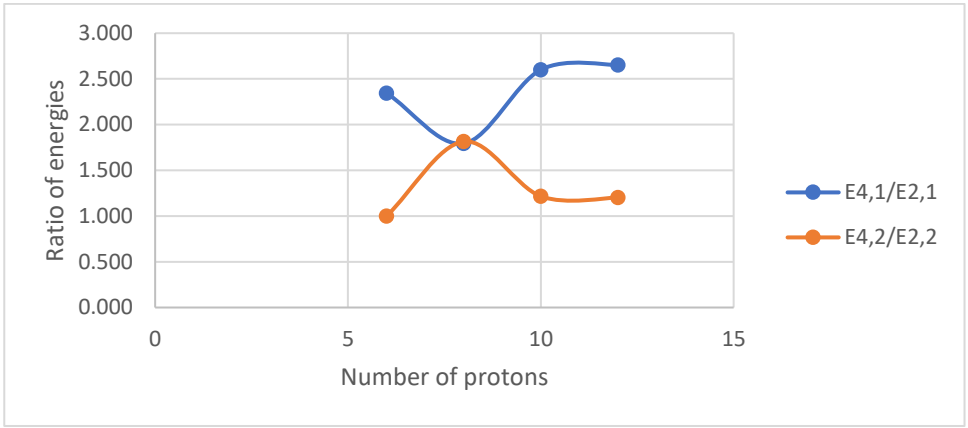

B

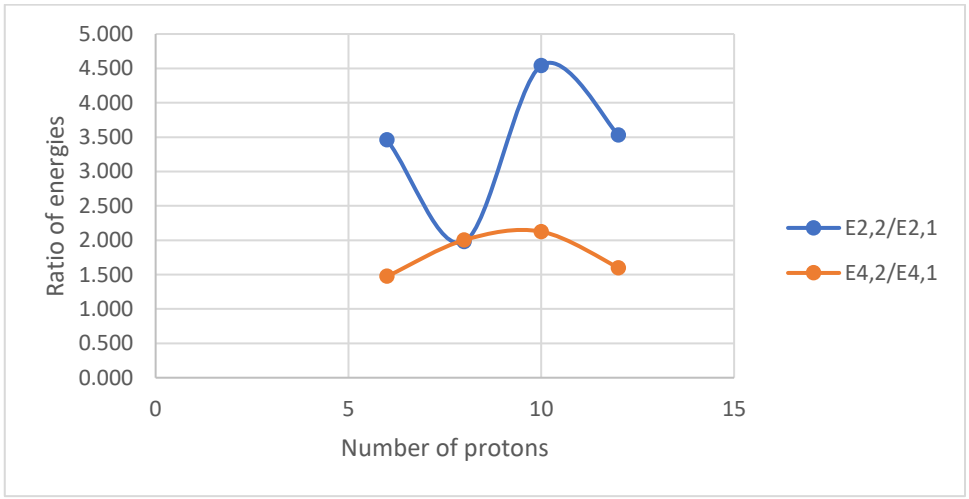

C

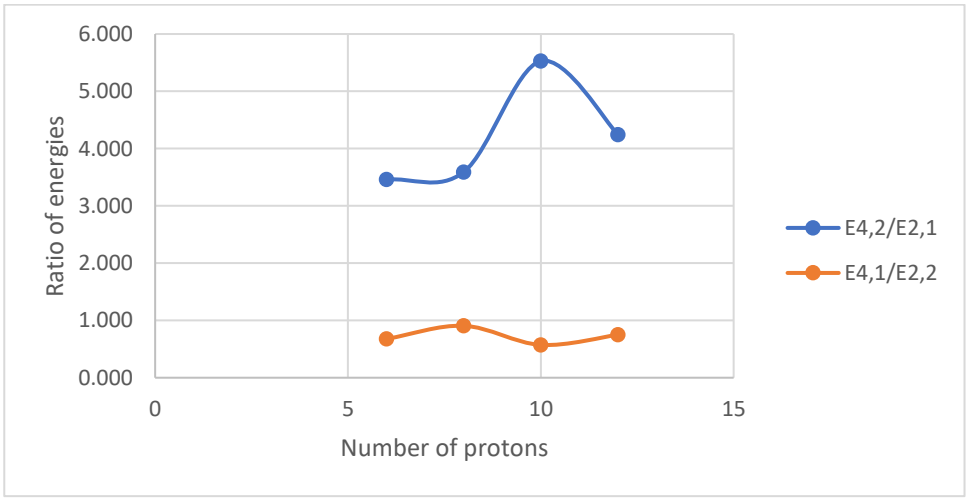

D

Figure V. 5 (color online) Panel **A** represents the comparison of the experimental energy levels of the lowest 2_1^+, 2_2^+, 4_1^+ and 4_2^+ states for the chain of N=10 isotones. Panels **B, C, D** represent the comparison of the experimental energy ratios ($E_{4_1^+}/E_{2_1^+}$ and $E_{4_2^+}/E_{2_2^+}$), ($E_{2_2^+}/E_{2_1^+}$ and $E_{4_2^+}/E_{4_1^+}$) and ($E_{4_2^+}/E_{2_1^+}$ and $E_{4_1^+}/E_{2_2^+}$), respectively, for the chain of N=10 isotones.

Isotones (N=12)

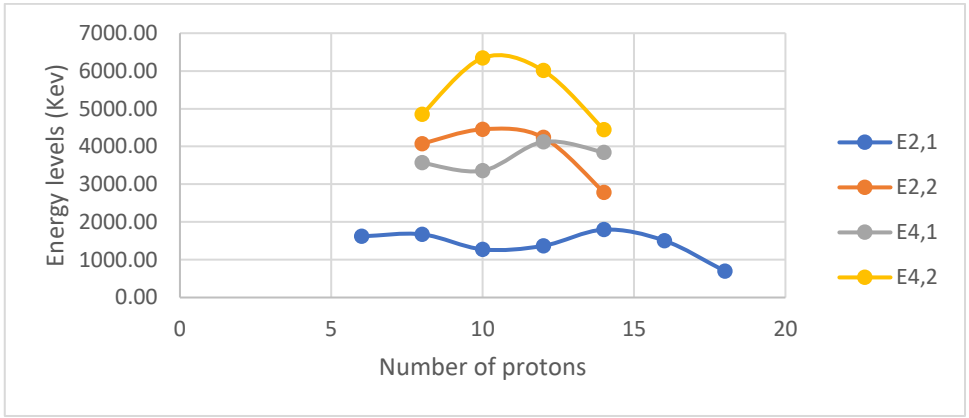

A

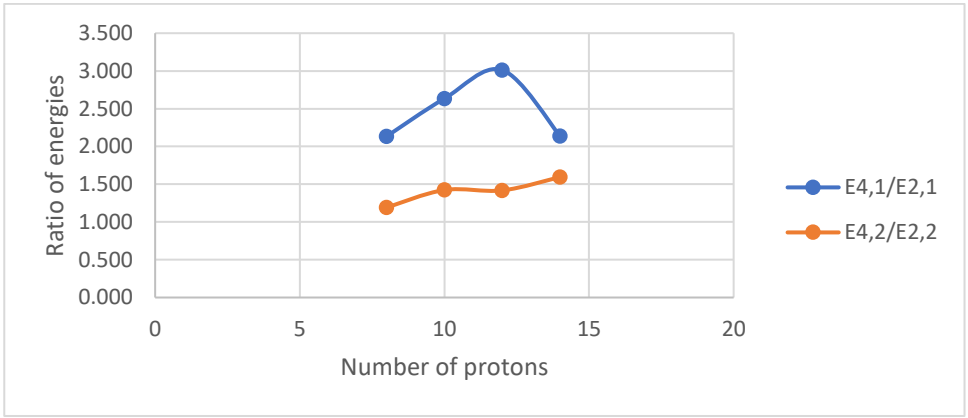

B

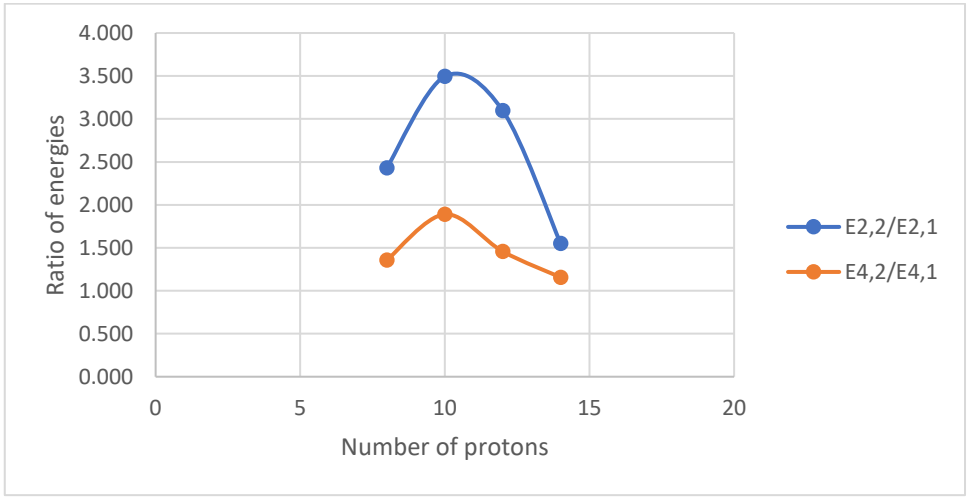

C

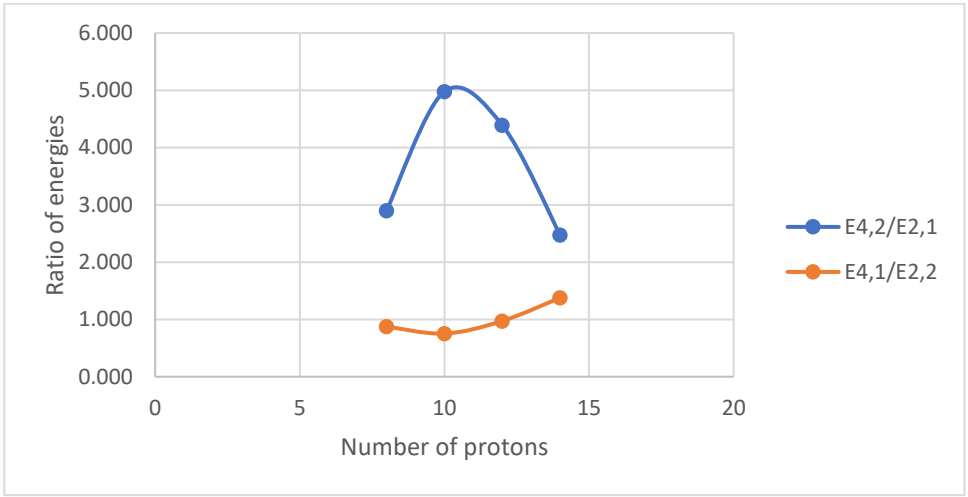

D

Figure V. 6 (color online) Panel **A** represents the comparison of the experimental energy levels of the lowest 2_1^+, 2_2^+, 4_1^+ and 4_2^+ states for the chain of N=12 isotones. Panels **B, C, D** represent the comparison of the experimental energy ratios ($E_{4_1^+}/E_{2_1^+}$ and $E_{4_2^+}/E_{2_2^+}$), ($E_{2_2^+}/E_{2_1^+}$ and $E_{4_2^+}/E_{4_1^+}$) and ($E_{4_2^+}/E_{2_1^+}$ and $E_{4_1^+}/E_{2_2^+}$), respectively, for the chain of N=12 isotones.

Isotones (N=14)

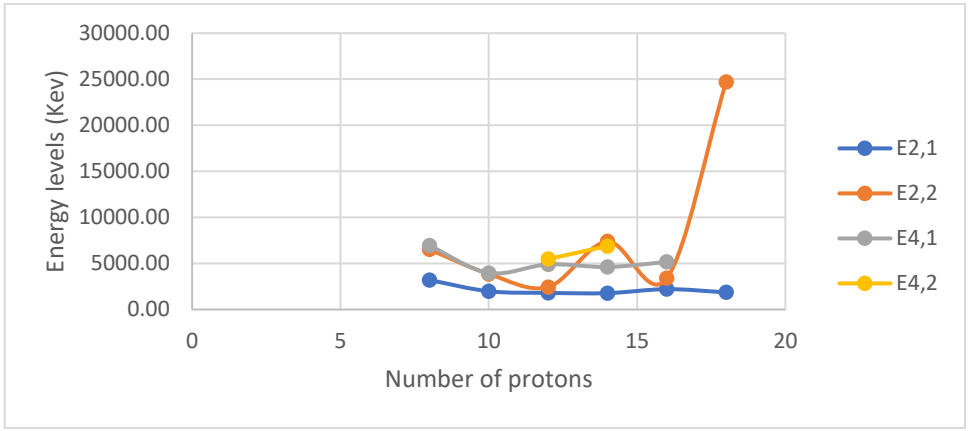

A

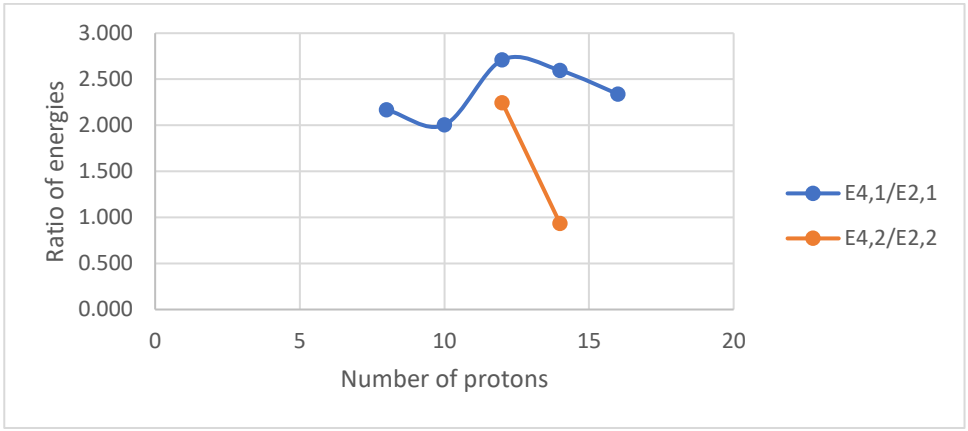

B

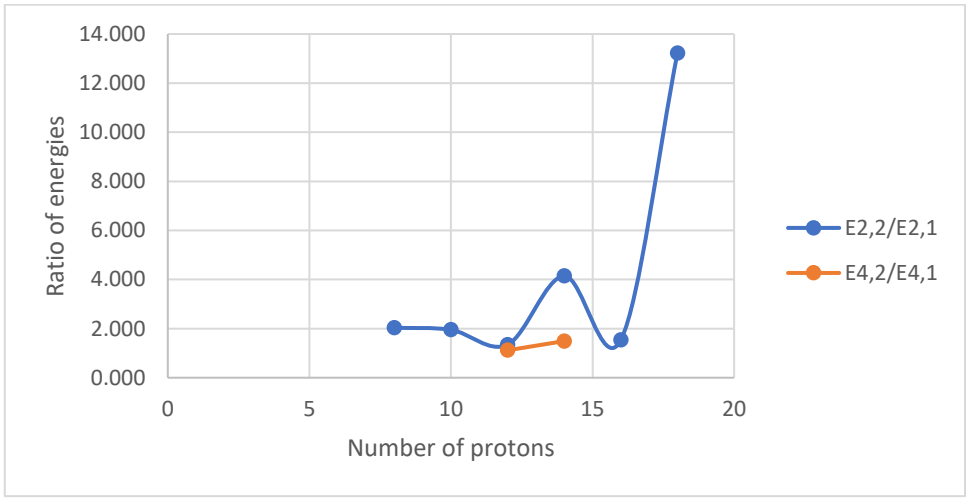

C

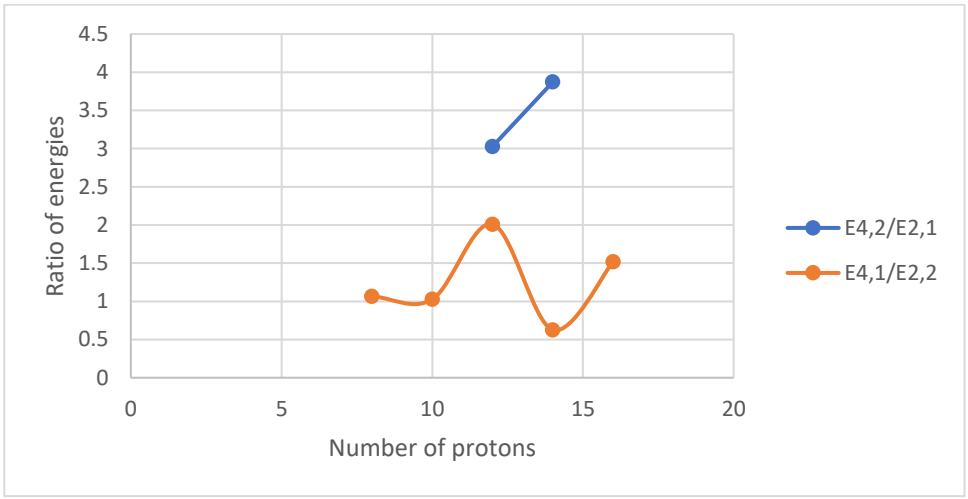

D

Figure V. 7 (color online) Panel **A** represents the comparison of the experimental energy levels of the lowest 2_1^+, 2_2^+, 4_1^+ and 4_2^+ states for the chain of N=14 isotones. Panels **B, C, D** represent the comparison of the experimental energy ratios ($E_{4_1^+}/E_{2_1^+}$ and $E_{4_2^+}/E_{2_2^+}$), ($E_{2_2^+}/E_{2_1^+}$ and $E_{4_2^+}/E_{4_1^+}$) and ($E_{4_2^+}/E_{2_1^+}$ and $E_{4_1^+}/E_{2_2^+}$), respectively, for the chain of N=14 isotones.

Isotones (N=16)

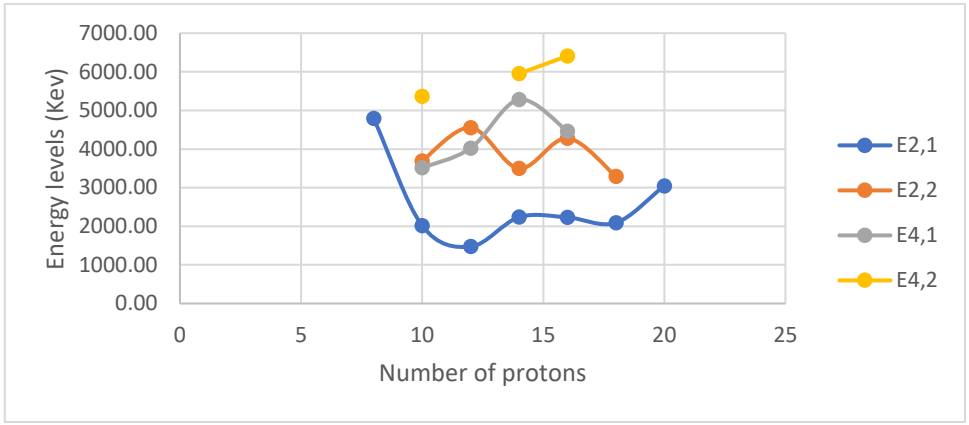

A

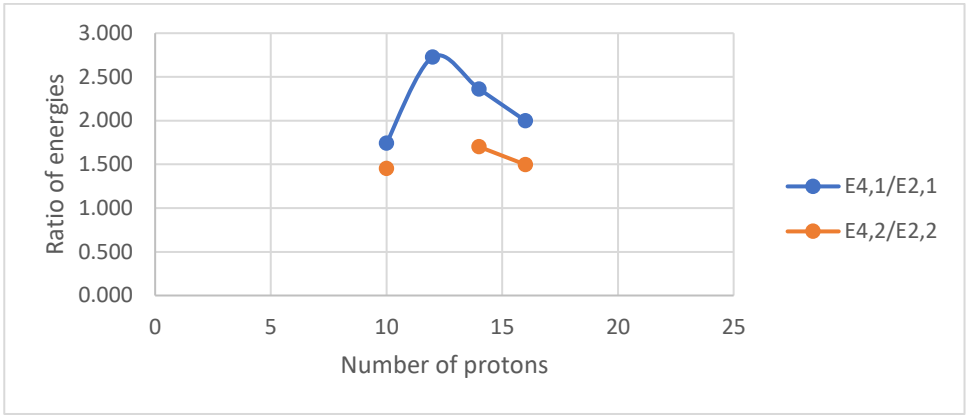

B

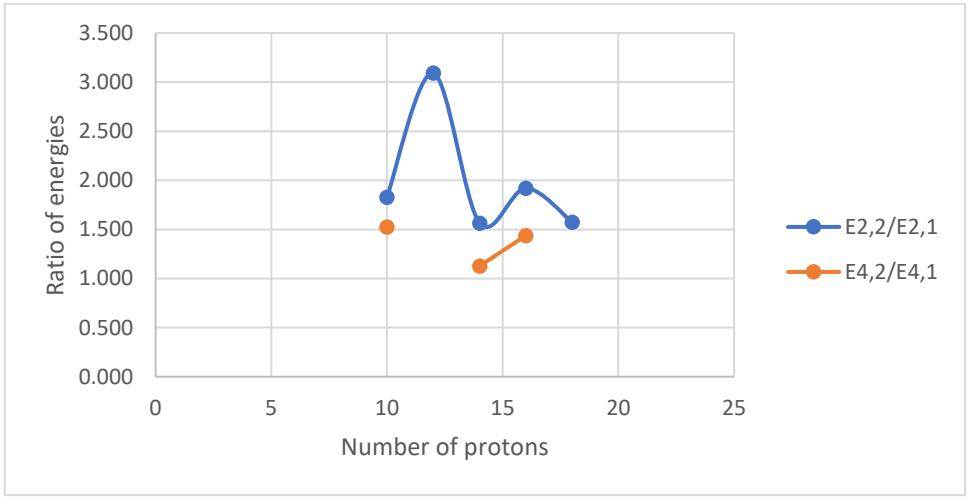

C

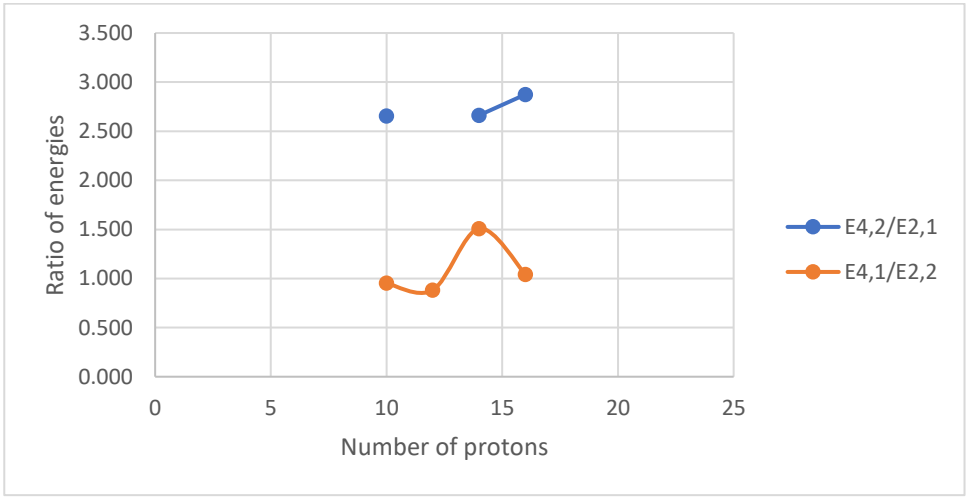

D

Figure V. 8 (color online) Panel **A** represents the comparison of the experimental energy levels of the lowest 2_1^+, 2_2^+, 4_1^+ and 4_2^+ states for the chain of N=16 isotones. Panels **B, C, D** represent the comparison of the experimental energy ratios ($E_{4_1^+}/E_{2_1^+}$ and $E_{4_2^+}/E_{2_2^+}$), ($E_{2_2^+}/E_{2_1^+}$ and $E_{4_2^+}/E_{4_1^+}$) and ($E_{4_2^+}/E_{2_1^+}$ and $E_{4_1^+}/E_{2_2^+}$), respectively, for the chain of N=16 isotones.

Isotones (N=18)

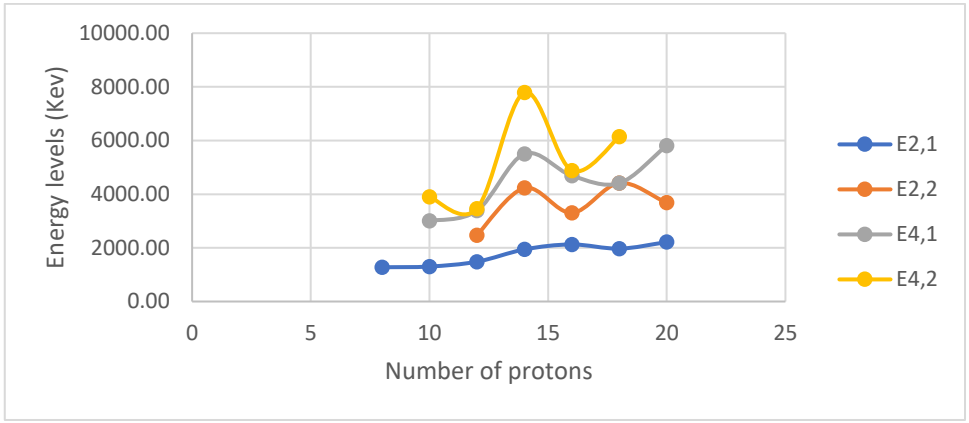

A

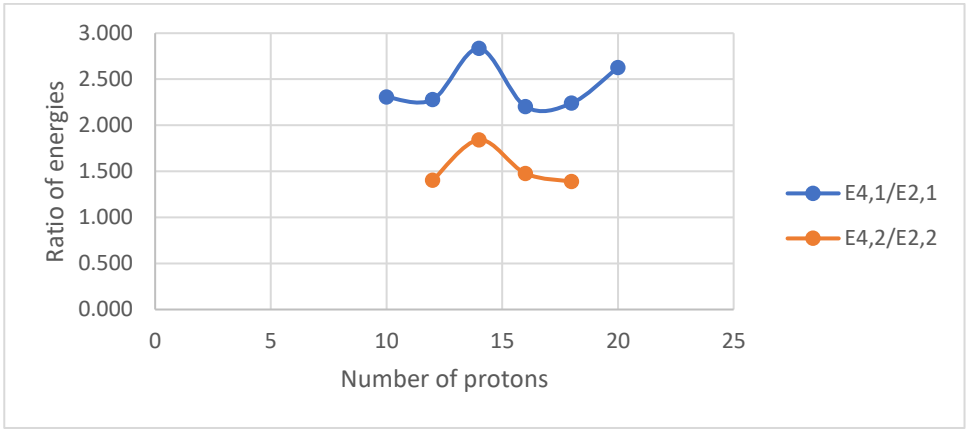

B

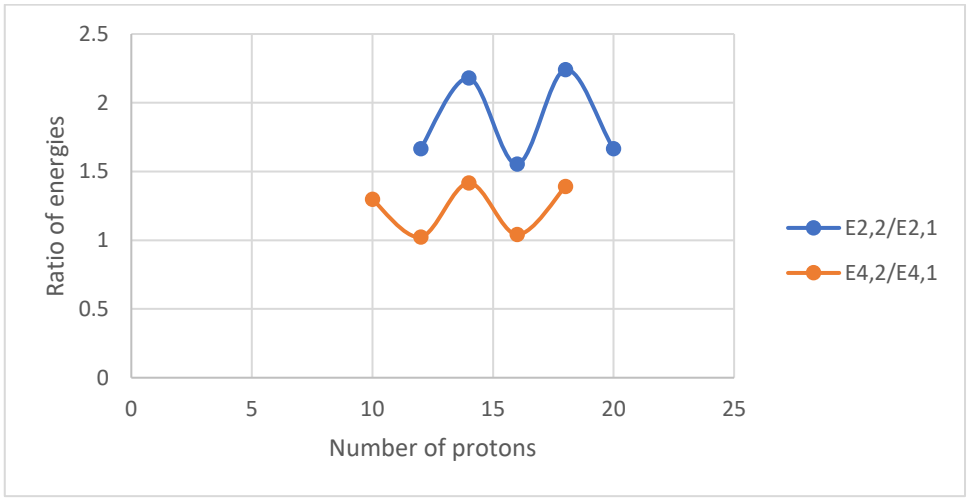

C

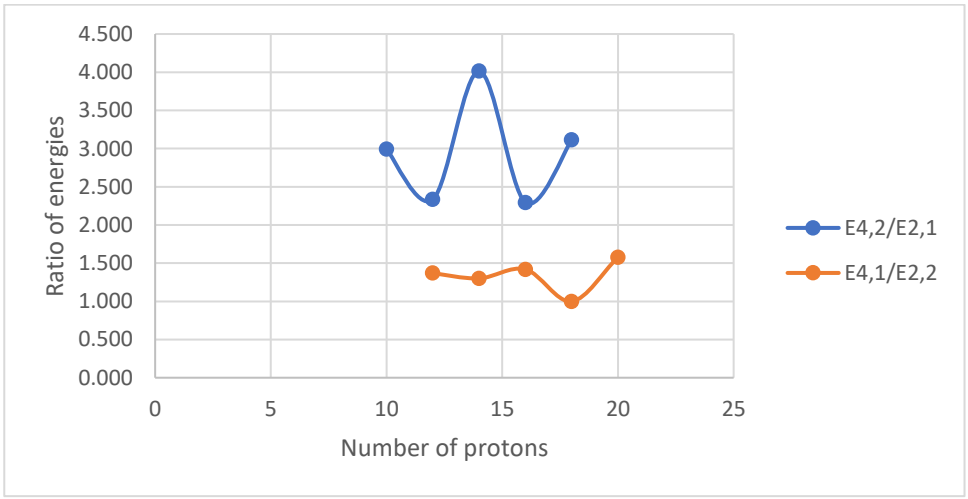

D

Figure V. 9 (color online) Panel **A** represents the comparison of the experimental energy levels of the lowest 2_1^+, 2_2^+, 4_1^+ and 4_2^+ states for the chain of N=18 isotones. Panels **B, C, D** represent the comparison of the experimental energy ratios ($E_{4_1^+}/E_{2_1^+}$ and $E_{4_2^+}/E_{2_2^+}$), ($E_{2_2^+}/E_{2_1^+}$ and $E_{4_2^+}/E_{4_1^+}$) and ($E_{4_2^+}/E_{2_1^+}$ and $E_{4_1^+}/E_{2_2^+}$), respectively, for the chain of N=18 isotones.

Isotones (N=20)

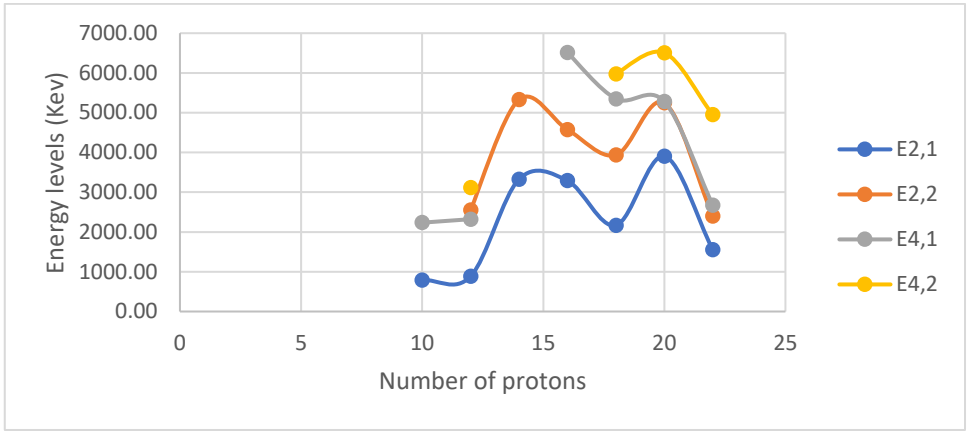

A

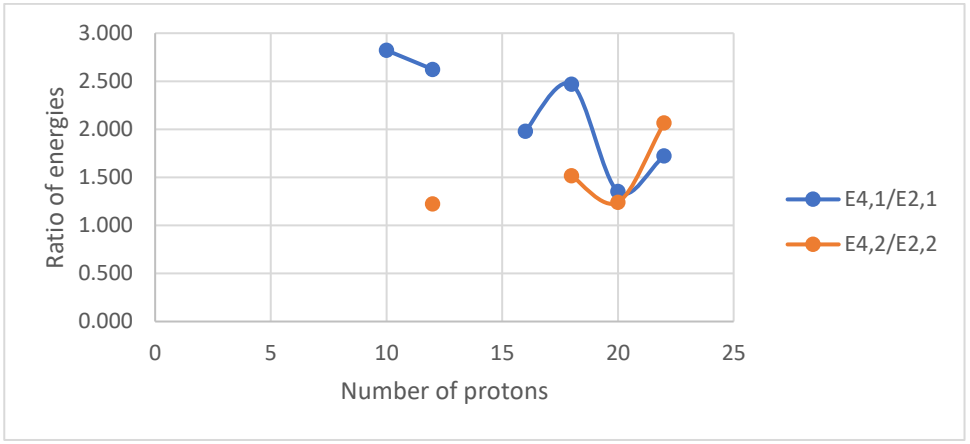

B

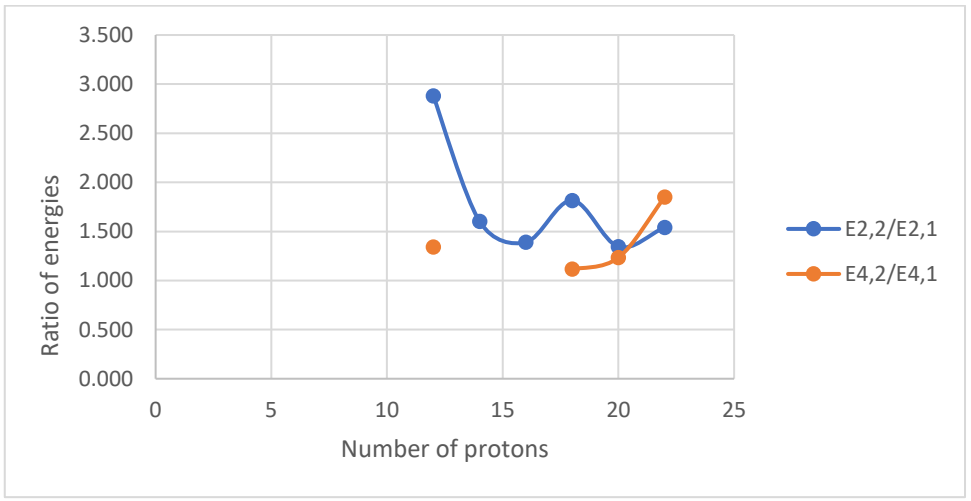

C

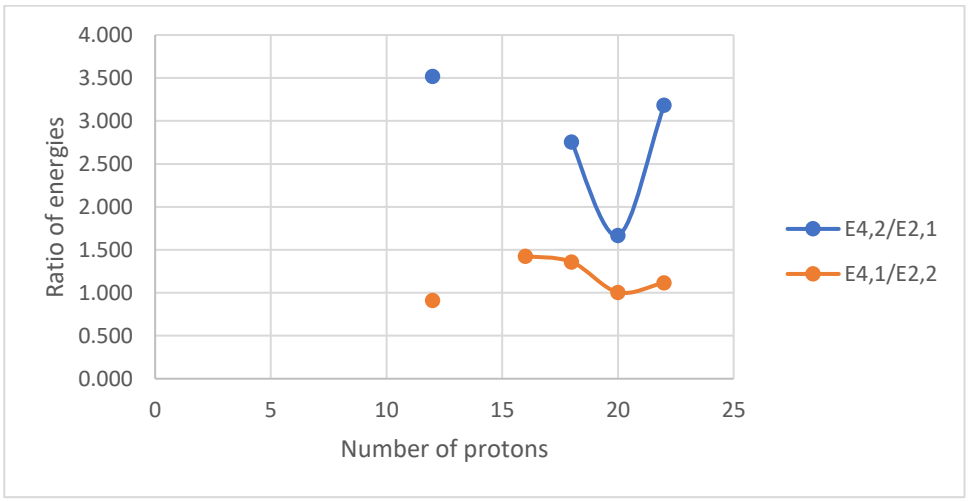

D

Figure V. 10 (color online) Panel **A** represents the comparison of the experimental energy levels of the lowest 2_1^+, 2_2^+, 4_1^+ and 4_2^+ states for the chain of N=20 isotones. Panels **B, C, D** represent the comparison of the experimental energy ratios ($E_{4_1^+}/E_{2_1^+}$ and $E_{4_2^+}/E_{2_2^+}$), ($E_{2_2^+}/E_{2_1^+}$ and $E_{4_2^+}/E_{4_1^+}$) and ($E_{4_2^+}/E_{2_1^+}$ and $E_{4_1^+}/E_{2_2^+}$), respectively, for the chain of N=20 isotones.

Isotones (N=22)

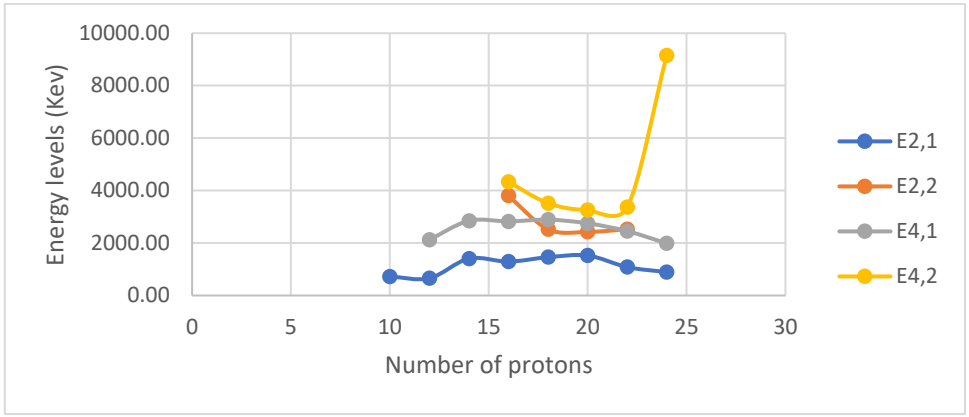

A

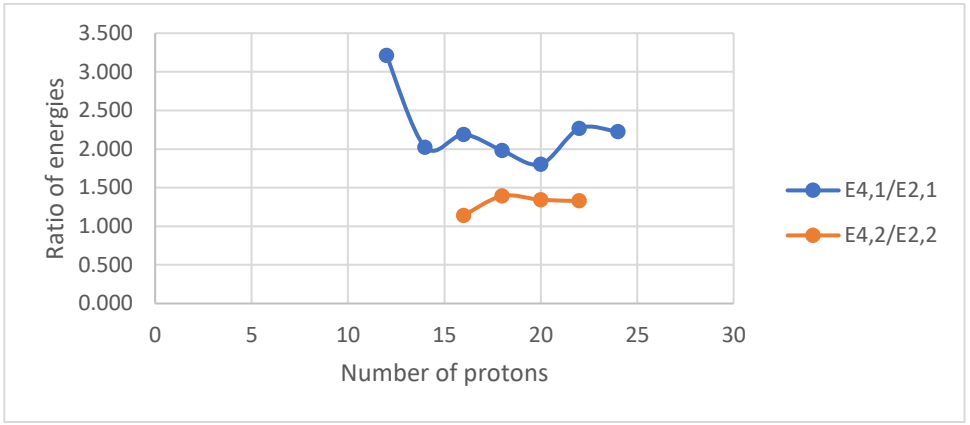

B

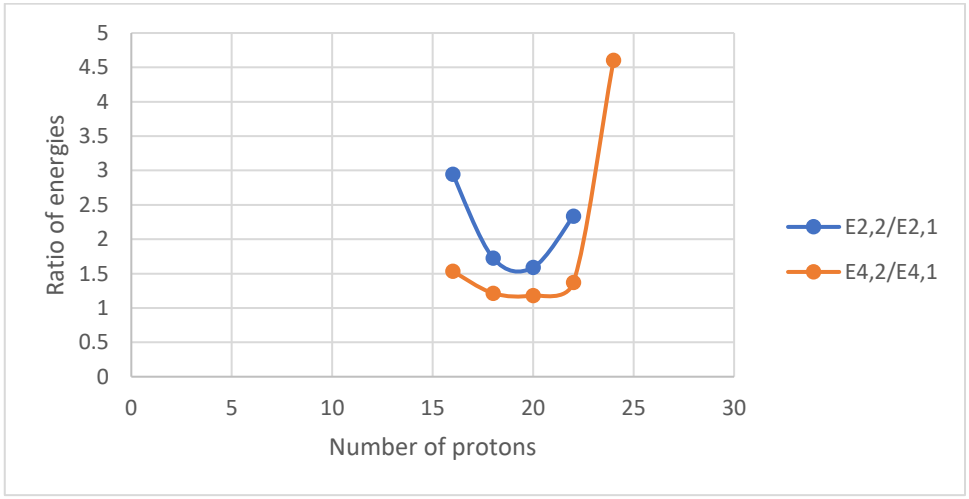

C

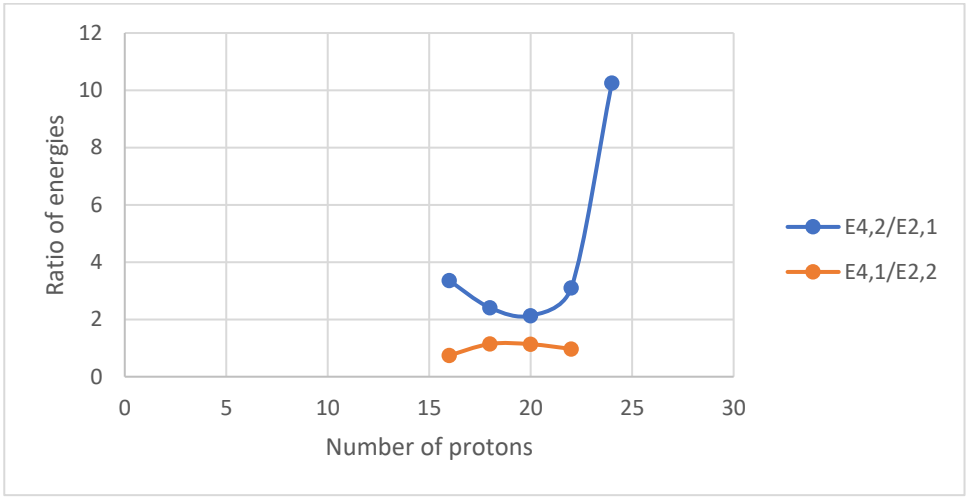

D

Figure V. 11 (color online) Panel **A** represents the comparison of the experimental energy levels of the lowest 2_1^+, 2_2^+, 4_1^+ and 4_2^+ states for the chain of N=22 isotones. Panels **B, C, D** represent the comparison of the experimental energy ratios ($E_{4_1^+}/E_{2_1^+}$ and $E_{4_2^+}/E_{2_2^+}$), ($E_{2_2^+}/E_{2_1^+}$ and $E_{4_2^+}/E_{4_1^+}$) and ($E_{4_2^+}/E_{2_1^+}$ and $E_{4_1^+}/E_{2_2^+}$), respectively, for the chain of N=22 isotones.

Isotones (N=24)

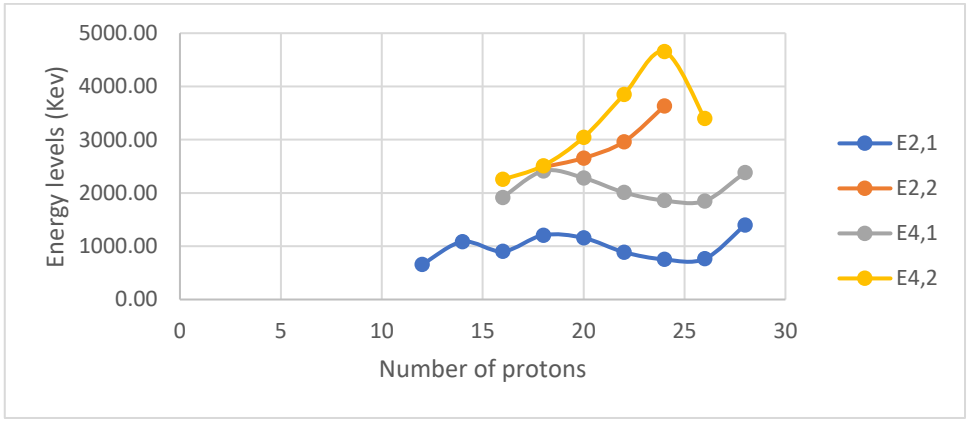

A

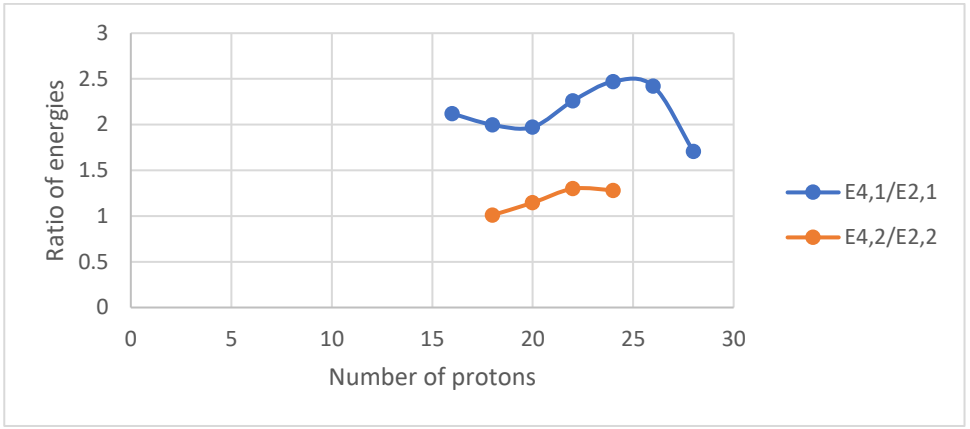

B

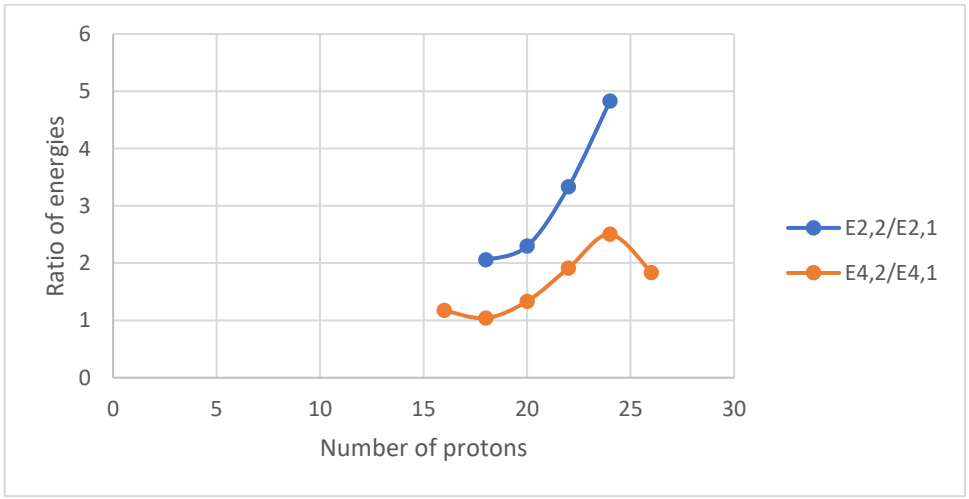

C

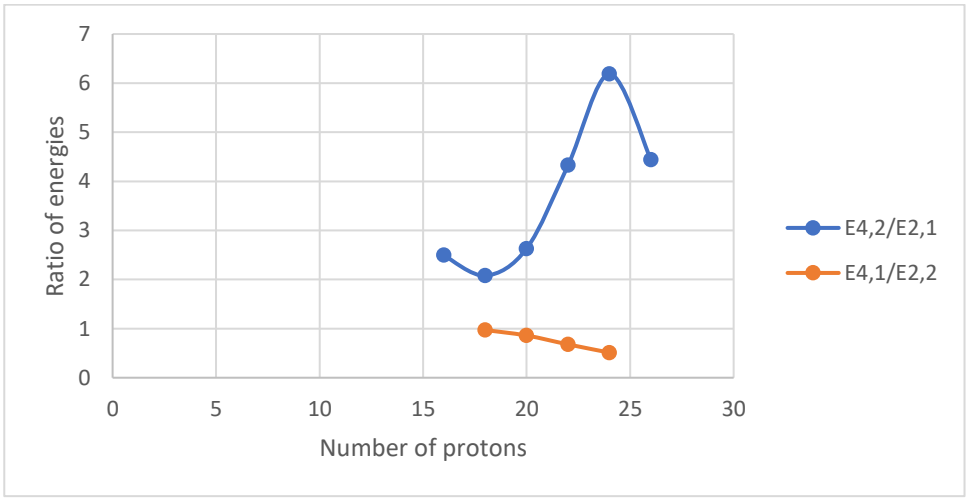

D

Figure V. 12 (color online) Panel **A** represents the comparison of the experimental energy levels of the lowest 2_1^+, 2_2^+, 4_1^+ and 4_2^+ states for the chain of N=24 isotones. Panels **B, C, D** represent the comparison of the experimental energy ratios ($E_{4_1^+}/E_{2_1^+}$ and $E_{4_2^+}/E_{2_2^+}$), ($E_{2_2^+}/E_{2_1^+}$ and $E_{4_2^+}/E_{4_1^+}$) and ($E_{4_2^+}/E_{2_1^+}$ and $E_{4_1^+}/E_{2_2^+}$), respectively, for the chain of N=24 isotones.

Isotones (N=26)

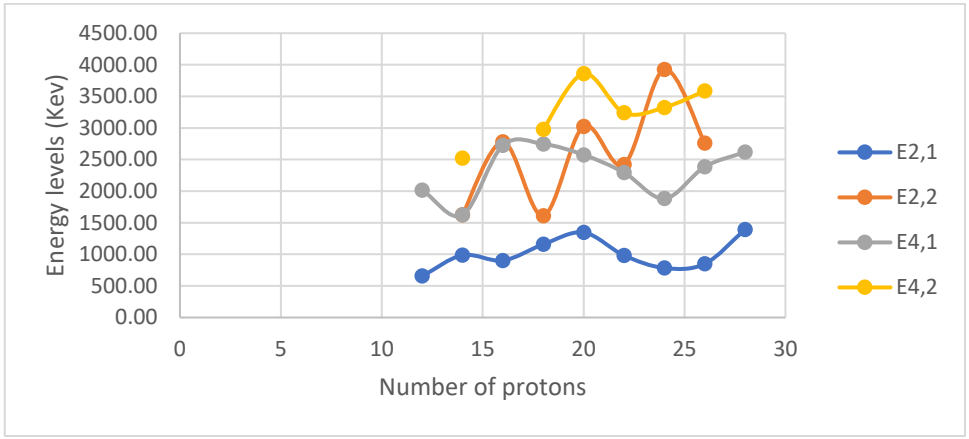

A

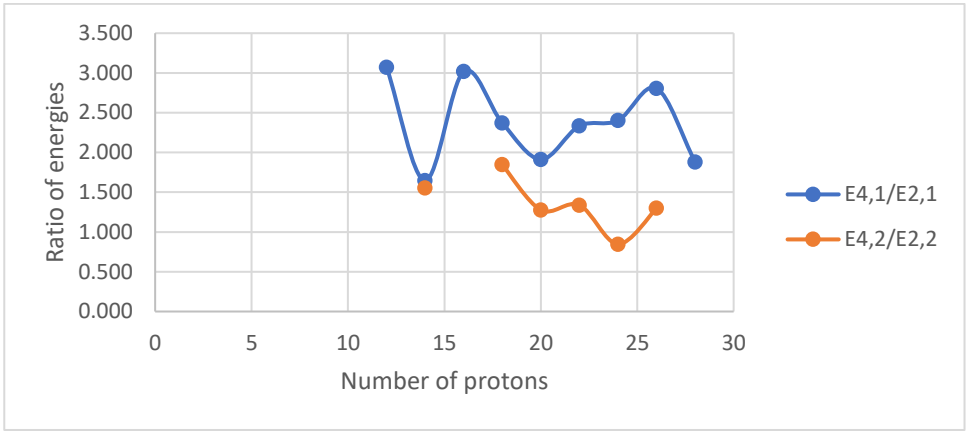

B

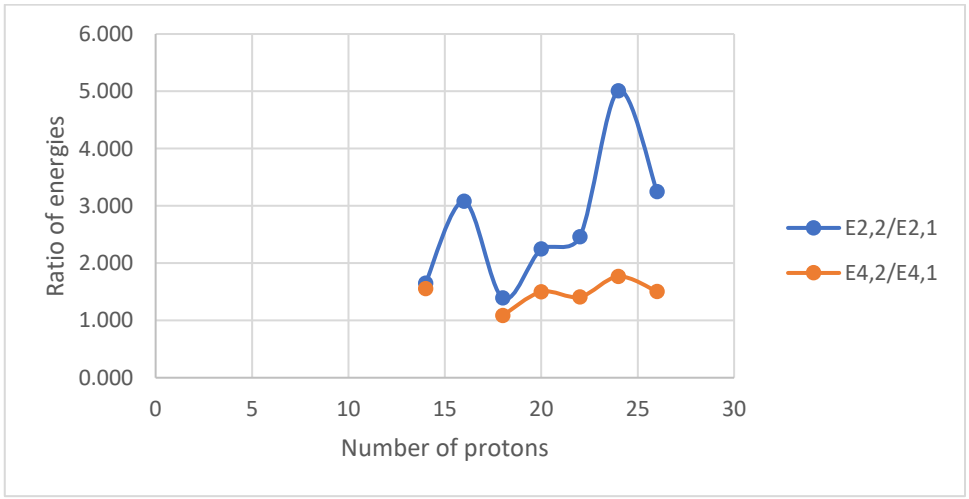

C

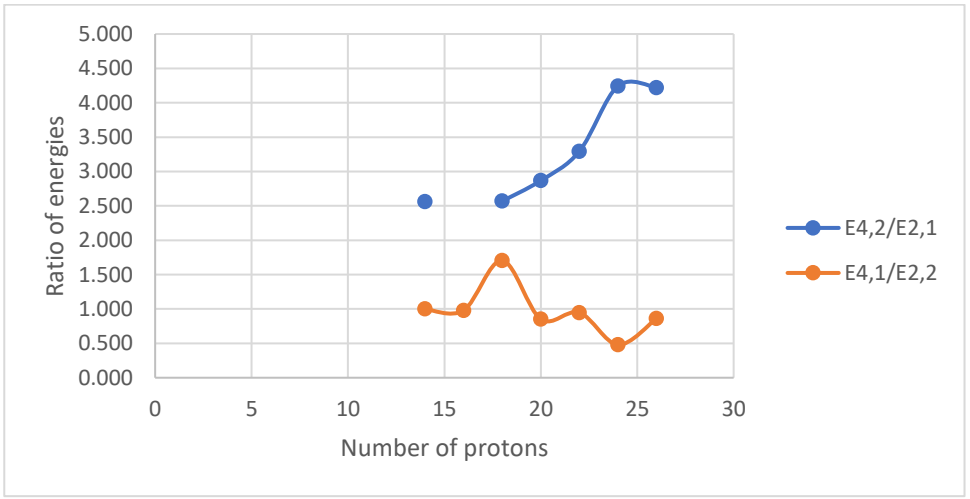

D

Figure V. 13 (color online) Panel **A** represents the comparison of the experimental energy levels of the lowest 2_1^+, 2_2^+, 4_1^+ and 4_2^+ states for the chain of N=26 isotones. Panels **B, C, D** represent the comparison of the experimental energy ratios ($E_{4_1^+}/E_{2_1^+}$ and $E_{4_2^+}/E_{2_2^+}$), ($E_{2_2^+}/E_{2_1^+}$ and $E_{4_2^+}/E_{4_1^+}$) and ($E_{4_2^+}/E_{2_1^+}$ and $E_{4_1^+}/E_{2_2^+}$), respectively, for the chain of N=26 isotones.

Isotones (N=28)

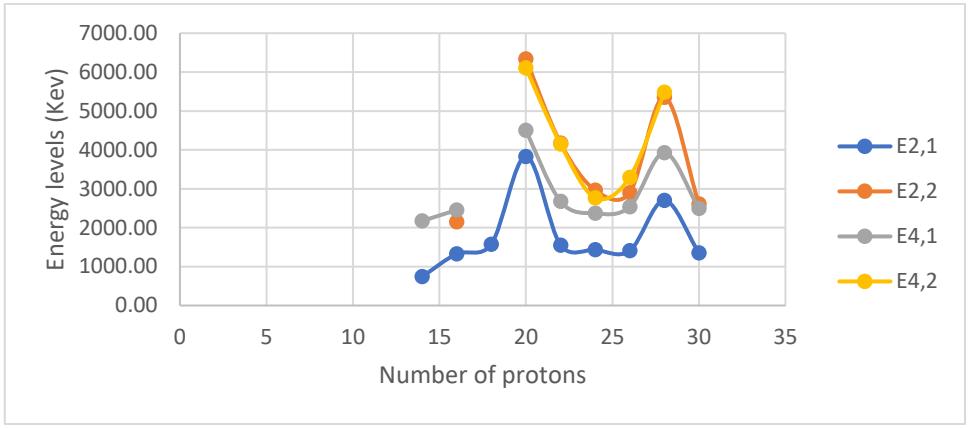

A

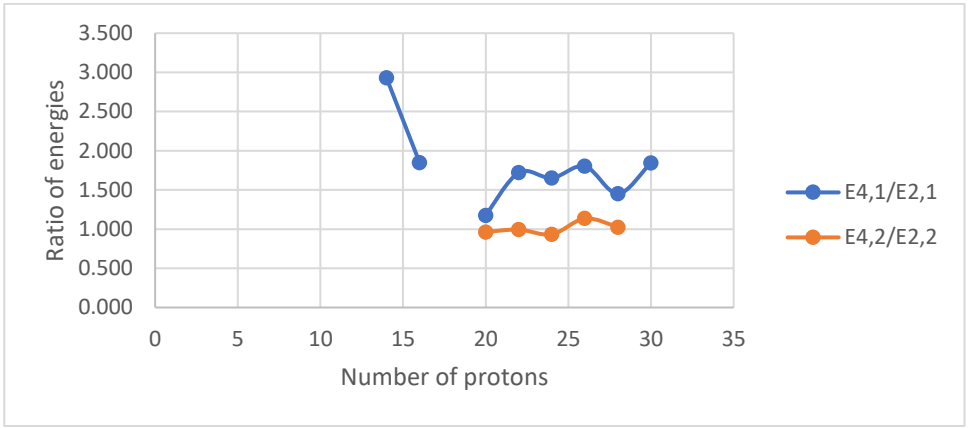

B

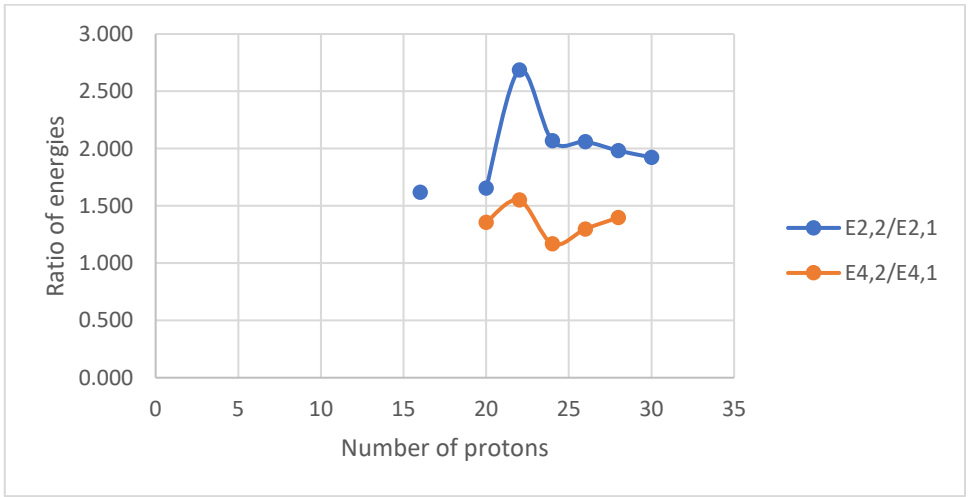

C

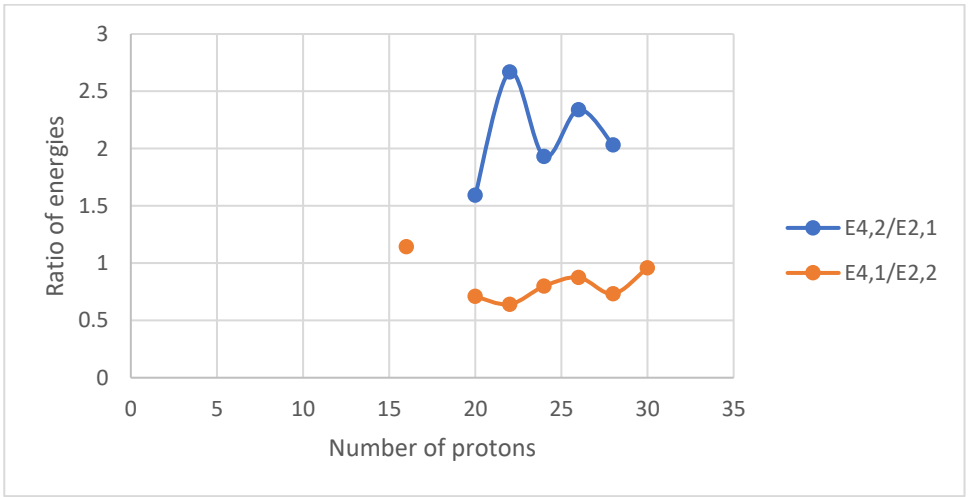

D

Figure V. 14 (color online) Panel **A** represents the comparison of the experimental energy levels of the lowest 2_1^+, 2_2^+, 4_1^+ and 4_2^+ states for the chain of N=28 isotones. Panels **B, C, D** represent the comparison of the experimental energy ratios ($E_{4_1^+}/E_{2_1^+}$ and $E_{4_2^+}/E_{2_2^+}$), ($E_{2_2^+}/E_{2_1^+}$ and $E_{4_2^+}/E_{4_1^+}$) and ($E_{4_2^+}/E_{2_1^+}$ and $E_{4_1^+}/E_{2_2^+}$), respectively, for the chain of N=28 isotones.

Isotones (N=30)

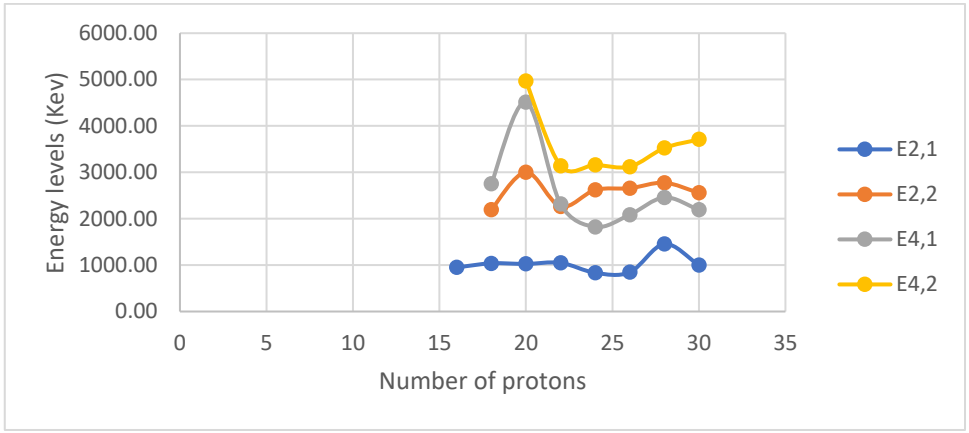

A

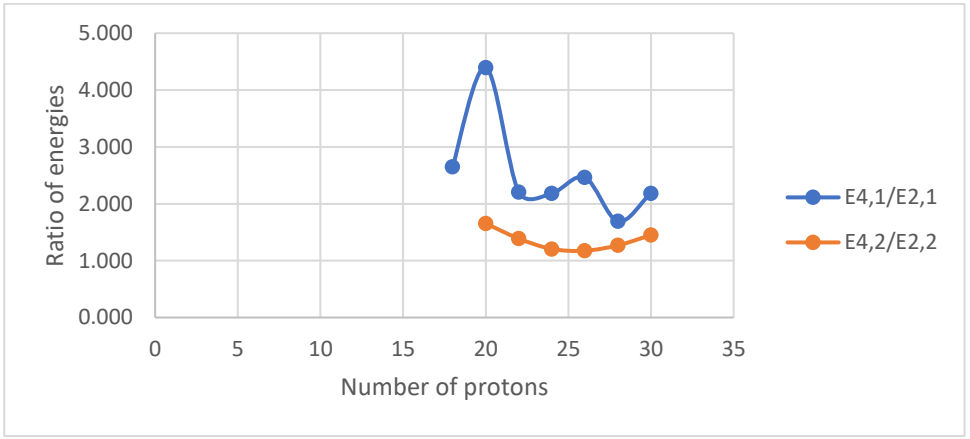

B

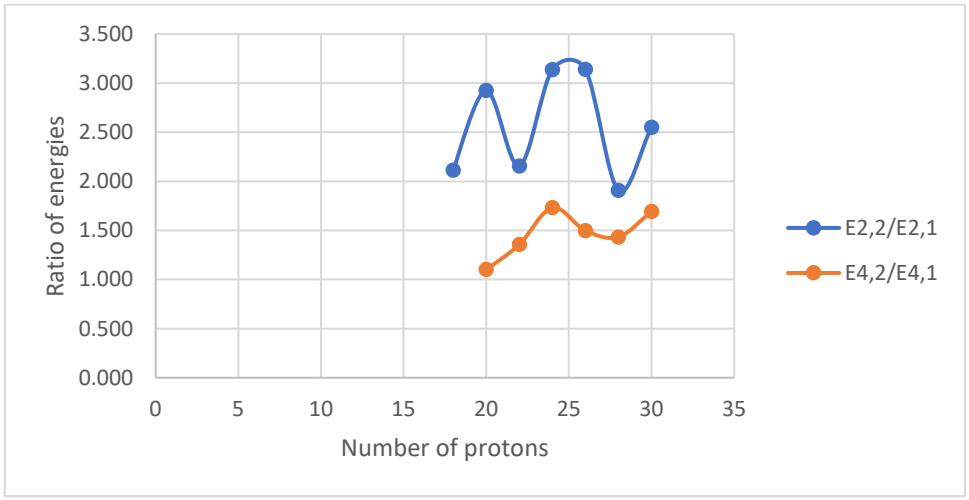

C

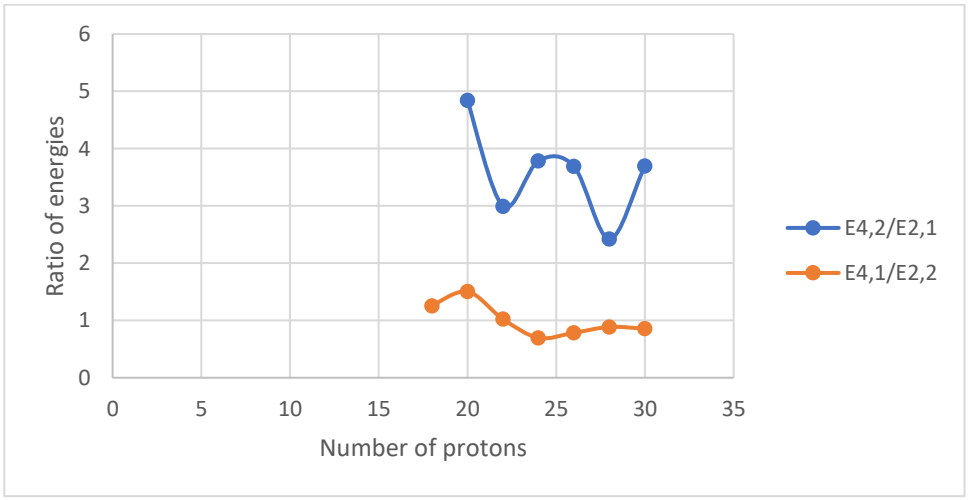

D

Figure V. 15 (color online) Panel **A** represents the comparison of the experimental energy levels of the lowest 2_1^+, 2_2^+, 4_1^+ and 4_2^+ states for the chain of N=30 isotones. Panels **B, C, D** represent the comparison of the experimental energy ratios ($E_{4_1^+}/E_{2_1^+}$ and $E_{4_2^+}/E_{2_2^+}$), ($E_{2_2^+}/E_{2_1^+}$ and $E_{4_2^+}/E_{4_1^+}$) and ($E_{4_2^+}/E_{2_1^+}$ and $E_{4_1^+}/E_{2_2^+}$), respectively, for the chain of N=30 isotones.

Isotones (N=32)

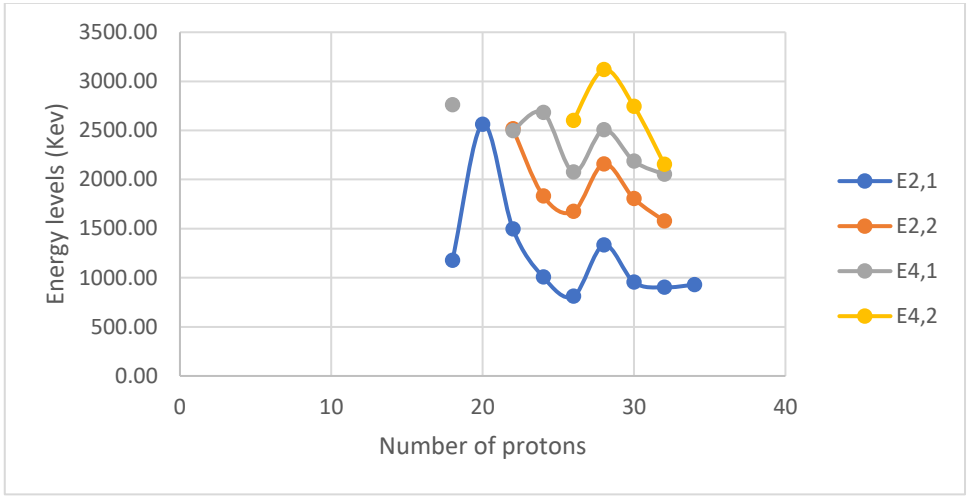

A

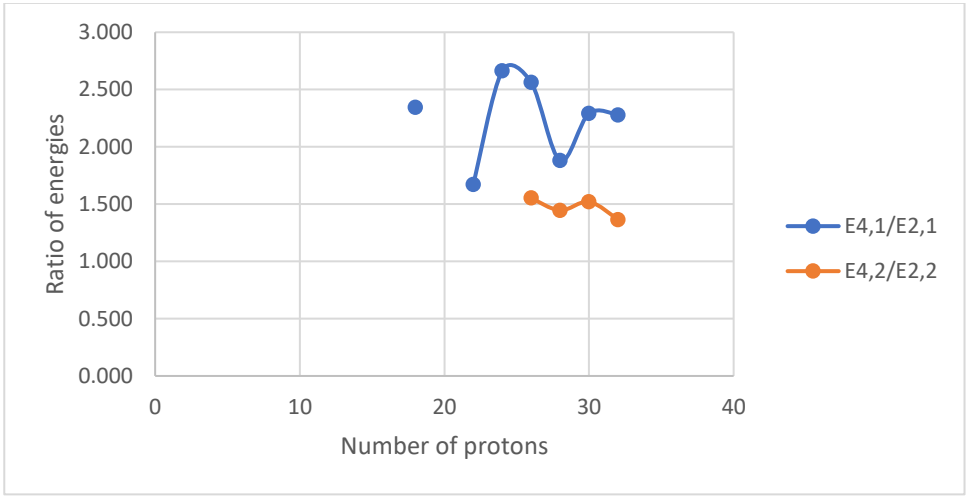

B

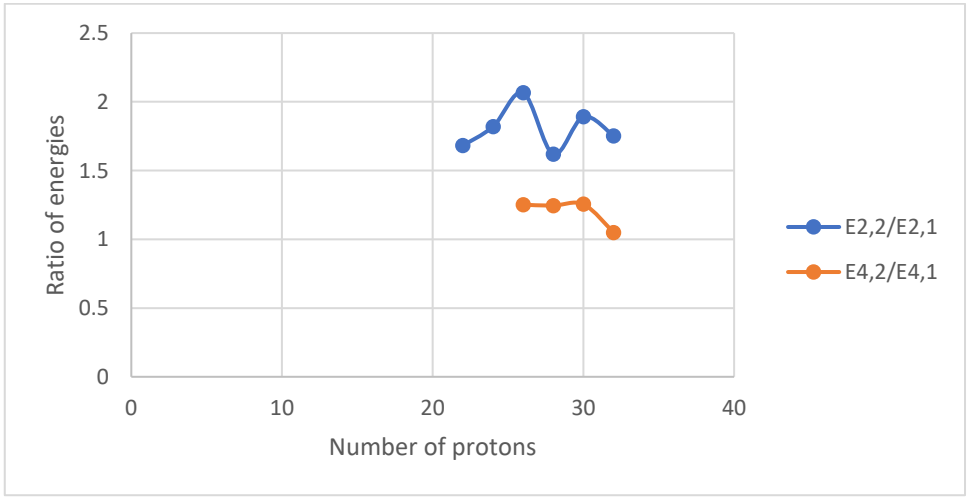

C

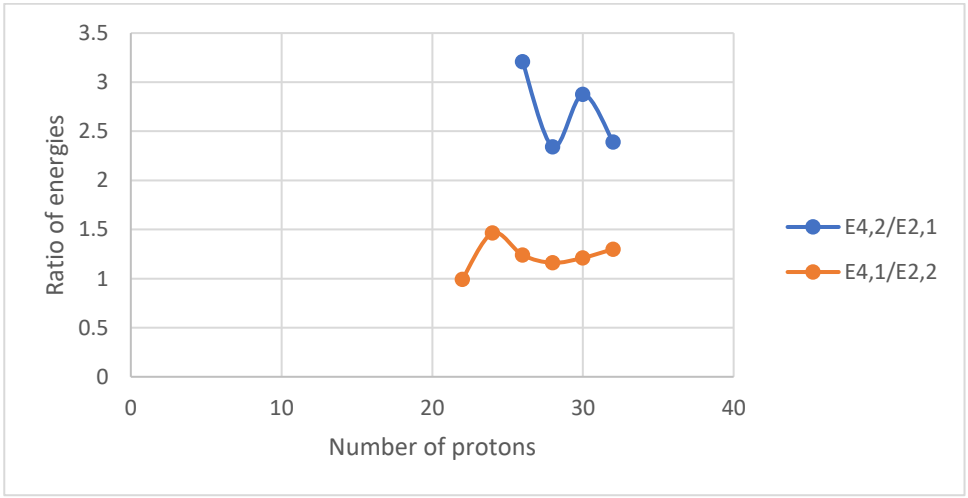

D

Figure V. 16 (color online) Panel **A** represents the comparison of the experimental energy levels of the lowest 2_1^+, 2_2^+, 4_1^+ and 4_2^+ states for the chain of N=32 isotones. Panels **B, C, D** represent the comparison of the experimental energy ratios ($E_{4_1^+}/E_{2_1^+}$ and $E_{4_2^+}/E_{2_2^+}$), ($E_{2_2^+}/E_{2_1^+}$ and $E_{4_2^+}/E_{4_1^+}$) and ($E_{4_2^+}/E_{2_1^+}$ and $E_{4_1^+}/E_{2_2^+}$), respectively, for the chain of N=32 isotones.

Isotones (N=34)

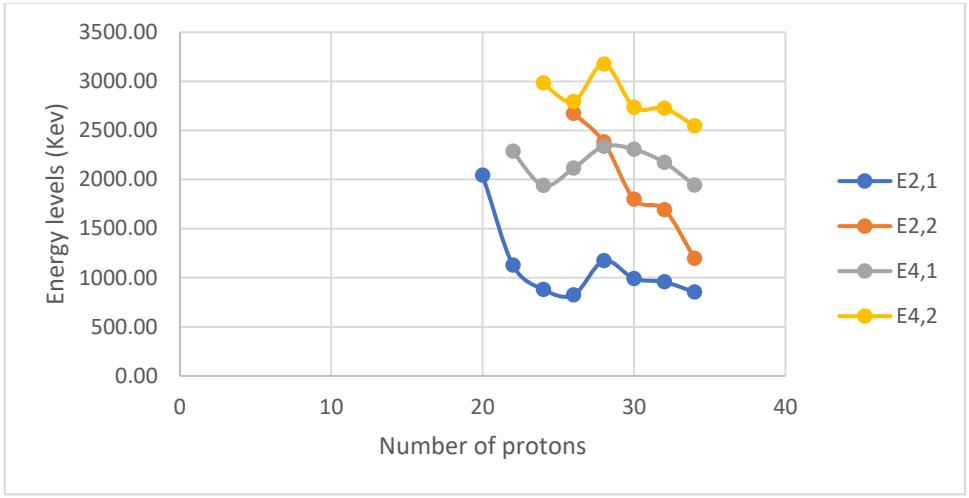

A

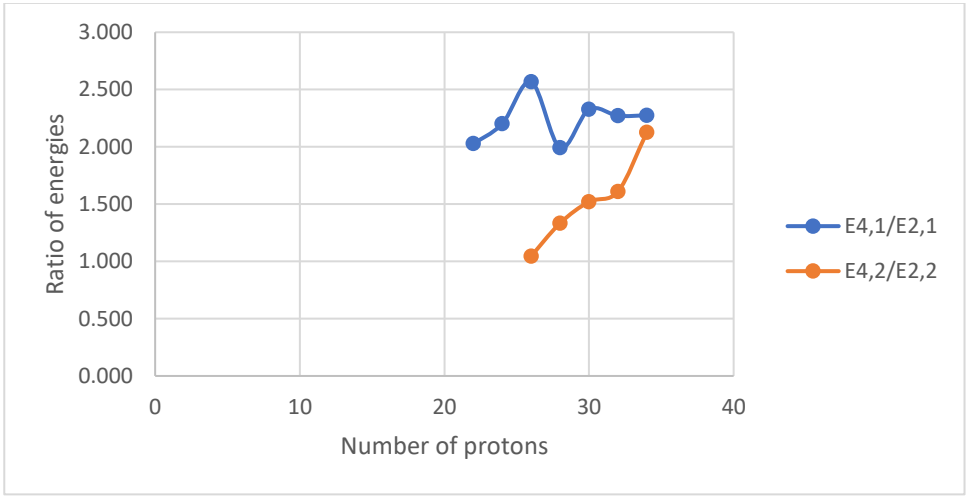

B

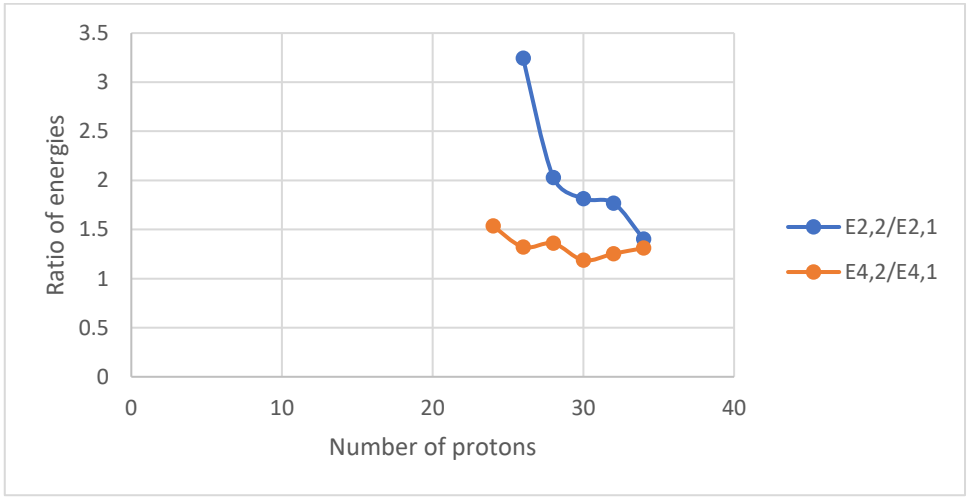

C

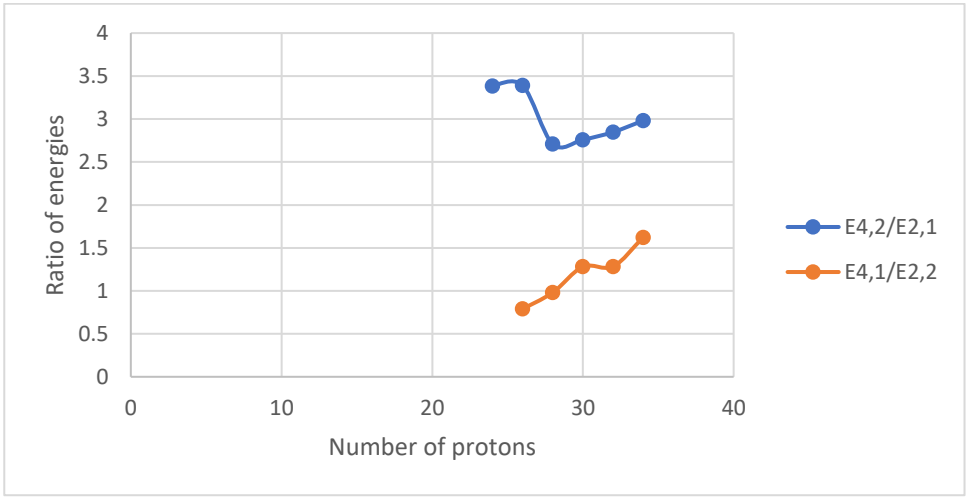

D

Figure V. 17 (color online) Panel **A** represents the comparison of the experimental energy levels of the lowest 2_1^+, 2_2^+, 4_1^+ and 4_2^+ states for the chain of N=34 isotones. Panels **B, C, D** represent the comparison of the experimental energy ratios ($E_{4_1^+}/E_{2_1^+}$ and $E_{4_2^+}/E_{2_2^+}$), ($E_{2_2^+}/E_{2_1^+}$ and $E_{4_2^+}/E_{4_1^+}$) and ($E_{4_2^+}/E_{2_1^+}$ and $E_{4_1^+}/E_{2_2^+}$), respectively, for the chain of N=34 isotones.

Isotones (N=36)

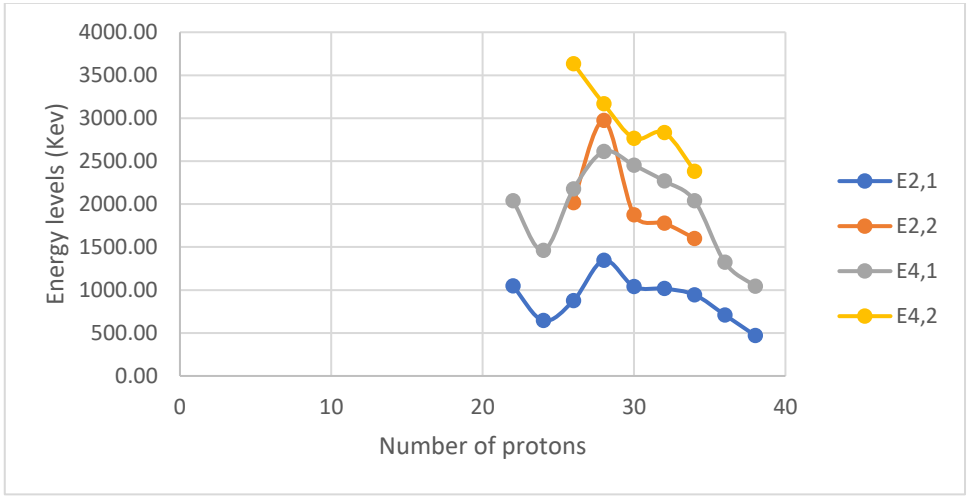

A

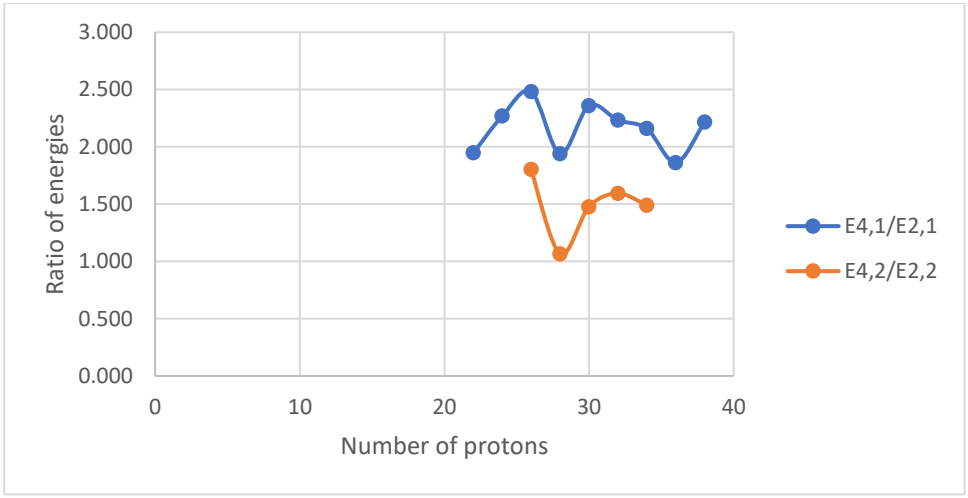

B

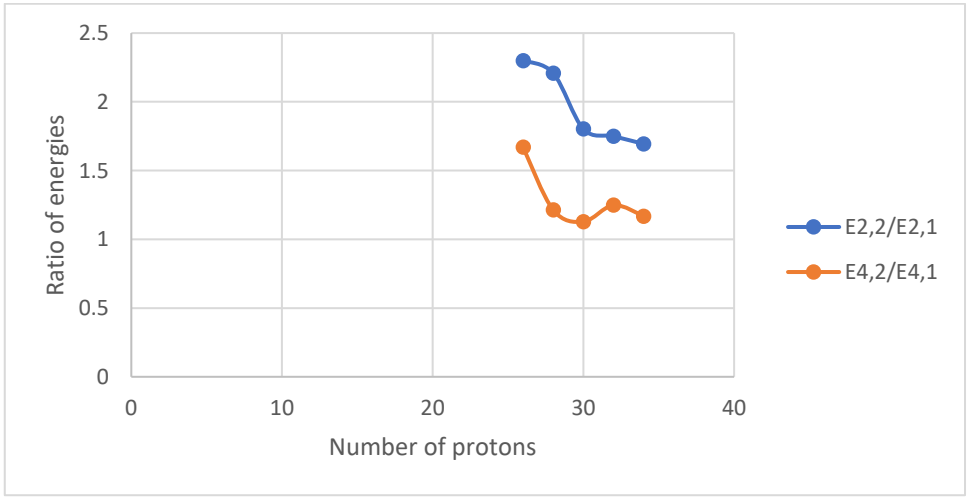

C

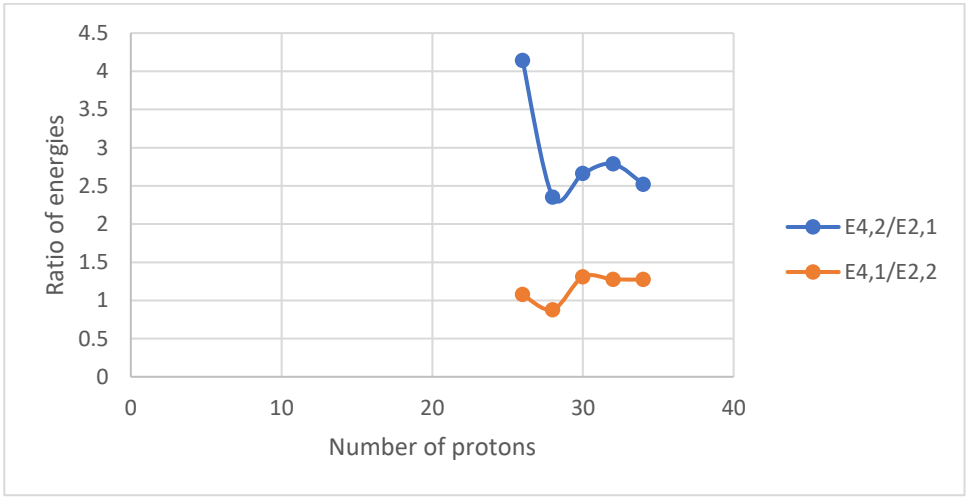

D

Figure V. 18 (color online) Panel **A** represents the comparison of the experimental energy levels of the lowest 2_1^+, 2_2^+, 4_1^+ and 4_2^+ states for the chain of N=36 isotones. Panels **B, C, D** represent the comparison of the experimental energy ratios ($E_{4_1^+}/E_{2_1^+}$ and $E_{4_2^+}/E_{2_2^+}$), ($E_{2_2^+}/E_{2_1^+}$ and $E_{4_2^+}/E_{4_1^+}$) and ($E_{4_2^+}/E_{2_1^+}$ and $E_{4_1^+}/E_{2_2^+}$), respectively, for the chain of N=36 isotones.

Isotones (N=38)

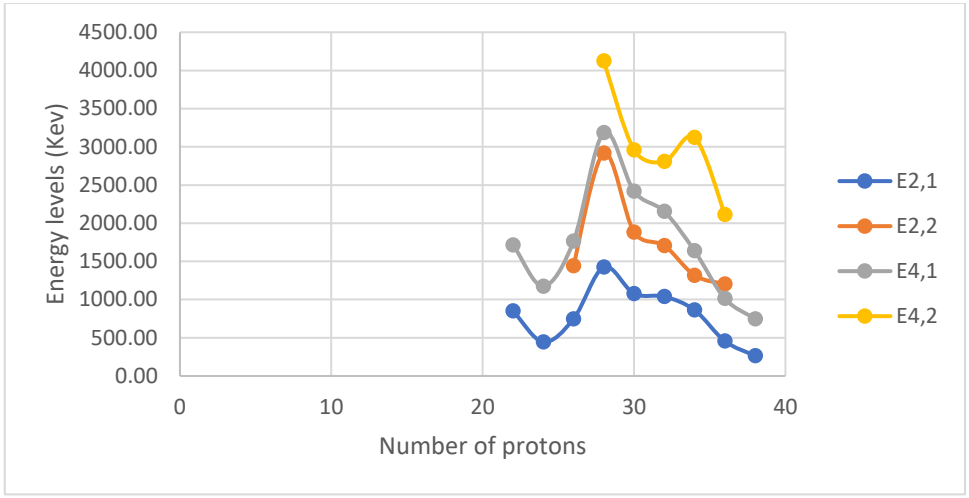

A

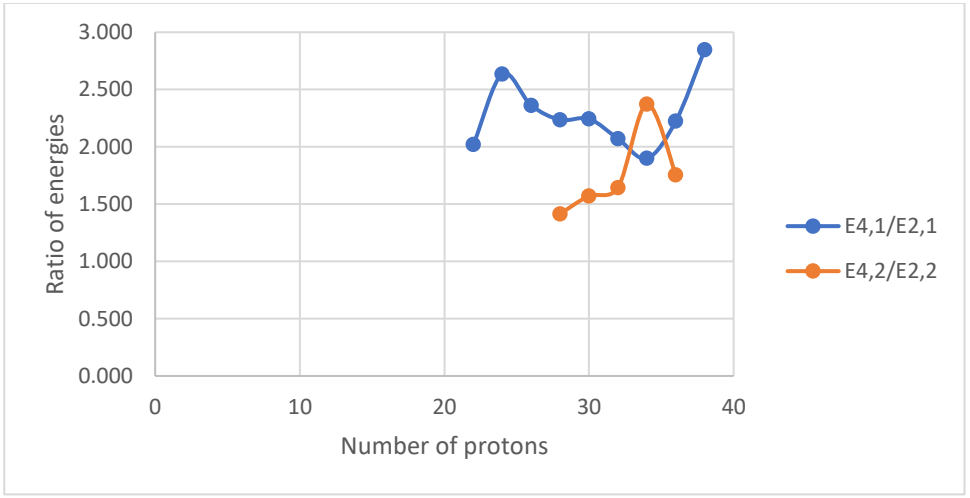

B

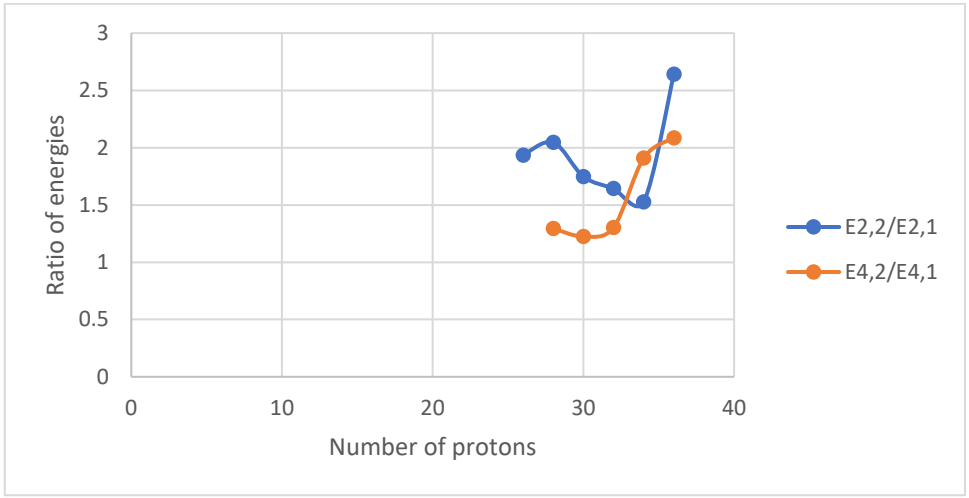

C

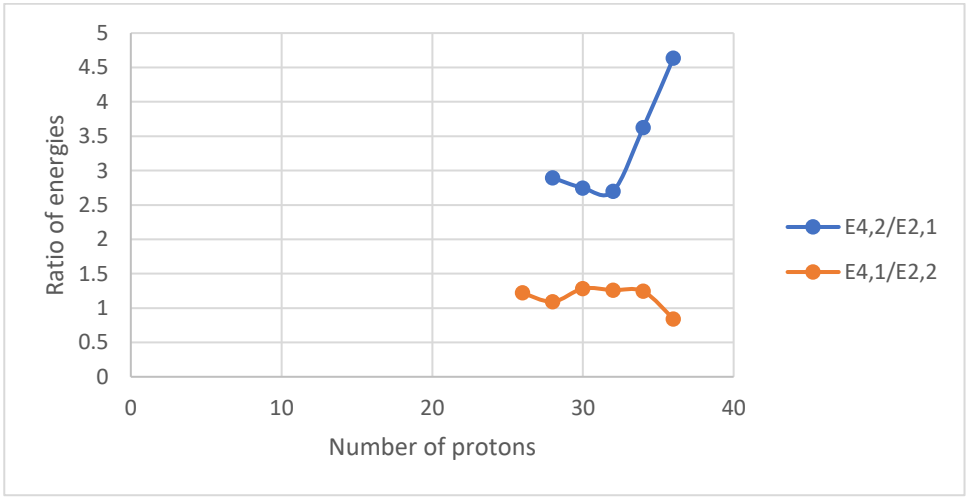

D

Figure V. 19 (color online) Panel **A** represents the comparison of the experimental energy levels of the lowest 2_1^+, 2_2^+, 4_1^+ and 4_2^+ states for the chain of N=38 isotones. Panels **B, C, D** represent the comparison of the experimental energy ratios ($E_{4_1^+}/E_{2_1^+}$ and $E_{4_2^+}/E_{2_2^+}$), ($E_{2_2^+}/E_{2_1^+}$ and $E_{4_2^+}/E_{4_1^+}$) and ($E_{4_2^+}/E_{2_1^+}$ and $E_{4_1^+}/E_{2_2^+}$), respectively, for the chain of N=38 isotones.

Isotones (N=40)

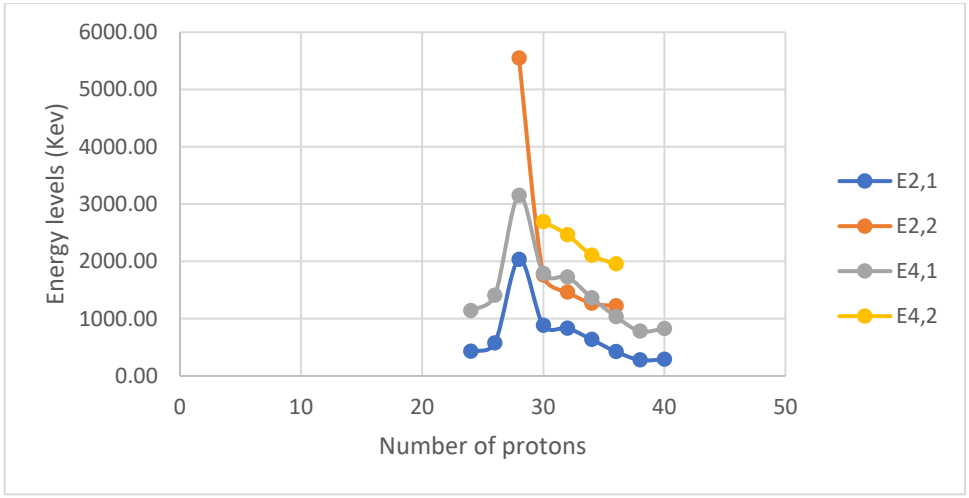

A

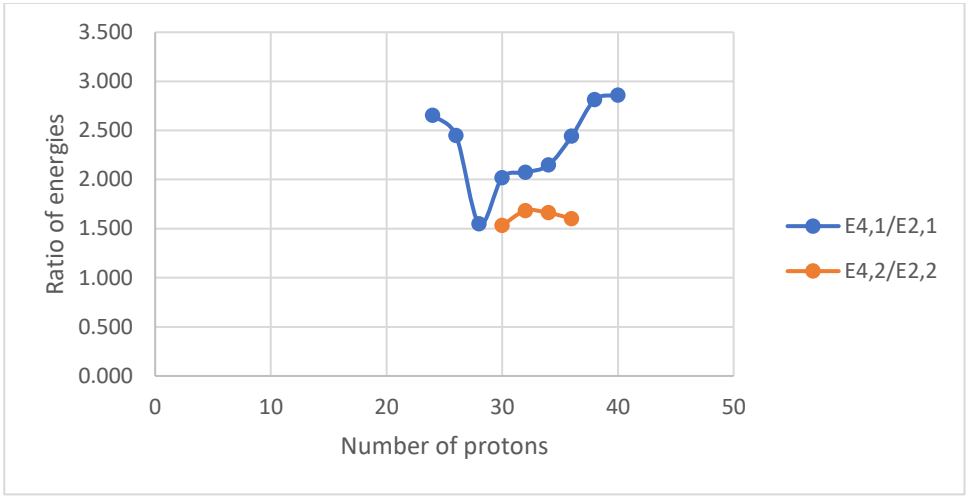

B

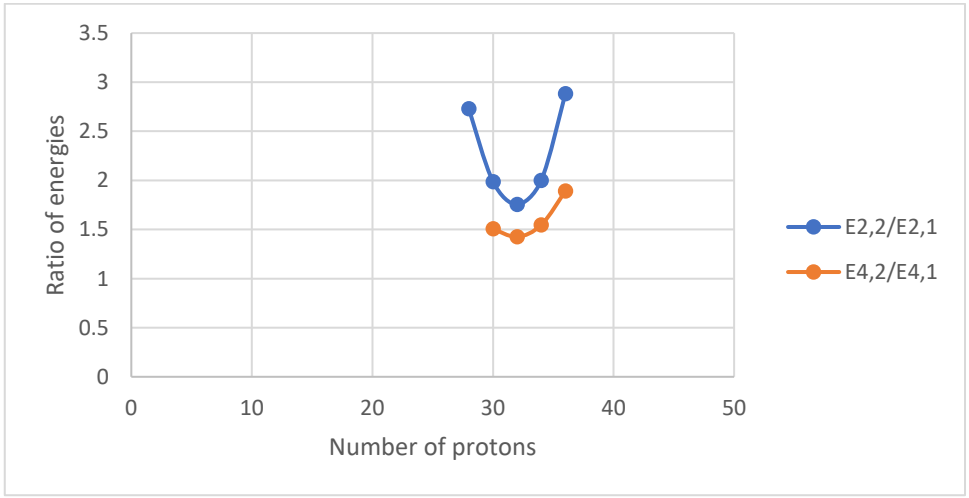

C

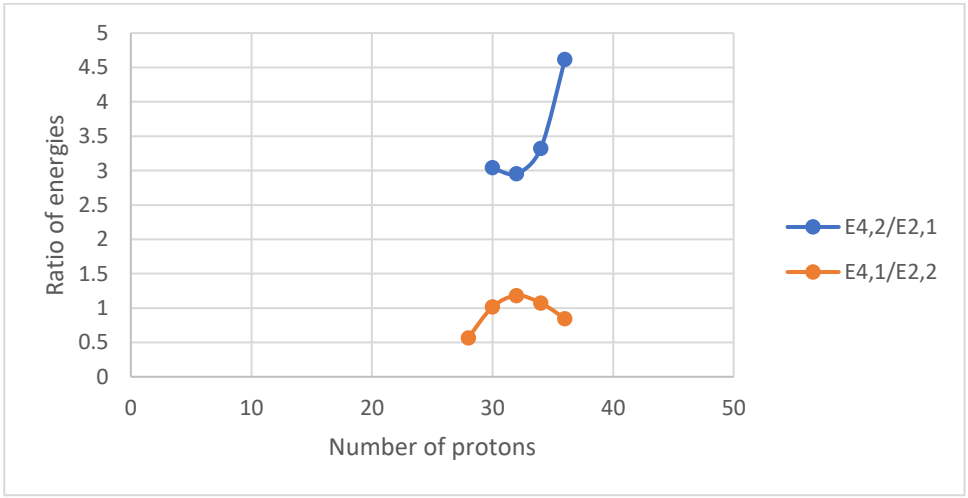

D

Figure V. 20 (color online) Panel **A** represents the comparison of the experimental energy levels of the lowest 2_1^+, 2_2^+, 4_1^+ and 4_2^+ states for the chain of N=40 isotones. Panels **B, C, D** represent the comparison of the experimental energy ratios ($E_{4_1^+}/E_{2_1^+}$ and $E_{4_2^+}/E_{2_2^+}$), ($E_{2_2^+}/E_{2_1^+}$ and $E_{4_2^+}/E_{4_1^+}$) and ($E_{4_2^+}/E_{2_1^+}$ and $E_{4_1^+}/E_{2_2^+}$), respectively, for the chain of N=40 isotones.

Isotones (N=42)

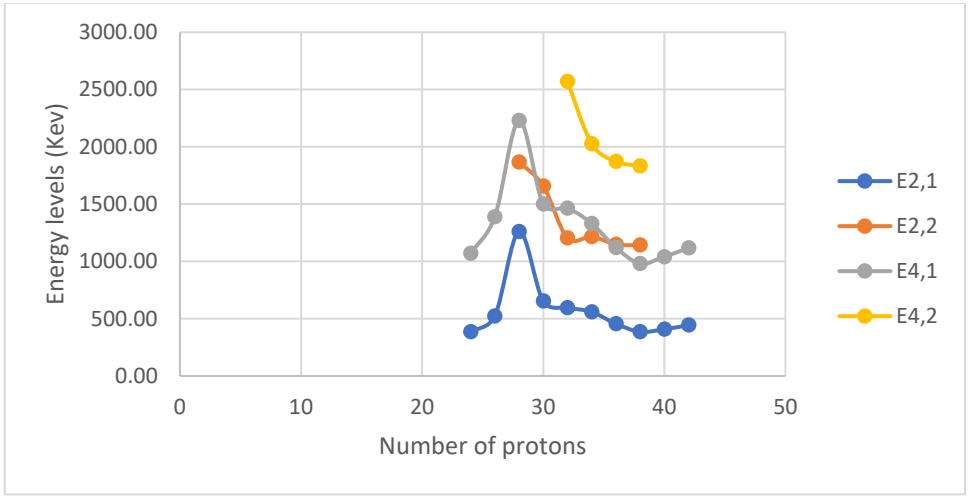

A

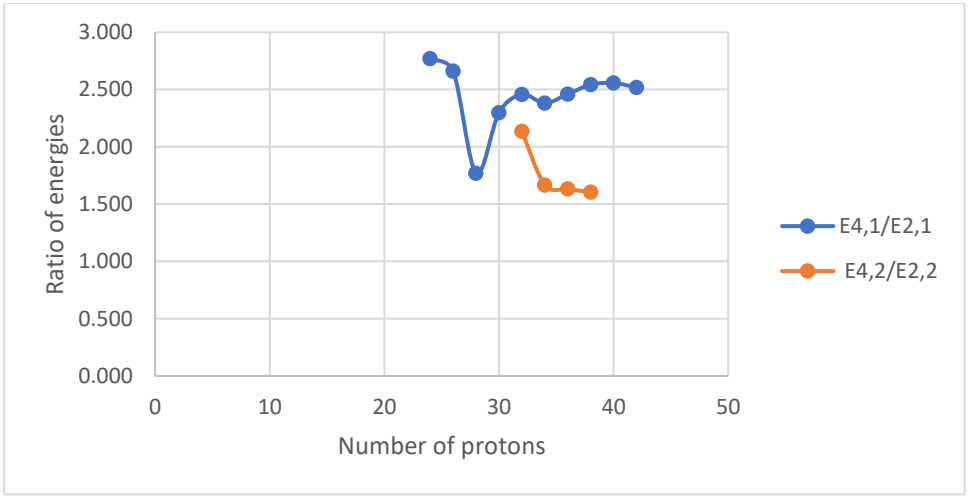

B

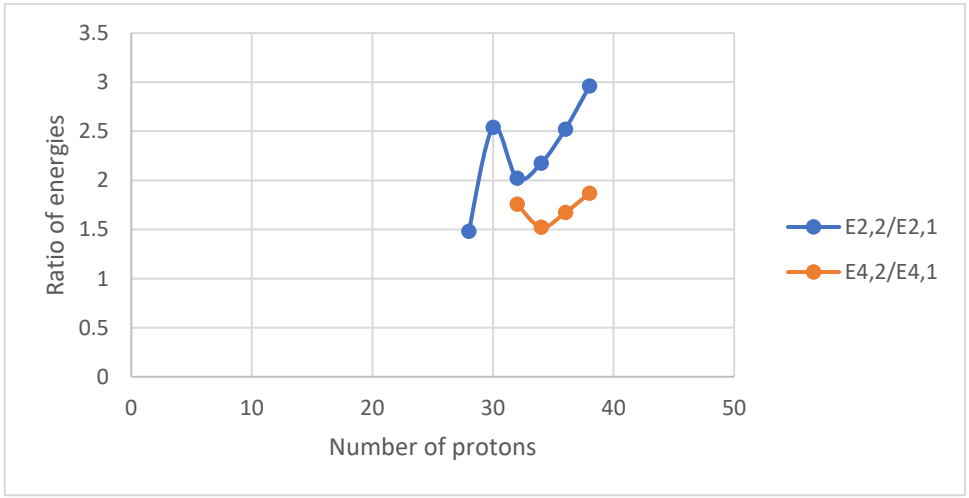

C

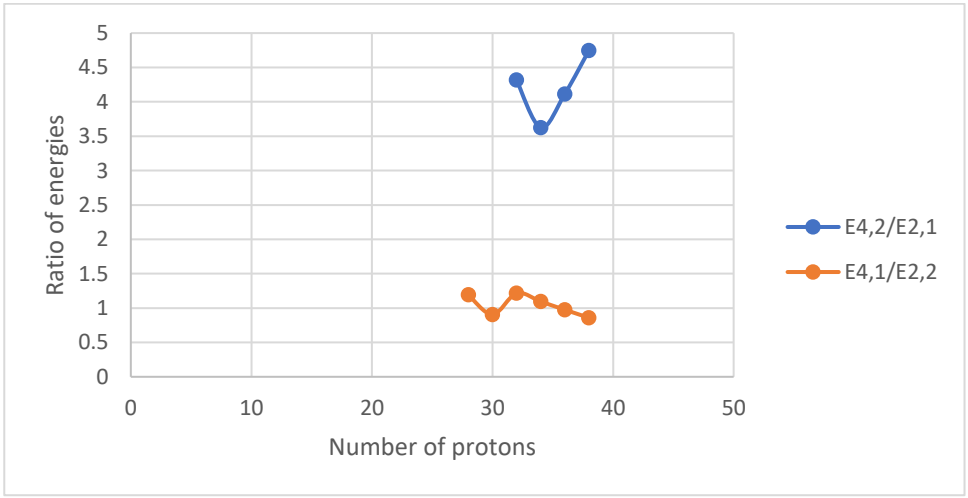

D

Figure V. 21 (color online) Panel **A** represents the comparison of the experimental energy levels of the lowest 2_1^+, 2_2^+, 4_1^+ and 4_2^+ states for the chain of N=42 isotones. Panels **B, C, D** represent the comparison of the experimental energy ratios ($E_{4_1^+}/E_{2_1^+}$ and $E_{4_2^+}/E_{2_2^+}$), ($E_{2_2^+}/E_{2_1^+}$ and $E_{4_2^+}/E_{4_1^+}$) and ($E_{4_2^+}/E_{2_1^+}$ and $E_{4_1^+}/E_{2_2^+}$), respectively, for the chain of N=42 isotones.

Isotones (N=44)

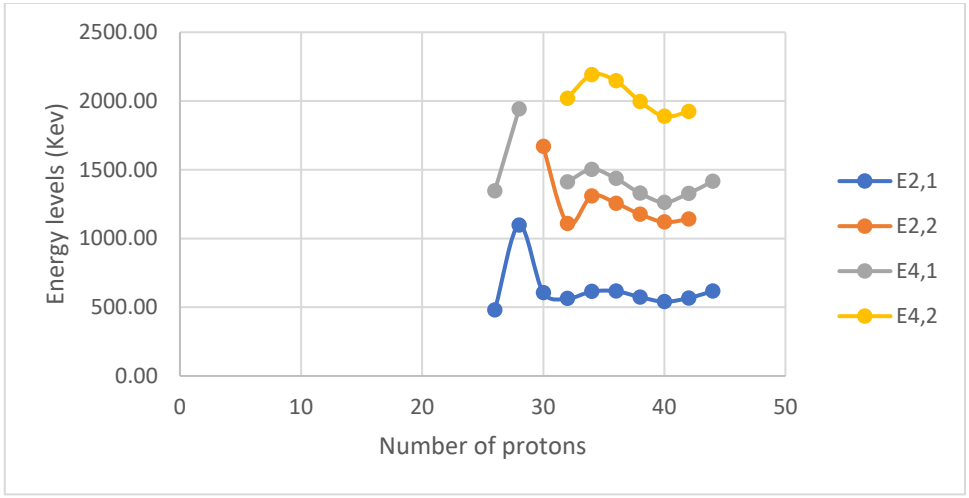

A

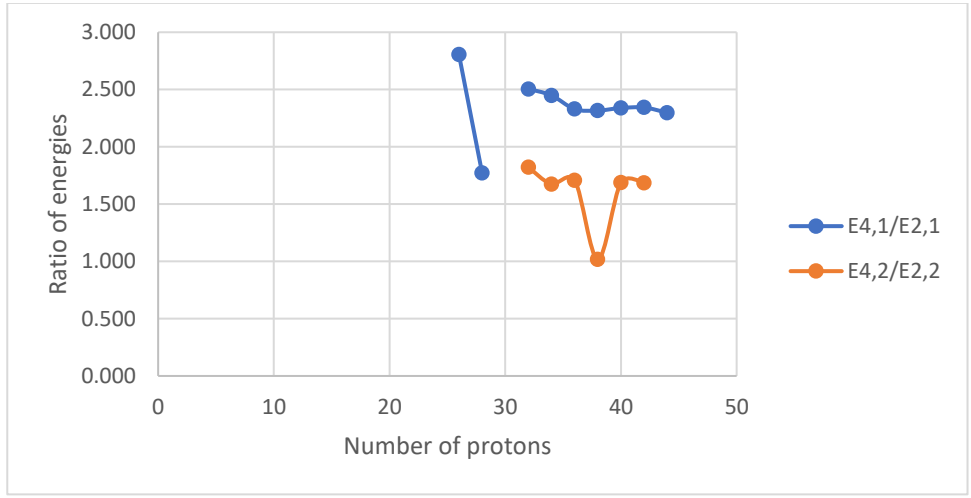

B

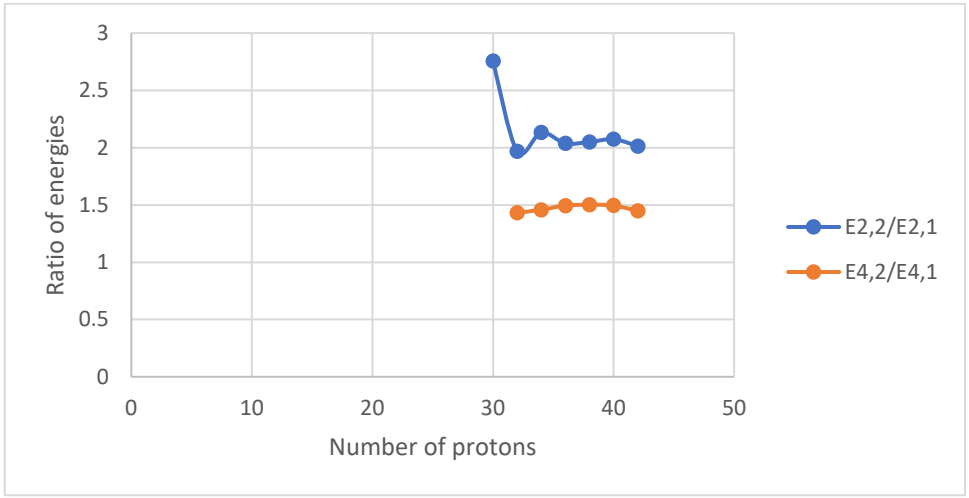

C

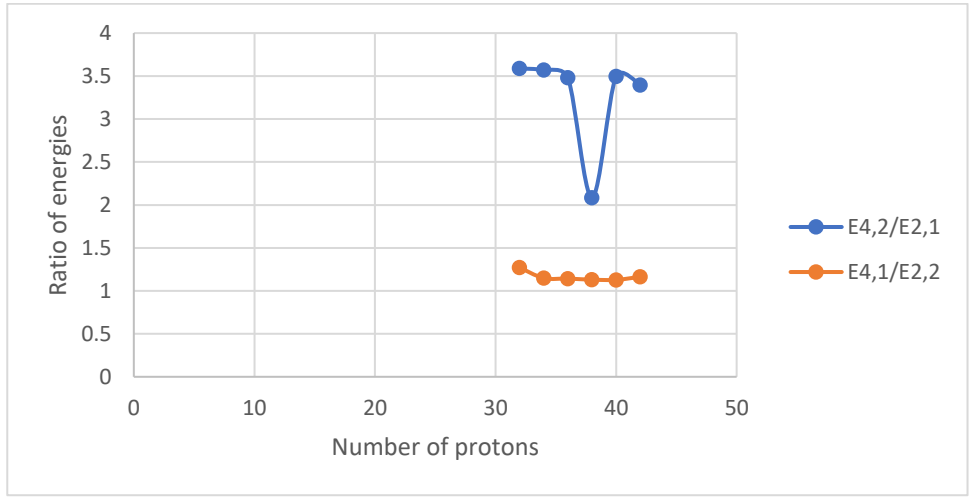

D

Figure V. 22 (color online) Panel **A** represents the comparison of the experimental energy levels of the lowest 2_1^+, 2_2^+, 4_1^+ and 4_2^+ states for the chain of N=44 isotones. Panels **B, C, D** represent the comparison of the experimental energy ratios ($E_{4_1^+}/E_{2_1^+}$ and $E_{4_2^+}/E_{2_2^+}$), ($E_{2_2^+}/E_{2_1^+}$ and $E_{4_2^+}/E_{4_1^+}$) and ($E_{4_2^+}/E_{2_1^+}$ and $E_{4_1^+}/E_{2_2^+}$), respectively, for the chain of N=44 isotones.

Isotones (N=46)

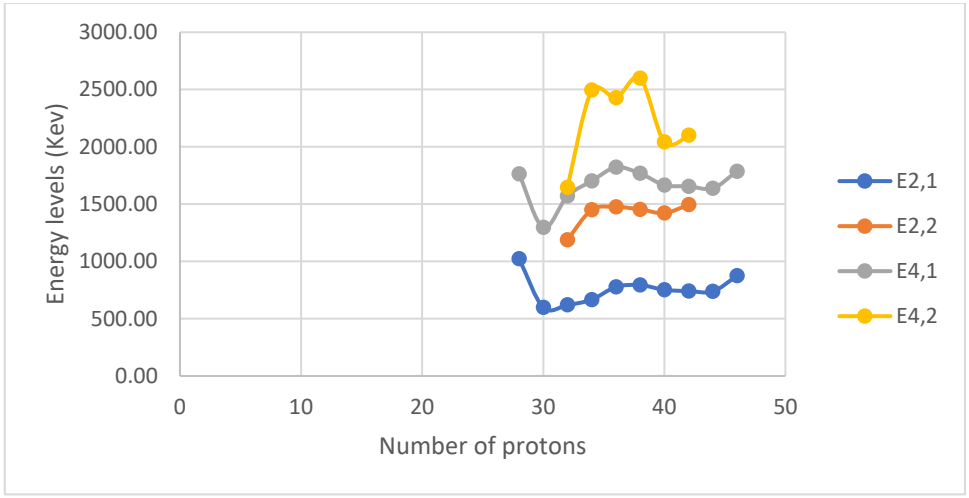

A

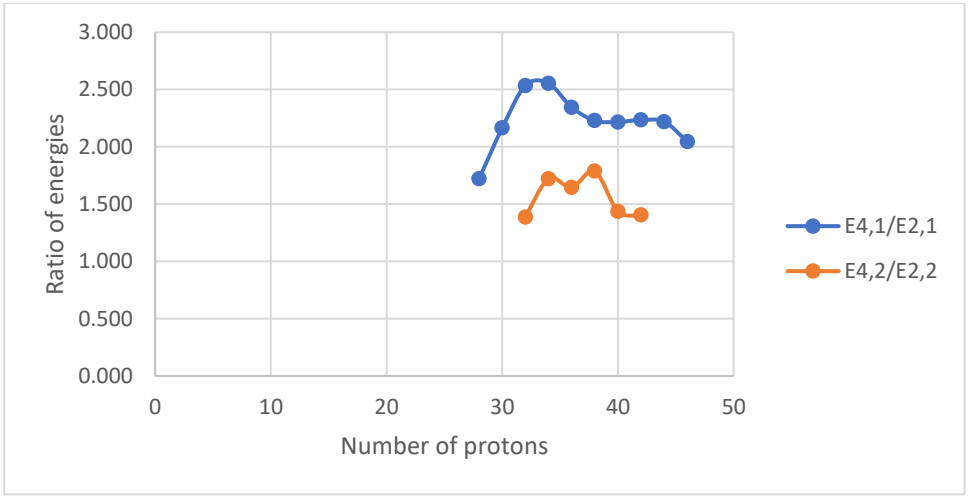

B

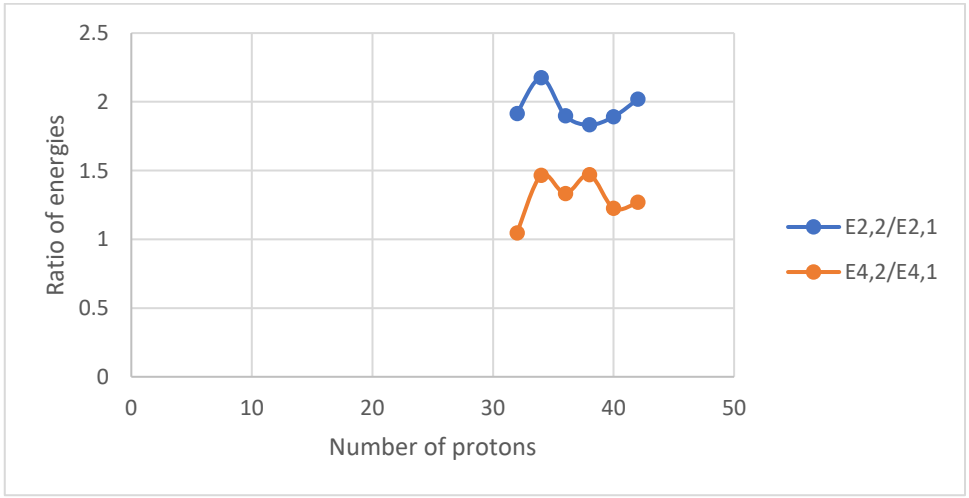

C

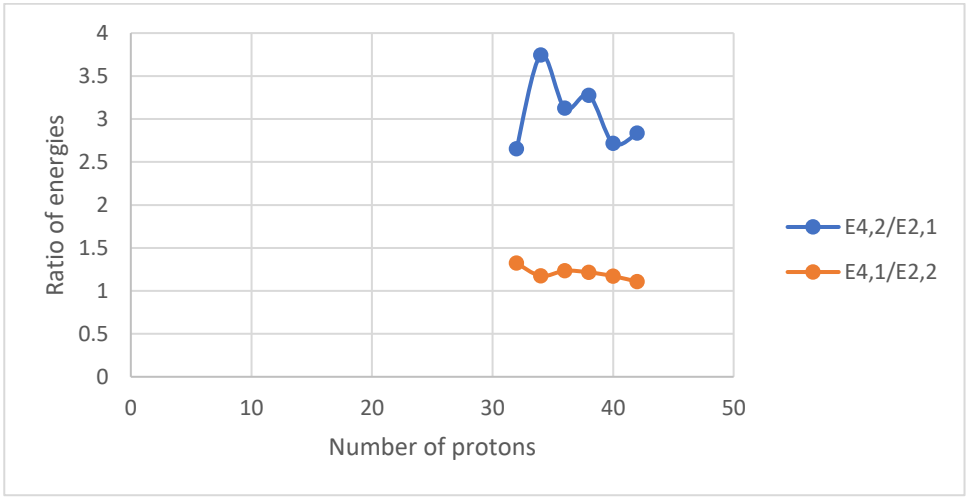

D

Figure V. 23 (color online) Panel **A** represents the comparison of the experimental energy levels of the lowest 2_1^+, 2_2^+, 4_1^+ and 4_2^+ states for the chain of N=46 isotones. Panels **B, C, D** represent the comparison of the experimental energy ratios ($E_{4_1^+}/E_{2_1^+}$ and $E_{4_2^+}/E_{2_2^+}$), ($E_{2_2^+}/E_{2_1^+}$ and $E_{4_2^+}/E_{4_1^+}$) and ($E_{4_2^+}/E_{2_1^+}$ and $E_{4_1^+}/E_{2_2^+}$), respectively, for the chain of N=46 isotones.

Isotones (N=48)

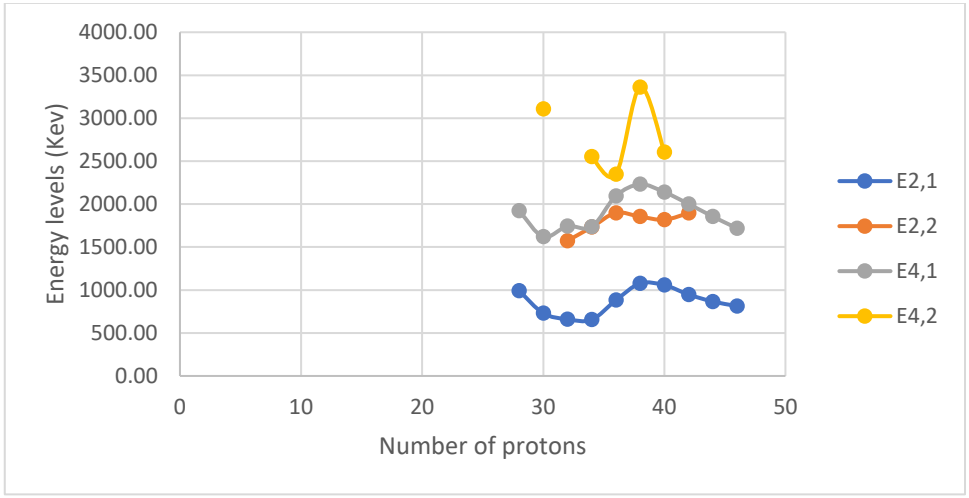

A

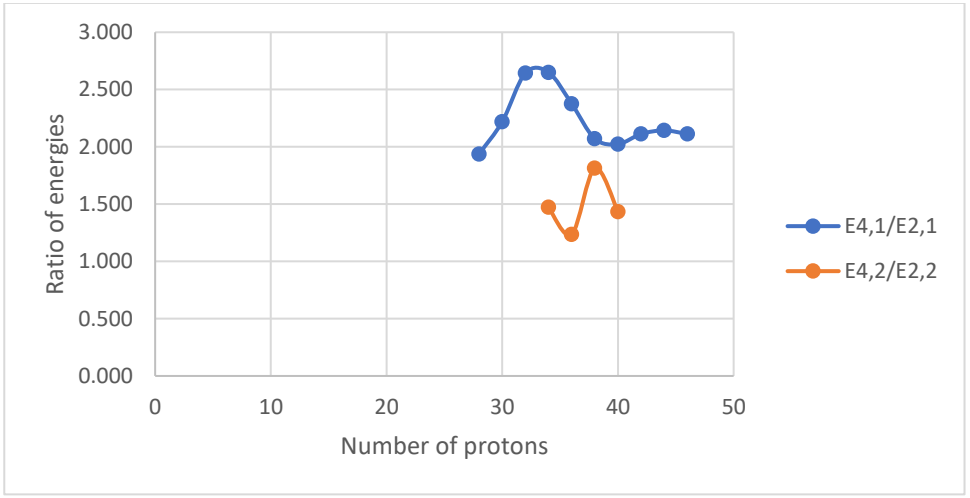

B

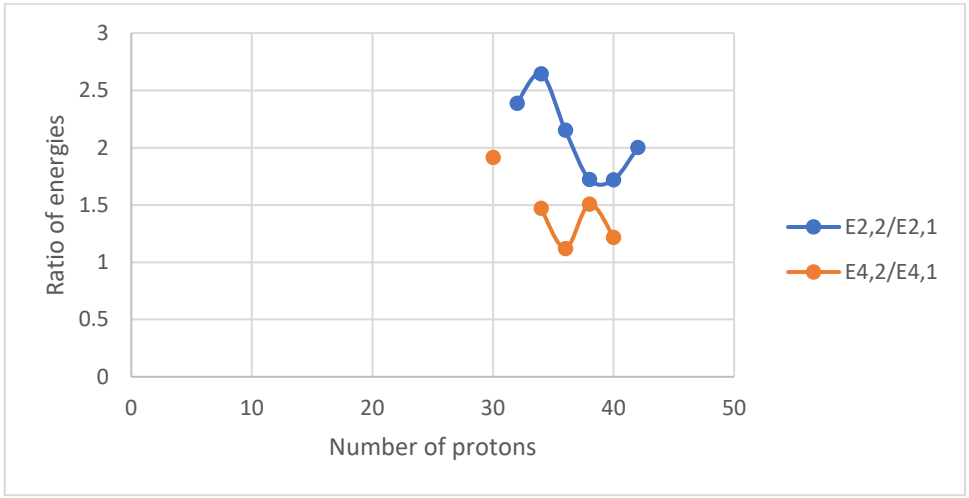

C

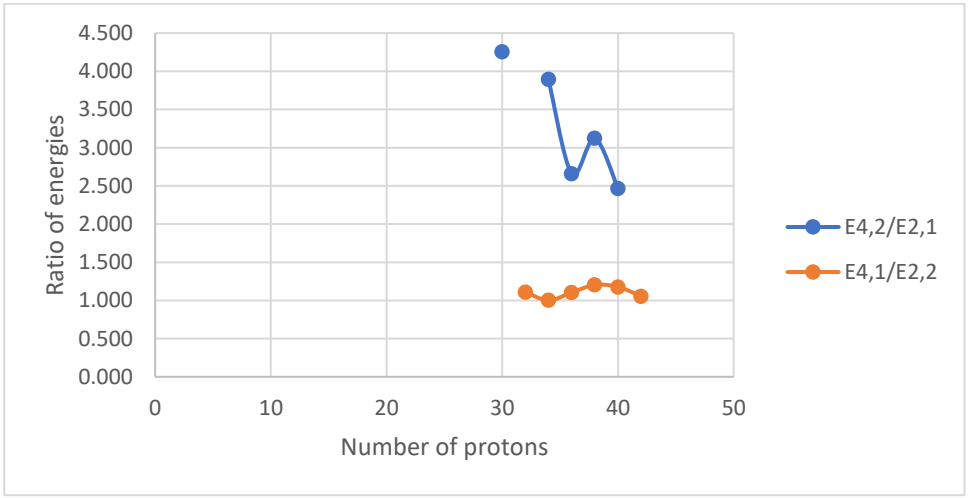

D

Figure V. 24 (color online) Panel **A** represents the comparison of the experimental energy levels of the lowest 2_1^+, 2_2^+, 4_1^+ and 4_2^+ states for the chain of N=48 isotones. Panels **B, C, D** represent the comparison of the experimental energy ratios ($E_{4_1^+}/E_{2_1^+}$ and $E_{4_2^+}/E_{2_2^+}$), ($E_{2_2^+}/E_{2_1^+}$ and $E_{4_2^+}/E_{4_1^+}$) and ($E_{4_2^+}/E_{2_1^+}$ and $E_{4_1^+}/E_{2_2^+}$), respectively, for the chain of N=48 isotones.

Isotones (N=50)

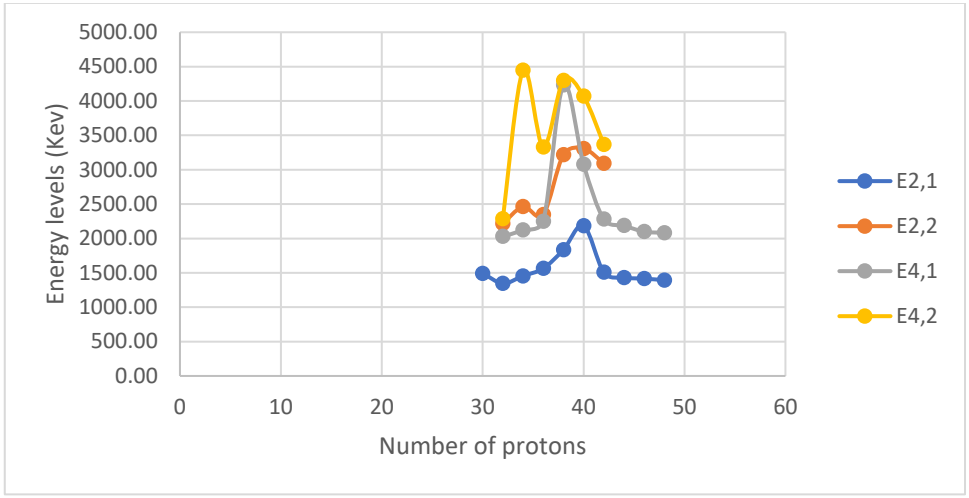

A

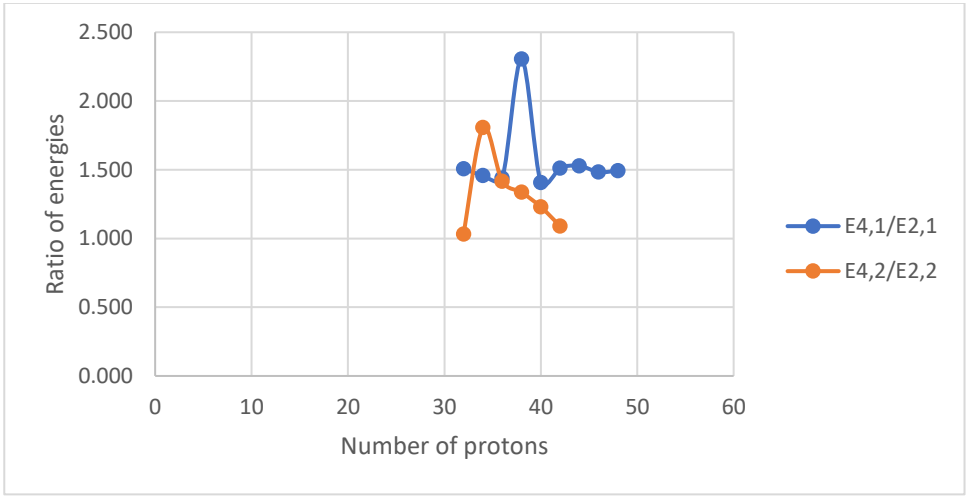

B

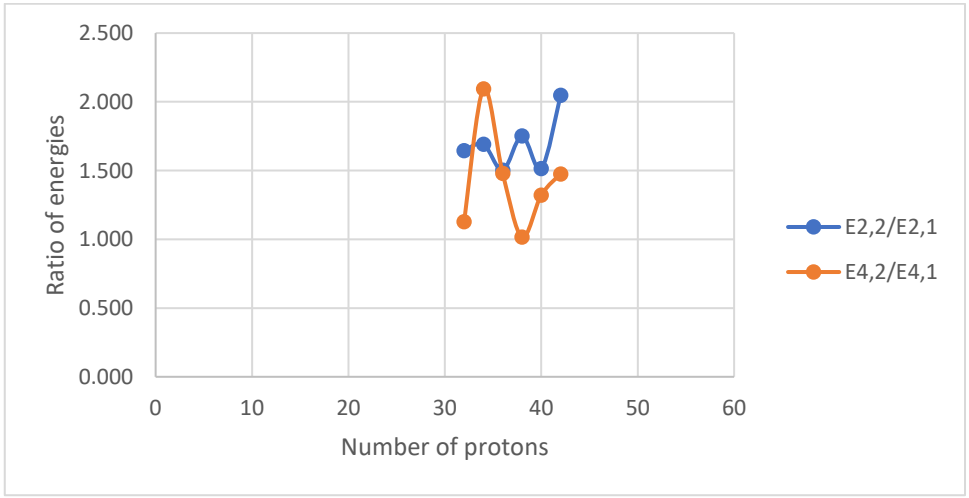

C

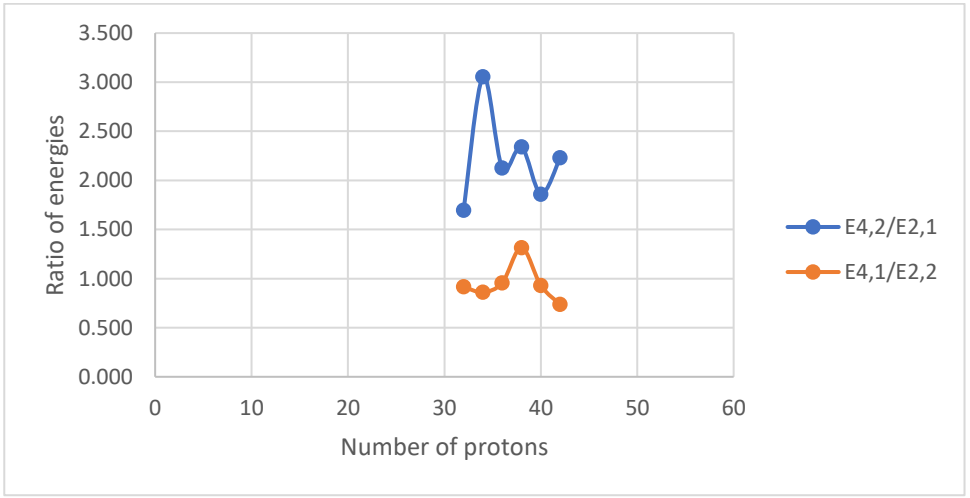

D

Figure V. 25 (color online) Panel **A** represents the comparison of the experimental energy levels of the lowest 2_1^+, 2_2^+, 4_1^+ and 4_2^+ states for the chain of N=50 isotones. Panels **B, C, D** represent the comparison of the experimental energy ratios ($E_{4_1^+}/E_{2_1^+}$ and $E_{4_2^+}/E_{2_2^+}$), ($E_{2_2^+}/E_{2_1^+}$ and $E_{4_2^+}/E_{4_1^+}$) and ($E_{4_2^+}/E_{2_1^+}$ and $E_{4_1^+}/E_{2_2^+}$), respectively, for the chain of N=50 isotones.

Isotones (N=52)

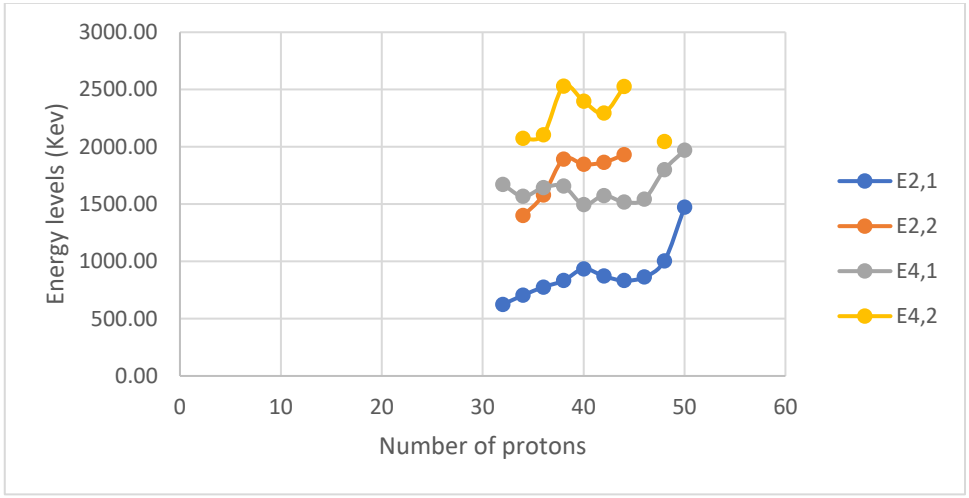

A

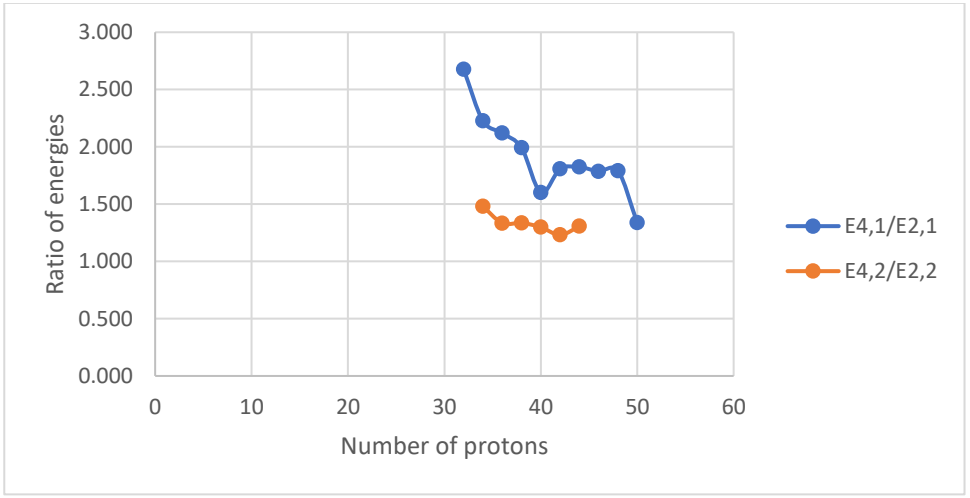

B

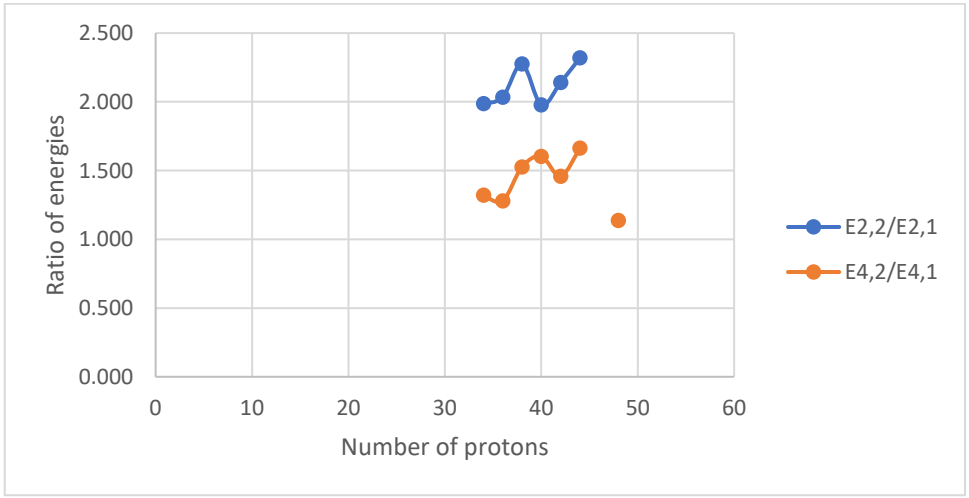

C

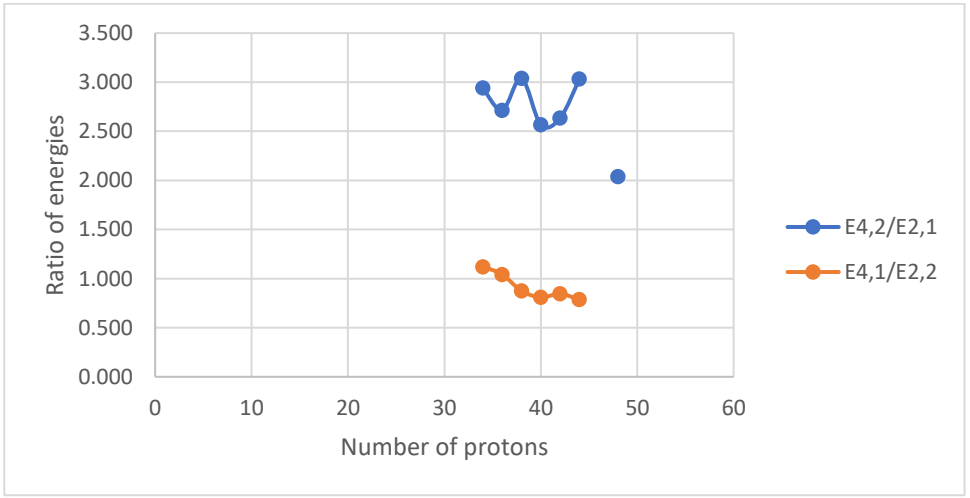

D

Figure V. 26 (color online) Panel **A** represents the comparison of the experimental energy levels of the lowest 2_1^+, 2_2^+, 4_1^+ and 4_2^+ states for the chain of N=52 isotones. Panels **B, C, D** represent the comparison of the experimental energy ratios ($E_{4_1^+}/E_{2_1^+}$ and $E_{4_2^+}/E_{2_2^+}$), ($E_{2_2^+}/E_{2_1^+}$ and $E_{4_2^+}/E_{4_1^+}$) and ($E_{4_2^+}/E_{2_1^+}$ and $E_{4_1^+}/E_{2_2^+}$), respectively, for the chain of N=52 isotones.

Isotones (N=54)

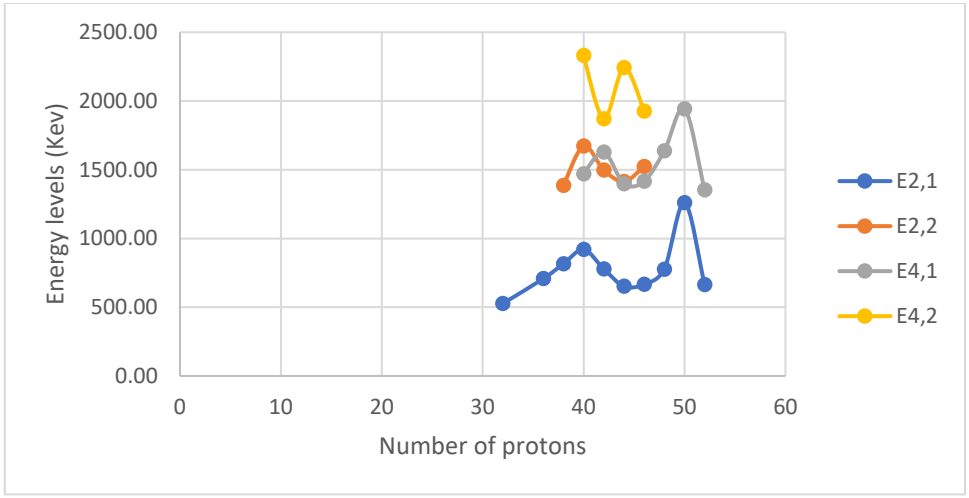

A

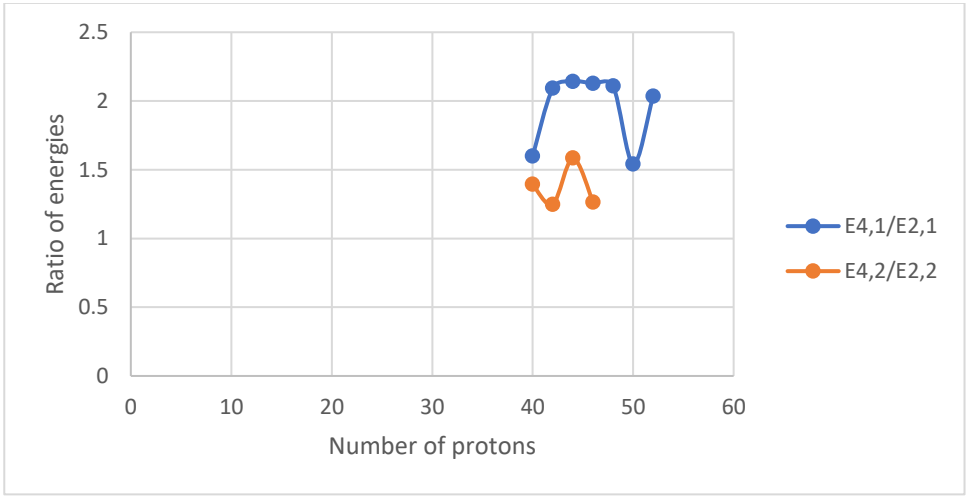

B

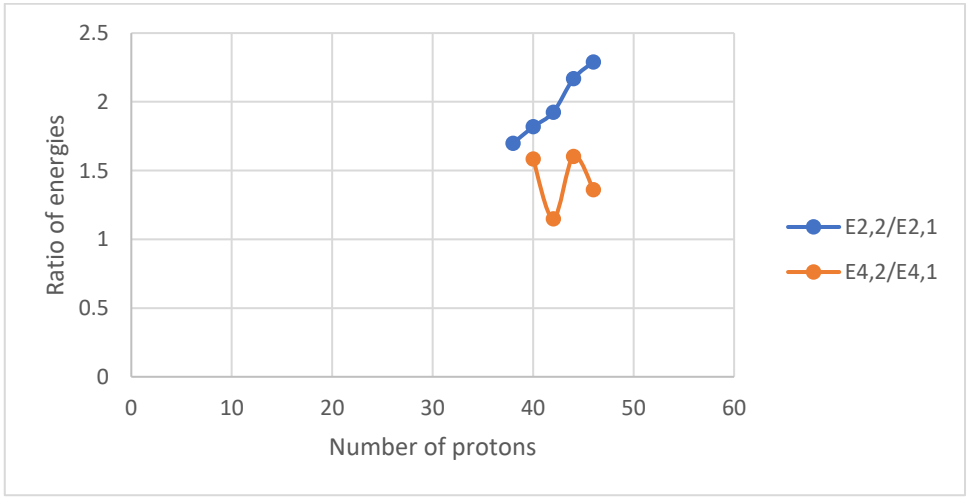

C

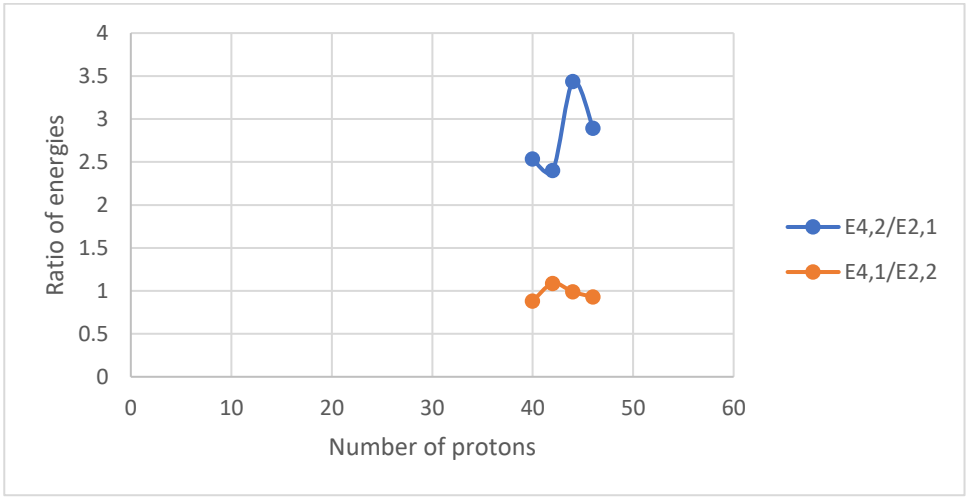

D

Figure V. 27 (color online) Panel **A** represents the comparison of the experimental energy levels of the lowest 2_1^+, 2_2^+, 4_1^+ and 4_2^+ states for the chain of N=54 isotones. Panels **B, C, D** represent the comparison of the experimental energy ratios ($E_{4_1^+}/E_{2_1^+}$ and $E_{4_2^+}/E_{2_2^+}$), ($E_{2_2^+}/E_{2_1^+}$ and $E_{4_2^+}/E_{4_1^+}$) and ($E_{4_2^+}/E_{2_1^+}$ and $E_{4_1^+}/E_{2_2^+}$), respectively, for the chain of N=54 isotones.

Isotones (N=56)

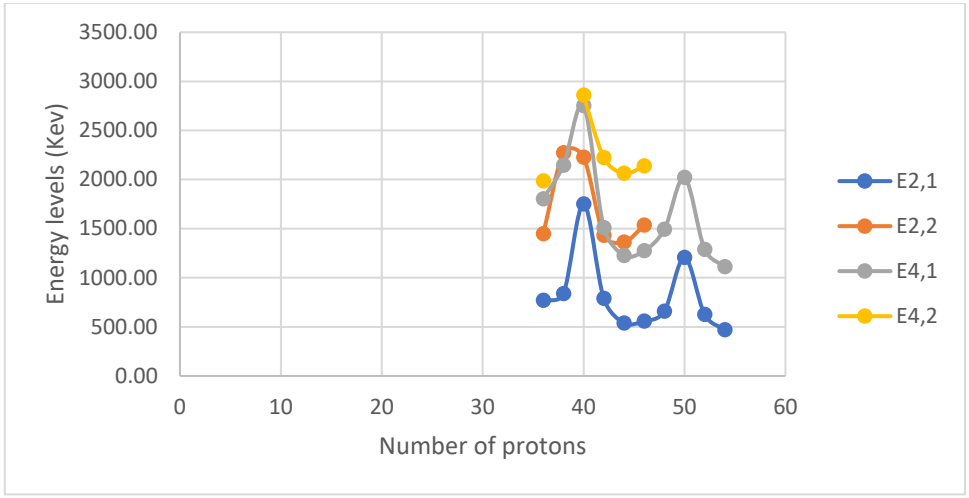

A

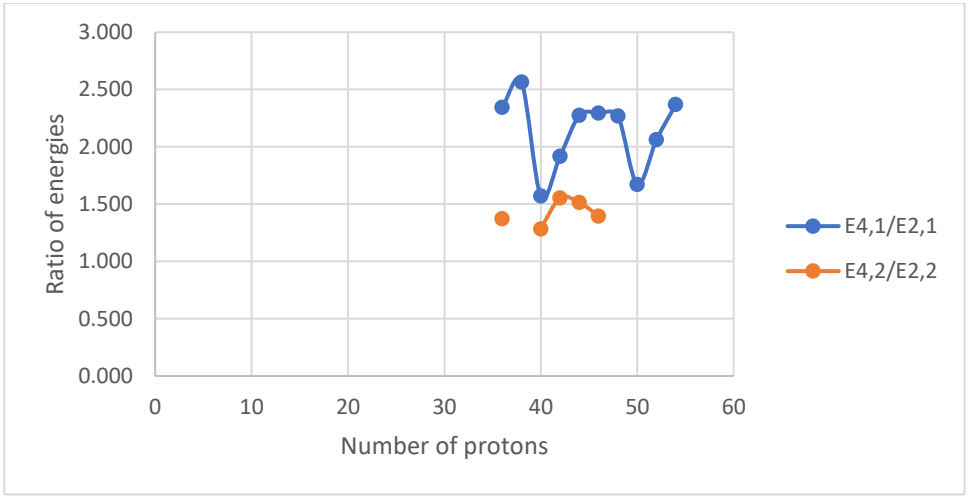

B

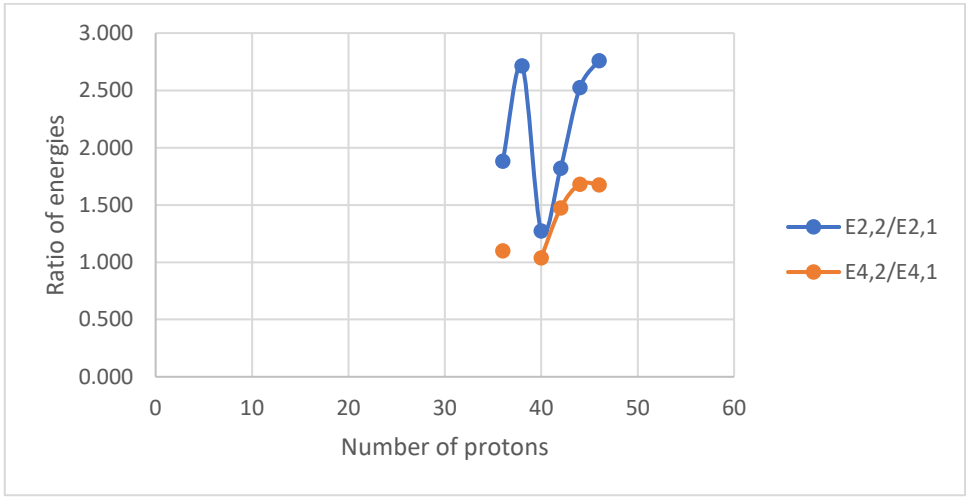

C

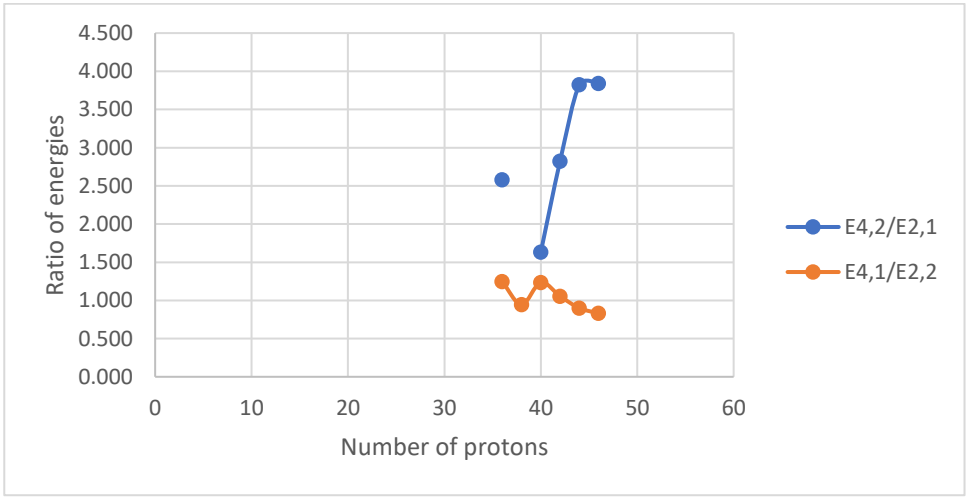

D

Figure V. 28 (color online) Panel **A** represents the comparison of the experimental energy levels of the lowest 2_1^+, 2_2^+, 4_1^+ and 4_2^+ states for the chain of N=56 isotones. Panels **B, C, D** represent the comparison of the experimental energy ratios ($E_{4_1^+}/E_{2_1^+}$ and $E_{4_2^+}/E_{2_2^+}$), ($E_{2_2^+}/E_{2_1^+}$ and $E_{4_2^+}/E_{4_1^+}$) and ($E_{4_2^+}/E_{2_1^+}$ and $E_{4_1^+}/E_{2_2^+}$), respectively, for the chain of N=56 isotones.

Isotones (N=58)

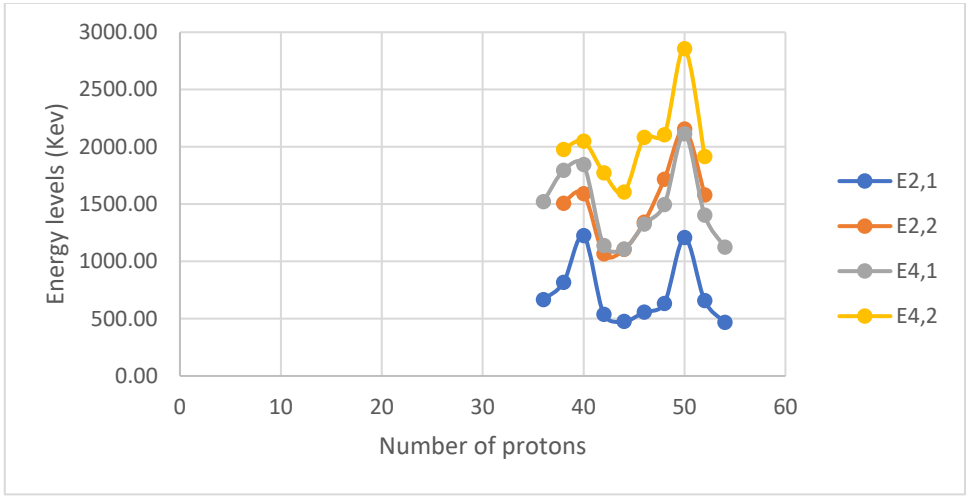

A

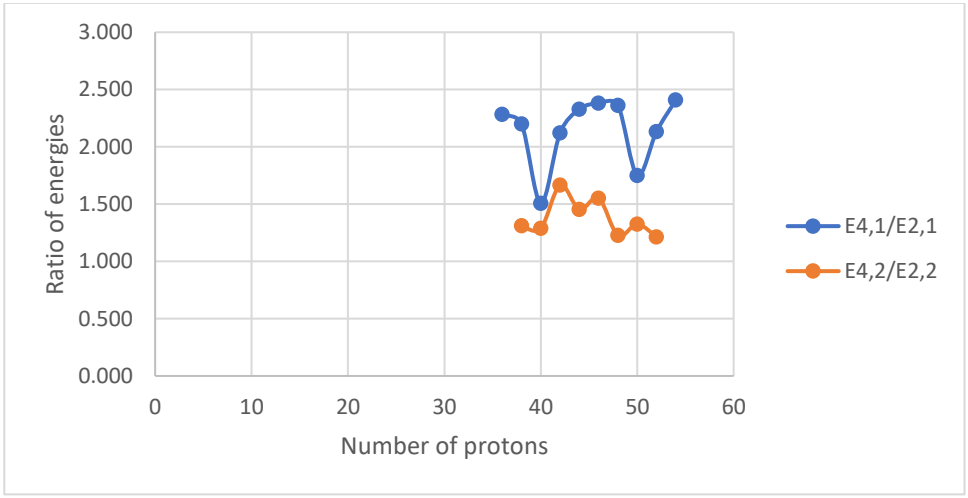

B

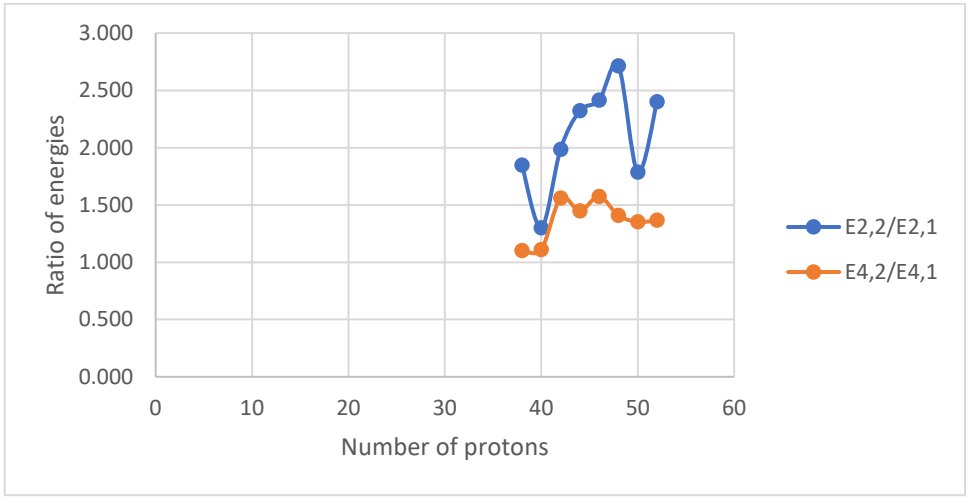

C

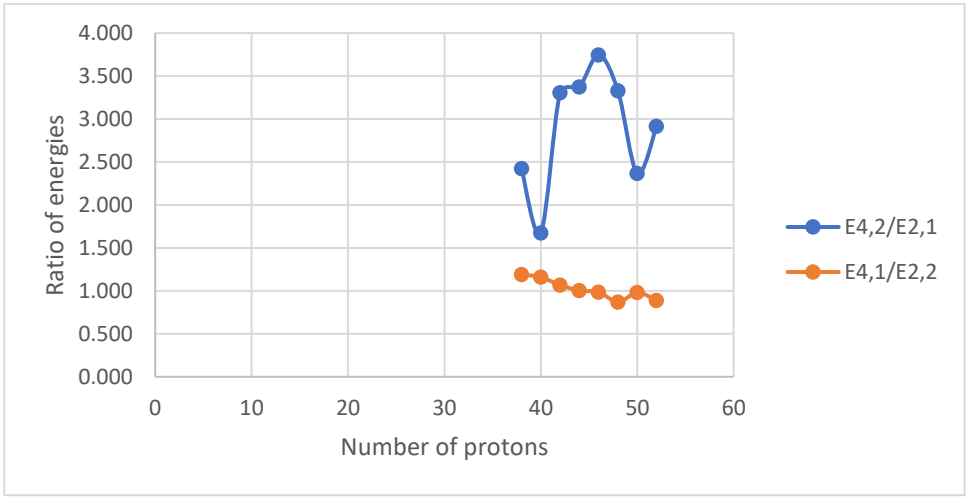

D

Figure V. 29 (color online) Panel **A** represents the comparison of the experimental energy levels of the lowest 2_1^+, 2_2^+, 4_1^+ and 4_2^+ states for the chain of N=58 isotones. Panels **B, C, D** represent the comparison of the experimental energy ratios ($E_{4_1^+}/E_{2_1^+}$ and $E_{4_2^+}/E_{2_2^+}$), ($E_{2_2^+}/E_{2_1^+}$ and $E_{4_2^+}/E_{4_1^+}$) and ($E_{4_2^+}/E_{2_1^+}$ and $E_{4_1^+}/E_{2_2^+}$), respectively, for the chain of N=58 isotones.

Isotones (N=60)

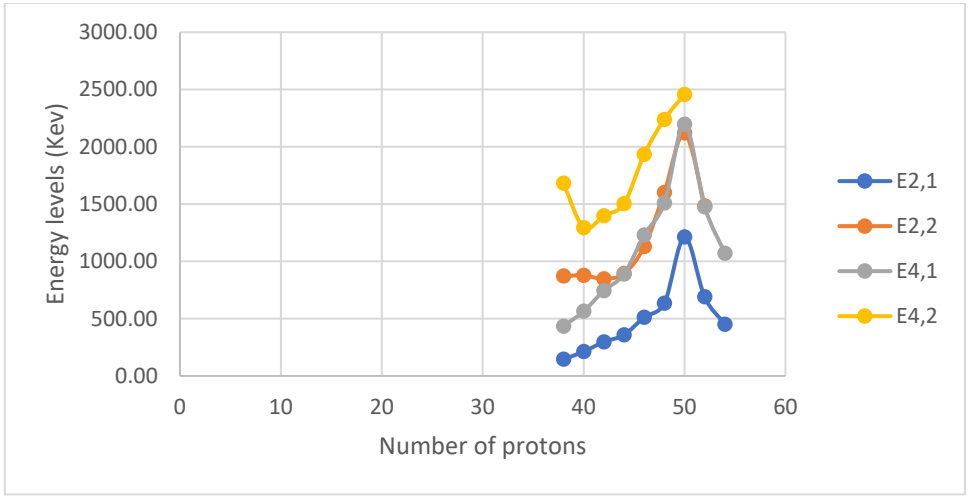

A

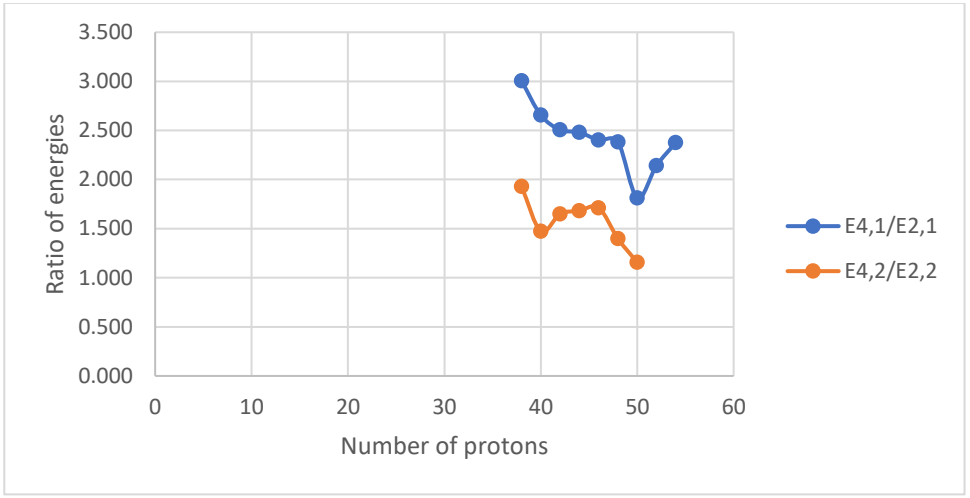

B

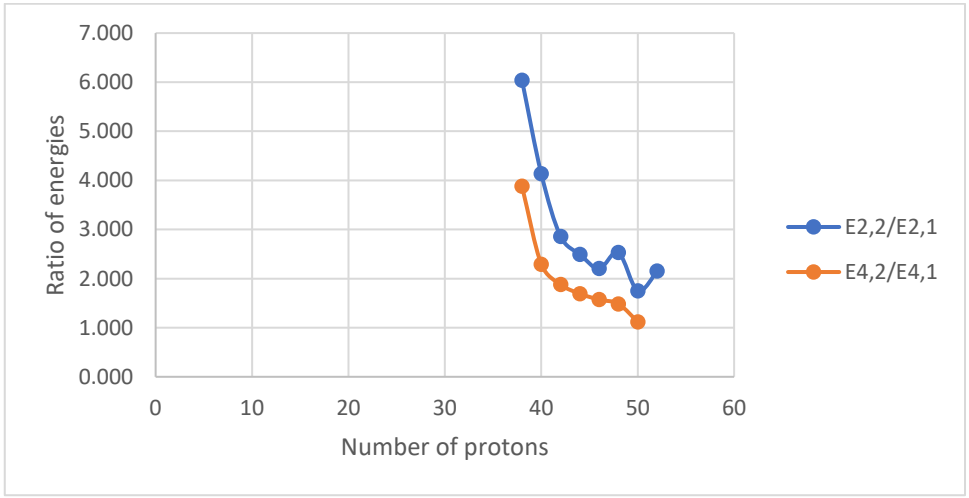

C

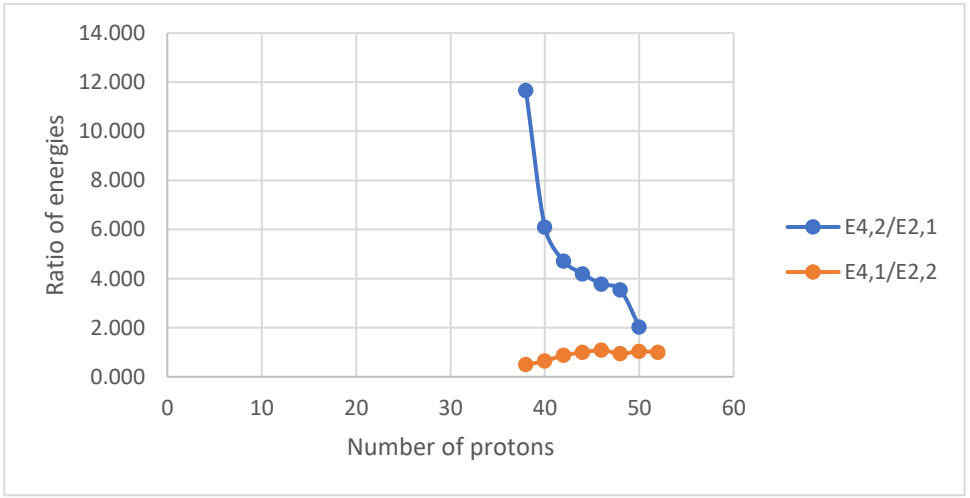

D

Figure V. 30 (color online) Panel **A** represents the comparison of the experimental energy levels of the lowest 2_1^+, 2_2^+, 4_1^+ and 4_2^+ states for the chain of N=60 isotones. Panels **B, C, D** represent the comparison of the experimental energy ratios ($E_{4_1^+}/E_{2_1^+}$ and $E_{4_2^+}/E_{2_2^+}$), ($E_{2_2^+}/E_{2_1^+}$ and $E_{4_2^+}/E_{4_1^+}$) and ($E_{4_2^+}/E_{2_1^+}$ and $E_{4_1^+}/E_{2_2^+}$), respectively, for the chain of N=60 isotones.

Isotones (N=62)

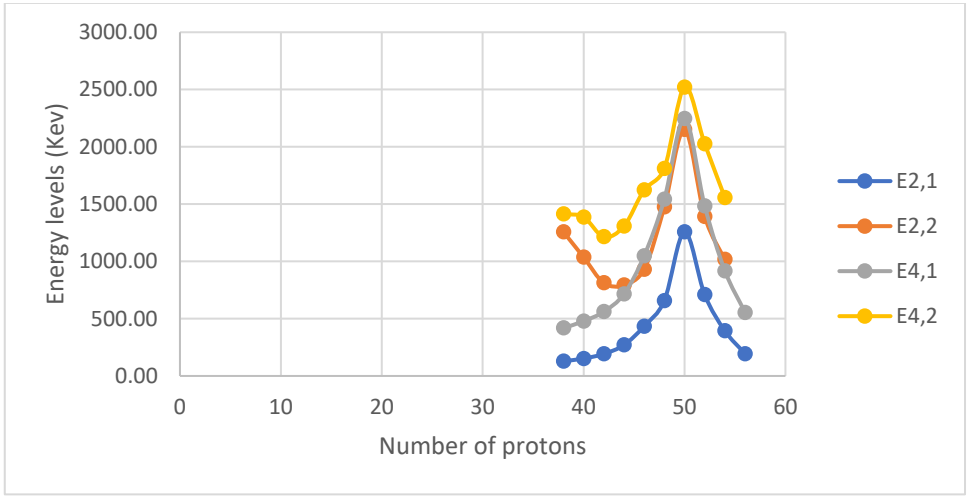

A

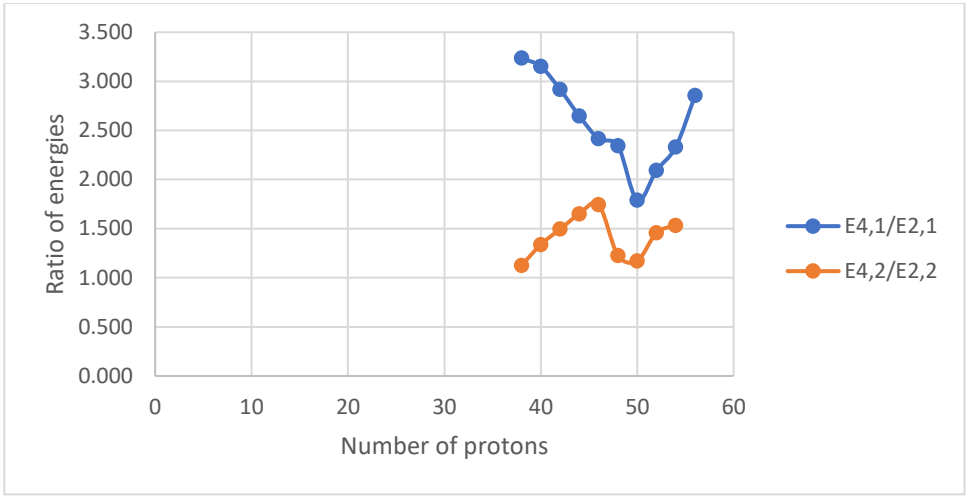

B

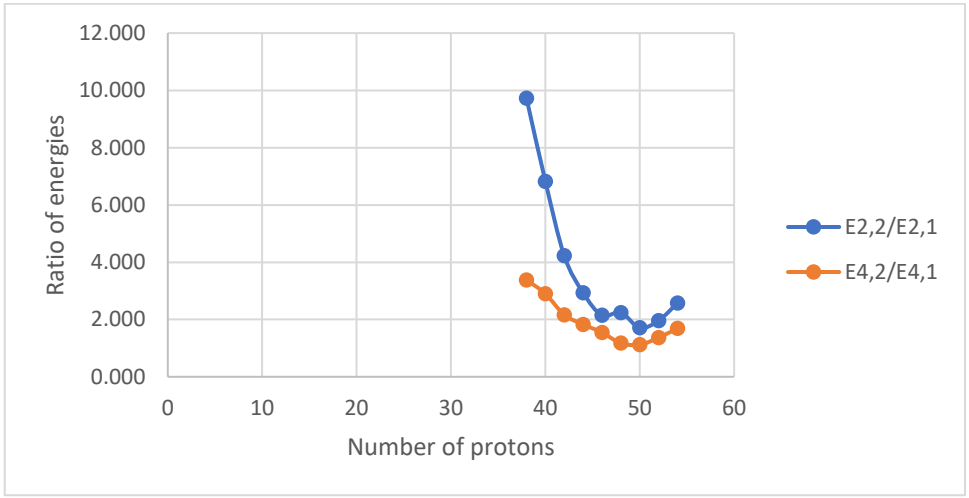

C

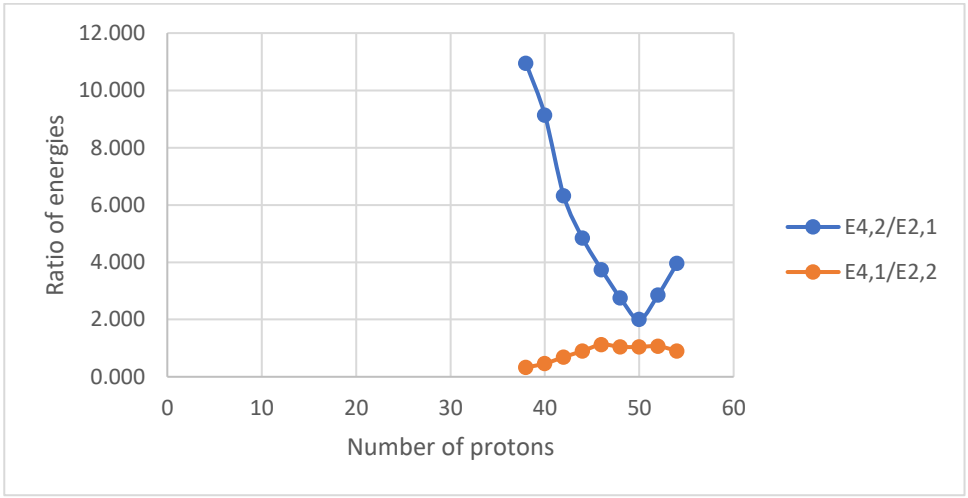

D

Figure V. 31 (color online) Panel **A** represents the comparison of the experimental energy levels of the lowest 2_1^+, 2_2^+, 4_1^+ and 4_2^+ states for the chain of N=62 isotones. Panels **B, C, D** represent the comparison of the experimental energy ratios ($E_{4_1^+}/E_{2_1^+}$ and $E_{4_2^+}/E_{2_2^+}$), ($E_{2_2^+}/E_{2_1^+}$ and $E_{4_2^+}/E_{4_1^+}$) and ($E_{4_2^+}/E_{2_1^+}$ and $E_{4_1^+}/E_{2_2^+}$), respectively, for the chain of N=62 isotones.

Isotones (N=64)

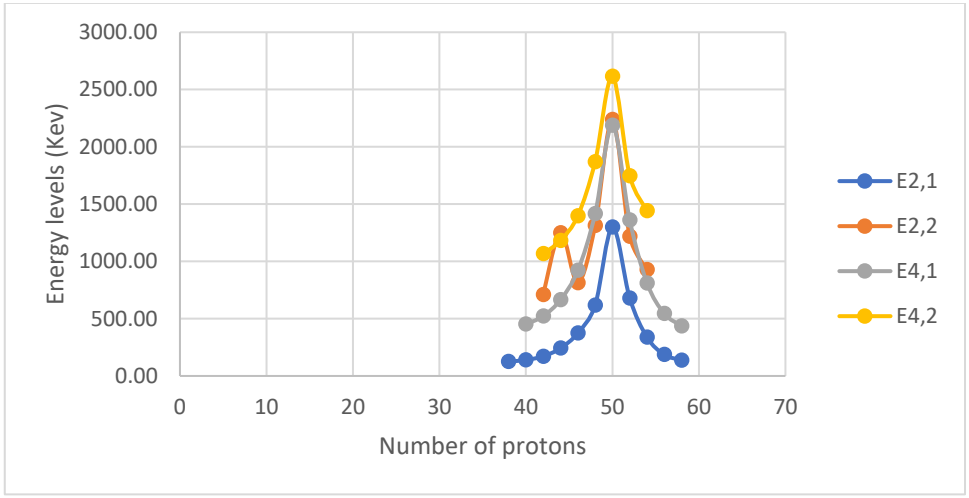

A

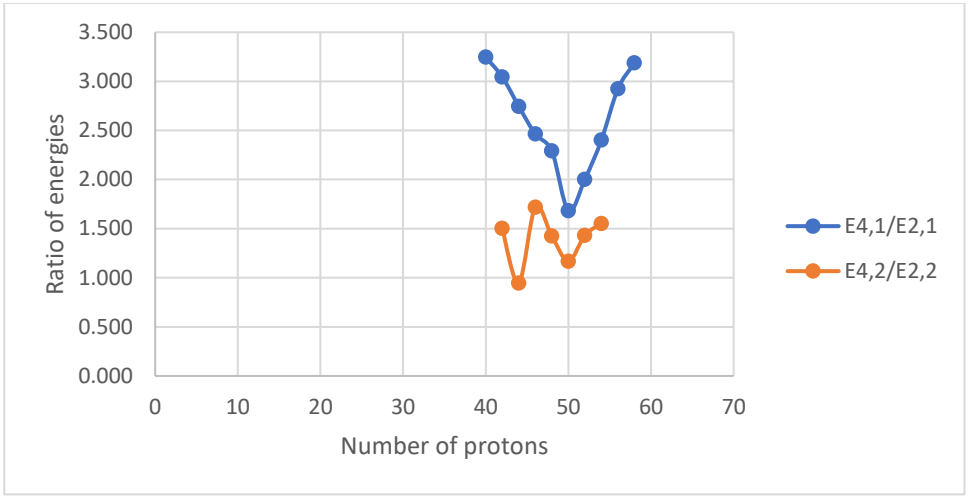

B

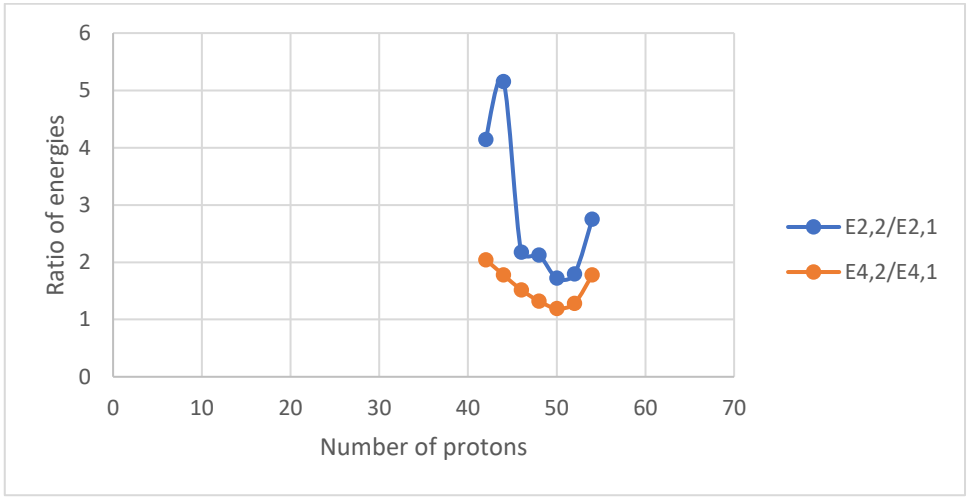

C

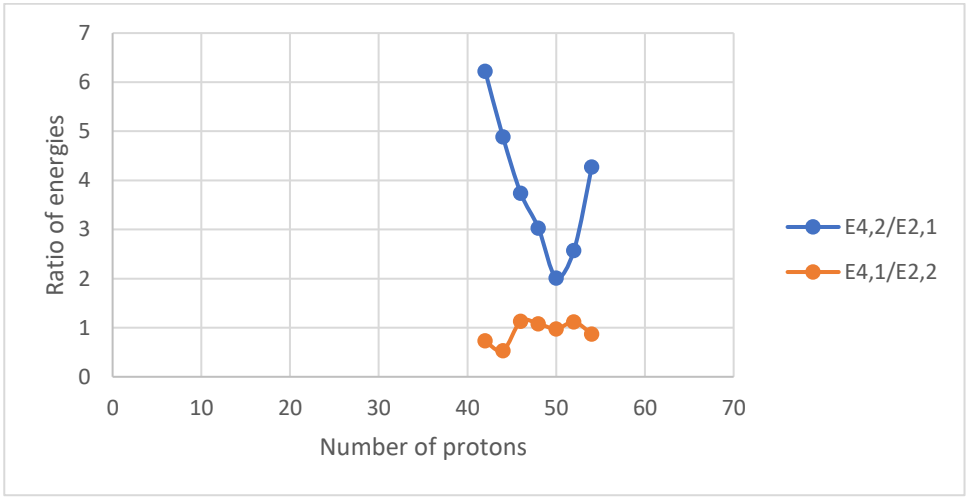

D

Figure V. 32 (color online) Panel **A** represents the comparison of the experimental energy levels of the lowest 2_1^+, 2_2^+, 4_1^+ and 4_2^+ states for the chain of N=64 isotones. Panels **B, C, D** represent the comparison of the experimental energy ratios ($E_{4_1^+}/E_{2_1^+}$ and $E_{4_2^+}/E_{2_2^+}$), ($E_{2_2^+}/E_{2_1^+}$ and $E_{4_2^+}/E_{4_1^+}$) and ($E_{4_2^+}/E_{2_1^+}$ and $E_{4_1^+}/E_{2_2^+}$), respectively, for the chain of N=64 isotones.

Isotones (N=66)

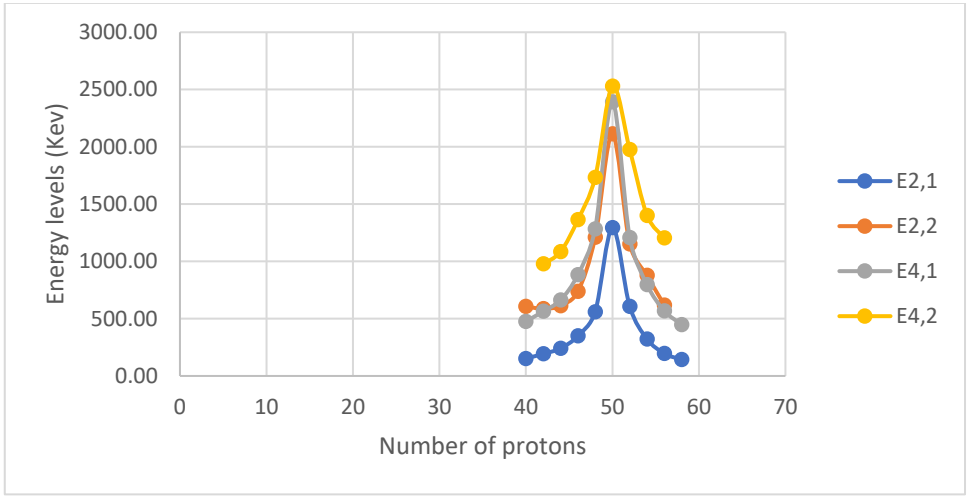

A

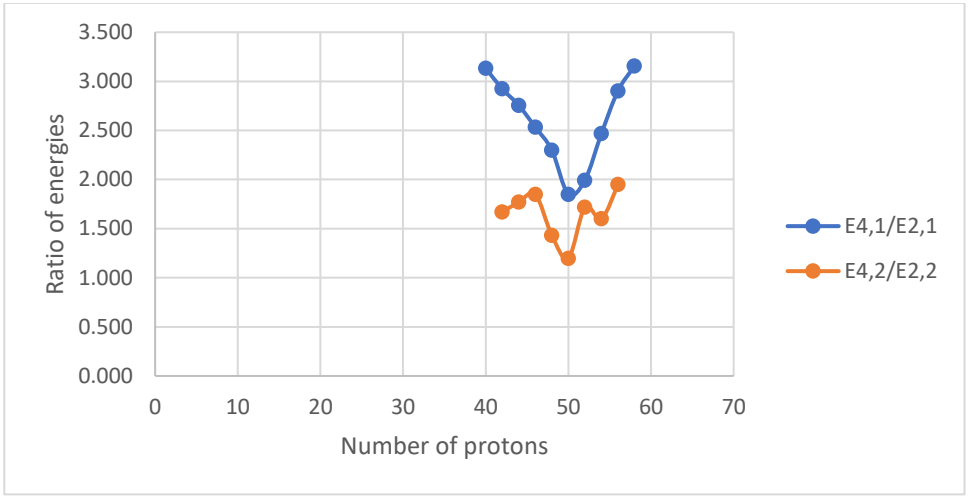

B

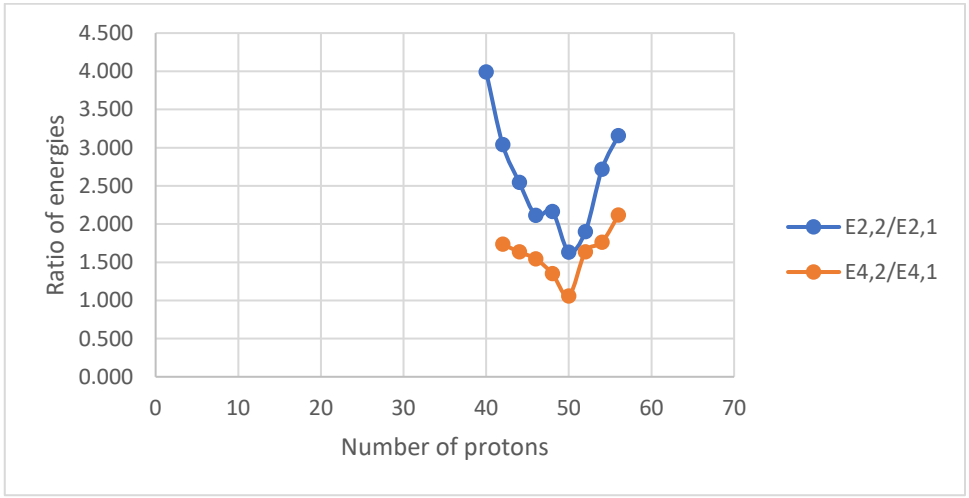

C

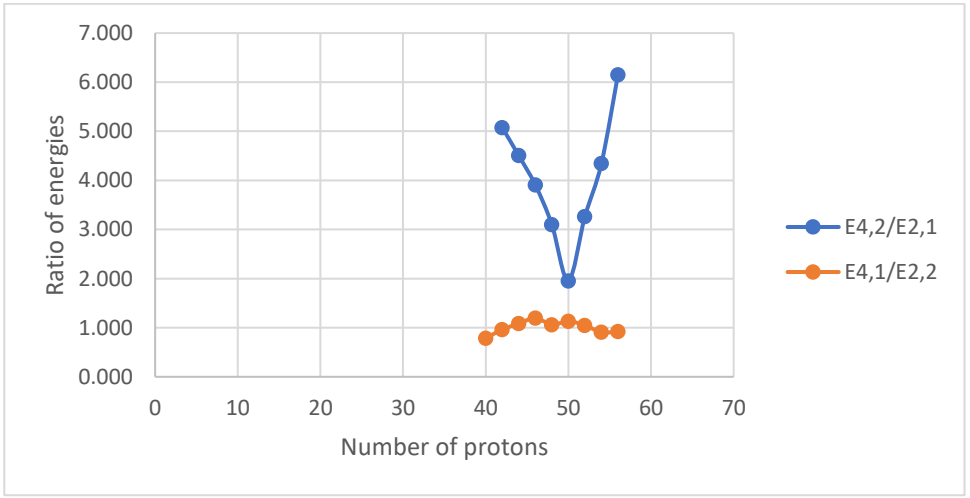

D

Figure V. 33 (color online) Panel **A** represents the comparison of the experimental energy levels of the lowest 2_1^+, 2_2^+, 4_1^+ and 4_2^+ states for the chain of N=66 isotones. Panels **B, C, D** represent the comparison of the experimental energy ratios ($E_{4_1^+}/E_{2_1^+}$ and $E_{4_2^+}/E_{2_2^+}$), ($E_{2_2^+}/E_{2_1^+}$ and $E_{4_2^+}/E_{4_1^+}$) and ($E_{4_2^+}/E_{2_1^+}$ and $E_{4_1^+}/E_{2_2^+}$), respectively, for the chain of N=66 isotones.

Isotones (N=68)

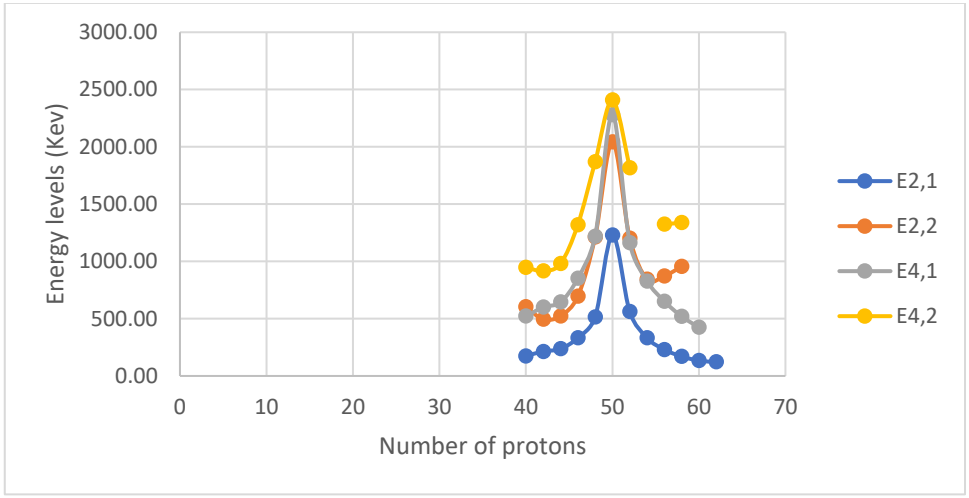

A

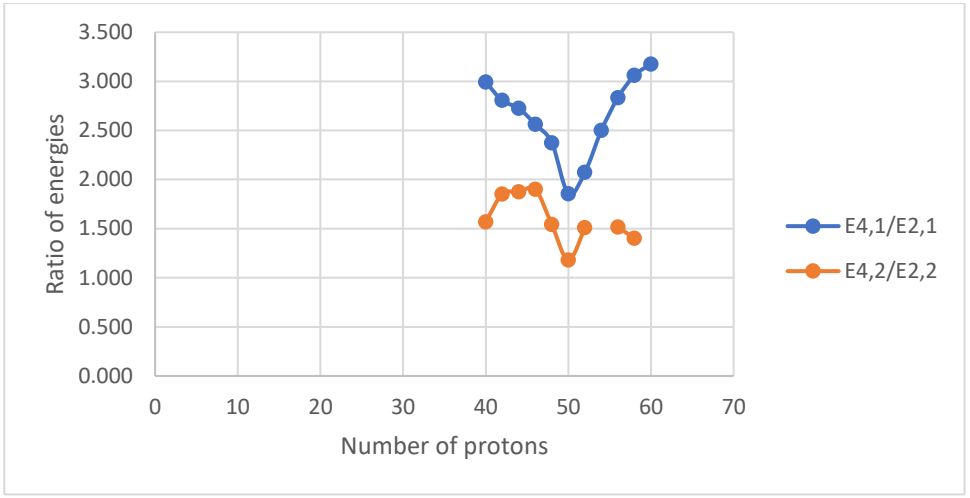

B

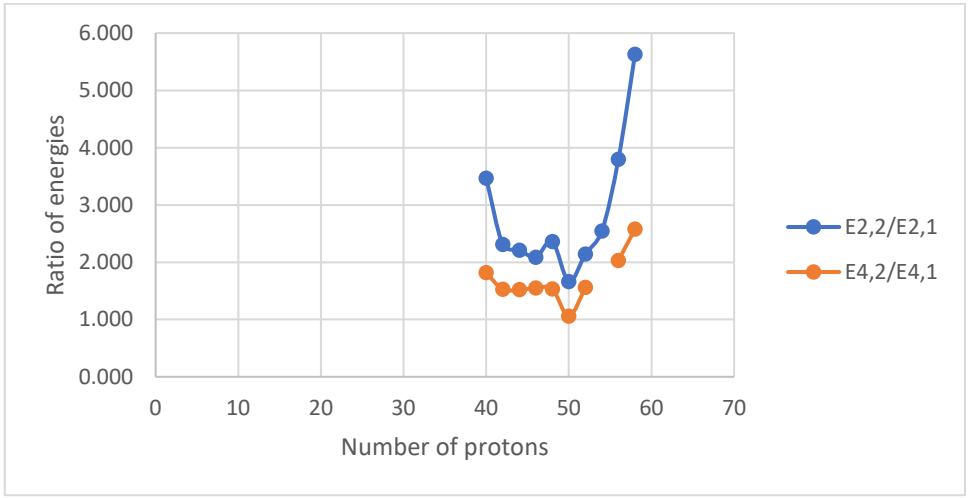

C

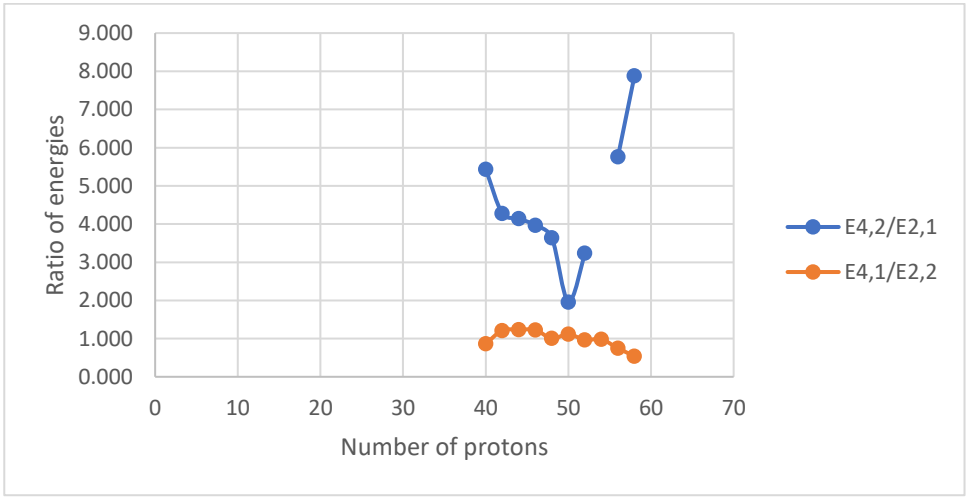

D

Figure V. 34 (color online) Panel **A** represents the comparison of the experimental energy levels of the lowest 2_1^+, 2_2^+, 4_1^+ and 4_2^+ states for the chain of N=68 isotones. Panels **B, C, D** represent the comparison of the experimental energy ratios ($E_{4_1^+}/E_{2_1^+}$ and $E_{4_2^+}/E_{2_2^+}$), ($E_{2_2^+}/E_{2_1^+}$ and $E_{4_2^+}/E_{4_1^+}$) and ($E_{4_2^+}/E_{2_1^+}$ and $E_{4_1^+}/E_{2_2^+}$), respectively, for the chain of N=68 isotones.

Isotones (N=70)

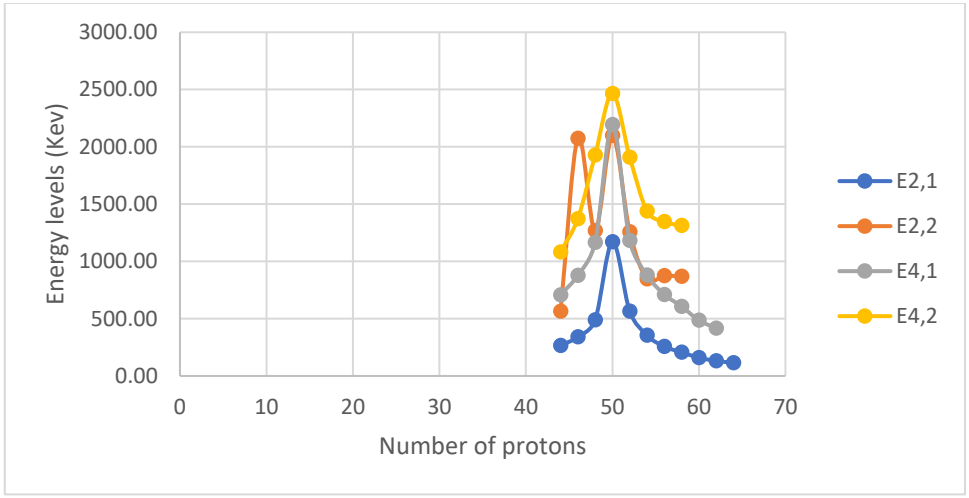

A

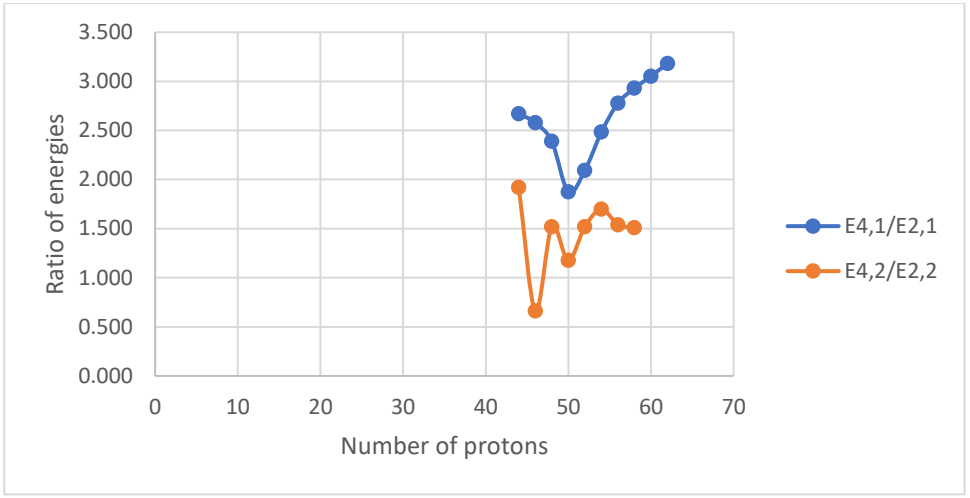

B

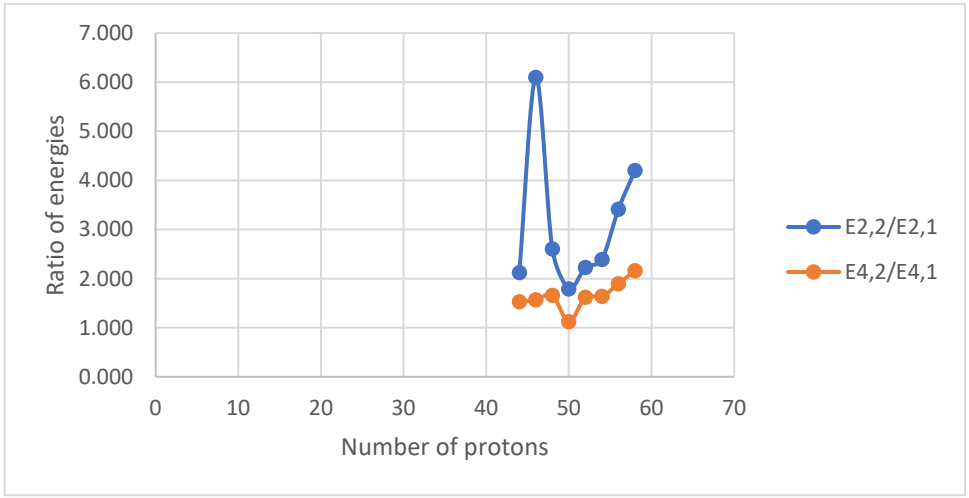

C

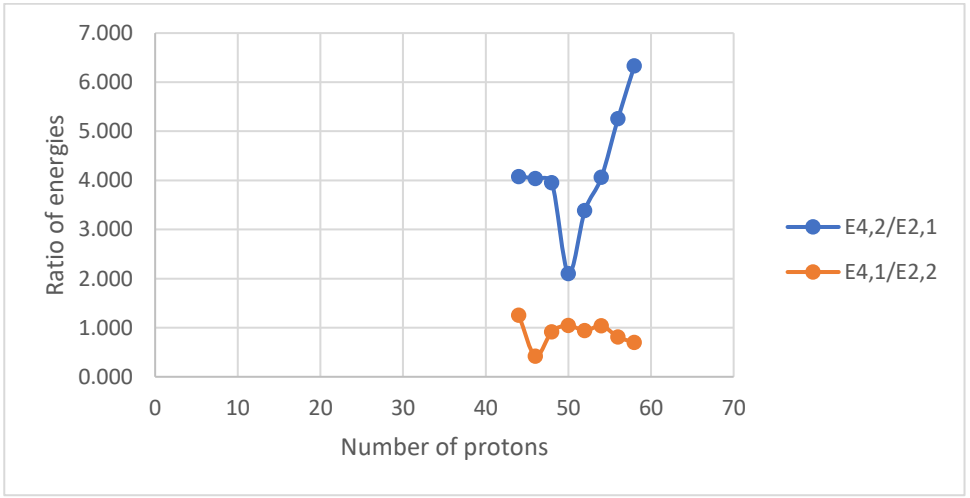

D

Figure V. 35 (color online) Panel **A** represents the comparison of the experimental energy levels of the lowest 2_1^+, 2_2^+, 4_1^+ and 4_2^+ states for the chain of N=70 isotones. Panels **B, C, D** represent the comparison of the experimental energy ratios ($E_{4_1^+}/E_{2_1^+}$ and $E_{4_2^+}/E_{2_2^+}$), ($E_{2_2^+}/E_{2_1^+}$ and $E_{4_2^+}/E_{4_1^+}$) and ($E_{4_2^+}/E_{2_1^+}$ and $E_{4_1^+}/E_{2_2^+}$), respectively, for the chain of N=70 isotones.

Isotones (N=72)

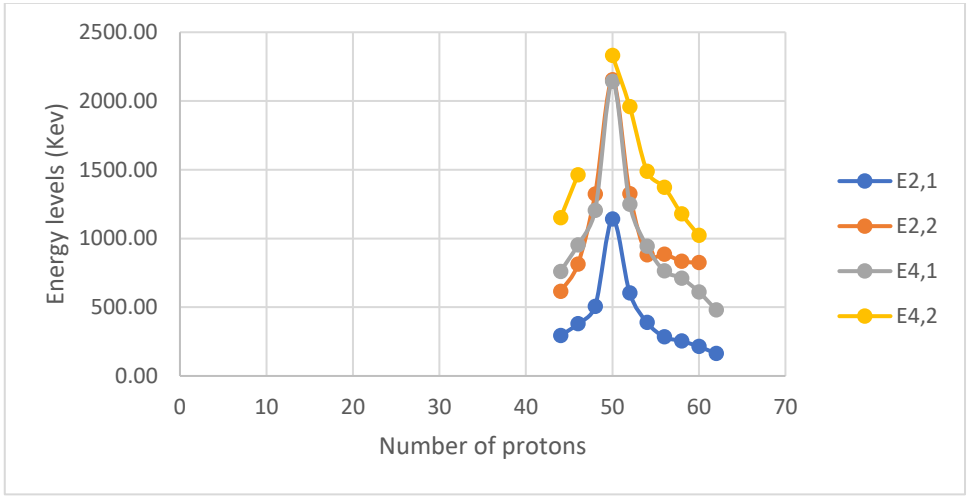

A

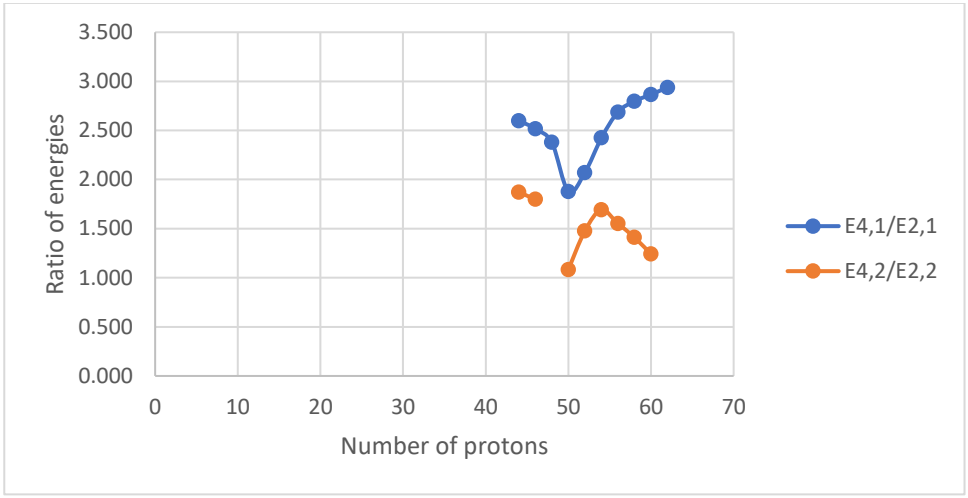

B

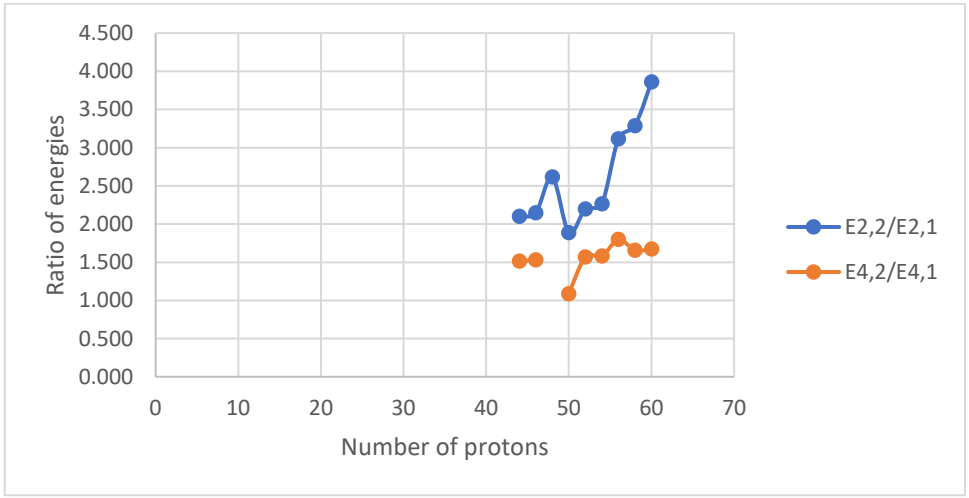

C

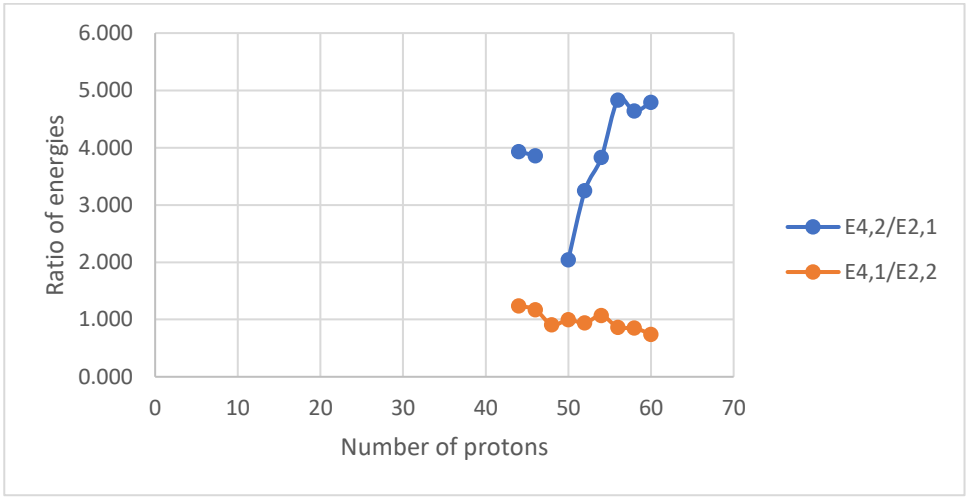

D

Figure V. 36 (color online) Panel **A** represents the comparison of the experimental energy levels of the lowest 2_1^+, 2_2^+, 4_1^+ and 4_2^+ states for the chain of N=72 isotones. Panels **B, C, D** represent the comparison of the experimental energy ratios ($E_{4_1^+}/E_{2_1^+}$ and $E_{4_2^+}/E_{2_2^+}$), ($E_{2_2^+}/E_{2_1^+}$ and $E_{4_2^+}/E_{4_1^+}$) and ($E_{4_2^+}/E_{2_1^+}$ and $E_{4_1^+}/E_{2_2^+}$), respectively, for the chain of N=72 isotones.

Isotones (N=74)

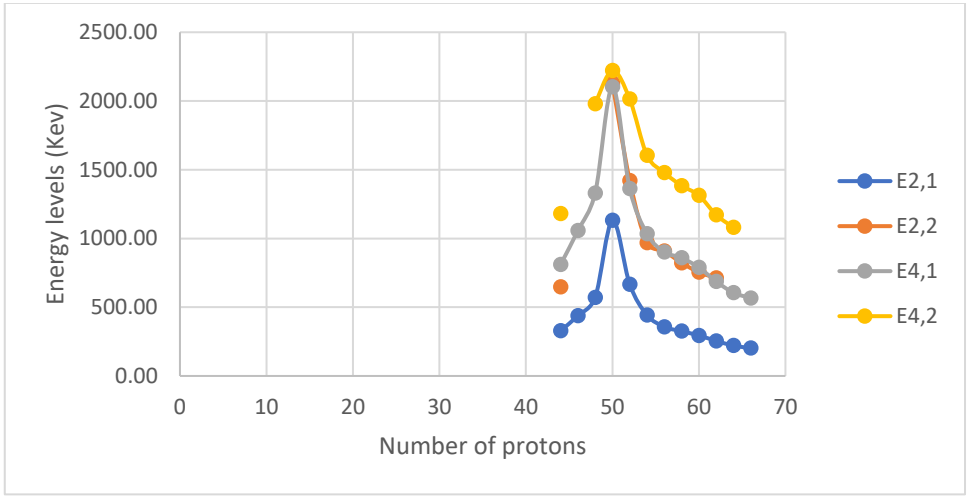

A

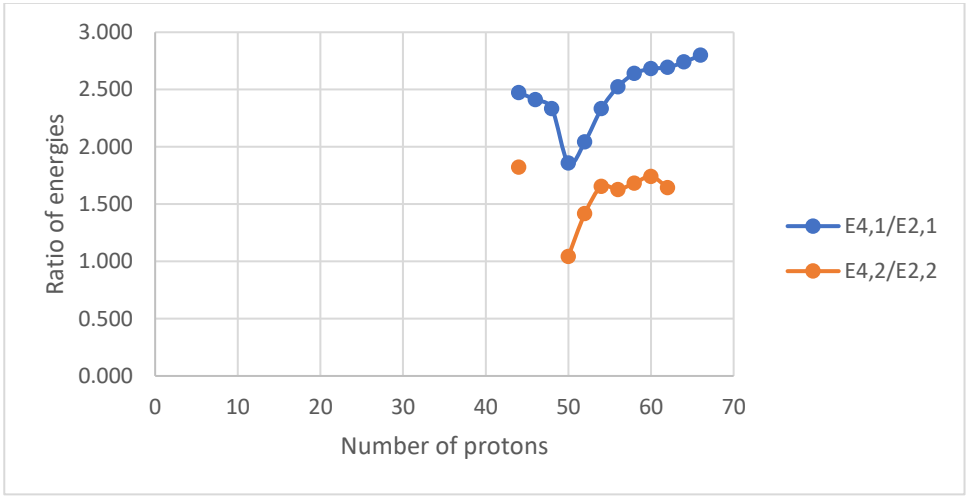

B

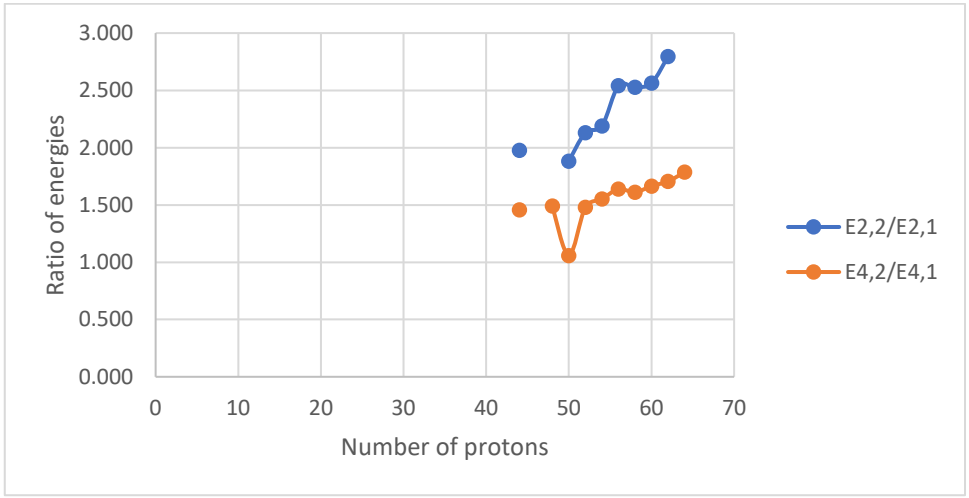

C

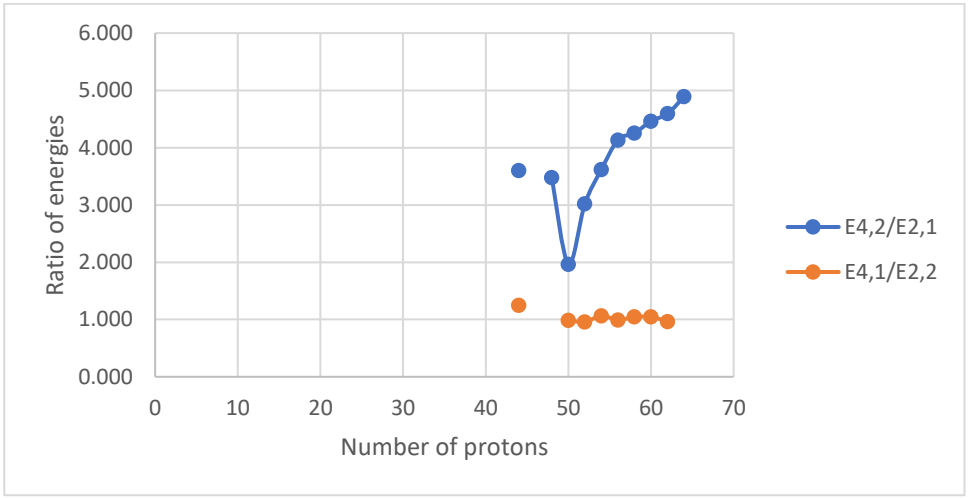

D

Figure V. 37 (color online) Panel **A** represents the comparison of the experimental energy levels of the lowest 2_1^+, 2_2^+, 4_1^+ and 4_2^+ states for the chain of N=74 isotones. Panels **B, C, D** represent the comparison of the experimental energy ratios ($E_{4_1^+}/E_{2_1^+}$ and $E_{4_2^+}/E_{2_2^+}$), ($E_{2_2^+}/E_{2_1^+}$ and $E_{4_2^+}/E_{4_1^+}$) and ($E_{4_2^+}/E_{2_1^+}$ and $E_{4_1^+}/E_{2_2^+}$), respectively, for the chain of N=74 isotones.

Isotones (N=76)

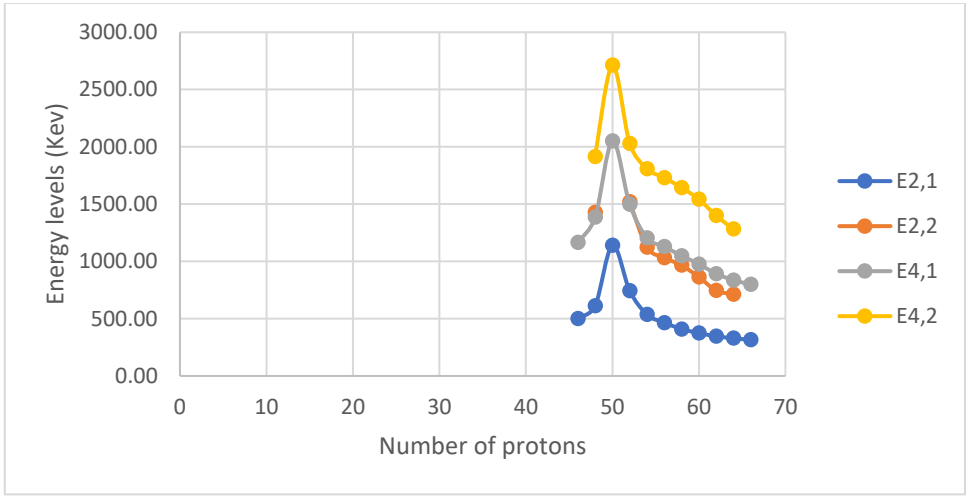

A

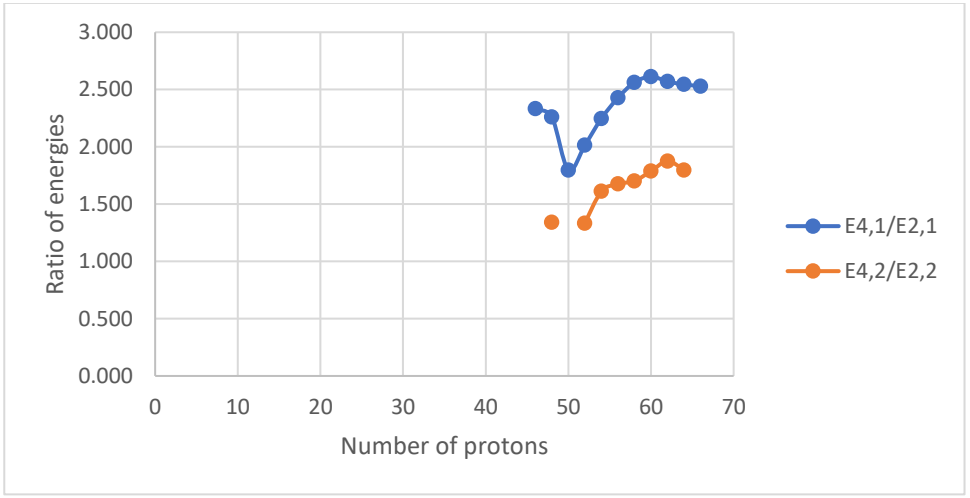

B

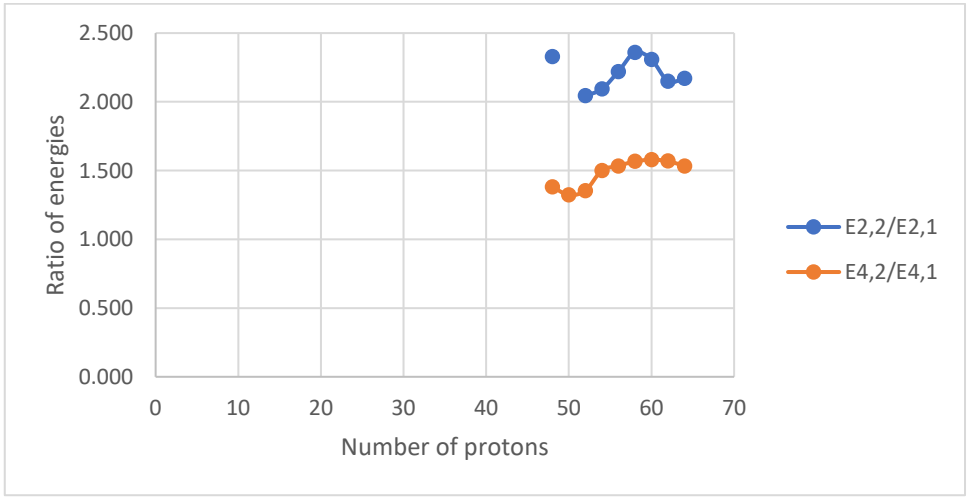

C

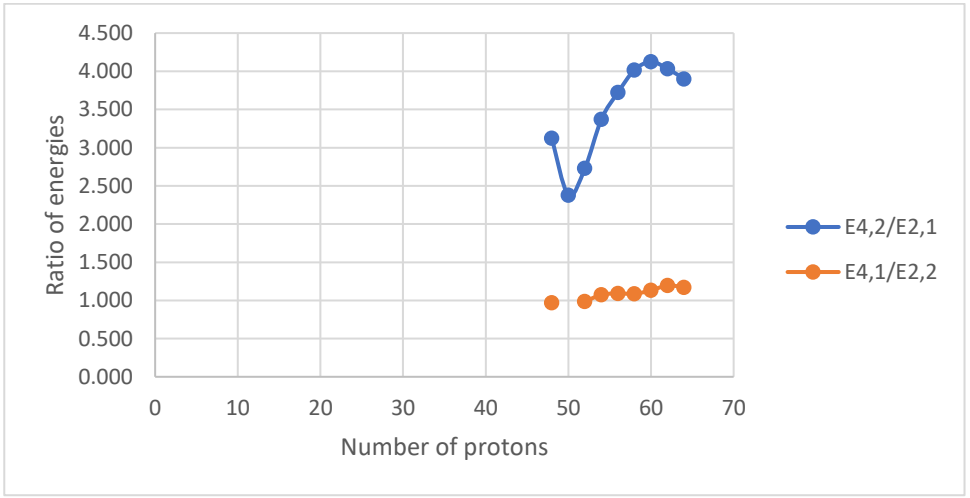

D

Figure V. 38 (color online) Panel **A** represents the comparison of the experimental energy levels of the lowest 2_1^+, 2_2^+, 4_1^+ and 4_2^+ states for the chain of N=76 isotones. Panels **B, C, D** represent the comparison of the experimental energy ratios ($E_{4_1^+}/E_{2_1^+}$ and $E_{4_2^+}/E_{2_2^+}$), ($E_{2_2^+}/E_{2_1^+}$ and $E_{4_2^+}/E_{4_1^+}$) and ($E_{4_2^+}/E_{2_1^+}$ and $E_{4_1^+}/E_{2_2^+}$), respectively, for the chain of N=76 isotones.

Isotones (N=78)

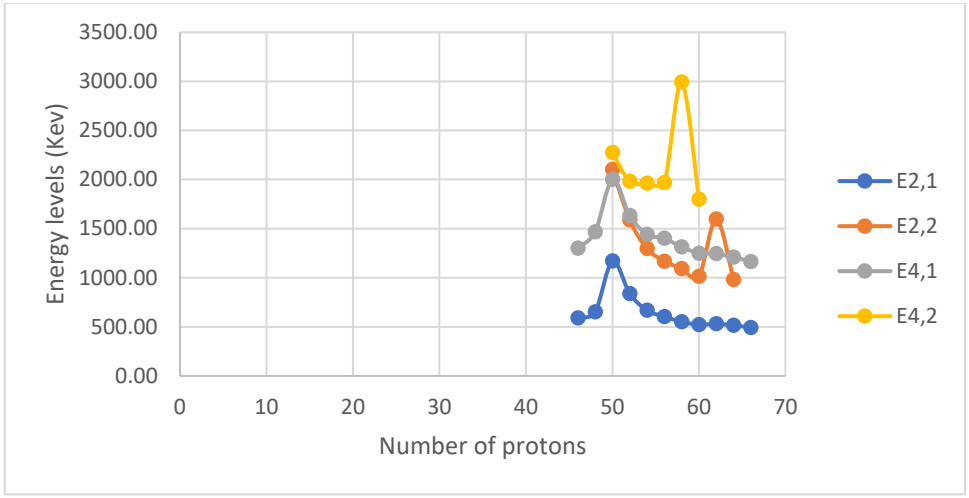

A

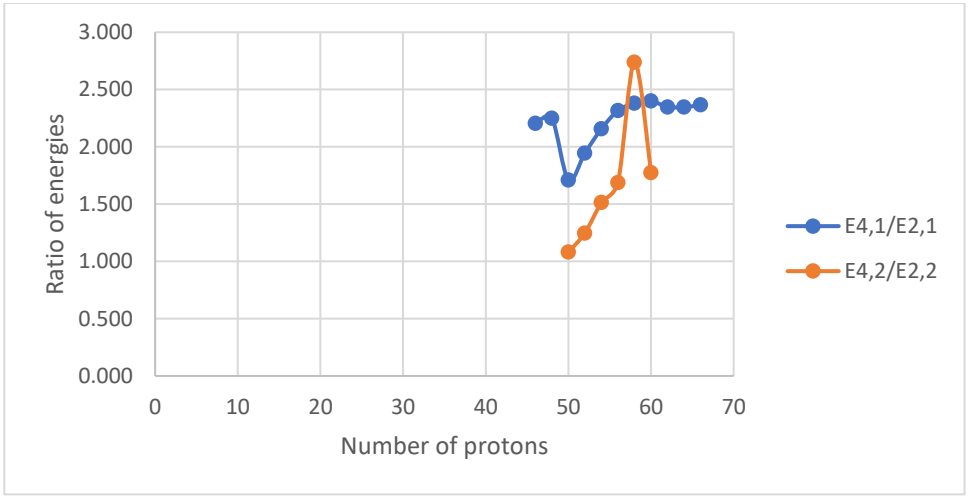

B

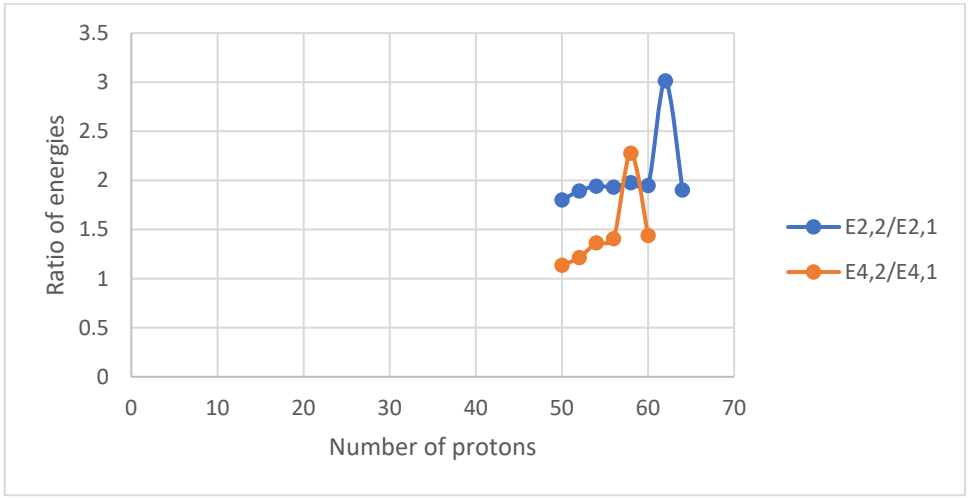

C

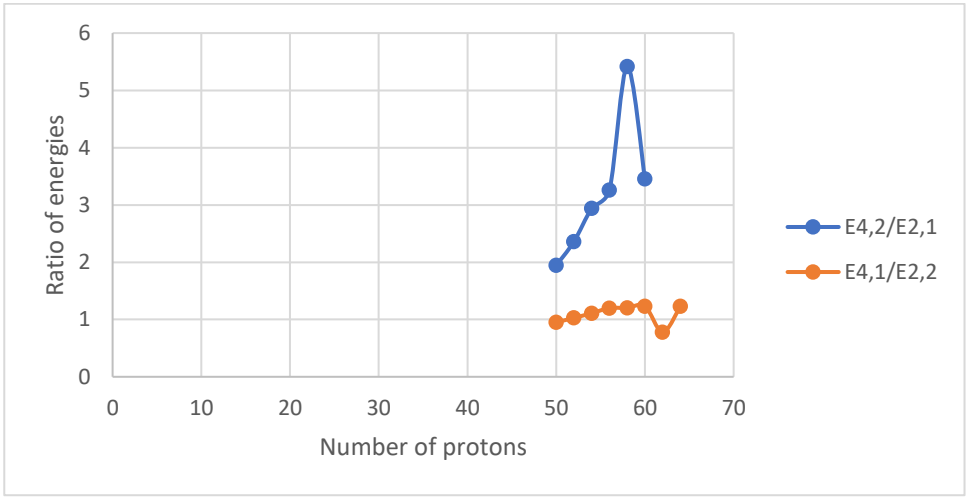

D

Figure V. 39 (color online) Panel **A** represents the comparison of the experimental energy levels of the lowest 2_1^+, 2_2^+, 4_1^+ and 4_2^+ states for the chain of N=78 isotones. Panels **B, C, D** represent the comparison of the experimental energy ratios ($E_{4_1^+}/E_{2_1^+}$ and $E_{4_2^+}/E_{2_2^+}$), ($E_{2_2^+}/E_{2_1^+}$ and $E_{4_2^+}/E_{4_1^+}$) and ($E_{4_2^+}/E_{2_1^+}$ and $E_{4_1^+}/E_{2_2^+}$), respectively, for the chain of N=78 isotones.

Isotones (N=80)

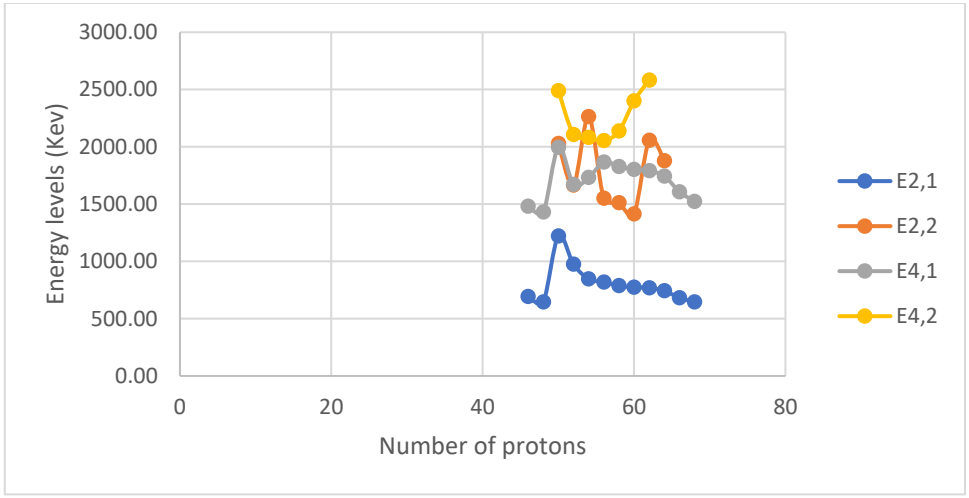

A

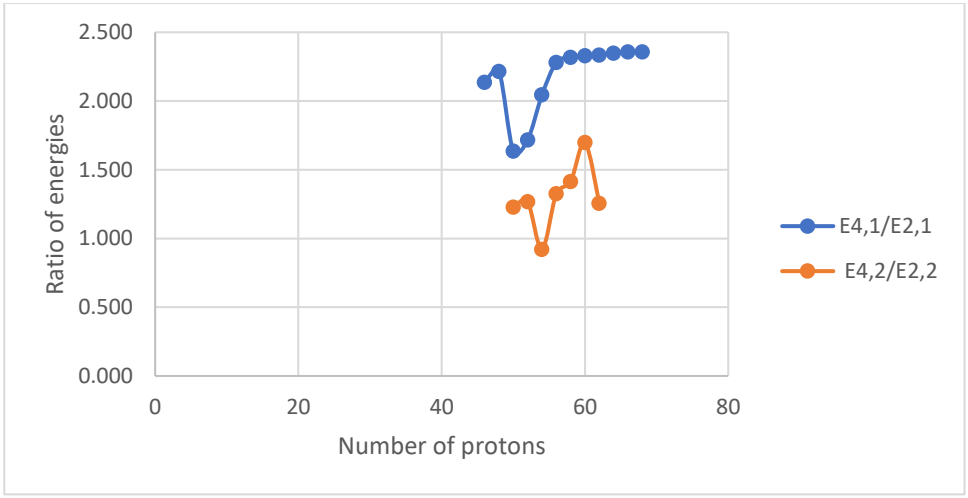

B

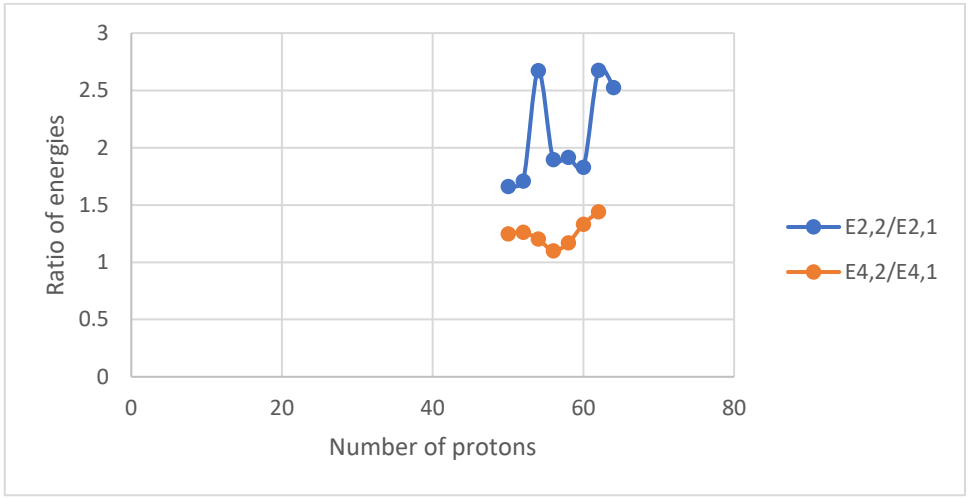

C

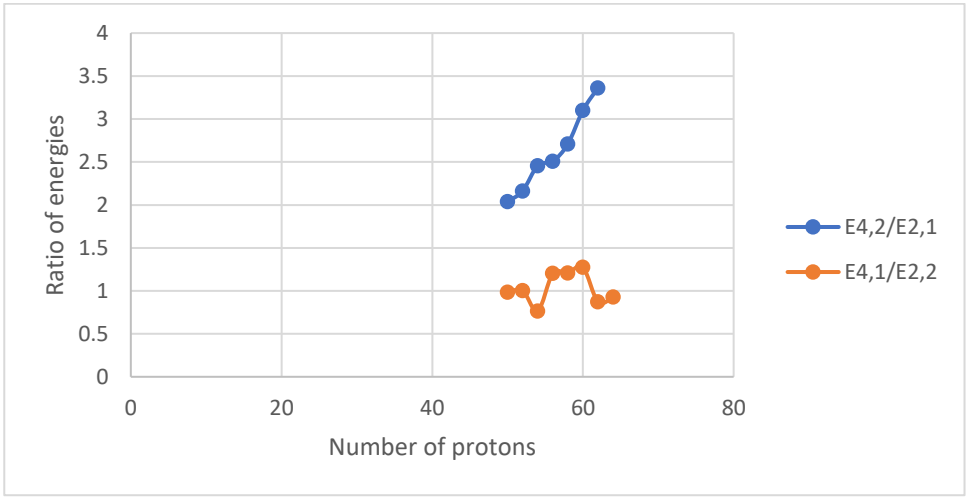

D

Figure V. 40 (color online) Panel **A** represents the comparison of the experimental energy levels of the lowest 2_1^+, 2_2^+, 4_1^+ and 4_2^+ states for the chain of N=80 isotones. Panels **B, C, D** represent the comparison of the experimental energy ratios ($E_{4_1^+}/E_{2_1^+}$ and $E_{4_2^+}/E_{2_2^+}$), ($E_{2_2^+}/E_{2_1^+}$ and $E_{4_2^+}/E_{4_1^+}$) and ($E_{4_2^+}/E_{2_1^+}$ and $E_{4_1^+}/E_{2_2^+}$), respectively, for the chain of N=80 isotones.

Isotones (N=82)

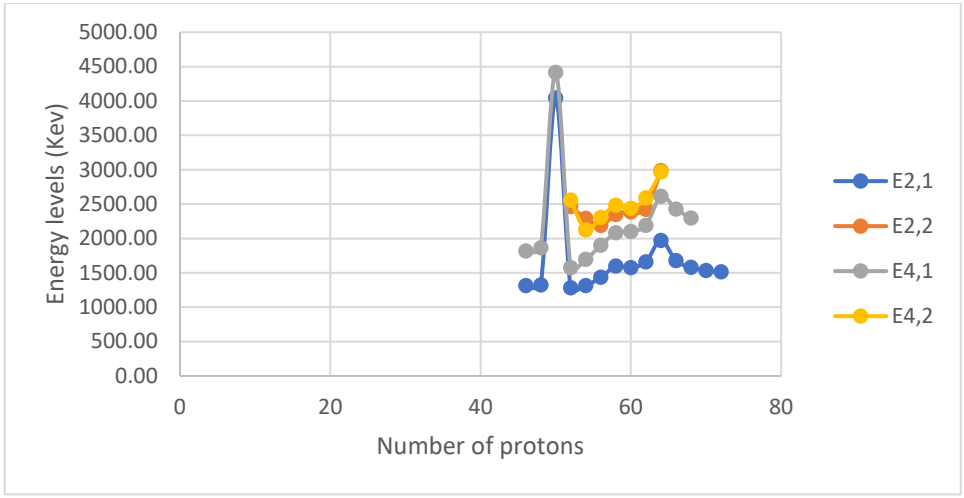

A

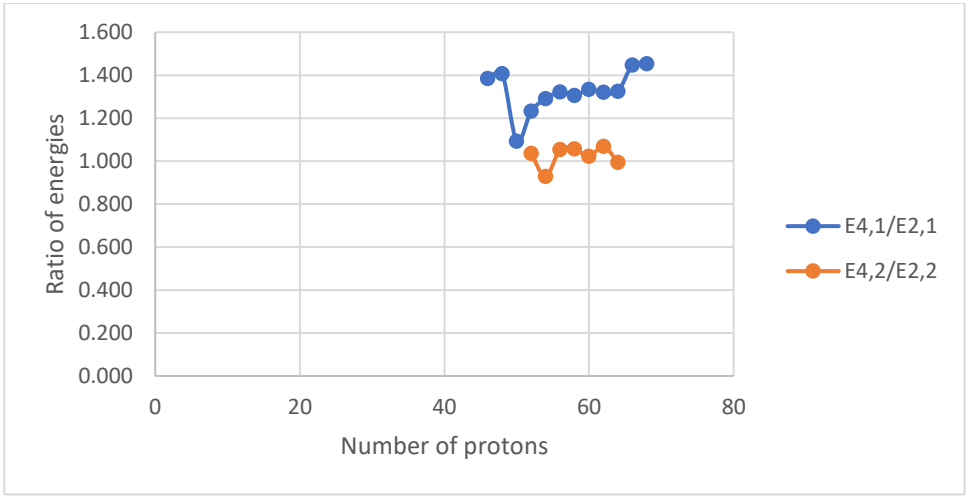

B

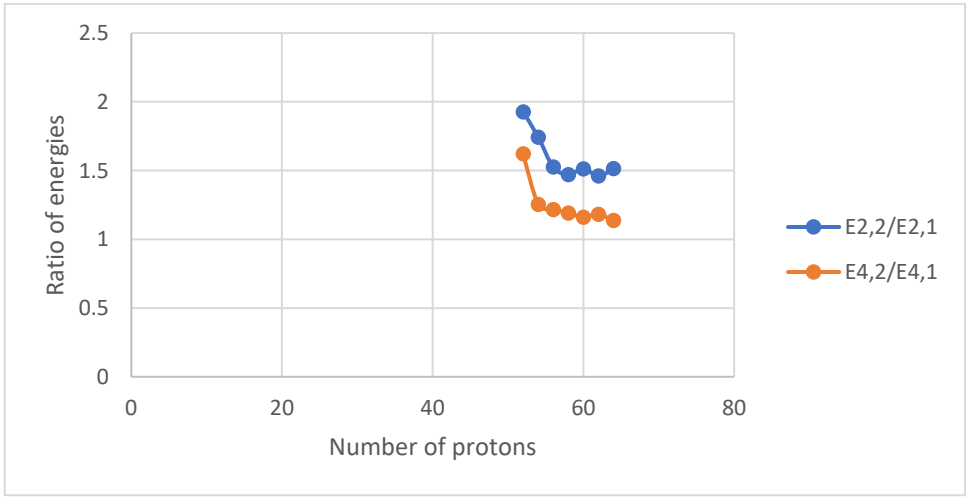

C

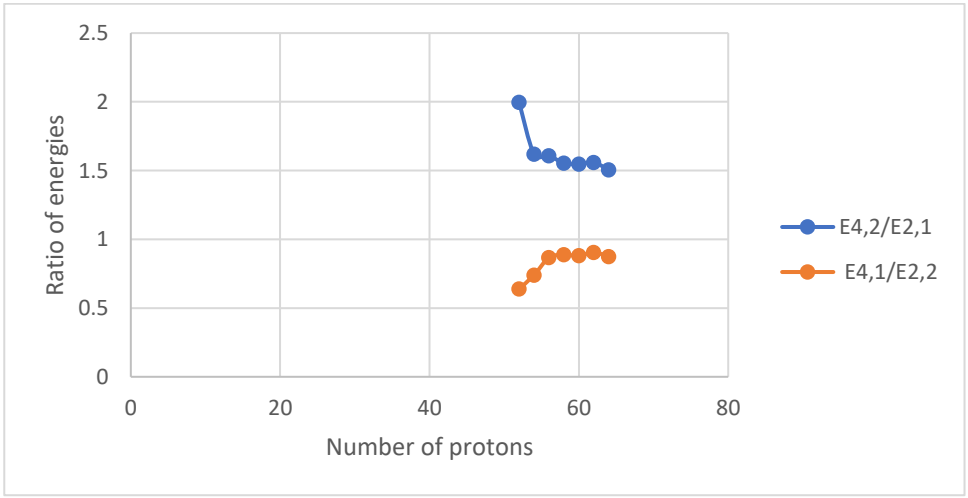

D

Figure V. 41 (color online) Panel **A** represents the comparison of the experimental energy levels of the lowest 2_1^+, 2_2^+, 4_1^+ and 4_2^+ states for the chain of N=82 isotones. Panels **B, C, D** represent the comparison of the experimental energy ratios ($E_{4_1^+}/E_{2_1^+}$ and $E_{4_2^+}/E_{2_2^+}$), ($E_{2_2^+}/E_{2_1^+}$ and $E_{4_2^+}/E_{4_1^+}$) and ($E_{4_2^+}/E_{2_1^+}$ and $E_{4_1^+}/E_{2_2^+}$), respectively, for the chain of N=82 isotones.

Isotones (N=84)

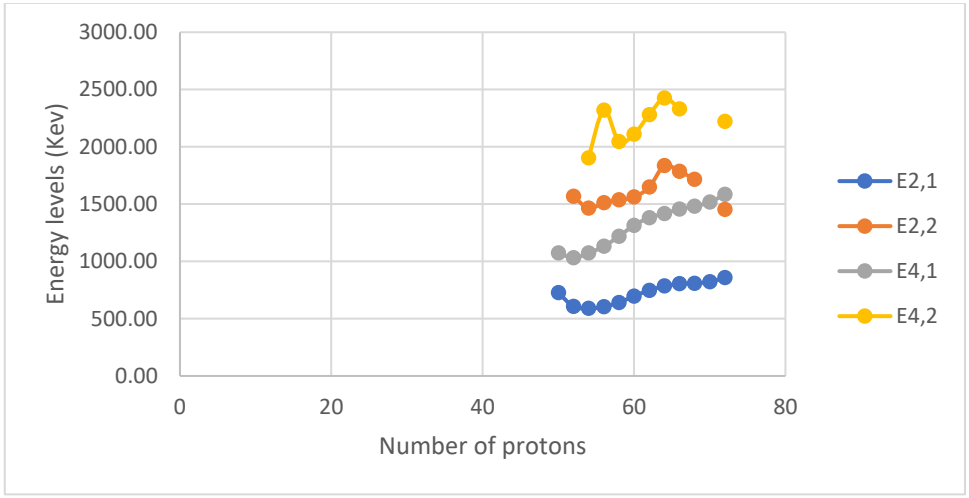

A

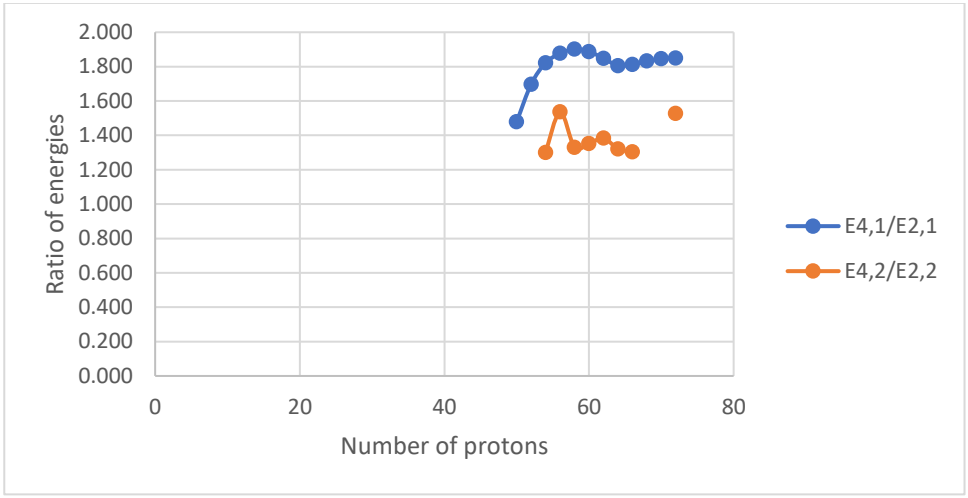

B

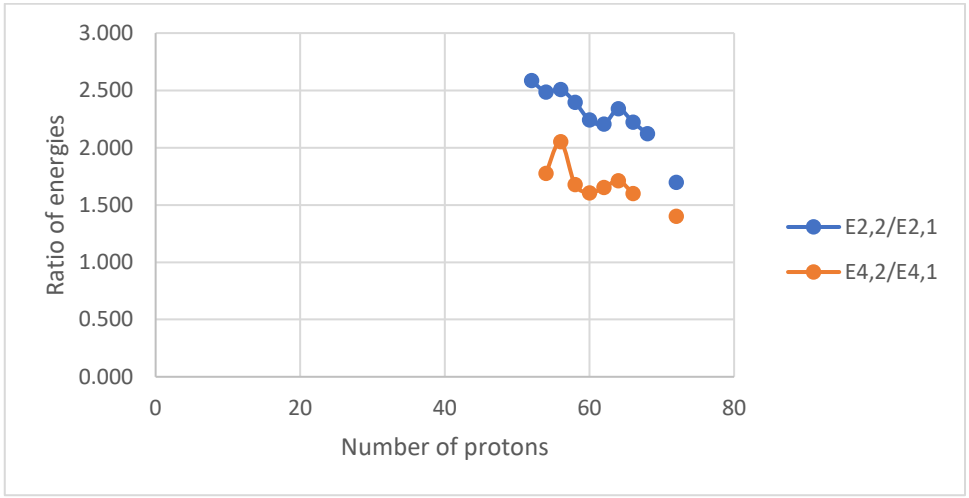

C

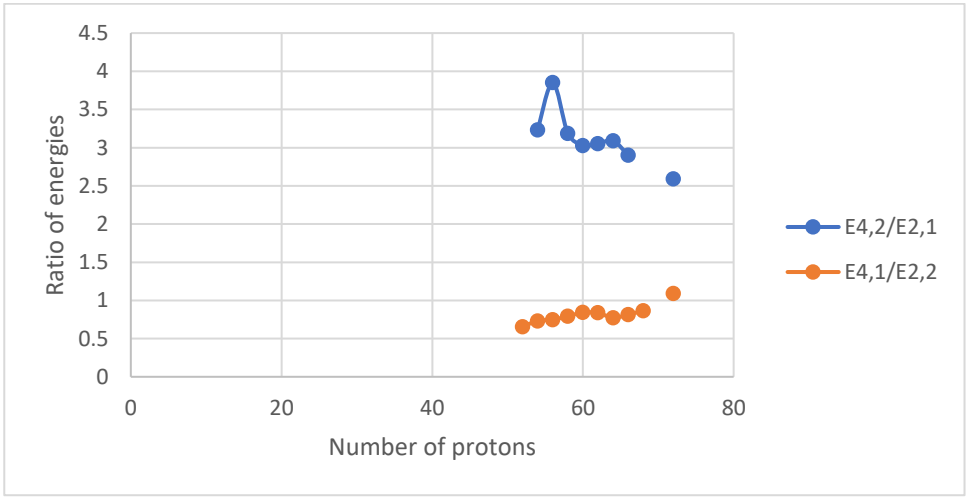

D

Figure V. 42 (color online) Panel **A** represents the comparison of the experimental energy levels of the lowest 2_1^+, 2_2^+, 4_1^+ and 4_2^+ states for the chain of N=84 isotones. Panels **B, C, D** represent the comparison of the experimental energy ratios ($E_{4_1^+}/E_{2_1^+}$ and $E_{4_2^+}/E_{2_2^+}$), ($E_{2_2^+}/E_{2_1^+}$ and $E_{4_2^+}/E_{4_1^+}$) and ($E_{4_2^+}/E_{2_1^+}$ and $E_{4_1^+}/E_{2_2^+}$), respectively, for the chain of N=84 isotones.

Isotones (N=86)

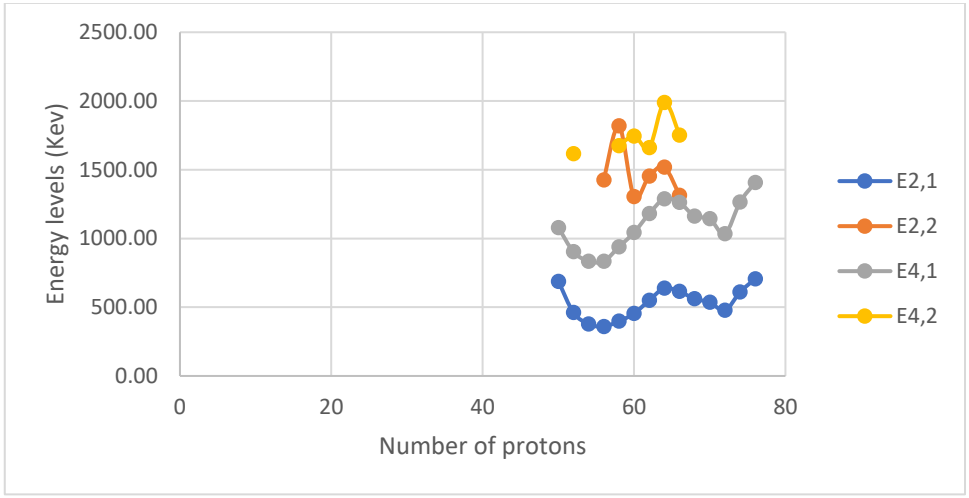

A

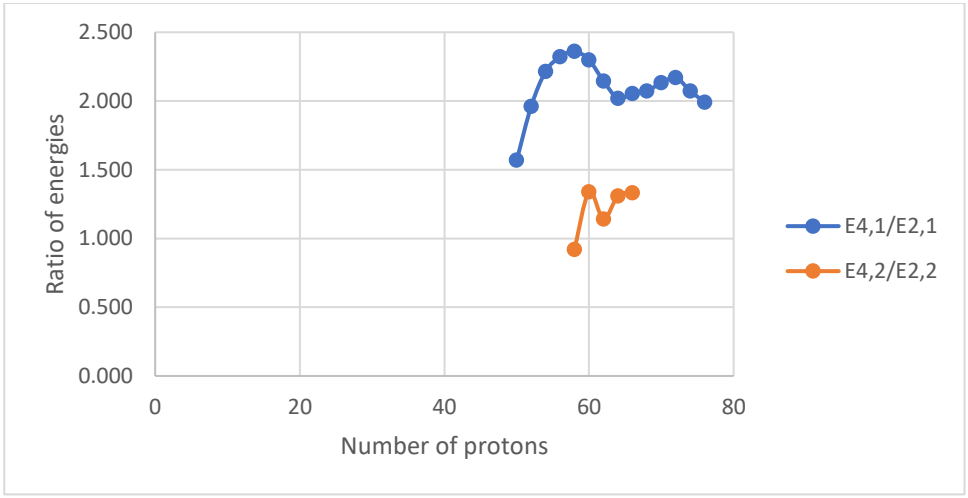

B

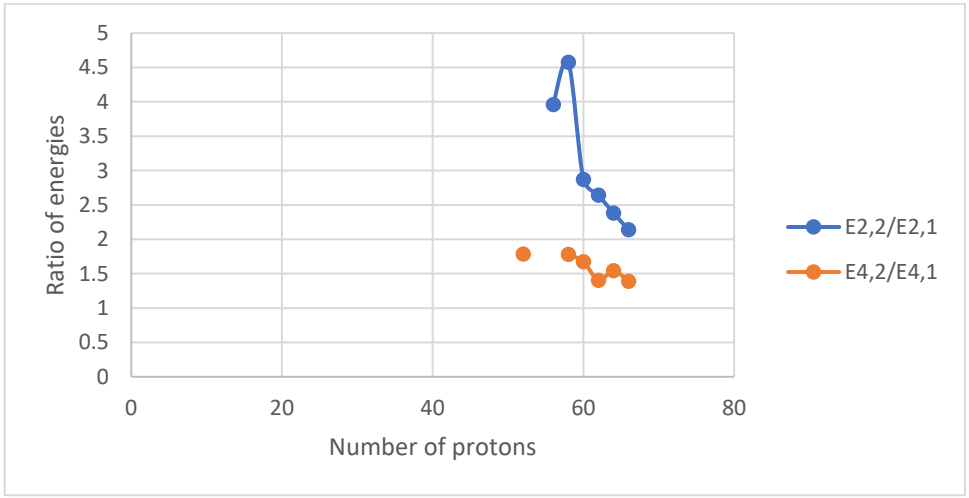

C

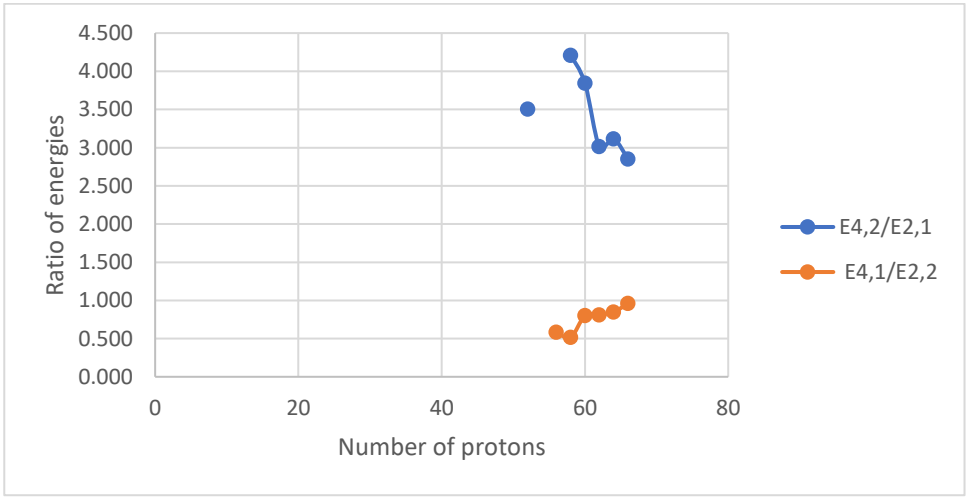

D

Figure V. 43 (color online) Panel **A** represents the comparison of the experimental energy levels of the lowest 2_1^+, 2_2^+, 4_1^+ and 4_2^+ states for the chain of N=86 isotones. Panels **B, C, D** represent the comparison of the experimental energy ratios ($E_{4_1^+}/E_{2_1^+}$ and $E_{4_2^+}/E_{2_2^+}$), ($E_{2_2^+}/E_{2_1^+}$ and $E_{4_2^+}/E_{4_1^+}$) and ($E_{4_2^+}/E_{2_1^+}$ and $E_{4_1^+}/E_{2_2^+}$), respectively, for the chain of N=86 isotones.

Isotones (N=88)

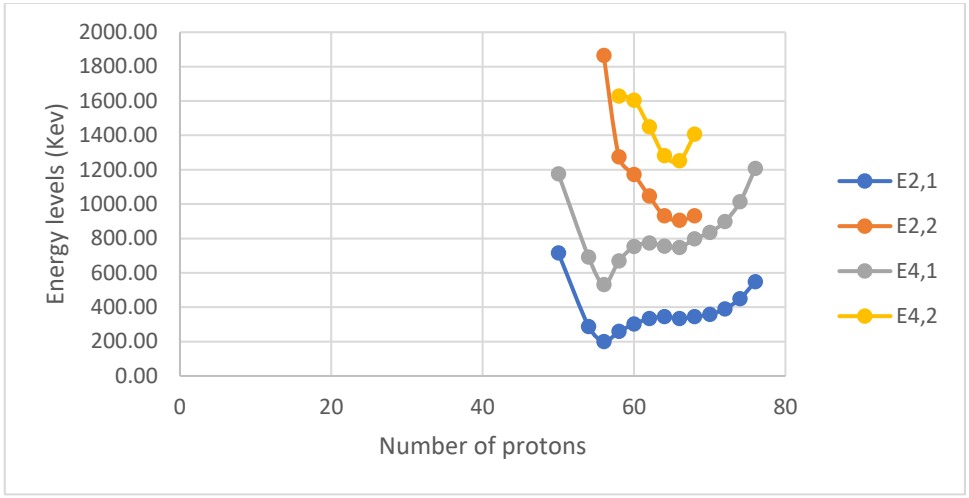

A

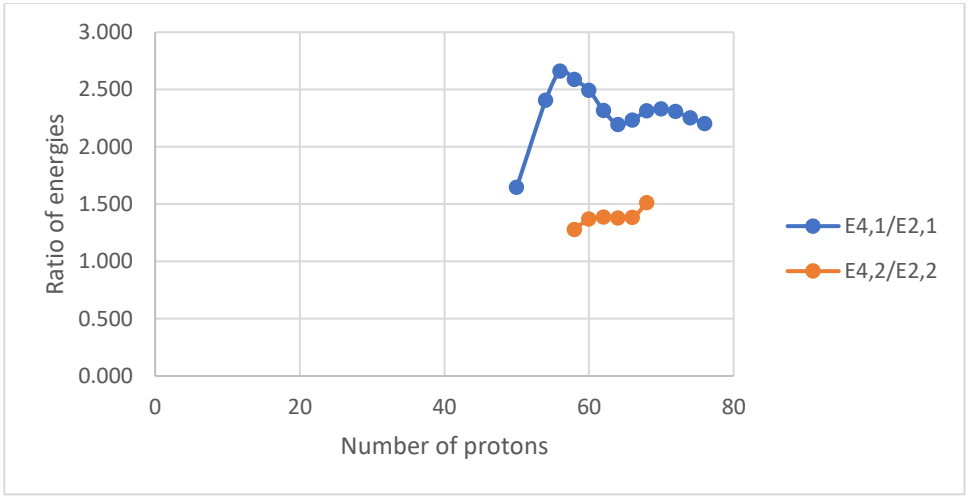

B

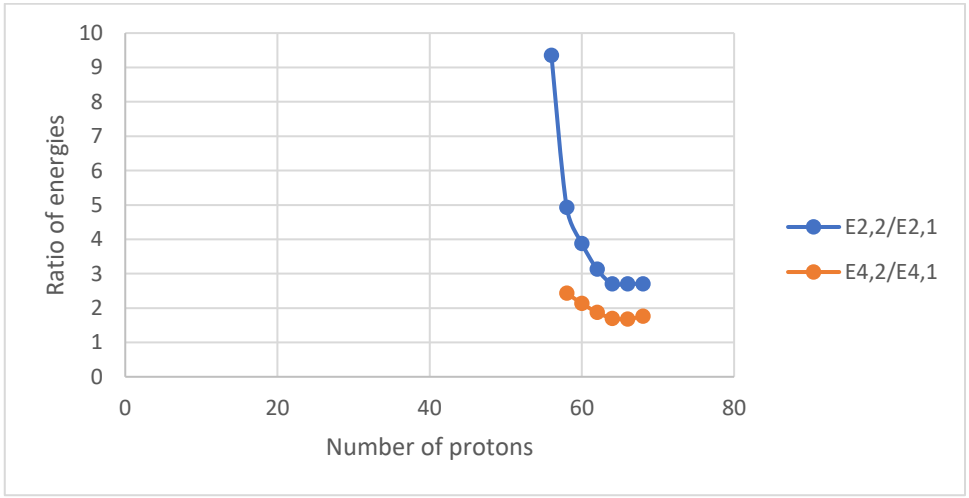

C

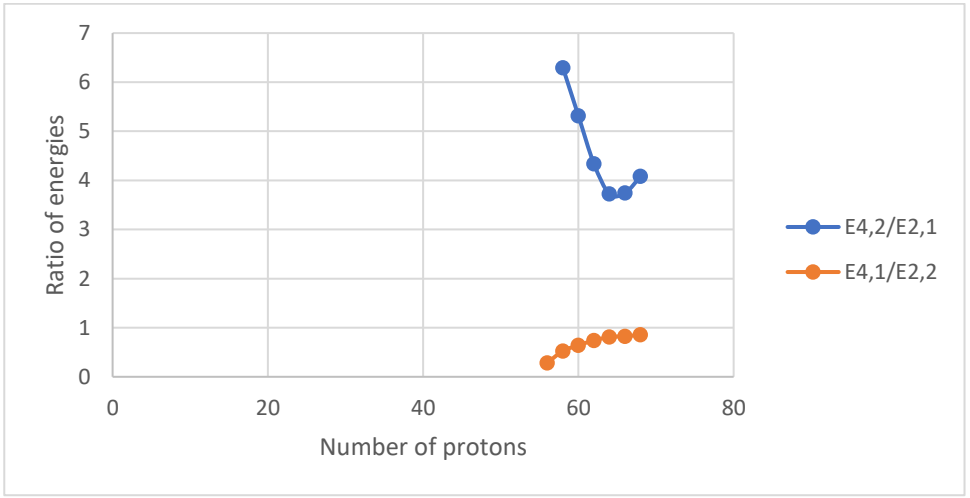

D

Figure V. 44 (color online) Panel **A** represents the comparison of the experimental energy levels of the lowest 2_1^+, 2_2^+, 4_1^+ and 4_2^+ states for the chain of N=88 isotones. Panels **B, C, D** represent the comparison of the experimental energy ratios ($E_{4_1^+}/E_{2_1^+}$ and $E_{4_2^+}/E_{2_2^+}$), ($E_{2_2^+}/E_{2_1^+}$ and $E_{4_2^+}/E_{4_1^+}$) and ($E_{4_2^+}/E_{2_1^+}$ and $E_{4_1^+}/E_{2_2^+}$), respectively, for the chain of N=88 isotones.

Isotones (N=90)

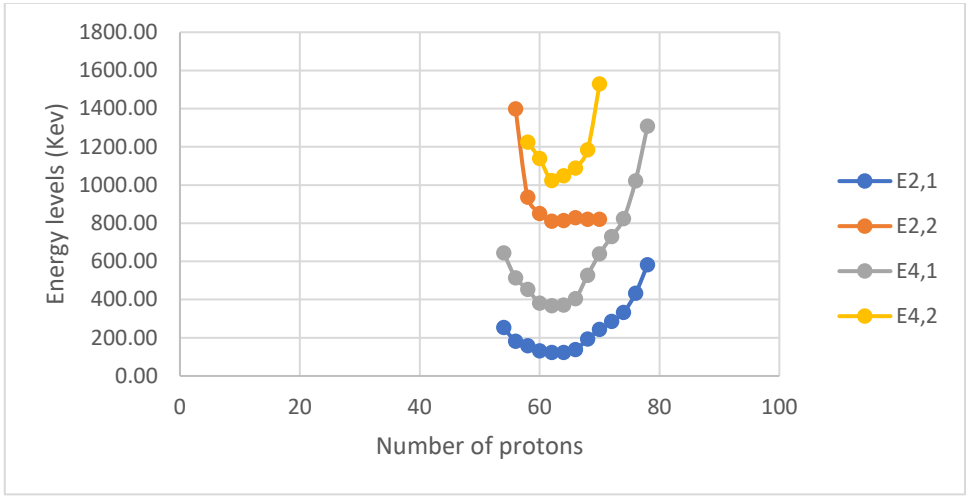

A

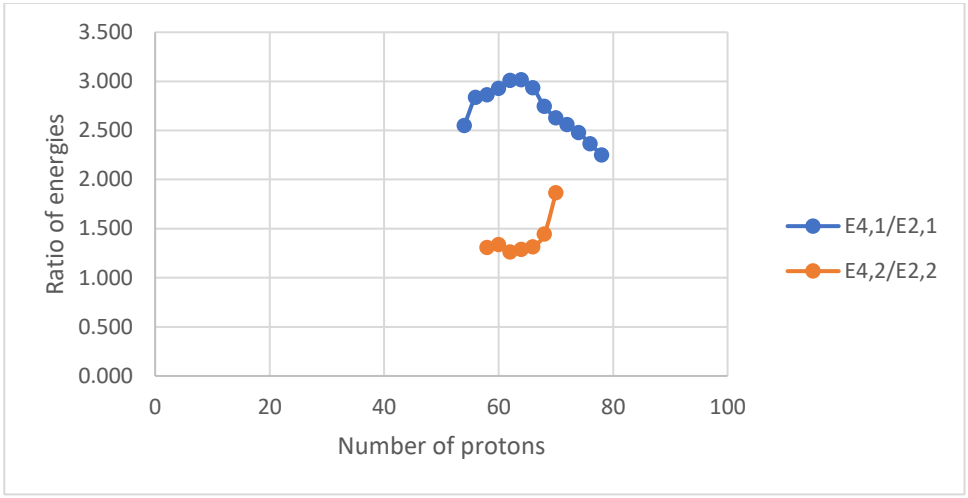

B

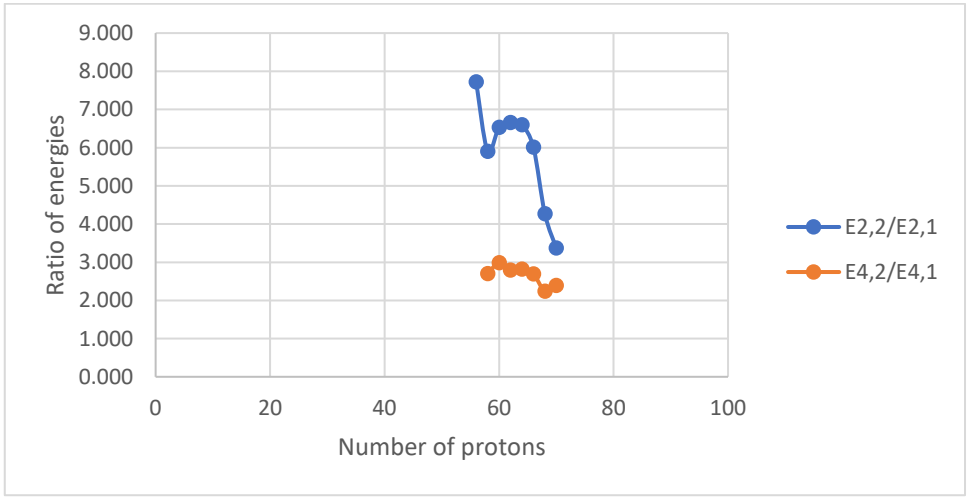

C

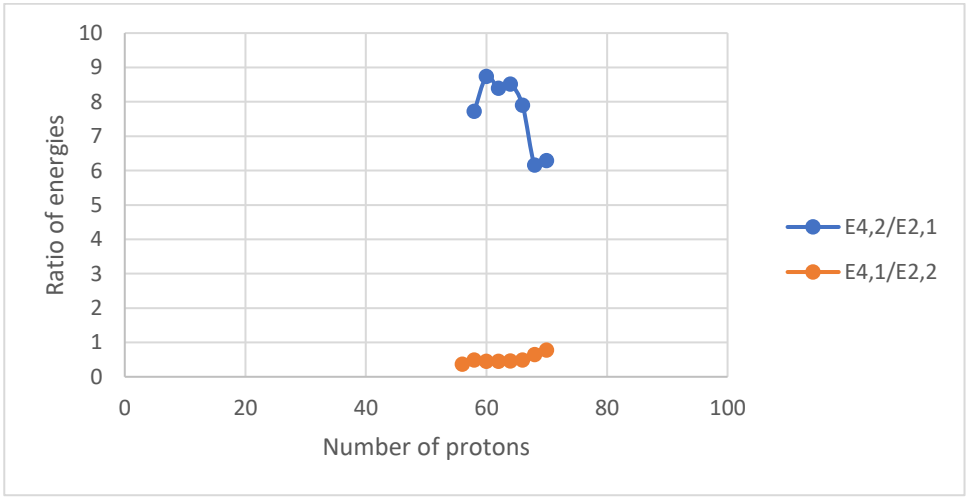

D

Figure V. 45 (color online) Panel **A** represents the comparison of the experimental energy levels of the lowest 2_1^+, 2_2^+, 4_1^+ and 4_2^+ states for the chain of N=90 isotones. Panels **B, C, D** represent the comparison of the experimental energy ratios ($E_{4_1^+}/E_{2_1^+}$ and $E_{4_2^+}/E_{2_2^+}$), ($E_{2_2^+}/E_{2_1^+}$ and $E_{4_2^+}/E_{4_1^+}$) and ($E_{4_2^+}/E_{2_1^+}$ and $E_{4_1^+}/E_{2_2^+}$), respectively, for the chain of N=90 isotones.

Isotones (N=92)

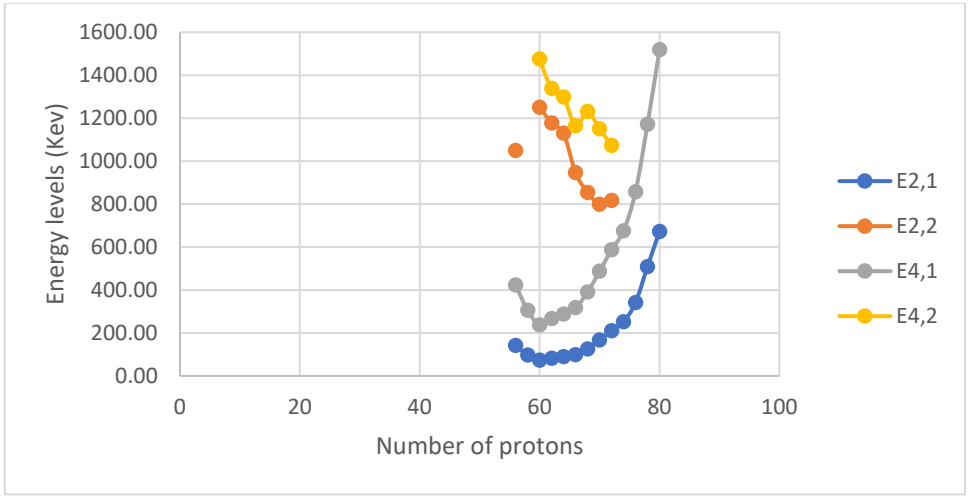

A

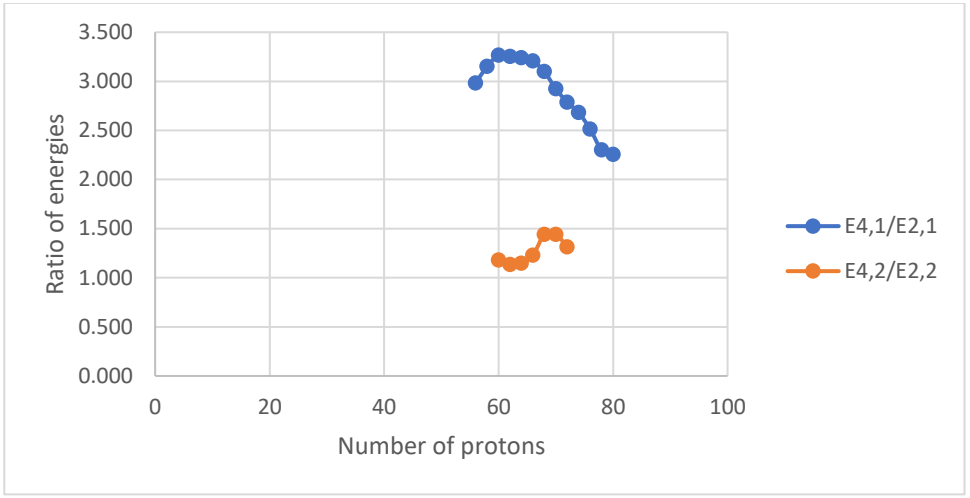

B

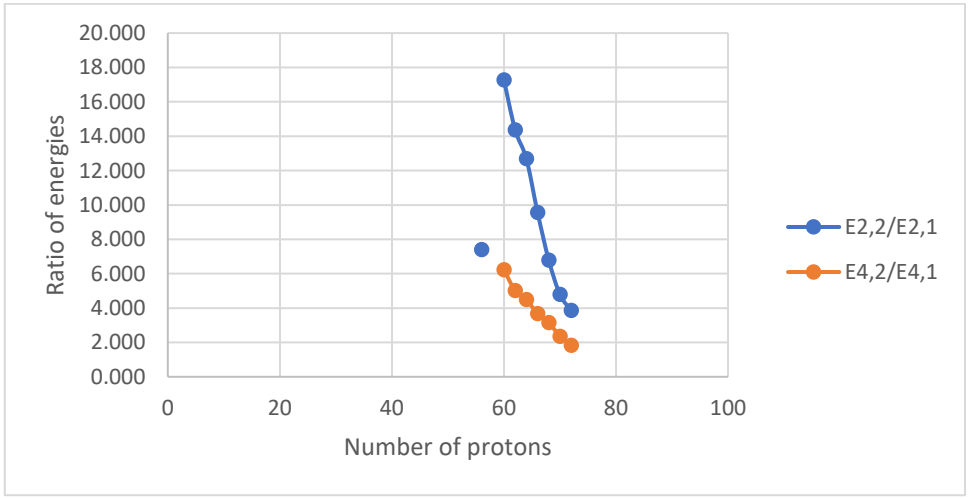

C

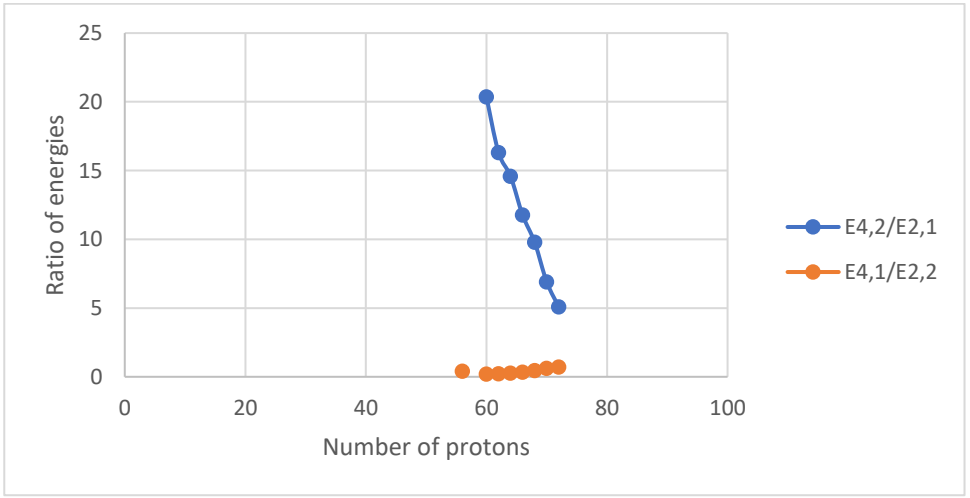

D

Figure V. 46 (color online) Panel **A** represents the comparison of the experimental energy levels of the lowest 2_1^+, 2_2^+, 4_1^+ and 4_2^+ states for the chain of N=92 isotones. Panels **B, C, D** represent the comparison of the experimental energy ratios ($E_{4_1^+}/E_{2_1^+}$ and $E_{4_2^+}/E_{2_2^+}$), ($E_{2_2^+}/E_{2_1^+}$ and $E_{4_2^+}/E_{4_1^+}$) and ($E_{4_2^+}/E_{2_1^+}$ and $E_{4_1^+}/E_{2_2^+}$), respectively, for the chain of N=92 isotones.

Isotones (N=94)

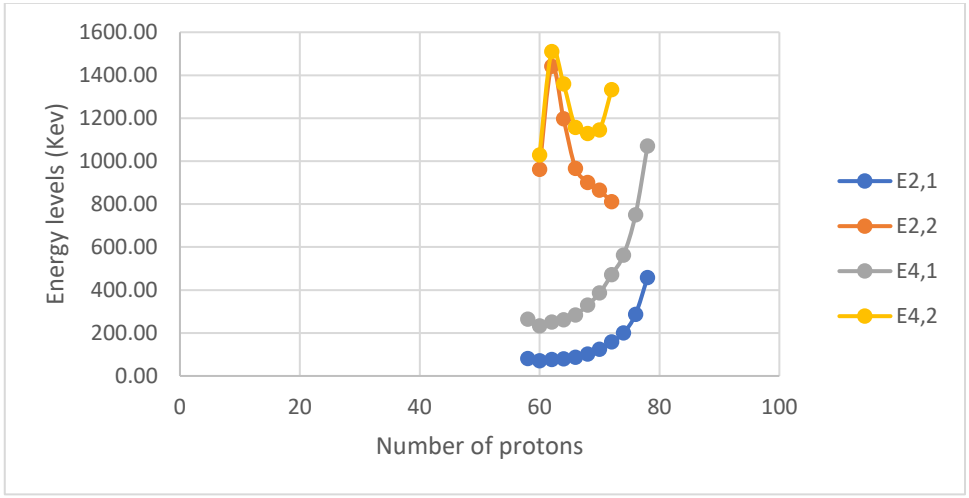

A

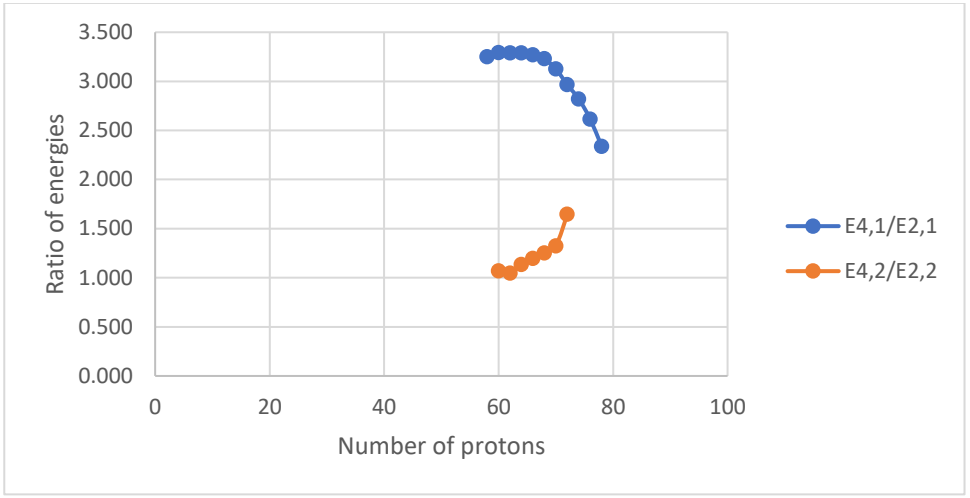

B

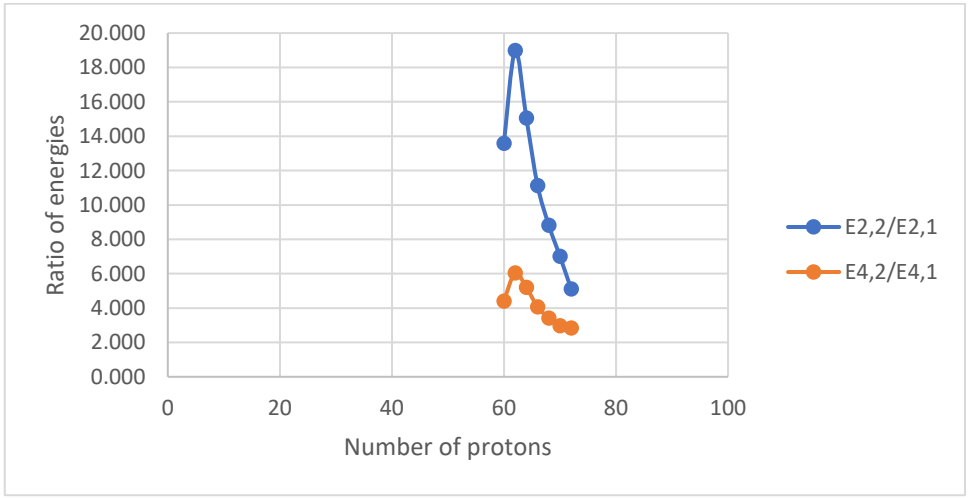

C

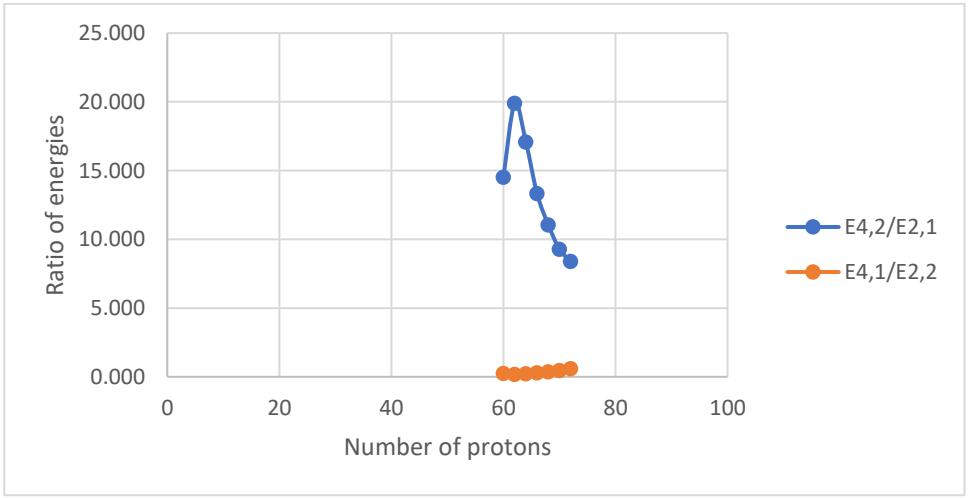

D

Figure V. 47 (color online) Panel **A** represents the comparison of the experimental energy levels of the lowest 2_1^+, 2_2^+, 4_1^+ and 4_2^+ states for the chain of N=94 isotones. Panels **B, C, D** represent the comparison of the experimental energy ratios ($E_{4_1^+}/E_{2_1^+}$ and $E_{4_2^+}/E_{2_2^+}$), ($E_{2_2^+}/E_{2_1^+}$ and $E_{4_2^+}/E_{4_1^+}$) and ($E_{4_2^+}/E_{2_1^+}$ and $E_{4_1^+}/E_{2_2^+}$), respectively, for the chain of N=94 isotones.

Isotones (N=96)

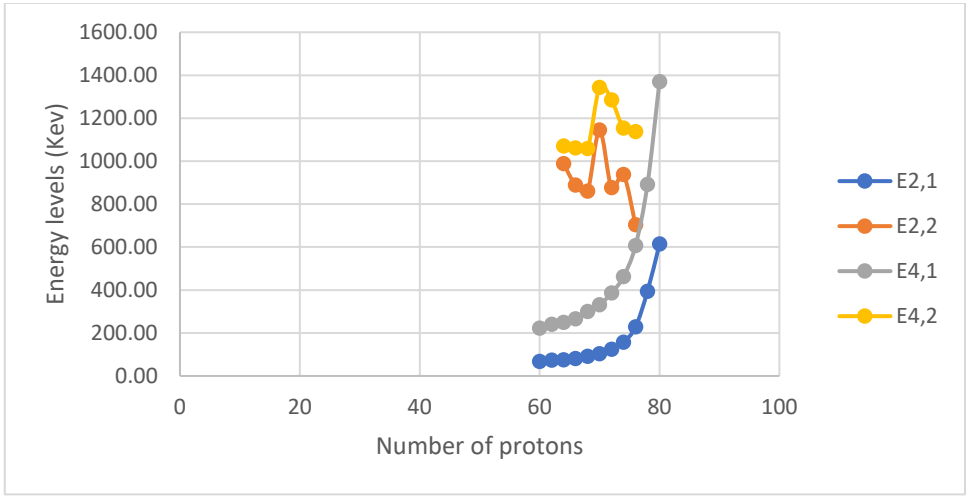

A

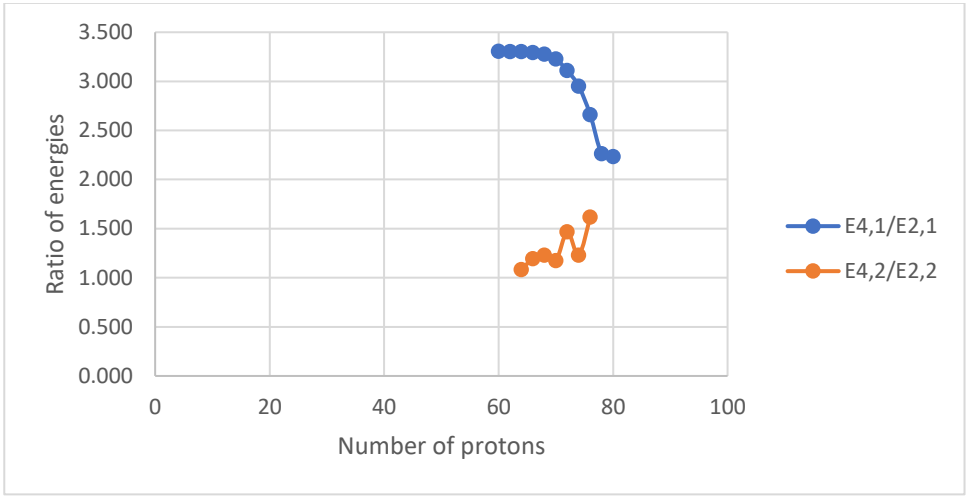

B

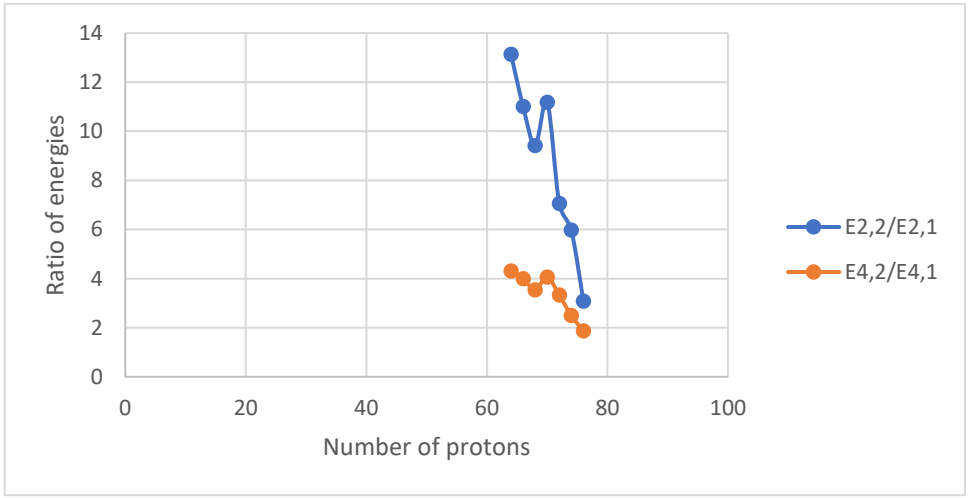

C

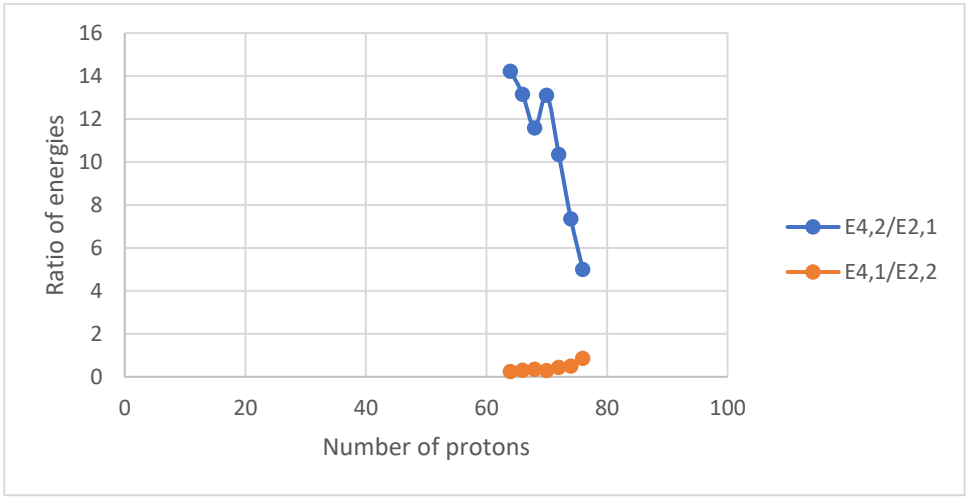

D

Figure V. 48 (color online) Panel **A** represents the comparison of the experimental energy levels of the lowest 2_1^+, 2_2^+, 4_1^+ and 4_2^+ states for the chain of N=96 isotones. Panels **B, C, D** represent the comparison of the experimental energy ratios ($E_{4_1^+}/E_{2_1^+}$ and $E_{4_2^+}/E_{2_2^+}$), ($E_{2_2^+}/E_{2_1^+}$ and $E_{4_2^+}/E_{4_1^+}$) and ($E_{4_2^+}/E_{2_1^+}$ and $E_{4_1^+}/E_{2_2^+}$), respectively, for the chain of N=96 isotones.

Isotones (N=98)

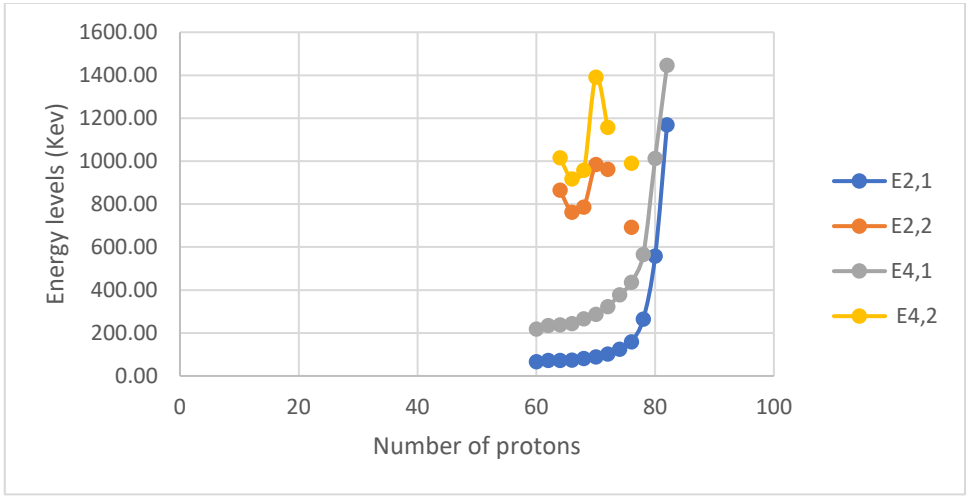

A

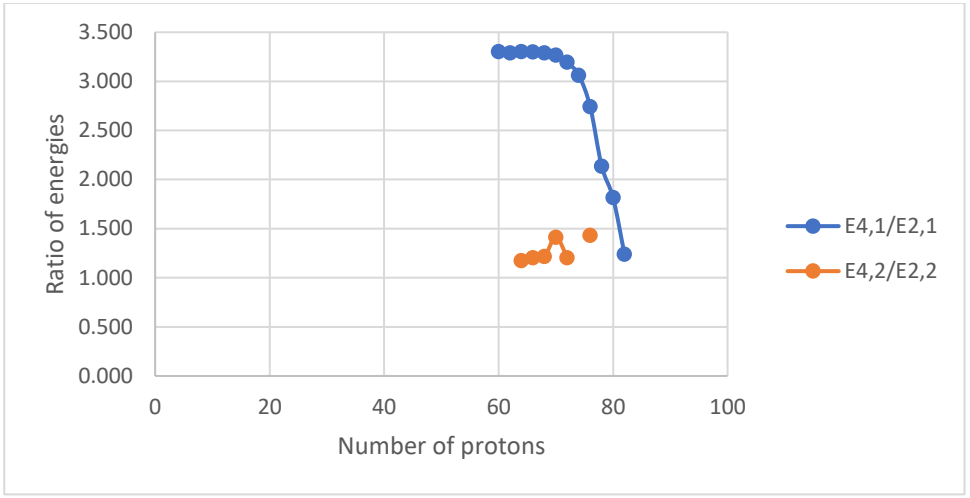

B

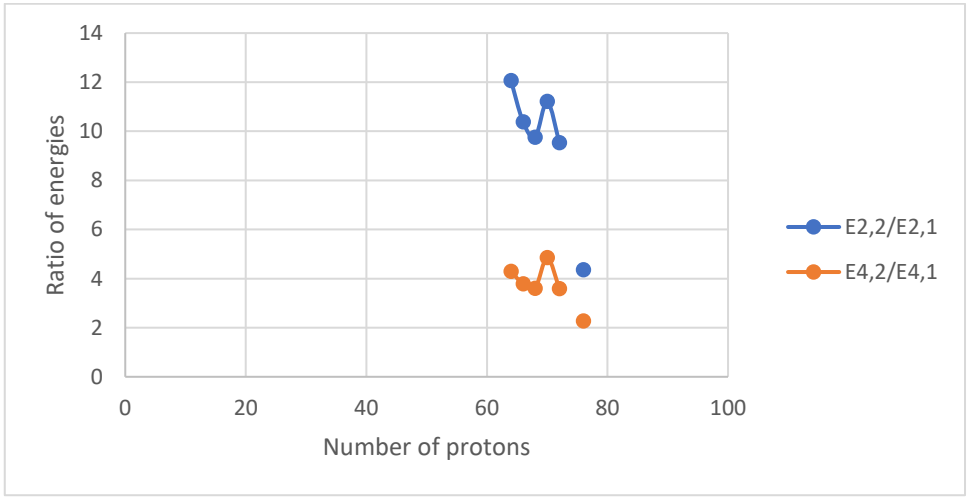

C

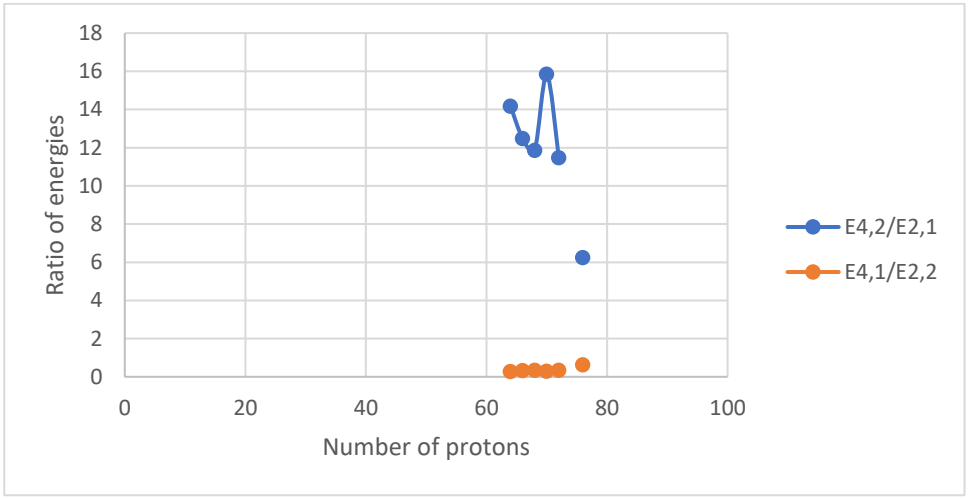

D

Figure V. 49 (color online) Panel **A** represents the comparison of the experimental energy levels of the lowest 2_1^+, 2_2^+, 4_1^+ and 4_2^+ states for the chain of N=98 isotones. Panels **B, C, D** represent the comparison of the experimental energy ratios ($E_{4_1^+}/E_{2_1^+}$ and $E_{4_2^+}/E_{2_2^+}$), ($E_{2_2^+}/E_{2_1^+}$ and $E_{4_2^+}/E_{4_1^+}$) and ($E_{4_2^+}/E_{2_1^+}$ and $E_{4_1^+}/E_{2_2^+}$), respectively, for the chain of N=98 isotones.

Isotones (N=100)

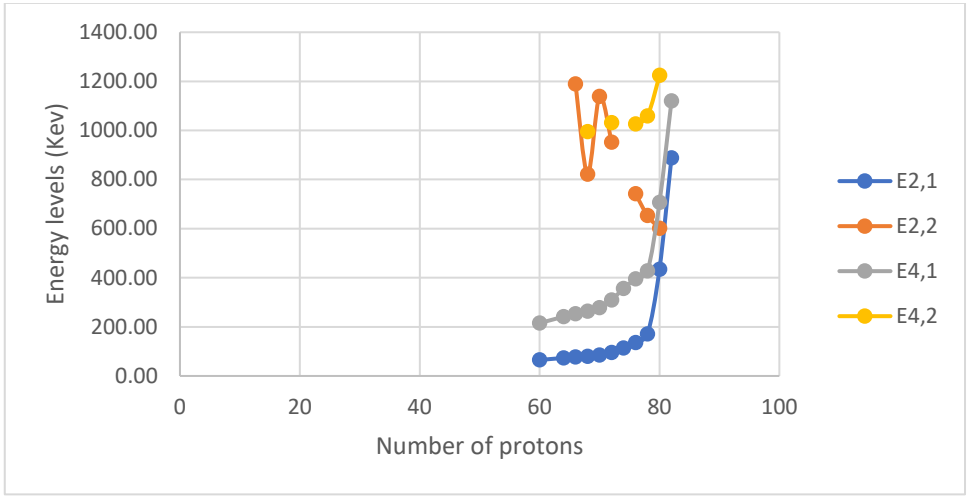

A

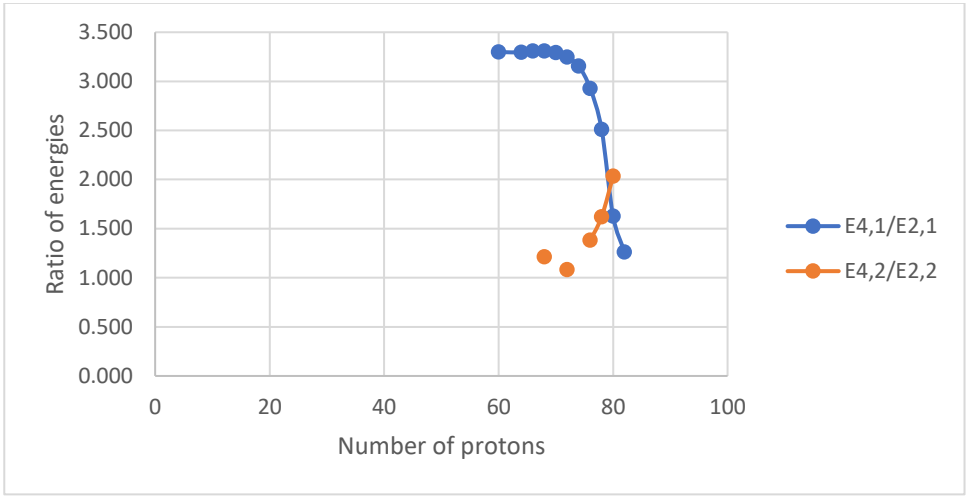

B

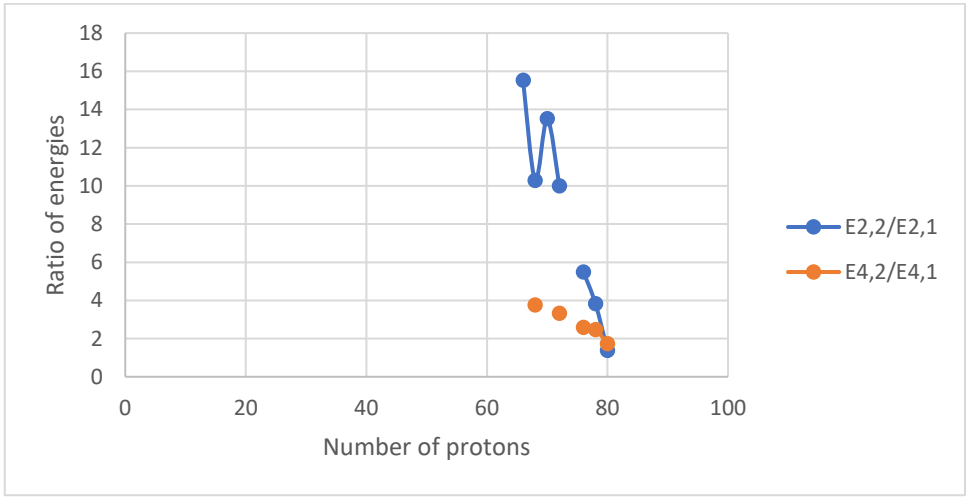

C

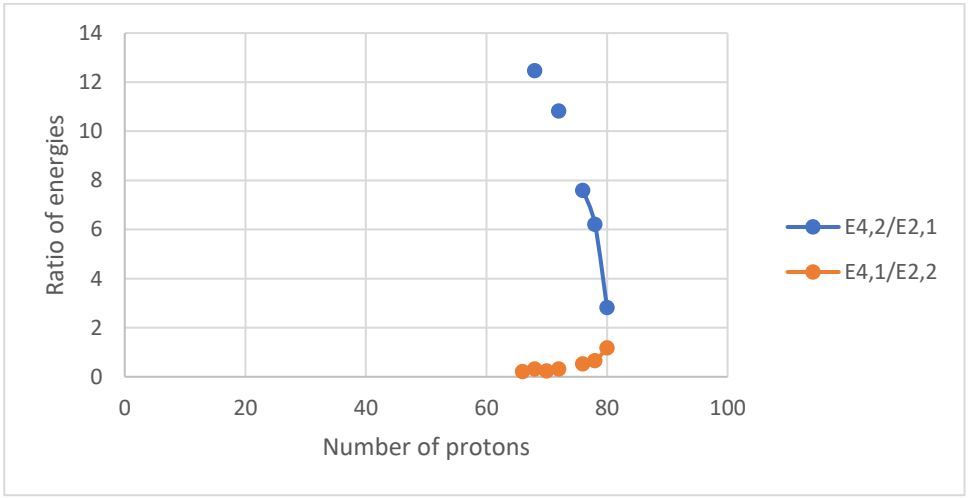

D

Figure V. 50 (color online) Panel **A** represents the comparison of the experimental energy levels of the lowest 2_1^+, 2_2^+, 4_1^+ and 4_2^+ states for the chain of N=100 isotones. Panels **B, C, D** represent the comparison of the experimental energy ratios ($E_{4_1^+}/E_{2_1^+}$ and $E_{4_2^+}/E_{2_2^+}$), ($E_{2_2^+}/E_{2_1^+}$ and $E_{4_2^+}/E_{4_1^+}$) and ($E_{4_2^+}/E_{2_1^+}$ and $E_{4_1^+}/E_{2_2^+}$), respectively, for the chain of N=100 isotones.

Isotones (N=102)

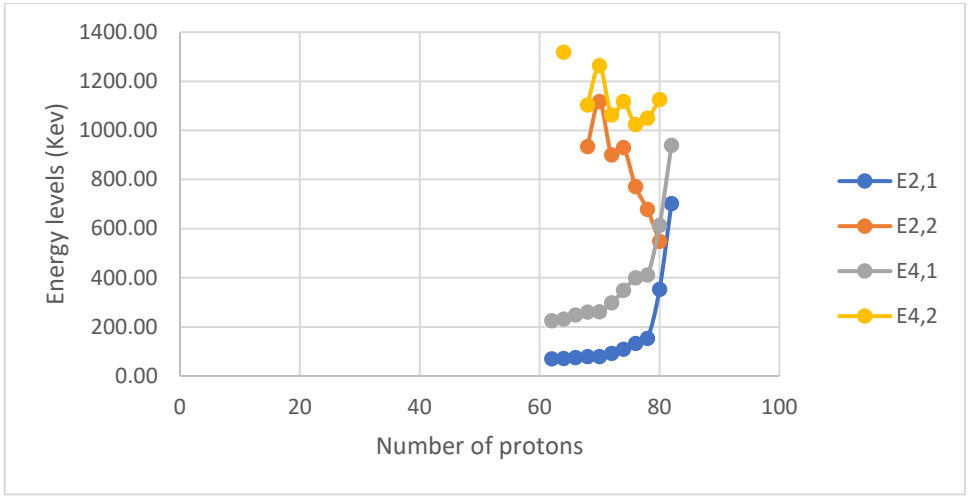

A

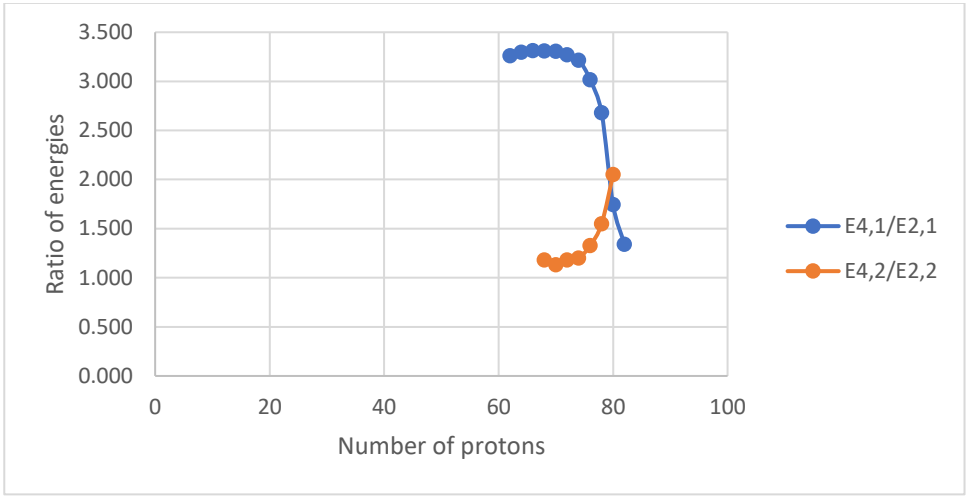

B

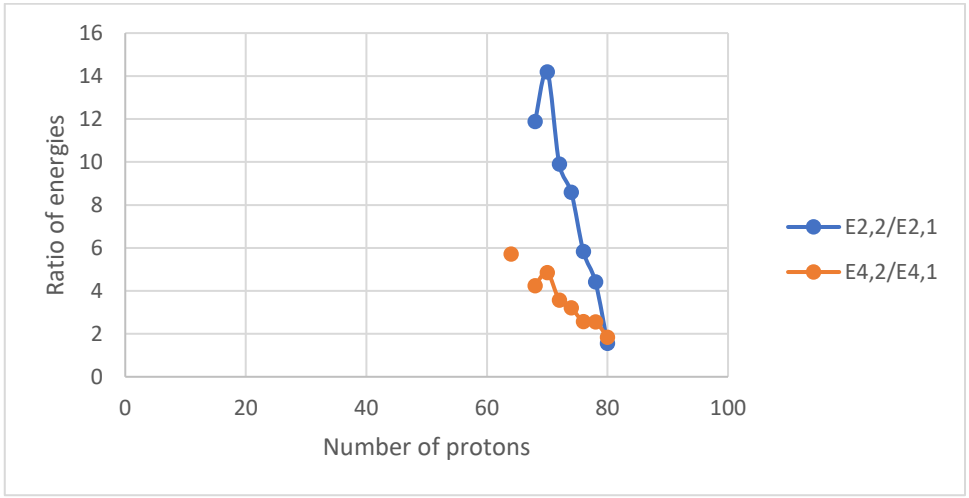

C

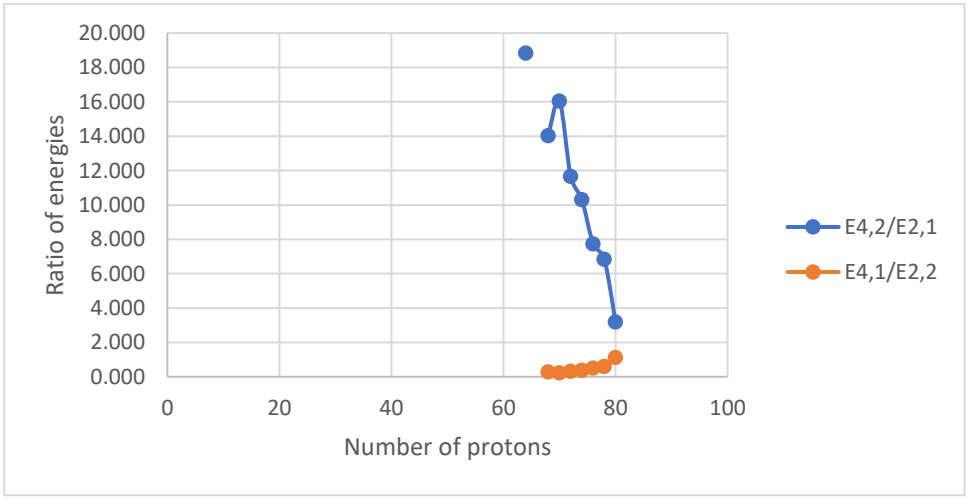

D

Figure V. 51 (color online) Panel **A** represents the comparison of the experimental energy levels of the lowest 2_1^+, 2_2^+, 4_1^+ and 4_2^+ states for the chain of N=102 isotones. Panels **B, C, D** represent the comparison of the experimental energy ratios ($E_{4_1^+}/E_{2_1^+}$ and $E_{4_2^+}/E_{2_2^+}$), ($E_{2_2^+}/E_{2_1^+}$ and $E_{4_2^+}/E_{4_1^+}$) and ($E_{4_2^+}/E_{2_1^+}$ and $E_{4_1^+}/E_{2_2^+}$), respectively, for the chain of N=102 isotones.

Isotones (N=104)

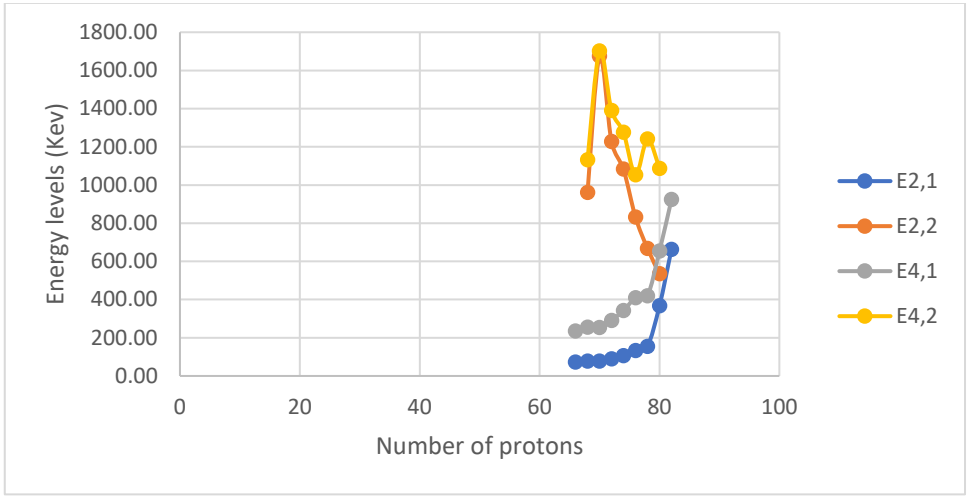

A

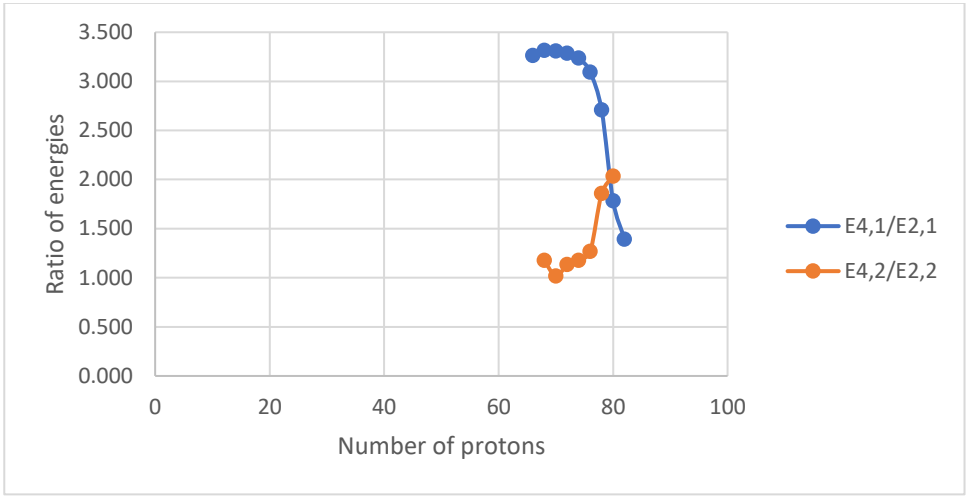

B

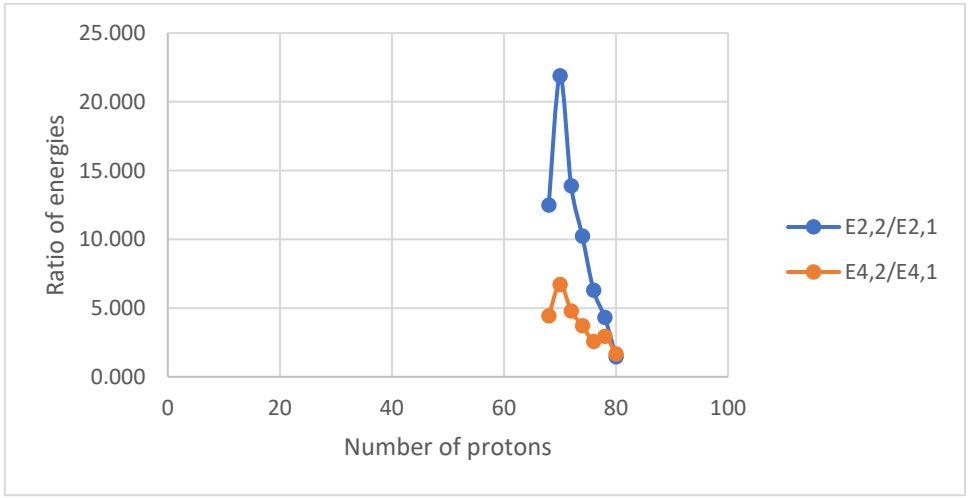

C

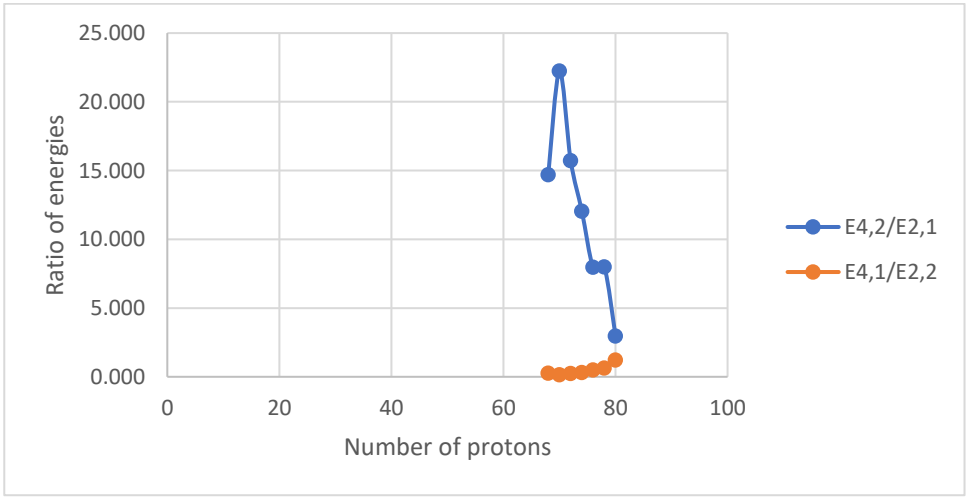

D

Figure V. 52 (color online) Panel **A** represents the comparison of the experimental energy levels of the lowest 2_1^+, 2_2^+, 4_1^+ and 4_2^+ states for the chain of N=104 isotones. Panels **B, C, D** represent the comparison of the experimental energy ratios ($E_{4_1^+}/E_{2_1^+}$ and $E_{4_2^+}/E_{2_2^+}$), ($E_{2_2^+}/E_{2_1^+}$ and $E_{4_2^+}/E_{4_1^+}$) and ($E_{4_2^+}/E_{2_1^+}$ and $E_{4_1^+}/E_{2_2^+}$), respectively, for the chain of N=104 isotones.

Isotones (N=106)

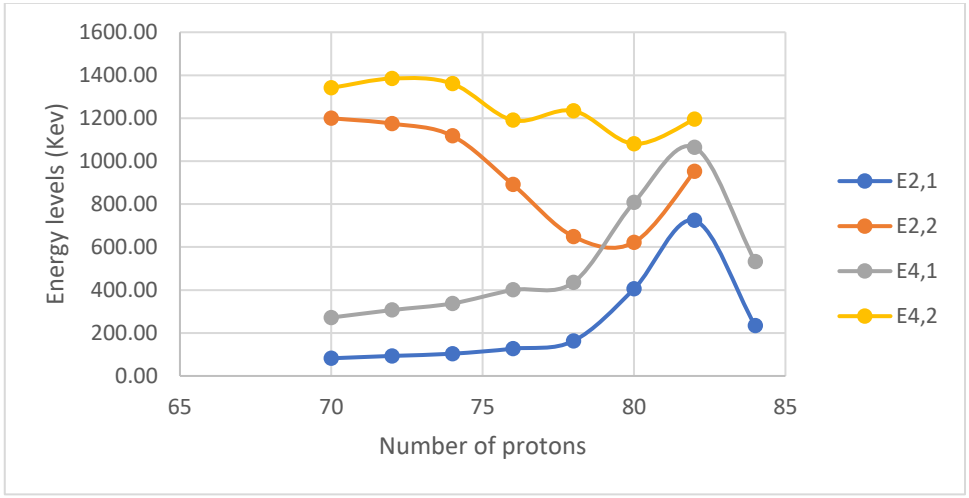

A

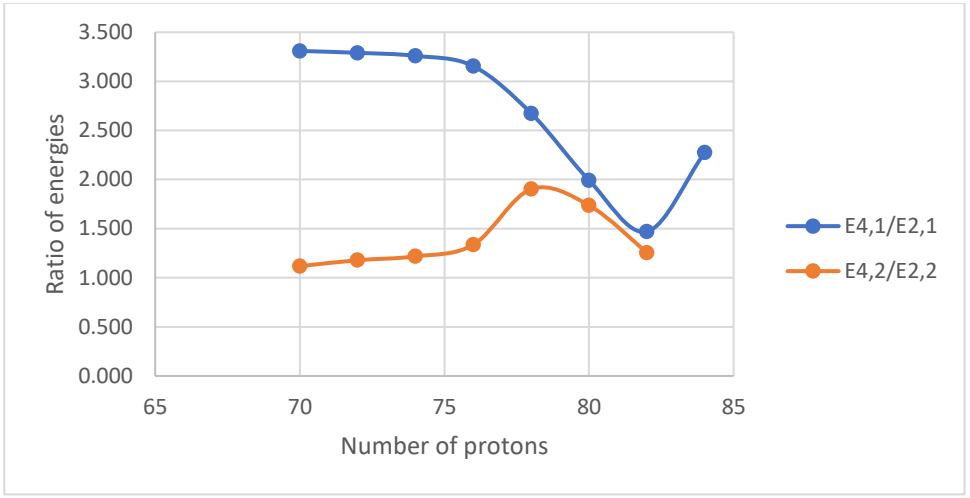

B

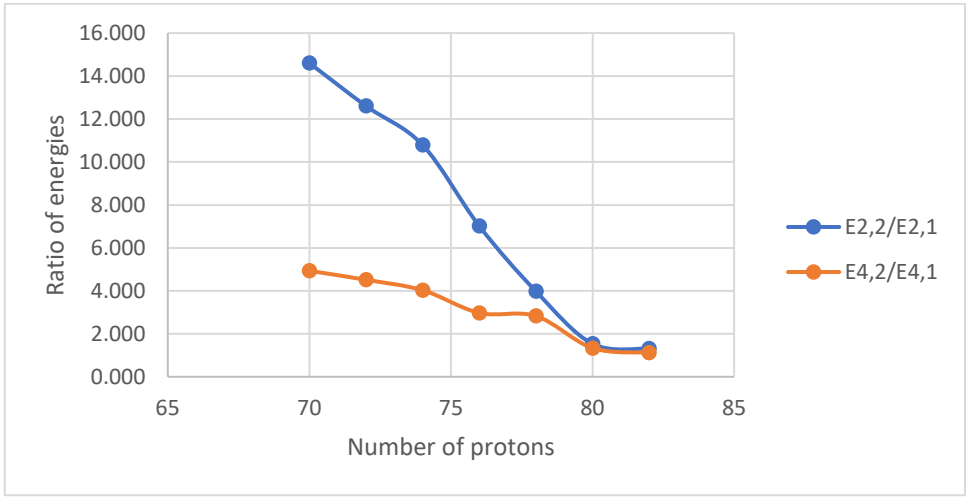

C

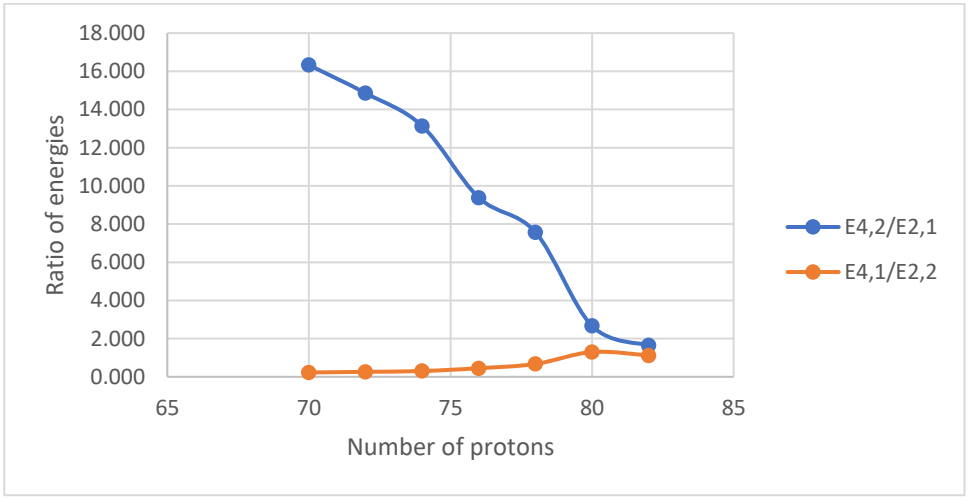

D

Figure V. 53 (color online) Panel **A** represents the comparison of the experimental energy levels of the lowest 2_1^+, 2_2^+, 4_1^+ and 4_2^+ states for the chain of N=106 isotones. Panels **B, C, D** represent the comparison of the experimental energy ratios ($E_{4_1^+}/E_{2_1^+}$ and $E_{4_2^+}/E_{2_2^+}$), ($E_{2_2^+}/E_{2_1^+}$ and $E_{4_2^+}/E_{4_1^+}$) and ($E_{4_2^+}/E_{2_1^+}$ and $E_{4_1^+}/E_{2_2^+}$), respectively, for the chain of N=106 isotones.

Isotones (N=108)

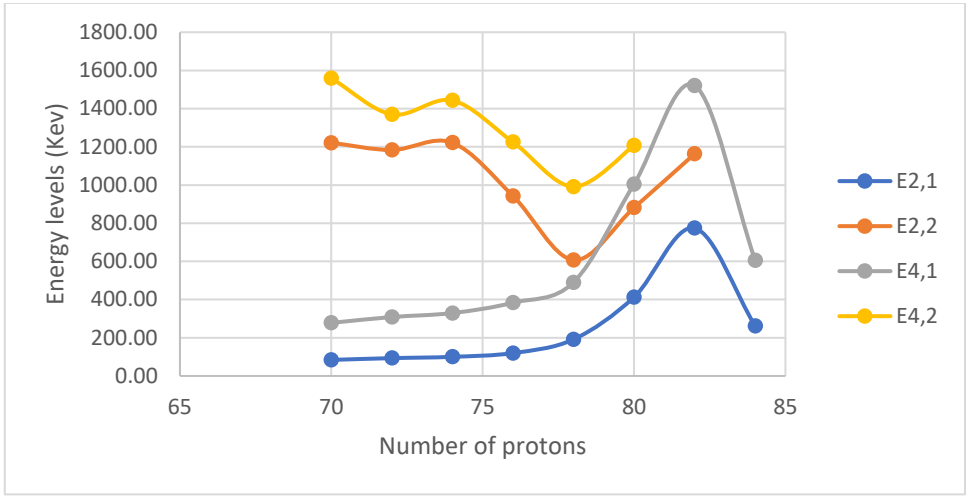

A

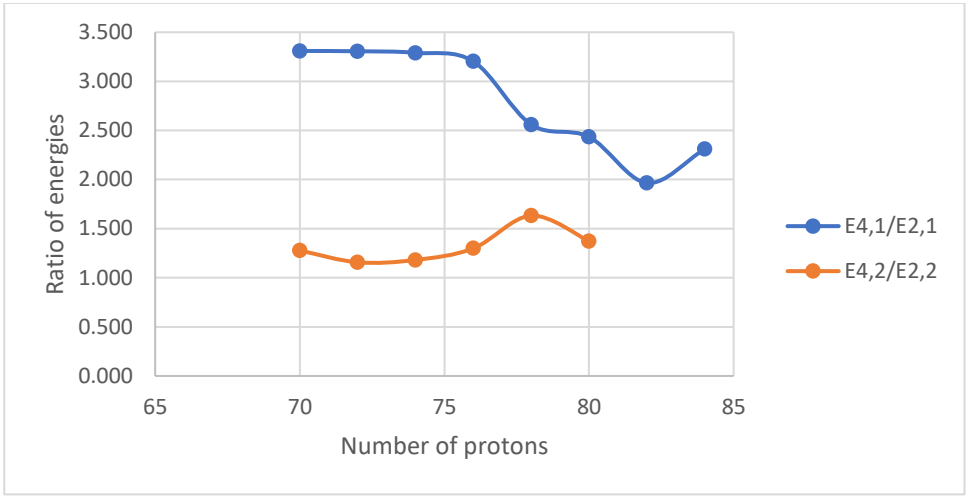

B

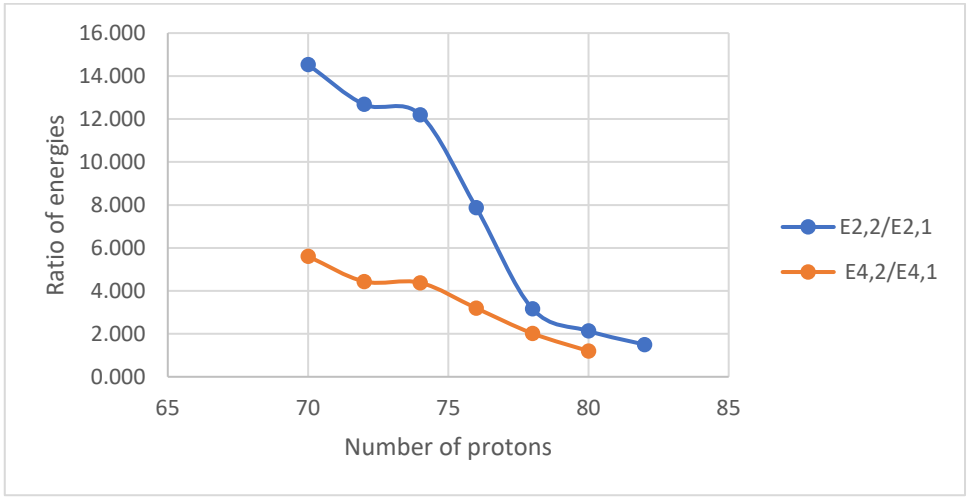

C

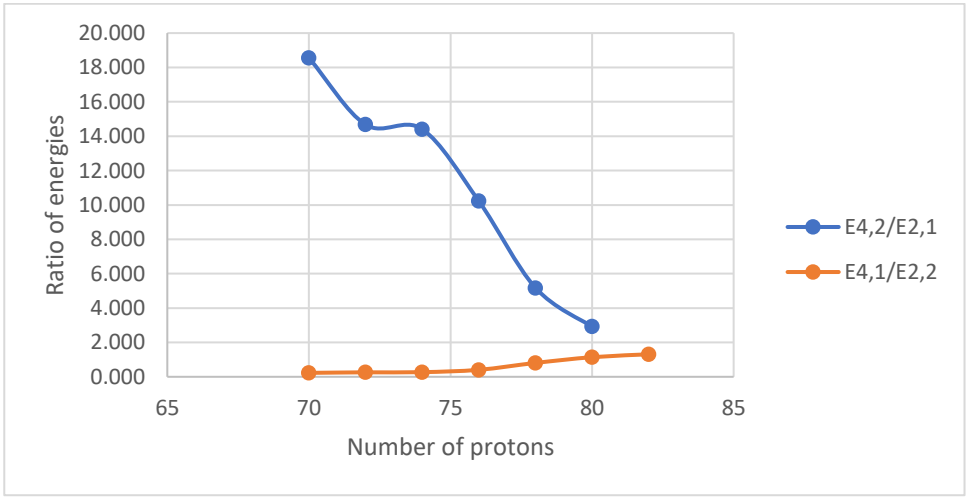

D

Figure V. 54 (color online) Panel **A** represents the comparison of the experimental energy levels of the lowest 2_1^+, 2_2^+, 4_1^+ and 4_2^+ states for the chain of N=108 isotones. Panels **B, C, D** represent the comparison of the experimental energy ratios ($E_{4_1^+}/E_{2_1^+}$ and $E_{4_2^+}/E_{2_2^+}$), ($E_{2_2^+}/E_{2_1^+}$ and $E_{4_2^+}/E_{4_1^+}$) and ($E_{4_2^+}/E_{2_1^+}$ and $E_{4_1^+}/E_{2_2^+}$), respectively, for the chain of N=108 isotones.

Isotones (N=110)

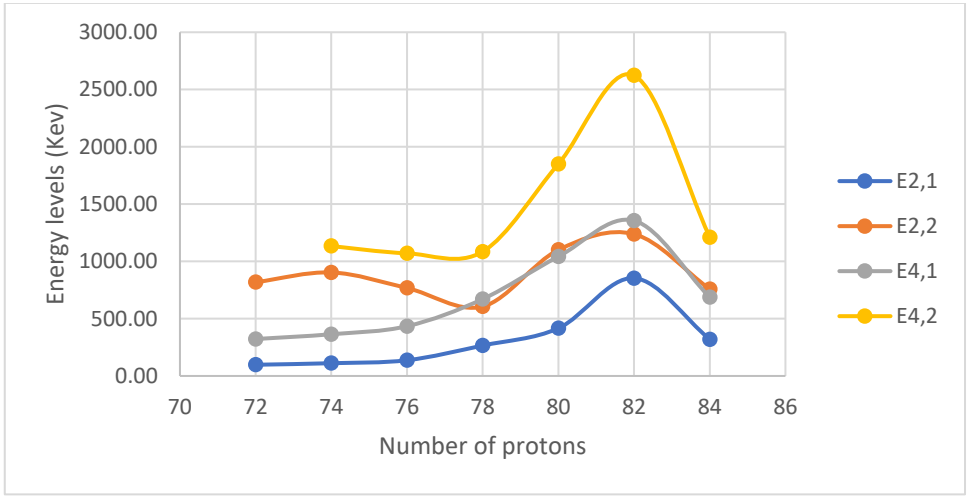

A

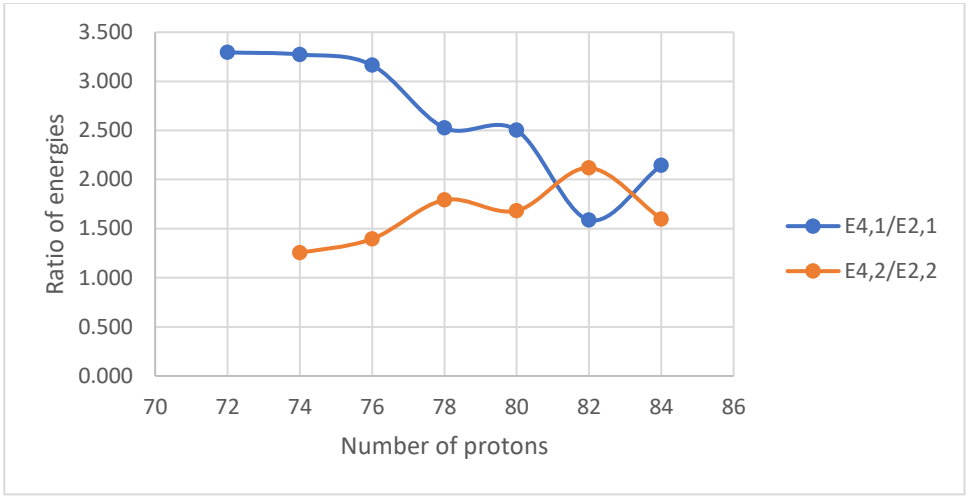

B

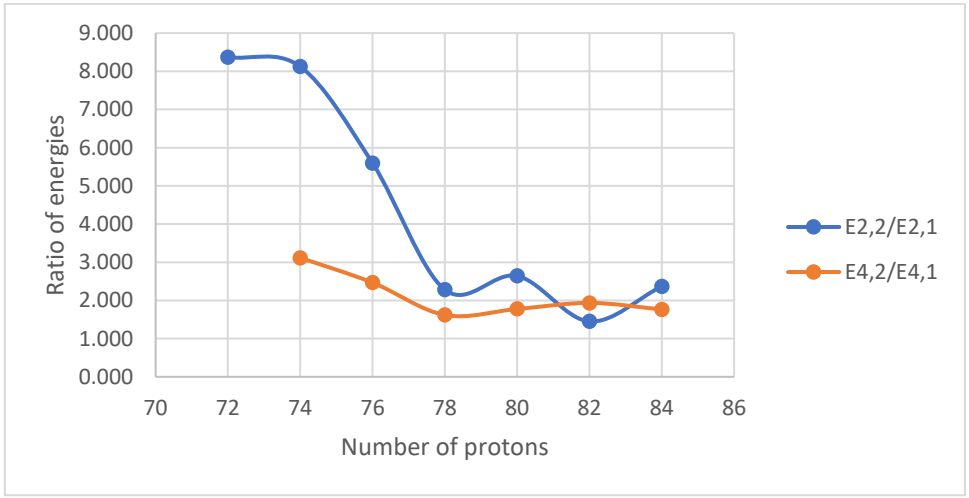

C

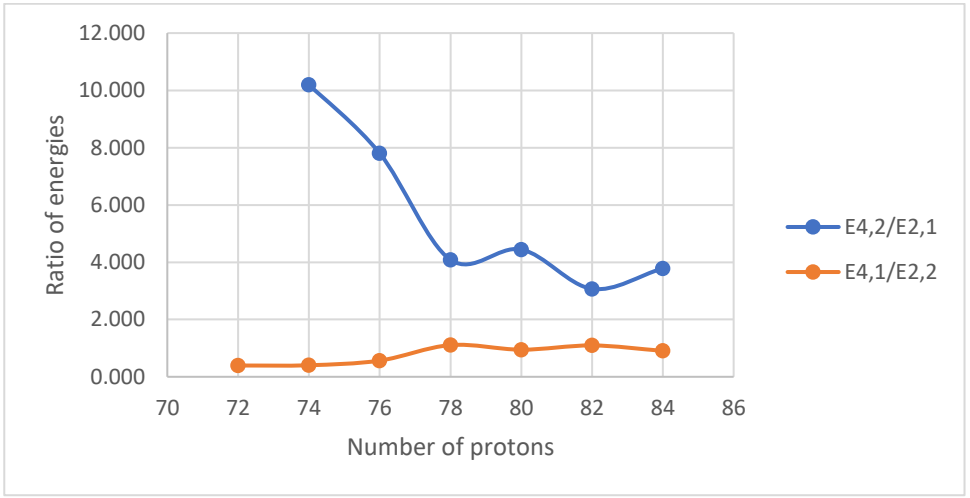

D

Figure V. 55 (color online) Panel **A** represents the comparison of the experimental energy levels of the lowest 2_1^+, 2_2^+, 4_1^+ and 4_2^+ states for the chain of N=110 isotones. Panels **B, C, D** represent the comparison of the experimental energy ratios ($E_{4_1^+}/E_{2_1^+}$ and $E_{4_2^+}/E_{2_2^+}$), ($E_{2_2^+}/E_{2_1^+}$ and $E_{4_2^+}/E_{4_1^+}$) and ($E_{4_2^+}/E_{2_1^+}$ and $E_{4_1^+}/E_{2_2^+}$), respectively, for the chain of N=110 isotones.

Isotones (N=112)

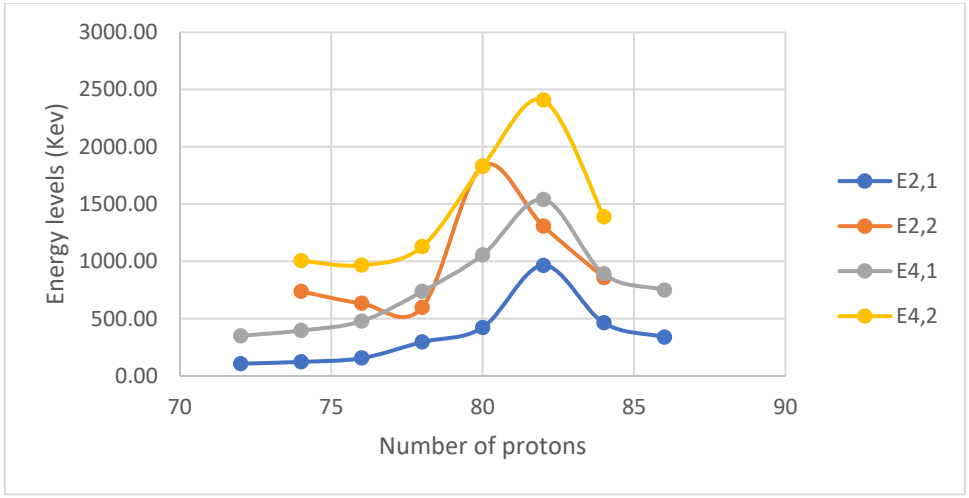

A

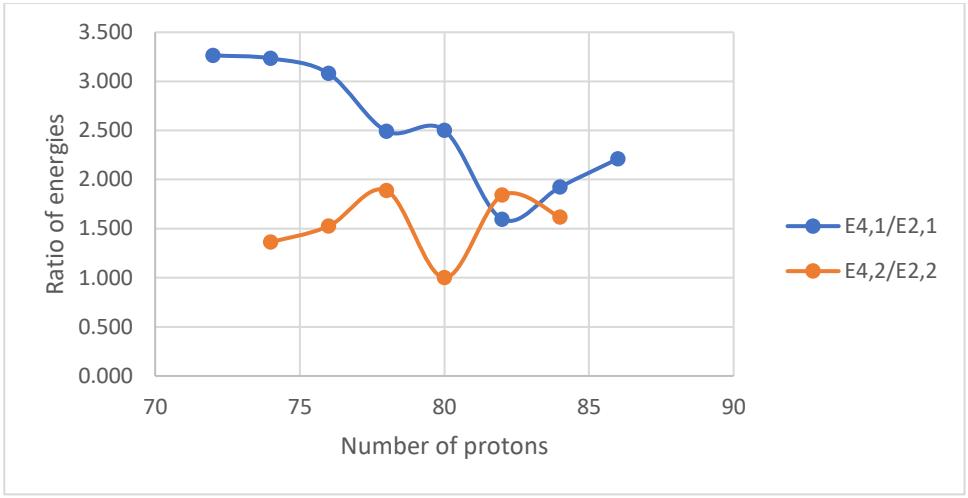

B

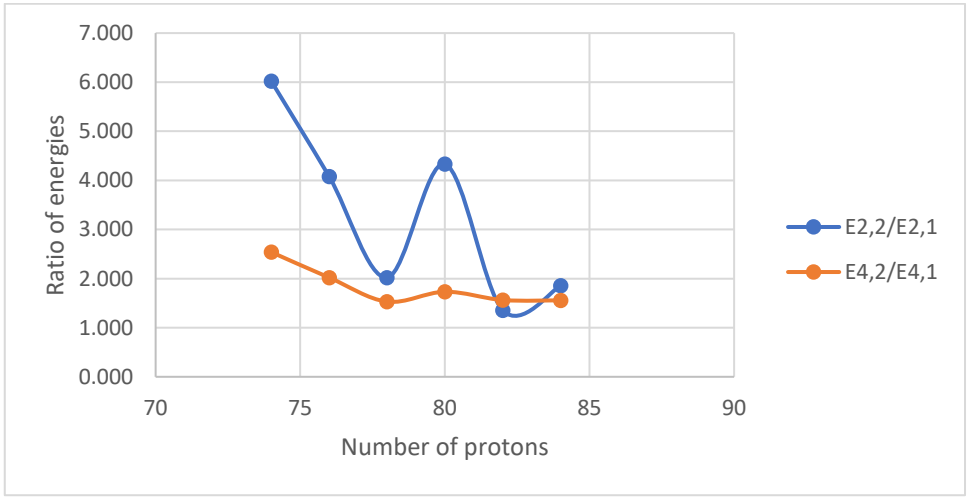

C

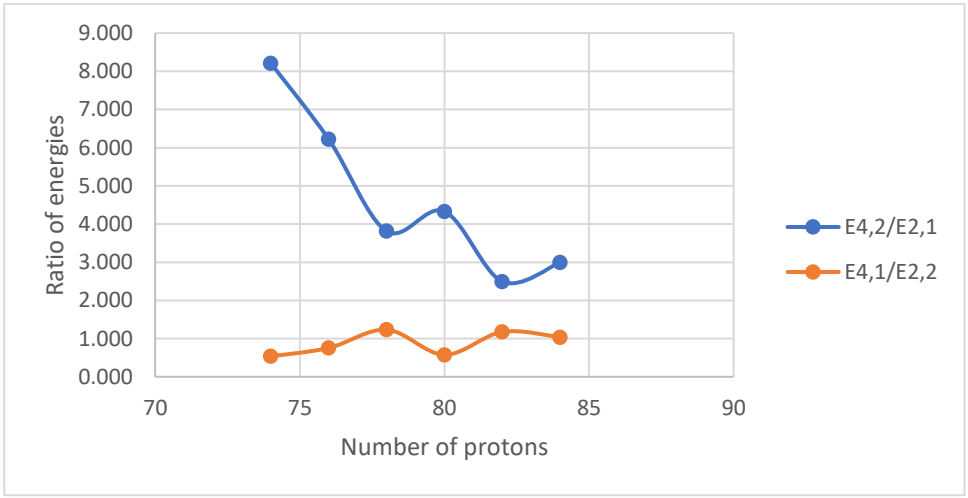

D

Figure V. 56 (color online) Panel **A** represents the comparison of the experimental energy levels of the lowest 2_1^+, 2_2^+, 4_1^+ and 4_2^+ states for the chain of N=112 isotones. Panels **B, C, D** represent the comparison of the experimental energy ratios ($E_{4_1^+}/E_{2_1^+}$ and $E_{4_2^+}/E_{2_2^+}$), ($E_{2_2^+}/E_{2_1^+}$ and $E_{4_2^+}/E_{4_1^+}$) and ($E_{4_2^+}/E_{2_1^+}$ and $E_{4_1^+}/E_{2_2^+}$), respectively, for the chain of N=112 isotones.

Isotones (N=114)

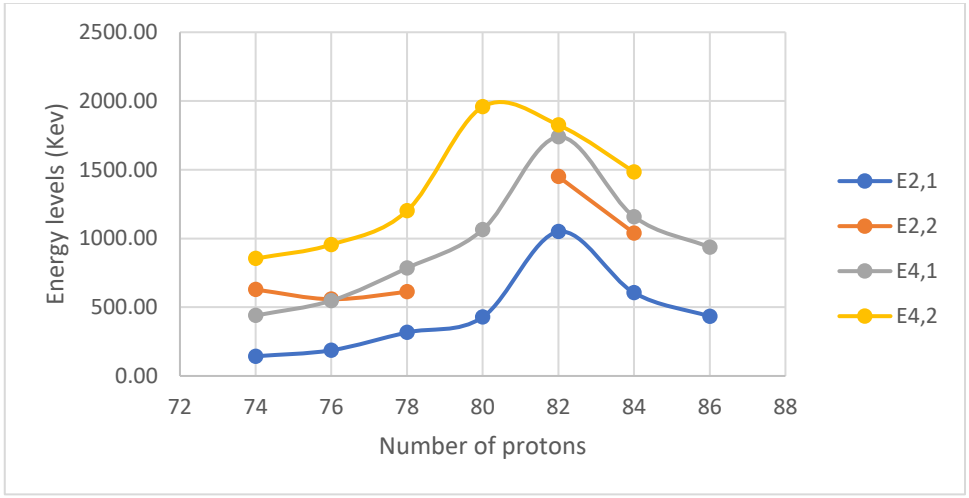

A

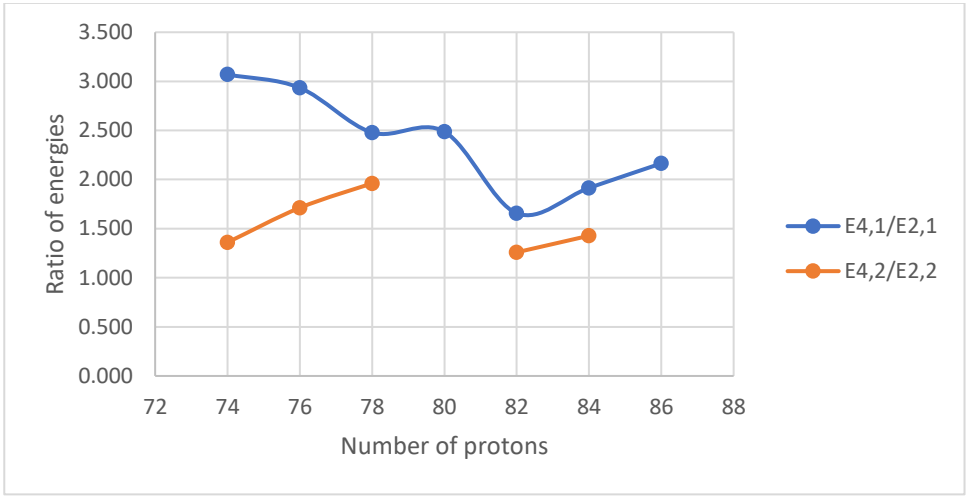

B

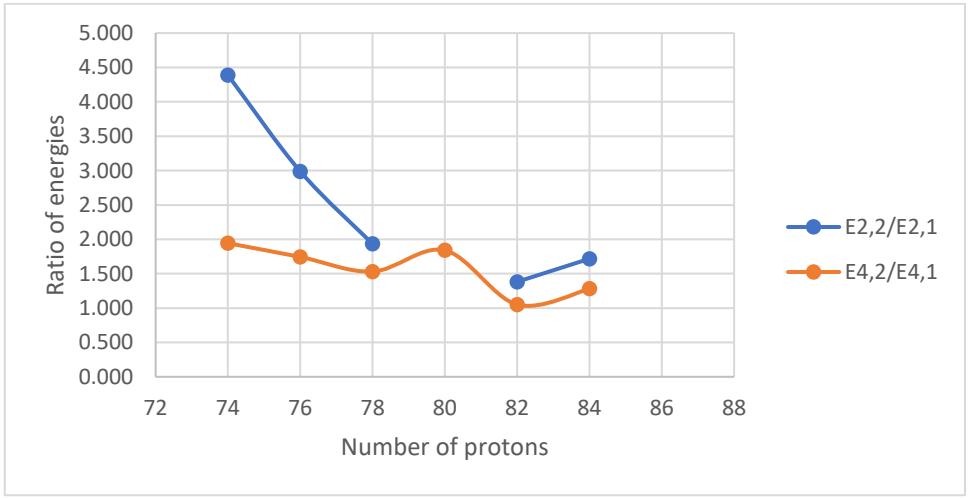

C

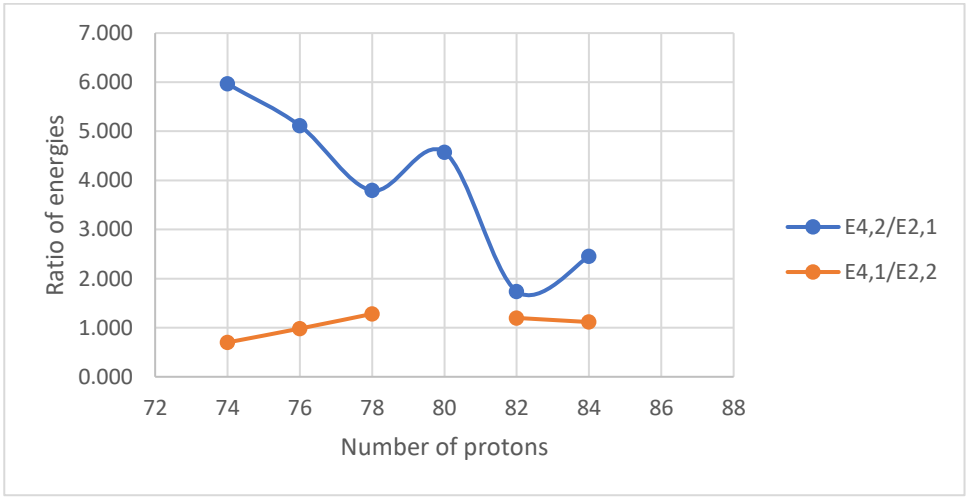

D

Figure V. 57 (color online) Panel **A** represents the comparison of the experimental energy levels of the lowest 2_1^+, 2_2^+, 4_1^+ and 4_2^+ states for the chain of N=114 isotones. Panels **B, C, D** represent the comparison of the experimental energy ratios ($E_{4_1^+}/E_{2_1^+}$ and $E_{4_2^+}/E_{2_2^+}$), ($E_{2_2^+}/E_{2_1^+}$ and $E_{4_2^+}/E_{4_1^+}$) and ($E_{4_2^+}/E_{2_1^+}$ and $E_{4_1^+}/E_{2_2^+}$), respectively, for the chain of N=114 isotones.

Isotones (N=116)

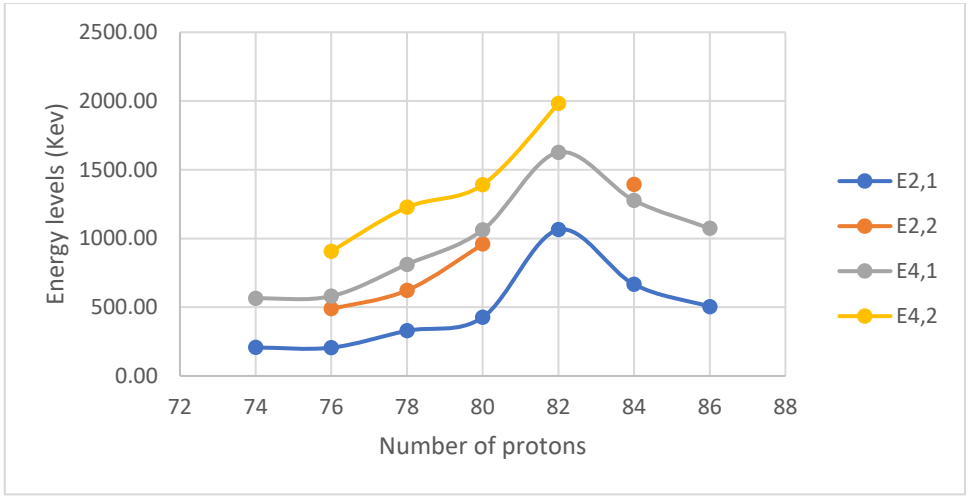

A

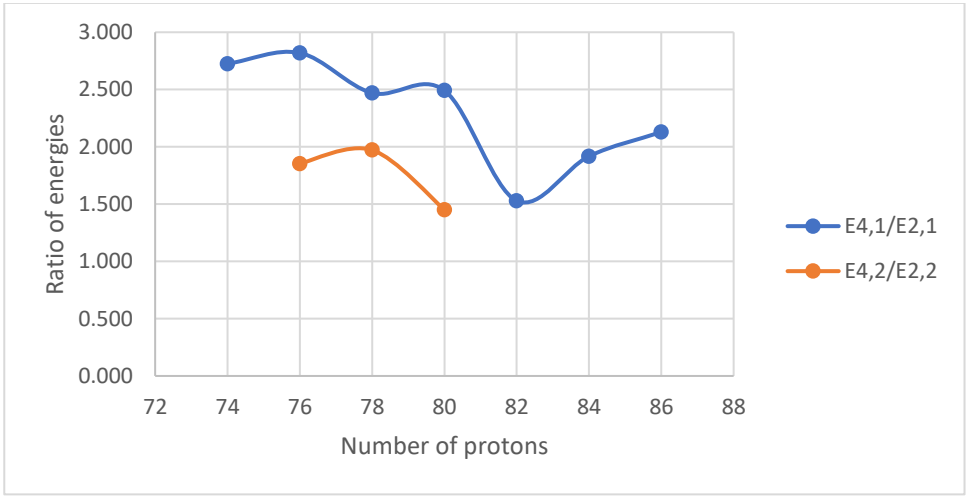

B

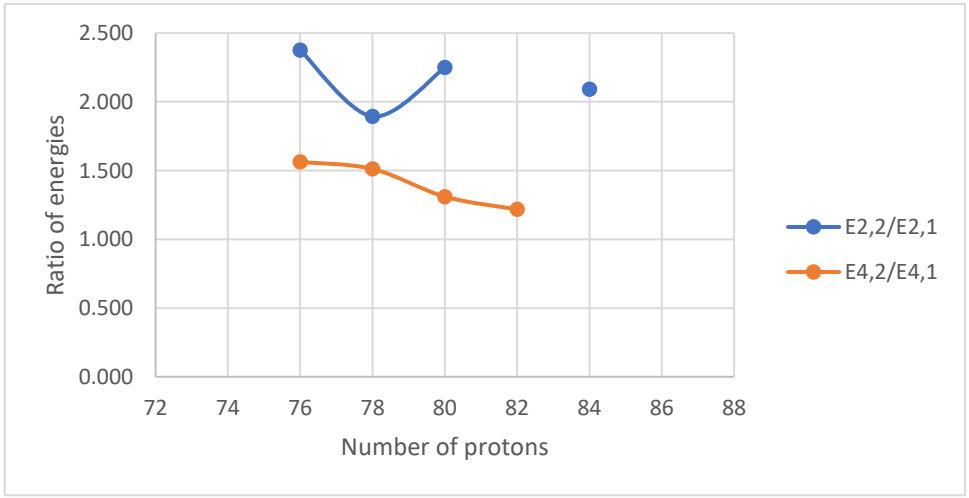

C

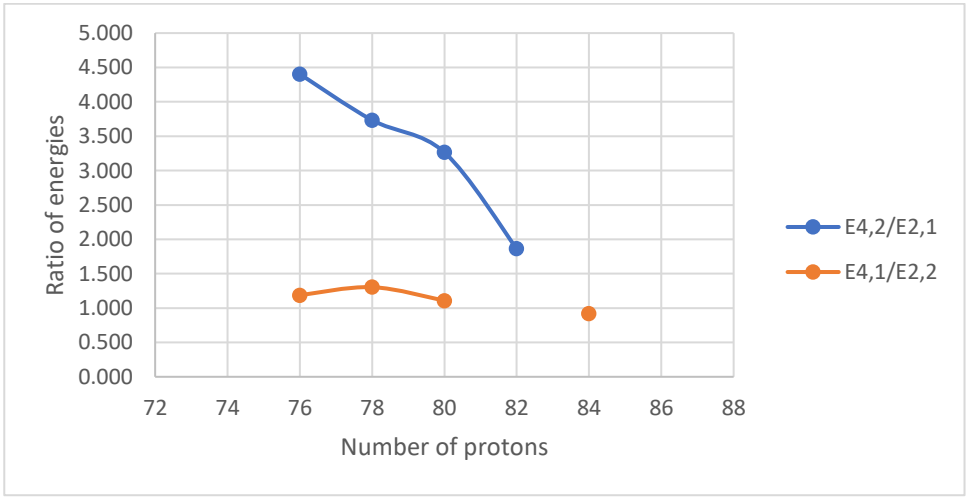

D

Figure V. 58 (color online) Panel **A** represents the comparison of the experimental energy levels of the lowest 2_1^+, 2_2^+, 4_1^+ and 4_2^+ states for the chain of N=116 isotones. Panels **B, C, D** represent the comparison of the experimental energy ratios ($E_{4_1^+}/E_{2_1^+}$ and $E_{4_2^+}/E_{2_2^+}$), ($E_{2_2^+}/E_{2_1^+}$ and $E_{4_2^+}/E_{4_1^+}$) and ($E_{4_2^+}/E_{2_1^+}$ and $E_{4_1^+}/E_{2_2^+}$), respectively, for the chain of N=116 isotones.

Isotones (N=118)

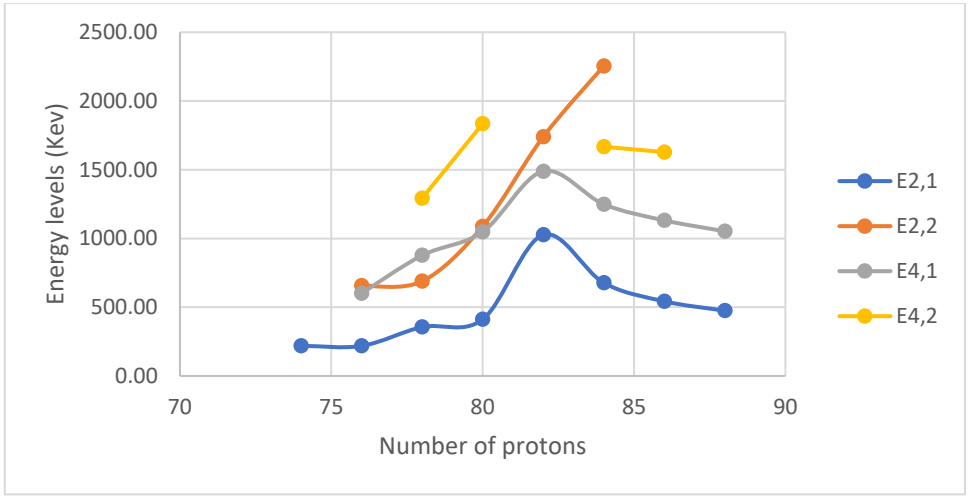

A

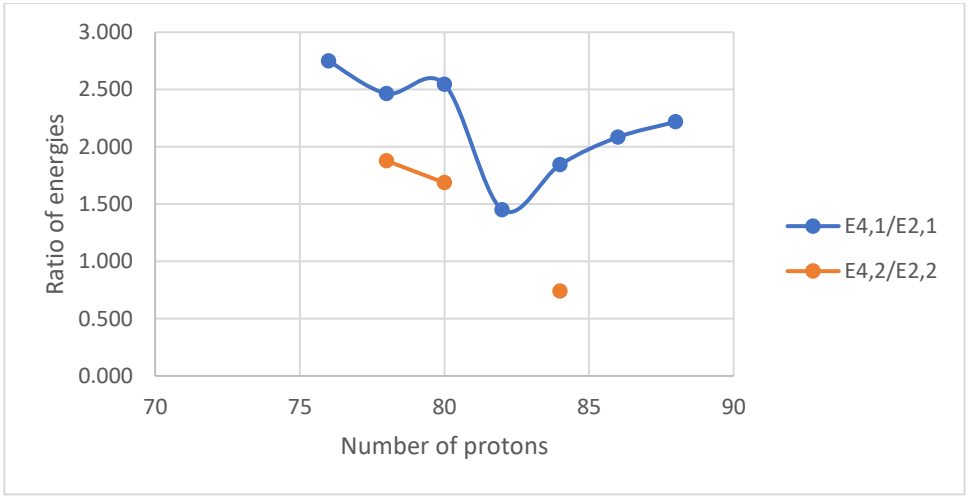

B

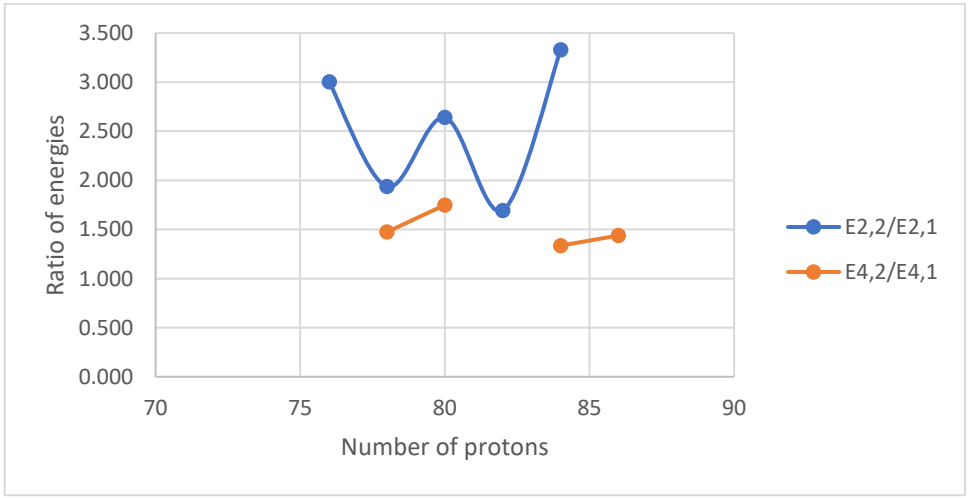

C

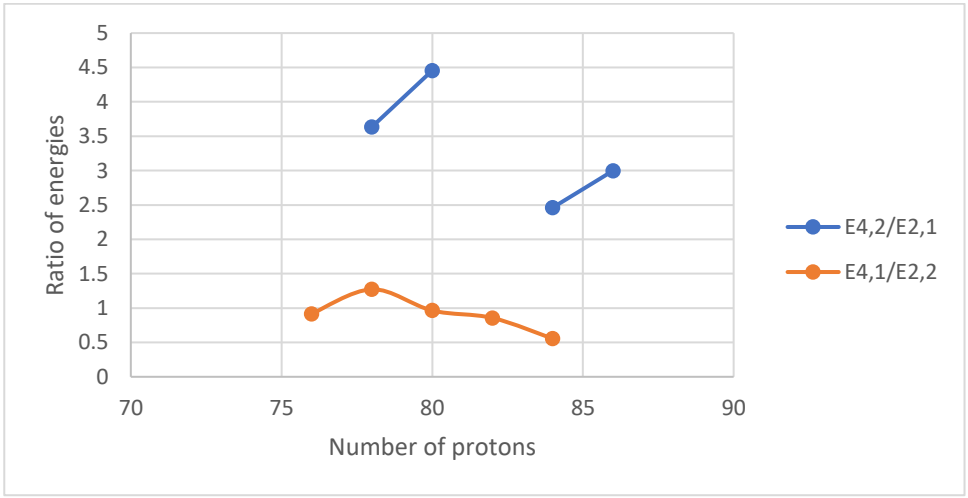

D

Figure V. 59 (color online) Panel **A** represents the comparison of the experimental energy levels of the lowest 2_1^+, 2_2^+, 4_1^+ and 4_2^+ states for the chain of N=118 isotones. Panels **B, C, D** represent the comparison of the experimental energy ratios ($E_{4_1^+}/E_{2_1^+}$ and $E_{4_2^+}/E_{2_2^+}$), ($E_{2_2^+}/E_{2_1^+}$ and $E_{4_2^+}/E_{4_1^+}$) and ($E_{4_2^+}/E_{2_1^+}$ and $E_{4_1^+}/E_{2_2^+}$), respectively, for the chain of N=118 isotones.

Isotones (N=120)

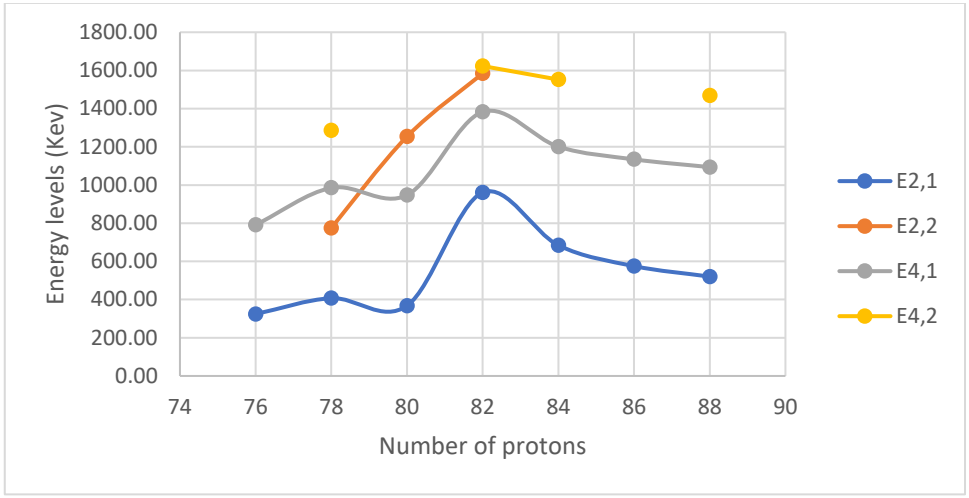

A

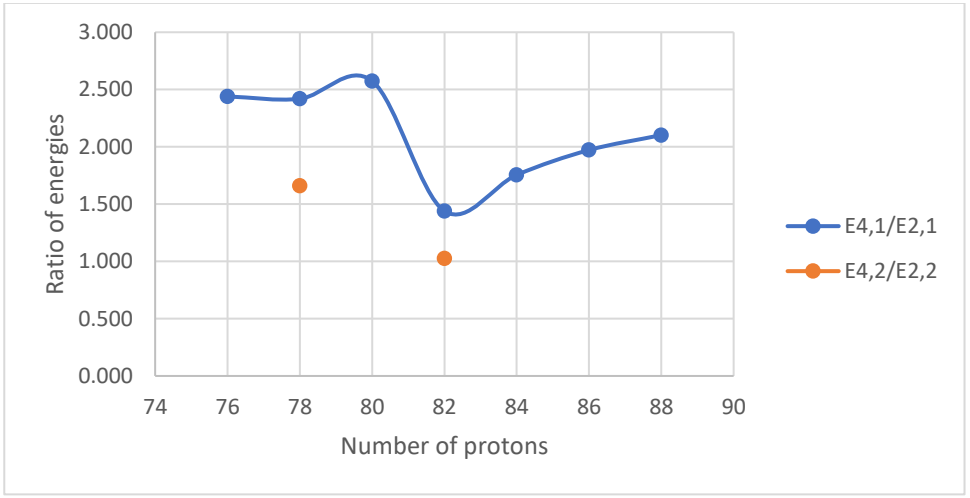

B

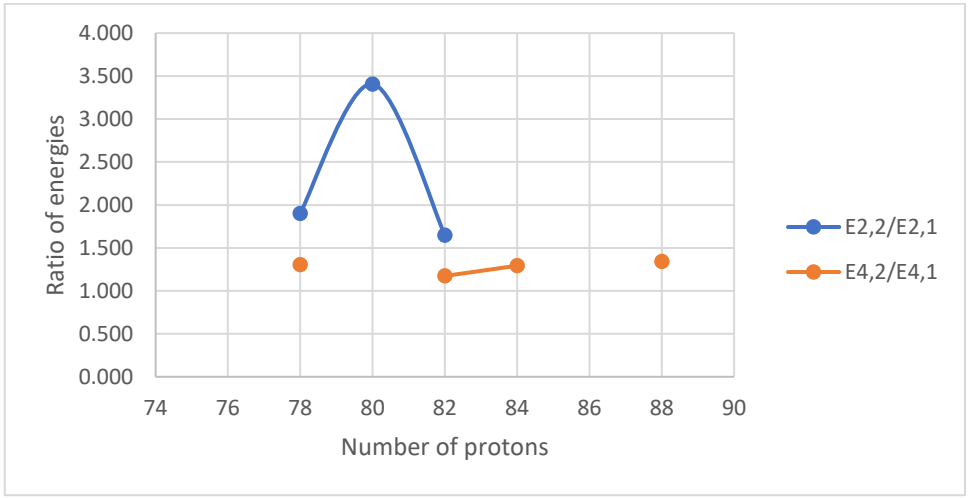

C

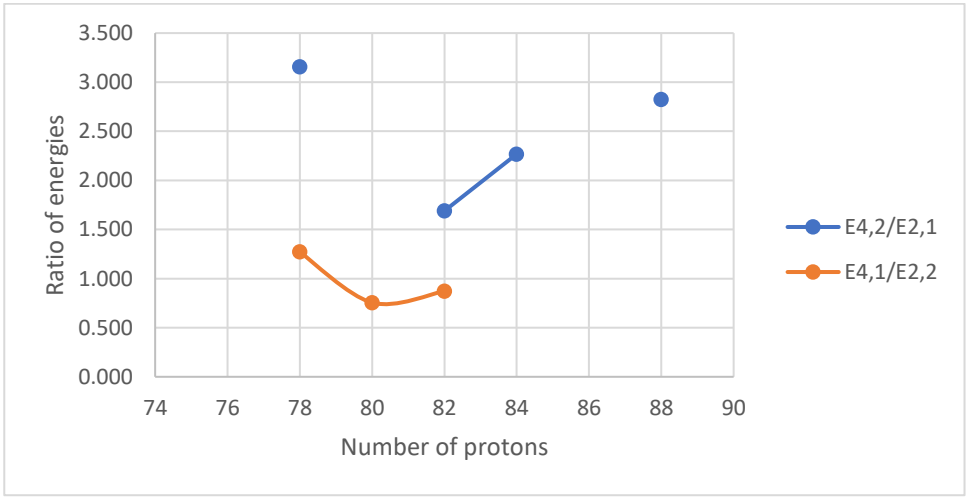

D

Figure V. 60 (color online) Panel **A** represents the comparison of the experimental energy levels of the lowest 2_1^+, 2_2^+, 4_1^+ and 4_2^+ states for the chain of N=120 isotones. Panels **B, C, D** represent the comparison of the experimental energy ratios ($E_{4_1^+}/E_{2_1^+}$ and $E_{4_2^+}/E_{2_2^+}$), ($E_{2_2^+}/E_{2_1^+}$ and $E_{4_2^+}/E_{4_1^+}$) and ($E_{4_2^+}/E_{2_1^+}$ and $E_{4_1^+}/E_{2_2^+}$), respectively, for the chain of N=120 isotones.

Isotones (N=122)

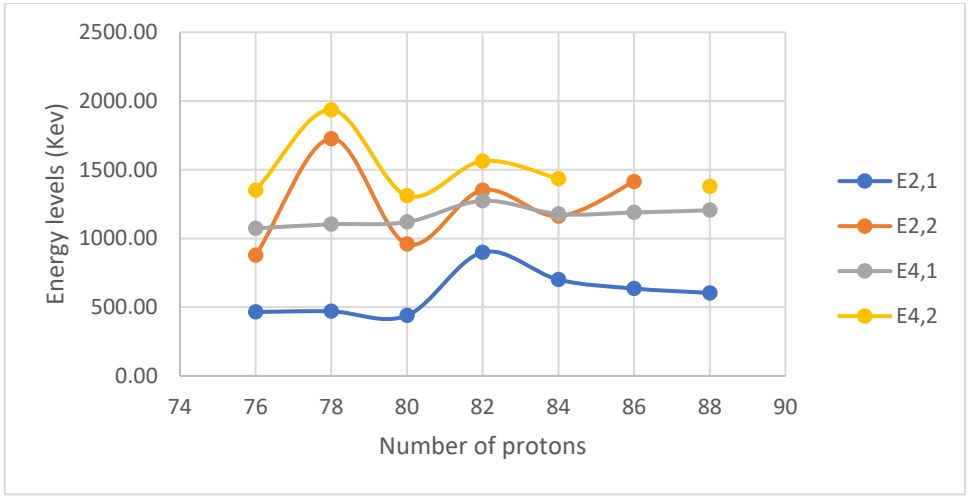

A

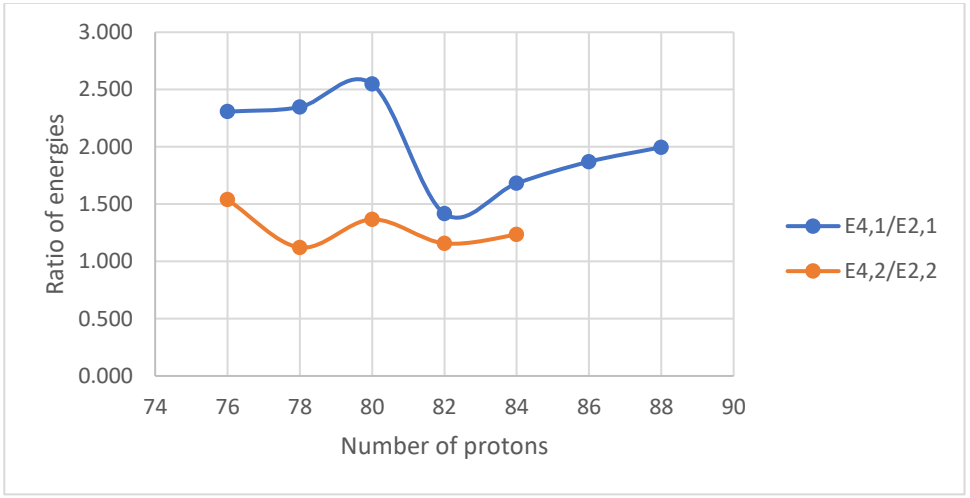

B

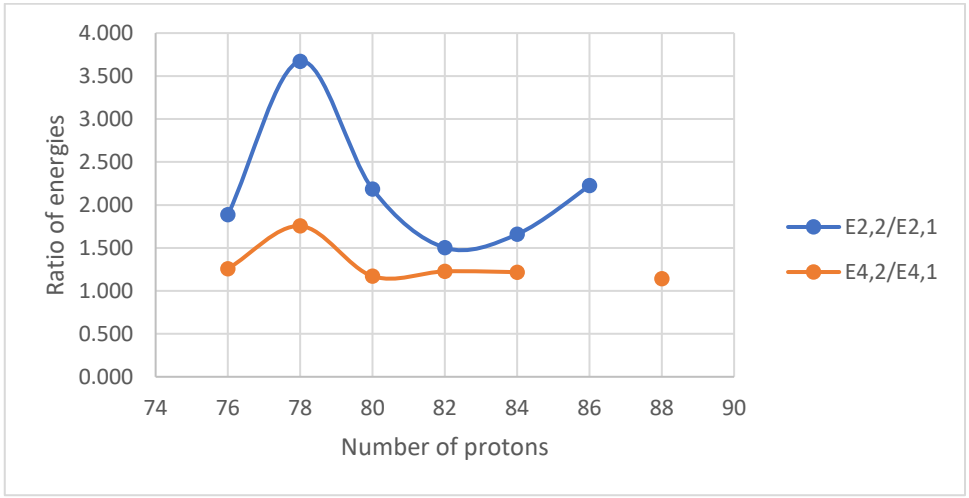

C

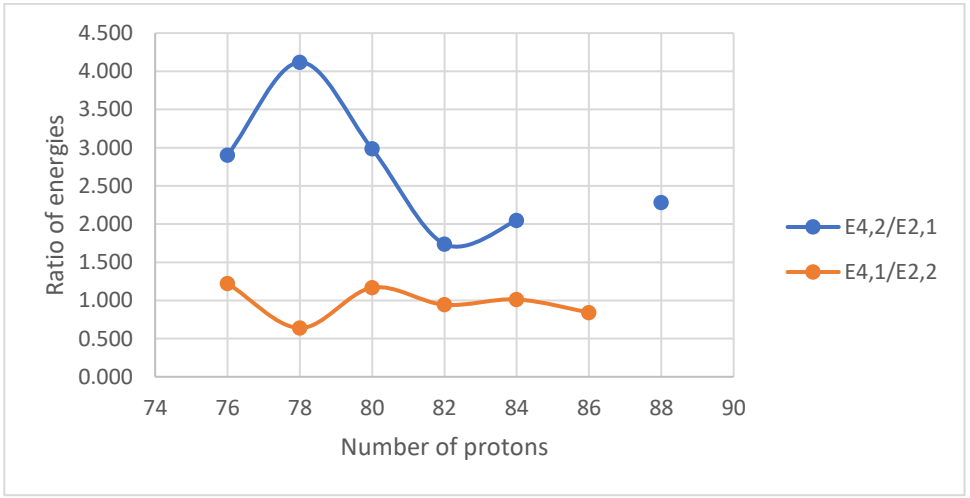

D

Figure V. 61 (color online) Panel **A** represents the comparison of the experimental energy levels of the lowest 2_1^+, 2_2^+, 4_1^+ and 4_2^+ states for the chain of N=122 isotones. Panels **B, C, D** represent the comparison of the experimental energy ratios ($E_{4_1^+}/E_{2_1^+}$ and $E_{4_2^+}/E_{2_2^+}$), ($E_{2_2^+}/E_{2_1^+}$ and $E_{4_2^+}/E_{4_1^+}$) and ($E_{4_2^+}/E_{2_1^+}$ and $E_{4_1^+}/E_{2_2^+}$), respectively, for the chain of N=122 isotones.

Isotones (N=124)

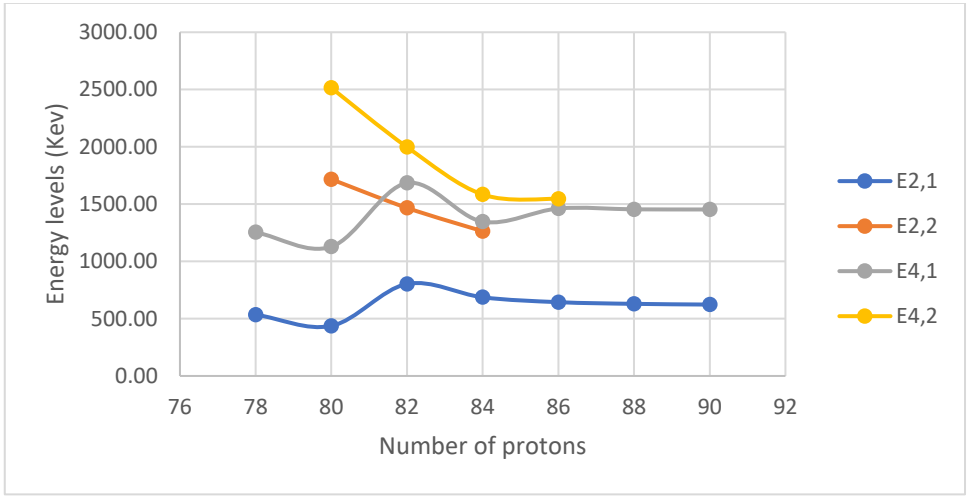

A

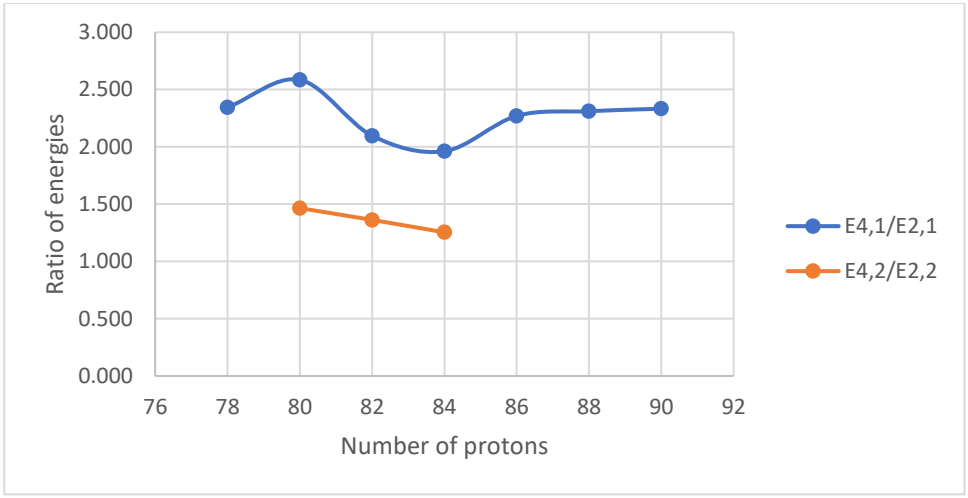

B

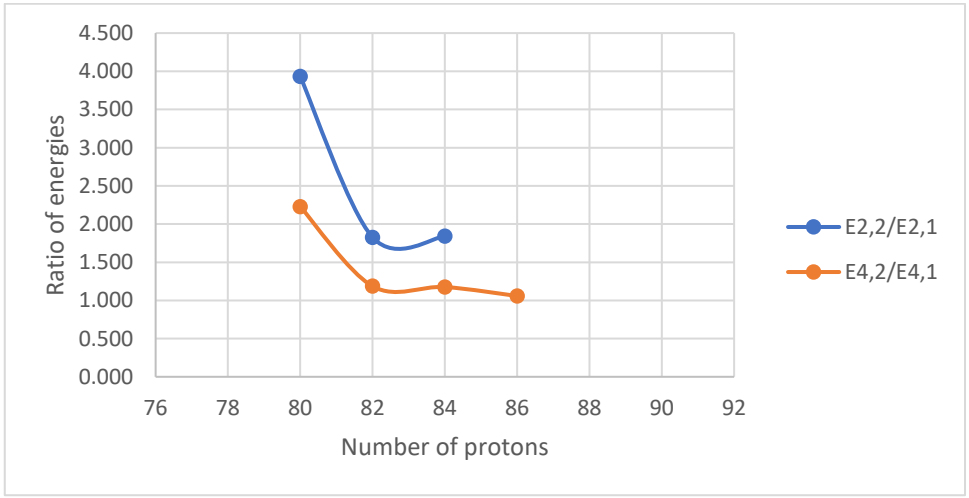

C

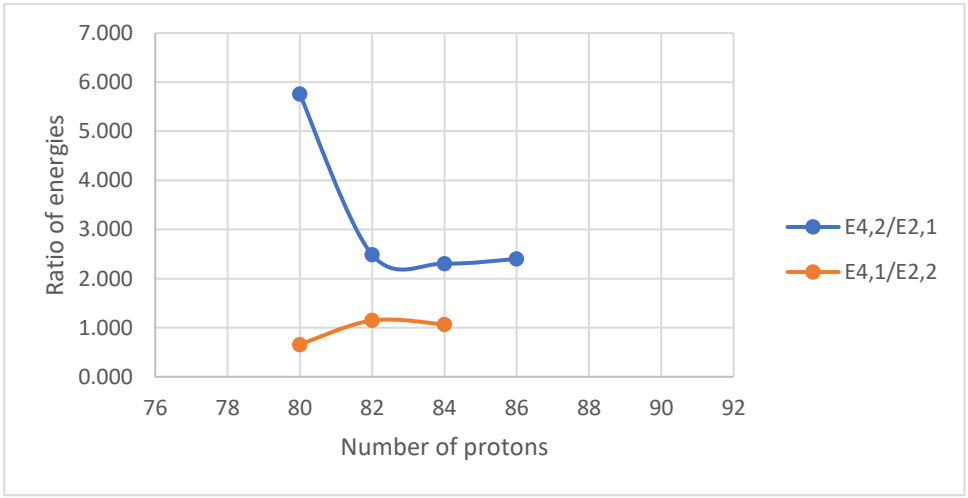

D

Figure V. 62 (color online) Panel **A** represents the comparison of the experimental energy levels of the lowest 2_1^+, 2_2^+, 4_1^+ and 4_2^+ states for the chain of N=124 isotones. Panels **B, C, D** represent the comparison of the experimental energy ratios ($E_{4_1^+}/E_{2_1^+}$ and $E_{4_2^+}/E_{2_2^+}$), ($E_{2_2^+}/E_{2_1^+}$ and $E_{4_2^+}/E_{4_1^+}$) and ($E_{4_2^+}/E_{2_1^+}$ and $E_{4_1^+}/E_{2_2^+}$), respectively, for the chain of N=124 isotones.

Isotones (N=126)

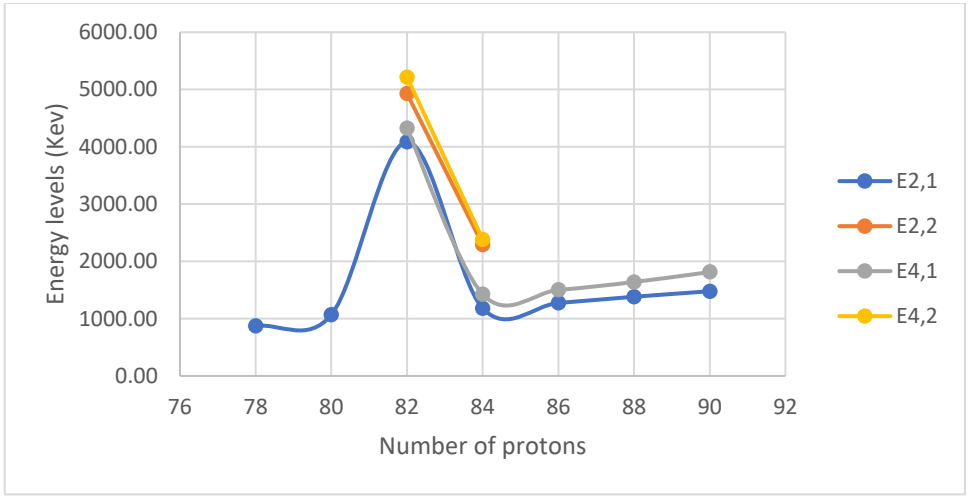

A

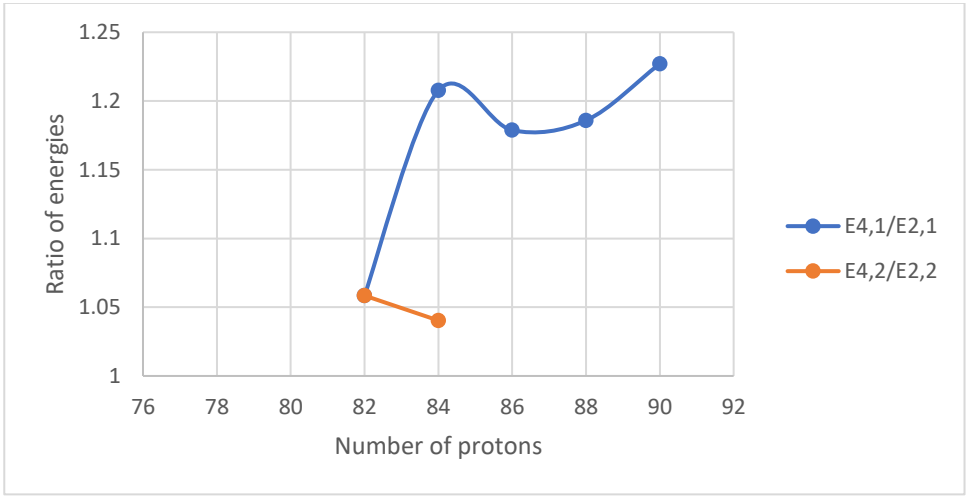

B

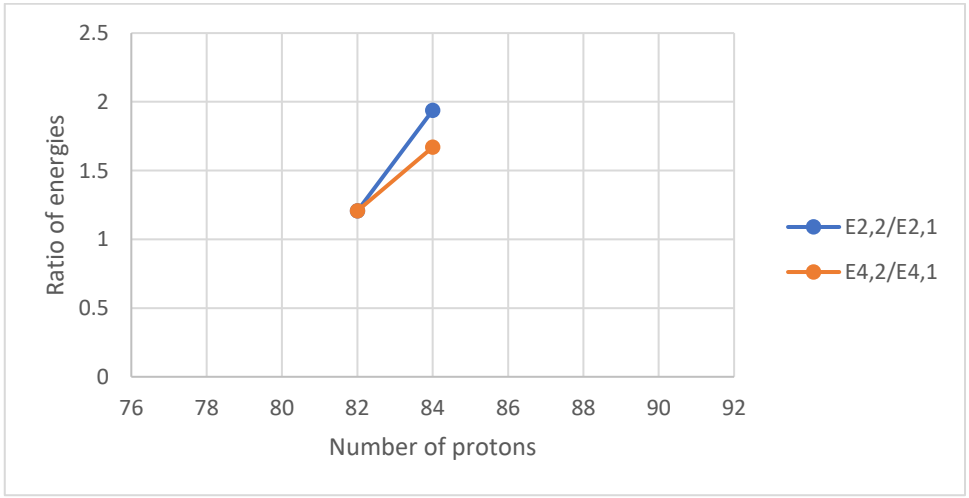

C

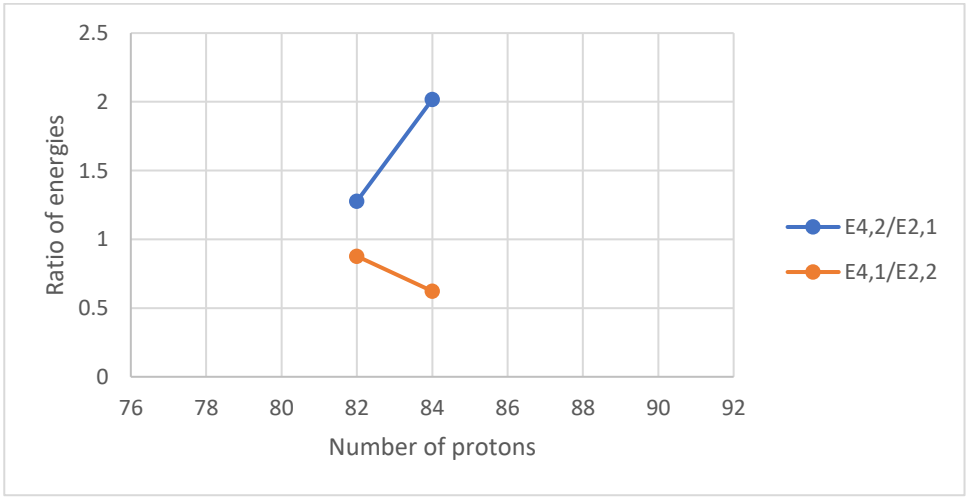

D

Figure V. 63 (color online) Panel **A** represents the comparison of the experimental energy levels of the lowest 2_1^+, 2_2^+, 4_1^+ and 4_2^+ states for the chain of N=126 isotones. Panels **B, C, D** represent the comparison of the experimental energy ratios ($E_{4_1^+}/E_{2_1^+}$ and $E_{4_2^+}/E_{2_2^+}$), ($E_{2_2^+}/E_{2_1^+}$ and $E_{4_2^+}/E_{4_1^+}$) and ($E_{4_2^+}/E_{2_1^+}$ and $E_{4_1^+}/E_{2_2^+}$), respectively, for the chain of N=126 isotones.

Isotones (N=128)

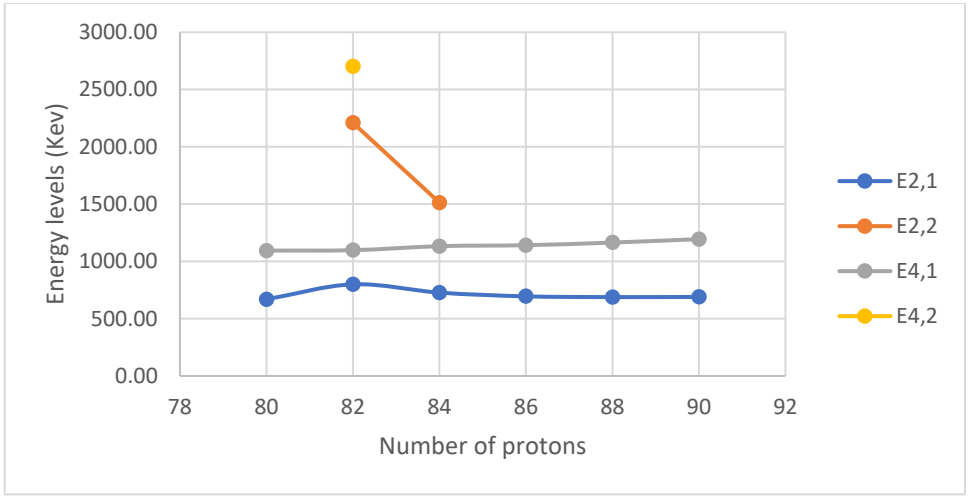

A

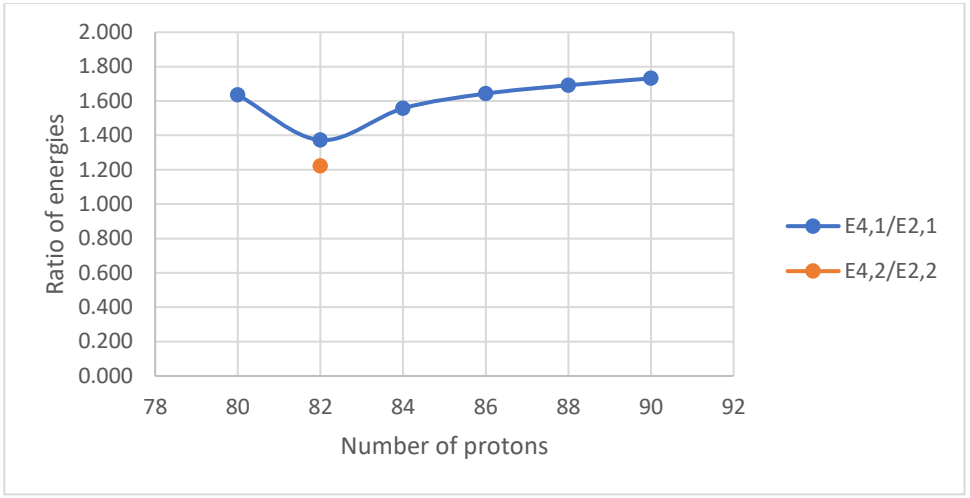

B

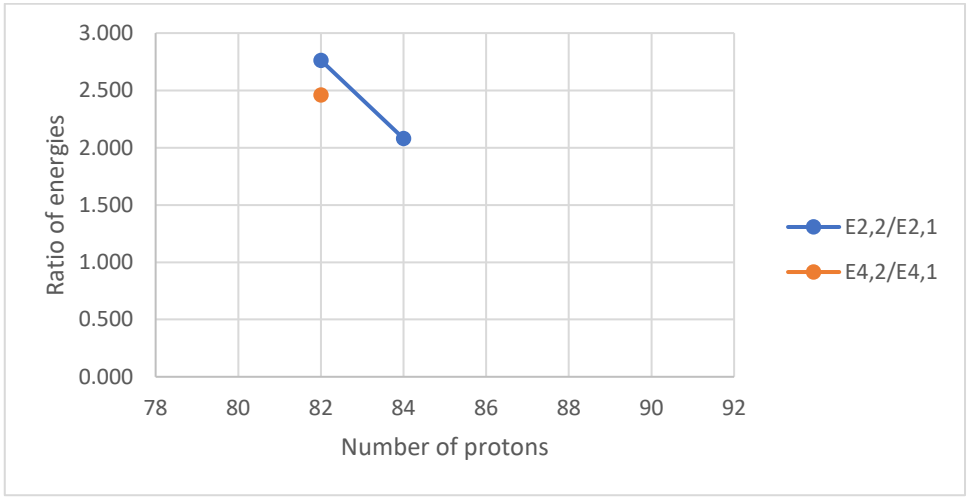

C

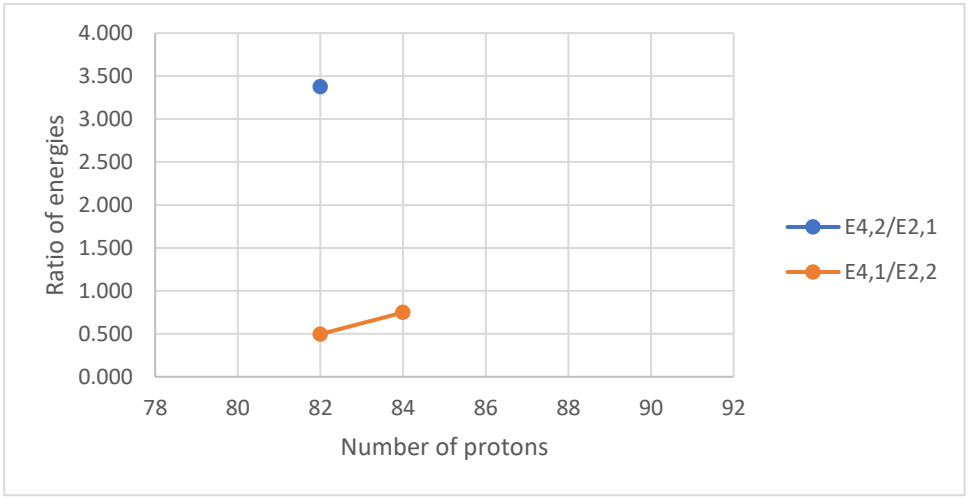

D

Figure V. 64 (color online) Panel **A** represents the comparison of the experimental energy levels of the lowest 2_1^+, 2_2^+, 4_1^+ and 4_2^+ states for the chain of N=128 isotones. Panels **B, C, D** represent the comparison of the experimental energy ratios ($E_{4_1^+}/E_{2_1^+}$ and $E_{4_2^+}/E_{2_2^+}$), ($E_{2_2^+}/E_{2_1^+}$ and $E_{4_2^+}/E_{4_1^+}$) and ($E_{4_2^+}/E_{2_1^+}$ and $E_{4_1^+}/E_{2_2^+}$), respectively, for the chain of N=128 isotones.

Isotones (N=130)

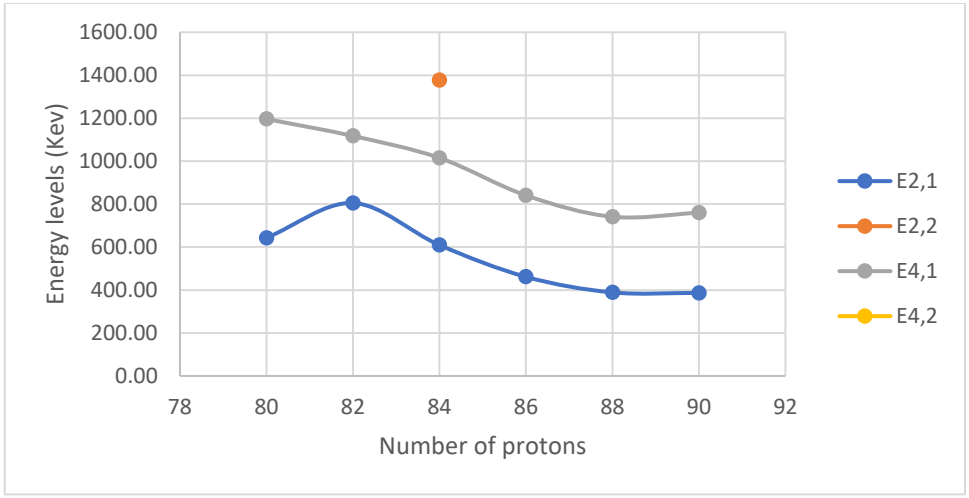

A

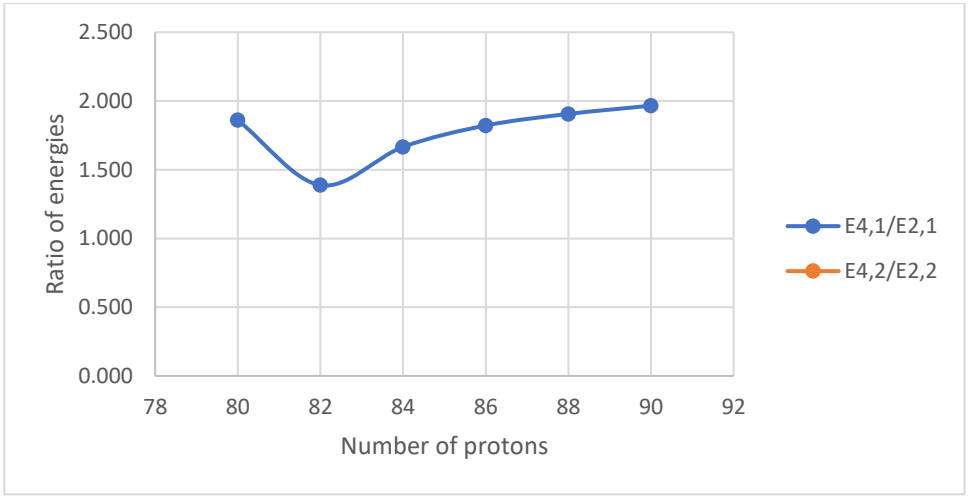

B

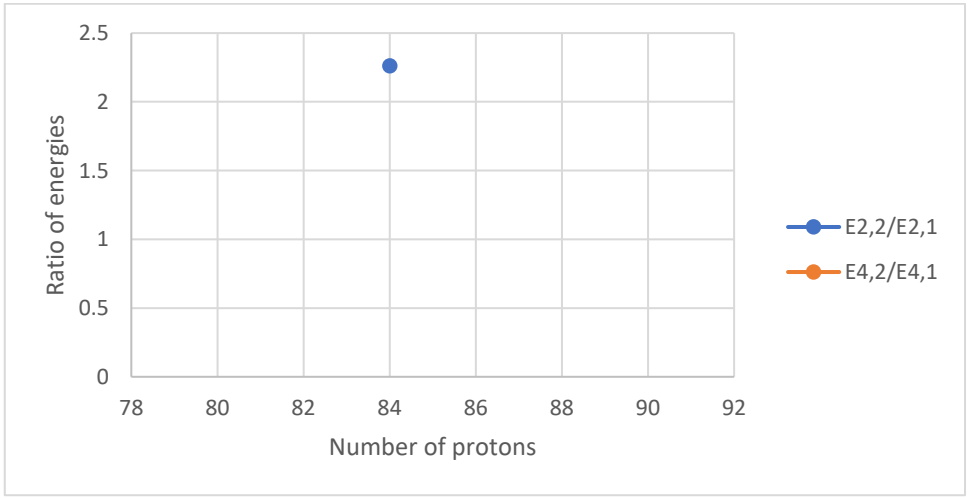

C

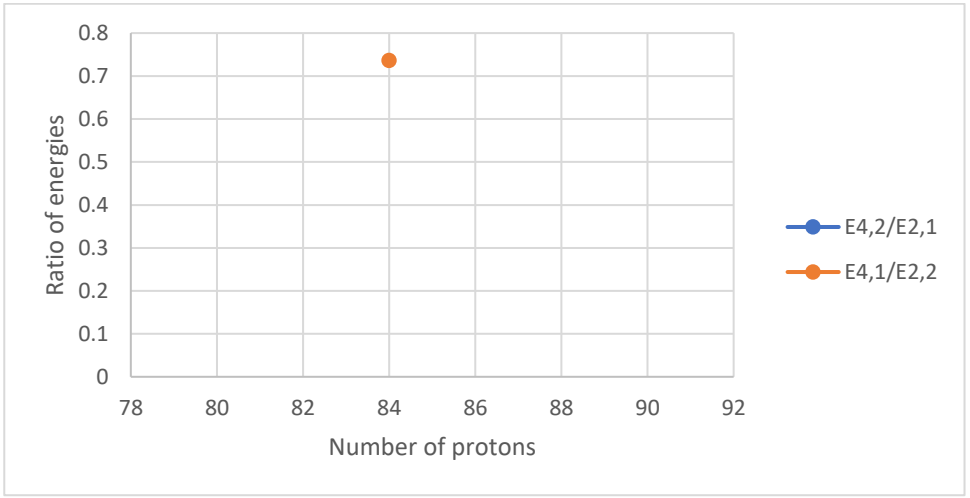

D

Figure V. 65 (color online) Panel **A** represents the comparison of the experimental energy levels of the lowest 2_1^+, 2_2^+, 4_1^+ and 4_2^+ states for the chain of N=130 isotones. Panels **B, C, D** represent the comparison of the experimental energy ratios ($E_{4_1^+}/E_{2_1^+}$ and $E_{4_2^+}/E_{2_2^+}$), ($E_{2_2^+}/E_{2_1^+}$ and $E_{4_2^+}/E_{4_1^+}$) and ($E_{4_2^+}/E_{2_1^+}$ and $E_{4_1^+}/E_{2_2^+}$), respectively, for the chain of N=130 isotones.

Isotones (N=132)

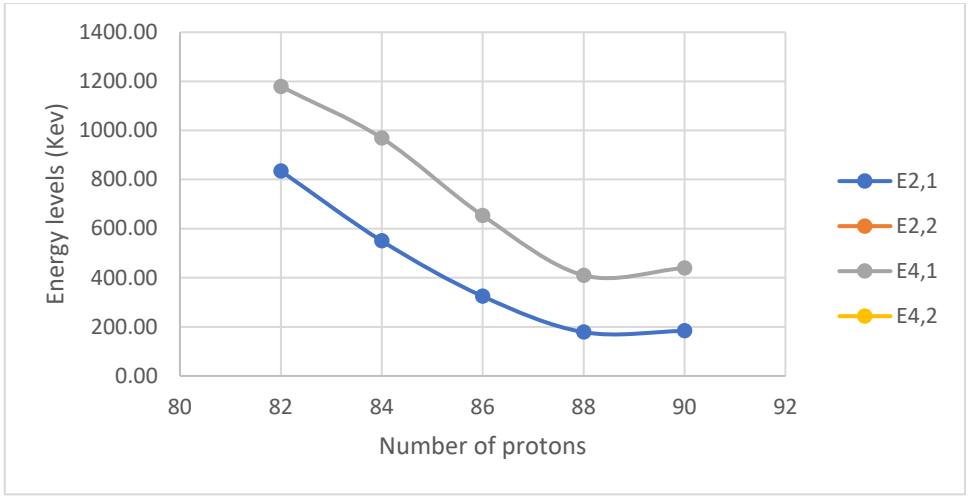

A

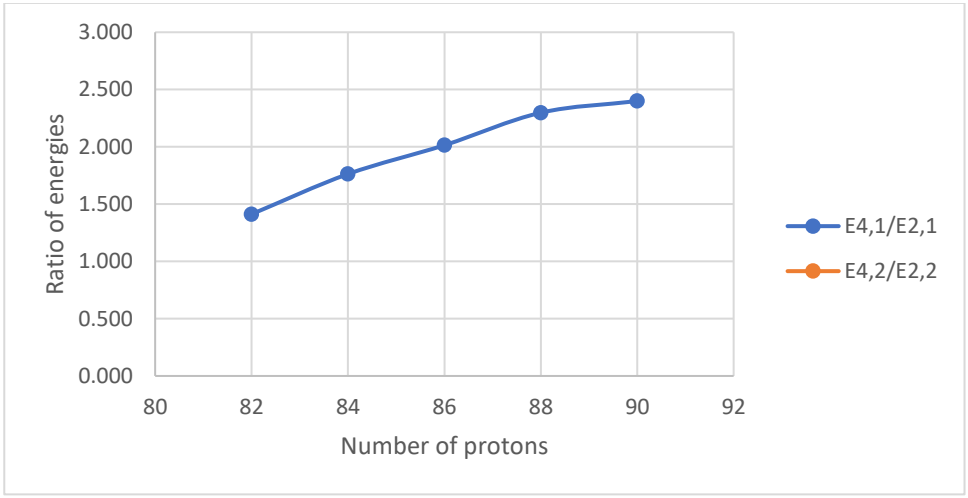

B

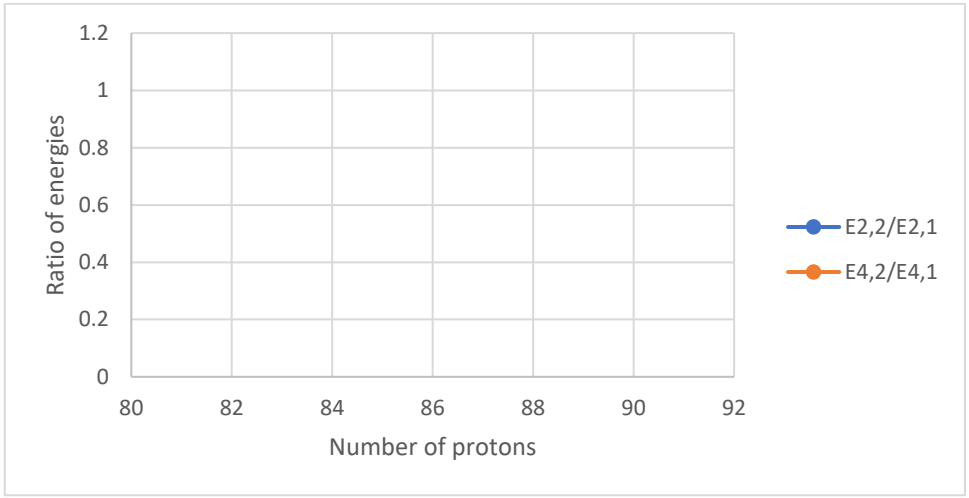

C

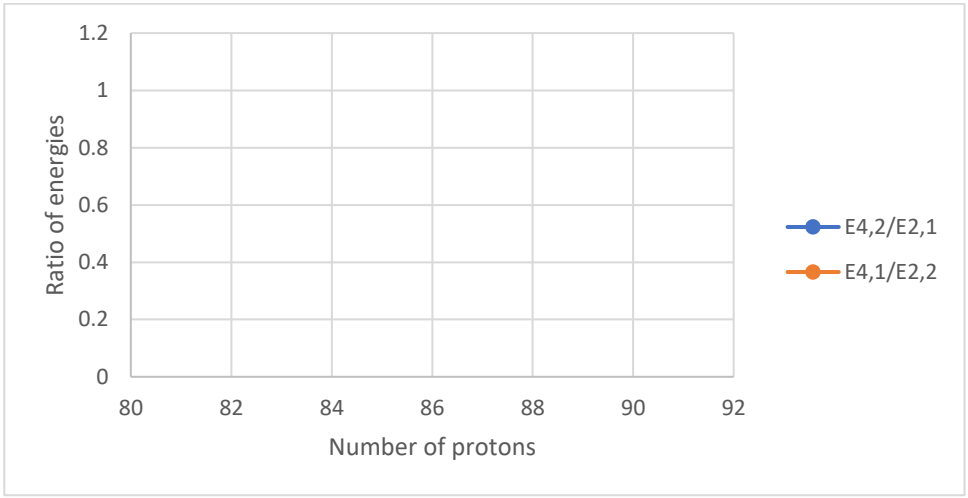

D

Figure V. 66 (color online) Panel **A** represents the comparison of the experimental energy levels of the lowest 2_1^+, 2_2^+, 4_1^+ and 4_2^+ states for the chain of N=132 isotones. Panels **B, C, D** represent the comparison of the experimental energy ratios ($E_{4_1^+}/E_{2_1^+}$ and $E_{4_2^+}/E_{2_2^+}$), ($E_{2_2^+}/E_{2_1^+}$ and $E_{4_2^+}/E_{4_1^+}$) and ($E_{4_2^+}/E_{2_1^+}$ and $E_{4_1^+}/E_{2_2^+}$), respectively, for the chain of N=132 isotones.

Isotones (N=134)

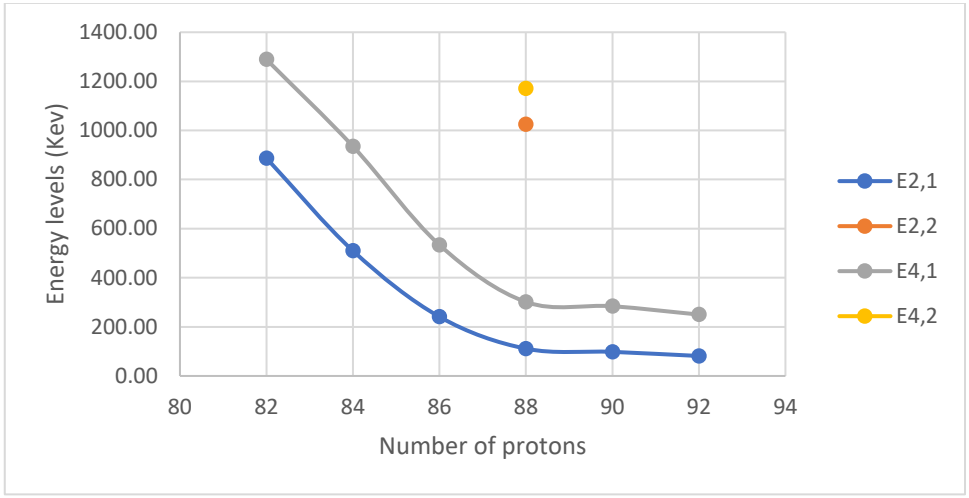

A

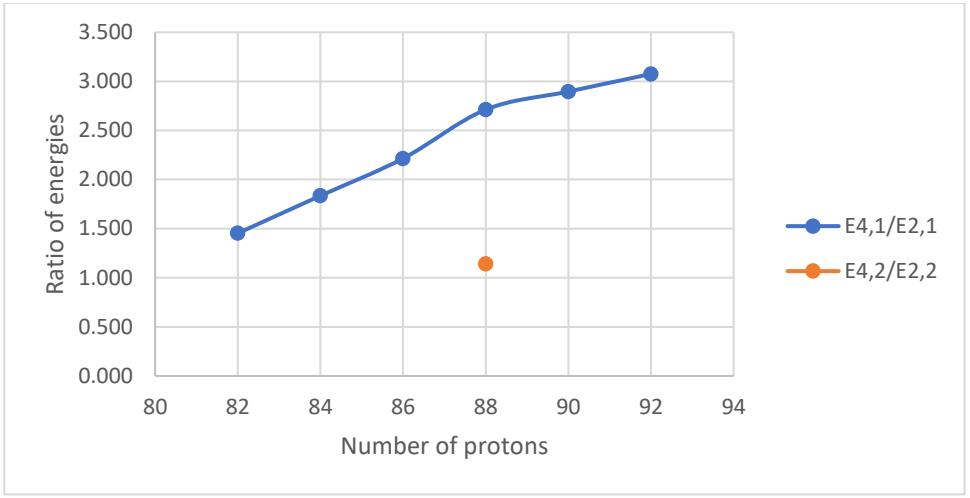

B

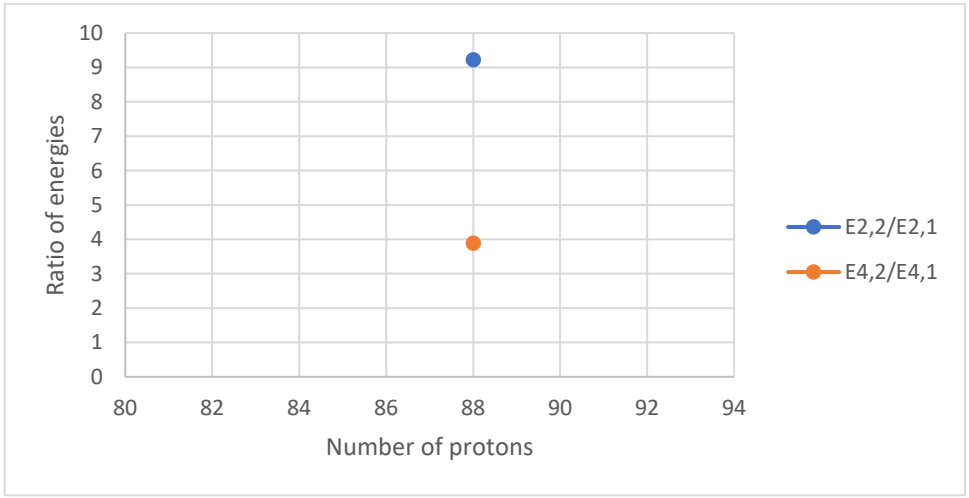

C

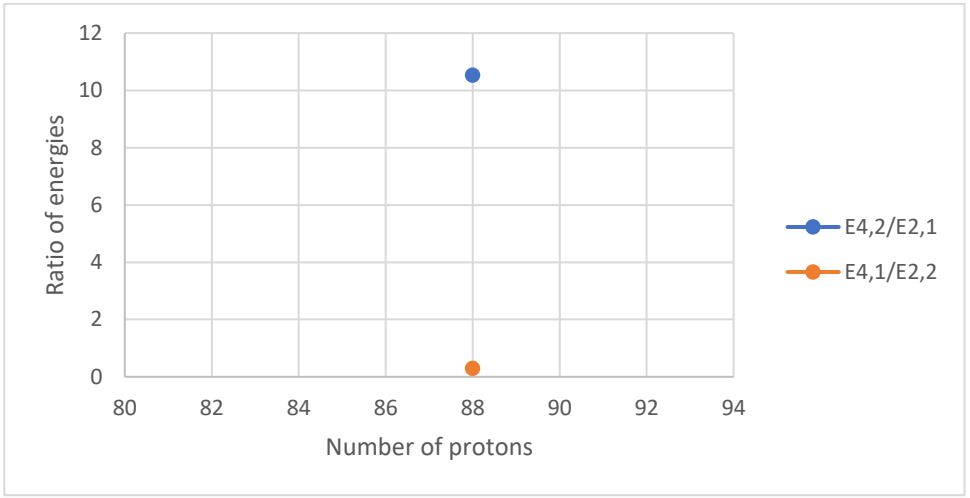

D

Figure V. 67 (color online) Panel **A** represents the comparison of the experimental energy levels of the lowest 2_1^+, 2_2^+, 4_1^+ and 4_2^+ states for the chain of N=134 isotones. Panels **B, C, D** represent the comparison of the experimental energy ratios ($E_{4_1^+}/E_{2_1^+}$ and $E_{4_2^+}/E_{2_2^+}$), ($E_{2_2^+}/E_{2_1^+}$ and $E_{4_2^+}/E_{4_1^+}$) and ($E_{4_2^+}/E_{2_1^+}$ and $E_{4_1^+}/E_{2_2^+}$), respectively, for the chain of N=134 isotones.

Isotones (N=136)

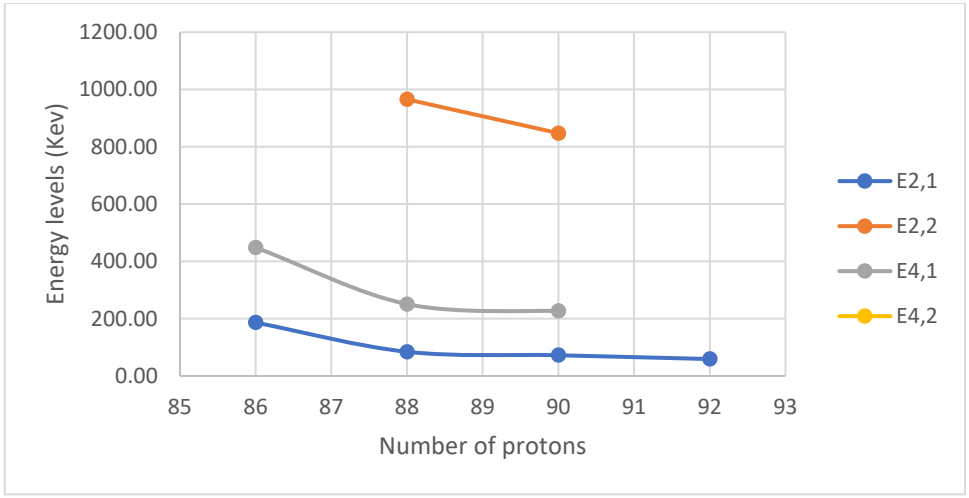

A

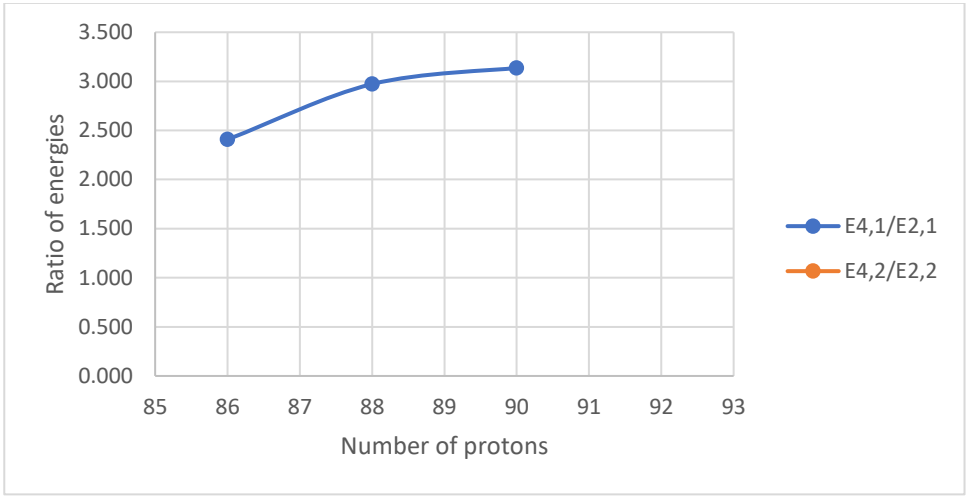

B

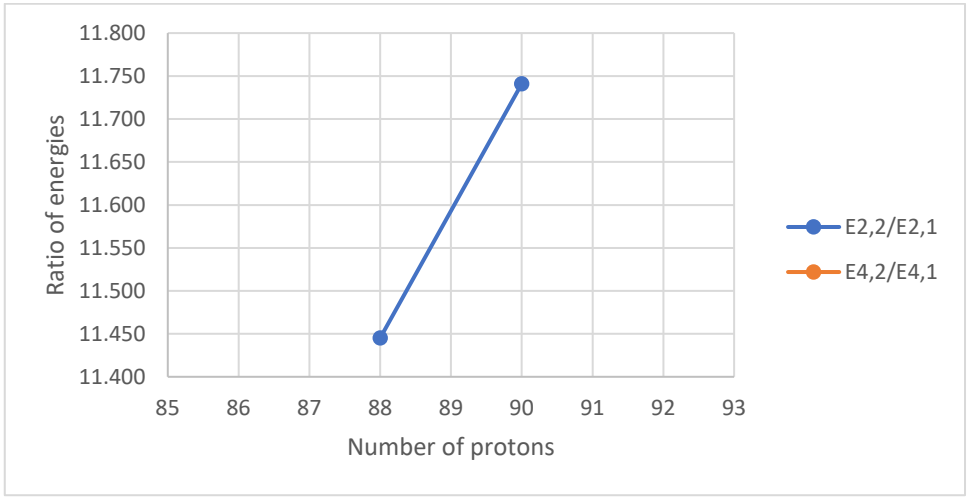

C

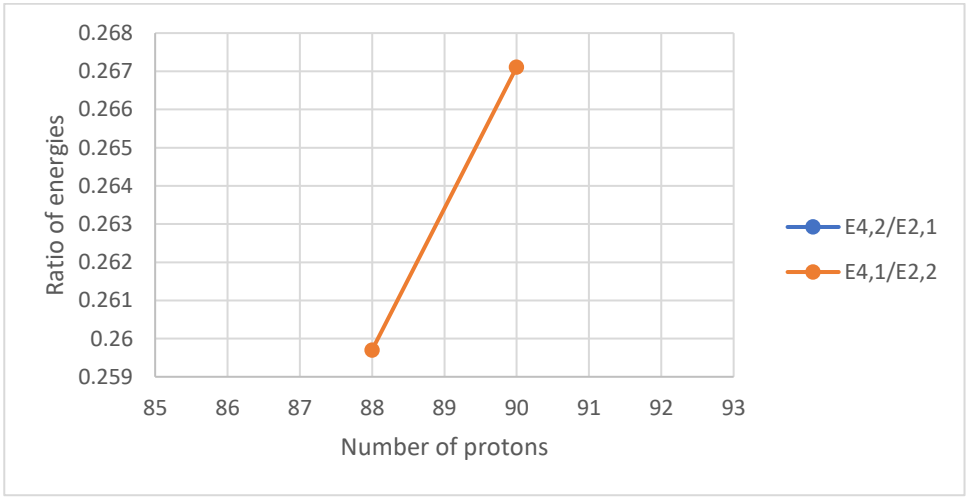

D

Figure V. 68 (color online) Panel **A** represents the comparison of the experimental energy levels of the lowest 2_1^+, 2_2^+, 4_1^+ and 4_2^+ states for the chain of N=136 isotones. Panels **B, C, D** represent the comparison of the experimental energy ratios ($E_{4_1^+}/E_{2_1^+}$ and $E_{4_2^+}/E_{2_2^+}$), ($E_{2_2^+}/E_{2_1^+}$ and $E_{4_2^+}/E_{4_1^+}$) and ($E_{4_2^+}/E_{2_1^+}$ and $E_{4_1^+}/E_{2_2^+}$), respectively, for the chain of N=136 isotones.

Isotones (N=138)

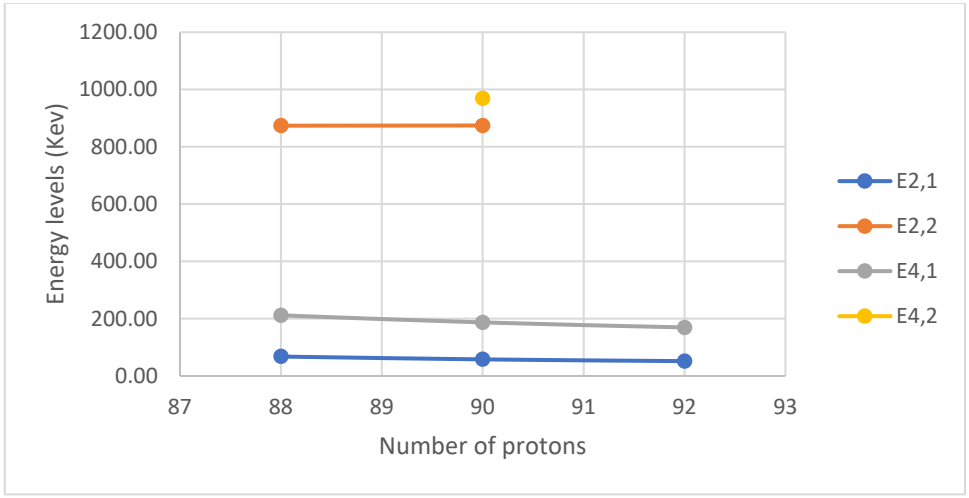

A

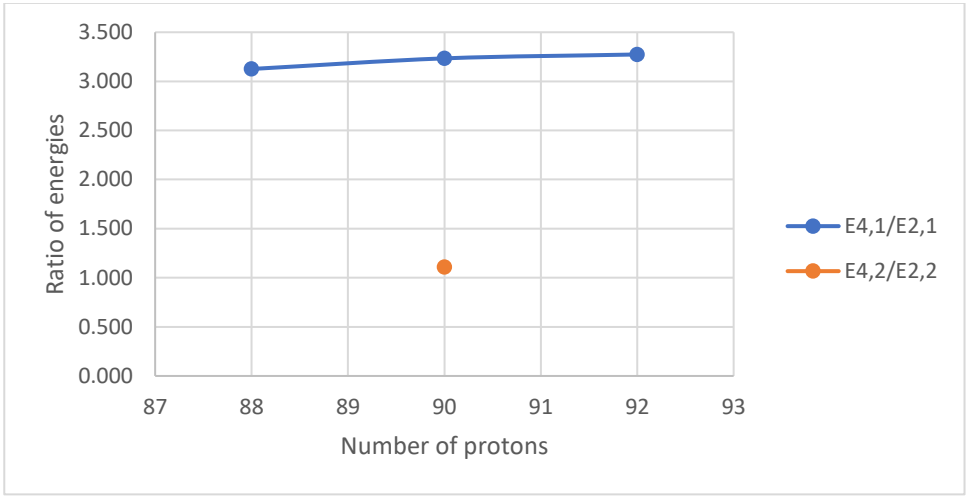

B

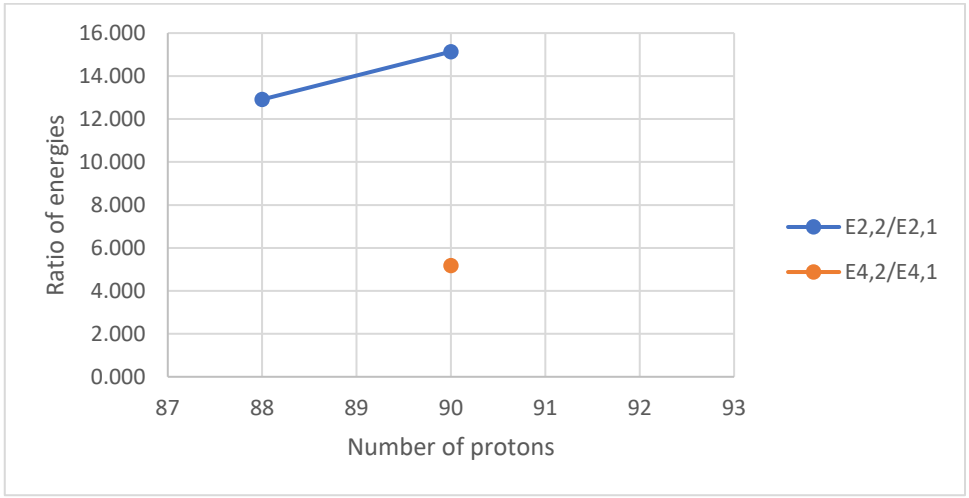

C

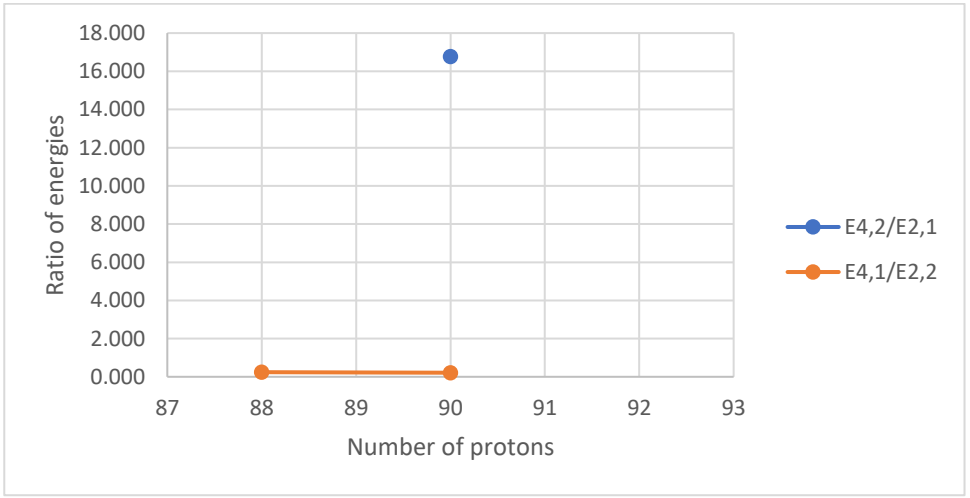

D

Figure V. 69 (color online) Panel **A** represents the comparison of the experimental energy levels of the lowest 2_1^+, 2_2^+, 4_1^+ and 4_2^+ states for the chain of N=138 isotones. Panels **B, C, D** represent the comparison of the experimental energy ratios ($E_{4_1^+}/E_{2_1^+}$ and $E_{4_2^+}/E_{2_2^+}$), ($E_{2_2^+}/E_{2_1^+}$ and $E_{4_2^+}/E_{4_1^+}$) and ($E_{4_2^+}/E_{2_1^+}$ and $E_{4_1^+}/E_{2_2^+}$), respectively, for the chain of N=138 isotones.

Isotones (N=140)

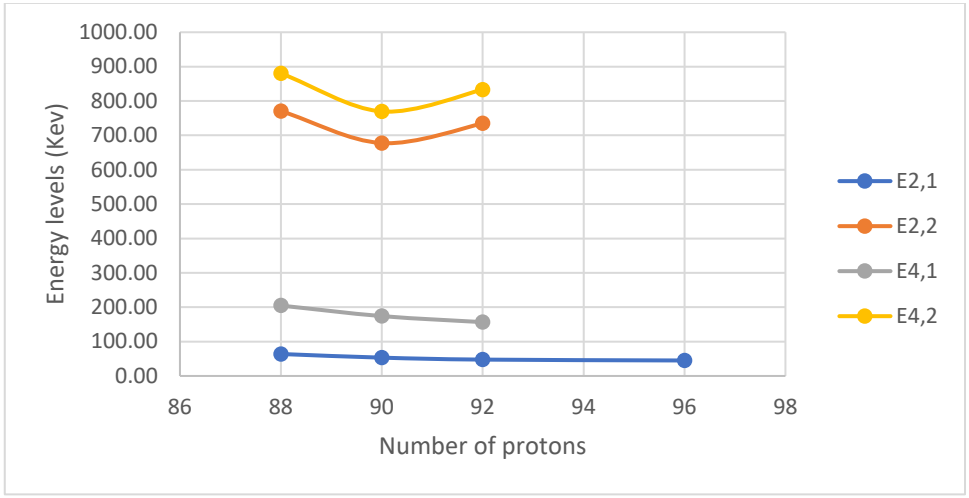

A

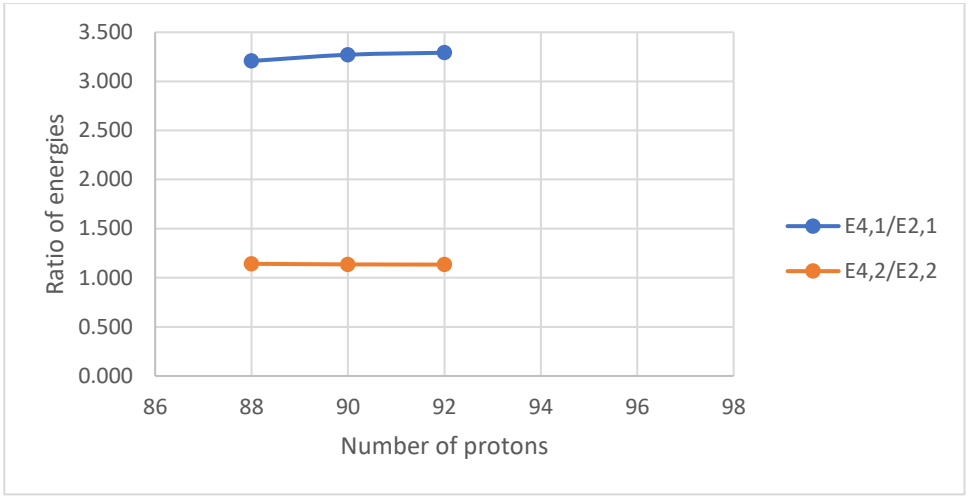

B

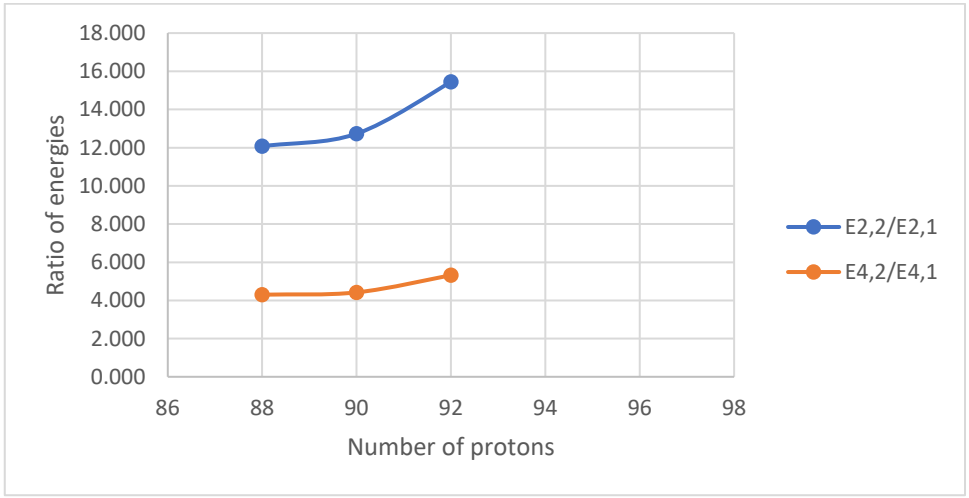

C

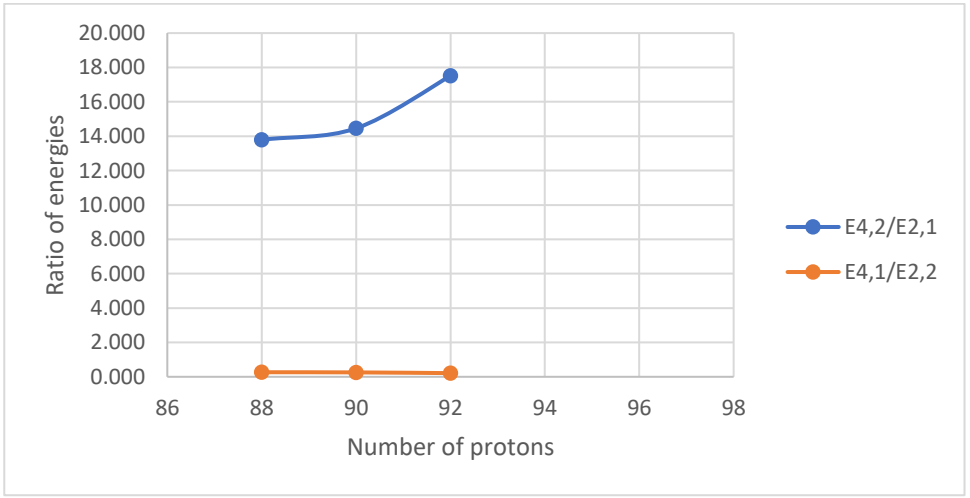

D

Figure V. 70 (color online) Panel **A** represents the comparison of the experimental energy levels of the lowest 2_1^+, 2_2^+, 4_1^+ and 4_2^+ states for the chain of N=140 isotones. Panels **B, C, D** represent the comparison of the experimental energy ratios ($E_{4_1^+}/E_{2_1^+}$ and $E_{4_2^+}/E_{2_2^+}$), ($E_{2_2^+}/E_{2_1^+}$ and $E_{4_2^+}/E_{4_1^+}$) and ($E_{4_2^+}/E_{2_1^+}$ and $E_{4_1^+}/E_{2_2^+}$), respectively, for the chain of N=140 isotones.

Isotones (N=142)

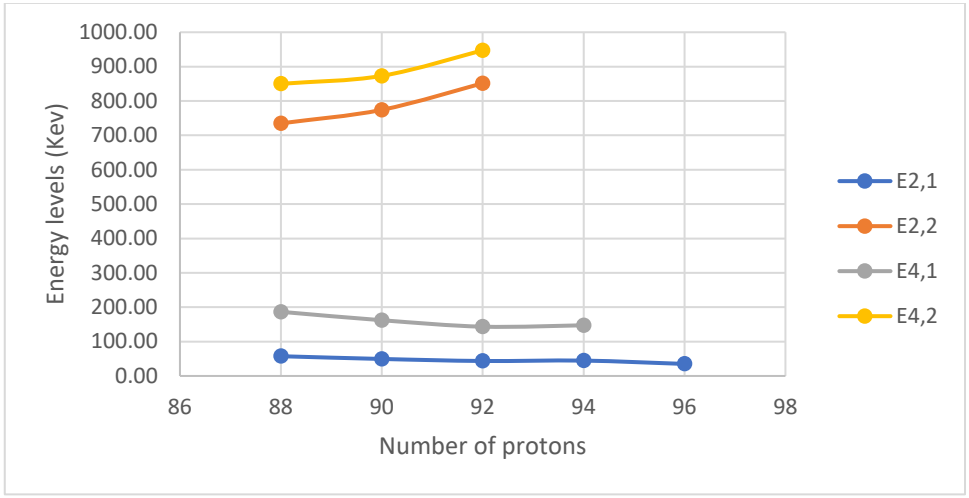

A

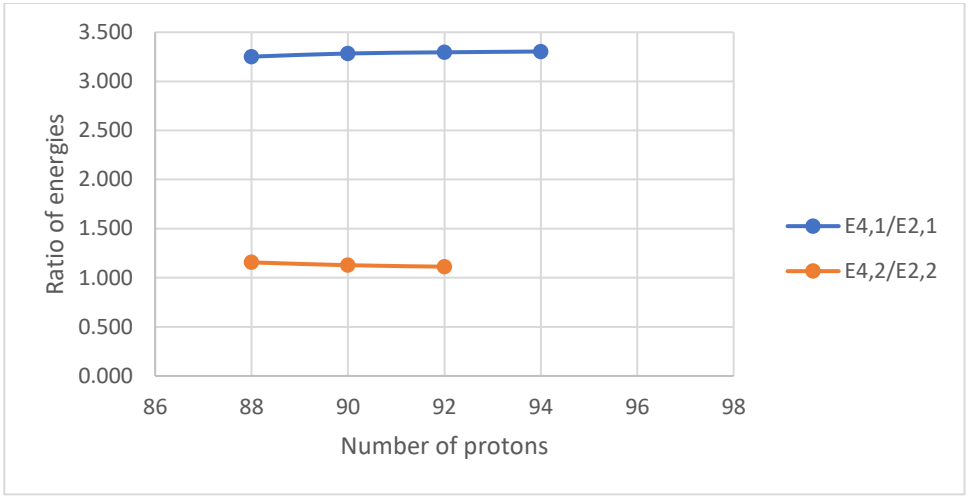

B

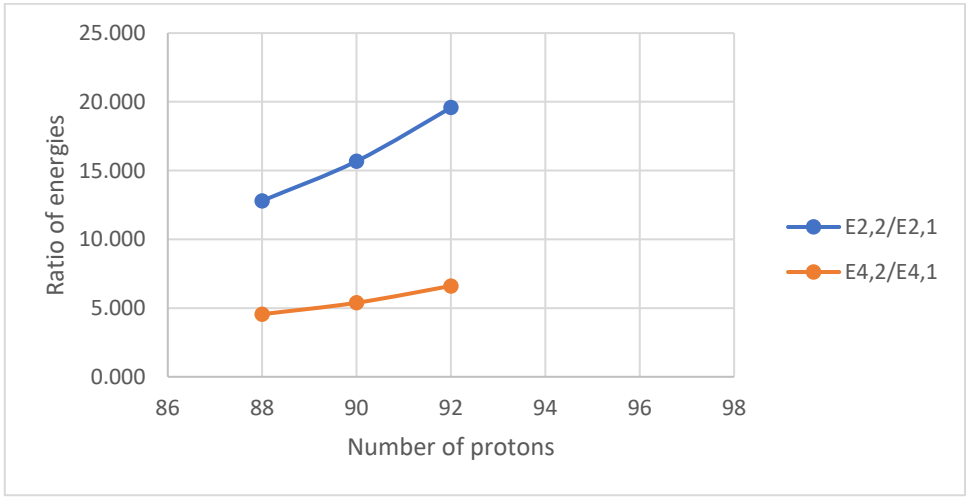

C

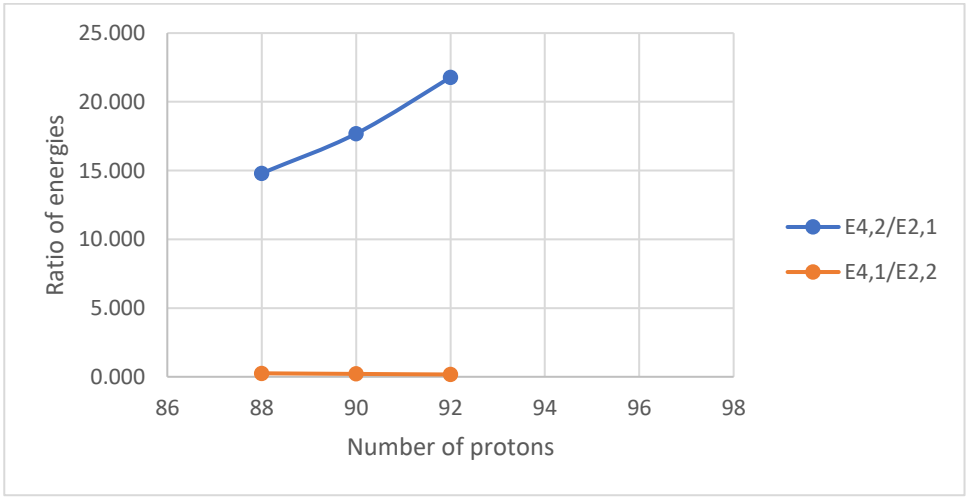

D

Figure V. 71 (color online) Panel **A** represents the comparison of the experimental energy levels of the lowest 2_1^+, 2_2^+, 4_1^+ and 4_2^+ states for the chain of N=142 isotones. Panels **B, C, D** represent the comparison of the experimental energy ratios ($E_{4_1^+}/E_{2_1^+}$ and $E_{4_2^+}/E_{2_2^+}$), ($E_{2_2^+}/E_{2_1^+}$ and $E_{4_2^+}/E_{4_1^+}$) and ($E_{4_2^+}/E_{2_1^+}$ and $E_{4_1^+}/E_{2_2^+}$), respectively, for the chain of N=142 isotones.

Isotones (N=144)

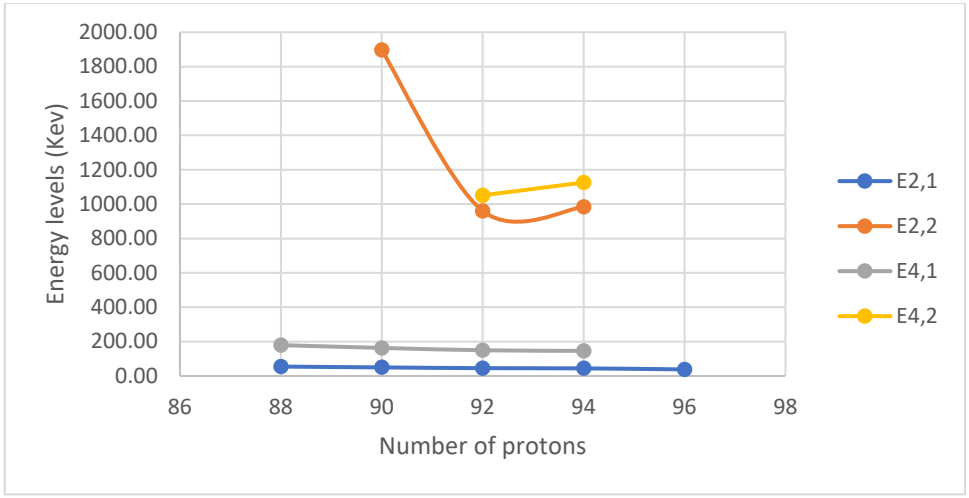

A

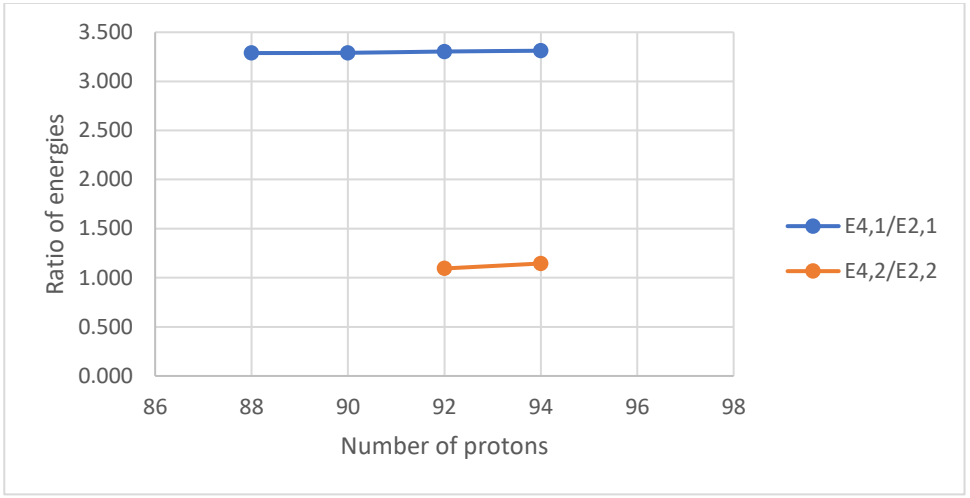

B

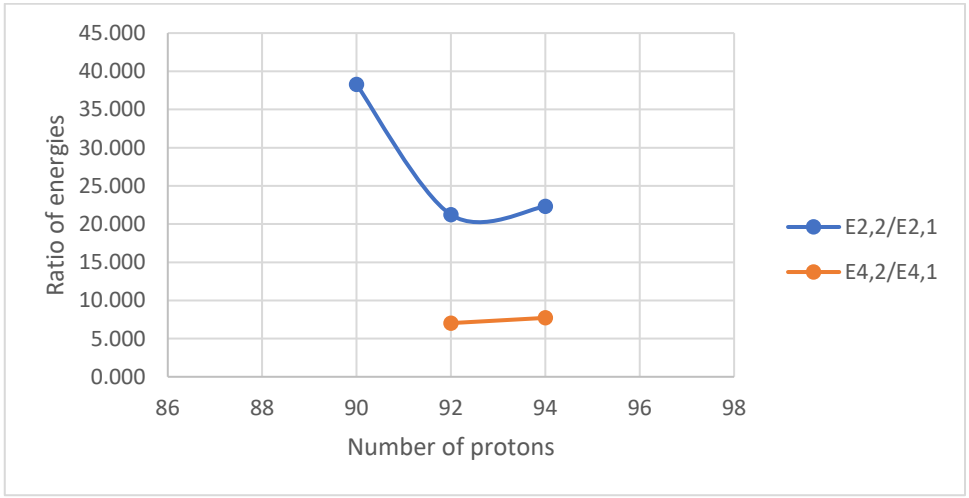

C

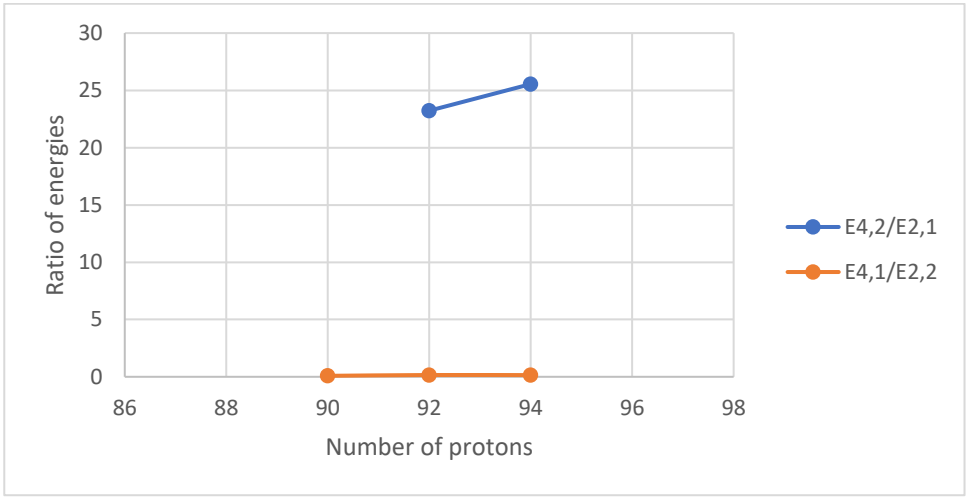

D

Figure V. 72 (color online) Panel **A** represents the comparison of the experimental energy levels of the lowest 2_1^+, 2_2^+, 4_1^+ and 4_2^+ states for the chain of N=144 isotones. Panels **B, C, D** represent the comparison of the experimental energy ratios ($E_{4_1^+}/E_{2_1^+}$ and $E_{4_2^+}/E_{2_2^+}$), ($E_{2_2^+}/E_{2_1^+}$ and $E_{4_2^+}/E_{4_1^+}$) and ($E_{4_2^+}/E_{2_1^+}$ and $E_{4_1^+}/E_{2_2^+}$), respectively, for the chain of N=144 isotones.

Isotones (N=146)

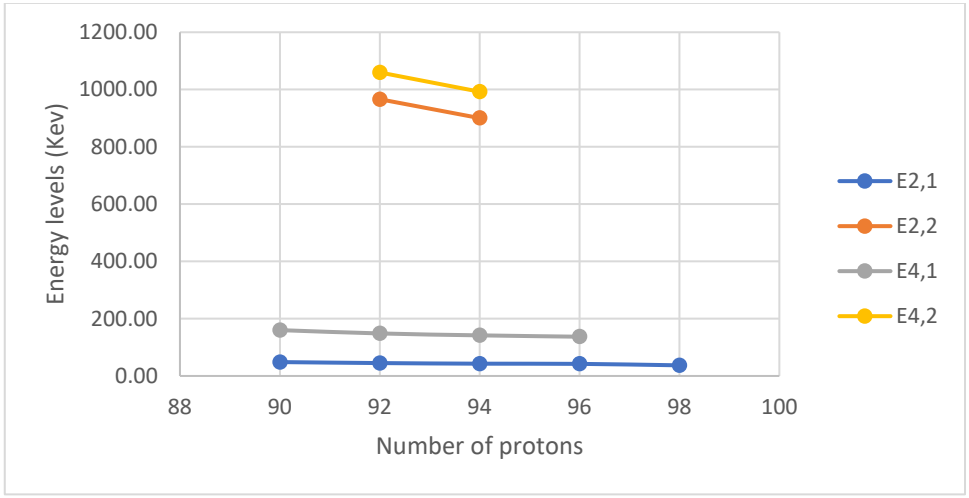

A

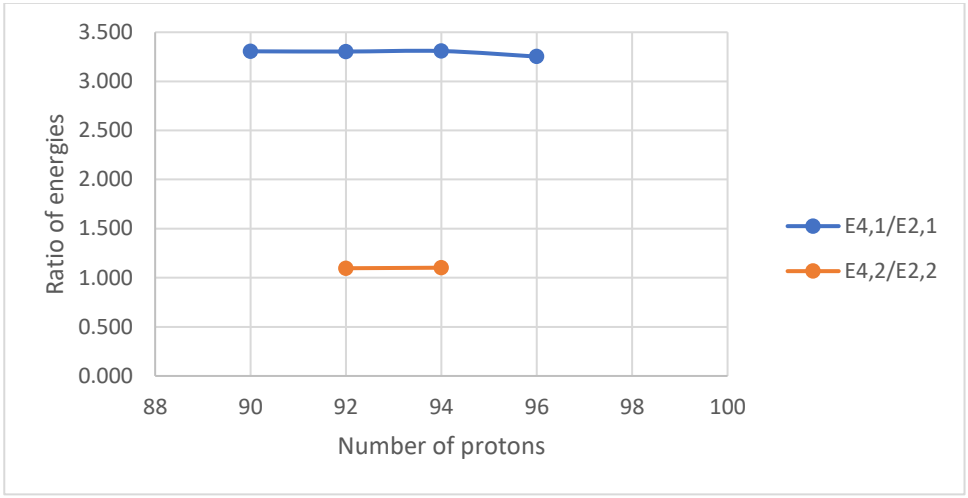

B

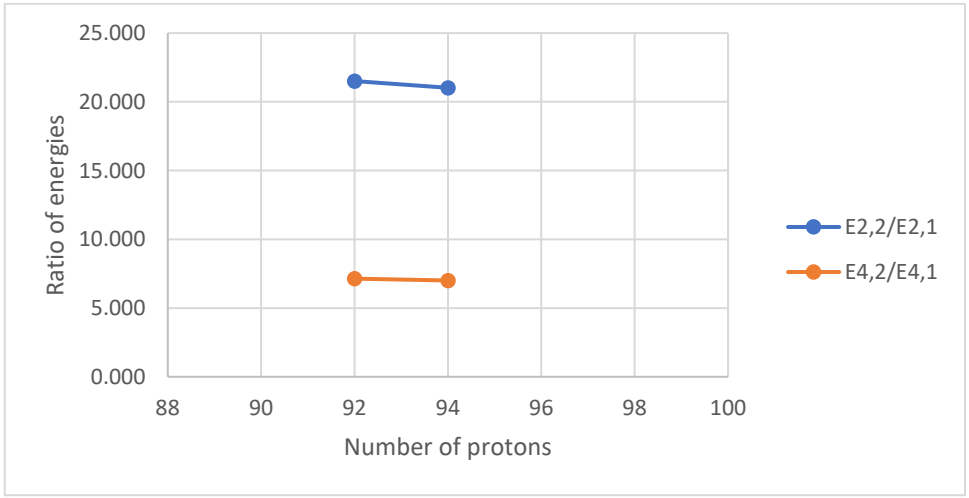

C

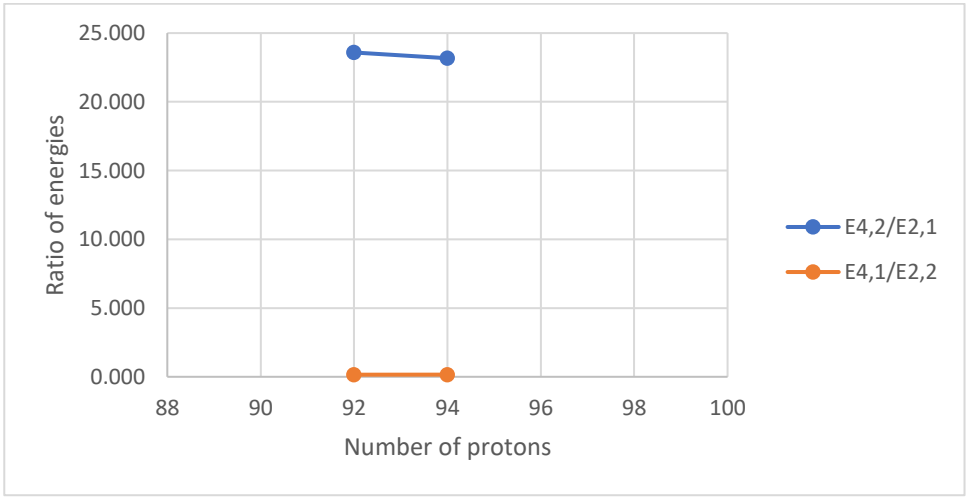

D

Figure V. 73 (color online) Panel **A** represents the comparison of the experimental energy levels of the lowest 2_1^+, 2_2^+, 4_1^+ and 4_2^+ states for the chain of N=146 isotones. Panels **B, C, D** represent the comparison of the experimental energy ratios ($E_{4_1^+}/E_{2_1^+}$ and $E_{4_2^+}/E_{2_2^+}$), ($E_{2_2^+}/E_{2_1^+}$ and $E_{4_2^+}/E_{4_1^+}$) and ($E_{4_2^+}/E_{2_1^+}$ and $E_{4_1^+}/E_{2_2^+}$), respectively, for the chain of N=146 isotones.

Isotones (N=148)

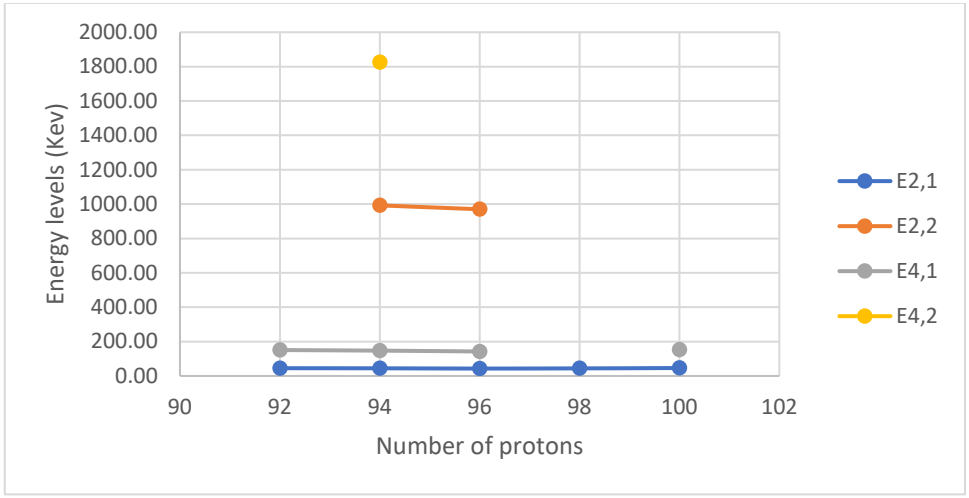

A

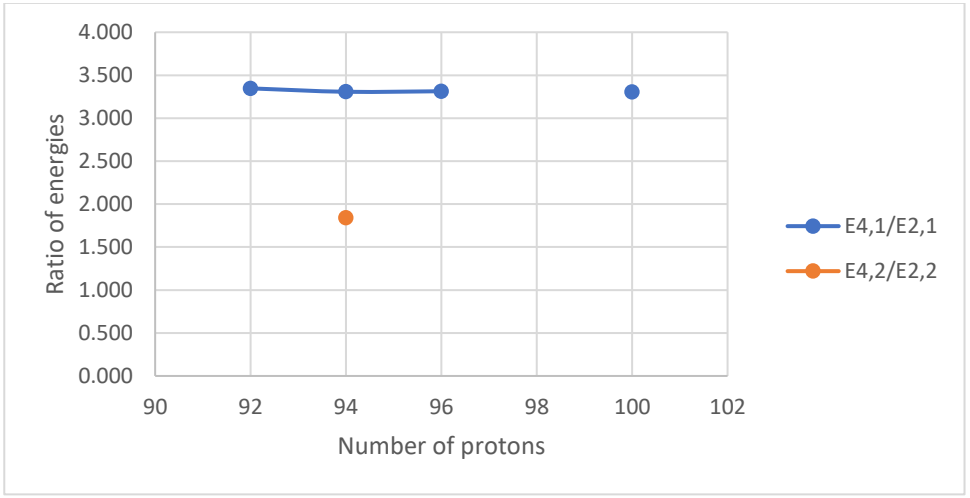

B

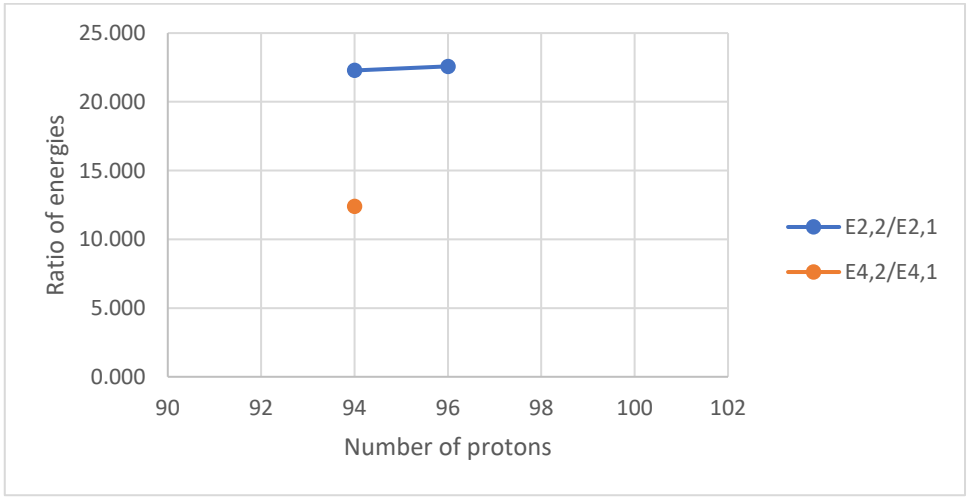

C

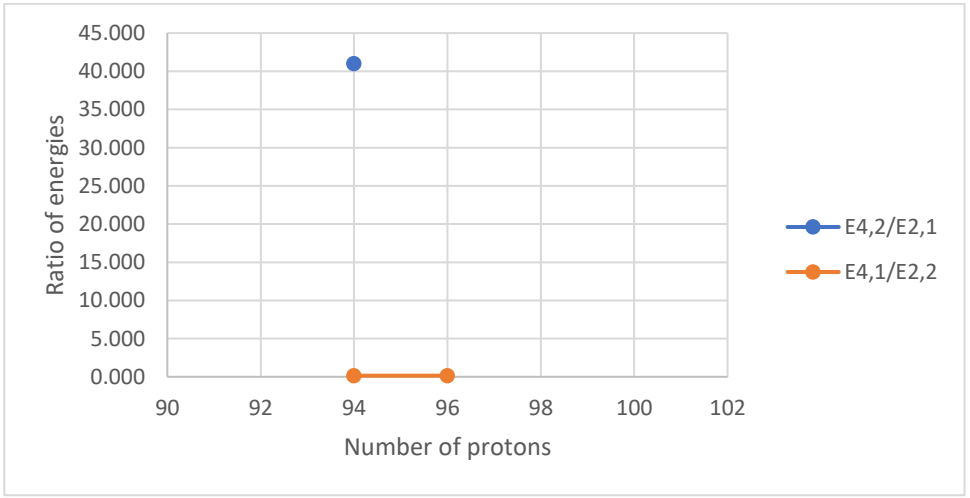

D

Figure V. 74 (color online) Panel **A** represents the comparison of the experimental energy levels of the lowest 2_1^+, 2_2^+, 4_1^+ and 4_2^+ states for the chain of N=148 isotones. Panels **B, C, D** represent the comparison of the experimental energy ratios ($E_{4_1^+}/E_{2_1^+}$ and $E_{4_2^+}/E_{2_2^+}$), ($E_{2_2^+}/E_{2_1^+}$ and $E_{4_2^+}/E_{4_1^+}$) and ($E_{4_2^+}/E_{2_1^+}$ and $E_{4_1^+}/E_{2_2^+}$), respectively, for the chain of N=148 isotones.

Isotones (N=150)

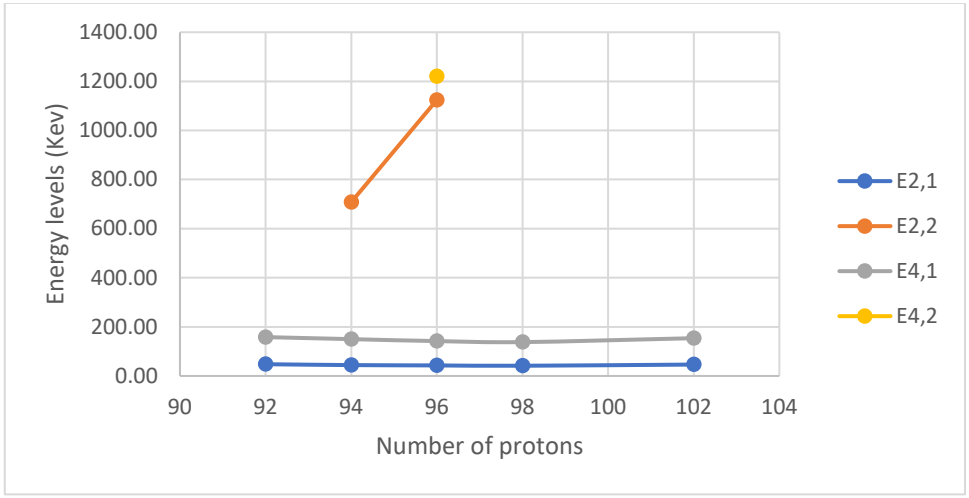

A

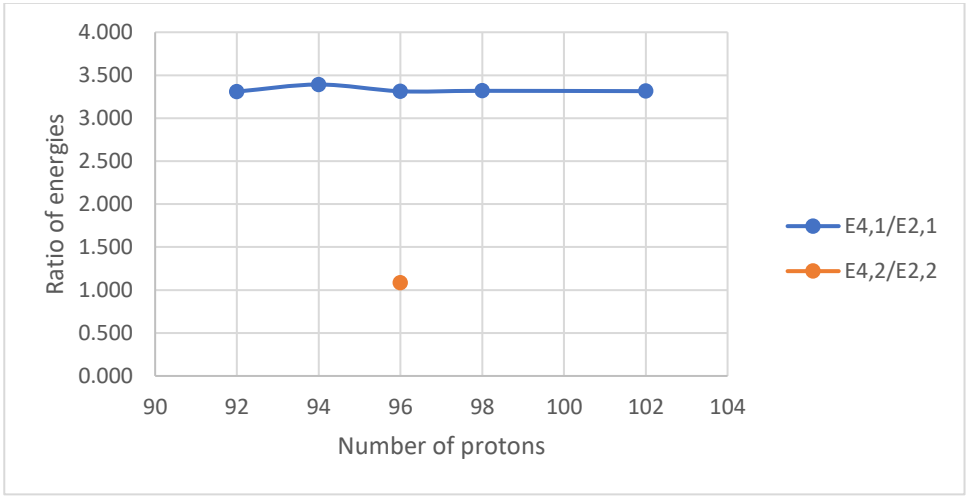

B

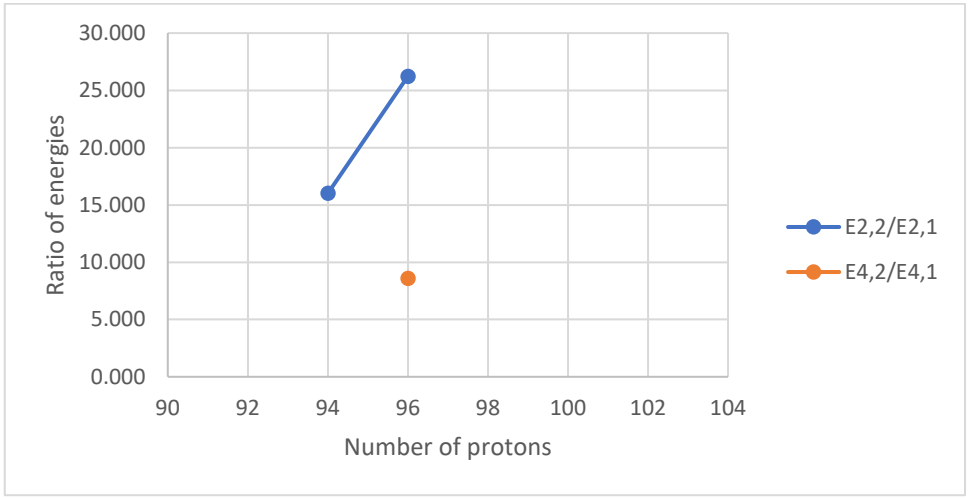

C

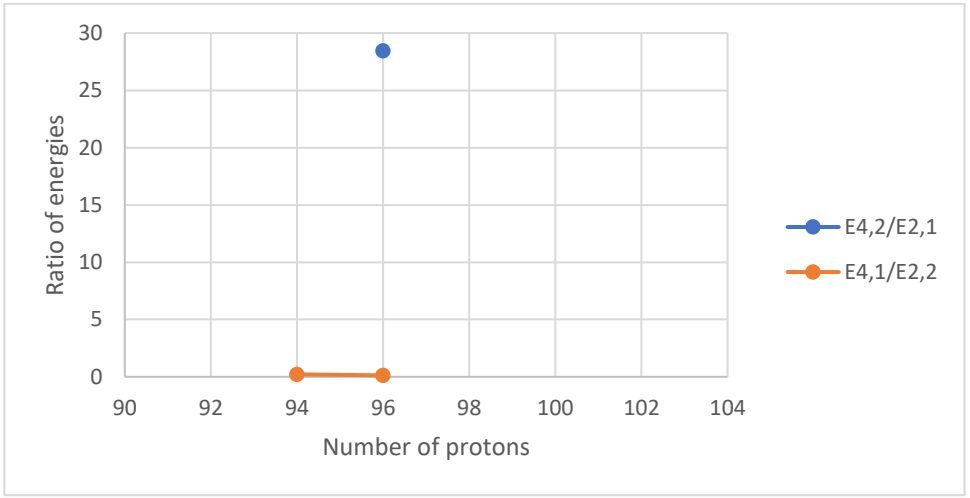

D

Figure V. 75 (color online) Panel **A** represents the comparison of the experimental energy levels of the lowest 2_1^+, 2_2^+, 4_1^+ and 4_2^+ states for the chain of N=150 isotones. Panels **B, C, D** represent the comparison of the experimental energy ratios ($E_{4_1^+}/E_{2_1^+}$ and $E_{4_2^+}/E_{2_2^+}$), ($E_{2_2^+}/E_{2_1^+}$ and $E_{4_2^+}/E_{4_1^+}$) and ($E_{4_2^+}/E_{2_1^+}$ and $E_{4_1^+}/E_{2_2^+}$), respectively, for the chain of N=150 isotones.

Isotones (N=152)

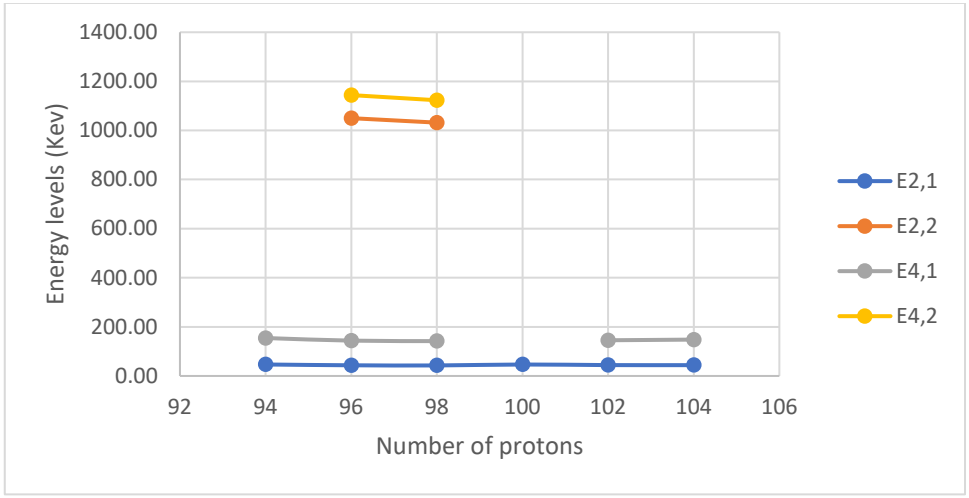

A

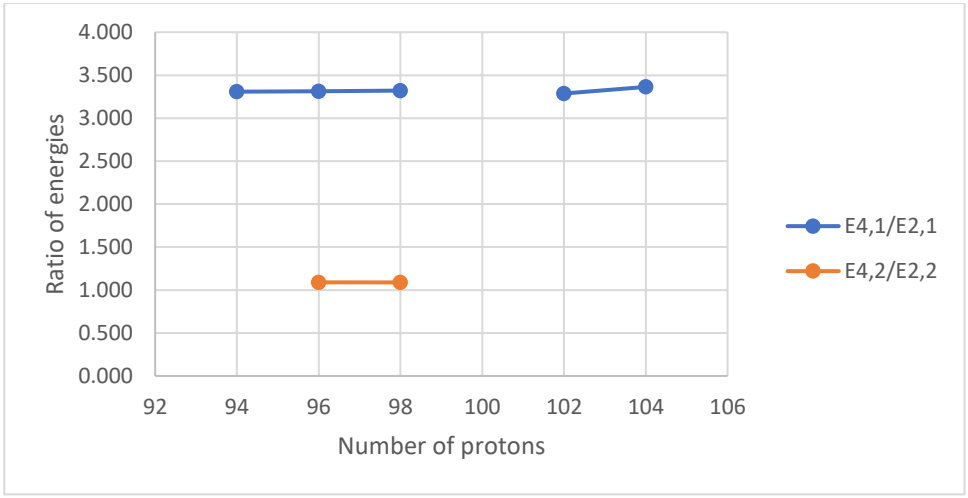

B

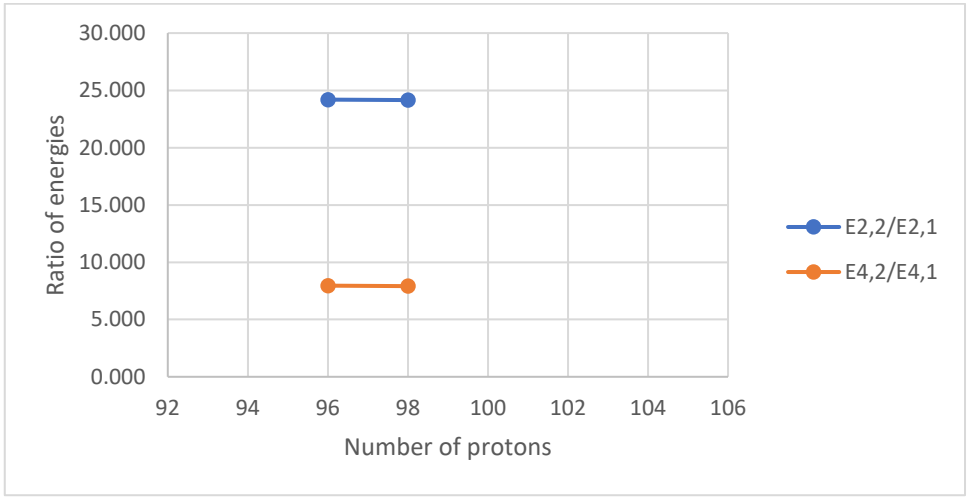

C

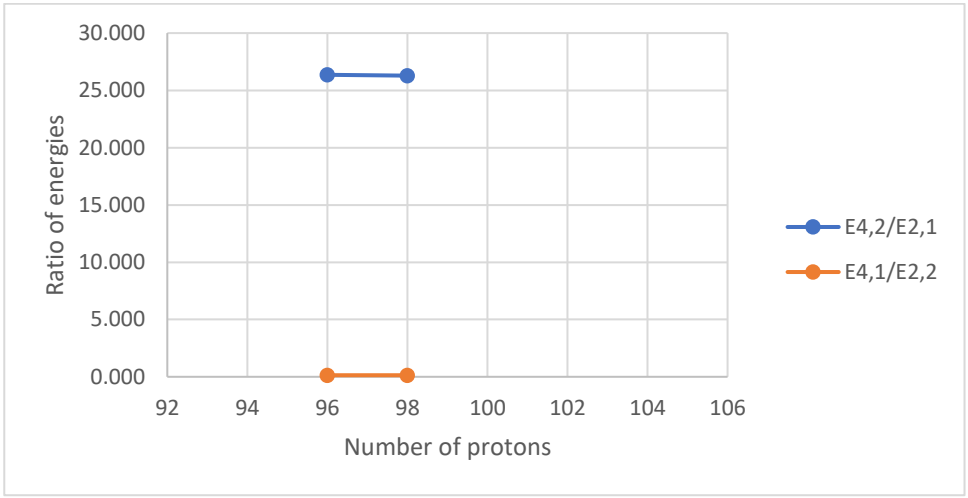

D

Figure V. 76 (color online) Panel **A** represents the comparison of the experimental energy levels of the lowest 2_1^+, 2_2^+, 4_1^+ and 4_2^+ states for the chain of N=152 isotones. Panels **B, C, D** represent the comparison of the experimental energy ratios ($E_{4_1^+}/E_{2_1^+}$ and $E_{4_2^+}/E_{2_2^+}$), ($E_{2_2^+}/E_{2_1^+}$ and $E_{4_2^+}/E_{4_1^+}$) and ($E_{4_2^+}/E_{2_1^+}$ and $E_{4_1^+}/E_{2_2^+}$), respectively, for the chain of N=152 isotones.

Isotones (N=154)

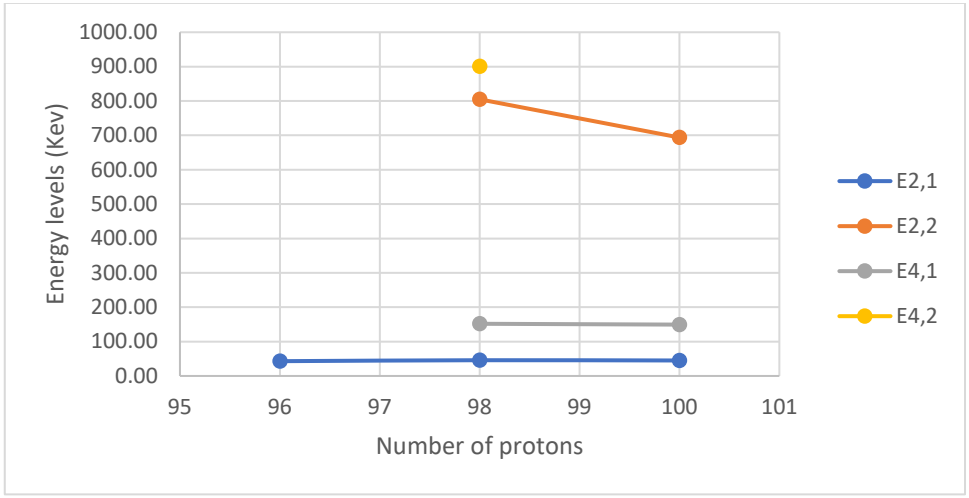

A

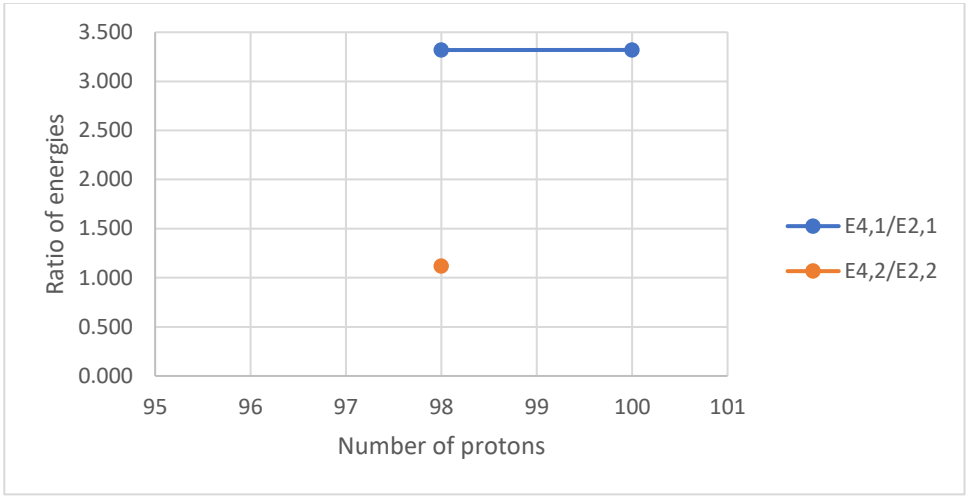

B

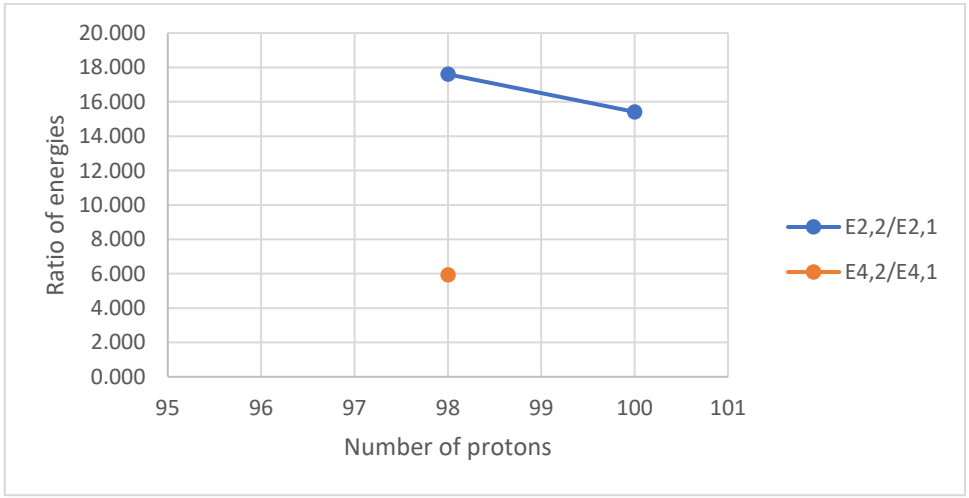

C

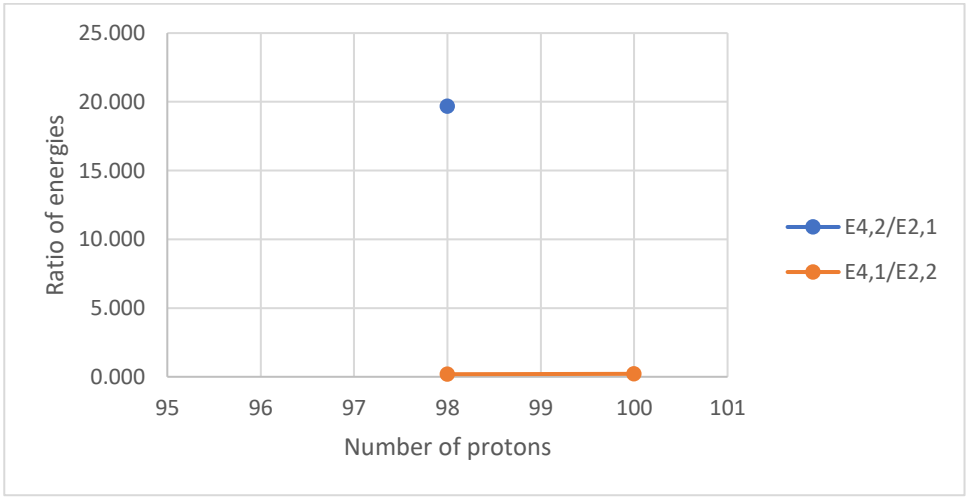

D

Figure V. 77 (color online) Panel **A** represents the comparison of the experimental energy levels of the lowest 2_1^+, 2_2^+, 4_1^+ and 4_2^+ states for the chain of N=154 isotones. Panels **B, C, D** represent the comparison of the experimental energy ratios ($E_{4_1^+}/E_{2_1^+}$ and $E_{4_2^+}/E_{2_2^+}$), ($E_{2_2^+}/E_{2_1^+}$ and $E_{4_2^+}/E_{4_1^+}$) and ($E_{4_2^+}/E_{2_1^+}$ and $E_{4_1^+}/E_{2_2^+}$), respectively, for the chain of N=154 isotones.

Isotones (N=156)

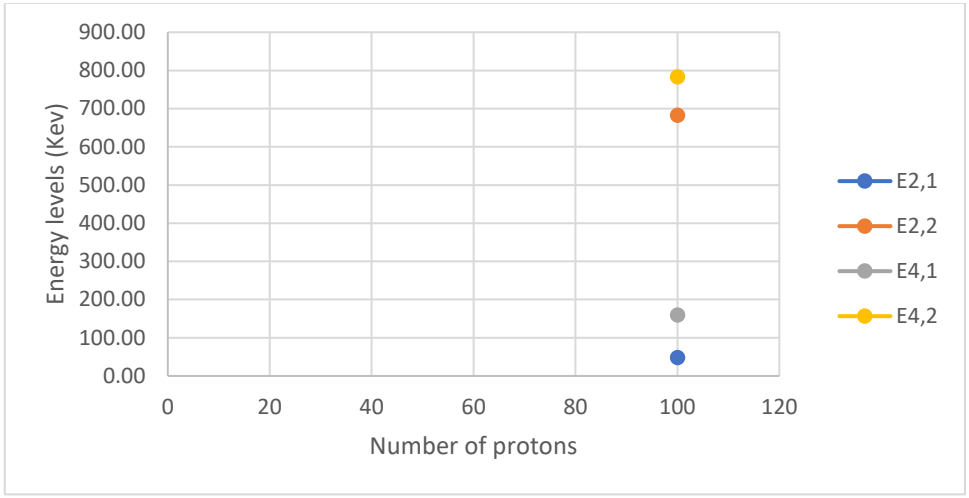

A

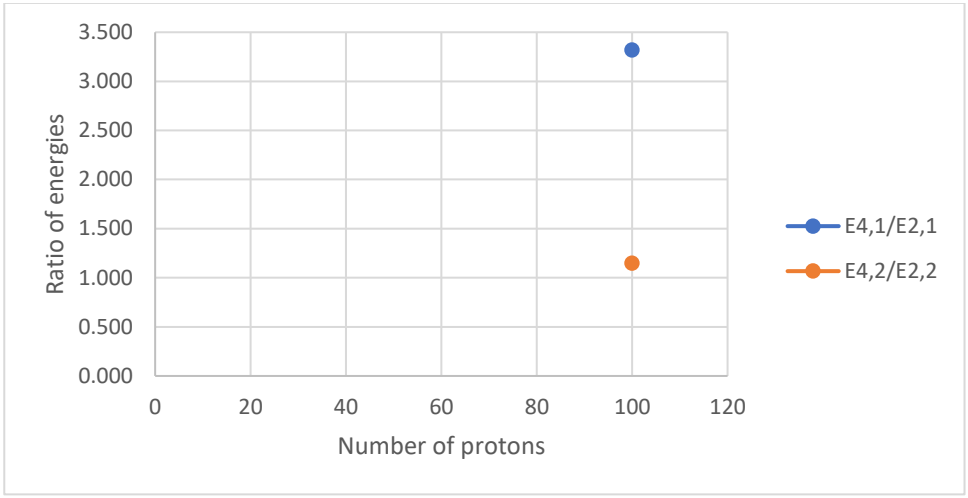

B

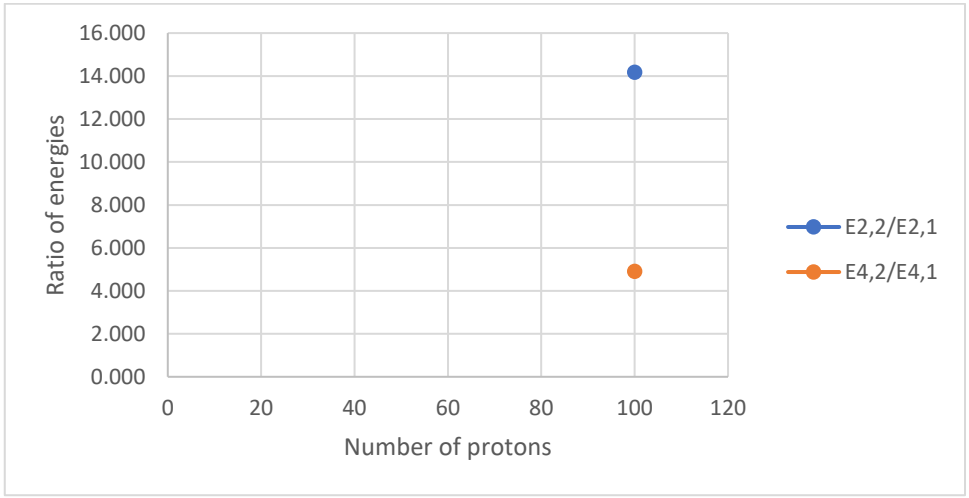

C

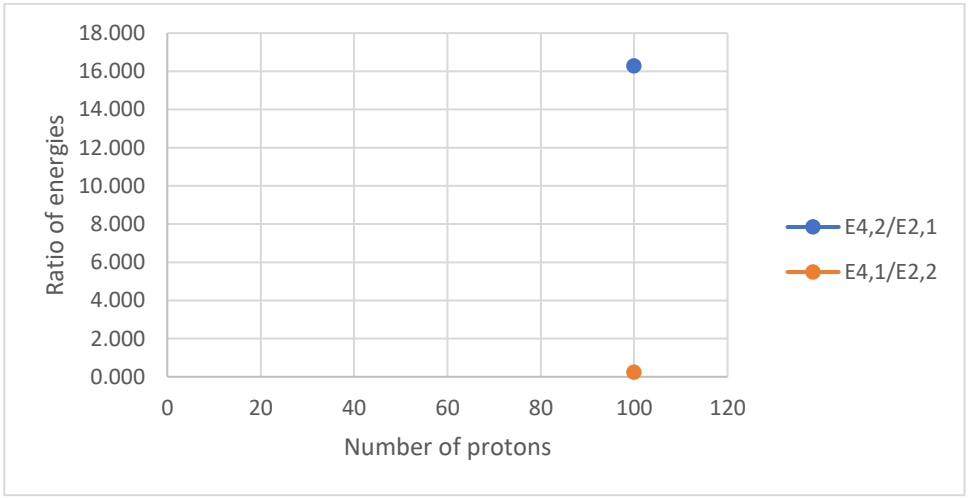

D

Figure V. 78 (color online) Panel **A** represents the comparison of the experimental energy levels of the lowest 2_1^+, 2_2^+, 4_1^+ and 4_2^+ states for the chain of N=156 isotones. Panels **B, C, D** represent the comparison of the experimental energy ratios ($E_{4_1^+}/E_{2_1^+}$ and $E_{4_2^+}/E_{2_2^+}$), ($E_{2_2^+}/E_{2_1^+}$ and $E_{4_2^+}/E_{4_1^+}$) and ($E_{4_2^+}/E_{2_1^+}$ and $E_{4_1^+}/E_{2_2^+}$), respectively, for the chain of N=156 isotones.

Chapter VI

Scatter plots showing relationship between the values of energy levels 2_1^+, 2_2^+, 4_1^+ and 4_2^+ for all even–even nuclei.

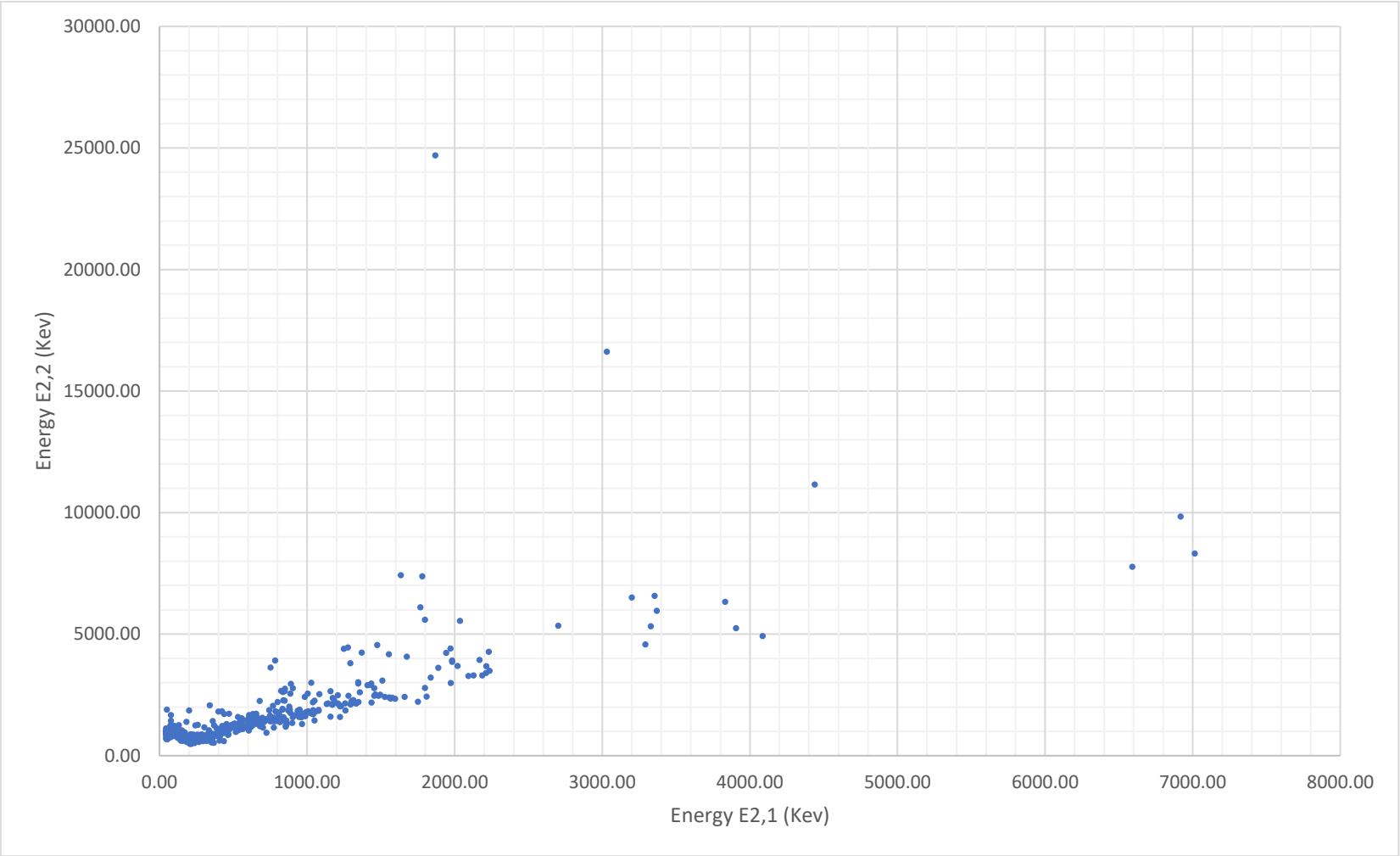

Figure VI. 1 (color online) Scatter plot showing relationship between the $E_{2_1^+}$ along the x axis and $E_{2_2^+}$ along the y axis for all even–even nuclei.

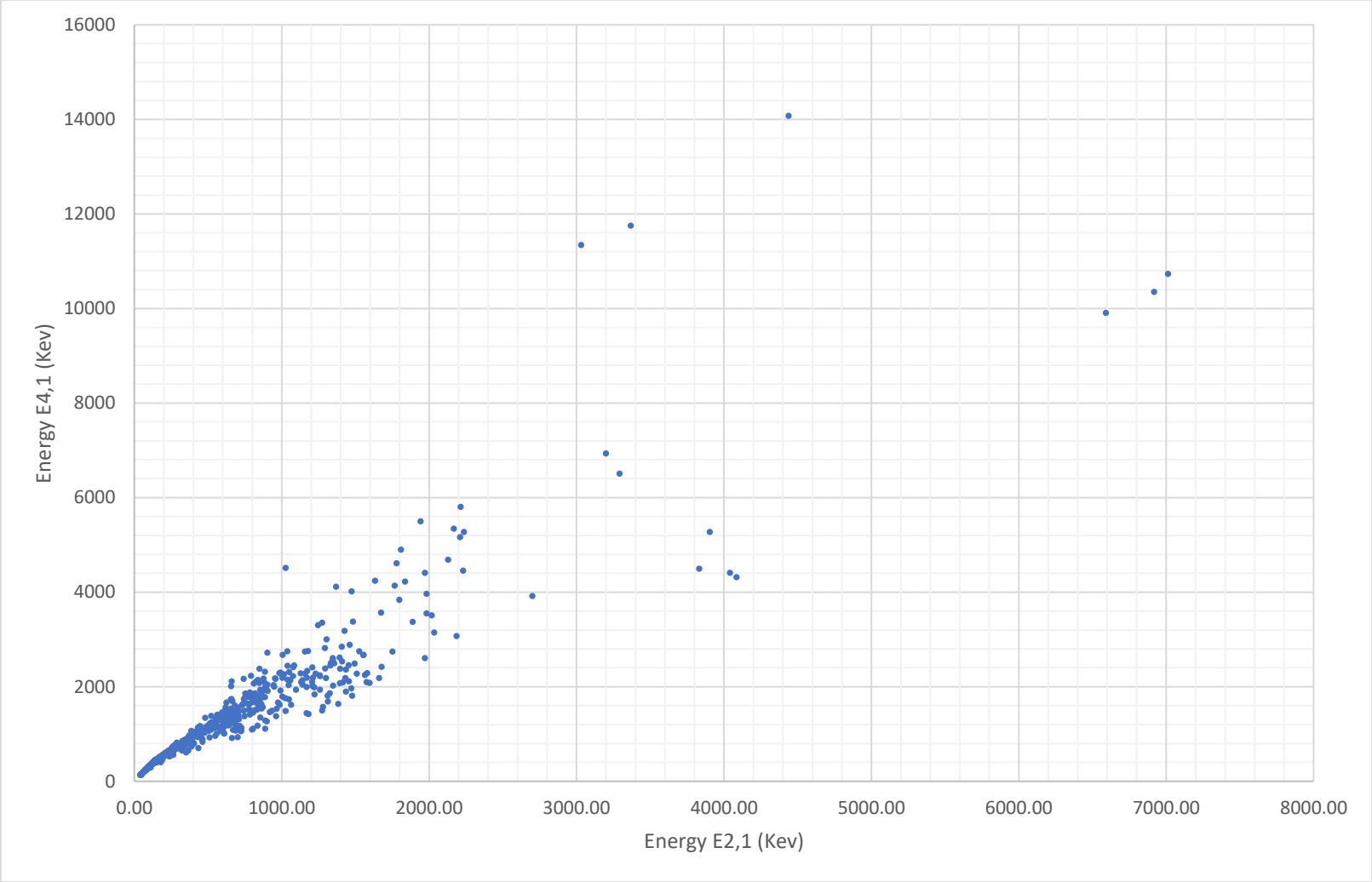

Figure VI. 2 (color online) Scatter plot showing relationship between the $E_{2_1^+}$ along the x axis and $E_{4_1^+}$ along the y axis for all even–even nuclei.

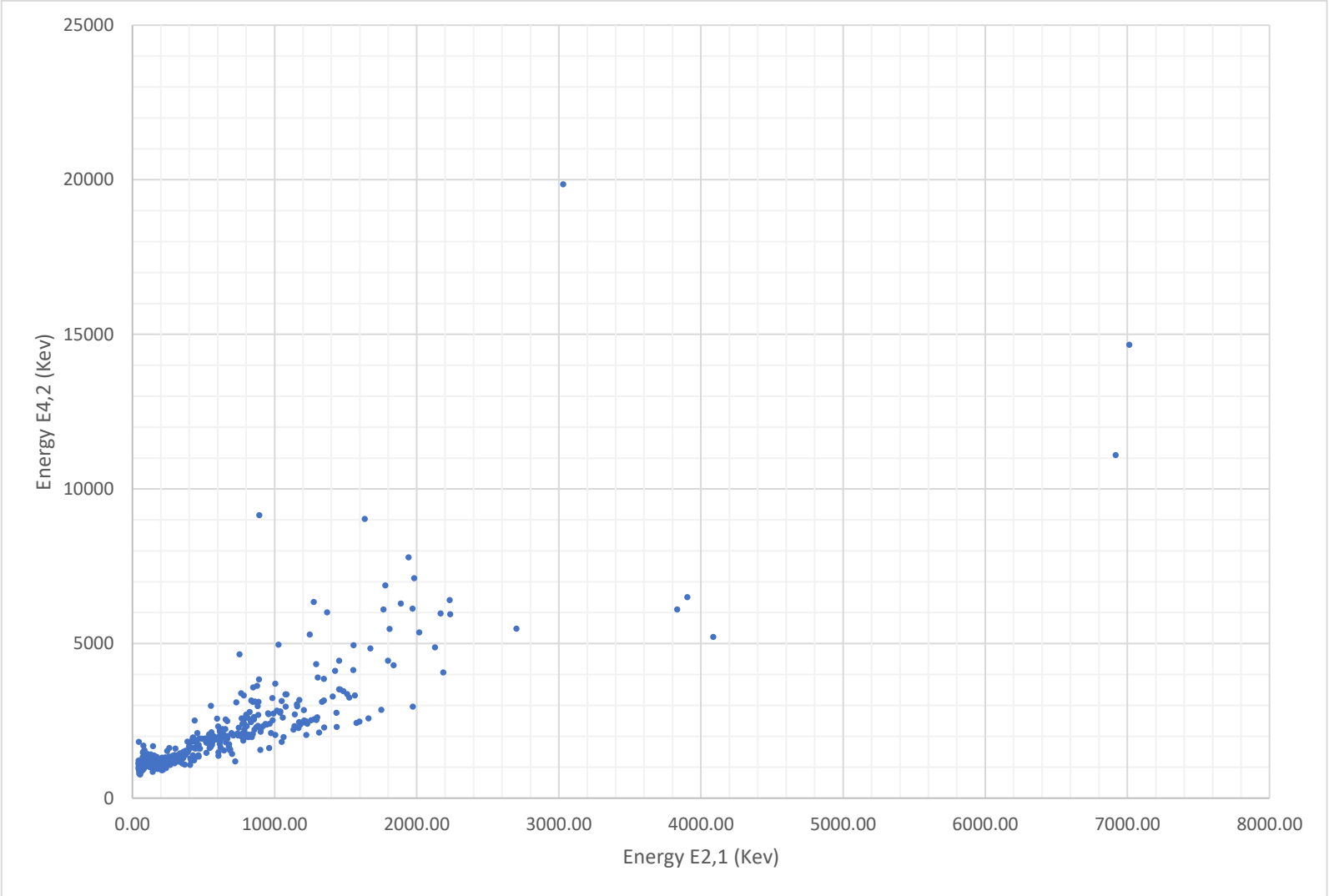

Figure VI. 3 (color online) Scatter plot showing relationship between the $E_{2_1^+}$ along the x axis and $E_{4_2^+}$ along the y axis for all even–even nuclei.

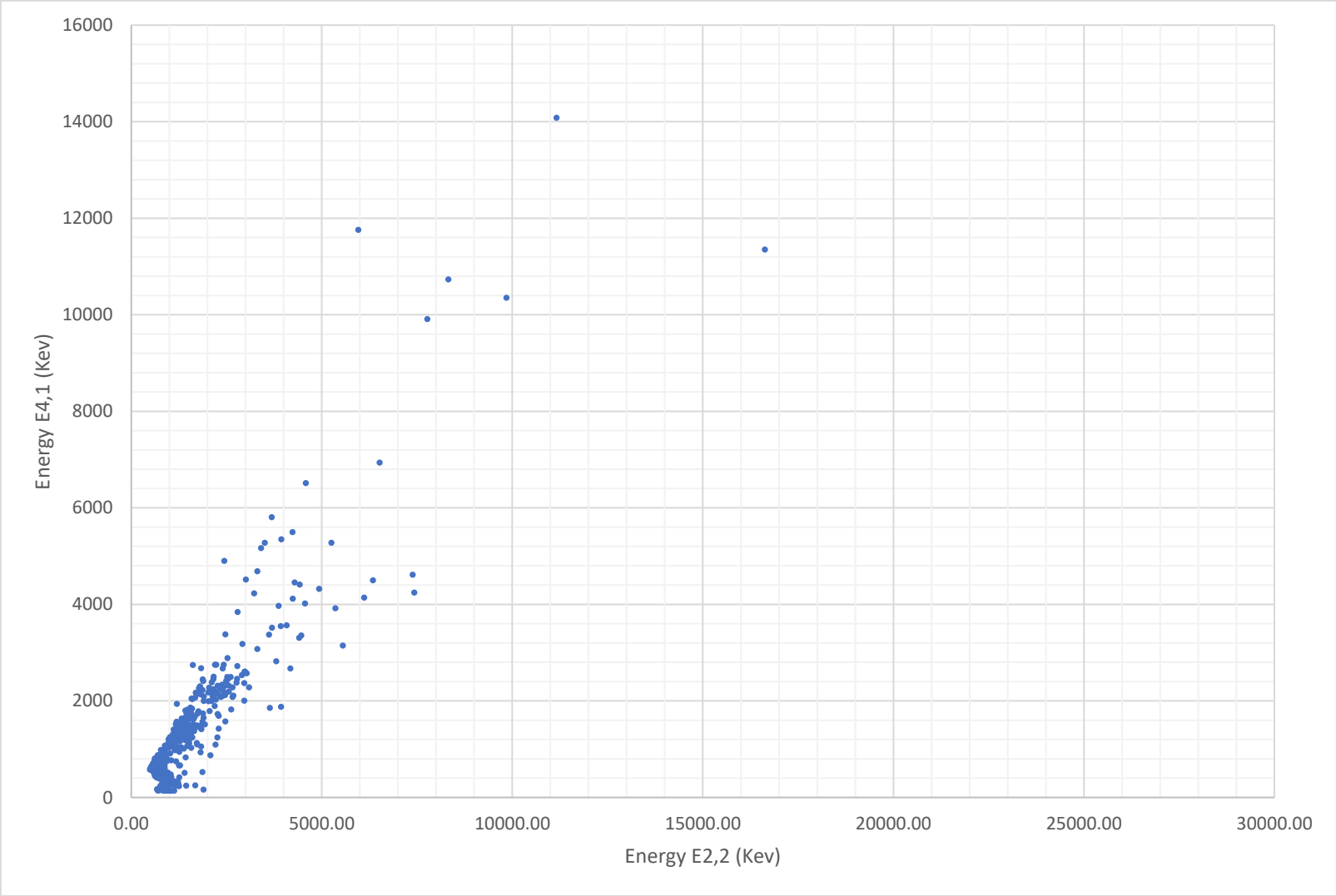

Figure VI. 4 (color online) Scatter plot showing relationship between the $E_{2_2^+}$ along the x axis and $E_{4_1^+}$ along the y axis for all even–even nuclei.

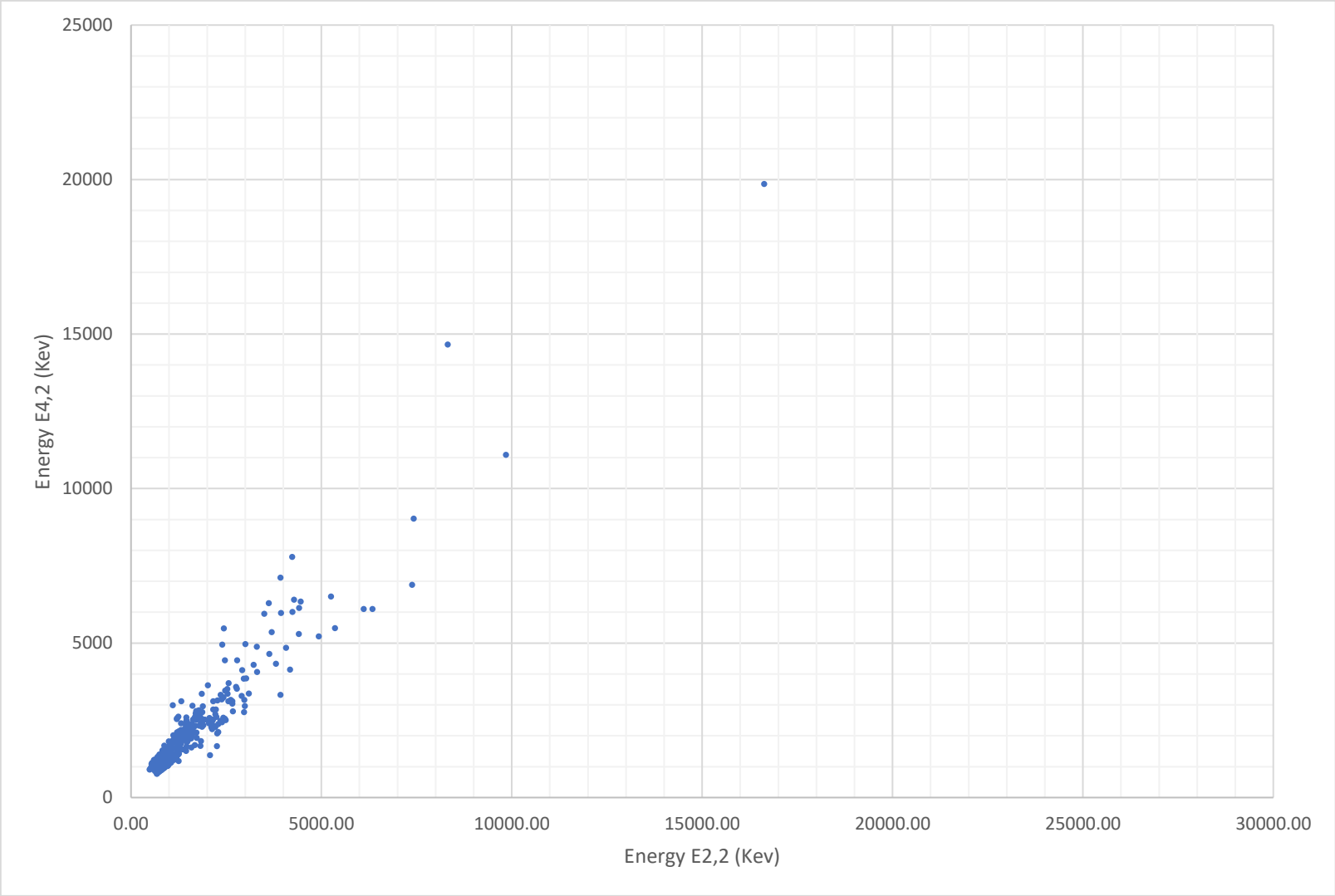

Figure VI. 5 (color online) Scatter plot showing relationship between the $E_{4_2^+}$ along the x axis and $E_{2_2^+}$ along the y axis for all even–even nuclei.

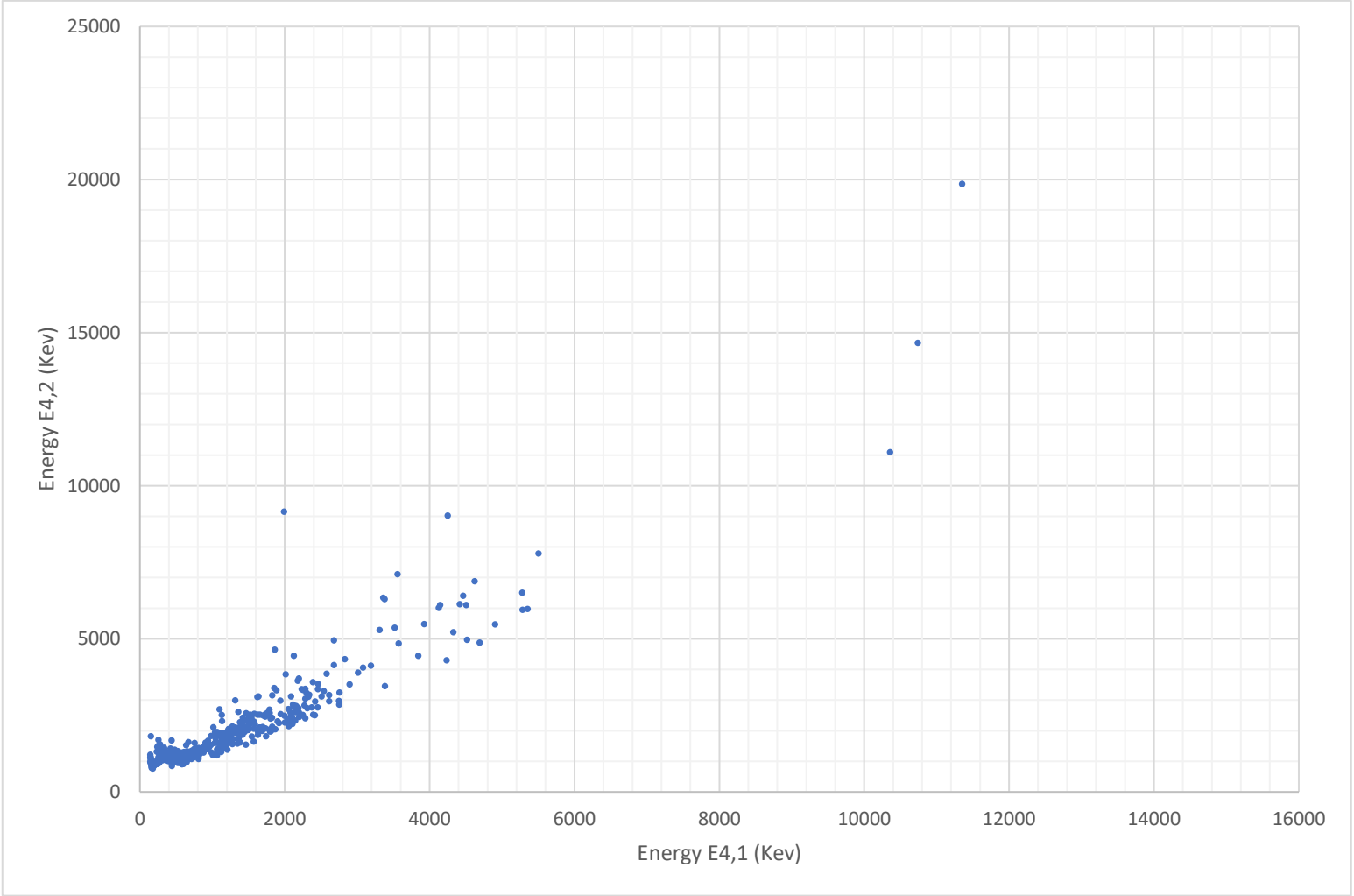

Figure VI. 6 (color online) Scatter plot showing relationship between the $E_{4_2^+}$ along the x axis and $E_{4_1^+}$ along the y axis for all even–even nuclei.

Chapter VII

Table of experimental data. In order are given: the nuclide, Z, N, A, $E_{2,1}$, $E_{2,2}$, $E_{4,1}$, $E_{4,2}$, $\frac{E_{4,2}}{E_{2,1}}$, $\frac{E_{4,2}}{E_{2,2}}$, $\frac{E_{4,2}}{E_{4,1}}$, $\frac{E_{4,1}}{E_{2,1}}$, $\frac{E_{4,1}}{E_{2,2}}$, $\frac{E_{2,2}}{E_{2,1}}$, and reference.

Nuclide	Z	N	A	$E_{2,1}$	$E_{2,2}$	$E_{4,1}$	$E_{4,2}$	$\frac{E_{4,2}}{E_{2,1}}$	$\frac{E_{4,2}}{E_{2,2}}$	$\frac{E_{4,2}}{E_{4,1}}$	$\frac{E_{4,1}}{E_{2,1}}$	$\frac{E_{4,1}}{E_{2,2}}$	$\frac{E_{2,2}}{E_{2,1}}$	Refrences
He	2	2	4	27420.00	28670.00								1.05	[167]
He	2	4	6	1797.00	5600.00								3.12	[168]
He	2	6	8	3100.00										[169]
He	2	8	10	3240.00										[169]
Be	4	2	6	1670.00										[168]
Be	4	4	8	3030.00	16626.00	11350.00	19860.00	6.55	1.19	1.75	3.75	0.68	5.49	[169]
Be	4	6	10	3368.03	5958.40	11760.00					3.49	1.97	1.77	[169]
Be	4	8	12	2102.00										[170]
C	6	4	10	3353.70	6580.00								1.96	[169]
C	6	6	12	4438.91	11160.00	14083.00					3.17	1.26	2.51	[170]
C	6	8	14	7012.00	8317.90	10736.00	14667.00	2.09	1.76	1.37	1.53	1.29	1.19	[171]
C	6	10	16	1766.00	6109.00	4142.00	6109.00	3.46	1.00	1.47	2.35	0.68	3.46	[172]
C	6	12	18	1620.00										[173]
O	8	6	14	6590.00	7768.00	9915.00					1.50	1.28	1.18	[171]
O	8	8	16	6917.14	9844.50	10356.00	11096.70	1.60	1.13	1.07	1.50	1.05	1.42	[172]
O	8	10	18	1982.07	3920.44	3554.84	7116.90	3.59	1.82	2.00	1.79	0.91	1.98	[173]
O	8	12	20	1673.68	4072.00	3570.00	4850.00	2.90	1.19	1.36	2.13	0.88	2.43	[174]
O	8	14	22	3199.00	6512.00	6938.00					2.17	1.07	2.04	[175]
O	8	16	24	4790.00										[176]
O	8	18	26	1277.00										[177]
Ne	10	6	16	1690.00										[172]
Ne	10	8	18	1887.30	3616.40	3376.20	6297.00	3.34	1.74	1.87	1.79	0.93	1.92	[173]
Ne	10	10	20	1633.67	7421.40	4247.70	9031.00	5.53	1.22	2.13	2.60	0.57	4.54	[174]
Ne	10	12	22	1274.54	4456.20	3357.20	6345.10	4.98	1.42	1.89	2.63	0.75	3.50	[175]
Ne	10	14	24	1981.60	3868.00	3972.00					2.00	1.03	1.95	[176]
Ne	10	16	26	2018.00	3690.80	3517.10	5360.60	2.66	1.45	1.52	1.74	0.95	1.83	[177]
Ne	10	18	28	1304.00		3010.00	3904.00	2.99		1.30	2.31			[178]
Ne	10	20	30	792.00		2235.00					2.82			[179]
Ne	10	22	32	722.00										[180]
Mg	12	8	20	1598.00										[166]
Mg	12	10	22	1247.02	4402.00	3308.22	5293.10	4.24	1.20	1.60	2.65	0.75	3.53	[175]

Nuclide	Z	N	A	$E_{2,1}$	$E_{2,2}$	$E_{4,1}$	$E_{4,2}$	$\frac{E_{4,2}}{E_{2,1}}$	$\frac{E_{4,2}}{E_{2,2}}$	$\frac{E_{4,2}}{E_{4,1}}$	$\frac{E_{4,1}}{E_{2,1}}$	$\frac{E_{4,1}}{E_{2,2}}$	$\frac{E_{2,2}}{E_{2,1}}$	Refrences
Mg	12	12	24	1368.67	4238.20	4122.89	6010.80	4.39	1.42	1.46	3.01	0.97	3.10	[176]
Mg	12	14	26	1808.74	2438.30	4901.44	5476.10	3.03	2.25	1.12	2.71	2.01	1.35	[177]
Mg	12	16	28	1473.54	4554.60	4021.00					2.73	0.88	3.09	[178]
Mg	12	18	30	1482.80	2468.40	3381.20	3461.10	2.33	1.40	1.02	2.28	1.37	1.66	[179]
Mg	12	20	32	885.30	2551.00	2322.30	3117.00	3.52	1.22	1.34	2.62	0.91	2.88	[180]
Mg	12	22	34	660.00		2120.00					3.21			[181]
Mg	12	24	36	660.00										[182]
Mg	12	26	38	656.00		2016.00					3.07			[183]
Si	14	10	24	1879.00										[176]
Si	14	12	26	1797.30	2787.10	3842.20	4446.40	2.47	1.60	1.16	2.14	1.38	1.55	[177]
Si	14	14	28	1779.03	7380.51	4617.86	6887.65	3.87	0.93	1.49	2.60	0.63	4.15	[178]
Si	14	16	30	2235.32	3498.50	5279.37	5950.73	2.66	1.70	1.13	2.36	1.51	1.57	[179]
Si	14	18	32	1941.40	4230.80	5502.00	7793.00	4.01	1.84	1.42	2.83	1.30	2.18	[180]
Si	14	20	34	3327.14	5330.40								1.60	[181]
Si	14	22	36	1408.00		2850.00					2.02			[182]
Si	14	24	38	1084.00										[183]
Si	14	26	40	986.00	1624.00	1624.00	2524.00	2.56	1.55	1.55	1.65	1.00	1.65	[184]
Si	14	28	42	742.00		2173.00					2.93			[185]
S	16	12	28	1507.00										[178]
S	16	14	30	2210.60	3402.60	5168.00					2.34	1.52	1.54	[179]
S	16	16	32	2230.57	4281.80	4459.10	6411.00	2.87	1.50	1.44	2.00	1.04	1.92	[180]
S	16	18	34	2127.56	3304.21	4688.98	4882.00	2.29	1.48	1.04	2.20	1.42	1.55	[181]
S	16	20	36	3290.90	4575.20	6514.40					1.98	1.42	1.39	[182]
S	16	22	38	1292.00	3805.00	2825.20	4336.00	3.36	1.14	1.53	2.19	0.74	2.95	[183]
S	16	24	40	903.69		1916.84	2254.80	2.50		1.18	2.12			[184]
S	16	26	42	903.00	2779.00	2725.00					3.02	0.98	3.08	[185]
S	16	28	44	1329.00	2150.00	2457.00					1.85	1.14	1.62	[186]
S	16	30	46	952.00										[187]
Ar	18	12	30	700.00										[166]
Ar	18	14	32	1867.00	24700.00								13.23	[180]
Ar	18	16	34	2091.10	3287.70								1.57	[181]

Nuclide	Z	N	A	$E_{2,1}$	$E_{2,2}$	$E_{4,1}$	$E_{4,2}$	$\frac{E_{4,2}}{E_{2,1}}$	$\frac{E_{4,2}}{E_{2,2}}$	$\frac{E_{4,2}}{E_{4,1}}$	$\frac{E_{4,1}}{E_{2,1}}$	$\frac{E_{4,1}}{E_{2,2}}$	$\frac{E_{2,2}}{E_{2,1}}$	Refrences
Ar	18	18	36	1970.38	4414.40	4414.40	6136.50	3.11	1.39	1.39	2.24	1.00	2.24	[182]
Ar	18	20	38	2167.64	3936.40	5349.40	5974.80	2.76	1.52	1.12	2.47	1.36	1.82	[183]
Ar	18	22	40	1460.85	2524.10	2892.65	3515.00	2.41	1.39	1.22	1.98	1.15	1.73	[184]
Ar	18	24	42	1208.22	2485.90	2413.80	2512.50	2.08	1.01	1.04	2.00	0.97	2.06	[185]
Ar	18	26	44	1157.97	1610.00	2746.20	2975.90	2.57	1.85	1.08	2.37	1.71	1.39	[186]
Ar	18	28	46	1577.00										[187]
Ar	18	30	48	1038.00	2194.00	2753.00					2.65	1.25	2.11	[188]
Ar	18	32	50	1178.00		2760.00					2.34			[189]
Ca	20	16	36	3045.00										[182]
Ca	20	18	38	2213.13	3683.70	5810.00					2.63	1.58	1.66	[183]
Ca	20	20	40	3904.38	5248.70	5278.80	6507.80	1.67	1.24	1.23	1.35	1.01	1.34	[184]
Ca	20	22	42	1524.71	2424.40	2752.40	3253.89	2.13	1.34	1.18	1.81	1.14	1.59	[185]
Ca	20	24	44	1157.02	2656.50	2283.11	3044.27	2.63	1.15	1.33	1.97	0.86	2.30	[186]
Ca	20	26	46	1346.00	3022.60	2574.70	3859.70	2.87	1.28	1.50	1.91	0.85	2.25	[187]
Ca	20	28	48	3831.72	6336.80	4503.14	6104.70	1.59	0.96	1.36	1.18	0.71	1.65	[188]
Ca	20	30	50	1026.72	3002.10	4515.02	4970.00	4.84	1.66	1.10	4.40	1.50	2.92	[189]
Ca	20	32	52	2563.00										[190]
Ca	20	34	54	2043.00										[191]
Ti	22	20	42	1554.60	2396.10	2676.60	4950.00	3.18	2.07	1.85	1.72	1.12	1.54	[185]
Ti	22	22	44	1083.06	2531.00	2454.33	3364.00	3.11	1.33	1.37	2.27	0.97	2.34	[186]
Ti	22	24	46	889.29	2961.80	2009.85	3848.00	4.33	1.30	1.91	2.26	0.68	3.33	[187]
Ti	22	26	48	983.54	2421.05	2295.65	3239.78	3.29	1.34	1.41	2.33	0.95	2.46	[188]
Ti	22	28	50	1553.78	4172.50	2674.91	4147.00	2.67	0.99	1.55	1.72	0.64	2.69	[189]
Ti	22	30	52	1050.06	2264.50	2318.19	3143.00	2.99	1.39	1.36	2.21	1.02	2.16	[190]
Ti	22	32	54	1494.80	2515.80	2496.00					1.67	0.99	1.68	[191]
Ti	22	34	56	1128.20		2288.20					2.03			[192]
Ti	22	36	58	1047.00		2038.00					1.95			[193]
Ti	22	38	60	850.00		1716.00					2.02			[194]
Cr	24	22	46	892.16		1987.10	9152.00	10.26		4.61	2.23			[187]
Cr	24	24	48	752.19	3632.30	1858.47	4653.00	6.19	1.28	2.50	2.47	0.51	4.83	[188]
Cr	24	26	50	783.32	3924.30	1881.31	3324.60	4.24	0.85	1.77	2.40	0.48	5.01	[189]

Nuclide	Z	N	A	$E_{2,1}$	$E_{2,2}$	$E_{4,1}$	$E_{4,2}$	$\frac{E_{4,2}}{E_{2,1}}$	$\frac{E_{4,2}}{E_{2,2}}$	$\frac{E_{4,2}}{E_{4,1}}$	$\frac{E_{4,1}}{E_{2,1}}$	$\frac{E_{4,1}}{E_{2,2}}$	$\frac{E_{2,2}}{E_{2,1}}$	Refrences
Cr	24	28	52	1434.09	2964.00	2369.63	2767.80	1.93	0.93	1.17	1.65	0.80	2.07	[190]
Cr	24	30	54	834.86	2619.70	1823.93	3159.60	3.78	1.21	1.73	2.18	0.70	3.14	[191]
Cr	24	32	56	1006.61	1831.60	2681.70					2.66	1.46	1.82	[192]
Cr	24	34	58	880.70		1938.60	2981.80	3.39		1.54	2.20			[193]
Cr	24	36	60	643.90		1460.70					2.27			[194]
Cr	24	38	62	446.00		1175.00					2.63			[195]
Cr	24	40	64	430.00		1141.00					2.65			[196]
Cr	24	42	66	386.00		1069.00					2.77			[166]
Fe	26	24	50	764.90		1851.50	3397.20	4.44		1.83	2.42			[189]
Fe	26	26	52	849.45	2758.80	2384.55	3585.00	4.22	1.30	1.50	2.81	0.86	3.25	[190]
Fe	26	28	54	1408.19	2900.00	2538.10	3294.80	2.34	1.14	1.30	1.80	0.88	2.06	[191]
Fe	26	30	56	846.78	2657.60	2085.10	3123.00	3.69	1.18	1.50	2.46	0.78	3.14	[192]
Fe	26	32	58	810.77	1674.73	2076.52	2600.39	3.21	1.55	1.25	2.56	1.24	2.07	[193]
Fe	26	34	60	823.83	2672.90	2114.60	2792.70	3.39	1.04	1.32	2.57	0.79	3.24	[194]
Fe	26	36	62	877.31	2017.00	2176.47	3633.50	4.14	1.80	1.67	2.48	1.08	2.30	[195]
Fe	26	38	64	746.40	1443.60	1763.12					2.36	1.22	1.93	[196]
Fe	26	40	66	574.40		1407.00					2.45			[197]
Fe	26	42	68	522.00		1389.00					2.66			[198]
Fe	26	44	70	480.00		1346.00					2.80			[199]
Ni	28	24	52	1397.00		2385.00					1.71			[190]
Ni	28	26	54	1392.30		2619.70					1.88			[191]
Ni	28	28	56	2700.60	5352.50	3923.60	5483.70	2.03	1.02	1.40	1.45	0.73	1.98	[192]
Ni	28	30	58	1454.21	2775.42	2459.21	3524.00	2.42	1.27	1.43	1.69	0.89	1.91	[193]
Ni	28	32	60	1332.51	2158.60	2505.75	3119.87	2.34	1.45	1.25	1.88	1.16	1.62	[194]
Ni	28	34	62	1172.98	2381.80	2336.52	3176.70	2.71	1.33	1.36	1.99	0.98	2.03	[195]
Ni	28	36	64	1345.75	2972.08	2610.10	3166.10	2.35	1.07	1.21	1.94	0.88	2.21	[196]
Ni	28	38	66	1424.80	2916.00	3185.44	4125.00	2.90	1.41	1.29	2.24	1.09	2.05	[197]
Ni	28	40	68	2034.08	5550.20	3149.20					1.55	0.57	2.73	[198]
Ni	28	42	70	1259.55	1867.40	2229.44					1.77	1.19	1.48	[199]
Ni	28	44	72	1096.00		1941.00					1.77			[200]
Ni	28	46	74	1024.00		1763.00					1.72			[166]

Nuclide	Z	N	A	$E_{2,1}$	$E_{2,2}$	$E_{4,1}$	$E_{4,2}$	$\frac{E_{4,2}}{E_{2,1}}$	$\frac{E_{4,2}}{E_{2,2}}$	$\frac{E_{4,2}}{E_{4,1}}$	$\frac{E_{4,1}}{E_{2,1}}$	$\frac{E_{4,1}}{E_{2,2}}$	$\frac{E_{2,2}}{E_{2,1}}$	Refrences
Ni	28	48	76	992.00		1922.00					1.94			[166]
Zn	30	28	58	1356.00	2609.00	2499.00					1.84	0.96	1.92	[166]
Zn	30	30	60	1003.90	2559.00	2193.00	3710.00	3.70	1.45	1.69	2.18	0.86	2.55	[194]
Zn	30	32	62	953.84	1804.70	2186.06	2743.80	2.88	1.52	1.26	2.29	1.21	1.89	[195]
Zn	30	34	64	991.56	1799.40	2306.75	2736.50	2.76	1.52	1.19	2.33	1.28	1.81	[196]
Zn	30	36	66	1039.22	1872.80	2451.01	2765.60	2.66	1.48	1.13	2.36	1.31	1.80	[197]
Zn	30	38	68	1077.37	1883.20	2417.40	2959.50	2.75	1.57	1.22	2.24	1.28	1.75	[198]
Zn	30	40	70	884.92	1759.20	1786.75	2693.40	3.04	1.53	1.51	2.02	1.02	1.99	[199]
Zn	30	42	72	652.70	1657.30	1499.58					2.30	0.90	2.54	[200]
Zn	30	44	74	605.90	1670.30								2.76	[201]
Zn	30	46	76	598.68		1296.46					2.17			[202]
Zn	30	48	78	730.20		1620.70	3106.00	4.25		1.92	2.22			[203]
Zn	30	50	80	1492.00										[204]
Ge	32	32	64	901.70	1578.70	2052.60	2154.80	2.39	1.36	1.05	2.28	1.30	1.75	[196]
Ge	32	34	66	956.94	1693.20	2173.29	2725.70	2.85	1.61	1.25	2.27	1.28	1.77	[197]
Ge	32	36	68	1015.81	1777.43	2267.83	2831.90	2.79	1.59	1.25	2.23	1.28	1.75	[198]
Ge	32	38	70	1039.51	1707.70	2153.08	2806.30	2.70	1.64	1.30	2.07	1.26	1.64	[199]
Ge	32	40	72	834.01	1463.99	1728.30	2463.90	2.95	1.68	1.43	2.07	1.18	1.76	[200]
Ge	32	42	74	595.85	1204.20	1463.76	2572.00	4.32	2.14	1.76	2.46	1.22	2.02	[201]
Ge	32	44	76	562.93	1108.40	1410.08	2019.90	3.59	1.82	1.43	2.50	1.27	1.97	[202]
Ge	32	46	78	619.36	1186.50	1570.20	1644.58	2.66	1.39	1.05	2.54	1.32	1.92	[203]
Ge	32	48	80	659.15	1573.60	1742.55					2.64	1.11	2.39	[204]
Ge	32	50	82	1347.51	2214.90	2028.60	2286.30	1.70	1.03	1.13	1.51	0.92	1.64	[205]
Ge	32	52	84	624.30		1670.40					2.68			[206]
Ge	32	54	86	527.00										[207]
Se	34	32	66	929.00										[197]
Se	34	34	68	853.75	1196.70	1942.10	2545.10	2.98	2.13	1.31	2.27	1.62	1.40	[198]
Se	34	36	70	944.52	1599.90	2038.80	2382.50	2.52	1.49	1.17	2.16	1.27	1.69	[199]
Se	34	38	72	862.07	1316.70	1636.86	3124.04	3.62	2.37	1.91	1.90	1.24	1.53	[200]
Se	34	40	74	634.74	1269.00	1363.17	2108.00	3.32	1.66	1.55	2.15	1.07	2.00	[201]
Se	34	42	76	559.10	1216.10	1330.86	2026.00	3.62	1.67	1.52	2.38	1.09	2.18	[202]

Nuclide	Z	N	A	$E_{2,1}$	$E_{2,2}$	$E_{4,1}$	$E_{4,2}$	$\frac{E_{4,2}}{E_{2,1}}$	$\frac{E_{4,2}}{E_{2,2}}$	$\frac{E_{4,2}}{E_{4,1}}$	$\frac{E_{4,1}}{E_{2,1}}$	$\frac{E_{4,1}}{E_{2,2}}$	$\frac{E_{2,2}}{E_{2,1}}$	Refrences
Se	34	44	78	613.73	1308.60	1502.83	2190.70	3.57	1.67	1.46	2.45	1.15	2.13	[203]
Se	34	46	80	666.27	1449.40	1701.45	2494.80	3.74	1.72	1.47	2.55	1.17	2.18	[204]
Se	34	48	82	654.75	1731.50	1735.12	2550.30	3.90	1.47	1.47	2.65	1.00	2.64	[205]
Se	34	50	84	1454.55	2461.40	2121.65	4445.20	3.06	1.81	2.10	1.46	0.86	1.69	[206]
Se	34	52	86	704.30	1398.90	1567.71	2072.80	2.94	1.48	1.32	2.23	1.12	1.99	[207]
Kr	36	36	72	709.72		1321.40					1.86			[200]
Kr	36	38	74	455.61	1203.20	1013.32	2112.00	4.64	1.76	2.08	2.22	0.84	2.64	[201]
Kr	36	40	76	423.96	1221.70	1034.62	1957.30	4.62	1.60	1.89	2.44	0.85	2.88	[202]
Kr	36	42	78	455.03	1147.90	1119.48	1872.90	4.12	1.63	1.67	2.46	0.98	2.52	[203]
Kr	36	44	80	616.60	1256.20	1436.09	2145.90	3.48	1.71	1.49	2.33	1.14	2.04	[204]
Kr	36	46	82	776.52	1474.90	1820.53	2426.88	3.13	1.65	1.33	2.34	1.23	1.90	[205]
Kr	36	48	84	881.62	1897.80	2095.00	2345.50	2.66	1.24	1.12	2.38	1.10	2.15	[206]
Kr	36	50	86	1564.61	2349.50	2250.01	3328.10	2.13	1.42	1.48	1.44	0.96	1.50	[207]
Kr	36	52	88	775.32	1577.40	1643.78	2103.80	2.71	1.33	1.28	2.12	1.04	2.03	[208]
Kr	36	54	90	707.13										[209]
Kr	36	56	92	769.10	1446.30	1804.00	1985.00	2.58	1.37	1.10	2.35	1.25	1.88	[210]
Kr	36	58	94	665.50		1518.70					2.28			[166]
Sr	38	36	74	471.00		1043.00					2.21			[201]
Sr	38	38	76	262.30		746.70					2.85			[202]
Sr	38	40	78	277.60		780.80					2.81			[203]
Sr	38	42	80	385.88	1142.10	980.68	1832.60	4.75	1.60	1.87	2.54	0.86	2.96	[204]
Sr	38	44	82	573.54	1175.70	1328.54	1996.02	2.09	1.02	1.50	2.32	1.13	2.05	[205]
Sr	38	46	84	793.22	1453.90	1767.69	2598.20	3.28	1.79	1.47	2.23	1.22	1.83	[206]
Sr	38	48	86	1076.68	1854.20	2229.81	3362.11	3.12	1.81	1.51	2.07	1.20	1.72	[207]
Sr	38	50	88	1836.09	3218.28	4232.00	4299.52	2.34	1.34	1.02	2.30	1.31	1.75	[208]
Sr	38	52	90	831.68	1892.36	1655.91	2527.90	3.04	1.34	1.53	1.99	0.88	2.28	[209]
Sr	38	54	92	814.98	1384.79								1.70	[210]
Sr	38	56	94	836.90	2271.20	2146.00					2.56	0.94	2.71	[166]
Sr	38	58	96	814.93	1506.80	1792.77	1975.70	2.42	1.31	1.10	2.20	1.19	1.85	[211]
Sr	38	60	98	144.23	871.10	433.52	1681.50	11.66	1.93	3.88	3.01	0.50	6.04	[212]
Sr	38	62	100	129.16	1257.00	417.98	1414.40	10.95	1.13	3.38	3.24	0.33	9.73	[213]

Nuclide	Z	N	A	$E_{2,1}$	$E_{2,2}$	$E_{4,1}$	$E_{4,2}$	$\frac{E_{4,2}}{E_{2,1}}$	$\frac{E_{4,2}}{E_{2,2}}$	$\frac{E_{4,2}}{E_{4,1}}$	$\frac{E_{4,1}}{E_{2,1}}$	$\frac{E_{4,1}}{E_{2,2}}$	$\frac{E_{2,2}}{E_{2,1}}$	Refrences
Sr	38	64	102	126.00										[214]
Zr	40	40	80	288.90		825.80					2.86			[204]
Zr	40	42	82	407.00		1040.84					2.56			[205]
Zr	40	44	84	539.92	1119.30	1262.81	1887.90	3.50	1.69	1.49	2.34	1.13	2.07	[206]
Zr	40	46	86	751.75	1421.80	1666.57	2041.90	2.72	1.44	1.23	2.22	1.17	1.89	[207]
Zr	40	48	88	1057.03	1817.90	2139.59	2605.20	2.46	1.43	1.22	2.02	1.18	1.72	[208]
Zr	40	50	90	2186.27	3308.80	3076.93	4068.00	1.86	1.23	1.32	1.41	0.93	1.51	[166]
Zr	40	52	92	934.51	1847.27	1495.46	2398.36	2.57	1.30	1.60	1.60	0.81	1.98	[210]
Zr	40	54	94	918.75	1671.40	1469.62	2329.90	2.54	1.39	1.59	1.60	0.88	1.82	[215]
Zr	40	56	96	1750.50	2225.80	2750.00	2857.40	1.63	1.28	1.04	1.57	1.24	1.27	[211]
Zr	40	58	98	1222.92	1590.70	1843.45	2047.60	1.67	1.29	1.11	1.51	1.16	1.30	[212]
Zr	40	60	100	212.53	878.60	564.49	1294.85	6.09	1.47	2.29	2.66	0.64	4.13	[213]
Zr	40	62	102	151.78	1036.30	478.28	1386.70	9.14	1.34	2.90	3.15	0.46	6.83	[214]
Zr	40	64	104	139.30		452.10					3.25			[216]
Zr	40	66	106	152.10	607.00	476.50					3.13	0.79	3.99	[217]
Zr	40	68	108	174.30	604.10	521.50	947.60	5.44	1.57	1.82	2.99	0.86	3.47	[218]
Mo	42	42	84	443.90		1117.30					2.52			[206]
Mo	42	44	86	566.60	1140.90	1327.50	1923.40	3.39	1.69	1.45	2.34	1.16	2.01	[207]
Mo	42	46	88	740.54	1495.00	1654.83	2100.70	2.84	1.41	1.27	2.23	1.11	2.02	[208]
Mo	42	48	90	947.97	1896.50	2002.06					2.11	1.06	2.00	[209]
Mo	42	50	92	1509.51	3091.40	2282.61	3368.70	2.23	1.09	1.48	1.51	0.74	2.05	[210]
Mo	42	52	94	871.10	1864.31	1573.76	2294.80	2.63	1.23	1.46	1.81	0.84	2.14	[215]
Mo	42	54	96	778.24	1497.78	1628.19	1869.60	2.40	1.25	1.15	2.09	1.09	1.92	[211]
Mo	42	56	98	787.38	1432.20	1510.04	2223.85	2.82	1.55	1.47	1.92	1.05	1.82	[212]
Mo	42	58	100	535.56	1063.80	1136.09	1771.44	3.31	1.67	1.56	2.12	1.07	1.99	[213]
Mo	42	60	102	296.61	847.90	743.73	1398.40	4.71	1.65	1.88	2.51	0.88	2.86	[214]
Mo	42	62	104	192.19	812.40	560.68	1214.80	6.32	1.50	2.17	2.92	0.69	4.23	[216]
Mo	42	64	106	171.55	710.50	522.32	1067.80	6.22	1.50	2.04	3.04	0.74	4.14	[217]
Mo	42	66	108	192.79	586.00	563.69	978.30	5.07	1.67	1.74	2.92	0.96	3.04	[218]
Mo	42	68	110	213.77	494.20	599.69	915.50	4.28	1.85	1.53	2.81	1.21	2.31	[219]
Ru	44	44	88	616.20		1416.00					2.30			[208]

Nuclide	Z	N	A	$E_{2,1}$	$E_{2,2}$	$E_{4,1}$	$E_{4,2}$	$\frac{E_{4,2}}{E_{2,1}}$	$\frac{E_{4,2}}{E_{2,2}}$	$\frac{E_{4,2}}{E_{4,1}}$	$\frac{E_{4,1}}{E_{2,1}}$	$\frac{E_{4,1}}{E_{2,2}}$	$\frac{E_{2,2}}{E_{2,1}}$	Refrences
Ru	44	46	90	738.00		1638.11					2.22			[209]
Ru	44	48	92	865.70		1854.90					2.14			[210]
Ru	44	50	94	1430.71		2186.60					1.53			[215]
Ru	44	52	96	832.56	1931.10	1518.05	2524.85	3.03	1.31	1.66	1.82	0.79	2.32	[211]
Ru	44	54	98	652.44	1414.30	1397.82	2241.40	3.44	1.58	1.60	2.14	0.99	2.17	[212]
Ru	44	56	100	539.51	1362.16	1226.47	2062.64	3.82	1.51	1.68	2.27	0.90	2.52	[213]
Ru	44	58	102	475.10	1103.00	1106.43	1603.37	3.37	1.45	1.45	2.33	1.00	2.32	[214]
Ru	44	60	104	358.20	893.10	888.48	1502.60	4.19	1.68	1.69	2.48	0.99	2.49	[216]
Ru	44	62	106	270.07	792.30	714.69	1306.80	4.84	1.65	1.83	2.65	0.90	2.93	[217]
Ru	44	64	108	242.23	1249.17	665.10	1183.00	4.88	0.95	1.78	2.75	0.53	5.16	[218]
Ru	44	66	110	240.73	612.90	663.35	1084.40	4.50	1.77	1.63	2.76	1.08	2.55	[219]
Ru	44	68	112	236.69	523.50	644.97	980.70	4.14	1.87	1.52	2.72	1.23	2.21	[220]
Ru	44	70	114	265.19	563.30	708.20	1081.90	4.08	1.92	1.53	2.67	1.26	2.12	[221]
Ru	44	72	116	292.43	614.30	760.10	1150.10	3.93	1.87	1.51	2.60	1.24	2.10	[222]
Ru	44	74	118	327.60	647.80	809.90	1180.50	3.60	1.82	1.46	2.47	1.25	1.98	[166]
Pd	46	46	92	873.60		1786.00					2.04			[210]
Pd	46	48	94	813.80		1719.11					2.11			[215]
Pd	46	50	96	1415.31		2099.01					1.48			[211]
Pd	46	52	98	862.89		1541.40					1.79			[212]
Pd	46	54	100	665.50	1523.60	1416.15	1926.00	2.89	1.26	1.36	2.13	0.93	2.29	[213]
Pd	46	56	102	556.44	1534.50	1275.91	2138.00	3.84	1.39	1.68	2.29	0.83	2.76	[214]
Pd	46	58	104	555.81	1341.68	1323.59	2082.40	3.75	1.55	1.57	2.38	0.99	2.41	[216]
Pd	46	60	106	511.85	1128.00	1229.30	1932.30	3.78	1.71	1.57	2.40	1.09	2.20	[166]
Pd	46	62	108	433.94	931.20	1048.22	1624.20	3.74	1.74	1.55	2.42	1.13	2.15	[218]
Pd	46	64	110	373.80	813.60	920.78	1398.30	3.74	1.72	1.52	2.46	1.13	2.18	[219]
Pd	46	66	112	348.66	736.70	882.96	1362.40	3.91	1.85	1.54	2.53	1.20	2.11	[220]
Pd	46	68	114	332.61	694.60	852.37	1319.90	3.97	1.90	1.55	2.56	1.23	2.09	[221]
Pd	46	70	116	340.26	2074.10	877.58	1373.00	4.04	0.66	1.56	2.58	0.42	6.10	[222]
Pd	46	72	118	378.60	812.60	953.20	1461.60	3.86	1.80	1.53	2.52	1.17	2.15	[223]
Pd	46	74	120	438.00		1056.50					2.41			[224]
Pd	46	76	122	499.00		1164.00					2.33			[225]

Nuclide	Z	N	A	$E_{2,1}$	$E_{2,2}$	$E_{4,1}$	$E_{4,2}$	$\frac{E_{4,2}}{E_{2,1}}$	$\frac{E_{4,2}}{E_{2,2}}$	$\frac{E_{4,2}}{E_{4,1}}$	$\frac{E_{4,1}}{E_{2,1}}$	$\frac{E_{4,1}}{E_{2,2}}$	$\frac{E_{2,2}}{E_{2,1}}$	Refrences
Pd	46	78	124	590.00		1300.00					2.20			[226]
Pd	46	80	126	693.30		1481.00					2.14			[166]
Pd	46	82	128	1311.40		1815.80					1.38			[227]
Cd	48	50	98	1394.70		2082.30					1.49			[212]
Cd	48	52	100	1004.11		1799.00	2046.20	2.04		1.14	1.79			[213]
Cd	48	54	102	776.55		1637.90					2.11			[214]
Cd	48	56	104	658.00		1492.10					2.27			[216]
Cd	48	58	106	632.64	1716.50	1493.78	2104.50	3.33	1.23	1.41	2.36	0.87	2.71	[217]
Cd	48	60	108	632.99	1601.80	1508.47	2239.35	3.54	1.40	1.48	2.38	0.94	2.53	[218]
Cd	48	62	110	657.76	1475.79	1542.44	1809.48	2.75	1.23	1.17	2.34	1.05	2.24	[219]
Cd	48	64	112	617.52	1312.39	1415.48	1870.68	3.03	1.43	1.32	2.29	1.08	2.13	[220]
Cd	48	66	114	558.46	1209.70	1283.74	1732.20	3.10	1.43	1.35	2.30	1.06	2.17	[221]
Cd	48	68	116	513.49	1213.00	1219.45	1869.50	3.64	1.54	1.53	2.37	1.01	2.36	[222]
Cd	48	70	118	487.77	1269.60	1164.94	1929.10	3.95	1.52	1.66	2.39	0.92	2.60	[223]
Cd	48	72	120	505.94	1323.10	1203.70					2.38	0.91	2.62	[224]
Cd	48	74	122	569.45		1329.15	1979.30	3.48		1.49	2.33			[225]
Cd	48	76	124	612.80	1427.60	1385.10	1915.30	3.13	1.34	1.38	2.26	0.97	2.33	[226]
Cd	48	78	126	652.00		1467.00					2.25			[228]
Cd	48	80	128	645.80		1430.39					2.21			[227]
Cd	48	82	130	1325.00		1864.00					1.41			[229]
Sn	50	52	102	1472.00		1969.00					1.34			[214]
Sn	50	54	104	1260.10		1942.70					1.54			[216]
Sn	50	56	106	1207.70		2019.60					1.67			[217]
Sn	50	58	108	1206.07	2155.10	2111.11	2855.04	2.37	1.32	1.35	1.75	0.98	1.79	[218]
Sn	50	60	110	1212.02	2121.04	2197.05	2455.60	2.03	1.16	1.12	1.81	1.04	1.75	[219]
Sn	50	62	112	1256.69	2150.90	2247.39	2520.70	2.01	1.17	1.12	1.79	1.04	1.71	[220]
Sn	50	64	114	1299.91	2239.00	2187.60	2614.50	2.01	1.17	1.20	1.68	0.98	1.72	[221]
Sn	50	66	116	1293.56	2112.30	2390.88	2529.20	1.96	1.20	1.06	1.85	1.13	1.63	[222]
Sn	50	68	118	1229.66	2042.88	2280.34	2408.00	1.96	1.18	1.06	1.85	1.12	1.66	[223]
Sn	50	70	120	1171.27	2097.20	2194.30	2465.63	2.11	1.18	1.12	1.87	1.05	1.79	[224]
Sn	50	72	122	1140.51	2153.80	2142.06	2331.10	2.04	1.08	1.09	1.88	0.99	1.89	[225]

Nuclide	Z	N	A	$E_{2,1}$	$E_{2,2}$	$E_{4,1}$	$E_{4,2}$	$\frac{E_{4,2}}{E_{2,1}}$	$\frac{E_{4,2}}{E_{2,2}}$	$\frac{E_{4,2}}{E_{4,1}}$	$\frac{E_{4,1}}{E_{2,1}}$	$\frac{E_{4,1}}{E_{2,2}}$	$\frac{E_{2,2}}{E_{2,1}}$	Refrences
Sn	50	74	124	1131.74	2129.60	2101.71	2221.80	1.96	1.04	1.06	1.86	0.99	1.88	[226]
Sn	50	76	126	1141.15		2049.74	2712.10	2.38		1.32	1.80			[228]
Sn	50	78	128	1168.82	2104.10	2000.37	2274.10	1.95	1.08	1.14	1.71	0.95	1.80	[227]
Sn	50	80	130	1221.26	2028.30	1995.62	2490.90	2.04	1.23	1.25	1.63	0.98	1.66	[229]
Sn	50	82	132	4041.20		4416.29					1.09			[230]
Sn	50	84	134	725.60		1073.40					1.48			[231]
Sn	50	86	136	688.00		1079.00					1.57			[232]
Sn	50	88	138	715.00		1176.00					1.64			[233]
Te	52	54	106	664.80		1353.20					2.04			[217]
Te	52	56	108	625.20		1289.00					2.06			[218]
Te	52	58	110	657.20	1578.30	1401.80	1915.00	2.91	1.21	1.37	2.13	0.89	2.40	[219]
Te	52	60	112	689.00	1483.60	1476.10					2.14	0.99	2.15	[220]
Te	52	62	114	708.74	1391.34	1483.83	2027.00	2.86	1.46	1.37	2.09	1.07	1.96	[221]
Te	52	64	116	678.92	1219.10	1359.78	1746.00	2.57	1.43	1.28	2.00	1.12	1.80	[222]
Te	52	66	118	605.71	1150.80	1206.42	1976.18	3.26	1.72	1.64	1.99	1.05	1.90	[223]
Te	52	68	120	560.44	1201.30	1161.56	1815.10	3.24	1.51	1.56	2.07	0.97	2.14	[224]
Te	52	70	122	564.09	1256.95	1181.25	1909.61	3.39	1.52	1.62	2.09	0.94	2.23	[225]
Te	52	72	124	602.73	1325.50	1248.58	1957.90	3.25	1.48	1.57	2.07	0.94	2.20	[226]
Te	52	74	126	666.35	1420.20	1361.40	2013.20	3.02	1.42	1.48	2.04	0.96	2.13	[228]
Te	52	76	128	743.22	1520.00	1497.02	2027.80	2.73	1.33	1.35	2.01	0.98	2.05	[227]
Te	52	78	130	839.49	1588.30	1633.00	1981.50	2.36	1.25	1.21	1.95	1.03	1.89	[229]
Te	52	80	132	974.22	1665.20	1671.29	2108.00	2.16	1.27	1.26	1.72	1.00	1.71	[230]
Te	52	82	134	1279.11	2464.90	1576.13	2554.50	2.00	1.04	1.62	1.23	0.64	1.93	[231]
Te	52	84	136	606.64	1568.00	1030.00					1.70	0.66	2.58	[232]
Te	52	86	138	460.80		903.60	1615.30	3.51		1.79	1.96			[233]
Xe	54	56	110	469.70		1113.10					2.37			[219]
Xe	54	58	112	466.00		1122.10					2.41			[220]
Xe	54	60	114	450.08		1069.10					2.38			[221]
Xe	54	62	116	393.60	1015.80	917.90	1557.00	3.96	1.53	1.70	2.33	0.90	2.58	[222]
Xe	54	64	118	337.32	928.10	810.27	1441.20	4.27	1.55	1.78	2.40	0.87	2.75	[223]
Xe	54	66	120	322.61	876.10	796.10	1401.30	4.34	1.60	1.76	2.47	0.91	2.72	[224]

Nuclide	Z	N	A	$E_{2,1}$	$E_{2,2}$	$E_{4,1}$	$E_{4,2}$	$\frac{E_{4,2}}{E_{2,1}}$	$\frac{E_{4,2}}{E_{2,2}}$	$\frac{E_{4,2}}{E_{4,1}}$	$\frac{E_{4,1}}{E_{2,1}}$	$\frac{E_{4,1}}{E_{2,2}}$	$\frac{E_{2,2}}{E_{2,1}}$	Refrences
Xe	54	68	122	331.28	843.10	828.53					2.50	0.98	2.54	[225]
Xe	54	70	124	354.03	846.50	878.92	1437.96	4.06	1.70	1.64	2.48	1.04	2.39	[226]
Xe	54	72	126	388.63	879.87	942.00	1488.38	3.83	1.69	1.58	2.42	1.07	2.26	[228]
Xe	54	74	128	442.91	969.47	1033.15	1603.50	3.62	1.65	1.55	2.33	1.07	2.19	[227]
Xe	54	76	130	536.07	1122.10	1204.61	1808.20	3.37	1.61	1.50	2.25	1.07	2.09	[229]
Xe	54	78	132	667.72	1297.00	1440.32	1963.00	2.94	1.51	1.36	2.16	1.11	1.94	[230]
Xe	54	80	134	847.04	2262.70	1731.17	2082.00	2.46	0.92	1.20	2.04	0.77	2.67	[231]
Xe	54	82	136	1313.03	2289.50	1694.39	2125.70	1.62	0.93	1.25	1.29	0.74	1.74	[232]
Xe	54	84	138	588.83	1464.00	1072.53	1903.20	3.23	1.30	1.77	1.82	0.73	2.49	[233]
Xe	54	86	140	376.66		834.29					2.21			[234]
Xe	54	88	142	287.20		690.70					2.40			[235]
Xe	54	90	144	252.60		644.30					2.55			[236]
Ba	56	62	118	194.00		554.00					2.86			[166]
Ba	56	64	120	186.00		544.00					2.92			[224]
Ba	56	66	122	195.90	618.20	568.60	1205.20	6.15	1.95	2.12	2.90	0.92	3.16	[225]
Ba	56	68	124	229.91	873.20	651.66	1324.80	5.76	1.52	2.03	2.83	0.75	3.80	[226]
Ba	56	70	126	256.02	873.60	711.10	1345.50	5.26	1.54	1.89	2.78	0.81	3.41	[228]
Ba	56	72	128	284.00	884.50	763.32	1372.33	4.83	1.55	1.80	2.69	0.86	3.11	[227]
Ba	56	74	130	357.38	908.00	901.85	1477.50	4.13	1.63	1.64	2.52	0.99	2.54	[229]
Ba	56	76	132	464.51	1031.70	1127.62	1729.30	3.72	1.68	1.53	2.43	1.09	2.22	[230]
Ba	56	78	134	604.72	1168.00	1400.59	1969.90	3.26	1.69	1.41	2.32	1.20	1.93	[231]
Ba	56	80	136	818.50	1551.00	1866.55	2053.80	2.51	1.32	1.10	2.28	1.20	1.89	[232]
Ba	56	82	138	1435.81	2189.90	1898.59	2307.50	1.61	1.05	1.22	1.32	0.87	1.53	[233]
Ba	56	84	140	602.37	1510.70	1130.60	2320.50	3.85	1.54	2.05	1.88	0.75	2.51	[234]
Ba	56	86	142	359.60	1424.10	834.81					2.32	0.59	3.96	[235]
Ba	56	88	144	199.33	1864.25	530.19					2.66	0.28	9.35	[236]
Ba	56	90	146	181.04	1398.65	513.66					2.84	0.37	7.73	[237]
Ba	56	92	148	141.80	1049.20	423.10					2.98	0.40	7.40	[238]
Ce	58	64	122	136.40		434.70					3.19			[225]
Ce	58	66	124	141.90		447.80					3.16			[226]
Ce	58	68	126	169.59	954.40	519.04	1337.10	7.88	1.40	2.58	3.06	0.54	5.63	[228]

Nuclide	Z	N	A	$E_{2,1}$	$E_{2,2}$	$E_{4,1}$	$E_{4,2}$	$\frac{E_{4,2}}{E_{2,1}}$	$\frac{E_{4,2}}{E_{2,2}}$	$\frac{E_{4,2}}{E_{4,1}}$	$\frac{E_{4,1}}{E_{2,1}}$	$\frac{E_{4,1}}{E_{2,2}}$	$\frac{E_{2,2}}{E_{2,1}}$	Refrences
Ce	58	70	128	207.09	869.40	606.77	1312.10	6.34	1.51	2.16	2.93	0.70	4.20	[227]
Ce	58	72	130	253.85	834.60	710.37	1177.37	4.64	1.41	1.66	2.80	0.85	3.29	[229]
Ce	58	74	132	325.34	822.17	858.82	1384.06	4.25	1.68	1.61	2.64	1.04	2.53	[230]
Ce	58	76	134	409.20	965.70	1048.68	1643.50	4.02	1.70	1.57	2.56	1.09	2.36	[231]
Ce	58	78	136	552.20	1092.10	1314.15	2991.40	5.42	2.74	2.28	2.38	1.20	1.98	[232]
Ce	58	80	138	788.74	1510.80	1826.51	2137.00	2.71	1.41	1.17	2.32	1.21	1.92	[233]
Ce	58	82	140	1596.24	2347.90	2083.26	2480.90	1.55	1.06	1.19	1.31	0.89	1.47	[234]
Ce	58	84	142	641.28	1536.30	1219.37	2044.50	3.19	1.33	1.68	1.90	0.79	2.40	[235]
Ce	58	86	144	397.44	1819.00	938.65	1673.70	4.21	0.92	1.78	2.36	0.52	4.58	[236]
Ce	58	88	146	258.45	1274.30	668.38	1627.30	6.30	1.28	2.43	2.59	0.52	4.93	[237]
Ce	58	90	148	158.47	935.60	453.45	1224.00	7.72	1.31	2.70	2.86	0.48	5.90	[238]
Ce	58	92	150	97.00		305.70					3.15			[239]
Ce	58	94	152	81.20		264.00					3.25			[240]
Nd	60	68	128	133.66		424.47					3.18			[227]
Nd	60	70	130	159.05		485.50					3.05			[229]
Nd	60	72	132	213.16	823.50	610.85	1021.60	4.79	1.24	1.67	2.87	0.74	3.86	[230]
Nd	60	74	134	294.17	753.90	788.92	1313.00	4.46	1.74	1.66	2.68	1.05	2.56	[231]
Nd	60	76	136	373.72	862.40	976.37	1541.70	4.13	1.79	1.58	2.61	1.13	2.31	[232]
Nd	60	78	138	520.75	1013.80	1249.70	1799.70	3.46	1.78	1.44	2.40	1.23	1.95	[233]
Nd	60	80	140	773.73	1414.20	1801.90	2400.00	3.10	1.70	1.33	2.33	1.27	1.83	[234]
Nd	60	82	142	1575.70	2384.30	2100.79	2437.17	1.55	1.02	1.16	1.33	0.88	1.51	[235]
Nd	60	84	144	696.56	1560.90	1314.67	2109.79	3.03	1.35	1.60	1.89	0.84	2.24	[236]
Nd	60	86	146	453.84	1303.20	1043.21	1745.20	3.85	1.34	1.67	2.30	0.80	2.87	[237]
Nd	60	88	148	301.71	1171.00	752.29	1604.10	5.32	1.37	2.13	2.49	0.64	3.88	[238]
Nd	60	90	150	130.21	850.80	381.10	1137.80	8.74	1.34	2.99	2.93	0.45	6.53	[239]
Nd	60	92	152	72.40	1251.00	236.54	1474.60	20.37	1.18	6.23	3.27	0.19	17.28	[240]
Nd	60	94	154	70.80	961.60	233.20	1027.60	14.51	1.07	4.41	3.29	0.24	13.58	[241]
Nd	60	96	156	67.20		222.20					3.31			[242]
Nd	60	98	158	65.90		217.60					3.30			[243]
Nd	60	100	160	65.20		215.10					3.30			[166]
Sm	62	68	130	122.00										[229]

Nuclide	Z	N	A	$E_{2,1}$	$E_{2,2}$	$E_{4,1}$	$E_{4,2}$	$\frac{E_{4,2}}{E_{2,1}}$	$\frac{E_{4,2}}{E_{2,2}}$	$\frac{E_{4,2}}{E_{4,1}}$	$\frac{E_{4,1}}{E_{2,1}}$	$\frac{E_{4,1}}{E_{2,2}}$	$\frac{E_{2,2}}{E_{2,1}}$	Refrences
Sm	62	70	132	131.00		417.00					3.18			[230]
Sm	62	72	134	163.00		479.00					2.94			[231]
Sm	62	74	136	254.92	712.90	686.36	1170.98	4.59	1.64	1.71	2.69	0.96	2.80	[232]
Sm	62	76	138	346.71	745.70	891.25	1398.60	4.03	1.88	1.57	2.57	1.20	2.15	[233]
Sm	62	78	140	530.68	1598.79	1245.83					2.35	0.78	3.01	[234]
Sm	62	80	142	768.08	2055.50	1791.40	2582.20	3.36	1.26	1.44	2.33	0.87	2.68	[235]
Sm	62	82	144	1660.03	2423.20	2190.89	2587.78	1.56	1.07	1.18	1.32	0.90	1.46	[236]
Sm	62	84	146	747.17	1648.00	1381.29	2280.90	3.05	1.38	1.65	1.85	0.84	2.21	[237]
Sm	62	86	148	550.26	1454.12	1180.26	1659.40	3.02	1.14	1.41	2.14	0.81	2.64	[238]
Sm	62	88	150	333.96	1046.10	773.37	1449.20	4.34	1.39	1.87	2.32	0.74	3.13	[239]
Sm	62	90	152	121.78	810.45	366.48	1022.97	8.40	1.26	2.79	3.01	0.45	6.65	[240]
Sm	62	92	154	81.98	1177.80	266.82	1337.60	16.32	1.14	5.01	3.25	0.23	14.37	[241]
Sm	62	94	156	75.89	1441.00	249.71	1509.20	19.89	1.05	6.04	3.29	0.17	18.99	[242]
Sm	62	96	158	72.80		240.30					3.30			[243]
Sm	62	98	160	70.90		233.30					3.29			[244]
Sm	62	102	164	69.00		224.90					3.26			[245]
Gd	64	70	134	115.00										[231]
Gd	64	74	138	220.86		605.10	1080.40	4.89		1.79	2.74			[233]
Gd	64	76	140	328.60	713.30	836.20	1281.40	3.90	1.80	1.53	2.54	1.17	2.17	[234]
Gd	64	78	142	515.20	980.00	1208.80					2.35	1.23	1.90	[235]
Gd	64	80	144	743.00	1876.40	1744.52					2.35	0.93	2.53	[236]
Gd	64	82	146	1972.02	2986.40	2611.57	2967.52	1.50	0.99	1.14	1.32	0.87	1.51	[237]
Gd	64	84	148	784.43	1834.60	1416.38	2424.30	3.09	1.32	1.71	1.81	0.77	2.34	[238]
Gd	64	86	150	638.05	1518.36	1288.42	1987.95	3.12	1.31	1.54	2.02	0.85	2.38	[239]
Gd	64	88	152	344.28	930.54	755.40	1282.40	3.72	1.38	1.70	2.19	0.81	2.70	[166]
Gd	64	90	154	123.07	812.49	371.00	1047.59	8.51	1.29	2.82	3.01	0.46	6.60	[241]
Gd	64	92	156	88.97	1129.43	288.19	1297.80	14.59	1.15	4.50	3.24	0.26	12.69	[242]
Gd	64	94	158	79.51	1197.15	261.46	1358.70	17.09	1.13	5.20	3.29	0.22	15.06	[243]
Gd	64	96	160	75.26	988.40	248.52	1070.40	14.22	1.08	4.31	3.30	0.25	13.13	[244]
Gd	64	98	162	71.60	864.00	236.40	1015.00	14.18	1.17	4.29	3.30	0.27	12.07	[246]
Gd	64	100	164	73.27		241.40					3.29			[245]

Nuclide	Z	N	A	$E_{2,1}$	$E_{2,2}$	$E_{4,1}$	$E_{4,2}$	$\frac{E_{4,2}}{E_{2,1}}$	$\frac{E_{4,2}}{E_{2,2}}$	$\frac{E_{4,2}}{E_{4,1}}$	$\frac{E_{4,1}}{E_{2,1}}$	$\frac{E_{4,1}}{E_{2,2}}$	$\frac{E_{2,2}}{E_{2,1}}$	Refrences
Gd	64	102	166	70.00		230.80	1318.90	18.84		5.71	3.30			[247]
Dy	66	74	140	202.20		566.20					2.80			[234]
Dy	66	76	142	315.90		798.90					2.53			[235]
Dy	66	78	144	492.50		1165.00					2.37			[236]
Dy	66	80	146	682.62		1607.75					2.36			[237]
Dy	66	82	148	1677.30		2426.70					1.45			[238]
Dy	66	84	150	803.64	1786.37	1456.96	2330.80	2.90	1.30	1.60	1.81	0.82	2.22	[239]
Dy	66	86	152	613.83	1313.70	1261.20	1750.70	2.85	1.33	1.39	2.05	0.96	2.14	[240]
Dy	66	88	154	334.34	905.30	746.78	1251.52	3.74	1.38	1.68	2.23	0.82	2.71	[241]
Dy	66	90	156	137.77	828.64	404.19	1088.28	7.90	1.31	2.69	2.93	0.49	6.01	[242]
Dy	66	92	158	98.92	946.32	317.14	1163.75	11.76	1.23	3.67	3.21	0.34	9.57	[243]
Dy	66	94	160	86.79	966.20	283.82	1155.80	13.32	1.20	4.07	3.27	0.29	11.13	[244]
Dy	66	96	162	80.66	888.16	265.66	1060.99	13.15	1.19	3.99	3.29	0.30	11.01	[246]
Dy	66	98	164	73.39	761.80	242.23	916.00	12.48	1.20	3.78	3.30	0.32	10.38	[245]
Dy	66	100	166	76.59	1189.38	253.53					3.31	0.21	15.53	[247]
Dy	66	102	168	74.96		248.33					3.31			[248]
Dy	66	104	170	72.00		235.00					3.26			[249]
Er	68	80	148	645.89		1522.68					2.36			[238]
Er	68	82	150	1578.33		2293.90					1.45			[239]
Er	68	84	152	808.30	1715.40	1480.90					1.83	0.86	2.12	[240]
Er	68	86	154	560.80		1162.20					2.07			[241]
Er	68	88	156	344.53	930.50	797.39	1406.20	4.08	1.51	1.76	2.31	0.86	2.70	[242]
Er	68	90	158	192.15	820.10	527.22	1183.80	6.16	1.44	2.25	2.74	0.64	4.27	[243]
Er	68	92	160	125.80	854.40	389.90	1230.30	9.78	1.44	3.16	3.10	0.46	6.79	[244]
Er	68	94	162	102.04	900.72	329.62	1128.11	11.06	1.25	3.42	3.23	0.37	8.83	[246]
Er	68	96	164	91.38	860.25	299.43	1058.50	11.58	1.23	3.54	3.28	0.35	9.41	[245]
Er	68	98	166	80.58	785.91	264.99	956.20	11.87	1.22	3.61	3.29	0.34	9.75	[247]
Er	68	100	168	79.80	821.16	264.09	994.75	12.46	1.21	3.77	3.31	0.32	10.29	[248]
Er	68	102	170	78.60	934.03	260.15	1103.40	14.04	1.18	4.24	3.31	0.28	11.88	[249]
Er	68	104	172	77.00	961.40	255.20	1131.30	14.69	1.18	4.43	3.31	0.27	12.49	[250]
Yb	70	82	152	1531.40										[240]

Nuclide	Z	N	A	$E_{2,1}$	$E_{2,2}$	$E_{4,1}$	$E_{4,2}$	$\frac{E_{4,2}}{E_{2,1}}$	$\frac{E_{4,2}}{E_{2,2}}$	$\frac{E_{4,2}}{E_{4,1}}$	$\frac{E_{4,1}}{E_{2,1}}$	$\frac{E_{4,1}}{E_{2,2}}$	$\frac{E_{2,2}}{E_{2,1}}$	Refrences
Yb	70	84	154	821.30		1516.00					1.85			[241]
Yb	70	86	156	536.00		1143.20					2.13			[242]
Yb	70	88	158	358.20		835.20					2.33			[243]
Yb	70	90	160	243.10	820.40	638.40	1529.20	6.29	1.86	2.40	2.63	0.78	3.37	[244]
Yb	70	92	162	166.72	798.40	487.33	1150.20	6.90	1.44	2.36	2.92	0.61	4.79	[246]
Yb	70	94	164	123.31	863.90	385.56	1144.30	9.28	1.32	2.97	3.13	0.45	7.01	[245]
Yb	70	96	166	102.37	1144.29	330.48	1342.29	13.11	1.17	4.06	3.23	0.29	11.18	[247]
Yb	70	98	168	87.73	984.00	286.55	1390.12	15.85	1.41	4.85	3.27	0.29	11.22	[248]
Yb	70	100	170	84.25	1138.60	277.43					3.29	0.24	13.51	[249]
Yb	70	102	172	78.74	1117.87	260.27	1263.03	16.04	1.13	4.85	3.31	0.23	14.20	[250]
Yb	70	104	174	76.47	1674.82	253.12	1701.70	22.25	1.02	6.72	3.31	0.15	21.90	[251]
Yb	70	106	176	82.14	1199.60	271.85	1341.10	16.33	1.12	4.93	3.31	0.23	14.61	[252]
Yb	70	108	178	84.00	1221.00	278.00	1559.00	18.56	1.28	5.61	3.31	0.23	14.54	[253]
Hf	72	82	154	1513.00										[241]
Hf	72	84	156	857.20	1454.20	1585.20	2221.60	2.59	1.53	1.40	1.85	1.09	1.70	[242]
Hf	72	86	158	476.36		1033.33					2.17			[243]
Hf	72	88	160	389.40		898.26					2.31			[244]
Hf	72	90	162	285.00		729.50					2.56			[246]
Hf	72	92	164	210.70	816.00	587.10	1072.80	5.09	1.31	1.83	2.79	0.72	3.87	[245]
Hf	72	94	166	158.64	810.00	470.46	1332.40	8.40	1.64	2.83	2.97	0.58	5.11	[247]
Hf	72	96	168	124.10	875.94	385.92	1284.66	10.35	1.47	3.33	3.11	0.44	7.06	[248]
Hf	72	98	170	100.80	961.30	321.99	1156.60	11.47	1.20	3.59	3.19	0.33	9.54	[249]
Hf	72	100	172	95.22	952.40	309.24	1031.10	10.83	1.08	3.33	3.25	0.32	10.00	[250]
Hf	72	102	174	90.99	900.24	297.38	1062.17	11.67	1.18	3.57	3.27	0.33	9.89	[251]
Hf	72	104	176	88.35	1226.63	290.18	1390.19	15.74	1.13	4.79	3.28	0.24	13.88	[252]
Hf	72	106	178	93.18	1174.63	306.62	1384.46	14.86	1.18	4.52	3.29	0.26	12.61	[253]
Hf	72	108	180	93.32	1183.40	308.58	1369.70	14.68	1.16	4.44	3.31	0.26	12.68	[254]
Hf	72	110	182	97.79	818.40	322.17					3.29	0.39	8.37	[255]
Hf	72	112	184	107.10		349.60					3.26			[256]
W	74	86	160	609.90		1264.60					2.07			[244]
W	74	88	162	449.50		1012.50					2.25			[246]

Nuclide	Z	N	A	$E_{2,1}$	$E_{2,2}$	$E_{4,1}$	$E_{4,2}$	$\frac{E_{4,2}}{E_{2,1}}$	$\frac{E_{4,2}}{E_{2,2}}$	$\frac{E_{4,2}}{E_{4,1}}$	$\frac{E_{4,1}}{E_{2,1}}$	$\frac{E_{4,1}}{E_{2,2}}$	$\frac{E_{2,2}}{E_{2,1}}$	Refrences
W	74	90	164	331.90		822.40					2.48			[245]
W	74	92	166	252.00		675.70					2.68			[247]
W	74	94	168	199.30		562.30					2.82			[248]
W	74	96	170	156.72	937.10	462.33	1153.00	7.36	1.23	2.49	2.95	0.49	5.98	[249]
W	74	98	172	123.20		377.10					3.06			[250]
W	74	100	174	113.00		356.40					3.15			[251]
W	74	102	176	108.30	930.00	348.20	1117.00	10.31	1.20	3.21	3.22	0.37	8.59	[252]
W	74	104	178	105.90	1082.44	342.74	1275.09	12.04	1.18	3.72	3.24	0.32	10.22	[253]
W	74	106	180	103.56	1117.31	337.56	1360.50	13.14	1.22	4.03	3.26	0.30	10.79	[254]
W	74	108	182	100.11	1221.40	329.43	1442.80	14.41	1.18	4.38	3.29	0.27	12.20	[255]
W	74	110	184	111.22	903.31	364.07	1133.85	10.19	1.26	3.11	3.27	0.40	8.12	[256]
W	74	112	186	122.63	737.96	396.55	1006.70	8.21	1.36	2.54	3.23	0.54	6.02	[257]
W	74	114	188	143.16	628.14	439.49	854.10	5.97	1.36	1.94	3.07	0.70	4.39	[258]
W	74	116	190	207.00		564.00					2.72			[259]
W	74	118	192	219.00										[260]
Os	76	86	162	706.70		1406.50					1.99			[246]
Os	76	88	164	548.00		1206.30					2.20			[245]
Os	76	90	166	432.00		1021.00					2.36			[247]
Os	76	92	168	341.20		857.30					2.51			[248]
Os	76	94	170	286.70		749.90					2.62			[249]
Os	76	96	172	227.77	702.80	606.17	1137.00	4.99	1.62	1.88	2.66	0.86	3.09	[250]
Os	76	98	174	158.60	690.90	435.00	989.40	6.24	1.43	2.27	2.74	0.63	4.36	[251]
Os	76	100	176	135.10	742.40	395.50	1025.60	7.59	1.38	2.59	2.93	0.53	5.50	[252]
Os	76	102	178	132.20	771.00	398.79	1023.20	7.74	1.33	2.57	3.02	0.52	5.83	[253]
Os	76	104	180	132.11	831.10	408.63	1052.70	7.97	1.27	2.58	3.09	0.49	6.29	[254]
Os	76	106	182	126.89	890.61	400.29	1190.30	9.38	1.34	2.97	3.15	0.45	7.02	[255]
Os	76	108	184	119.77	942.90	383.68	1225.00	10.23	1.30	3.19	3.20	0.41	7.87	[256]
Os	76	110	186	137.16	767.48	434.09	1070.50	7.80	1.39	2.47	3.16	0.57	5.60	[257]
Os	76	112	188	155.21	633.00	477.96	965.70	6.22	1.53	2.02	3.08	0.76	4.08	[258]
Os	76	114	190	186.72	558.00	547.85	955.40	5.12	1.71	1.74	2.93	0.98	2.99	[259]
Os	76	116	192	205.79	489.10	580.28	906.50	4.40	1.85	1.56	2.82	1.19	2.38	[260]

Nuclide	Z	N	A	$E_{2,1}$	$E_{2,2}$	$E_{4,1}$	$E_{4,2}$	$\frac{E_{4,2}}{E_{2,1}}$	$\frac{E_{4,2}}{E_{2,2}}$	$\frac{E_{4,2}}{E_{4,1}}$	$\frac{E_{4,1}}{E_{2,1}}$	$\frac{E_{4,1}}{E_{2,2}}$	$\frac{E_{2,2}}{E_{2,1}}$	Refrences
Os	76	118	194	218.51	656.50	601.00					2.75	0.92	3.00	[261]
Os	76	120	196	324.40		791.40					2.44			[262]
Os	76	122	198	465.40	877.60	1073.60	1350.90	2.90	1.54	1.26	2.31	1.22	1.89	[263]
Pt	78	90	168	581.40		1307.30					2.25			[248]
Pt	78	92	170	508.90		1171.20					2.30			[249]
Pt	78	94	172	457.60		1069.98					2.34			[250]
Pt	78	96	174	394.20		891.80					2.26			[251]
Pt	78	98	176	264.00		564.10					2.14			[252]
Pt	78	100	178	170.30	653.20	427.40	1058.20	6.21	1.62	2.48	2.51	0.65	3.84	[253]
Pt	78	102	180	153.24	677.50	410.73	1049.30	6.85	1.55	2.55	2.68	0.61	4.42	[254]
Pt	78	104	182	154.97	667.80	419.62	1239.90	8.00	1.86	2.95	2.71	0.63	4.31	[255]
Pt	78	106	184	162.98	648.70	435.91	1234.33	7.57	1.90	2.83	2.67	0.67	3.98	[256]
Pt	78	108	186	191.53	607.20	490.33	991.50	5.18	1.63	2.02	2.56	0.81	3.17	[257]
Pt	78	110	188	265.63	605.70	671.02	1085.40	4.09	1.79	1.62	2.53	1.11	2.28	[258]
Pt	78	112	190	295.80	597.60	737.04	1128.20	3.81	1.89	1.53	2.49	1.23	2.02	[259]
Pt	78	114	192	316.51	612.50	784.58	1201.00	3.79	1.96	1.53	2.48	1.28	1.94	[260]
Pt	78	116	194	328.46	622.00	811.27	1226.50	3.73	1.97	1.51	2.47	1.30	1.89	[261]
Pt	78	118	196	355.68	688.70	876.87	1293.30	3.64	1.88	1.47	2.47	1.27	1.94	[262]
Pt	78	120	198	407.22	774.70	985.07	1286.10	3.16	1.66	1.31	2.42	1.27	1.90	[263]
Pt	78	122	200	470.10	1726.00	1103.30	1936.00	4.12	1.12	1.75	2.35	0.64	3.67	[264]
Pt	78	124	202	534.90		1253.60					2.34			[265]
Pt	78	126	204	872.00										[266]
Hg	80	92	172	672.80		1518.60					2.26			[166]
Hg	80	96	176	613.30		1369.70					2.23			[252]
Hg	80	98	178	558.00		1012.40					1.81			[253]
Hg	80	100	180	434.24	601.60	706.27	1223.80	2.82	2.03	1.73	1.63	1.17	1.39	[254]
Hg	80	102	182	351.70	548.30	613.20	1124.80	3.20	2.05	1.83	1.74	1.12	1.56	[255]
Hg	80	104	184	366.78	534.40	653.77	1086.60	2.96	2.03	1.66	1.78	1.22	1.46	[256]
Hg	80	106	186	405.33	621.80	807.99	1080.36	2.67	1.74	1.34	1.99	1.30	1.53	[257]
Hg	80	108	188	412.80	881.10	1004.89	1207.90	2.93	1.37	1.20	2.43	1.14	2.13	[258]
Hg	80	110	190	416.32	1099.94	1041.77	1850.78	4.45	1.68	1.78	2.50	0.95	2.64	[259]

Nuclide	Z	N	A	$E_{2,1}$	$E_{2,2}$	$E_{4,1}$	$E_{4,2}$	$\frac{E_{4,2}}{E_{2,1}}$	$\frac{E_{4,2}}{E_{2,2}}$	$\frac{E_{4,2}}{E_{4,1}}$	$\frac{E_{4,1}}{E_{2,1}}$	$\frac{E_{4,1}}{E_{2,2}}$	$\frac{E_{2,2}}{E_{2,1}}$	Refrences
Hg	80	112	192	422.79	1831.60	1057.58	1831.60	4.33	1.00	1.73	2.50	0.58	4.33	[260]
Hg	80	114	194	427.89		1064.19	1957.80	4.58		1.84	2.49			[261]
Hg	80	116	196	425.98	958.40	1061.44	1390.90	3.27	1.45	1.31	2.49	1.11	2.25	[262]
Hg	80	118	198	411.81	1087.60	1048.51	1834.90	4.46	1.69	1.75	2.55	0.96	2.64	[263]
Hg	80	120	200	367.94	1254.10	947.24					2.57	0.76	3.41	[264]
Hg	80	122	202	439.51	959.90	1119.80	1311.50	2.98	1.37	1.17	2.55	1.17	2.18	[265]
Hg	80	124	204	436.55	1716.80	1128.23	2514.40	5.76	1.46	2.23	2.58	0.66	3.93	[266]
Hg	80	126	206	1068.20										[267]
Hg	80	128	208	669.00		1093.90					1.64			[268]
Hg	80	130	210	643.00		1196.00					1.86			[269]
Pb	82	98	180	1168.00		1446.00					1.24			[254]
Pb	82	100	182	888.30		1119.50					1.26			[255]
Pb	82	102	184	701.50		938.90					1.34			[256]
Pb	82	104	186	662.40		923.00					1.39			[257]
Pb	82	106	188	723.60	952.50	1063.80	1195.10	1.65	1.25	1.12	1.47	1.12	1.32	[258]
Pb	82	108	190	773.90	1163.00	1521.30					1.97	1.31	1.50	[259]
Pb	82	110	192	853.64	1237.90	1355.50	2622.40	3.07	2.12	1.93	1.59	1.09	1.45	[260]
Pb	82	112	194	965.08	1308.20	1540.03	2407.60	2.49	1.84	1.56	1.60	1.18	1.36	[261]
Pb	82	114	196	1049.20	1449.87	1738.27	1825.60	1.74	1.26	1.05	1.66	1.20	1.38	[262]
Pb	82	116	198	1063.50		1625.90	1980.70	1.86		1.22	1.53			[263]
Pb	82	118	200	1026.61	1739.40	1488.95					1.45	0.86	1.69	[264]
Pb	82	120	202	960.67	1584.00	1382.84	1623.00	1.69	1.02	1.17	1.44	0.87	1.65	[265]
Pb	82	122	204	899.17	1351.20	1274.13	1563.40	1.74	1.16	1.23	1.42	0.94	1.50	[266]
Pb	82	124	206	803.05	1466.80	1683.99	1997.70	2.49	1.36	1.19	2.10	1.15	1.83	[267]
Pb	82	126	208	4085.52	4928.10	4323.95	5216.20	1.28	1.06	1.21	1.06	0.88	1.21	[268]
Pb	82	128	210	799.70	2209.00	1097.70	2701.00	3.38	1.22	2.46	1.37	0.50	2.76	[269]
Pb	82	130	212	804.90		1117.00					1.39			[270]
Pb	82	132	214	835.00		1179.00					1.41			[271]
Pb	82	134	216	887.00		1289.00					1.45			[166]
Po	84	106	190	234.10		532.40					2.27			[259]
Po	84	108	192	262.00		605.20					2.31			[260]

Nuclide	Z	N	A	$E_{2,1}$	$E_{2,2}$	$E_{4,1}$	$E_{4,2}$	$\frac{E_{4,2}}{E_{2,1}}$	$\frac{E_{4,2}}{E_{2,2}}$	$\frac{E_{4,2}}{E_{4,1}}$	$\frac{E_{4,1}}{E_{2,1}}$	$\frac{E_{4,1}}{E_{2,2}}$	$\frac{E_{2,2}}{E_{2,1}}$	Refrences
Po	84	110	194	319.80	757.80	686.50	1211.30	3.79	1.60	1.76	2.15	0.91	2.37	[261]
Po	84	112	196	463.12	859.10	890.99	1387.80	3.00	1.62	1.56	1.92	1.04	1.86	[262]
Po	84	114	198	604.94	1039.10	1158.39	1483.40	2.45	1.43	1.28	1.91	1.11	1.72	[263]
Po	84	116	200	665.90	1392.30	1276.90					1.92	0.92	2.09	[264]
Po	84	118	202	677.20	2254.10	1248.60	1667.40	2.46	0.74	1.34	1.84	0.55	3.33	[265]
Po	84	120	204	684.34		1200.66	1552.20	2.27		1.29	1.75			[266]
Po	84	122	206	700.66	1162.20	1177.80	1434.40	2.05	1.23	1.22	1.68	1.01	1.66	[267]
Po	84	124	208	686.53	1263.00	1346.56	1583.21	2.31	1.25	1.18	1.96	1.07	1.84	[268]
Po	84	126	210	1181.40	2290.10	1426.70	2382.50	2.02	1.04	1.67	1.21	0.62	1.94	[269]
Po	84	128	212	727.33	1512.70	1132.53					1.56	0.75	2.08	[270]
Po	84	130	214	609.32	1377.70	1015.04					1.67	0.74	2.26	[271]
Po	84	132	216	549.76		968.94					1.76			[272]
Po	84	134	218	509.70		935.20					1.83			[273]
Rn	86	112	198	339.00		749.50					2.21			[263]
Rn	86	114	200	432.60		936.30					2.16			[264]
Rn	86	116	202	504.00		1073.10					2.13			[265]
Rn	86	118	204	542.90		1131.50	1627.80	3.00		1.44	2.08			[266]
Rn	86	120	206	575.30		1134.30					1.97			[267]
Rn	86	122	208	635.80	1414.30	1188.90					1.87	0.84	2.22	[268]
Rn	86	124	210	643.90		1461.60	1546.10	2.40		1.06	2.27			[269]
Rn	86	126	212	1273.80		1501.50					1.18			[270]
Rn	86	128	214	694.70		1141.20					1.64			[271]
Rn	86	130	216	461.40		840.50					1.82			[272]
Rn	86	132	218	324.32		653.18					2.01			[273]
Rn	86	134	220	240.99		533.68					2.21			[274]
Rn	86	136	222	186.21		448.37					2.41			[275]
Ra	88	118	206	474.30		1052.10					2.22			[267]
Ra	88	120	208	520.20		1093.60	1468.40	2.82		1.34	2.10			[268]
Ra	88	122	210	603.70		1205.10	1377.80	2.28		1.14	2.00			[269]
Ra	88	124	212	629.30		1454.30					2.31			[270]
Ra	88	126	214	1382.40		1639.30					1.19			[271]

Nuclide	Z	N	A	$E_{2,1}$	$E_{2,2}$	$E_{4,1}$	$E_{4,2}$	$\frac{E_{4,2}}{E_{2,1}}$	$\frac{E_{4,2}}{E_{2,2}}$	$\frac{E_{4,2}}{E_{4,1}}$	$\frac{E_{4,1}}{E_{2,1}}$	$\frac{E_{4,1}}{E_{2,2}}$	$\frac{E_{2,2}}{E_{2,1}}$	Refrences
Ra	88	128	216	688.20		1164.10					1.69			[272]
Ra	88	130	218	388.90		741.10					1.91			[273]
Ra	88	132	220	178.47		410.07					2.30			[274]
Ra	88	134	222	111.12	1024.90	301.39	1170.40	10.53	1.14	3.88	2.71	0.29	9.22	[275]
Ra	88	136	224	84.37	965.65	250.78					2.97	0.26	11.45	[276]
Ra	88	138	226	67.67	873.70	211.54					3.13	0.24	12.91	[277]
Ra	88	140	228	63.82	770.70	204.70	880.30	13.79	1.14	4.30	3.21	0.27	12.08	[278]
Ra	88	142	230	57.40	734.90	186.64	849.90	14.81	1.16	4.55	3.25	0.25	12.80	[279]
Ra	88	144	232	54.50		179.20					3.29			[166]
Th	90	124	214	623.00		1453.00					2.33			[271]
Th	90	126	216	1478.20		1813.80					1.23			[272]
Th	90	128	218	689.60		1194.20					1.73			[273]
Th	90	130	220	386.50		759.80					1.97			[274]
Th	90	132	222	183.30		439.80					2.40			[275]
Th	90	134	224	98.10		284.10					2.90			[276]
Th	90	136	226	72.20	847.70	226.43					3.14	0.27	11.74	[277]
Th	90	138	228	57.77	874.50	186.84	968.50	16.76	1.11	5.18	3.23	0.21	15.14	[278]
Th	90	140	230	53.23	677.50	174.11	769.60	14.46	1.14	4.42	3.27	0.26	12.73	[279]
Th	90	142	232	49.37	774.20	162.12	873.00	17.68	1.13	5.38	3.28	0.21	15.68	[280]
Th	90	144	234	49.55	1896.30	163.05					3.29	0.09	38.27	[281]
Th	90	146	236	48.40		160.00					3.31			[282]
U	92	134	226	81.30		250.00					3.08			[277]
U	92	136	228	59.00										[278]
U	92	138	230	51.73		169.34					3.27			[279]
U	92	140	232	47.57	734.60	156.57	833.10	17.51	1.13	5.32	3.29	0.21	15.44	[280]
U	92	142	234	43.50	851.74	143.35	947.64	21.79	1.11	6.61	3.30	0.17	19.58	[281]
U	92	144	236	45.24	960.30	149.48	1050.90	23.23	1.09	7.03	3.30	0.16	21.22	[282]
U	92	146	238	44.92	966.13	148.38	1059.60	23.59	1.10	7.14	3.30	0.15	21.51	[283]
U	92	148	240	45.00		150.60					3.35			[284]
U	92	150	242	47.80		158.20					3.31			[285]
Pu	94	142	236	44.63		147.45					3.30			[282]

Nuclide	Z	N	A	$E_{2,1}$	$E_{2,2}$	$E_{4,1}$	$E_{4,2}$	$\frac{E_{4,2}}{E_{2,1}}$	$\frac{E_{4,2}}{E_{2,2}}$	$\frac{E_{4,2}}{E_{4,1}}$	$\frac{E_{4,1}}{E_{2,1}}$	$\frac{E_{4,1}}{E_{2,2}}$	$\frac{E_{2,2}}{E_{2,1}}$	Refrences
Pu	94	144	238	44.07	983.10	145.94	1125.80	25.55	1.15	7.71	3.31	0.15	22.31	[283]
Pu	94	146	240	42.82	900.30	141.69	992.40	23.17	1.10	7.00	3.31	0.16	21.02	[284]
Pu	94	148	242	44.54	992.50	147.30	1825.80	40.99	1.84	12.40	3.31	0.15	22.28	[285]
Pu	94	150	244	44.20	708.00	149.90					3.39	0.21	16.02	[286]
Pu	94	152	246	46.70		154.50					3.31			[287]
Cm	96	140	236	45.00										[282]
Cm	96	142	238	35.00										[166]
Cm	96	144	240	38.00										[284]
Cm	96	146	242	42.13		137.00					3.25			[285]
Cm	96	148	244	42.96	970.00	142.34					3.31	0.15	22.58	[286]
Cm	96	150	246	42.85	1124.01	141.99	1219.90	28.47	1.09	8.59	3.31	0.13	26.23	[287]
Cm	96	152	248	43.40	1050.00	143.80	1144.00	26.36	1.09	7.96	3.31	0.14	24.19	[288]
Cm	96	154	250	43.00										[289]
Cf	98	146	244	37.00										[286]
Cf	98	148	246	44.00										[287]
Cf	98	150	248	41.53		137.81					3.32			[288]
Cf	98	152	250	42.72	1031.90	141.88	1123.00	26.29	1.09	7.92	3.32	0.14	24.15	[289]
Cf	98	154	252	45.72	804.80	151.74	900.30	19.69	1.12	5.93	3.32	0.19	17.60	[290]
Fm	100	148	248	46.00		152.00					3.30			[288]
Fm	100	152	252	46.60										[290]
Fm	100	154	254	45.00	693.70	149.40					3.32	0.22	15.42	[291]
Fm	100	156	256	48.10	682.20	159.60	783.20	16.28	1.15	4.91	3.32	0.23	14.18	[292]
No	102	150	252	46.40		153.80					3.31			[290]
No	102	152	254	44.20		145.30					3.29			[291]
Rf	104	152	256	44.00		148.00					3.36			[292]

References

[1] E. Rutherford, *Philos. Mag.* **21,** 669 (1911).

[2] K. S. Krane, Introductory Nuclear Physics (Wiley, 1987).

[3] J. Erler, N. Birge, M. Kortelainen, W. Nazarewicz, E. Olsen, A. M. Perhac, and M. Stoitsov, *Nature* **486,** 509 (2012).

[4] W. Nazarewicz, *Nature Physics* **14,** 537 (2018).

[5] A. V. Afanasjev, S. E. Abgemava, D. Ray, and P. Ring, *Phys. Lett. B* **726,** 680 (2013).

[6] S. Cht. Mavrodiev and M.A. Deliyergiyev, *Int. J. Mod. Phys. E* **27,** 1850015 (2018).

[7] H. A. Bethe and R. F. Bacher, *Rev. Mod. Phys.* **8,** 82 (1936).

[8] N. Bohr and J. A. Wheeler, *Phys. Rev.* **56,** 426 (1939).

[9] N. Bohr, *Phys. Rev.* **55,** 418 (1939).

[10] M. G. Mayer, *Phys. Rev.* **74,** 235 (1948).

[11] M. G. Mayer, *Phys. Rev.* **75,** 1969 (1949).

[12] M. G. Mayer, *Phys. Rev.* **78,** 16 (1950).

[13] M. G. Mayer, *Phys. Rev.* **78,** 22 (1950).

[14] K. Heyde, Basic ideas and concepts in nuclear physics (CRC Press, 2004).

[15] W. Greiner and J. A. Maruhn, Nuclear Models (Springer-Verlag Berlin Heidelberg Copyright Holder, 1996).

[16] D. Bazin, *Nature* **486,** 330 (2012).

[17] G. Hagen and T. Papenbrock, *Nature* **569,** 49 (2019).

[18] A. Bohr and B. R. Mottelson, Nuclear Structure (World Scientific, 1998).

[19] D. J. Rowe, J. L. Wood, Fundamentals of Nuclear Models: Foundational Models (World Scientific, 2010).

[20] V. Zelevinsky and A. Volya, Physics of Atomic Nuclei (Wiley-VCH, Weinheim, 2017).

[21] E. Wigner, *Phys. Rev.* **51,** 106 (1937).

[22] J. P. Elliott, *Proc. Roy. Soc. A (London)* **245,** 128 (1958).

[23] J. P. Elliott, *Proc. Roy. Soc. A (London)* **245,** 562 (1958).

[24] G. Racah, *Phys. Rev.* **63,** 367 (1943).

[25] G. Racah, *Phys. Rev.* **76,** 1352 (1949).

[26] K. T. Hecht, *Nucl. Phys. A* **102,** 11 (1967).

[27] K. T. Hecht, *Nucl. Phys. A* **493,** 29 (1989).

[28] K. T. Hecht and A. Adler, *Nucl. Phys. A* **137,** 129 (1969).

[29] A. Arima, M. Harvey, and K. Shimizu, *Phys. Lett. B* **30,** 517 (1969).

[30] G. Rosensteel and D. J. Rowe, *Phys. Rev. Lett.* **38,** 10 (1977).

[31] P. Van Isacker, *Phys. Rev. Lett.* **83,** 4269 (1999).

[32] P. Van Isacker, *Rep. Prog. Phys.* **62,** 1661 (1999).

[33] A. Arima and F. Iachello, *Ann. Phys.* **99,** 253 (1976).

[34] A. Arima and F. Iachello, *Ann. Phys.* **111,** 201 (1978).

[35] O. Scholten, F. Iachello, and A. Arima, *Ann. Phys.* **115,** 325 (1978).

[36] A. Arima and F. Iachello, *Ann. Phys.* **123,** 468 (1979).

[37] A. Arima and F. Iachello, *Phys. Rev. Let.* **40,** 385 (1978).

[38] F. Iachello and A. Arima, The Interacting Boson Model (Cambridge University Press, Cambridge, 1987).

[39] D. A. Varshalovich, A. N. Moskalev, and V. K. Khersonskii, Quantum Theory of Angular Momentum (World Scientific, Singapore, 1988).

[40] K. Heyde, P. Van Isacker, M. Waroquier, G. Wenes, and Y. Gigase, *Nucl. Phys.* A **398,** 235 (1983).

[41] V. K. B. Kota, J. Van de Jeugt, H. De Meyer, and G. Vanden Berghe, *J. Math. Phys.* **28,** 1644 (1987).

[42] Y. D. Devi, V. K. B. Kota, and J. A. Sheikh, *Phys. Rev.* C **39,** 2057 (1989).

[43] Y. D. Devi and V. K. B. Kota, *Z. Phys.* A **337,** 15 (1990).

[44] P. Van Isacker and D. D. Warner, *J. Phys.* G*: Nuci. Part. Phys.* **20,** 853 (1994).

[45] A. Bouldjedri, P. Van Isacker, and S. Zerguine, *J. Phys.* G*: Nucl. Part. Phys.* **31,** 1329 (2005).

[46] D. Kusnezov, *J. Phys.* A **22,** 4271 (1989).

[47] G. Long, W. Zhang, H. Ji, and S. Zhu, *Sci. China A* **41,** 1296 (1998).

[48] Y. X. Liu, H. Z. Sun, and E. G. Zhao, *J. Phys. G* **20,** 407 (1994).

[49] M. A. Caprio, P. Cejnar, and F. Iachello, *Ann. Phys.* (*NY*) **323,** 1106 (2008).

[50] M. A. Caprio, J. H. Skrabacz, and F. Iachello, *J. Phys. A: Math. Theor.* **44,** 075303 (2011).

[51] V. K. B. Kota, *AIP Conf. Proc.* **1524,** 52 (2013).

[52] V K B Kota, *J. Math. Phys.* **38,** 6639 (1997).

[53] M. M. Hammad, S. M. Fawaz, M. N. El-Hammamy, H. A. Motaweh, and S. B. Doma, *J. Phys. Commun.* **2,** 085010 (2018).

[54] T. Otsuka, *Phys. Rev. Lett.* **46,** 710 (1981).

[55] P. Van Isacker, K. Heyde, J. Jolie, M. Waroquier, J. Moreau, and O. Scholten, *Phys. Lett. B.* **144,** 1 (1984).

[56] O. Scholten, K. Heyde, P. van Isacker, J. Jolie, J. Moreau, M. Waroquier, and J. Sau, *Nucl. Phys. A* **438,** 1 (1985).

[57] A. B. Balantekin and B. R. Barrett, *Phys. Rev. C* **32,** 288 (1985).

[58] P. Van Isacker, K. Heyde, J. Jolie, and A. Sevrin, *Ann. Phys.* **171,** 2 (1986).

[59] A. Leviatan and M. W. Kirson, *Ann. Phys.* **201,** 1 (1990).

[60] V.K.B. Kota, *Pramana-J. Phys.* **60,** 59 (2003).

[61] A. Frank and P. Van Isacker, Algebraic Methods in Molecular and Nuclear Structure Physics (Wiley, New York, 1994).

[62] F. Iachello and P. Van Isacker, The Interacting Boson–Fermion Model (Cambridge University Press, Cambridge, 1991).

[63] R. Bijker and F. Iachello, *Ann. Phys. (N.Y.)* **161,** 360 (1985).

[64] R. Bijker and V. K. B. Kota, *Ann. Phys. (N.Y.)* **187,** 148 (1988).

[65] A. B. Balantekin, I. Bars, and F. Iachello, *Nucl. Phys. A* **370,** 284 (1981).

[66] P. Van Isacker, A. Frank, and Hong-Zhou Sun, *Ann. Phys.* **157,** 183 (1984).

[67] Y. S. Ling, M. Zhang, J. M. Xu, M. Vallieres, R. Gilmore, D. H. Feng, and H.Z. Sun, *Phys. Lett. B* **148,** 13 (1984).

[68] A. K. Singh, G. Gangopadhyay, and D. Banerjee, *Phys. Rev. C* **53,** 2524 (1996).

[69] A. B. Balantekin, I. Bars, R. Bijker, and F. Iachello, *Phys. Rev. C* **27,** 1761 (1983).

[70] J. Jolie, K. Heyde, P. Van Isacker, and A. Frank, *Nucl. Phys. A* **466,** 1 (1987).

[71] I. Morrison and P. D. Jarvis, *Nucl. Phys. A* **435,** 461 (1985).

[72] M. M. Hammad, H. E. Shetawy, A. A. Aly, and S. B. Doma, Phys. Scr. **94,** 105207 (2019).

[73] R. N. Alvarez, D. Bonatsos, and Yu. F. Smirnov, *Phys. Rev. A* **50,** 1088 (1994).

[74] A. J. Majarshin, H. Sabri, and M. A. Jafarizadeh, *Eur. Phys. J. A* **54,** 36 (2018).

[75] D. Bonatsos, P. P. Raychev, R. P. Roussev, and Yu F. Smimov, *Chem. Phys. Lett*. **175,** 300 (1990).

[76] D. Bonatsos, A. Faessler, P. P. Raychev, R. P. Roussev, and Yu F. Smimov, *J. Phys. A: Math. Gen*. **25,** L267 (1992).

[77] D. Bonatsos, P. P. Raychev, and A. Faessler, *Chem. Phys. Lett*. **178,** 221 (1991).

[78] F. Pan, *Phys. Rev. C* **50,** 1876 (1994).

[79] M. A. Jafarizadeh, N. Amiri, N. Fouladi, M. Ghapanvari, and Z. Ranjbar, *Nucl. Phys. A* **972,** 86 (2018).

[80] M. A. Jafarizadeh, N. Amiri, M. Ghapanvari, and N. Fouladi, *Nucl. Phys. A* **977,** 129 (2018).

[81] R. K. Gupta, J. Cseh, A. Ludu, W. Greiner, and W. Scheid, *J. Phys. G: Nucl. Part. Phys*. **18,** L73 (1992).

[82] R. K. Gupta and A. Ludu, *Phys. Rev. C* **48,** 593 (1993).

[83] M. M. Hammad, S. M. Fawaz, M. N. El-Hammamy, H. A. Motaweh, and S. B. Doma, *J. Phys. Commun.* **3,** (2019).

[84] J. Cseh, *J. Phys. A: Math. Gen*. **25,** L1225 (1992).

[85] R. Gilmore, *J. Math. Phys.* **20,** 891 (1979).

[86] R. Gilmore and D. H. Feng, *Nucl. Phys. A* **301,** 189 (1978).

[87] R. Gilmore and D. H. Feng, *Phys. Lett. B* **76,** 26 (1978).

[88] P. Van Isacker and J. Q. chen, *Phys. Rev. C* **24,** 684 (1981).

[89] J. Meng, W. Zhang, S. G. Zhou, H. Toki, and L. S. Geng, *Eur. Phys. J. A* **25,** 23 (2005).

[90] Z. Q. Sheng and J. Y. Guo, *Mod. Phys. Lett. A* **20,** 2711 (2005).

[91] R. Fossion, D. Bonatsos, and G. A. Lalazissis, *Phys. Rev. C* **73,** 044310 (2006).

[92] Z. P. Li, T. Niksic, D. Vretenar, J. Meng, G. A. Lalazissis, and P. Ring, *Phys. Rev. C* **79,** 054301 (2009).

[93] J. Jolie, R. F. Casten, P. von Brentano, and V. Werner, *Phys. Rev. Lett.* **87,** 162501 (2001).

[94] J. Jolie and A. Linnemann, *Phys. Rev. C* **68,** 031301 (R) (2003).

[95] L. Bettermann, V. Werner, E. Williams, and R. J. Casperson, *Phys. Rev. C* **81,** 021303 (R) (2010).

[96] P. Cejnar and J. Jolie, *Phys. Rev. E* **61,** 6237 (2000).

[97] P. Cejnar, J. Jolie, and R. F. Casten, *Rev. Mod. Phys.* **82,** 2155 (2010).

[98] F. Pan, T. Wang, Y-S Huo, and J. P. Draayer, *J. Phys. G: Nucl. Part. Phys.* **35,** 125105 (2008).

[99] P. Van Isacker, A. Bouldjedri, and S. Zerguine, *Nucl. Phys. A* **836,** 225 (2010).

[100] M. A. Caprio and F. Iachello, *Phys. Rev. Lett.* **93,** 242502 (2004).

[101] M. A. Caprio and F. Iachello, *Ann. Phys. (N.Y.)* **318,** 454 (2005).

[102] J. M. Arias, J. E. Garcia-Ramos, and J. Dukelsky, *Phys. Rev. Lett.* **93,** 212501 (2004).

[103] A. Giannatiempo, L. Fortunato, and A. Vitturi, *Phys. Rev. C* **86,** 034311 (2012).

[104] P Cejnar, M Macek, S Heinze, J Jolie, and J Dobes, *J. Phys. A. Math. Gen.* **39,** L515 (2006).

[105] C. E. Alonso, J. M. Arias, and A. Vitturi, *Phys. Rev. C* **75,** 064316 (2007).

[106] J. Jolie, S. Heinze, P. Van Isacker, and R. F. Casten, *Phys. Rev. C* **70,** 011305 (R) (2004).

[107] C. E. Alonso, J. M. Arias, L. Fortunato, and A. Vitturi, *Phys. Rev. C* **72,** 061302 (R) (2005).

[108] C. E. Alonso, J. M. Arias, L. Fortunato, and A. Vitturi, *Phys. Rev. C* **79,** 014306 (2009).

[109] K. Heyde and J. L. Wood, *Rev. Mod. Phys.* **83,** 1467 (2011).

[110] F. Iachello, *Phys. Rev. Lett*. **85,** 3580 (2000).

[111] F. Iachello, *Phys. Rev. Lett*. **87,** 052502 (2001).

[112] R. F. Casten and N. V. Zamfir, *Phys. Rev. Lett*. **87,** 052503 (2001).

[113] R. M. Clark, M. Cromaz, M. A. Deleplanque, M. Descovich, R. M. Diamond, P. Fallon, R. B. Firestone, I. Y. Lee, A. O. Macchiavelli, H. Mahmud, E. Rodriguez-Vieitez, F. S. Stephens, and D. Ward, *Phys. Rev. C* **68,** 037301 (2003).

[114] R. F. Casten and N. V. Zamfir, *Phys. Rev. Lett*. **85,** 3584 (2000).

[115] R. M. Clark, M. Cromaz, M. A. Deleplanque, M. Descovich, R. M. Diamond, P. Fallon, I. Y. Lee, A. O. Macchiavelli, H. Mahmud, E. Rodriguez-Vieitez, F. S. Stephens, and D. Ward, *Phys. Rev. C* **69,** 064322 (2004).

[116] A. Frank, C. E. Alonso, and J. M. Arias, *Phys. Rev. C* **65,** 014301 (2001).

[117] N. V. Zamfir, M. A. Caprio, R. F. Casten, C. J. Barton, C. W. Beausang, Z. Berant, D. S. Brenner, W. T. Chou, J. R. Cooper, A. A. Hecht, R. Krücken, H. Newman, J. R. Novak, N. Pietralla, A. Wolf, and K. E. Zyromski, *Phys. Rev. C* **65,** 044325 (2002).

[118] M. A. Caprio, *Phys. Rev. C* **65,** 031304 (R) (2002).

[119] J. M. Arias, C. E. Alonso, A. Vitturi, J. E. García-Ramos, J. Dukelsky, and A. Frank, *Phys. Rev. C* **68,** 041302 (R) (2003).

[120] L. Fortunato and A. Vitturi, *J. Phys. G: Nucl. Part. Phys.* **29,** 1341 (2003).

[121] L. Fortunato and A. Vitturi, *J. Phys. G: Nucl. Part. Phys.* **30,** 627 (2004).

[122] V. K. B. Kota, *Pramana-J. Phys.* **82 ,**743 (2014).

[123] D. Bonatsos, D. Lenis, N. Minkov, P. P. Raychev, and P. A. Terziev, *Phys. Rev. C* **69,** 044316 (2004).

[124] D. Bonatsos, D. Lenis, N. Pietralla, and P. A. Terziev, *Phys. Rev. C* **74,** 044306 (2006).

[125] J. E. García-Ramos, J. Dukelsky, and J. M. Arias, *Phys. Rev. C* **72,** 037301 (2005).

[126] M. A. Caprio and F. Iachello, *Nucl. Phys. A* **781,** 26 (2007).

[127] R. Krücken, B. Albanna, C. Bialik, R. F. Casten, J. R. Cooper, A. Dewald, N. V. Zamfir, C. J. Barton, C. W. Beausang, M. A. Caprio, A. A. Hecht, T. Klug, J. R. Novak, N. Pietralla, and P. von Brentano, *Phys. Rev. Lett.* **88,** 232501 (2002).

[128] P. G. Bizzeti and A. M. Bizzeti-Sona, *Phys. Rev. C* **66,** 031301 (R) (2002).

[129] M. A. Caprio, N. V. Zamfir, R. F. Casten, C. J. Barton, C. W. Beausang, J. R. Cooper, A. A. Hecht, R. Krücken, H. Newman, J. R. Novak, N. Pietralla, A. Wolf, and K. E. Zyromski, *Phys. Rev. C* **66,** 054310 (2002).

[130] C. Hutter, R. Krücken, A. Aprahamian, C. J. Barton, C. W. Beausang, M. A. Caprio, R. F. Casten, W. T. Chou, R. M. Clark, D. Cline, J. R. Cooper, M. Cromaz, A. A. Hecht, A. O.

Macchiavelli, N. Pietralla, M. Shawcross, M. A. Stoyer, C. Y. Wu, and N. V. Zamfir, *Phys. Rev. C* **67,** 054315 (2003).

[131] D. Tonev, A. Dewald, T. Klug, P. Petkov, J. Jolie, A. Fitzler, O. Möller, S. Heinze, P. von Brentano, and R. F. Casten, *Phys. Rev. C* **69,** 034334 (2004).

[132] E. A. McCutchan, N. V. Zamfir, M. A. Caprio, R. F. Casten, H. Amro, C. W. Beausang, D. S. Brenner, A. A. Hecht, C. Hutter, S. D. Langdown, D. A. Meyer, P. H. Regan, J. J. Ressler, and A. D. Yamamoto, *Phys. Rev. C* **69,** 024308 (2004).

[133] D. Bonatsos, D. Lenis, N. Minkov, P. P. Raychev, and P. A. Terziev, *Phys. Rev. C* **69,** 014302 (2004).

[134] D. Bonatsos, D. Lenis, N. Minkov, D. Petrellis, P. P. Raychev, and P. A. Terziev, *Phys. Rev. C* **70,** 024305 (2004).

[135] A. Leviatan, *Phys. Rev. C* **72,** 031305 (R) (2005).

[136] M. Sugawara and H Kusakari, *Phys. Rev. C* **75,** 067302 (2007).

[137] F. Iachello, *Phys. Rev. Lett.* **91,** 132502 (2003).

[138] D. Bonatsos, D. Lenis, D. Petrellis, and P. A. Terziev, *Phys. Lett. B* **588,** 172 (2004).

[139] D. Bonatsos, D. Lenis, D. Petrellis, P. A. Terziev, I. Yigitoglu, *Phys. Lett. B* **632,** 238 (2006).

[140] Y. Zhang, F. Pan, Y. A. Luo, and J.P. Draayer, *Phys. Lett. B* **751,** 423 (2015).

[141] D. Bonatsos, D. Lenis, N. Minkov, D. Petrellis, and P. Yotov, *Phys. Rev. C* **71,** 064309 (2005).

[142] Y. Zhang, Z. Hou, and Y. Liu, *Phys. Rev. C* **76,** 011305 (R) (2007).

[143] L. R. Dai, F. Pan, L. Liu, L. X. Wang, and J. P. Draayer, *Phys. Rev. C* **86,** 034316 (2012).

[144] Y. Zhang, F. Pan, Y.A. Luo, Y.X. Liu, and J. P. Draayer, *Phys. Rev. C* **86,** 044312 (2012).

[145] F. Iachello, *Phys. Rev. Lett.* **95,** 052503 (2005).

[146] M. S. Fetea, R. B. Cakirli, R. F. Casten, D. D. Warner, E. A. McCutchan, D. A. Meyer, A. Heinz, H. Ai, G. Gürdal, J. Qian, and R. Winkler, *Phys. Rev. C* **73,** 051301 (R) (2006).

[147] C. E. Alonso, J. M. Arias, and A. Vitturi, *Phys. Rev. Lett.* **98,** 052501 (2007).

[148] Y. Zhang, F. Pan, Y. X. Liu, Z. F. Hou, and J. P. Draayer, Phys. Rev. C **82,** 034327 (2010).

[149] Y. Zhang, F. Pan, Y. X. Liu, Y. A. Luo, and J. P. Draayer, *Phys. Rev. C* **84,** 034306 (2011).

[150] J. A. Cizewski, *Phys. Lett. B* **219,** 189 (1989).

[151] D. Bonatsos, L. D. Skouras, and J. Rikovska, *Phys. Rev. C* **43,** R952 (1991).

[152] Y. Zhang, Z. Hou, and Y. Liu, *Sci. China Phys. Mech. Astron.* **54,** 88 (2011).

[153] R. F. Casten, N. V. Zamfir, and D. S. Brenner, *Phys. Rev. Lett.* **71,** 227 (1993).

[154] N. V. Zamfir and R. F. Casten, *Phys. Lett. B* **341,** 1 (1994).

[155] N. V. Zamfir, R. F. Casten, and D. S. Brenner, *Phys. Rev. Lett.***72,** 3480 (1994).

[156] D. Bucurescu, G. Căta-Danil, M. Ivaşcu, L. Stroe, and C. A. Ur, *Phys. Rev. C* **49,** R1759 (1994).

[157] D. Bucurescu, N. Mărginean, I. Căta-Danil, M. Ivaşcu, L. Stroe, and C. A. Ur, *Phys. Lett. B* **386,** 12 (1996).

[158] D. Bucurescu and N. Mărginean, *Phys. Rev. Lett.* **79,** 31 (1997).

[159] D. Bucurescu, N. V. Zamfir, G. Căta-Danil, M. Ivaşcu, L. Stroe, C. A. Ur, and R. F. Casten, *Phys. Lett. B* **376,** 1 (1996).

[160] D. Bucurescu, N. V. Zamfir, R. F. Casten, and W. T. Chou, *Phys. Rev. C* **60,** 044303 (1999).

[161] D. Bucurescu, N. V. Zamfir, G. Căta-Danil, M. Ivaşcu, and N. Mărginean, *Phys. Rev. C* **78,** 044322 (2008).

[162] C. A. Mallmann, *Phys. Rev. Lett.* **2,** 507 (1959).

[163] D. Bonatsos and A. Klein, *Phys. Rev. C* **29,** 1879 (1984).

[164] T. K. Das, R. M. Dreizler, and A. Klein, *Phys. Rev. C* **2,** 632 (1970).

[165] H. Ejiri, M. Ishihara, M. Sakai, K. Katori, and T. Inamura, *J. Phys. Soc. Jpn.* **24,** 1189 (1968).

[166] Evaluated Nuclear Structure Data File, https://www.nndc.bnl.gov/ensdf/

[167] J. H. Kelley, D. R. Tilley, H. R. Weller, and G. M. Hale, *Nucl. Phys. A* **541,** 1 (1992).

[168] D. R. Tilley, C. M. Cheves, J. L. Godwin, G. M. Hale, H. M. Hofmann, J. H. Kelley, C. G. Sheu, and H. R. Weller *Nucl. Phys. A* **708,** 3 (2002).

[169] D. R. Tilley, J. H. Kelley, J. L. Godwin, D. J. Millener, J. E. Purcell, C. G. Sheu, and H. R. Weller, *Nucl. Phys. A* **745,** 155 (2004).

[170] F. Ajzenberg-Selove, *Nucl. Phys. A* **506,** 1 (1990).

[171] F. Ajzenberg-Selove, *Nucl. Phys. A* **523,** 1 (1991).

[172] D. R. Tilley, H. R. Weller, and C. M. Cheves, *Nucl. Phys. A* **564,** 1 (1993).

[173] D. R. Tilley, H. R. Weller, C. M. Cheves, and R. M. Chasteler, *Nucl. Phys. A* **595,** 1 (1995).

[174] D. R. Tilley, C. M. Cheves, J. H. Kelley, S. Raman, and H. R. Weller, *Nucl. Phys. A* **636,** 249 (1998).

[175] M. S. Basunia, *Nucl. Data Sheets* **127,** 69 (2015).

[176] R. B. Firestone, *Nucl. Data Sheets* **108,** 2319 (2007).

[177] M. S. Basunia and A. M. Hurst, *Nucl. Data Sheets* **134,** 1 (2016).

[178] M. S. Basunia, *Nucl. Data Sheets* **114,** 1189 (2013).

[179] M. S. Basunia, *Nucl. Data Sheets* **111,** 2331 (2010).

[180] C. Ouellet and B. Singh, *Nucl. Data Sheets* **112,** 2199 (2011).

[181] N. Nica and B. Singh, *Nucl. Data Sheets* **113,** 1563 (2012).

[182] N. Nica, J. A. Cameron, and B. Singh, *Nucl. Data Sheets* **113,** 1 (2012).

[183] J. A. Cameron and B. Singh, *Nucl. Data Sheets* **109,** 1 (2008).

[184] J. Chen, *Nucl. Data Sheets* **140,** 1 (2017).

[185] J. Chen and B. Singh, *Nucl. Data Sheets* **135,** 1 (2016).

[186] J. Chen, B. Singh, and J. A. Cameron, *Nucl. Data Sheets* **112,** 2357 (2011).

[187] S. C. Wu, *Nucl. Data Sheets* **91,** 1 (2000).

[188] T. W. Burrows, *Nucl. Data Sheets* **107,** 1747 (2006).

[189] Z. Elekes, J. Timar, and B. Singh, *Nucl. Data Sheets* **112,** 1 (2011).

[190] Y. Dong and H. Junde, *Nucl. Data Sheets* **128,** 185 (2015).

[191] Y. Dong and H. Junde, *Nucl. Data Sheets* **121,** 1 (2014).

[192] H. Junde, H. Su, and Y. Dong, *Nucl. Data Sheets* **112,** 1513 (2011).

[193] C. D. Nesaraja, S. D. Geraedts, and B. Singh, *Nucl. Data Sheets* **111,** 897 (2010).

[194] E. Browne and J. K. Tuli, *Nucl. Data Sheets* **114,** 1849 (2013).

[195] A. L. Nichols, B. Singh, and J. K. Tuli, *Nucl. Data Sheets* **113,** 973 (2012).

[196] B. Singh, *Nucl. Data Sheets* **108,** 197 (2007).

[197] E. Browne and J. K. Tuli, *Nucl. Data Sheets* **111,** 1093 (2010).

[198] E. A. McCutchan, *Nucl. Data Sheets* **113,** 1735 (2012).

[199] G. Gurdal and E. A. McCutchan, *Nucl. Data Sheets* **136,** 1 (2016).

[200] D. Abriola and A. A. Sonzogni, *Nucl. Data Sheets* **111,** 1 (2010).

[201] B. Singh and A. R. Farhan, *Nucl. Data Sheets* **107,** 1923 (2006).

[202] B. Singh, *Nucl. Data Sheets* **74,** 63 (1995).

[203] A. R. Farhan and B. Singh, *Nucl. Data Sheets* **110,** 1917 (2009).

[204] B. Singh, *Nucl. Data Sheets* **105,** 223 (2005).

[205] J. K. Tuli, *Nucl. Data Sheets* **98,** 209 (2003).

[206] D. Abriola, M. Bostan, S. Erturk, M. Fadil, M. Galan, S. Juutinen, T. Kibédi, F. Kondev, A. Luca, A. Negret, N. Nica, B. Pfeiffer, B. Singh, A. Sonzogni, J. Timar, J. Tuli, T. Venkova, and K. Zuber, *Nucl. Data Sheets* **110,** 2815 (2009).

[207] A. Negret and B. Singh, *Nucl. Data Sheets* **124,** 1 (2015).

[208] E. A. McCutchan and A. A. Sonzogni, *Nucl. Data Sheets* **115,** 135 (2014).

[209] E. Browne, *Nucl. Data Sheets* **82,** 379 (1997).

[210] C. M. Baglin, *Nucl. Data Sheets* **113,** 2187 (2012).

[211] D. Abriola and A. A. Sonzogni, *Nucl. Data Sheets* **109,** 2501 (2008).

[212] B. Singh and Z. Hu, *Nucl. Data Sheets* **98,** 335 (2003).

[213] B. Singh, *Nucl. Data Sheets* **109,** 297 (2008).

[214] D. De Frenne, *Nucl. Data Sheets* **110,** 1745 (2009).

[215] D. Abriola, A. A. Sonzogni, *Nucl. Data Sheets* **107,** 2423 (2006).

[216] J. Blachot, *Nucl. Data Sheets* **108,** 2035 (2007).

[217] D. De Frenne and A. Negret, *Nucl. Data Sheets* **109,** 943 (2008).

[218] J. Blachot, *Nucl. Data Sheets* **91,** 135 (2000).

[219] G. Gurdal and F. G. Kondev, *Nucl. Data Sheets* **113,** 1315 (2012).

[220] S. Lalkovski and F. G. Kondev, *Nucl. Data Sheets* **124,** 157 (2015).

[221] J. Blachot, *Nucl. Data Sheets* **113,** 515 (2012).

[222] J. Blachot, *Nucl. Data Sheets* **111,** 717 (2010).

[223] K. Kitao, *Nucl. Data Sheets* **75,** 99 (1995).

[224] K. Kitao, Y. Tendow, and A. Hashizume, *Nucl. Data Sheets* **96,** 241 (2002).

[225] T. Tamura, *Nucl. Data Sheets* **108,** 455 (2007).

[226] J. Katakura and Z. D. Wu, *Nucl. Data Sheets* **109,** 1655 (2008).

[227] Z. Elekes and J. Timar, *Nucl. Data Sheets* **129,** 191 (2015).

[228] J. Katakura and K. Kitao, *Nucl. Data Sheets* **97,** 765 (2002).

[229] B. Singh, *Nucl. Data Sheets* **93,** 33 (2001).

[230] Yu. Khazov, A. A. Rodionov, S. Sakharov, and B. Singh, *Nucl. Data Sheets* **104,** 497 (2005).

[231] A. A. Sonzogni, *Nucl. Data Sheets* **103,** 1 (2004).

[232] A. A. Sonzogni, *Nucl. Data Sheets* **95,** 837 (2002).

[233] J. Chen, *Nucl. Data Sheets* **146,** 1 (2017).

[234] N. Nica, *Nucl. Data Sheets* **108,** 1287 (2007).

[235] T. D. Johnson, D. Symochko, M. Fadil, and J. K. Tuli, *Nucl. Data Sheets* **112,** 1949 (2011).

[236] A. A. Sonzogni, *Nucl. Data Sheets* **93,** 599 (2001).

[237] Yu. Khazov, A. Rodionov, and G. Shulyak, *Nucl. Data Sheets* **136,** 163 (2016).

[238] N. Nica, *Nucl. Data Sheets* **117,** 1 (2014).

[239] S. K. Basu and A. A. Sonzogni, *Nucl. Data Sheets* **114,** 435 (2013).

[240] M. J. Martin, *Nucl. Data Sheets* **114,** 1497 (2013).

[241] C. W. Reich, *Nucl. Data Sheets* **110,** 2257 (2009).

[242] C. W. Reich, *Nucl. Data Sheets* **113,** 2537 (2012).

[243] N. Nica, *Nucl. Data Sheets* **141,** 1 (2017).

[244] C. W. Reich, *Nucl. Data Sheets* **105,** 557 (2005).

[245] B. Singh and J. Chen, *Nucl. Data Sheets* **147,** 1 (2018).

[246] C. W. Reich, *Nucl. Data Sheets* **108,** 1807 (2007).

[247] C. M. Baglin, *Nucl. Data Sheets* **109,** 1103 (2008).

[248] C. M. Baglin, *Nucl. Data Sheets* **111,** 1807 (2010).

[249] C. M. Baglin, *Nucl. Data Sheets* **96,** 611 (2002).

[250] B. Singh, *Nucl. Data Sheets* **75,** 199 (1995).

[251] E. Browne and H. Junde, *Nucl. Data Sheets* **87,** 15 (1999).

[252] M. S. Basunia, *Nucl. Data Sheets* **107,** 791 (2006).

[253] E. Achterberg, O. A. Capurro, and G. V. Marti, *Nucl. Data Sheets* **110,** 1473 (2009).

[254] E. A. McCutchan, *Nucl. Data Sheets* **126,** 151 (2015).

[255] B. Singh, *Nucl. Data Sheets* **130,** 21 (2015).

[256] C. M. Baglin, *Nucl. Data Sheets* **111,** 275 (2010).

[257] C. M. Baglin, *Nucl. Data Sheets* **99,** 1 (2003).

[258] F. G. Kondev, S. Juutinen, and D. J. Hartley, *Nucl. Data Sheets* **150,** 1 (2018).

[259] B. Singh, *Nucl. Data Sheets* **99,** 275 (2003).

[260] C. M. Baglin, *Nucl. Data Sheets* **113,** 1871 (2012).

[261] B. Singh, *Nucl. Data Sheets* **107,** 1531 (2006).

[262] H. Xiaolong, *Nucl. Data Sheets* **108,** 1093 (2007).

[263] H. Xiaolong and K. Mengxiao, *Nucl. Data Sheets* **133,** 221 (2016).

[264] F. G. Kondev and S. Lalkovski, *Nucl. Data Sheets* **108,** 1471 (2007).

[265] S. Zhu and F. G. Kondev, *Nucl. Data Sheets* **109,** 699 (2008).

[266] C. J. Chiara and F. G. Kondev, *Nucl. Data Sheets* **111,** 141 (2010).

[267] F. G. Kondev, *Nucl. Data Sheets* **109,** 1527 (2008).

[268] M. J. Martin, *Nucl. Data Sheets* **108,** 1583 (2007).

[269] M. S. Basunia, *Nucl. Data Sheets* **121,** 561 (2014).

[270] E. Browne, *Nucl. Data Sheets* **104,** 427 (2005).

[271] S. C. Wu, *Nucl. Data Sheets* **110,** 681 (2009).

[272] S. C. Wu, *Nucl. Data Sheets* **108,** 1057 (2007).

[273] A. K. Jain and B. Singh, *Nucl. Data Sheets* **107,** 1027 (2006).

[274] E. Browne and J. K. Tuli, *Nucl. Data Sheets* **112,** 1115 (2011).

[275] S. Singh, A. K. Jain, and J. K. Tuli, *Nucl. Data Sheets* **112,** 2851 (2011).

[276] S. Singh and B. Singh, *Nucl. Data Sheets* **130,** 127 (2015).

[277] Y. A. Akovali, *Nucl. Data Sheets* **77,** 433 (1996).

[278] K. Abusaleem, *Nucl. Data Sheets* **116,** 163 (2014).

[279] E. Browne and J. K. Tuli, *Nucl. Data Sheets* **113,** 2113 (2012).

[280] E. Browne, *Nucl. Data Sheets* **107,** 2579 (2006).

[281] E. Browne and J. K. Tuli, *Nucl. Data Sheets* **108,** 681 (2007).

[282] E. Browne and J. K. Tuli, *Nucl. Data Sheets* **107,** 2649 (2006).

[283] E. Browne and J. K. Tuli, *Nucl. Data Sheets* **127,** 191 (2015).

[284] B. Singh and E. Browne, *Nucl. Data Sheets* **109,** 2439 (2008).

[285] Y. A. Akovali, *Nucl. Data Sheets* **96,** 177 (2002).

[286] C. D. Nesaraja, *Nucl. Data Sheets* **146,** 387 (2017).

[287] E. Browne and J. K. Tuli, *Nucl. Data Sheets* **112,** 1833 (2011).

[288] M. J. Martin, *Nucl. Data Sheets* **122,** 377 (2014).

[289] Y. A. Akovali, *Nucl. Data Sheets* **94,** 131 (2001).

[290] N. Nica, *Nucl. Data Sheets* **106,** 813 (2005).

[291] A. Bhagwat, N. J. Thompson, and J. K. Tuli, *Nucl. Data Sheets* **105,** 959 (2005).

[292] B. Singh, *Nucl. Data Sheets* **141,** 327 (2017).